(2)

A [illegible]

Volume [illegible]

AD-A143 619



[illegible] NAVAL [illegible]

[illegible]

84 07 10 016

2

SECURITY CLASSIFICATION OF THIS PAGE (When Data Entered)

REPORT DOCUMENTATION PAGE		READ INSTRUCTIONS BEFORE COMPLETING FORM
1 REPORT NUMBER	2 GOVT ACCESSION NO. AD-A143 619	3 RECIPIENT'S CATALOG NUMBER
4. TITLE (and Subtitle) A TREATISE ON ACOUSTIC RADIATION VOLUME II-ACOUSTIC TRANSDUCERS		5 TYPE OF REPORT & PERIOD COVERED Book
		6. PERFORMING ORG REPORT NUMBER
7. AUTHOR(s) Dr. Sam Hanish		8 CONTRACT OR GRANT NUMBER(s)
9. PERFORMING ORGANIZATION NAME AND ADDRESS Naval Research Laboratory Code 5104 Washington, DC 20375		10 PROGRAM ELEMENT, PROJECT, TASK AREA & WORK UNIT NUMBERS 62711N SF11-121-601 51-C001-X-3 61153N RR023-03-01 51-1445-0-3
11. CONTROLLING OFFICE NAME AND ADDRESS Naval Sea Systems Command Undersea Warfare Systems Group Washington, DC 20362		12 REPORT DATE 1983
		13 NUMBER OF PAGES 516
14 MONITORING AGENCY NAME & ADDRESS(if different from Controlling Office)		15 SECURITY CLASS. (of this report) UNCLASSIFIED
		15a DECLASSIFICATION/DOWNGRADING SCHEDULE

16. DISTRIBUTION STATEMENT (of this Report)

Approved for public release; distribution unlimited.

17. DISTRIBUTION STATEMENT (of the abstract entered in Block 20, if different from Report)

18. SUPPLEMENTARY NOTES

DTIC ELECTE JUL 3 0 1984 S E D

19. KEY WORDS (Continue on reverse side if necessary and identify by block number)

general theory of acoustic transducers
fiber-optic hydrophones
composite material transducers
Helmholtz radiator
metglass transducers
directional hydrophones

20. ABSTRACT (Continue on reverse side if necessary and identify by block number)

This book is a second volume of the author's series on Acoustic Radiation. The first two chapters review standard theory of equivalent circuits, with a substantial introduction to bond-graph theory as applied to transducers. Chapters 3-8 and 10 discuss special topics in current acoustic transducer practice. Chapter 9 is devoted to basic generalizations which relate acoustic transducer mechanical impedances to acoustic radiation.

DD FORM 1 JAN 73 1473 EDITION OF 1 NOV 65 IS OBSOLETE
S/N 0102-014-6601

SECURITY CLASSIFICATION OF THIS PAGE (When Data Entered)

A Treatise on Acoustic Radiation

Volume II — Acoustic Transducers

S. HANISH, Ph.D.

Senior Scientist and Consultant
Naval Research Laboratory
Washington, D.C.

1983

Accession For
NTIS GRA&I [X]
DTIC TAB [ ]
Unannounced [ ]
Justification
By
Distribution/
Availability Codes
Dist | Avail and/or Special
A-1





NAVAL RESEARCH LABORATORY
Washington, D.C.

Approved for public release; distribution unlimited.

PREFACE

Volume II is a continuation of Volume I of a "Treatise on Acoustic Radiation" published 1982 at the Naval Research Laboratory, Washington, DC. In Volume I the source strengths of simple and complex surface and volume radiators were assumed known. In Volume II the theory of acoustic transduction is reviewed in detail to expose the underlying energy conversion processes which generate the source strengths used earlier in Volume I. The closely allied theory of acoustic receivers (particularly hydrophones) also is discussed. Emphasis is placed on methodology of analyzing transducers to show interrelations between structure and acoustic performance. Examples are selected primarily to illuminate this methodology. Fuller descriptions of sonar transducers used by the U.S. Navy are reserved for Volume III of this series.

ACKNOWLEDGMENT

The author acknowledges with gratitude the financial support and encouragement in the production of this book of Mr. Charles Walker, U.S. Naval Ship Systems Command, and Drs. Robert Pohanka, Nicholas Basdekas, and A. Ellinthorpe of the U.S. Office of Naval Research.

CONTENTS

PREFACE iv

ACKNOWLEDGMENT iv

1.0 INTRODUCTION TO TRANSDUCERS PICTURED AS ENERGY CONVERTERS 1

1.2 EQUIVALENT CIRCUIT MODELING OF ACOUSTIC TRANSDUCERS 2

1.3 MECHANICAL NETWORKS 3

1.4 MECHANICAL CIRCUIT ELEMENTS 5

1.5 MUTUAL MASS ELEMENTS 5

1.6 GROUNDING OF MASS E..EMENT IN MECHANICAL CIRCUITS 8

1.7 REPRESENTATION OF ACOUSTIC LOAD AS A MECHANICAL CIRCUIT ELEMENT 8

1.8 EXCHANGE OF SOURCES 15

1.9 DISTINCTION BETWEEN MECHANICAL ELEMENTS IN SERIES/PARALLEL FORM AND IN DUAL FORM 18

1.10 CIRCUIT LAWS FOR MECHANICAL NETWORKS 18

1.11 EXAMPLES OF V-F REPRESENTATIONS OF SIMPLE MECHANICAL SYSTEMS 19

1.12 ACOUSTICAL NETWORKS 23

1.13 MODELING OF AN ACOUSTIC TRANSDUCER BY A MATRIX EQUATION 30

1.14 EXAMPLE OF MATRIX MODELING FOR AN ACOUSTIC PROJECTOR 31

1.15 MATRIX MODELING OF AN ACOUSTIC RECEIVER 32

1.16 ELECTROACOUSTIC ANALOGIES 33

1.17 INTRODUCTION TO CONSTRUCTION OF EQUIVALENT CIRCUITS 35

1.18 A GENERAL PROCEDURE FOR CONSTRUCTING EQUIVALENT CIRCUITS OF MECHANICAL NETWORKS 35

1.19 EXAMPLES OF MECHANICAL NETWORKS AND THEIR EQUIVALENT CIRCUITS 36

1.20 SUMMARY OF PROCEDURE FOR CONSTRUCTING REPRESENTATIONS OF MECHANICAL CIRCUITS AS SECONDARY COMPONENTS OF AN ELECTROMECHANICAL TRANSDUCER 40

1.21 BLACK BOX DESCRIPTIONS OF TRANSDUCER COMPONENTS 45

1.22 EQUIVALENT CIRCUITS OF CONTINUOUS ELASTIC SYSTEMS 49

1.23 UNIFICATION OF CIRCUITS INTO ALL PRIMARY OR ALL SECONDARY COORDINATES 52

1.24 EXAMPLE OF TRANSFER OF SECONDARY CIRCUITS INTO PRIMARY CIRCUITS 55

1.25 METHODS OF ANALYZING ONE-CONNECTION AND MULTIPLE-CONNECTION MECHANICAL SYSTEMS 57

1.26 GENERALIZED ONE-CONNECTION SYSTEMS AND THEIR THEVENIN AND NORTON EQUIVALENTS 57

1.27 BOND GRAPHS OF EQUIVALENT SOURCES 58

1.28 ANALYSIS OF ONE-CONNECTION SYSTEMS 59

1.29 ANALYSIS OF TWO-CONNECTION SYSTEMS BY USE OF EQUIVALENT π OR T NETWORKS 60

1.30 ANALYSIS OF TWO-CONNECTION SYSTEMS BY USE OF FOUR-POLE PARAMETERS 62

1.31 ANALYSIS OF TWO-CONNECTION MECHANICAL SYSTEMS BY IMPEDANCE AND ADMITTANCE PARAMETERS 63

1.32 CONVERSION OF ONE-CONNECTION INTO TWO-CONNECTION SYSTEMS AND COMBINATIONS OF SIMPLE SYSTEMS 64

1.33 BASIC THEORY OF COUPLED ELECTRICAL CIRCUITS 68

1.34 BASIC FORM OF MUTUAL-INDUCTIVE COUPLED CIRCUITS; SPECIFIC CASES OF SIMPLE PRIMARIES AND SECONDARIES 69

1.35 CAPACITIVE AND DIRECT INDUCTIVE COUPLING OF PRIMARY TO SECONDARY CIRCUITS 76

1.36 DUAL CIRCUITS AND SERIES-PARALLEL INVERSIONS 77

1.37 COEFFICIENT OF ELECTROMECHANICAL COUPLING 79

1.38 EXPERIMENTAL DETERMINATION OF ELECTROMECHANICAL COUPLING 81

1.39 MATERIAL COUPLING COEFFICIENTS 84

1.40 COEFFICIENT OF ELECTROMECHANICAL COUPLING AS A MEASURE OF WORK DONE IN A WORK CYCLE 84

1.41 EFFECTIVE COEFFICIENT OF ELECTROMECHANICAL COUPLING (k_{eff}) 87

1.42 STATIC AND DYNAMIC ELECTROMECHANICAL COUPLING FACTORS 89

1.43 INDUCTANCE COUPLED INTO THE ELECTRICAL MESH FROM THE MECHANICAL MESH OF A TWO-MESH SYSTEM 90

1.44 CANONICAL CIRCUITS 91

1.45 TWO-MESH CIRCUITS WITH SYMMETRICAL TRANSDUCTION 91

1.46 TRANSDUCTION COEFFICIENTS IN RECIPROCAL TRANSDUCTION SYSTEMS 93

1.47 TURNS-RATIO DISCUSSION 94

1.48 TRANSDUCTION COEFFICIENTS IN ANTIRECIPROCAL SYSTEMS 96

1.49 INTRODUCTION TO ANALYSIS OF TRANSDUCERS BY VARIATIONAL METHODS 97

1.50 GENERALIZED COORDINATES, GENERALIZED FORCES, VARIATIONAL PRINCIPLE 97

1.51 EXAMPLES OF ANALYSIS OF TRANSDUCERS BY USE OF THE VARIATIONAL PRINCIPLE 107

1.52 TRANSDUCER ANALYSIS VIA SIGNAL FLOW GRAPHS AND BLOCK DIAGRAMS 109

1.53 DYNAMICAL EQUATIONS OF TRANSDUCER OPERATION IN ABSTRACT FORM FOR SYSTEMS EXHIBITING COUPLING BETWEEN n-MESHES 114

1.54 ANALYSIS OF A MULTIMODE—MULTIELECTRODE PIEZOACTIVE SYSTEM BY USE OF GREEN'S FUNCTIONS 115

STATE MODELS OF DISCRETE SYSTEMS

1.55 LOW FREQUENCY ACOUSTIC TRANSDUCTION 119

1.56 MEASUREMENT DIAGRAMS 120

1.57 IDEALIZED TERMINAL-PAIRS AND THEIR COMPONENT-EQUATIONS 123

1.58 MIXED (OR HYBRID) COMPONENT EQUATIONS 124

1.59 ENERGY-CONVERSION TRANSDUCERS AS TWO-PORT COMPONENTS 126

1.60 STATE SYSTEMS, SYSTEM GRAPHS, TREES AND COTREES 128

1.61 CIRCUIT EQUATIONS ON THE ACROSS-VARIABLES 129

1.62 SUPERNODE (OR CUT SET) EQUATIONS ON THE THROUGH-VARIABLES 131

1.63 THE PRIMARY MATHEMATICAL MODEL 132

1.64 THE STATE MODEL 133

1.65 EXAMPLES OF CONSTRUCTION OF STATE MODELS 136

1.66 ACOUSTIC PORTS IN STATE MODEL THEORY 145

1.67 ANALYSIS BY USE OF EQUATIONS OF MOTION AND EQUIVALENT CIRCUITS 146

1.68 THEORY AND APPLICATION OF BOND GRAPHS 148

1.69 EXAMPLES OF INTERCONNECTED BOND GRAPHS 157

1.70 ANALYSIS OF MULTIPORT SYSTEMS USING INTEGRAL CAUSALITY 168

1.71 ANALYSIS OF MULTIPORT SYSTEMS BY FIRST-ORDER DIFFERENTIAL EQUATIONS 176

1.72 BOND GRAPHS AND IMPEDANCE METHODS FOR 2-PORTS 178

2.1 PROJECTORS AND RECEIVERS 187

2.2 MAGNETIC FIELDS AND DRIVES 187

2.3 FUNDAMENTAL EQUATIONS OF PIEZOMAGNETIC ACTIVITY 192

2.4 PHYSICAL INTERPRETATION OF PIEZOMAGNETIC COUPLING 194

2.5 FUNDAMENTAL CONSTITUTIVE EQUATIONS OF PIEZOACTIVE COUPLING 196

2.6 COEFFICIENTS OF ELECTROMECHANICAL COUPLING FOR DIELECTRIC-TYPE TRANSDUCERS 197

2.7 ELASTIC STRUCTURES WHICH EXHIBIT MULTIPLE VELOCITY RESONANCES 198

2.8 VELOCITY RESONANCE IN ELECTROACOUSTIC TRANSDUCTION 200

2.9 DISTINCTION BETWEEN ELECTRICAL AND MECHANICAL RESONANCE 202

2.10 DISTINCTION BETWEEN CONSTANT-B AND CONSTANT-H DRIVE OF A MAGNETOSTRICTIVE TRANSDUCER 203

2.11 SUMMARY OF NOMENCLATURE USED BY VARIOUS AUTHORS TO DESCRIBE RESONANCE IN ELECTROMECHANICAL TRANSDUCERS 209

2.12 MECHANICAL AND ELECTRICAL BOUNDARY CONDITIONS IN PIEZOELECTRIC TRANSDUCERS 211

2.13 LIST OF COMMONLY USED MODES OF VIBRATION OF PIEZOELECTRIC TRANSDUCERS AND THEIR EQUIVALENT CIRCUITS 213

2.14 STANDARD EQUIVALENT CIRCUITS 216

2.15 INTRODUCTION TO DESIGN AIDS 220

2.16 FREQUENCY OF MAXIMUM MOTIONAL IMPEDANCE AND FREQUENCY OF MAXIMUM MOTIONAL ADMITTANCE 224

2.17 GEOMETRICAL CONSIDERATIONS OF MOTIONAL IMPEDANCE AND MOTIONAL ADMITTANCE CIRCLES 225

2.18 TURNS-RATIO IN EQUIVALENT CIRCUITS OF PIEZOELECTRIC TRANSDUCERS 228

2.19 RESONANT FREQUENCIES AT CONSTANT CURRENT AND CONSTANT VOLTAGE DRIVE 229

2.20 QUARTER-WAVE AND HALF-WAVE LONGITUDINAL VIBRATORS 230

2.21 THE MASON EQUIVALENT CIRCUIT OF THE LONGITUDINAL TRANSDUCER 232

2.22 LONGITUDINAL BAR TRANSDUCER CLAMPED AT ONE END 239

2.23 A LONGITUDINAL BAR TRANSDUCER WITH ONE END FREE AND ONE END DRIVING A LOAD 240

2.24 INTRODUCTION TO BANDPASS AND BANDREJECT PROPERTIES OF TRANSDUCERS 243

2.25 PARALLEL RESONANT MECHANICAL CIRCUITS 243

2.26 SERIES-CONNECTED RESONANT MECHANICAL CIRCUITS 248

2.27 SERIES/PARALLEL-CONNECTED MECHANICAL CIRCUIT 252

2.28 MECHANICAL AND ACOUSTICAL WAVE FILTERS 254

2.29 THEORY OF ACOUSTICAL AND MECHANICAL TRANSMISSION LINES 269

2.30 DISTRIBUTED PARAMETER TRANSMISSION LINES 280

2.31 DISTRIBUTED PARAMETER TRANSMISSION LINE WITH LUMPED IMPEDANCE AT ONE TERMINUS 283

2.32 AN ELECTRICAL CIRCUIT WHICH IS THE EQUIVALENT OF A MASS-LOADED PIEZOELECTRIC BAR 285

2.33 RESONANT TRANSDUCER INTERPRETED AS A BAND-PASS FILTER 287

2.34 INTRODUCTION TO DESIGN OF RECEIVERS 293

2.35 FUNDAMENTALS OF MOVING-ARMATURE SYSTEMS 293

2.36 EQUIVALENT CIRCUIT OF A MOVING-ARMATURE TRANSDUCER 295

2.37 THE DYNAMICS OF A LENGTH EXPANDER BAR WITH BIASING FIELD PARALLEL TO LENGTH 296

2.38 FUNDAMENTALS OF ELECTROSTATIC TRANSDUCERS 299

2.39 EQUIVALENT CIRCUIT OF ELECTROSTATIC TRANSDUCERS 301

2.40 PARAMETERS OF STANDARD HYDROPHONE DESIGNS BASED ON POLARIZED PIEZOACTIVE CERAMIC MATERIALS IN CONVENTIONAL GEOMETRIES 303

3.1 INTRODUCTION TO THE UNDERWATER HELMHOLTZ RESONATOR 309

3.2 CONSTRUCTION FEATURES OF AN UNDERWATER HELMHOLTZ ACOUSTIC RADIATOR 309

3.3 ANALYSIS OF OPERATION OF A HELMHOLTZ RESONATOR ACTING AS A SOURCE OF SOUND 310

3.4 GENERIC MODEL OF HELMHOLTZ RESONATOR SOUND SOURCE 314

3.5 EXPLICIT FORMS OF THE ACOUSTICAL IMPEDANCES OF THE HELMHOLTZ RADIATOR SOUND SOURCE 315

3.6 THE CYLINDRICAL PIEZOCERAMIC HELMHOLTZ RESONATOR SOUND SOURCE 320

3.7 CORRECTIONS TO CAVITY AND ORIFICE INERTANCE 327

4.1 INTRODUCTION TO POLYMER FILM TRANSDUCERS 331

4.2 PHENOMENOLOGICAL THEORY OF PIEZOELECTRICITY IN POLYMER FILMS 331

4.3 STRUCTURE AND PROPERTIES OF PVF_2 IN 31 MODE 333

4.4 PIEZOELECTRIC PROPERTIES OF PVDF IN THE 33 MODE 337

4.5 FURTHER DISCUSSION ON THE ORIGIN OF PIEZOELECTRICITY IN PVDF 339

4.6 PIEZOELECTRIC POLYMER HYDROPHONE 340

4.7 ANALYSIS OF THE OPEN-CIRCUIT VOLTAGE OF A DISK HYDROPHONE 342

5.1 ACOUSTO-OPTIC MATERIALS AND THEIR MODELS 347

5.2 STRESS-STRAIN RELATIONS IN A LONG FUSED SILICA FIBER 349

5.3 PRESSURE-INDUCED PHASE CHANGES IN A BARE LIGHT-CARRYING FIBER 349

5.4 NUMERICAL ESTIMATES OF THE ACOUSTIC PRESSURE SENSITIVITY OF A BARE FUSED SILICA FIBER 351

5.5 PRESSURE-INDUCED CHANGES IN A FIBER-OPTIC ACOUSTIC SENSOR WITH COMPOSITE STRUCTURE 352

5.6 FIBER-OPTIC HYDROPHONE—THEORY AND EXPERIMENTAL RESULTS 357

5.7 FIBER-OPTIC HYDROPHONE—PROTECTION AGAINST ENVIRONMENTAL NOISE 362

5.8 SIGNAL/NOISE RATIO OF FIBER-OPTIC HYDROPHONES 366

5.9 INTENSITY MODULATED FIBER OPTIC SENSORS 373

6.1 INTRODUCTION TO UNDERWATER LASER DOPPLER HYDROPHONE 377

6.2 HOMODYNE AND HETERODYNE SYSTEMS OF DETECTION 377

6.3 PREDICTION OF THE LOWEST LEVEL ACOUSTIC SIGNALS THAT CAN BE DETECTED 381

6.4 DESCRIPTION OF A LABORATORY EXPERIMENT IN THE DETECTION OF UNDERWATER ACOUSTIC SIGNALS BY USE OF A LASER HETERODYNE DETECTOR 382

6.5 DETECTION OF ACOUSTIC FIELDS IN WATER BY USE OF A LASER HETERODYNE DETECTOR-EXPERIMENTAL RESULTS 384

6.6 DESIGN CONSIDERATIONS FOR A REMOTE-SENSING LASER HETERODYNE HYDROPHONE 385

6.7 COMPARISON OF THE LASER HETERODYNE DETECTOR WITH THE LASER DOPPLER VELOCIMETER 394

7.1 INTRODUCTION TO METALLIC-GLASS TRANSDUCER 399

7.2 MAGNETOSTRICTION IN METALS—SUMMARY OF PROPERTIES OF USE IN ACOUSTIC TRANSDUCER 399

7.3 MAGNETOSTRICTIVITY 400

7.4 COEFFICIENT OF MAGNETOELASTIC COUPLING 402

7.5 ΔE EFFECT 404

7.6 TRANSDUCTION LOSSES 407

7.7 TRANSDUCTION RATIO 407

7.8 MAGNETOELASTIC PROPERTIES OF METALLIC GLASSES 408

7.9 ALTERNATIVE SOLUTION OF THE DYNAMIC PROBLEM RAISED BY THE EXPERIMENT IN SEC. 7.8 413

7.10 EXPERIMENTAL RESULTS OF MAGNETOMECHANICAL TESTS ON METALLIC GLASS RIBBONS 415

7.11 ELECTROMECHANICAL TRANSDUCERS MADE OF MAGNETOSTRICTIVE RARE EARTH-IRON ALLOYS 418

8.1 PARTICLE VELOCITY AND PRESSURE GRADIENT AT A POINT IN AN ACOUSTIC FIELD 423

8.2 PRESSURE-DIFFERENCE BETWEEN TWO POINTS IN A SOUND FIELD 424

8.3 PRESSURE DIFFERENCE BETWEEN TWO PAIRS OF POINTS ORIENTED IN AN ARBITRARY DIRECTION 427

8.4 "PRESSURE-GRADIENT" MICROPHONE AND ITS EQUIVALENT CIRCUIT IN ELEMENTARY FORM 428

8.5 DIFFRACTION EFFECTS IN PRESSURE-GRADIENT MICROPHONES 433

8.6 DIFFRACTION CONSTANT FOR PRESSURE-GRADIENT SENSORS 448

8.7 EQUIVALENT CIRCUIT OF A SPHERICAL-SHELL PRESSURE GRADIENT HYDROPHONE 451

8.8 FIBER OPTIC PRESSURE-GRADIENT HYDROPHONE 452

8.9 ERROR ANALYSIS IN MEASUREMENT OF PARTICLE VELOCITY BY PRESSURE-GRADIENT HYDROPHONES 458

8.10 ERRORS DUE TO NOISE AND ARBITRARY PHASE SHIFTS 461

8.11 ERRORS IN INTENSITY MEASUREMENTS DUE TO INTEGRATION TIME 463

9.0 INTRODUCTION TO THE GENERAL THEORY OF ELECTROACOUSTIC TRANSDUCTION 467

9.1 ELECTROMECHANICAL TRANSDUCTION 467

9.2 ELECTROACOUSTIC TRANSDUCTION 468

9.3 ACOUSTIC PRESSURE IN AN INFINITE MEDIUM RADIATED BY A TRANSDUCER IN A BAFFLE IN THE PRESENCE OF DISTANT SOUND SOURCES 470

9.4 TRANSDUCER RECEIVING RESPONSE 471

9.5 TRANSDUCER TRANSMITTING RESPONSE 472

9.6 THE RECIPROCITY THEOREM FOR ELECTROACOUSTIC TRANSDUCERS 473

9.7 PASSIVE LINEAR ACOUSTIC TRANSDUCERS WITH FIXED VELOCITY DISTRIBUTION 475

10.0 INTRODUCTION TO TRANSDUCERS MADE OF COMPOSITE MATERIALS 485

10.1 HYDROPHONE FIGURE-OF-MERIT 485

10.2 CONNECTIVITY OF PHASES COMPOSITE STRUCTURES 487

10.3 SERIES, PARALLEL CONNECTIVITIES; HYDROSTATIC PIEZOELECTRIC CONSTANTS 488

10.4 PREPARATION PROCEDURES FOR COMPOSITE MATERIALS 492

10.5 SUMMARY OF MEASUREMENTS ON FERROELECTRIC COMPOSITES FOR HYDROPHONES 492

10.6 LEAD ZIRCONATE TITANATE/POLYMER COMPOSITES FOR HIGH FREQUENCY AFPLICATIONS 498

Chapter 1
REPRESENTATION AND ANALYSIS OF ACOUSTIC TRANSDUCERS

A. Representation by Equivalent Circuits

1.0 INTRODUCTION

Transducers that convert primary sources of energy such as mechanical, electrical, hydraulic, thermal or chemical into sound, are most efficiently designed, calculated, constructed and tested on the basis of equivalent graphs. In classical transducer technology the equivalent graph is chosen to be an electrical circuit. This is a choice justified by the existence of the copious tools of electric circuit theory which can be made available to the acoustic designer. But, however advantageous this choice is, there is equal or better justification to model acoustic transducers by employing the concepts of state system theory, or bond graphs. These latter approachs are taken up in Sections 1.52, and 1.68. Here the theory of equivalent electrical circuits is reviewed in order to provide a background for newer methods to be discussed later.

TRANSDUCERS PICTURED AS ENERGY CONVERTERS

Acoustic transducers can be categorized in several ways: in reference to direction of energy flow, as transmitters or receivers; in reference to frequency spectrum, as broadband or narrowband; in reference to power, as high power or low; in reference to transduction as mechanical, hydraulic, electromagnetic, etc.; and in reference to frequency, as high frequency or low. However, no matter in what context the word acoustic transducer is used, its ultimate construction as a device can be epitomized as a finite chain of components in which energy in different guises flows from one component to another. Generally two species of energy are being interchanged: "primary" (or source) energy such as mechanical, electrical, hydraulic, etc. which have been briefly mentioned above, and "secondary" energy or mechanico-acoustical, whose nature will be more thoroughly discussed in later parts of this chapter. Each energy type, primary and secondary, is stored during part of the vibration cycle in a characteristic storage component. Each storage component is associated with a source or a load. In addition to these components there is a special component which describes how primary energy is converted into secondary energy, and vice versa. This is the transduction component. All components are essentially representations of mathematical relations whose variables can be categorized by sets of *energy coordinates* peculiar to the specific type of energy flowing. For example, the coordinates of the secondary mechanical energy are force f (units: N) and velocity v (units: ms^{-1}); of the secondary acoustical energy, pressure p (units: Nm^{-2}) and volume velocity q (units: m^3s^{-1}). The coordinates for the primary energy are various depending on the specific energy (hydraulic, electromagnetic, chemical, etc.). For convenience these are generalized into the "intensive" coordinate e, and the "extensive" coordinate i. Thus the transducer chain represents a transfer of energy among coordinates e, i, f, v, p, q from component to component.

For quick construction of chains, components are drawn as rectangular boxes with attached terminals. Terminals must be associated in pairs (each pair a "port") because one energy coordinate must be "across" the component and the other must flow "through" the component. Source components have two terminals to serve as energy output; similarly, load components have two terminals to serve as energy absorbers. Passive components receive energy on two (or more) terminals and deliver energy on two (or more) terminals. Thus components are 2-pole (or 1-port), 4-pole (or 2-port), or multipole

(or *n*'th order port). This classification idealizes many otherwise complicated primary and secondary structures, but has the great advantage of giving quick understanding of the physics involved in energy transfer. It is used in the next section.

1.2 EQUIVALENT CIRCUIT MODELING OF ACOUSTIC TRANSDUCERS

The introduction has described how acoustic transducers can be modeled as chains or 'cascades' of 2-pole, 4-pole and multiple components. For convenience in exposition we treat here the case of a 1-dimensional cascade. A simple means of identifying terminals, (hence components) is to label them with integers. [Reichhardt (1)]. The chain is then drawn in the following way:

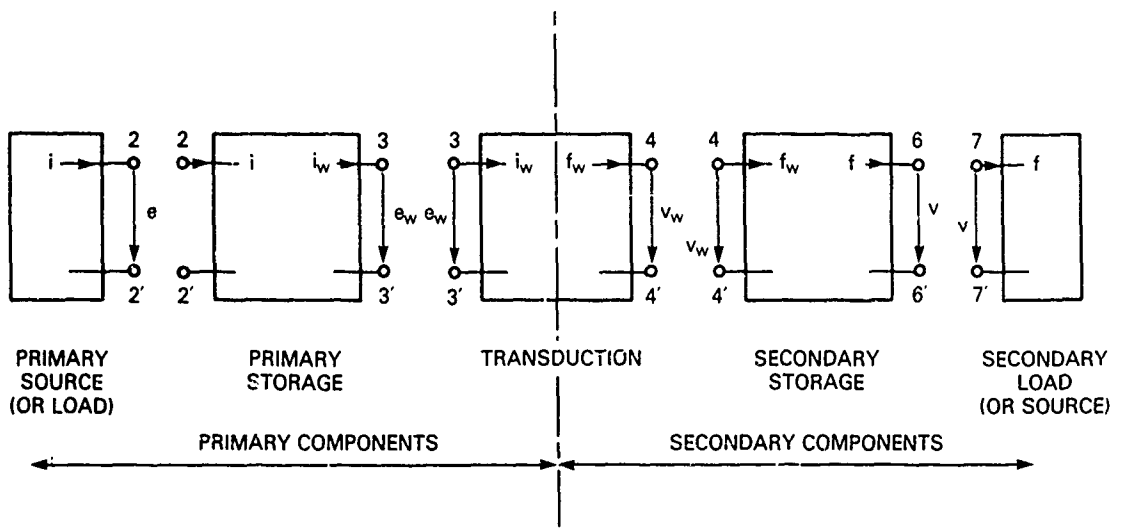


Fig. 1.2.1 — An acoustic transducer modeled as a cascade of components

The numbering sequence is based on the transmitter cascade. The primary source has several physical embodiments: a piston (mechanical, hydraulic), or an explosion (chemical), or an electric generator, or a magnetic field, etc. It is represented by an across-coordinate e at terminals 2,2′ which drives a through-coordinate i into the 2,2′ terminals of the primary storage. This is a 4-pole which stores the energy of the source during part of the drive cycle and releases it during the rest. It may be a flywheel (mechanical), a capacitor (electrical), an inductor (magnetic), an accumulator (hydraulic), etc. It drives flow-coordinate i_ω into the terminals 3,3′ of the transduction component. This 4-pole converts primary energy with coordinates e_ω, i_ω into secondary mechanical energy with coordinates f_ω, v_ω. The secondary storage component 4,4′,6,6′ stores the mechanical energy during part of the driven cycle, and releases it during the rest. Finally the secondary load component (7,7′) is the acoustic load with coordinates f, v related to acoustic coordinates p, q through the area S ($f = pS$, $q = vS$).

When the transducer is a receiver, the cascade operates in reverse: a secondary source (at 7,7′) with coordinates p, q drives the secondary storage component (4,4′,6,6′). The energy is then converted at 4,4′ into primary energy, stored in (4,4′,3,3′), and finally delivered to the load at 2,2′.

The analysis of the chain of components of Fig. 1.2.1 is greatly facilitated by converting energy coordinates of various kinds into one type by means of analogies. In the classical approach the analogous type is voltage e, current i. Thus the equivalent circuit is electrical. The selection of analogs is always purely symbolic: there are no physical considerations which underlie choices. Thus the relation between primary coordinates and analogs may be framed as either of the following pairs 1,2;3,4.

$$\text{pair}\begin{cases}(1)\ \ e \rightarrow f;\ \ i \rightarrow \mathrm{v} \\ (2)\ \ e \rightarrow \mathrm{v};\ \ i \rightarrow f\end{cases} \qquad \text{pair}\begin{cases}(3)\ \ e \rightarrow p;\ \ i \rightarrow q \\ (4)\ \ e \rightarrow q;\ \ i \rightarrow p\end{cases}$$

The symbol $e \rightarrow f$ is read, "the voltage e is analogous to force f," etc. The actual construction of analogs is done by first writing the mathematical expressions which relate the across quantity to the through quantity of single energy element, then comparing them with voltage-current relations of lumped electrical elements. If the mathematical symbols stand in identical relation to one to another, then an analog is permissible. A simple example is acceleration of mass,

$$f = m\ \mathrm{dv/dt}$$

A similar-*looking* electrical form is,

$$i = c\ \mathrm{de/dt}$$

The analogy can then be made as follows:

$$(1)\ \ i \rightarrow f \quad (2)\ e \rightarrow \mathrm{v} \quad (3)\ \ c \rightarrow m$$

There are no priviledged or "best" coordinates: Fig. 1.2.1 can be represented either in all primary, or in all secondary coordinates. We discuss next an all secondary representation of Fig. 1.2.1 and begin with a brief review of mechanical circuits.

1.3 MECHANICAL NETWORKS

Let an acoustic transmitter, or receiver, be represented as a purely mechanical network of lumped elements (that is, concentrated mass, spring, damper) whose dynamic response to a steady state forcing function is desired. A first step in the calculation of this response is advantageously made by constructing a mechanical circuit. It is begun by decomposing the actual mechanical system into a collection of elements representing active sources and passive loads. These elements have the following representational characteristics built into them to achieve a desired simplicity in form and illustration:

- elements are represented as "boxes" provided with terminals to connect them to the external world.

- a 2-terminal box represents a simple relation between the energy coordinate "across" an element to the energy coordinate "through" the element. A 4-terminal box represents a relation between energy coordinates f_1, v_1 at the input terminals to energy coordinates f_2, v_2 at the output terminals. If f_1, v_1 belongs to a different energy system than that of f_2, v_2, the 4-terminal box becomes a *transducer.* A 6-terminal box represents a relation between f_1, v_1 at the input, and two outputs, f_2, v_2, f_3, v_3. Higher order multi-terminal boxes may be similarly constructed. Figure 1.3.1 shows these element representations,

- an *input source* is an element that delivers a known and controllable energy coordinate (force or velocity) to a passive load independent of the reaction of the load. Thus a *force source* delivers a known and controllable force to a specific point of a load, and a *velocity source* delivers a known and controllable velocity to that same point.

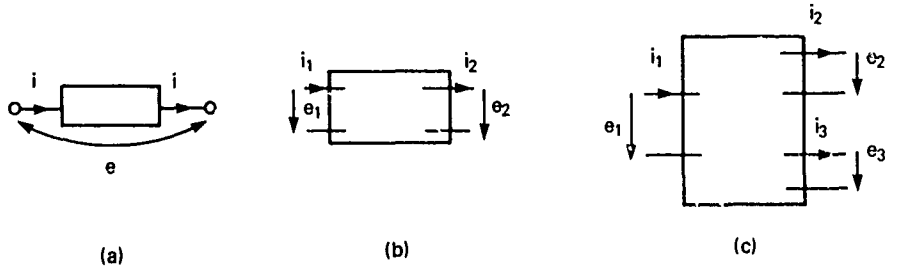


Fig. 1.3.1 — Component elements idealized as two-terminal (a) four-terminal, (b) six terminal, (c) "black boxes," or block diagrams

- a group of passive load elements so connected as to possess a common through-quantity is said to be mechanically in series relative to that quantity. It is called a *branch.* The ends of a branch are called nodes.

- branches so connected as to possess a common across-quantity between a node pair are said to be mechanically in parallel relative to that quantity. A parallel branch that couples two circuits is called a *4-terminal coupler.*

- a group of branches connected in series and forming a closed circuit is called a *loop.* In the formation of loops an input source is treated as a branch.

- a group of interconnected loops in dynamic equilibrium constitutes a *network.*

The construction of mechanical circuits from a collection of interconnected elements may be done in two ways: in the first, the force is taken to be the through-quantity and the velocity the across-quantity; in the second, the roles of force and velocity are reversed. While the choice is arbitrary, there is an advantage in acoustic circuits in selecting velocity as the across-quantity. The reason is that an acoustic source, designed to generate sound, is most physically represented as a velocity device. In addition, as will be discussed later, this choice permits a pictorial similarity between a mechanical circuit and an electrical analogous circuit: that is, when velocity is the across element, a mechanical series circuit will be represented by an electrical series circuit, and a mechanical parallel circuit by an electrical parallel circuit. This fact would not be true if the force coordinate were chosen to be the across-quantity, analogous to voltage.

In this treatise, therefore, mechanical circuits will preferably be constructed with velocity as the across-quantity and force as the through-quantity. They will be called *VF* (velocity-force) circuits. On occasion, however, when there is evident advantage, the opposite force-velocity, *FV*, circuit will be used.

Mechanical networks, like electrical networks, are made to conform to conventions in assignment of directions of across-quantity drop (that is, potential drop) and through-quantity flow (that is, current flow). A list of conventions follows:

- the direction of across-quantities will be shown by an arrow whose tail is at "high" (potential) and whose head is at "low" (potential).

- the direction of flow quantities in a loop will be clockwise.

- potential drops are positive in the direction of flow and negative if their assigned arrows are pointed opposite to the flow.

These conventions are arbitrary. They are adopted here to provide consistency in network representation and analysis.

1.4 MECHANICAL CIRCUIT ELEMENTS

The mechanical lumped circuit elements in common use are mass M, spring N and damper B if the system is in translational motion, and rotational mass J, spring N_r and damper B_r if the system is in rotational motion. The energy coordinates in translational motion are F, v, and in rotational motion are τ (torque), $\dot{\theta}$ (angular velocity).

These elements, when in series with each other, are pictured as 2-terminal boxes, and when in parallel with adjacent branches, as 4-terminal boxes (couplers). They are mathematically modeled by selecting one of the two energy coordinates (F or v, τ or $\dot{\theta}$) as the independent variable, and the other as the dependent variable. In VF networks, if force (or torque) is the independent variable, and velocity (or angular velocity) is the dependent variable, the element models have the forms:

Translational (V across, F through)	Rotational ($\dot{\theta}$ across, τ through)
$\mathrm{v}_M = \frac{1}{M}\int^T F_M(t')\,dt'$	$\dot{\theta}_J = \frac{1}{J}\int^t \tau_J(t')\,dt'$
$\mathrm{v}_N = N\,\frac{dF_N}{dt}(t)$	$\dot{\theta}_{N_r} = N_r\,\frac{d\tau_{N_r}}{dt}(t)$
$\mathrm{v}_B = \frac{F_B}{B}(t)$	$\dot{\theta}_{B_r} = \frac{\tau_{B_r}}{B_r}$

(1.4.1)

An analysis of a VF network containing such elements is then conducted on a *loop* basis, that is, conducted in terms of velocities. If the roles of the energy coordinates are reversed, then the element models have the forms:

Translational (V across, F through)	Rotational ($\dot{\theta}$ across, τ through)
$F_M = M\,\frac{d\mathrm{v}_M}{dt}(t)$	$\tau_J = J\frac{d\dot{\theta}_J}{dt}(t)$
$F_N = \frac{1}{N}\int^t \mathrm{v}_N(t')\,dt'$	$\tau_{N_r} = \frac{1}{N_r}\int^t \dot{\theta}_{N_r}(t')\,dt'$
$F_B = B\mathrm{v}_B(t)$	$\tau_{B_r} = B_r\dot{\theta}_{B_r}(t)$

(1.4.2)

An analysis of a VF network containing such elements is then conducted on a *node* basis, that is, conducted in terms of forces. It will be noted that in all forms the element N (or N_r) represents a compliance. Also, it is seen from Eqs. 1.4.1, 1.4.2 that whenever M and N are both in a network, N will appear in reciprocal form if M is direct form, or M is in reciprocal form if N is direct. Such representations, while arbitrary, make the symbols of mechanical elements and their electrical analogs (inductance L and capacitance C) more nearly alike. Moreover, they agree with rules of causality in bond graph theory as discussed in Sect. 1.68 below.

1.5 MUTUAL MASS ELEMENTS

In certain mechanical elements the force at a terminal may be proportional not only to the acceleration of a mass (say M_1) at that terminal but also proportional to the acceleration of a mass (call it mutual mass M) at another terminal. This is the case of a rigid bar suspended on springs at its ends. Its dynamic motion is analyzed in the following way.

A rigid bar, length l, mass M_b, with its center of gravity (cg) a distance l_1 from end 1, and l_2 from end 2, has a radius of gyration r_g about the cg. It is suspended in space by springs n_1, n_2, one at each end. Under the action of end forces it can be modeled as two lumped masses M_{11} M_{22} joined by a mutual mass M_{12}. Mass M_{11} is the self mass "seen" by the attachment point 1. When accelerated this mass develops a force $M_{11}dv_1/dt$ at point 1. Similarly, M_{22} is the self mass seen by point 2 where, upon acceleration, it develops a force $M_{22}dv_2/dt$. The mutual mass M_{12} is the (lumped) mass of the bar which converts the acceleration of point 2 into a force $M_{12}dv_2/dt$ at point 1, or the acceleration of point 1 into a force (of the same magnitude) at point 2. The values of M_{11}, M_{22} and M_{12} are found by coupling the dynamic motions in translation and rotation with kinematic relations of displacement and angular twist. Thus, in node analysis [2]

$$f_{12} = M_{12}\frac{dv_2}{dt};\quad f_{21} = M_{21}\frac{dv_1}{dt};\quad M_{12} = M_{21}$$

$$M_{12} = M_b\frac{l_1 l_2 - r_g^2}{l^2}. \tag{1.5.1}$$

The self-masses are,

$$M_{11} = M_b\frac{l_2^2 + r_g^2}{l^2};\quad M_{22} = M_b\frac{l_1^2 + r_g^2}{l^2}. \tag{1.5.2}$$

Similarly, in loop analysis,

$$v_{12} = \frac{1}{\tilde{M}_{12}}\int f_2(t)\,dt;\quad v_{21} = \frac{1}{\tilde{M}_{21}}\int f_1(t)\,dt$$

$$\tilde{M}_{12} = \frac{1}{M_b}\frac{M_{12}}{M_1M_2 - M_{12}^2} = \frac{1}{M_b}\frac{l_1 l_2 - r_g^2}{r_g^2} \tag{1.5.3}$$

$$v_1 = \frac{1}{\tilde{M}_{11}}\int f_1(t)\,dt;\quad v_2 = \frac{1}{\tilde{M}_{22}}\int f_2(t)\,dt$$

$$\tilde{M}_{11}^{-1} = \frac{1}{M_b}\frac{l_1^2 + r_g^2}{r_g^2};\quad \tilde{M}_{22}^{-1} = \frac{1}{M_b}\frac{l_2^2 + r_g^2}{r_g^2}.$$

Since the bar is rotating around the cg, one of its ends is (instantaneously) translating in a direction opposite to the other end. Hence the forces at the ends are given by,

$$f_1 = M_{11}\frac{dv_1}{dt} - M_{12}\frac{dv_2}{dt}$$

$$f_2 = -\tilde{M}_{21}\frac{dv_1}{dt} + \tilde{M}_{22}\frac{dv_2}{dt}. \tag{1.5.4}$$

Mutual mass can also be exhibited in rotational mechanical systems. An example, Fig. 1.5.1, is a mechanical element consisting of three external shafts (labeled 1, 2, 3) connected west-east-north with

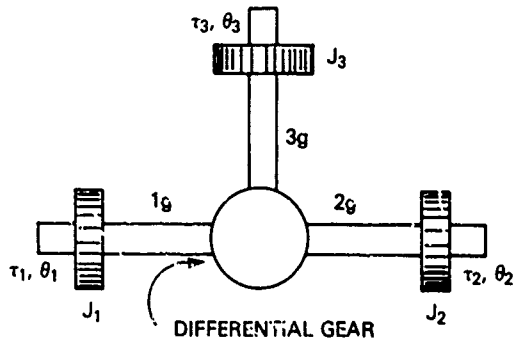


Fig. 1.5.1 — Three shafts of a differential gear illustrating mutual rotational mass

the internal shafts 1_g, 2_g, 3_g of a differential gear. The external shafts have torques τ_1, τ_2, τ_3, angular velocities $\dot{\theta}_1$, $\dot{\theta}_2$, $\dot{\theta}_3$, and moments of inertia J_1, J_2, J_3 respectively. The differential gear delivers the kinematic relation $\theta_3 = c(\theta_1 - \theta_2)$, c = const. The dynamic motion of the group of shafts may be visualized as follows: internal shaft 1_g delivers a torque τ_{1g} opposing external τ_1; internal shaft 2_g delivers the same torque τ_{1g} aiding external τ_2; internal shaft 3_g delivers the torque $\tau_{3g} = \tau_{1g}/c$ aiding external τ_3. These assigned directions of torque are arbitrary but consistent. Upon forming the equations of (rotational) motion for external shafts 1, 2 in terms of $\dot{\theta}_1$, $\dot{\theta}_2$, τ_1, τ_2, τ_3 it is found that these two shafts are coupled dynamically through a mutual moment of inertia of value $J_m = c^2 J_3$, and that shaft 1 is actually driven by $T_1 = \tau_1 + c\tau_3$, and shaft 2 by $T_2 = \tau_2 - c\tau_3$. The equations of motion then reduce to the set [Ref. 2, page 72],

$$T_1 = J_{11} \frac{d\dot{\theta}_2}{dt} - J_m \frac{d\dot{\theta}_2}{dt} \tag{1.5.5}$$

$$T_2 = J_{22} \frac{d\dot{\theta}_2}{dt} - J_m \frac{d\dot{\theta}_1}{dt}$$

in which the self moments of inertia are given by,

$$J_{11} = J_1 + J_m, \quad \text{(shaft 2 fixed)} \tag{1.5.6}$$

$$J_{22} = J_2 + J_m, \quad \text{(shaft 1 fixed)}.$$

These are the relations for analyzing a differential gear and attached external shafts on a node basis.

When the same mechanical rotational system is analyzed on a loop basis, the mathematical models of the differential gear and attached shafts are,

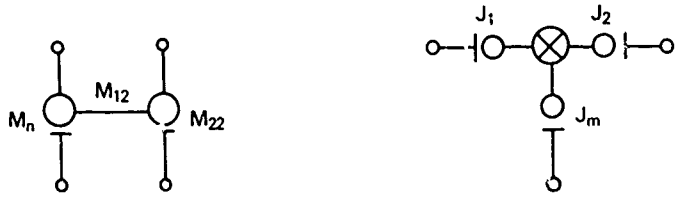
$$\dot{\theta}_1 = \frac{1}{\tilde{J}_{11}} \int^t T_1(t')\,dt' - \frac{1}{\tilde{J}_m} \int^t T_2(t')\,dt' \tag{1.5.7}$$

$$\dot{\theta}_2 = \frac{1}{\tilde{J}_{22}} \int^2 T_2(t')\,dt' - \frac{1}{\tilde{J}_m} \int^2 T_1(t')\,dt'$$

in which the self and mutual moments of inertia are given by,

$$\begin{cases} \tilde{J}_{11}^{-1} = \dfrac{J_{22}}{J_{11}J_{22} - J_m^2}; \\ \text{shaft 2 free} \end{cases} \quad \begin{cases} \tilde{J}_{22}^{-1} = \dfrac{J_{11}}{J_{11}J_{22} - J_m^2}; \quad J_m = C^2 J_3 \\ \text{shaft 1 free.} \end{cases} \tag{1.5.8}$$

The diagrammatic symbols given to mutual mass are the 4-terminal (translational), and the 3-terminal (rotational) shown in Fig. 1.5.2:



(a) TRANSLATIONAL (b) ROTATIONAL

Fig. 1.5.2 — Diagrammatic symbols for mutual mass

1.6 GROUNDING OF MASS ELEMENT IN MECHANICAL CIRCUITS

In a *V-F* circuit representation of a mechanical system the across-quantity is a velocity 'drop' between the terminals of elements. For a mass this velocity drop is calculated with reference to the earth where the velocity is zero. Hence, *one terminal of a mass element must be at ground.* By contrast, in a *F-V* circuit representation the across-quantity is force, for which no particular reference (force) is physically needed. Both terminals of a mass may then be above ground.

This principle may be stated in an alternative formulation: when a gravitational mass shares a common force with a spring or damper its dynamic motion is described by velocity difference relative to ground velocity. Hence one of its terminal must be at ground. When it shares a common velocity its dynamic motion is described by force difference. No restriction on its terminals with respect to ground is mandatory.

In systems with rotary inertia the angular velocity of the earth is involved only through the Coriolis force. If this is negligible (as it is in most acoustical transducers) no grounding rules are mandatory

The theory of bond graphs also observes these precautions (see Sections 1.68 through 1.72). There it is shown that an inertance can be bonded either to a common force junction or a common velocity junction.

1.7 REPRESENTATION OF ACOUSTIC LOAD AS A MECHANICAL CIRCUIT ELEMENT

Transducers designed to radiate (or receive) sound must include the acoustic load as a circuit element.

The calculation of acoustic loading may be quite difficult when the characteristic dimension of the radiating surface is comparable to a wavelength. It is then required to solve an integral-differential equation to determine this loading. However, for present purposes a lumped parameter approach, valid near mechanical resonances of the transmitting or receiving system, is used to arrive quickly at key results.

An acoustic load may be inserted into a *VF* mechanical network in *parallel form* if nodal (that is, force) analysis is used to solve the circuit, or inserted in *series form* if loop (that is, velocity) analysis is to be used.

We consider the parallel form first.

A differential surface of area dS, when mechanically driven in forced harmonic vibration (time given by $\exp j\omega t$) will experience a reaction of the medium. The ratio of the reaction force f_{RAD} exerted by the medium on this surface to the corresponding normal component of surface velocity v_{RAD} is the mechanical radiation impedance Z_{RAD}. Specific forms of Z_{RAD} for specific shapes of the radiating surface are obtained by solution of the equations of motion of the entire surface. Since the medium reacts by imposing a mass load M_{RAD} and a resistive load R_{RAD} on the moving surface the form of mechanical radiation impedance obtained by solving the equations of motion for M_{RAD} and R_{RAD} is,

$$Z_{RAD}(\omega) = \frac{f_{RAD}}{v_{RAD}} = R_{RAD}(\omega) + j\omega M_{RAD}(\omega) \quad \text{(units: Nsm}^{-1}\text{)} \tag{1.7.1}$$

In lumped acoustic circuits f_{RAD} and v_{RAD} are replaced by acoustic pressure $p_{RAD} = f_{RAD}S^{-1}$ and volume velocity $q_{RAD} = v_{RAD}S$. Hence, in acoustic circuits, Z_{RAD} is replaced by the acoustic impedance $\mathscr{Z}_{RAD}$,

$$\text{(a)}\quad \mathscr{Z}_{RAD} = \frac{p_{RAD}}{q_{RAD}} = \frac{Z_{RAD}}{S^2} = \mathscr{R}_{RAD}(\omega) + j\omega\mathscr{M}_{RAD}(\omega), \quad \text{(units: Nsm}^{5}\text{)} \tag{1.7.2}$$

$$\text{(b)}\quad \mathscr{R}_{RAD}(\omega) = \frac{R_{RAD}(\omega)}{S^2}; \quad \mathscr{M}_{RAD}(\omega) = \frac{M_{RAD}}{S^2}.$$

In Eq. 1.7.2a the acoustic resistance and acoustic mass are represented as forming the in-phase and quadrature phase components of pressure relative to volume velocity taken as reference (with zero phase). According to previously noted definitions (in Section 1.3 above) these acoustical elements of resistance and mass form a parallel network in a *VF* circuit. They can thus be written with superscripts p, and appear as $\mathscr{R}^{(p)}$, $\mathscr{M}^{(p)}$. In a *VF* representation these acoustical elements (which are the ones actually found by analyzing acoustical circuits) must be replaced by their corresponding mechanical forms. Figure 1.7.1 shows this representation together with its 'bond graph' (see Sect. 1.68).

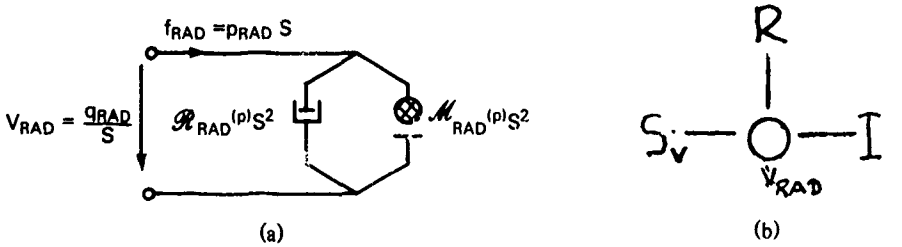


Fig. 1.7.1 — A VF representation of an acoustical load in parallel form

We next consider the series representation of acoustical load. This is obtained by inverting Z_{RAD}, and writing,

$$\text{(a)}\quad q_{RAD} = \mathscr{Y}_{RAD}\, p_{RAD}$$

$$\text{(b)}\quad \mathscr{Y}_{RAD} = \mathscr{G}^{(s)}_{RAD}(\omega) - j\mathscr{B}^{(s)}_{RAD} = \mathscr{Z}^{-1}_{RAD} \quad \text{(units: } m^5N^{-1}s^{-1}\text{)} \tag{1.7.3}$$

$$\text{(c)}\quad \mathscr{G}_{RAD}(\omega) = \frac{\mathscr{R}^{(p)}_{RAD}}{\mathscr{R}^{(p)2}_{RAD} + \omega^2\mathscr{M}^{(p)2}_{RAD}};\ \mathscr{B}_{RAD} = \frac{\omega\mathscr{M}^{(p)}_{RAD}}{\mathscr{R}^{(p)2}_{RAD} + \omega^2\mathscr{M}^{(p)2}_{RAD}}.$$

In Eqs. 1.7.3 the (inverse) acoustic resistance and (inverse) acoustic mass are considered to form the in-phase and quadrature-phase components of the volume velocity relative to acoustic pressure acting as reference (zero phase). By a simple rearrangement one can write these equations in another useful form,

$$\text{(a)}\quad q_{RAD} = \left(\mathscr{G}^{(s)}_{RAD} + \frac{1}{j\omega\mathscr{M}^{(s)}_{RAD}}\right) p_{RAD}$$

$$\text{(b)}\quad \mathscr{M}^{(s)}_{RAD} = \frac{\mathscr{R}^{(p)2}_{RAD} + \omega^2\mathscr{M}^{(p)2}_{RAD}}{\omega^2\mathscr{M}^{(p)}_{RAD}} \quad \text{(units: } Ns^2m^{-5}\text{)}. \tag{1.7.4}$$

The *VF* circuit representation of this series form of acoustical load is shown in Fig. 1.7.2 together with its bond graph (see Sect. 1.68). An example of these two representations is discussed next.

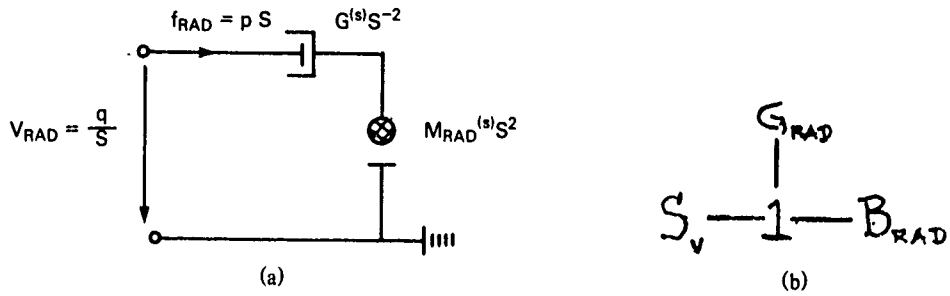


Fig. 1.7.2 — A VF representation of an acoustical load in series form

VF Representation of the Acoustic Load of a Monopole Spherical Radiator

In accord with the concepts of the previous section we consider the case of a monopole spherical radiator, both because of its wide applicability and because its radiation physics is well known. For a specified source strength the ratio of the mechanical force F_{RAD} required to generate the radial velocity U_{RAD} on a spherical surface of radius a, radiating into a medium of mass density ρ, sound speed c, at frequency $\omega = kc$, $k = \frac{2\pi}{\lambda}$ (λ = wavelength) is:

$$Z_{RAD} = \frac{F_{RAD}}{U_{RAD}} = R_{RAD} + jX_{RAD}$$

$$R_{RAD} = \rho c\, 4\pi a^2 \frac{k^2a^2}{1 + k^2a^2};\quad X_{RAD} = \frac{\omega\rho\, 4\pi a^3}{1 + k^2a^2} \quad \text{(units: Nsm}^{-1}\text{)} \tag{1.7.5}$$

$$X_{RAD} = \omega M_{RAD}.$$

The acoustical impedance is obtained from this by division by the square of the area,

$$\mathscr{Z}_{RAD} = \frac{p_{RAD}}{q_{RAD}} = \mathscr{R}_p + j\mathscr{X}_p = \mathscr{R}_p + j\omega\mathscr{M}_p \tag{1.7.6}$$

$$\mathscr{R}_p = \frac{\rho c k^2 a^2}{(1 + k^2a^2)4\pi a^2};\quad \mathscr{M}_p = \frac{\rho}{(1 + k^2a^2)4\pi a};\quad \text{(units: Nsm}^{-5}\text{)}.$$

In *VF* representations Eq. 1.7.5, written in the form,

$$F_{RAD} = (R_{RAD} + jX_{RAD})\, U_{RAD} \tag{1.7.7}$$

is a ***nodal equation*** whose pictorial form is given by Fig. 1.7.3 below:

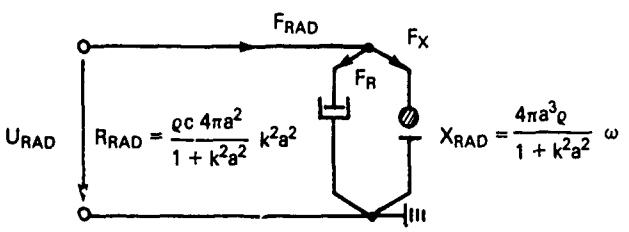


Fig. 1.7.3 — VF representation of the acoustic load of a monopole spherical radiator considered to be in parallel form

Because of the *VF* parallel form one obtains $F_R = RU$, $F_X = jXU$. This is analogous to $I = YE$ in electrical circuits. By use of Eq. 1.7.3 one converts the acoustic load to series form, Fig. 1.7.4, in which Eq. 1.7.7 is a loop equation:

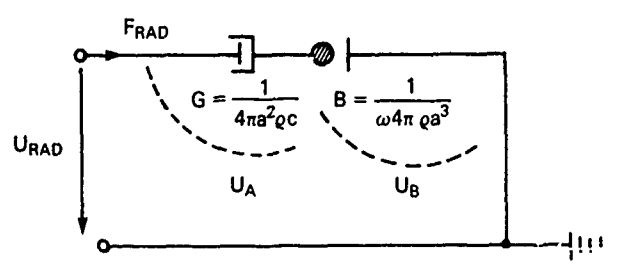


Fig. 1.7.4 — VF representation of the acoustic load of a monopole spherical radiator considered to be in series form

Because of the *VF* series form one obtains $U_G = F_{RAD}G$, $U_B = -jF_{RAD}B$, so that $U_{RAD} = U_G + U_B$. This is analogous to $E = IZ$ in electrical circuits.

It is to be noted that the choice between Figs. 1.7.3 and 1.7.4 is a matter of convenience only in circuit analysis: there may be a physical basis for a choice, but a particular choice is arbitrary.

Summary of Forms that Represent Acoustic Load in Equivalent Circuits

We consider here acoustic loads represented by mechanical radiation impedance Z_L, or by mechanical radiation mobility Y_L,

$$\text{(a)} F/V = Z_L = R_{RAD} + jX_{RAD}, \quad X_{RAD} = \omega M_{RAD}$$

$$\text{(b)} \quad V/F = Y_L = G_{RAD} - jB_{RAD}, \tag{1.7.8}$$

$$\text{(c)} \quad G_{RAD} = \frac{R_{RAD}}{R_{RAD}^2 + jX_{RAD}^2}; \quad B_{RAD} = \frac{X_{RAD}}{R_{RAD}^2 + X_{RAD}^2}$$

These two forms can appear in either *FV* mechanical circuits (=*F* across, v through) or *VF* mechanical circuits (v across, *F* through). In such circuits they are sketched in series or in parallel according to the following rules:

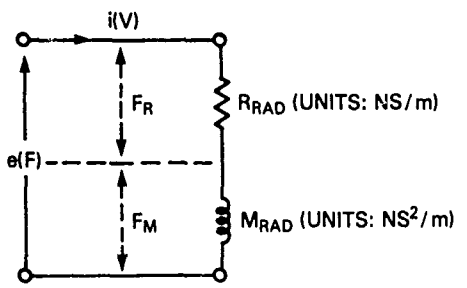


Fig. 1.7.5a — Acoustic loading of a sphere represented by force drops in an equivalent circuit featuring the *e/F* analogy

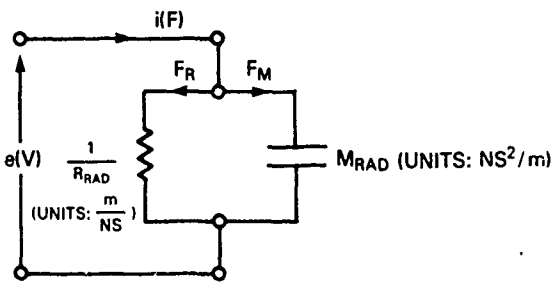


Fig. 1.7.5b — Acoustic loading of a sphere represented by nodal forces in an equivalent circuit featuring *e/V* analogy

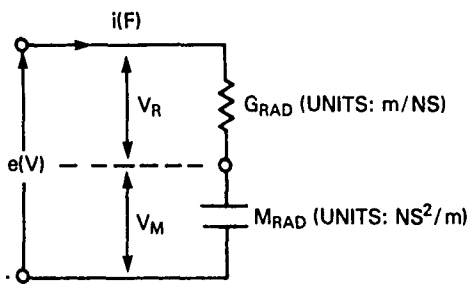


Fig. 1.7.5c — Acoustic loading of a sphere represented by velocity drops in an equivalent circuit featuring the *e/V* analogy

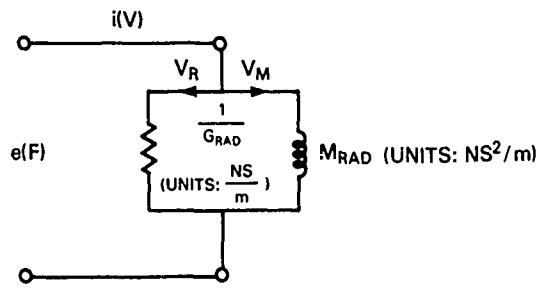


Fig. 1.7.5d — Acoustic loading of a sphere represented by nodal velocities in an equivalent circuit featuring the *e/F* analogy

1a. the formula $F = Z_L v$ is inte.preted as a sum of force "drops" in an electrically equivalent *FV* circuit hence pictured to be in series, Fig. 1.7.5a

or

1b. the formula $F = Z_L v$ is interpreted as a sum of nodal forces in an electrically equivalent *VF* circuit, hence pictured to be in parallel, Fig. 1.7.5b

2a. the formula $v = FY_L$ is interpreted as a sum of velocity drops in an electrically equivalent *VF* circuit, hence pictured to be in series, Fig. 1.7.5c

or

2b. the formula $v = FY_L$ is interpreted as a sum of nodal velocities in an electrically equivalent *FV* circuit, hence pictured to be in parallel, Fig. 1.7.5d

To illustrate these rules we repeat the example of the acoustic loading of a pulsating sphere of radius a:

$$\text{(a)}\quad R_{\text{RAD}} = \frac{\rho c(4\pi a^2)(ka)^2}{1+(ka)^2};\quad X_{\text{RAD}} = \frac{\rho c(4\pi a^2)ka}{1+(ka)^2} = \frac{\omega\rho 4\pi a^3}{1+k^2a^2}$$

$$\text{(b)}\quad G_{\text{RAD}} = \frac{1}{\rho c(4\pi a^2)};\quad B_{\text{RAD}} = \frac{1}{(ka)\rho c(4\pi a^2)} = \frac{1}{\omega\rho 4\pi a^3}$$

$$\text{(c)}\quad \mathrm{M}_{\text{RAD}} = \frac{\rho 4\pi a^3}{1+k^2a^2}\left[\text{units: } \frac{Ns^2}{m}\right];\quad \mathcal{M}_{\text{RAD}} = 4\pi a^3\rho\left[\text{units: } \frac{Ns^2}{m}\right] \tag{1.7.9}$$

$$\text{(d)}\quad F = V[R_{\text{RAD}} + j\omega M_{\text{RAD}}]$$

$$\text{(e)}\quad V = F\left[G_{\text{RAD}} + \frac{1}{j\omega\mathcal{M}_{\text{RAD}}}\right].$$

We note that R_{RAD}, M_{RAD} are functions of frequency (in the factor k) while G_{RAD}, M_{RAD} are not.

Since these representations of acoustic loading are purely symbolic, a choice in a specific application rests on simple considerations: if force is an across-variable one chooses the series representation Fig. 1.7.5a, or the parallel representation Fig. 1.7.5d. If force is a through-variable one chooses the parallel representation Fig. 1.7.5b, or the series representation, Fig. 1.7.5c. The relation between 1.7.5a and 1.7.5b is that of a *dual*, as is the relation between Fig. 1.7.5c and 1.7.5d. The relation between Fig 1.7.5a and Fig. 1.7.5d is that of *series-parallel inversion*, as is that of Fig. 1.7.5b and Fig. 1.7.5c. The distinction between *dual* and *series-parallel* inversion must be carefully noted. Duality implies an exchange of analogy including sources, while series-parallel inversion does not. The use of duals occurs naturally in canonical circuits. We note for example in Fig. 1.45.14 that an impedance Z_m in shunt position of the mechanical branch causes the appearance of $-T^2/Z_m$ in series position of the electrical branch. Since Z_m and $1/Z_m$ in this case are reciprocals it is seen that force and velocity exchange roles by reason of the dimensions of the turns ratio. One can immediately represent the acoustic load by Fig. 1.7.5d in the mechanical branch and by Fig. 1.7.5c multiplied by $-T^2$ in the electrical branch, where it appears in series position.

In all cases the symbols R, M, G, and $\mathscr{M}$ represent parameters associated with *impedances*. For example, in Fig. 1.7.5d one may deduce that $F = V_R(1/G_{RAD}) = V_M j\omega M_{RAD}$. Similarly in Fig. 1.7.5c it is seen that $V = FG_{RAD} + F/j\omega\mathscr{M}_{RAD}$. While these symbols have been applied to a sphere they can be interpreted simply as the radiation impedance and radiation mobility of an arbitrary radiator. Thus for a plane circular piston, radius a, in an infinite baffle,

$$R_{RAD} = \pi a^2 \rho c \left[1 - \frac{J_1(ka)}{ka}\right]; \quad X_{RAD} = \frac{\pi a^2 \rho c K_1(2ka)}{2(ka)^2}$$

in which J_1 is a Bessel function of the first kind, and K_1 is a special function defined by Raleigh [18]. A lumped circuit representation of this impedance in the form of two analogies is shown in Fig. 1.7.6a,b,c,d.

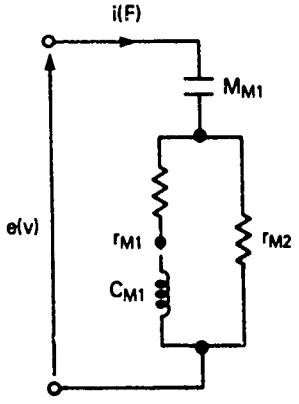


Fig. 1.7.6a — Acoustic loading on a piston in an infinite baffle represented by velocity drops in an equivalent circuit based on e/V analogy

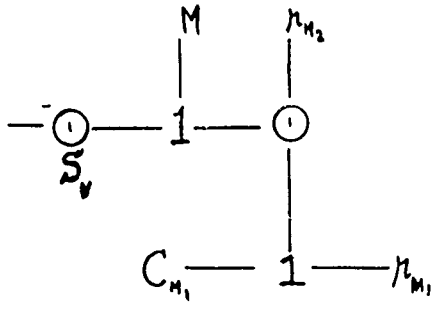


Fig. 1.7.6b — Bond graph of Fig. 1.7.6a

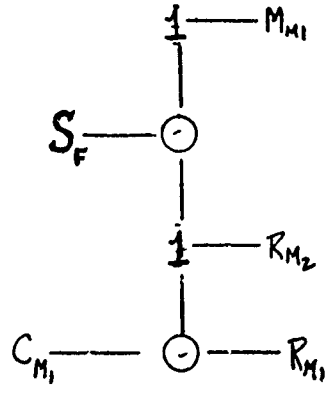


Fig. 1.7.6c — Bond graph of Fig. 1.7.6d

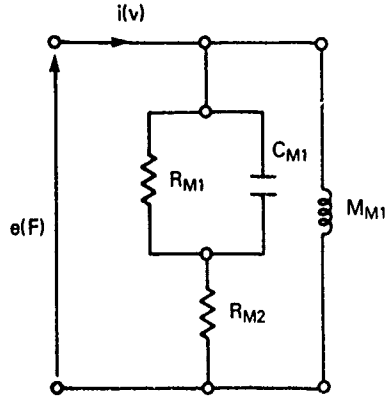


Fig. 1.7.6d — Acoustic loading on a piston in an infinite baffle represented by force drops in an equivalent circuit based on the e/F analogy

$$M_{M1} = \frac{8}{3} a^3 \rho \text{ (units: } Ns^2/m)$$

$$r_{M1} = 0.721\, a^2 \rho c \ (Ns/m)$$

$$r_{M1} = \frac{1}{\pi a^2 \rho c} = \frac{0.318}{a^2 \rho c} \left[\text{units: } \frac{m}{Ns}\right]$$

$$C_{M1} = \frac{0.6}{a \rho c^2} \text{ (units: } m/N)$$

$$R_{M1} = 1.386\, a^2 \rho c \left[\text{units: } \frac{Ns}{m}\right]$$

$$R_{M2} = \pi a^2 \rho c \left[\text{units: } \frac{Ns}{m}\right]$$

These circuits hold equally well for a piston at the end of a long (rigid wall) tube if the elements are chosen to have the values:

M_{M1}	=	$0.6133\, \pi a^3 \rho_0$	(Ns^2/m)
r_{M1}	=	$0.633/a^2 \rho_0 c$	(m/Ns)
r_{M2}	=	$1/\pi a^2 \rho_0 c$	(m/Ns)
C_{M1}	=	$0.55/a\, \rho_0 c^2$	(m/N)
R_{M1}	=	$0.504\, \pi a^2 \rho_0 c$	(Ns/m)
R_{M2}	=	$\pi a^2 \rho_0 c$	(Ns/m)

1.8 EXCHANGE OF SOURCES

A flow source (say q_s) and an effort source (say p_s) are related, and can be exchanged one for the other according to a simple rule best illustrated by an example. In Fig. 1.8.0 the source q_s is a *known* function of time in series with an acoustic mass M_1 and acoustic resistance R_1. Using Table 1.12.1 below we can express q_s in terms of the time dependent mobility forms given:

$$q_s(t) = \frac{1}{\mathscr{M}} \int_0^t p_s(t)\, dt + \frac{1}{\mathscr{R}} p_s(t). \tag{1.8.1}$$

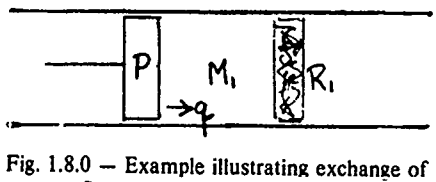


Fig. 1.8.0 — Example illustrating exchange of flow source and effort source

This formula states that the dual source p_s is related to the volume source q_s through an integral equation. Since this equation is linear and since $p_s = 0$ for $t < 0$, it may be solved by the method of the Laplace transform. Let $Q_s(s)$, $P_s(s)$ be the Laplace transforms of $q_s(t)$, $p_s(t)$ respectively. then,

$$P_s(s) = \frac{Q_s(s)}{\frac{1}{sM_1} + \frac{1}{R_1}}, \quad p_s(t) = \mathcal{L}^{-1}\{P_s(s)\}. \tag{1.8.2}$$

From the form of this equation it is seen that p_s is a flow source in parallel with mass $\mathcal{M}_1$, and resistance $\mathcal{R}_1$.

In general, a flow source q_s can be replaced by a pressure source p_s which is obtainable by solving an integral-differential equation of the form,

$$q_s(t) = \frac{1}{\mathcal{M}} \int_0^t p_s(t)\,dt + \frac{1}{\mathcal{R}}\, p_s(t) + \mathcal{N} \frac{dp_s}{dt}\,(t) \tag{1.8.3}$$

(subject to initial conditions). The relation of this formula to the concept of Helmholtz equivalent sources is discussed next.

1.8.1 Helmholtz Equivalent Sources

Sources deliver voltages across loads, or currents through loads, the magnitude of such voltages or currents being independent of load. In the theory of small signal linear analysis, voltage sources and current soures are interchangeable. The only requirement is that the current delivered by a voltage source to a load and the voltage delivered by a current source to the load be unchanged in switching from source to source. This requirement is summarized in *Helmholtz's theorem of equivalent sources:*

An ideal voltage source V (that is, source with no series internal impedance) acting in series with an impedance Z (which includes the source's internal impedance) is equivalent to an ideal current source $I = V/Z$ (that is, a source with no parallel internal impedance) acting in parallel with an admittance $Y = 1/Z$ (which includes the admittance of the source).

The proof of this theorem is easily demonstrated by circuit analysis of the sources as represented by Figs. 1.8.1.

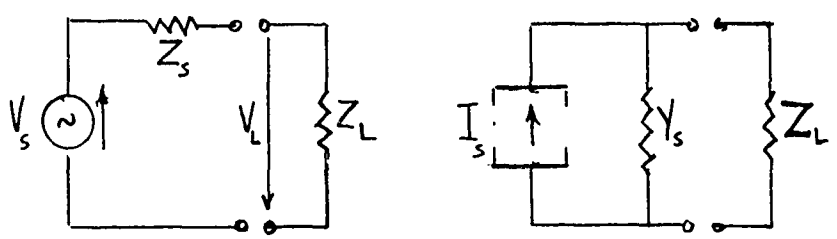


Fig 1.8 1 — Circuit representations of sources and loads, (a) voltage source and load, (b) current source and load

Proof: In (a),

$$Z_s I_L + V_L = V_s. \tag{1.8.4}$$

Divide by Z_s:

$$I_L + \frac{V_L}{Z_s} = \frac{V_s}{Z_s} = I_s, \text{ or } I_L + Y_s V_L = I_s. \tag{1.8.5}$$

This is the node law of (b). Since V_L, I_L are delivered to the load by both sources, they are equivalent and the proof is complete.

In this proof the only constraint is that the current I delivered by the current source have a (complex) magnitude V/Z_s, $(V = |V| \angle 0)$.

A more general procedure for exchange of sources is needed for arbitrary time-varying sources. The procedure is outlined below:

- By Eq. 1.8.5 the flow source $f_s(t)$ and effort source $e_s(t)$ are related in a simple way,

$$Y(t)\ \{e_s(t)\} = f_s(t) \tag{1.8.6}$$

in which $Y(t)$ is an integral-differential operator.

- Using the Laplace transform one obtains

$$Y(s)\ \mathbf{e}_s(s) = f_s(s). \tag{1.8.7}$$

If $e_s(t)$ is known then the inverse Laplace transform gives $f_s(t)$. If $f_s(t)$ is known then

$$\mathbf{e}_s(s) = \frac{f_s(s)}{Y(s)} \tag{1.8.8}$$

and the inverse transform gives $e_s(t)$.

As an example, let us suppose $e_s(t)$ with initial conditions in known and the source impedance is an inertance M, a resistance R, and capacitance N in series. Then

$$Y(t) = \frac{1}{M}\int (\ )\ dt + \frac{1}{R} + N\frac{d}{dt} \tag{1.8.9}$$

and

$$\left(\frac{1}{sM} + \frac{1}{R} + sN\right)\mathbf{e}_s(s) + \frac{e_s^{(-1)}(0+)}{sM} - Ne_s(0+) = \mathbf{f}_s(s). \tag{1.8.10}$$

If initial conditions are zero then the inverse gives the flow source explicitly:

$$L^{-1}\left\{\left(\frac{1}{sM} + \frac{1}{R} + sN\right)\mathbf{e}_s(s)\right\} = f_s(t). \tag{1.8.11}$$

1.9 DISTINCTION BETWEEN MECHANICAL ELEMENTS IN SERIES/PARALLEL FORM AND IN DUAL FORM

In a *VF* mechanical circuit (*V* across, *F* through) the nodal equation $F = \sum_i F_i = V \sum_i Z_i$ can be interpreted as a circuit in which a force source *F* drives an assembly of parallel branches characterized by impedances Z_i. If one solves for $V = F/\sum_i Z_i = \sum_i V_i$, which also can be written $1/Y = \Sigma 1/Y_i$, the result can be interpreted as a circuit in which the *same* force source drives an assembly of branches in series, of mobility $1/\sum_i Z_i$. From the point of view of the source the response of the circuit is the same whether parallel or series forms are used. The crucial point in such series/parallel interchange is that the form of the source remains constant.

Let us suppose now that the force source *F*, in association with a set of parallel branches, is transformed into a velocity source *V*, in series with a set of series connected branches. In performing the transformation let the following rules be obeyed:

- force source is replaced by a velocity source by use of methods described in Section 1.8.
- mass *M*, compliance C_M, resistance R_M of a translational system are replaced by reciprocals M^{-1}, C_M^{-1}, R_M^{-1}.
- differentiation (d/dt) is replaced by integration $(\int \ldots dt)$, and vice versa.
- the variable *F* is replaced by the variable *V*, and *V* by *F*.

The circuit resulting from this transformation is the *dual* of the original.

Thus it is seen that dual transformations differ from series/parallel transformations not only in the fact that sources are interchanged, but also in the fact that their mechanical element coefficients are simple element-by-element transformations instead of complex reciprocals of groups of elements.

1.10 CIRCUIT LAWS FOR MECHANICAL NETWORKS

In a mechanical system driven by force sources one is required to determine the velocities through each circuit element. Alternatively, if it is driven by velocity sources, one is required to find the forces through each circuit element. Adopting velocity sources as the rule in modeling mechanical networks we can construct *V-F* diagrams and use circuit laws to find unknown quantities. These laws are:

• *Loop Law*: In a complex series-parallel mechanical system whose *V-F* network representation has $i = 1, 2, \ldots. Q$ loops, and $j = 1, 2, \ldots. Q$ forces, the sum of all velocity 'drops' in each loop must be zero. In symbols, for a translational system,

$$\sum_{j=1}^{Q} \mathrm{V}_{ij}(f_i) - \mathrm{V}_{(g)l} = 0, \quad i = 1, 2, \ldots. Q. \tag{1.10.1}$$

Here, the symbol V_{ij} denotes the elements in a matrix of integrodifferential operators,

$$\mathrm{V}_{ij} = \{\mathrm{V}_{11}, \mathrm{V}_{12}, \ldots. \mathrm{V}_{QQ}\}$$

$$V_{11} = \sum_e \left(\frac{1}{M_1^{(e)}} \int \ldots dt + \frac{1}{B_1^{(e)}} + N_1^{(e)} \frac{d}{dt} \right) f_1 + \sum_{k=1}^{Q} \frac{1}{\tilde{M}_{1k}} \int f_k dt$$

$$V_{12} = \sum_e \left(\frac{1}{M_1^{(e)}} \int \ldots dt + \frac{1}{B_1^{(e)}} + N_1^{(e)} \frac{d}{dt} \right) f_2 + \sum_{k=1}^{Q} \frac{1}{\tilde{M}_{2k}} \int f_k dt \qquad (1.10.2)$$

$V_{(g)i}$ is a vector whose elements are applied velocity sources, $\tilde{M}_{ik}$ are mutual masses and superscript e signifies the element in question.

The loop law for a rotational system is easily obtained by exchange of symbols:

(1) $\dot{\Theta}_{ij}$ for V_{ij}
(2) τ for F
(3) J for M (1.10.3)
(4) B_r for B
(5) N_r for N

• *Node Law*: In a *V-F* mechanical network which has $i = 1, 2, \ldots Q$ nodes and $j = 1, 2, \ldots Q$ forces the sum of all forces at a node must be zero. In symbols, for a translational system,

$$\sum_{j=1}^{Q} F_{ij}(v_j) - F_{(g)i} = 0, \quad i = 1, 2, \ldots Q \qquad (1.10.4)$$

in which the symbol F_{ij} denotes the elements in a matrix of integrodifferential operators,

$$F_{ij} = \{F_{11}, F_{12}, \ldots F_{QQ}\}$$

$$F_{11} = \sum_e \left(M_1^{(e)} \frac{d}{dt} + B_1^{(e)} + \frac{1}{N_1^{(e)}} \int \ldots dt \right) v_1 + \sum_{k=1}^{Q} M_{1k} \frac{dv_k}{dt}$$

$$F_{12} = \sum_e \left(M_1^{(e)} \frac{d}{dt} + B_1^{(e)} + \frac{1}{N_1^{(e)}} \int \ldots dt \right) v_2 + \sum_{k=1}^{Q} M_{2k} \frac{dv_k}{dt} \qquad (1.10.5)$$

$F_{(g)}$ is a vector whose elements are applied force sources, M_{ik} are mutual masses, and superscript e signifies the element in question.

The node law for rotational systems is obtainable from translational systems by exchange of symbols, Eq. ! 10.3.

Two examples of *V-F* circuits will now be presented.

1.11 EXAMPLES OF *V-F* REPRESENTATIONS OF SIMPLE MECHANICAL SYSTEMS

Example # 1

Fig. 1.11.1 shows a MNB translational system driven through the mass by a force source $F_{(g)}(t)$. Its bond graph (see Sect. 1.68) Fig. 1.11.2b is based on the idea that the velocity of the mass M relative

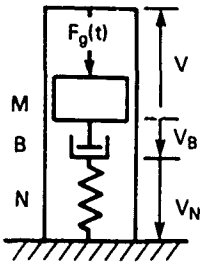


Fig. 1.11.1 — A MNB system driven by $F(t)$ through the mass

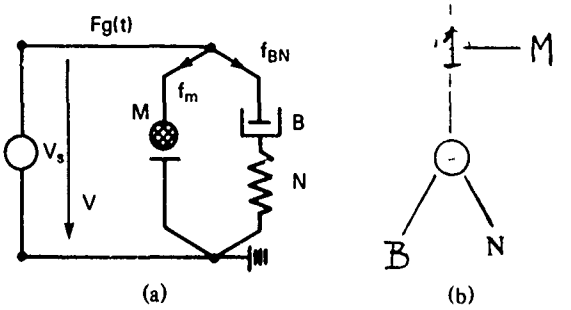


Fig. 1.11.2 — (a) a VF network representation (b) Bond graph of Fig. 1.11 1

to ground is the same as the velocity of the damper-spring relative to ground. Its V-F network representation is shown in Fig. 1.11.2a. In this representation one terminal of the mass m must be grounded. Hence the mass M is mechanically in parallel with the series branch BN, the terminals of which are connected in agreement with the *physical connections* shown. The (known) force source has an unknown velocity v across it. To solve for v one applies the node law (1.10.4).

$$f_M(\mathrm{v}) + f_{BN}(\mathrm{v}) = F_g(t) \tag{1.11.1}$$

in which only f_M is directly relatable to v by means of (1.4.2):

$$f_M = M \frac{d\mathrm{v}}{dt}. \tag{1.11.2}$$

In the series NB branch we first apply the loop law (1.10.1) with v acting as a source,

$$\mathrm{v}_B + \mathrm{v}_N = \mathrm{v}. \tag{1.11.3}$$

From (1.4.1) this equation reduces to,

$$f_{BN} = \frac{\mathrm{v}}{N\frac{d}{dt} + \frac{1}{B}}. \tag{1.11.4}$$

Thus, the node law requires that,

$$\left[M\frac{d}{dt} + \frac{1}{N\frac{d}{dt} + \frac{1}{B}}\right]\mathrm{v} = F_g(t). \tag{1.11.5}$$

Example #2

The MNB system of Fig. 1.11.1 is detached from the ground and is placed on a platform which is then driven by a known velocity $\mathrm{v}_g(t)$, Fig. 1.11.3. The bond graph Fig. 1.11.3b, is based on the idea

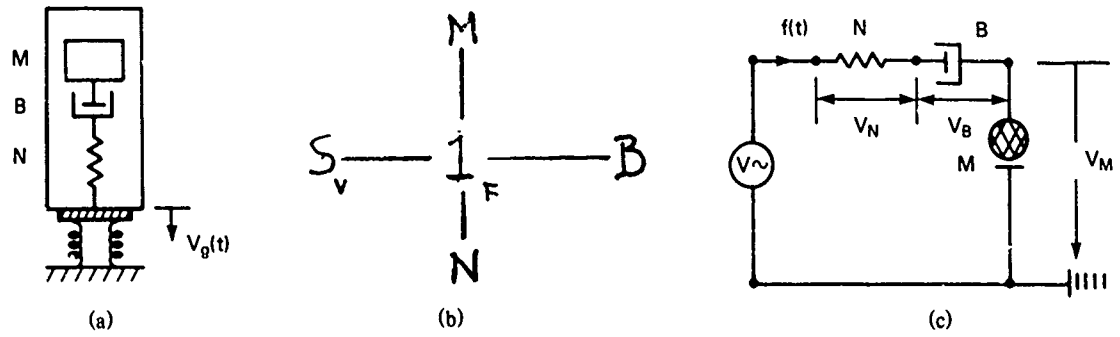


Fig. 1.11.3 — (a) A MNB system driven by a velocity source $V_g(t)$
(b) bond graph (c) a VF representation

that the force f is common to *M, B, N.* These elements are therefore mechanically in series. In constructing the *V-F* mechanical circuit it is noticed that all terminals are above ground, except for the element mass which again must have one terminal at ground, and the element of the velocity sources, which also must have one terminal at ground, Fig. 1.11.3c.

Since $v_g(t)$ is known we solve for $f(t)$ by application of the loop law (1.10.1),

$$v_N + v_B + v_M - v_g = 0. \tag{1.11.6}$$

By use of (1.4.1) this equation reduces to the form,

$$N\frac{df}{dt} + \frac{f}{B} + \frac{1}{M}\int f(t)\,dt = v_g(t). \tag{1.11.7}$$

Examples #1 and #2 illustrate an important rule that, appearances not withstanding, an MNB system in a *V-F* representation may be a parallel, or a series circuit depending on the nature of the driving input source, as well as upon its point of application.

Bond Flow Charts

A simple, but useful, modification of the above procedure for deriving circuit representations of physical systems is to construct bond flow charts (already mentioned in Examples #1 and #2 above) showing how the "through" quantity (force or velocity) branches out to form a "tree." If, for example, the source is a known force (taken as a flow quantity on *VF* chart) one constructs a *force flow chart* showing how the force branches through all the elements of the physical system. On the other hand, if the source is a known velocity (again taken as a flow quantity on a *FV* chart) one constructs a similar bond *velocity flow chart.* Such modifications of procedure allow one directly to construct dual representations of a given physical network.

An example will explain the procedure. Figure 1.11.4a is a mechanical system consisting of a massless rigid bar A driven by a known force $F(t)$ and restrained in its motion of the springs n_1, n_2, n_3, n_4, mass m and damper h as shown. By inspection we construct the *V-F* force flow chart, Fig. 1.11.4b. Here a circle 0 represents a velocity and a 1 represents a force.

Assuming bar A moves only in translation it is seen that all elements are in parallel relative to velocity (that is, all branches have the same velocity taken as an across-quantity). Thus, Fig. 1.11.4b consists of five branches in parallel, relative to velocity, the force acting as a through quantity.

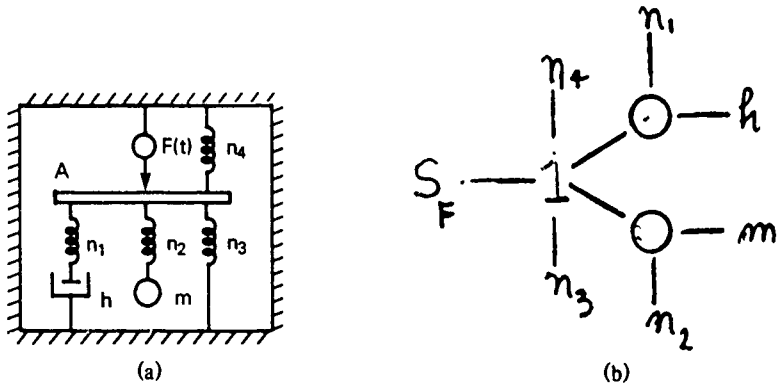


Fig. 1.11.4 — (a) A translational mechanical system and (b) its bond graph (see Sect. 1.68)

We next reverse the roles of F, V and consider the driver to generate a known velocity which is taken to be a through quantity. Using Fig. 1.11.4a we construct an FV velocity flow chart from a VF force flow chart according to the following rules:

(1) N independent loops in a VF network transform to N independent node pairs ($= N + 1$ nodes) in the dual FV network.

(2) Elements (or branches or subsystems) in series (i.e., possessing common force) in a VF network become elements in parallel (i.e., also possessing common force) in the dual FV network. Elements in parallel (i.e., having common velocity) in a VF network become elements in series (i.e., also have common velocity) in the dual FV network.

(3) Force sources are replaced by velocity sources.

(4) Each passive element is replaced by its dual, that is, by its reciprocal.

(5) The element of mass in a flow force, that is, VF, chart must have one terminal grounded.

Since Fig. 1.11.4b consists of 5 branches in parallel (relative to velocity) its dual FV network is 5 elements in series, shown in Fig. 1.11.4d. A pictorial representation of Fig. 1.11.4b is shown in Fig. 1.11.4c. Additional examples of flow charts will be discussed in several later sections of this chapter.

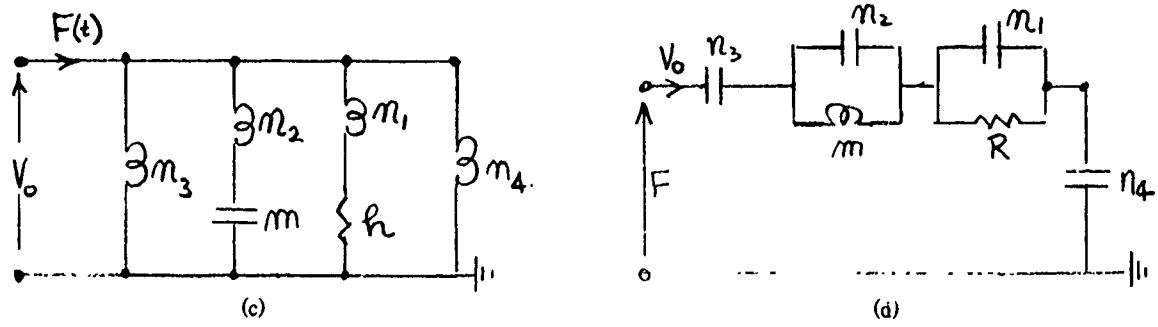


Fig. 1.11.4 — (c) a VF equivalent circuit and (d) a FV equivalent circuit

1.12 ACOUSTICAL NETWORKS

Sound generators and receivers often incorporate acoustical elements (acoustic mass, acoustic resistance, acoustic compliance) in their internal structure. For purposes of analysis it is convenient to represent such elements in an acoustical circuit in lumped parameter form. This representation is valid whenever the acoustical wavelength is large relative to the physical size of the source or receiver, or relative to the physical sizes of the internal structural components that makeup the circuit.

Explicit mathematical forms taken by acoustical elements depend on the choice of circuit across-variable (velocity V or force F in mechanical circuits, or volume velocity q or pressure p in acoustic circuits), and on the choice of circuit analysis, either nodal or loop. Since in this treatise we strive to use V (or q) as across-variable, and F (or p) as the through variable it is seen that nodal analysis leads to parallel-branch networks with pressure as the flow-through quantity, while loop analysis leads to series-branch networks, also with pressure as the flow-through quantity.

The simplest mathematical models of acoustical mass, compliance and resistance are pictured in Fig. 1.12.1.

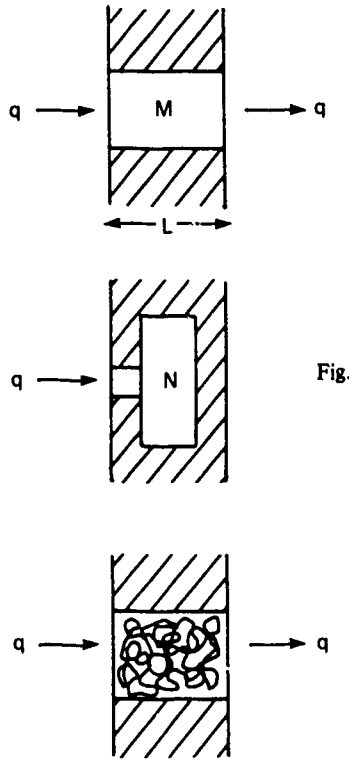


Fig. 1.12.1 — Simple pictures of acoustic mass, compliance, and resistance

Table 1.12.1 gives explicit mathematical forms of acoustical circuit elements excited by harmonic signals (time given by exp $j\omega t$), applicable to a circuit in which q is the across-quantity, and p is the through-quantity. In VF circuits the impedance form $p = p(q)$ is used in nodal analysis, while the mobility form $q = q(p)$ is used in loop analysis. Here superscript y indicates "mobility."

Elements in impedance form are related to elements in mobility form. In the simplest case where circuit branches contain only one element listed in Table 1.12.1 it is seen that,

$$\mathcal{M}^{(y)} = \frac{1}{\omega \mathrm{N}}; \mathcal{N}^{(y)} = \frac{1}{\omega^2 \mathcal{M}}; \mathcal{R}^{(y)} = \frac{1}{\mathcal{R}} = \mathcal{G} \tag{1.12.1}$$

Table 1.12.1 — Mathematical Models of Acoustic Circuit Elements

Impedance Form	Time Dependent Form	Mobility Form	Time Dependent Form
$p = \mathcal{M} j\omega q$	$p = \mathcal{M} \frac{dq}{dt}$	$q = \mathcal{N}^{(y)} j\omega p$	$q = \mathcal{N}^{(y)} \frac{dp(t)}{dt}$
$p = q/j\omega \mathcal{N}$	$p = \int \frac{q(t)\,dt}{\mathcal{N}}$	$q = \frac{p}{j\omega \mathcal{M}^{(g)}}$	$q = \frac{1}{\mathcal{M}^{(y)}} \int p(t)\,dt$
$p = \mathcal{R} q$	$p = \mathcal{R} q(t)$	$q = \mathcal{G} p$	$q = \frac{1}{\mathcal{R}^{(y)}} p(t)$

In words: when a branch consisting of a spring (or mass) in impedance form is conver' 1 to mobility form, it appears as an equivalent mass (or spring) respectively. When, however, branches contain several elements one can find the relation between parallel and series forms by use of the identity $\mathcal{Y} = \mathcal{Z}^{-1}$ (acoustical mobility equals inverse acoustical impedance). Thus, if an acoustic network in a *qp* acoustic circuit (*q* "across," *p* "through") is a parallel net of three branches $\mathcal{R}$, $\mathcal{M}$, and $\mathcal{N}$, represented by the nodal equation,

$$p = \left[\mathcal{R} + j\left(\omega \mathcal{M} - \frac{1}{\omega \mathcal{N}}\right)\right] q = (\mathcal{R} + jX) q = \mathcal{Z} q \tag{1.12.2}$$

then in the *same qp* circuit the corresponding series form of the three branches may be expressed by the loop equation,

$$q = \left[\mathcal{R}^{(y)} - j\left(\omega \mathcal{N}^{(y)} - \frac{1}{\omega \mathcal{M}^{(y)}}\right)\right] p = (\mathcal{G} - j\mathcal{B}) p = \mathcal{Y} p. \tag{1.12.3}$$

Since $\mathcal{Y} = \mathcal{Z}^{-1}$, it is seen that,

$$\text{(a)}\ \mathcal{G} = \frac{\mathcal{R}}{\mathcal{R}^2 + X^2};\ \text{(b)}\ \mathcal{N}^{(y)} = \frac{\mathcal{M}}{\mathcal{R}^2 + \left(\omega \mathcal{M} - \frac{1}{\omega \mathcal{N}}\right)^2};\ \mathcal{M}^{(y)} = \mathcal{N}\left[\mathcal{R}^2 + \left(\omega \mathcal{M} - \frac{1}{\omega \mathcal{N}}\right)^2\right]. \tag{1.12.4}$$

Near mechanical resonance ($\omega = \omega_r$), where the lumped form of mass and compliance is valid, one has,

$$\omega_r^2 \cong \frac{1}{\mathcal{M}.\mathcal{N}}. \tag{1.12.5}$$

Thus near and at mechanical resonance,

$$\mathcal{N}^{(y)} \simeq \frac{\mathcal{M}}{\mathcal{R}^2} \left[\text{units: } \frac{\text{in}^5}{\mathcal{N}}\right];\quad \mathcal{M}^{(y)} \simeq \mathcal{N}\mathcal{R}^2 \left[\text{units: } \frac{\mathcal{N}\text{s}^2}{\text{m}^5}\right]. \tag{1.12.6}$$

At frequencies of forced drive far below mechanical resonance, the mobility compliance and mass are given by,

$$\mathcal{N}^{(y)} \to \frac{\omega^2 \mathcal{N}^2 \mathcal{M}}{1 + \omega^2 \mathcal{N}^2 \mathcal{R}^2} \to \omega^2 \mathcal{N}^2 \mathcal{M};\ \mathcal{M}^{(y)} = \frac{1}{\omega^2 \mathcal{N}} (1 + \omega^2 \mathcal{N}^2 \mathcal{R}^2) \to \frac{1}{\omega^2 \mathcal{N}}. \tag{1.12.7}$$

A noticeable feature is that these mobility forms of compliance and mass are functions of frequency, except near mechanical resonance.

Acoustic Flow Charts

The construction of acoustic flow charts follows a few simple rules. These are illustrated by the example sketched in Fig. 1.12.2a. For this network one begins by constructing a bond graph flow chart, Fig. 1.12.2b. In this chart the piston accumulator combination is modeled as a (constant) pressure source $p_{\sim}$ driving a variable volume velocity through the series connected acoustic mass M, and acoustic resistance R. At terminal c the volume velocity divides into q_1 going into the acoustic compliance N, and q_2 going into acoustic mass M_2. From the nature of the physical connections both N and M_2 are grounded (meaning one terminal of each has zero volume velocity). The nodal equation describing this flow is $q = q_1 + q_2$. Each acoustic element describes a pressure drop: p_{M_1} is the drop across M_1, p_R across R, and p_N is the drop across N or across M_2 since these are in parallel (relative to acoustic volume velocity).

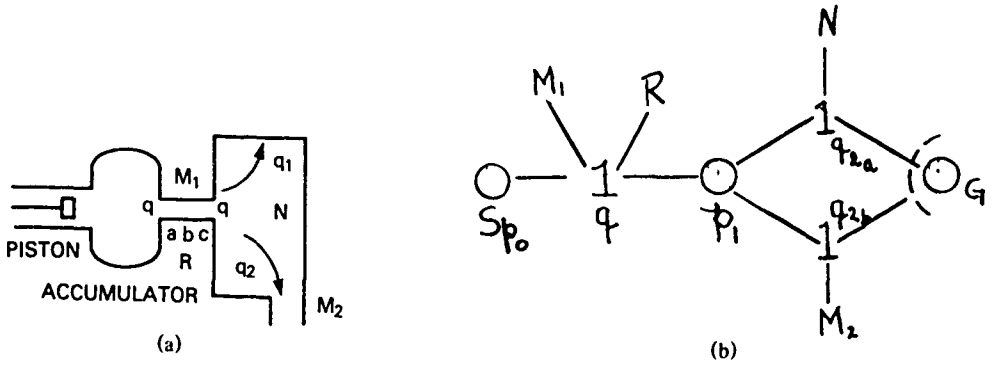


Fig. 1.12.2 — (a) A physical system of acoustic elements and (b) its bond graph

We next omit the accumulator and consider the piston to be a (constant) volume velocity source $q_{\sim}$ and construct an acoustic pressure flow chart. This is the *dual* of the volume velocity flow chart.

This amounts to constructing a *VF* chart from a given *FV* chart. The rules for construction of the dual are:

(1) exchange all common effort junctions (= 0-junctions) for common flow junctions and all common flow junctions for common effort junctions, *retaining the identification tags.*

(2) exchange all effort sources for flow sources and vice versa; and exchange all effort sinks for flow sinks, and vice versa.

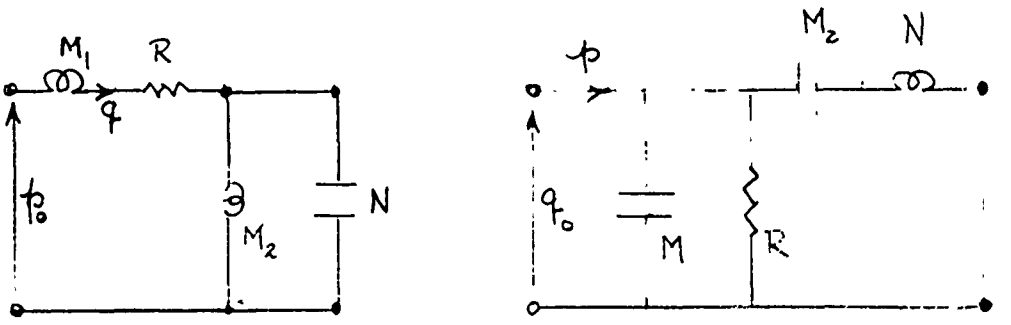
(3) identify inertance as reciprocal capacitance having the same numerical value and same units.

identify capacitance as reciprocal inertance having the same numerical value and same units

identify resistance as reciprocal conductance having the same numerical value and same units.

The acoustic pressure flow chart that is the dual of Fig. 1.12.2b is shown in Fig. 1.12.2c.

The (*VF*) loop equation of Fig. 1.12.2c is $q = q_1 + q_2$. The (*VF*) node equation is $p = p_{M^{-1}} + p_{R^{-1}} + p_{N^{-1}M_2^{-1}}$.

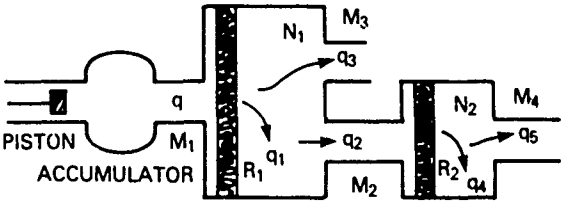


(c)

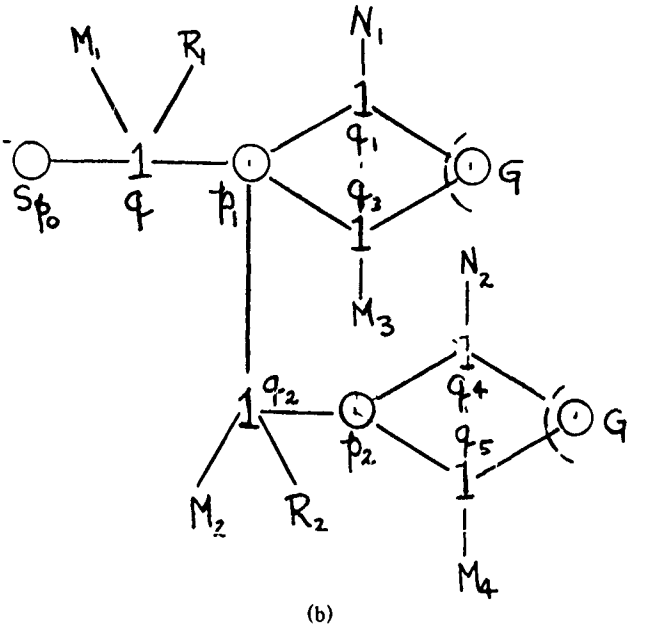
Fig. 1.12.2 — (c) dual equivalent circuits

A second example is the acoustic network shown in Fig. 1.12.3a.

We model this physical network by first *assuming* that the motion of the piston and accumulator constitute a source of constant pressure $p_{\sim}$. The volume velocity flow chart then takes on the appearance of Fig. 1.12.3b.



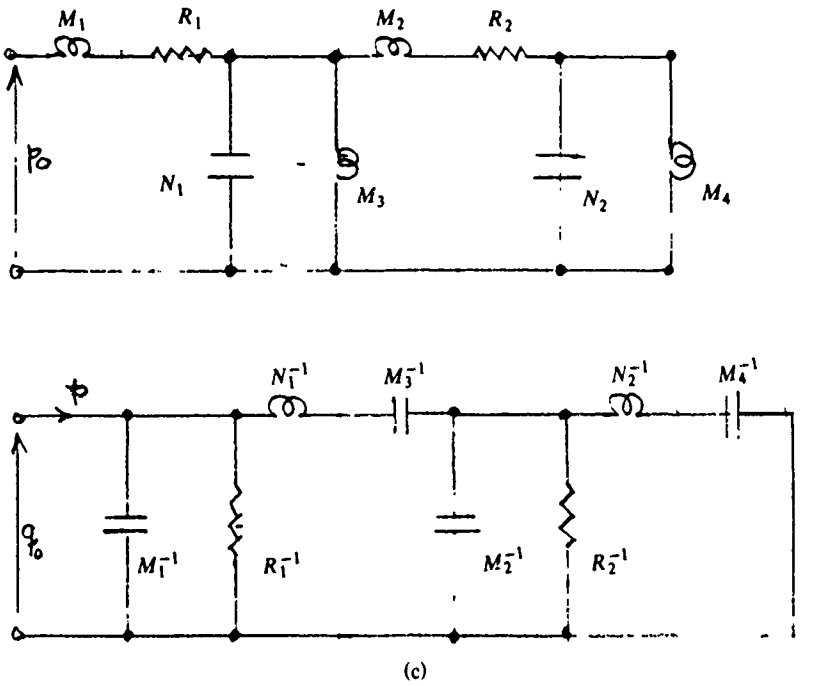
(a)



(b)

Fig. 1.12.3 — (a) A complex acoustical system and (b) its bond graph in *PQ* form

The dual of this flow chart, based on omission of the accumulator, with subsequent piston motion modeled as a velocity source, is easily obtained by use of the rules noted above. It is shown in Fig. 1.12.3c.



(c)

Fig. 1.12.3 (c) Dual equivalent circuits

Duality between Figs. 1.12.3b and 1.12.3c implies these rules: the equation $q = q_1 + q_2 + q_3$ is a *nodal* equation on a *FV* volume velocity flow chart and a *loop* equation on a pressure flow (or *VF*) chart. The equation $p = p_M + p_R + P_{NM}$ is a *nodal* equation on a *VF* pressure flow chart and a *loop* equation on an *FV* volume velocity flow chart. These relations are summarized in the following table.

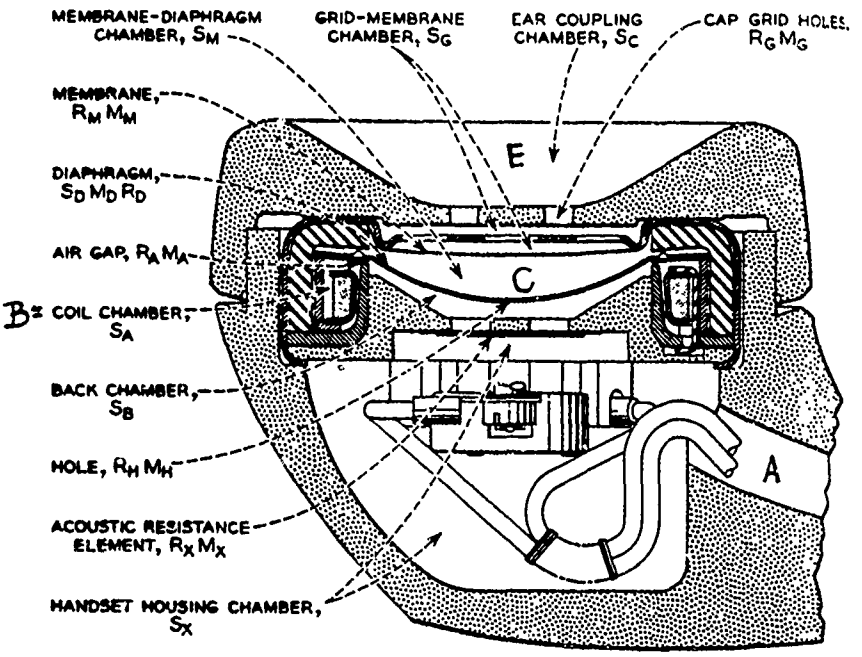
Table 1.12.2

Equation	Analysis using an *FV* Volume Velocity Flow Chart	Analysis using a *VF* Pressure Flow Chart
$p = \sum_i Z_i q_i$	loop	nodal
$q = \sum_i Y_i p_i$	nodal	loop

The Representation of the Ring Armature Telephone Receiver by Means of Flow Charts

A third example of an acoustical network is the ring armature telephone receiver shown in Fig. 1.12.4a.

The operation of this device is briefly this: the voice message, in electrical form, enters wires A which excite coil B of the ring armature, which couples to the diaphragm C through the air gap causing it to vibrate thus delivering the message in acoustic form to the ear coupling chamber E. The device is essentially an acoustic projector.



(a)

Fig. 1.12.4 — (a) The Ring Armature Telephone Receiver [14]. E. E. Mott and R. C. Miner, *The Bell System Technical Journal*, 31 (1951), ©1951 AT&T; by permission.

The idealized (lumped element) acoustic network will first be sketched as a volume velocity bond graph 1.12.4b driven by an (assumed) pressure (or force) source $p(t)$. The branching of volume velocity is explained as follows:

1. The full source velocity $q_s = q$ passes through the elastance S_D, mass M_D and resistance R_D (in series relative to velocity) of the diaphragm C.

2. q divides into three branches: the first q_{MD} goes into the membrane-diaphragm chamber (elastance S_M); the second q_M goes into the membrane (resistance R_M, mass M_M); the third q_H goes into the hole (resistance R_H, mass M_H).

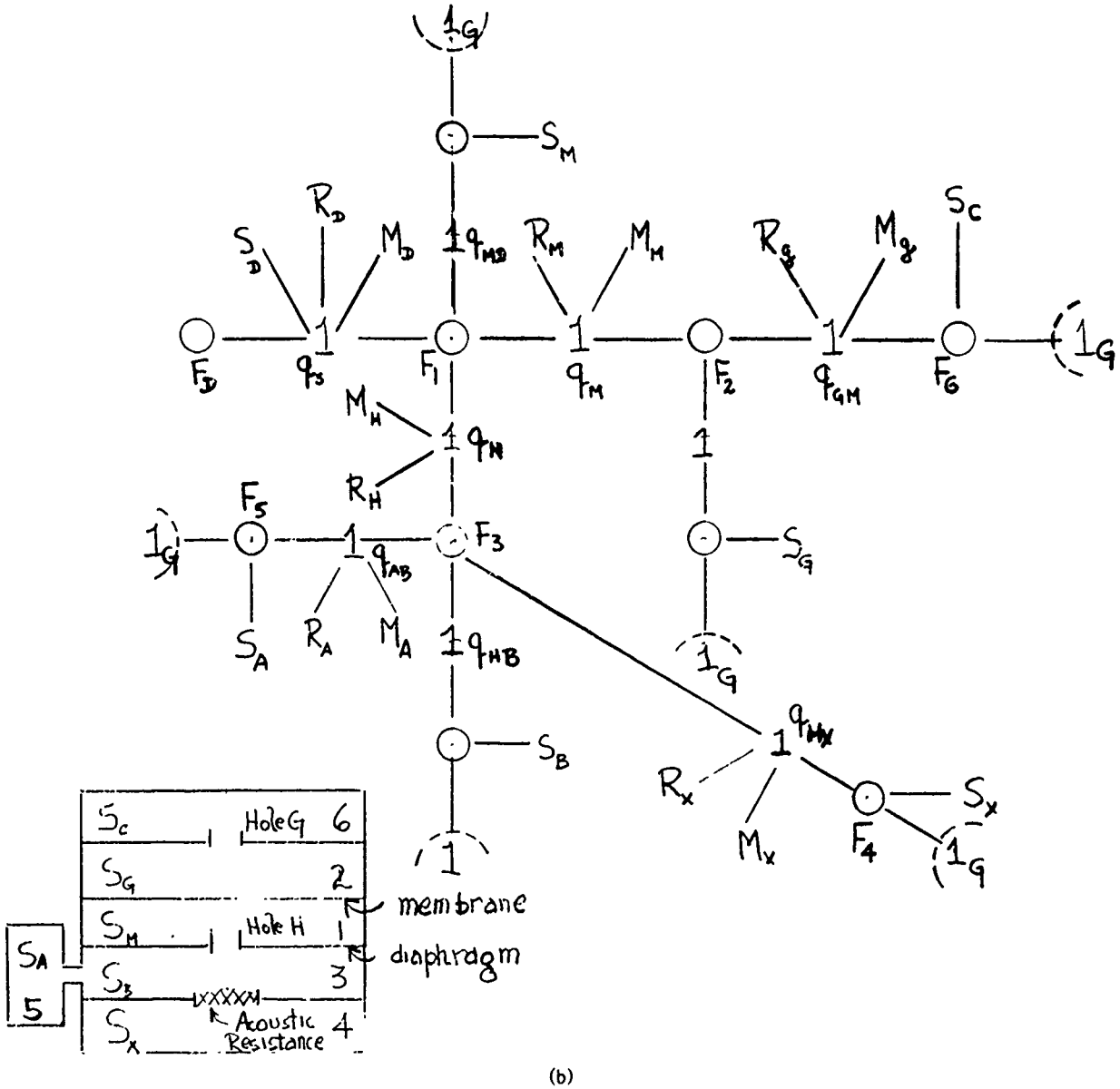
3. q_M divides into two branches: one, q_{MG} into the grid-membrane chamber (elastance S_G), and the other q_{GM} into the cap grid holes (resistance R_G, mass M_G), through the ear-coupling chamber (elastance S_c), then into the human ear.

4. q_H divides into three branches: one q_{HB} going into the back chamber (elastance S_B); the second q_{AB} going into the air gap (resistance R_A, mass M_A), then through the coil chamber (elastance S_A); the third q_{HX} going into the acoustic resistance element (resistance R_X, mass M_X), then through the handset housing chamber (elastance S_X).

Based on this branching the volume velocity bond graph has the following appearance, Fig. 1.12.4b.

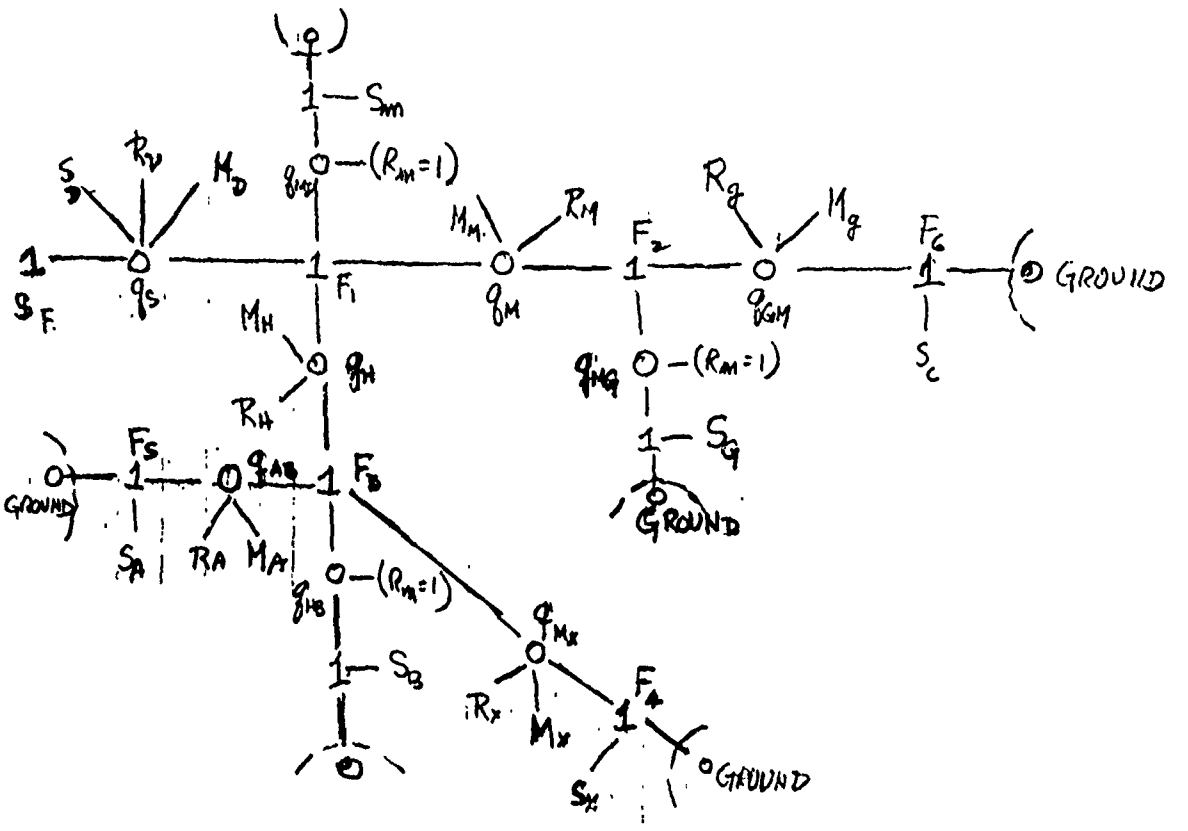
Inspection of this chart shows it to consist of an above-ground series branch (R_D, M_D, S_D) in series with a nest of five parallel branches (all grounded). All elements are listed in *impedance* form.

The acoustic pressure bond graph, which is the dual of the volume velocity bond graph, is constructed by application of the rules cited above. It appears as Fig. 1.12.4c.



(b)

Fig. 1.12.4 — (b) Bond graph of Fig. 1.12.4a



(c)

Fig. 1.12.4 — (c) Bond graph which is the dual of Fig. 1.12.4b

This type of chart gives the pressure flow across each acoustic element. All elements are listed in *mobility* form.

1.13 MODELING OF AN ACOUSTIC TRANSDUCER BY A MATRIX EQUATION

We return now to Fig. 1.2.1 in which the acoustic transducer is modeled as a cascade of component boxes. Each component box is an assemblage of network elements whose forms have been described in Sections 1.3 and 1.12. For the n'th box whose input energy coordinates are e_{IN}, i_{IN}, and whose output energy coordinates are e_{OUT}, i_{OUT}, the interrelation of these variables may be formulated as a matrix equation,

$$\mathbf{U}_n \begin{bmatrix} e_{IN} \\ i_{IN} \end{bmatrix} = \begin{bmatrix} e_{OUT} \\ i_{OUT} \end{bmatrix} \tag{1.13.1}$$

in which $\mathbf{U}_n$ is a matrix of impedance or mobility elements of the n'th box. If there are N boxes in cascade, the final output coordinates are given by,

$$\mathbf{U}_1\mathbf{U}_2 \ldots . \mathbf{U}_N \begin{bmatrix} e_1 \\ i_1 \end{bmatrix} = \begin{bmatrix} e_N \\ i_N \end{bmatrix}. \tag{1.13.2}$$

For the case where the input vector is (e_1, i_1) and output vector contains many components the interrelation is written in the more general form,

$$\mathbf{U}\mathbf{w}_{IN} = \mathbf{w}_{OUT} \tag{1.13.3}$$

where $\mathbf{w}_{IN} = (e_1, i_1, 0, 0, 0 \ldots.)^t$ and $\mathbf{w}_{OUT} = e_2, i_2, e_3, i_3, \ldots.)^t$, and the superscript t means "transpose."

Fig. 1.2.1 shows a transducer represented as a single-row-cascade. In the general case the representation takes the form of a multiplicity of interconnected cascades.

Several cases of matrix modeling are presented in the following Sections.

1.14 EXAMPLE OF MATRIX MODELING FOR AN ACOUSTIC PROJECTOR

To illustrate the modeling of acoustic projectors by use of Fig. 1.2.1 let us take the case of an acoustic projector whose primary circuit stores energy in the form of electric charge on a capacitor. Choose the energy coordinates to be voltage e, current i, and let zero potential be ground. For simplicity let this capacitor be the only element in the storage matrix, Fig. 1.14.1. The transmission matrix a relates e_w, i_w to e, i, that is, output energy coordinate to input coordinates. Using Kirchoff's current law, one has,

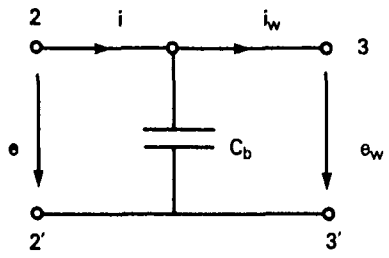


Fig. 1.14.1 — Matrix modeling illustrated by capacitor storage

$$\mathbf{A}\begin{pmatrix} e \\ i \end{pmatrix} = \begin{pmatrix} e_w \\ i_w \end{pmatrix}, \quad \mathbf{A} = \begin{pmatrix} 1 & 0 \\ -j\omega C_b & 1 \end{pmatrix}. \tag{1.14.1}$$

Next, primary coordinates e_w, i_w in Fig. 1.2.1 must be transduced in secondary coordinates. Since the secondary circuit is mechanical, it is seen that the transduction matrix must convert e_w, i_w into f_w, v_w. The way it does this depends on the physical laws of energy conversion. For an *electric field transducer* the laws are contained in transduction formulas to be described later. For the present we use the simplified forms involving the transduction coefficient y:

$$e_w = y f_w$$

$$i_w = \frac{1}{y} v_w. \tag{1.14.2}$$

We must at this junction choose which coordinate of f_w, v_w is to be considered as the through-coordinate. Arbitrarily, let f_w be the through-coordinate. The equations therefore signify that an across quantity e_w is transduced into a through quantity f_w by means of a transduction coefficient y, and a through quantity i_w is transduced into an across quantity v_w by means of y^{-1}. Generally, y is a complex number. Here for simplicity it is taken to be real. The transduction matrix equation can thus be written,

$$\mathbf{B}\begin{pmatrix} e_w \\ i_w \end{pmatrix} = \begin{pmatrix} f_w \\ v_w \end{pmatrix}, \quad \mathbf{B}\begin{pmatrix} y^{-1} & 0 \\ 0 & y \end{pmatrix}. \tag{1.14.3}$$

Next the secondary coordinates f_w, v_w in Fig. 1.2.1 are cascaded through the secondary storage matrix. This is generally a combination of mechanical mass m, spring n, and damper r. Assume these have all the same velocity. Then, since force is the through (or flowing) quantity and velocity is the across-

quantity, these mechanical elements appear in parallel, meaning their mechanical impedances are additive. The secondary storage thus receives f_w, v_w and delivers f, v; in matrix form, one has,

$$\mathbf{C}\begin{pmatrix} f_w \\ v_w \end{pmatrix} = \begin{pmatrix} f \\ v \end{pmatrix}, \qquad \mathbf{C} = \begin{pmatrix} 1 & -Z_m \\ 0 & 1 \end{pmatrix} \tag{1.14.4}$$

$$Z_m = j\omega m + \frac{1}{j\omega_n} + r = \frac{f}{v}.$$

Finally the energy described by f, v enters into the acoustic load. For simplicity calculate this load as if it were the loading on a uniformly vibrating sphere, radius a, at frequency $\omega = kc$, $k = 2\pi/\lambda$. Assume the acoustic mass and resistance have the same velocity and that $\lambda >> a$. Then since $f(= pS$, S is the radiating area) is the through-quantity, Fig. 1.14.2 applies. Setting $v = qS^{-1}$, one has the circuit,

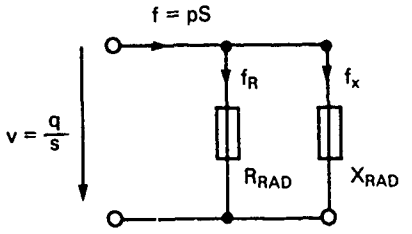


Fig. 1.14.2 — Matrix modeling illustrated by an acoustic load

$$X_{RAD} = \omega S^2 \mathscr{M}_p = \omega \frac{4\pi\rho a^3}{1 + k^2a^2} \tag{1.14.5}$$

$$R_{RAD} = S^2 \mathscr{R}_p = \frac{4\pi a^2 \rho c k^2 a^2}{1 + k^2a^2}$$

$$f = f_R + f_X = (R_{RAD} + jX_{RAD})v_{RAD}.$$

The full matrix equation of both primary and secondary circuits is obtained by cascading **A**, **B**, and **C**:

$$\mathbf{CBA}\begin{pmatrix} e \\ i \end{pmatrix} = \begin{pmatrix} f_{RAD} \\ v_{RAD} \end{pmatrix} = \begin{pmatrix} (R_{RAD} + j\omega M_{RAD})v_{RAD} \\ v_{RAD} \end{pmatrix} = v_{RAD}\begin{pmatrix} R_{RAD} + j\omega M_{RAD} \\ 1 \end{pmatrix}. \tag{1.14.6}$$

For known voltage source $e = e_S$, this equation is solved for v_{RAD}, which then allows a calculation of complex power delivered to the load,

$$W = |v_{RAD}|^2 \{R_{RAD} + j\omega M_{RAD}\} \tag{1.14.7}$$

This completes the circuit description of the acoustic projector.

1.15 MATRIX MODELING OF AN ACOUSTIC RECEIVER

When the transducer is an acoustic receiver, the terminals 7,7′ in Fig. 1.2.1 constitute a secondary source of force F_b and source admittance h_r, Fig. 1.15.1, The force F_b, or blocked force, is equal to the incident acoustic pressure multiplied by the active area S of the receiver. A factor g is inserted into the formula for F_b to account for the increase in pressure on the active surface caused by reflection of the incident sound wave. Its magnitude lies between 1 and 2, where 2 means that the surface of the receiver is acoustically hard, and 1 means that the surface is acoustically "transparent," that is, it has the same mechanical independence as the incident wave. Values of g are obtained from graphs (see Chap. 8 and Ref. [4]). The complex source admittanc h_r is modeled on the assumption that the across-

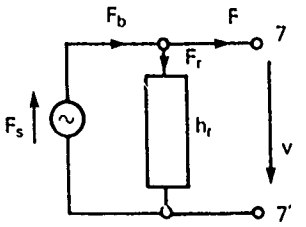


Fig. 1.15.1 — Source input circuit of an acoustic receiver modeled as a force source (F_s) in parallel with an acoustic admittance (h_r)

quantity of the acoustic load is the velocity v common to both acoustic mass and acoustic resistance, hence modeled as a parallel circuit with F as the through quantity (see Fig. 1.14.2). Thus,

$$h_r = \frac{v_r}{F_r} = \frac{1}{j\omega M_{RAD} + R_{RAD}} \quad \text{(units: } mN^{-1}s^{-1}\text{)}. \tag{1.15.1}$$

The (mobility) admittance h_r is inserted to account for the reradiation of sound by the receiver caused by motion of the receiving surface, hence a reduction of available force from F_b to F. The force lost to acoustic reradiation is given by,

$$F_{RAD} = v_{RAD}(j\omega M_{RAD} + R_{RAD}). \tag{1.15.2}$$

It is common practice in designing receivers to keep v_{RAD} very small, and also to keep the receiver surface very small. This combination makes F_{RAD} negligible so that the force delivered is very nearly F_b itself.

All remaining matrices of the receiver are the same as those of the transmitter with exception that at terminals 2,2' the primary source is replaced by a primary load, usually a passive electrical network which develop a receiver voltage or current for further signal processing.

1.16 ELECTROACOUSTIC ANALOGIES

The cascade model of an acoustic transducer shown in Fig. 1.2.1 features primary components (left of the transduction block) and secondary components (right of the transduction block). Analysis of such a model is advantageously made by changing the form of (say) all secondary components to simulate those of primary components, or vice versa. For example, if the transducer is electroacoustic in nature it may be modeled with all components in electrical form, or all components in mechanical form.

A simple way to achieve this transformation for an acoustic transducer whose primary energy storage is electrical is to use electromechanical or electroacoustic analogies. These are element for element analogies based on a purely formal similarity of mathematical models of electrical and mechanical (acoustical) elements, generally constructed without regard to physical correspondences. An example will illustrate the procedure. Let $\mathcal{M}$ be an acoustic fluid mass (units: Ns^2m^{-5}) which is being accelerated through a hole of finite depth by a pressure differential p (units: Nm^{-2}) resulting in a flow q_m (units: m^3s^{-1}). The mobility equation which relates the parameters of this mass effect is

$$q_m = \frac{1}{\mathcal{M}} \int p_m(t)\,dt. \tag{1.16.1}$$

In forming a model of a mechanical circuit element of this equation we can choose q_m to be the through-variable and p_m to be the across-variable, or vice versa. Now to form analogies it is noted that a similar choice is available in electrical circuits. There we can choose between e and i to be through or across variables. Thus if we write an electrical equation of the same appearance as 1.4.10,

$$e = \frac{1}{C}\int i dt \tag{1.16.2}$$

we may draw the following analogies simply by inspection: $q_m \rightarrow e$, $\mathcal{M} \rightarrow C$, $p(t) \rightarrow i(t)$. There is no implication that these quantities are physically similar. If we reverse the roles of e and i, we can write,

$$i = \frac{1}{L}\int e(t)\,dt. \tag{1.16.3}$$

Then we draw a different set of analogies: $q_m \rightarrow i$, $M \rightarrow L$, $p_m \rightarrow e$. Here q_m is now a through variable and p_m is an across-variable. Again the choice between 1.16.2 and 1.16.3 is purely a mathematical convenience in conducting loop or nodal analysis of circuits: no physical reasoning should suggest that acoustic mass is better modeled as electrical inductance or as electrical capacitance.

The procedure of forming analogies outlined above permits one to construct Table 1.16.1

Table 1.16.1 — Electromechanical Analogies

	Electrical Equations	$e = \frac{1}{C}\int i dt$ $i = C\frac{de}{dt}$	$e = L\frac{di}{dt}$ $i = \frac{1}{L}\int e(t)\,dt$	$e = iR$ $i = \frac{e}{R}$
(1)	Mechanical Equations	$v = \frac{1}{m}\int f(t)\,dt$	$v = n\frac{df}{dt}$	$v = \frac{f}{r}$
	Analogs for choices $\begin{cases} f \rightarrow i \\ v \rightarrow e \end{cases}$	$m \rightarrow C$	$n \rightarrow L$	$r \rightarrow \frac{1}{R}$
(2)	Mechanical Equations	$f = m\frac{dV(t)}{dt}$	$f = \frac{1}{n}\int v(t)\,dt$	$f = vr$
	Analogs for choices $\begin{cases} f \rightarrow e \\ v \rightarrow i \end{cases}$	$m \rightarrow L$	$n \rightarrow C$	$r \rightarrow R$

m = mechanical mass, n = mechanical compliance, r = mechanical resistance
C = electrical capacitance, L = electrical inductance, R = electrical resistance

	Acoustical Equations	$q = \frac{1}{\mathcal{M}}\int p(t)\,dt$	$q = \mathcal{N}\frac{dp}{dt}$	$q = \frac{p}{\mathcal{R}}$
(3)	Analogs for choices $\begin{cases} p \rightarrow i \\ q \rightarrow e \end{cases}$	$\mathcal{M} \rightarrow C$	$\mathcal{N} \rightarrow L$	$\mathcal{R} \rightarrow \frac{1}{R}$
	Acoustical Equations	$p = \mathcal{M}\frac{dp}{dt}$	$p = \frac{1}{\mathcal{N}}\int q(t)\,dt$	$p = \mathcal{R}q$
(4)	Analogs for choices $\begin{cases} p \rightarrow e \\ q \rightarrow i \end{cases}$	$\mathcal{M} \rightarrow L$	$\mathcal{N} \rightarrow C$	$\mathcal{R} \rightarrow R$

q = volume velocity, p = acoustic pressure, $\mathcal{R}$ = acoustic resistance

In this chart the units of electrical, mechanical and acoustical elements are all different. Hence in the process of forming models of transducrs in all primary or all secondary elements an adjustment must be made to render all element components in consistent units. The adjustment of units between electrical and mechanical components is contained in the transduction coefficient. An example of this coefficient is the electric field transduction y given in Eq. 1.4.2, which has the units $y = m/C$, (meter/coulomb). The units adjustment for this case becomes

$$\frac{e}{i} \times \frac{1}{y^2} = \frac{f}{\mathrm{v}} \quad \text{or } Z_e = y^2 Z_m.$$

$$Z_e = \text{electrial impedance (units: } V/A \text{ or } Vs/C) \tag{1.16.4}$$

$$Z_m = \text{mechanical impedance (units: } f/\mathrm{v} \text{ or } Ns/m).$$

Thus a mechanical impedance is transformed to electrical impedance by multiplication by y^2. Similarly the adjustment of units between mechanical and acoustical components is achieved by the use of spatial area (S),

$$\frac{f}{\mathrm{v}} \times \frac{1}{S^2} = \frac{p}{q}, \text{ or } Z_m = S^2 Z_A, \; Z_A = \frac{p}{q}. \tag{1.16.5}$$

1.17 INTRODUCTION TO CONSTRUCTION OF EQUIVALENT CIRCUITS

In this treatise conversion of energy from a primary storage component into energy in a secondary storage component, and ultimately into acoustic energy, is brought about by use of mechanical networks. These generally make up the secondary circuits, but may also be found in primary circuits. In analysis of these networks it is very advantageous to represent mechanical networks with symbols drawn from electrical circuit theory. Such a representation requires the selection of an electromechanical analogy. We choose here $e \triangleq F$, $i \triangleq V$. The networks described below will be FV (force across, velocity through). Thus spring, mass, damper will be represented by the electrical symbols of a condenser, a coil, and a resistor respectively.

While simple in principle the construction of an equivalent circuit of a given mechanism requires a detailed knowledge of its operation. In the following discussion a number of networks are analyzed to illustrate the general method of making equivalences. It should be recognized however that mechanical elements share more than one characterization, namely springs contain mass, masses are elastic, resistances are spring-like, etc. with the result that different equivalent circuits are possible for each network. Judgement is therefore needed to make best choices.

1.18 A GENERAL PROCEDURE FOR CONSTRUCTING EQUIVALENT CIRCUITS OF MECHANICAL NETWORKS

Electromechanical transducers used in acoustical engineering generally consist of electrical/mechanical elements interconnected in complicated ways. A first step in analysis is to assign a lumped parameter characterization to each element independent of frequency. This assignment always rests on an approximation and is valid only over a limited range of frequencies (of forced drive) To improve the approximation these parameters are made functions of frequency. Even so, it is generally not possible to use the lumped parameter approach over very broad ranges of frequency.

The next step in analysis is to analyze the transducer's operation by tracking the flow of force and velocity from element to element. By definition, elements possessing common velocity appear in series

in *FV* diagrams, while those posessing common force appear in parallel. Thus the equivalent network is a chain of nodes and loops. The velocity V_i in the ith loop, and the force F_j across the jth node pair constitute the tracking variables. At each node the node law requires that,

$$V_i = \sum_{\alpha} V_\alpha + V_{i+1} \qquad i = 1, 2 \ldots . \tag{1.18.1}$$

in which V_α is the velocity of the alpha element connected to the node. In general V_α can be written in terms of F_α across the node pair containing element, multiplied by the mechanical mobility (or admittance) ($\mathcal{M}$) of the element. Thus, for m elements between a node pair,

$$V_i = F_\alpha \sum_{m} Y_m + V_{i+1} \qquad i = 1, 2, \ldots . \tag{1.18.2}$$

Since F_α is the force between nodes of a pair it is seen that in an *FV* diagram the term containing F_α is in *shunt* position, while V_i, and V_{i+1} are in series position. Thus in tracking velocities, those that must be written in terms of forces between node pairs are to be considered in shunt position. Similarly in the ith loop, the loop law requires that

$$F_i = \sum_{\alpha} F_\alpha + F_{i+1} \qquad i = 1, 2, \ldots . \tag{1.18.3}$$

in which F_α is the force across the alpha element of the loop. In general F_α can be written as a product of the loop velocity V_α and the mechanical impedance of the element ($= Z_\alpha$). For m such elements,

$$F_i = V_\alpha \sum_{m} Z_m + F_{i+1} \tag{1.18.4}$$

Since V_α is the loop velocity it is seen that in an *FV* diagram the term containing V_α is in series position while F_i, F_{i+1} are measured across nodes in shunt position.

Equations 1.18.1 through 1.18.4 are the ones used in tracking force and velocity.

In the simplest case let $m = 1$. Then the tracking sequence is given in Fig. 1.18.1.

$F_0 = V_1 Z_1 + F_\alpha$	$V_1 = F_\alpha U_1 + V_2$
$F_\alpha = V_2 Z_2 + F_\beta$	$V_2 = F_\beta U_2 + V_3$
$F_\beta = V_3 Z_3 + F_\gamma$	$V_3 = F_\gamma U_3 + V_4$
(a) tracking force	(b) tracking velocity

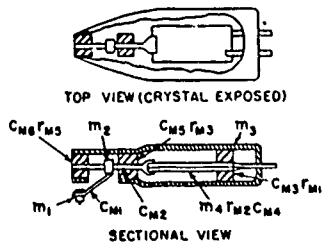
Fig. 1.18.1 — Tracking sequences

In this procedure all mobilities $\mathcal{M}_j$ and associated forces F_j are in shunt position and all impedance Z_j and associated velocities V_j are in series position.

We consider next several examples of constructing equivalent circuits.

1.19 EXAMPLES OF MECHANICAL NETWORKS AND THEIR EQUIVALENT CIRCUITS

Figure 1.19.1a shows cross-sectional views of a low noise wide range crystal pick-up used in phonographs. The operation of this pickup is quite complex. In simple terms one may track the force, or velocity, or both, in the following way:



(a)

Fig. 1.19.1 (a) — Schematic of a low-noise wide-range crystal pick-up [15]. H. F. Olson, *Acoustical Engineering* (3ed) (1957), ©1957 D. Van Nostrand Co. Inc.; by permission.

• a Thevenin's equivalent source consisting of a force f_M (delivered by the phonograph groove) in parallel with the mechanical impedance Z_{MR} of the record groove, applies a force F_0 to mass m_1 of the pick-up stylus.

• force F_0 develops a velocity V_1 in the mass impedance $Z_1 = j\omega m_1$. From previous discussion V_1 is seen to be the loop velocity, hence it is in series position. The mass m_1 delivers a force to the spring C_{M1} which *reacts* with a force F_α,

$$F_0 = j\omega m_1 V_1 + F_\alpha.$$

The force F_α is in shunt position.

• At the first node, the mobility of the spring is $j\omega C_{M1}$. The nodal law is then,

$$V_1 = F_\alpha j\omega C_{M1} + V_2, \quad \text{or } F_\alpha = (V_1 - V_2)/j\omega C_{M1}.$$

Thus the stylus spring C_{M1} is represented as being in the shunt branch.

• the spring C_{M1} delivers the force F_α to the mass m_2, developing in it a velocity V_2, and a force to the next contacting element. This element reacts with a force F_β,

$$F_\alpha = j\omega m_2 V_2 + F_\beta.$$

F_β is the reactive force developed by mass m_3 of the pick-up and the tone arm.

• At the second node

$$V_2 = F_\beta\left(\frac{1}{j\omega m_3}\right) + V_3, \quad \text{or} \quad F_\beta = (V_2 - V_3)\, j\omega m_3.$$

Thus m_3 is in shunt position. It can be regarded as a hollow mass moving in opposition to m_2 within which the crystal assembly is vibrating.

• The force F_β drives the lossy front-bearing compliance C_{M6}, developing within it a velocity V_3 and a force to the next contacting element, the compliance C_{M2} of the chuck. The chuck reacts with a force F_γ

$$F_\beta = \left(r_{M5} + \frac{1}{j\omega C_{M6}}\right) V_3 + F_\gamma.$$

- At the third node,

$$V_3 = F_\gamma \, j\omega C_{M2} + V_4.$$

Thus C_{M2} is in shunt position.

- The reactive force F_γ is also across the lossy compliance C_{M3} of the crystal support. Thus the fourth node is the same as the third node and C_{M3} is in shunt position.

- The force F_γ between the two compliances C_{M2}, C_{M3} drives the crystal, developing within it a velocity V_5, and a reactive force F_δ.

$$F_\gamma = \left(j\omega m_4 + \frac{1}{j\omega C_{M4}} + r_{M2}\right) V_5 + F_\delta$$

- The force F_δ drives the lossy rear bearing C_{M5}.

$$F_\delta = \left(r_{M3} + \frac{1}{j\omega C_{M5}}\right) V_5$$

The completed mechanical network is shown in Fig. 1.19.1b

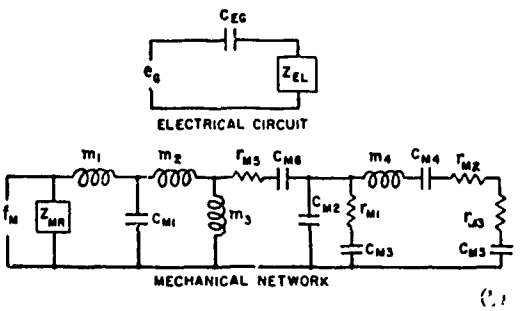


Fig. 1.19.1 (b) – Equivalent mechanical network using electrical circuit symbols [15]. H. F. Olson, *Acoustical Engineering* (3ed) (1957), ©1957 D. Van Nostrand Co. Inc.; by permission.

Example 2

Figure 1.19.2a is a cross-sectional view of a single-button carbon microphone. The essential features of operation of this transducer can be codified in an equivalent circuit by tracking velocity, or force, or both. The tracking is summarized here:

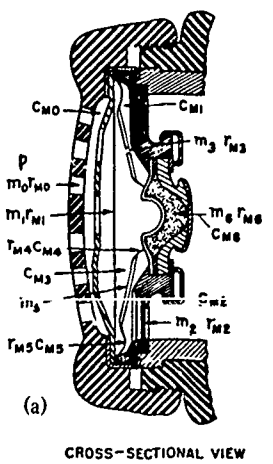


Fig. 1.19.2a – A cross-sectional view of a carbon microphone [15]. H. F. Olson, *Acoustical Engineering* (3ed) (1957), ©1957 D. Van Nostrand Co. Inc.; by permission.

• The driving force F_M is a voice-induced, transient acoustic pressure p acting over the area S of the face of the microphone. This force drives air through the hol[illegible]e face. A small mass of air m_0 is given a velocity V_1, accompanied by a resistance r_0 of the holes. The force balance is,

$$F_M = V_1(j\omega m_0 + r_0) + F_\alpha$$

in which F_α is the reactive force (of the cavity) impeding the motion of the air.

• At the first node the velocity balance is

$$V_1 = F_\alpha \mathcal{M}_1 + V_2 = F_\alpha(j\omega C_{M0}) + V_2.$$

Thus the cavity compliance C_{M0} is in shunt position while m_0, r_0 are in series position.

• The force F_α drives the lossy membrane, modelled here as a mass m_1 and resistance r_1, and gives it a velocity V_2,

$$F_\alpha = V_2(j\omega m_1 + r_1) + F_\beta.$$

in which F_β is the reactive force of the cavity compliance C_{M3}.

• At the second node the velocity balance is,

$$V_2 = F_\beta \mathcal{M}_2 + V_3.$$

The mobility $\mathcal{M}_2$ includes not only cavity compliance C_{M3} but also the impedance effect of the hole labelled m_3 r_{M3} in the diaphragm. This effect is discussed later.

• Force F_β drives the diaphragm labelled m_5 $r_{M5}C_{M5}$ giving it a velocity V_3 which is impeded by the reactive force F_γ of the coupling spring r_{M4} C_{M4}.

$$F_\beta = V_3\left(j\omega m_5 + r_{m5} + \frac{1}{j\omega C_{M5}}\right) + F_\gamma.$$

Since in an FV diagram forces are across-quantities and velocities are through-quantities it is seen that m_5, r_{m5}, C_{M5} are in series position while F_β, F_γ are in shunt position.

• At node three the velocity balance is,

$$V_3 = F_\gamma\left(\frac{1}{r_{M4} + j\omega C_{M4}}\right) + V_4$$

Thus r_{M4}, C_{M4} are in shunt position.

• The force F_γ across the coupling compliance C_{M4} drives the carbon cup and granules labeled m_6, r_{M6} C_{M6}, giving them the velocity V_4,

$$F_\gamma = V_4\left[j\omega m_6 + r_{M6} + \frac{1}{j\omega C_{M6}}\right].$$

- We account for the hole in the diaphragm by noting that the force F_β across the cavity compliance C_{M3} drives air through the hole giving a velocity V_5 to mass m_3 and resistance r_{M3},

$$F_\beta = V_5 [j\omega m_3 + r_{M3}] + F_\delta$$

in which F_δ is the reactive force the cavity compliance C_{M1}.

- At node 4 a balance of velocities leads to,

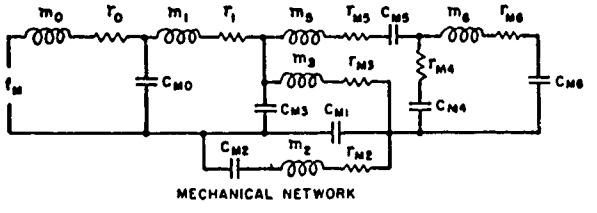
$$V_5 = F_\delta j\omega C_{M1} + V_6 \text{ or } F_\delta = (V_5 - V_6)/j\omega C_{M1}$$

in which V_6 is the velocity of the cloth diaphragm (labeled $m_2\ r_{M2}\ C_{M2}$).

- The force F_δ drives the cloth diaphragm with velocity V_6,

$$F_\delta = V_6\left[j\omega m_2 + \frac{1}{j\omega C_{M2}} + r_{M2}\right].$$

This completes the tracking of force and velocity through the mechanical network. The equivalent circuit is shown in Fig. 1.19.2b. The bandwidth characteristics of this microphone is plotted in Fig.1.19.3 in terms of response, dB re 1 volt per unit incident pressure (1 dyne/cm^2), versus frequency (Hz).



(b)

Fig. 1.19.2b — An equivalent circuit of Fig. 1.9.2a [15]. H. F. Olson, *Acoustical Engineering* (3ed) (1957), ©1957 D. Van Nostrand Co. Inc.; by permission.

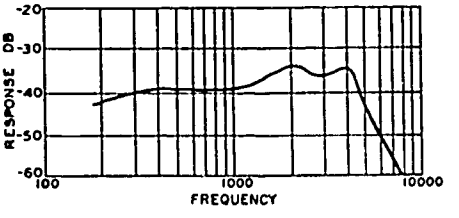


Fig. 1.19.3 — Open circuit voltage response (dB re 1 volt per dyne/cm^2) vs frequency of Fig. 1.19.2a

1.20 SUMMARY OF PROCEDURE FOR CONSTRUCTING REPRESENTATIONS OF MECHANICAL CIRCUITS AS SECONDARY COMPONENTS OF AN ELECTROMECHANICAL TRANSDUCER

A. *VF* Representation

Mechanical elements assembled in series/parallel circuits can be used as energy storage components in the secondary side of an electromechanical transducer. They are often purposely selected to provide desired characteristics of impedance (or mobility) response. We summarize here the design procedure and use a sequence of sketches to illustrate the method.

Suppose it is desired to have the secondary storage components of the transducer respond to a steady state applied force F, with a velocity V such that the mechanical impedance $(Z = F/V)$ $\left(\text{or mechanical mobility } \left(Y = \frac{V}{F}\right)\right)$ has the characteristics shown in Fig. 1.20.1.

Such a response is known to be given by the mechanical structure shown in Fig. 1.20.2.

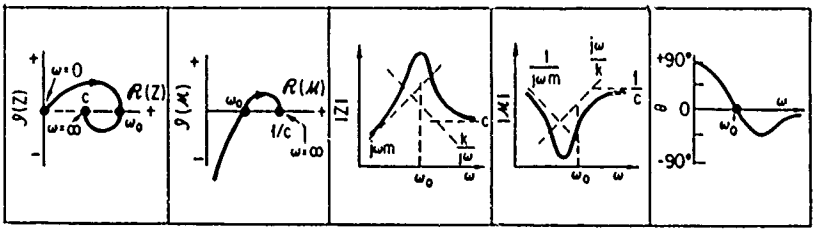


Fig. 1 20.1 — Desired response of a mechanical circuit, (a) plot of complex mechanical impedance with frequency as parameter, (b) plot of complex mobility, (c) magnitude of impedance versus frequency, (d) magnitude of mobility versus frequency, (e) phase angle of input velocity referred to the applied force [16]. C. M. Harris and C. E. Crede, *Shock and Vibration Handbook*, 1 (1961), ©1961 McGraw-Hill Book Co.; by permission.

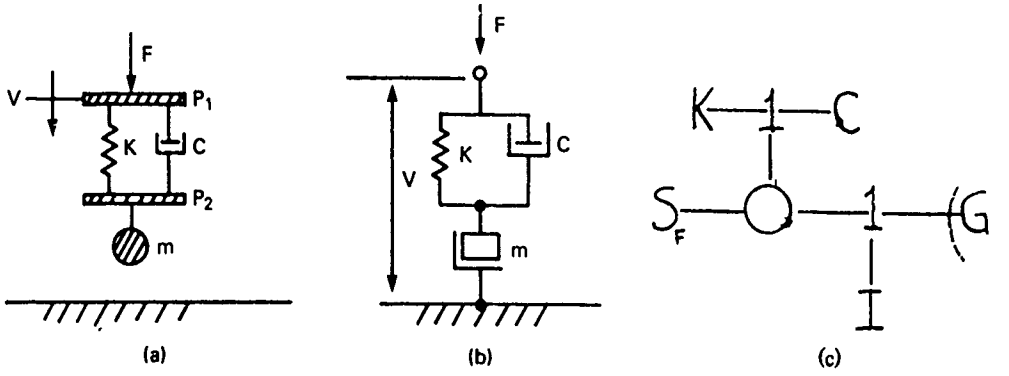


Fig. 1.20.2 — (a) mechanical structure which provides response of Fig. 1.20.1, (b) schematic (c) its bond graph

Here a spring (K), mass (m) and damping (c), connected through a massless rigid platform P_2, are driven by a force F through a massless rigid platform P_1. The physical structure is shown in (a) and a schematic of it is shown in (b). The structure is essentially series connected, hence a mobility analysis is advantageous. One therefore has,

$$(a)\quad V = F(\mathscr{M}_1 + \mathscr{M}_2) = F\mathscr{M}$$

$$(b)\quad Z = \frac{1}{\mathscr{M}}$$

$$(c)\quad \mathscr{M}_2 = \frac{1}{j\omega m};\ \mathscr{M}_1 = \frac{1}{\frac{K}{j\omega} + c} \tag{1.20.1}$$

$$(d)\quad \mathscr{M} = \frac{c + \frac{1}{j\omega m}\left[c^2 - \frac{K}{\omega}\left(\omega m - \frac{K}{\omega}\right)\right]}{c^2 + \left(\frac{K}{\omega}\right)^2}.$$

To represent the schematic (b) as the secondary circuit of the transducer we use the $i \triangleq F$, $e \triangleq V$ analogy. The series-parallel form in this analogy is preserved. The *representation* thus uses the analogies given by the following table:

Table 1.20.1 — Analogies to be Used In Converting *VF* Mechanical Networks Into *VF* Equivalent Electrical Networks as Applied to Fig. 1.20.2

electrical inductor L analogous to mechanical compliance $\left(\frac{1}{K}\right)$

electrical resistor R analogous to inverse damper $(1/c)$ (1.20.2)

electrical capacitor C analogous to mechanical mass (m)

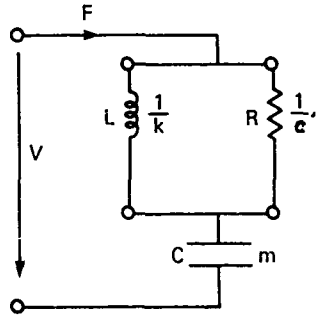


Fig. 1.20.3 — A VF representation of Fig. 1.20.2

Figure 1.20.3 shows the representation of the schematic circuit as a secondary storage element. It is seen by a simple derivation that the network of mechanical mobility specified by Fig. 1.20.1 is preserved. As with all such *VF* representations the electrical symbols used have the dimensions and units of mechanical components. They serve however to indicate the mathematical operations of differentiation and integration with respect to time, and thus are aptly suited to describing dynamic operation of the network.

B. *FV* Representation

The *FV* representation of Fig. 1.20.2 is the dual of Fig. 1.20.3. This is constructed according to these simple rules:

1. series branches are made parallel and parallel branches are made series.

2. lumped parameter elements are converted according to Table 1.20.2.

Table 1.20.2 — Analogies to be Used In Converting *VF* Mechanical Networks into Equivalent *FV* Electrical Networks

mechanical compliance $\frac{1}{K}$ is made analogous to to an electrical capacitor C

mechanical mass m is made analogous to an electrical inductor L (1.20.3)

damper c is made analogous to an { electrical resistor R in series position; electrical conductance $G = \frac{1}{C}$ in parallel position }

3. the analogy is $F \triangleq e$, $V \triangleq i$.

Figure 1.20.4 shows the *FV* representation. It is a useful model because with it one can apply all rules of electric circuit theory to calculate the response V for fixed F, or the response F for fixed V.

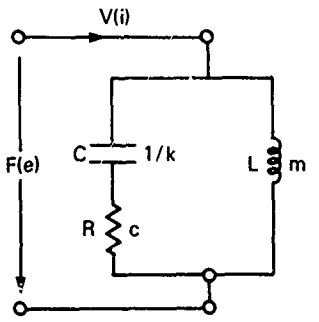


Fig. 1.20.4 — A FV representation of Fig. 1.20.2

To summarize: mechanical networks can be constructed to give desired frequency response, either exactly, or to some approximation. These networks are most conveniently pictured as *VF* diagrams (that is, with velocity as the across-quantity and force as the through-quantity). By selecting the analogy $i \triangleq F$, $e \triangleq V$, the mechanical network is *represented* by electrical symbols (inductance, capacitance, resistance) whole units however are mechanical. The dual of the *VF* diagram which features force F as the across quantity and velocity V as the through quantity is then constructed by use of the analogy $i \triangleq V$, $e \triangleq F$. The resultant *FV* diagram has a dynamic behavior for fixed force (or fixed velocity) that can be directly calculated by standard circuit theory.

For a network which is mechanically in parallel one sets $F = \Sigma F_i = V\mathrm{G}_i$. When making a *VF* representation the designer identifies G_i as an equivalent electrical mobility $\mathscr{M}_i$ according to the rules of Eq. 1.20.2. In contrast, when making a *FV* representation the designer considers G_i to be an equivalent electrical impedance Z_i according to the rules of Eq. 1.20.3. A *VF* representation preserves the original parallel form. A *FV* representation converts a parallel form to a series form.

For a network which is mechanically in series one sets $V = \Sigma\ V_i = F\ \Sigma\ \mathscr{Z}_i$. In a VF representation the symbol $\mathscr{Z}_i$ is an equivalent electrical impedance Z_i according to the rules of Eq. 1.20.2. In a *FV* representation the symbol $\mathscr{Z}_i$ is an equivalent electrical admittance (or mobility) $\mathscr{M}_i$ according to the rules of Eq. 1.20.3. Again a *VF* representation preserves the series form while an *FV* representation converts series to parallel.

It is important to note that in converting *VF* mechanical diagrams into equivalent *FV* electrical diagrams the impedance angle $+\theta$ is given a negative sign, meaning that lag angles become lead angles and vice versa.

Table 1.20.3 collects and displays all the cases previously noted.

Table 1.20.3 has another interpretation. If, for example, one is *given* a parallel electrical circuit one can conclude it is the possible equivalent circuit of two different mechanical networks: in the first, it is a parallel *VF* analog, hence the mechanical circuit corresponding to it is a parallel circuit with parameters given by Section I of the table. In the second interpretation, the parallel electrical circuit models a *FV* network. Hence it corresponds to a mechanical series network with parameters given by Section II of the Table. A few additional examples will serve to illustrate the uses of this table.

Case I. Given the series-parallel mechanical circuit, Fig. 1.20.5a, we are required to construct the electrical equivalent *FV* and *VF* networks. For *FV*, we first interchange series and parallel branches,

Table 1.20.3 — Formulas for Interconnecting *VF* and *FV* Circuits

I	
Equivalent Electrical Series *FV* Network	$e = i\left[R + j\omega L + \frac{1}{j\omega C}\right]$
Given: Mechanical Parallel Network	$F = V\left[c + j\omega m + \frac{K}{j\omega}\right]$
Equivalent Electrical Parallel *VF* Network	$i = e\left[\frac{1}{R} + j\omega C + \frac{1}{j\omega L}\right]$
II	
Equivalent Electrical Parallel *FV* Network	$i = e\left[\frac{1}{R} + j\omega C + \frac{1}{j\omega L}\right]$
Given: Mechanical Series Network	$V = F\left[\frac{1}{c} + \frac{j\omega}{K} + \frac{1}{j\omega m}\right]$
Equivalent Electrical Series *VF* Network	$e = i\left[R + j\omega L + \frac{1}{j\omega C}\right]$

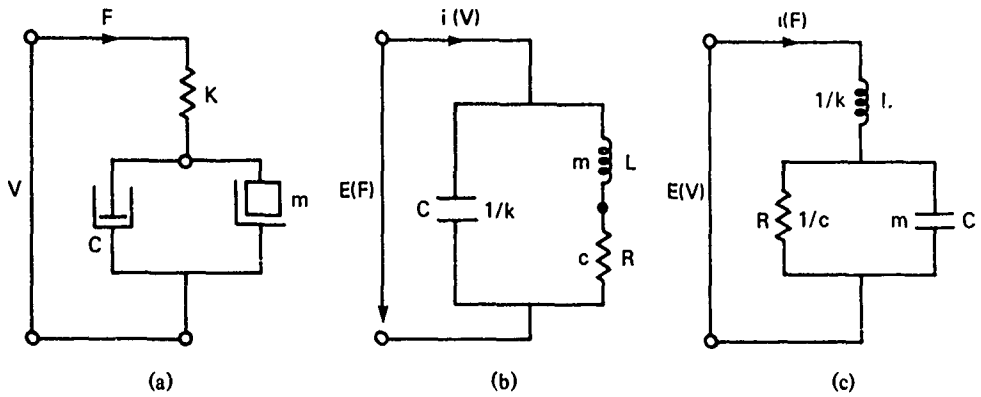


Fig. 1.20.5 — (a) Mechanical series-parallel network, (b) equivalent electrical network in FV form and (c) equivalent electrical network in VF form

that is, c and m are made series and the two are placed in parallel with K. Then series $\frac{1}{K}$ is replaced by electrical C as indicated in Section II of the table. Finally, mechanical c is replaced by electrical R and mechanical m by electrical L as indicated in Section I of Table 1.20.3. The completed equivalent *FV* network is shown in Fig. 1.20.5b. Because the original network (a) was a *VF* and the final network (b) is a *FV* network, the phase angle of (a) is given a negative sign to agree with (b).

For the *VF* network we recall that its *form* is unchanged Figs. 1.20.5c and 1.20.5a. From Section II of Table 1.20.3 it is found that $\frac{1}{K}$ is the analog of L; also from Section I the analog of C is $\frac{1}{R}$ and of m, it is C.

The dynamic response of this network is given in Fig. 1.20.5d through 1.20.5i.

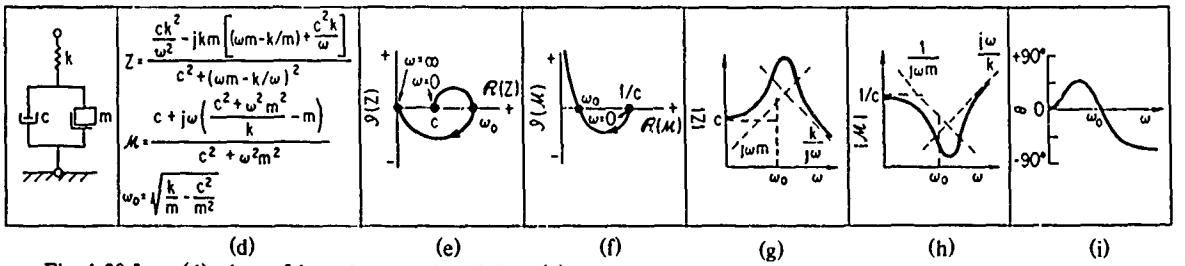


Fig. 1.20.5 — (d) plots of impedance and mobility, (e) plot of complex impedance, (f) plot of complex mobility, (g) magnitude of impedance, (h) magnitude of mobility and (i) phase angle of the mechanical circuit input velocity referred to the phase of applied force [16]. C. M. Harris and C. E. Crede, *Shock and Vibration Handbook*, 1 (1961), ©1961 McGraw-Hill Book Co.; by permission.

Case II: Using Table 1.20.3 convert the mechanical network of Fig. 1.20.6a into *FV* and *VF* electrical equivalents. Following the general rules we find the electrical equivalents to be Figs. 1.20.6b,c. The dynamic response of this network is given by Fig. 1.20.6d through 1.20.6i.

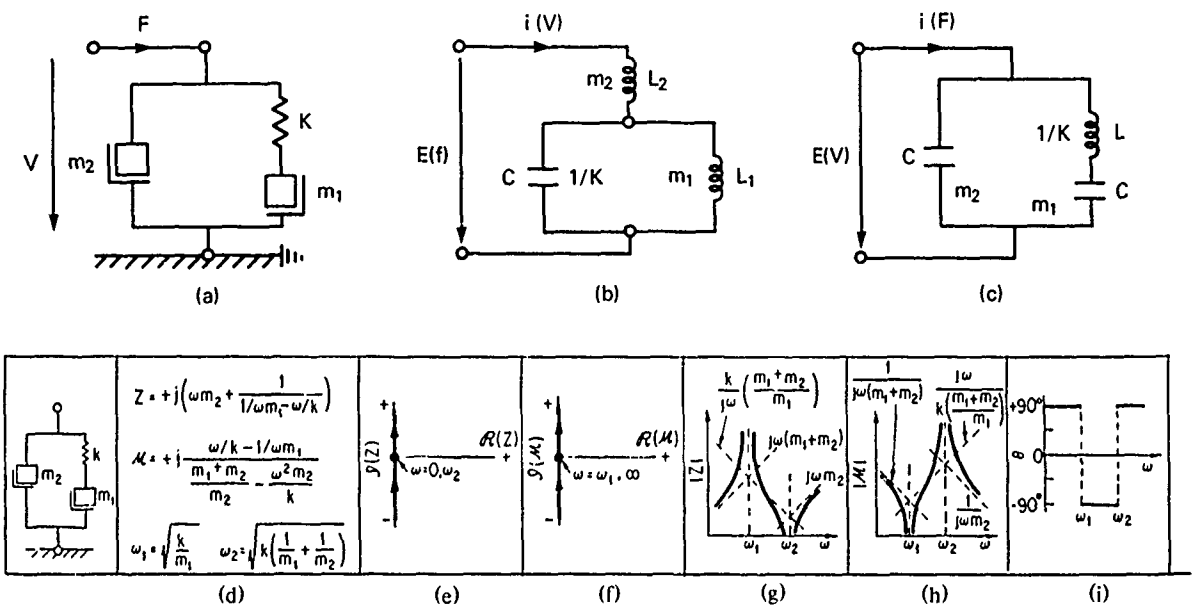


Fig. 1.20.6 — (a) Mechanical parallel network, (b) electrical equivalent circuit in FV form, (c) VF equivalent, (d) equations of impedance and mobility, (e) plot of complex impedance, (f) plot of complex mobility, (g) magnitude of impedance, (h) magnitude of mobility and (i) phase angle of velocity input referred to applied force [16]. C. M. Harris and C. E. Crede, *Shock and Vibration Handbook*, 1 (1961), ©1961 McGraw-Hill Book Co.; by permission.

Case III: A spring K and damper c_1 are connected mechanically in parallel, then the combination is connected in series with a second damper c_2, Fig. 1.20.7a. Again, by use of the Table 1.20.3, one finds the electrical equivalent *FV* diagram Fig. 1.20.7b; and the *VF* equivalent, (c). The dynamic response of this network is given by Fig. 1.20.7d through 1.20.7i.

Bond graphs of Cases I, II, III are shown in Fig. 1.20.8.

1.21 BLACK BOX DESCRIPTIONS OF TRANSDUCER COMPONENTS

In Sect. 1.1 of this treatise a transducer is decomposed into components visualized as 2-port networks connected in tandem. Other modes of connection of 2-ports are possible. These present the designer of transducers with opportunities to alter operational characteristics of their designs in a desired way. A few examples of ways to interconnect2-ports are discussed next.

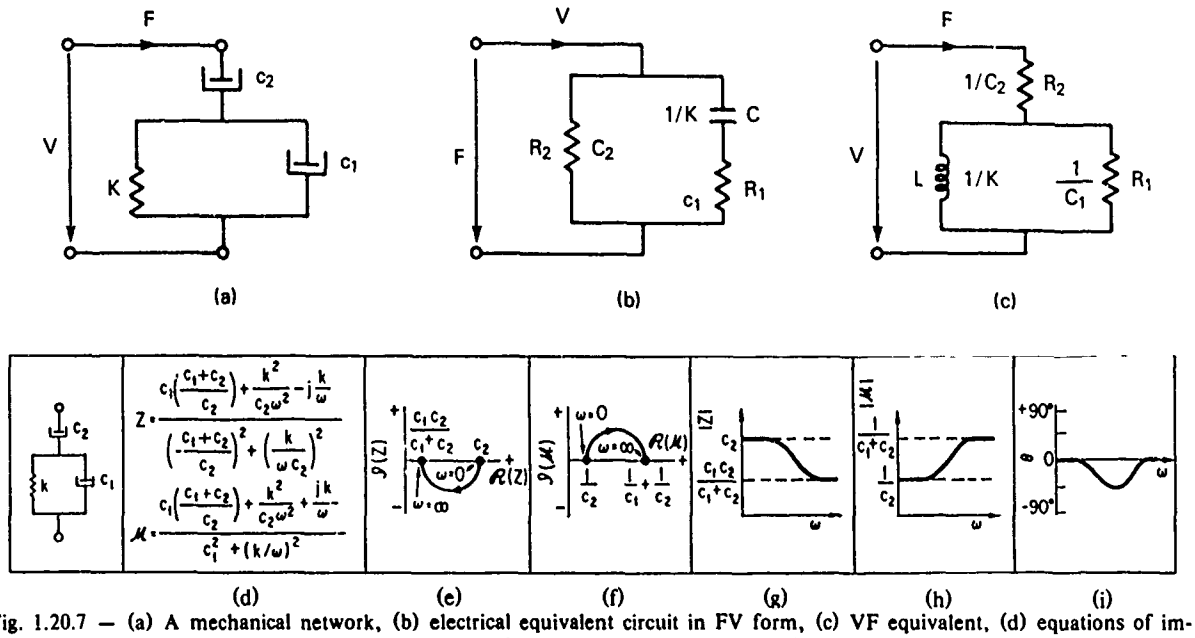
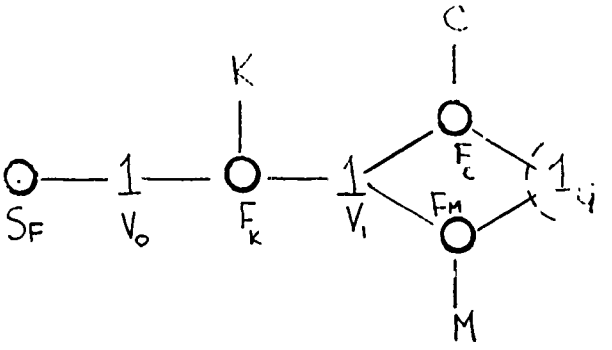
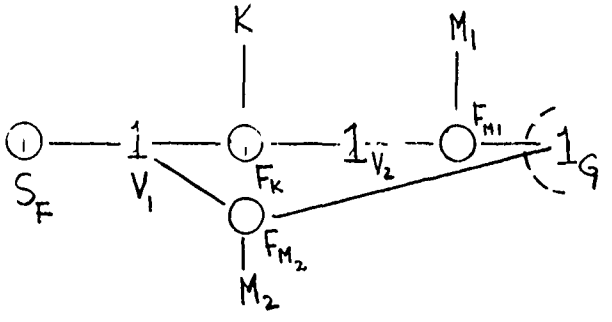


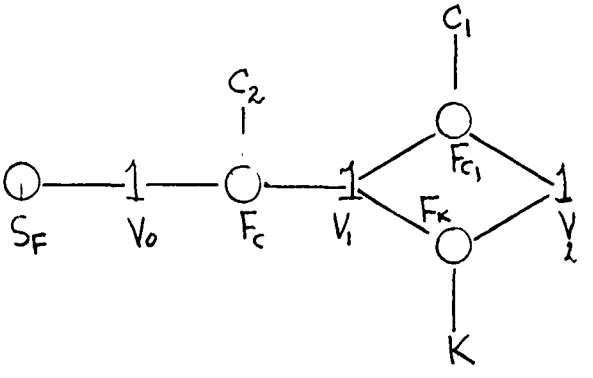
Fig. 1.20.7 — (a) A mechanical network, (b) electrical equivalent circuit in FV form, (c) VF equivalent, (d) equations of impedance and mobility, (e) plot of complex impedance, (f) plot of complex mobility, (g) plot of magnitude of impedance, (h) plot of magnitude of mobility and (i) phase of input velocity referred to applied force [16]. C. M. Harris and C. E. Crede, *Shock and Vibration Handbook*, 1 (1961), ©1961 McGraw-Hill Book Co.; by permission.



Case I



Case II

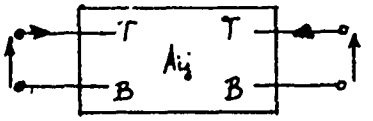


Case III

Fig. 1.20.8 — Bond graphs of Cases I, II, III above

Let each component of a transducer be a 2-port with the general description,

$$\begin{bmatrix} W_1 \\ W_2 \end{bmatrix} = \begin{bmatrix} a_{11}\ a \\ a_{21}\ a_{22} \end{bmatrix} \begin{bmatrix} X_1 \\ X_2 \end{bmatrix}$$ corresponds to the convention



(1.21.1)

(here symbols *T*, *B* are "TOP," "BOTTOM" respectively. Now *W* can be *V* or *I*, and *X* can also be *V* or *I*. There are thus four parameters V_1, V_2, I_1, I_2 from which 6 combination of input parameters two at a time, can be obtained: V_1V_2; V_1I_1; V_1I_2; $V_2\,I_1$; I_1, I_2; and $V_2\,I_2$. The last item can be eliminated since it has no subscript 1 to indicate an input quantity. Thus there are 5 input characterizations of 2-port networks. They are listed here together with descriptive names taken from the theory of electric circuits.

$$\begin{bmatrix} V_1 \\ V_2 \end{bmatrix} = \begin{bmatrix} z_{11}\ z_{12} \\ z_{21}\ z_{22} \end{bmatrix} \begin{bmatrix} I_1 \\ I_2 \end{bmatrix} \tag{1.21.2}$$

(a) Open-circuit impedance, *z* parameter

$$\begin{bmatrix} I_1 \\ I_2 \end{bmatrix} = \begin{bmatrix} y_{11}\ y_{12} \\ y_{21}\ y_{22} \end{bmatrix} \begin{bmatrix} V_1 \\ V_2 \end{bmatrix}$$

(b) Short-circuit admittance, *y* parameter

$$\begin{bmatrix} V_1 \\ V_2 \end{bmatrix} = \begin{bmatrix} h_{12}\ h_{12} \\ h_{21}\ h_{22} \end{bmatrix} \begin{bmatrix} I_1 \\ V_2 \end{bmatrix}$$

(c) Hybrid "*h*" parameters

$$\begin{bmatrix} I_1 \\ V_2 \end{bmatrix} = \begin{bmatrix} g_{11}\ g_{12} \\ g_{21}\ g_{22} \end{bmatrix} \begin{bmatrix} V_1 \\ I_2 \end{bmatrix}$$

(d) Hybrid *g* parameter

$$\begin{bmatrix} V_1 \\ I_1 \end{bmatrix} = \begin{bmatrix} AB \\ CD \end{bmatrix} \begin{bmatrix} V_2 \\ -I_2 \end{bmatrix}$$

(e) *ABCD* Parameters

(The negative $-I_2$ indicates a change in direction.) When two transducer components are visualized as 2-port black boxes (parameters *W*, *W'*; *X*, *X'*) and are connected series-series, parallel-parallel, series-parallel or parallel-series, a variety of new matrix equations (parameters *W''*, *X''*) are obtained. A *connection* in *series* means $V'' = V + V'$, and $I_1 = I'$; a *connection in parallel* means $I_1'' = I_1 + I_1'$ and $V_1 = V_1'$. The generic form of the combination is an enlarged black-box whose 2-port description is,

$$\begin{bmatrix} W_1'' \\ W_2'' \end{bmatrix} = \begin{bmatrix} a_{11}'' & a_{12}'' \\ a_{21}'' & a_{22}'' \end{bmatrix} \begin{bmatrix} X_1'' \\ X_2'' \end{bmatrix} \tag{1.21.3}$$

in which

$$a_{11}'' = a_{11} + a_{11}'; \; a_{12}'' = a_{12} + a_{12}', \text{ etc.}$$

Here it is seen that the transfer matrix A_{ij}'' is composed of elements which are simple sums of the elements of the original matrices, $A_{ij}'' = A_{ij} + A_{ij}'$. This additive property is useful in design because impedances (or admittances) can be increased, decreased or totally cancelled by such series/parallel combinations of components.

Fig. 1.21.1 shows 6 cases of addition of matrices by just such combinations.

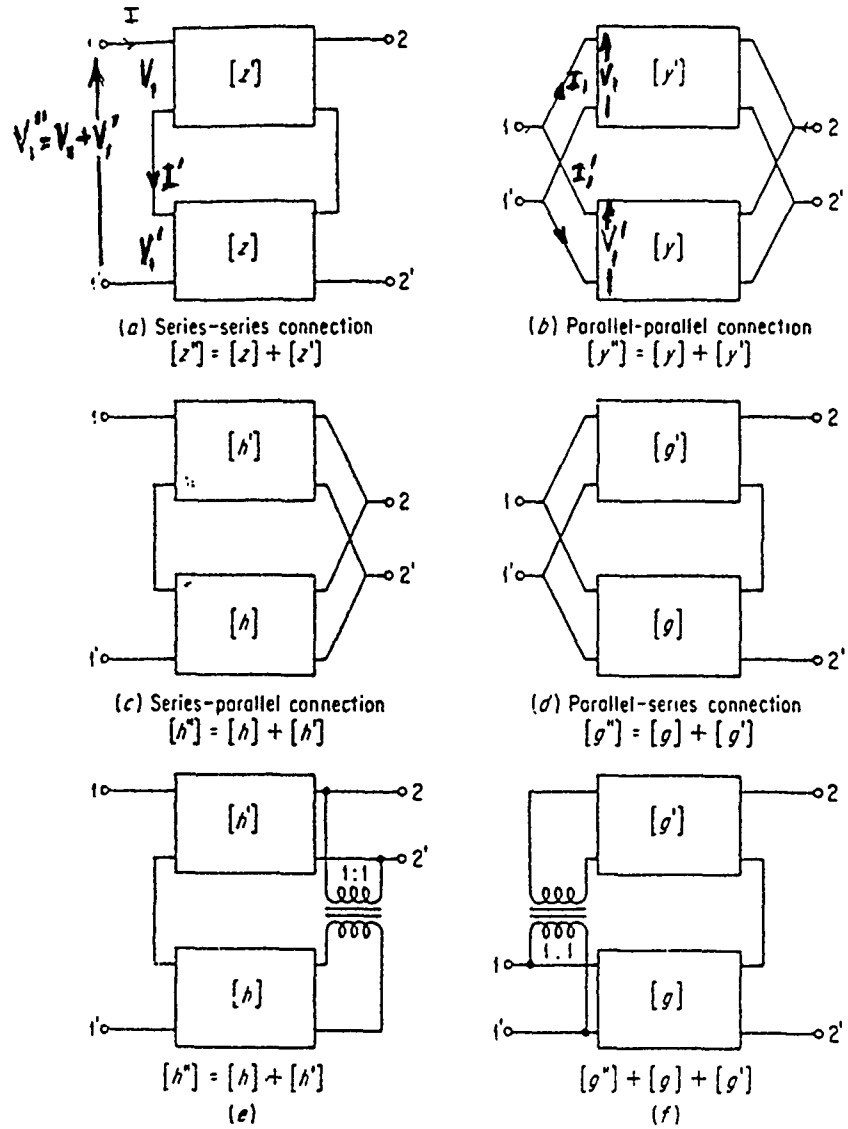


Fig. 1.21.1 — Series/parallel connections of transducer components illustrating changes in transfer matrices by addition of matrix elements

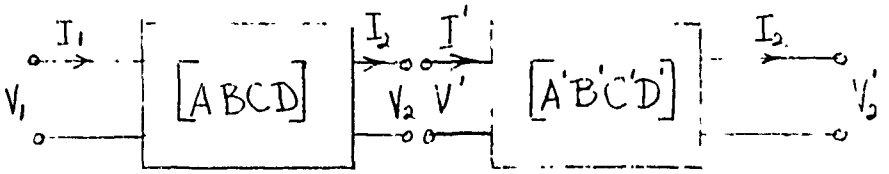


Fig. 1.21.2 — Connection of 2-Port Components in tandem

Instead of using series/parallel connections a designer may choose to connect 2-port components in tandem (= cascade). The most appropriate characterization is then the *ABCD* set, Fig. 1.21.2. By noting that $-I_2 = I_1'$ and $V_2 = V_1'$, it is readily seen that the transfer matrices multiply. The combined set is then,

$$\begin{bmatrix} V_1 \\ I_1 \end{bmatrix} = \begin{bmatrix} AB \\ CD \end{bmatrix} \begin{bmatrix} A' & B' \\ C' & D' \end{bmatrix} \begin{bmatrix} V_2' \\ -I_2' \end{bmatrix}. \tag{1.21.4}$$

The ratio V_2'/V_1 is called the *voltage gain* and the ratio $-I_2'/I_1$ is called the *current gain.*

The theory of electrical 2-ports may also be applied to mechanical 2-ports. Here the parameters F_1, F_2, v_1, v_2 can be assembled into 5 sets and series/parallel connections again formulated in the manner just described. In contrast to the electrical case a series connection means $F_1 = F_1'$, $v_1'' = v_1 + v_1'$ and a parallel connection means, $F_1'' = F_1 + F'$, $v_1 = v_1'$. The transfer matrix has elements which, in most cases, are lumped parameter representations of the dynamic mass, spring, and resistance of the mechanical components.

1.22 EQUIVALENT CIRCUITS OF CONTINUOUS ELASTIC SYSTEMS

The representation of acoustic transducers to this point has been done in terms of lumped parameters. This is useful not only intrinsically in accurately portraying the physical nature of discrete element transducers in selected frequency ranges, but also in helping improve the understanding of transducers constructed of continuous elastic members. We consider continuous systems here and choose a vibrating bar as our model.

The dynamic motion of a rectangular bar of elastic material, density ρ, length l, width w and thickness d in longitudinal motion can be described by a partial differential equation which has a unique solution in terms of prescribed boundary conditions. However a first approach to constructing an equivalent circuit of this bar is to return to a lumped parameter description and consider the motion to be approximated by a linear echelon of masses and springs. To begin the analysis, choose a single spring between two masses, and assume that across the spring there is a force source f_w generating a velocity difference V_w Fig. 1.22.1. This is a *tonpilz.* It is a fundamental structure occurring very fre-

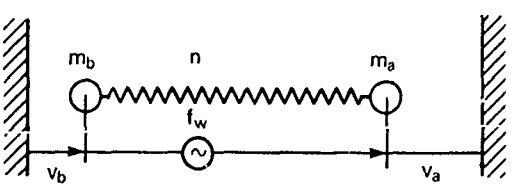
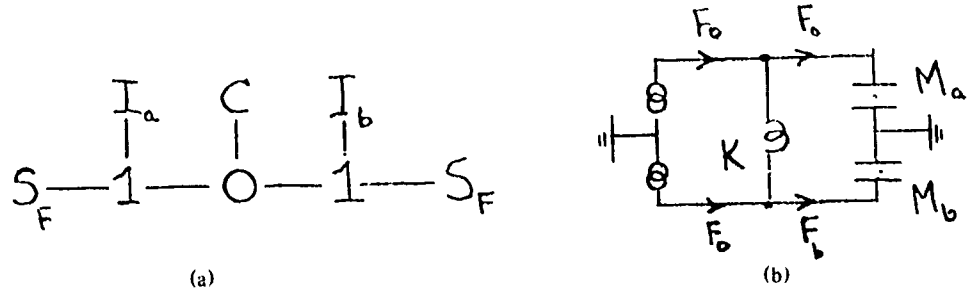


Fig. 1.22.1 — A two-mass system driven by a force source

quently in applications. The primitive bond graph *VF* flow chart Fig. 1.22.2a is based on the idea that the source, the spring and the masses all have a common velocity difference. It is thus seen to be three branches in parallel.

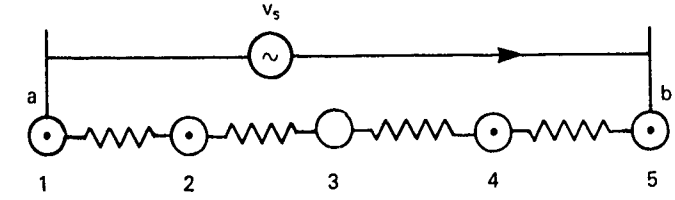


(a) (b)

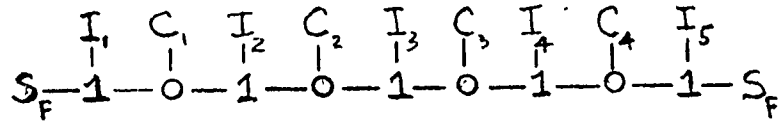
Fig. 1.22.2 — (a) Bond graph of Fig. 1.22.1 in dual form and (b) its VF equivalent circuit

The corresponding electrical circuit in its *VF* representation is shown in Fig. 1.22.2b. Here it is seen that the masses have one terminal (each) grounded, as required in *VF* circuits. At point a the mass m_a and spring n have a common velocity v_a. Hence they are pictured in parallel, meaning that the force f_w of the driver branches into the force f_n of the spring and f_{ma} of the the mass. Similarly at point b the branch forces f_n and f_{mb} combine to give f_w again.

We consider next four such tonpilzes connected as 5 masses and 4 springs, Fig. 1.22.3a. The primitive bond graph is shown in Fig. 1.22.3b. The *VF* mechanical circuit is shown in Fig. 1.22.4. This



(a)



(b)

Fig. 1.22.3 — (a) a five-mass, four-spring system and (b) its bond graph

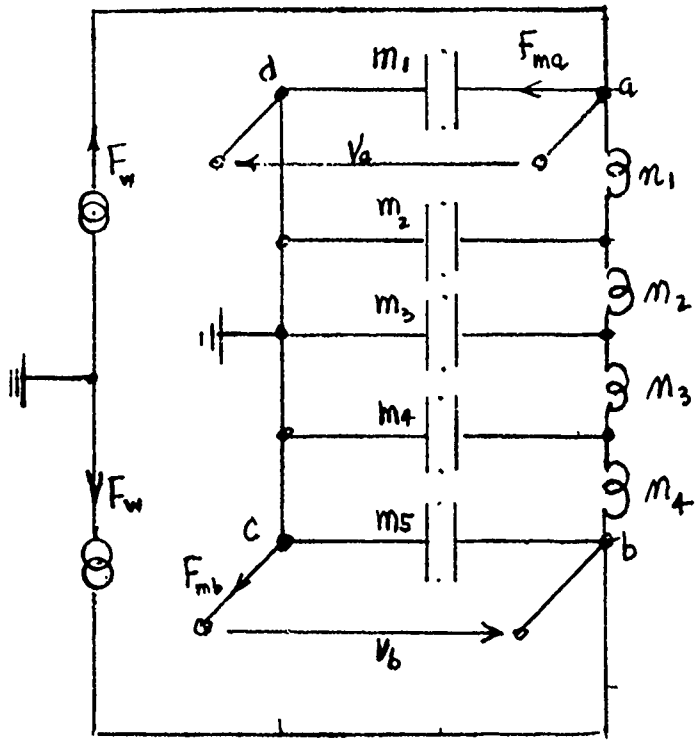


Fig. 1.22.4 — A mechanical VF circuit of the system in Fig. 1.22.3

combination of masses and springs has the appearance of a lumped element representation of a transmission line. Evidently the number of masses and springs can be increased indefinitely. In the limit of an elastic bar (width b, depth d, length l) the distributions of mass and spring become continuous functions of the length coordinate of the bar. Lumped elements then merge in such a way that the force f_w at point a divides into a force f_n to drive a distributed spring system of mechanical admittance $v_w/f_w = Y_1$, and force f_{ma} to drive a distributed mass system of mechanical admittance $v_a/f_a = Y_2$, Fig. 1.22.5. Similarly at point b the force f_{mb} drives the distributed mass of mechanical admittance $v_b/f_b = Y_3$, which for a symmetrical bar is equal to Y_2. The *VF* mechanical circuit is closely analogous to Fig. 1.22.2 with the exception that distributed parameters replace lumped parameters.

It is to be noted that "ground" has been removed from Fig. 1.22.5. It will be restored when various modes of loading the ends are discussed. Figure 1.22.5 is the dual of the Mason Circuit [3] of a longitudinal vibrator bar. In it, ω is the frequency of drive and c is the speed of sound in the material of the bar. At very low frequencies where $\omega l/c \ll 1$ one has,

$$Y_1 \rightarrow \frac{j\omega l}{wd\rho c^2} = j\omega n_k, \quad n_k = \frac{l^2}{MC^2}$$

$$Y_2 \rightarrow \frac{1}{j\omega wd\rho c\frac{\omega l}{2c}} = \frac{1}{j\omega\frac{M}{2}}$$

$$M = lwd\rho$$

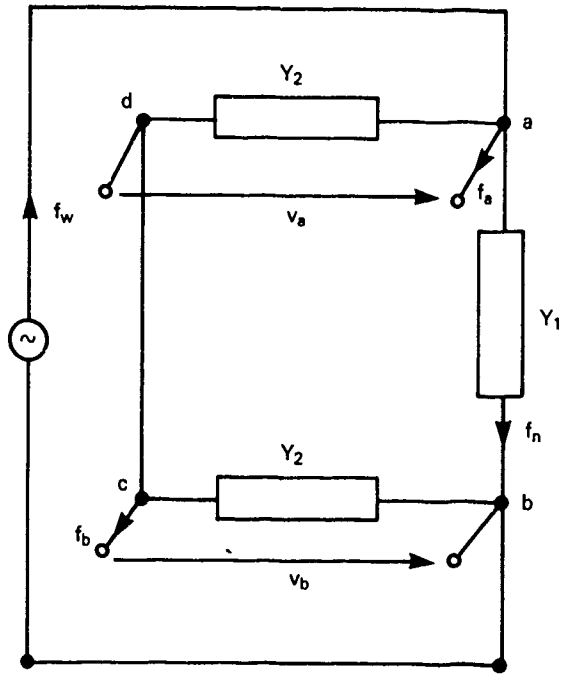


Fig. 1.22.5 — Distributed parameter VF mechanical circuit of a longitudinal elastic bar driven by a velocity difference between its ends

Here M, M_k are low frequency mass and compliance of the bar. By setting $M/2 = M_a = M_b$ and $n_k = n$ the equivalent circuit of the tonpilz is recovered (see Fig. 1.12(2)). Thus the longitudinally vibrating bar at low frequencies is very nearly a tonpilz. Several special, but important cases, can be derived from Figs. 1.22.5. These are concerned with driving the longitudinal bar near a mechanical resonance under various conditions of loading. A discussion will be found in Sect. 2.21.

1.23 UNIFICATION OF CIRCUITS INTO ALL PRIMARY OR ALL SECONDARY COORDINATES

This topic, briefly mentioned in Sect. 1.14, is treated here in greater detail.

Case of Gyrator Transduction

In the generalized acoustic transducer, Fig. 1.2.1 the number of energy coordinates is four, e, i, f, v, or six if the acoustic load p, q, is treated separately. A separate treatment of p, q can be reduced to f, v by use of the relations

$$p = \frac{f}{S};\ q = S\mathrm{v} \tag{1.23.1}$$

in which S is the surface through which the mechanical velocity v is flowing in a normal direction. It is often essential, and certainly convenient, to coalesce primary and secondary circuits and express the resultant network in primary e, i only, or in secondary f, v only.

To coalesce primary and secondary circuits one requires an explicit form of the transduction matrix. The elements of this matrix relate e_w, i_w to f_w, v_w Fig. 1.2.1. For almost all applications in acoustic transduction the relation is either linear, because of the inherent physical laws, or made linear

by procedures that come under the name of "polarization". In either case the formation of a unified circuit requires the selection of an analogy. It is convenient here to choose the current-force (i-f) analogy. Thus the mechanical circuits we shall draw will be *VF* (that is, velocity is the across-variable and force the through-variable). The physical laws of transduction can then be reduced to two general forms:

$$\text{VF Gyrator} \begin{cases} (1)\ e_w = y\, f_w \\ (2)\ i_w = \dfrac{1}{y}\, v_w \end{cases} \qquad \text{VF or Ideal Transformer} \begin{cases} (3)\ e_w = \dfrac{1}{X}\, v_w \\ (4)\ i_w = X\, f_w \end{cases} \tag{1.23.2}$$

In Eqs. (1), (2) of 1.23.2 the primary across-quantity e_w is linearly related to the secondary through-quantity f_w; and the primary through-quantity i_w is linearly related to the secondary across-quantity v_w. These relations define a VF form of *gyrator.* In Eqs. (3), (4) primary across-quantities are linearly related to secondary across-quantities, and primary through-quantities are linearly related to secondary through-quantities. These relations define a VF form of ideal *transformer.*

The procedure of coalescing primary and secondary circuits can now be easily described.

Case of the Ideal Gyrator

In the case of the gyrator, Eqs. (1), (2) of 1.23.2 can be combined to read:

$$\frac{e_w}{i_w} = y^2 \frac{f_w}{v_w} = y^2 z_m \tag{1.23.3}$$

in which z_m is the mechanical impedance of the secondary. This equation states that mechanical impedances are converted to electrical impedances by multiplication with y^2. Assuming that the masses m, compliances n and mechanical conductances h have the same velocity, we can write Eq. 1.23.3 in the form,

$$\frac{e_w}{i_w} = y^2 \left\{ j\omega m + \frac{1}{j\omega n} + \frac{1}{h} \right\}. \tag{1.23.4}$$

When force is the through-quantity (as here assumed), the impedance z_m is recognized as 3 parallel branches in which are flowing f_m, f_n and f_h respectively. Now to form an electrical equivalent circuit, choose by inspection the electrical primary elements L, C, R such that

$$\frac{e_w}{i_w} = j\omega L + \frac{1}{j\omega C} + R$$

$$L = y^2 m;\ C = \frac{n}{y^2};\ R = \frac{y^2}{h}. \tag{1.23.5}$$

With this choice the transduced secondary circuit elements appear electrically is series. Thus secondary elements connected mechanically in parallel (meaning they have the same velocity) become primary elements in series, with the analogs being mass/inductance, compliance/capacitance, conductance/resistance. This switching from parallel to series is traceable to the gyrator nature of the transduction coefficient, and the use of the i-f analogy in the secondary circuit.

Next we assume the secondary elements have a common force, that is, they are mechanically in series. The velocities across them are then,

$$q_m = f/j\omega m;\ q_n = ndf/dt;\ q_h = fh. \tag{1.23.6}$$

Using the gyrator transduction again one has,

$$\frac{i_w}{e_w} = \frac{1}{y^2}\left(\frac{1}{j\omega m} + j\omega n + h\right). \tag{1.23.7}$$

If we apply the correspondences (analogies) given by 1.23.5 and solve for i_w, that is, if we set,

$$i_w = \left(\frac{1}{j\omega L} + j\omega C + \frac{1}{R}\right) e_w \tag{1.23.8}$$

it is seen that the primary elements are in parallel. Thus secondary elements that are mechanically in series appear as elements in the primary connected in parallel.

Now we reverse the roles of primary and secondary components and apply Eq. (2) of 1.23.2. This shows that if the electrical elements are connected in series (namely having common electrical current) they will appear in the secondary to be connected in parallel (namely having common mechanical velocity). In symbols,

$$\frac{j\omega L_E}{y^2} + \frac{1}{j\omega C_E y^2} + \frac{R_E}{y^2} = j\omega m + \frac{1}{j\omega n} + \frac{1}{h} \tag{1.23.9}$$

from which one can make the same equivalences as given by 1.23.5. Similarly, from the relation that

$$y^2 \frac{i_w}{e_w} = \frac{v_w}{f_w} \tag{1.23.10}$$

it is seen that primary elements in parallel become secondary elements in series.

Summary: When the transduction matrix is a gyrator and the *i-f* analogy is used, all mechanical elements in a *VF* circuit representation which have common force (i.e. are in series) are transduced into electrical elements which have common voltage drop (i.e. are in parallel). This behavior mirrors Eq. (1) of 1.23.2. Also all mechanical elements which have a common velocity (i.e. are in parallel) are transduced into primary elements a common through-quantity (i.e. are in series). This behavior mirrors Eq. (2) of 1.23.2.

Case of Ideal Transformer Transduction

The procedure just used can also be applied to Eqs. (3), (4) of 1.23.2. Thus in the case of transduction through an *ideal transformer* it is seen that the following rules in the *i-f* analogy hold:

- All secondary mechanical elements in a *VF* circuit which are in parallel (i.e. have a common velocity) are transduced into primary elements whcih have a common across quantity (i.e. are also in parallel). This conclusion is drawn from the equations,

$$\frac{i_w}{e_w} = \frac{X^2 f_w}{v_w} = X^2 \left\{ j\omega m + \frac{1}{j\omega n} + \frac{1}{h} \right\}$$

$$\frac{i_w}{e_w} = \frac{X^2 f_w}{v_w} = j\omega C + \frac{1}{j\omega L} + R \qquad (1.23.11)$$

$$C = X^2 m;\ L_1 = \frac{n}{X^2};\ R = \frac{X^2}{h}$$

units $h : mN^{-1}s^{-1}$
$n : mN^{-1}$ $\quad X^2 : mAV^{-1}N^{-1}s^{-1}$
$m : Ns^2m^{-1}$

• All secondary mechanical elements in a *VF* circuit representation which have a common force (i.e. are in series) are transduced into primary elements which have a common through quantity (i.e. are in series). This conclusion is drawn from the following sets of equations,

$$\frac{e_w}{i_w} = X^{-2} \frac{v_w}{f_w} = \frac{1}{X^2} \left(\frac{1}{j\omega m} + j\omega n + h \right)$$

$$\frac{e_w}{i_w} = \frac{1}{j\omega C} + j\omega L + R^{-1}. \qquad (1.23.12)$$

These conclusions show the advantage of the *i-f* analogy which, in transformer type transduction, allows parallel-parallel, and series-series element transformations in unifying primary and secondary circuits.

1.24 EXAMPLE OF TRANSFER OF SECONDARY CIRCUITS INTO PRIMARY CIRCUITS

As an example of circuit unification we select the case of a condenser microphone Fig. 1.24.1. The cascade of matrices (Fig. 1.2.1) applied to this case appears as Fig. 1.24.2.

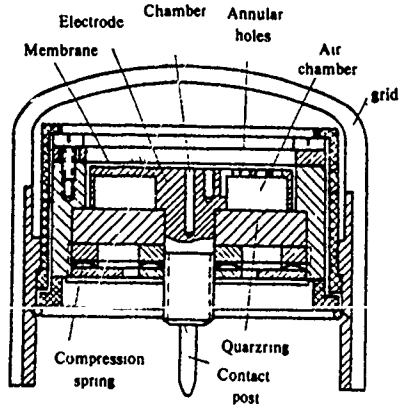


Fig. 1.24.1 — A condenser microphone

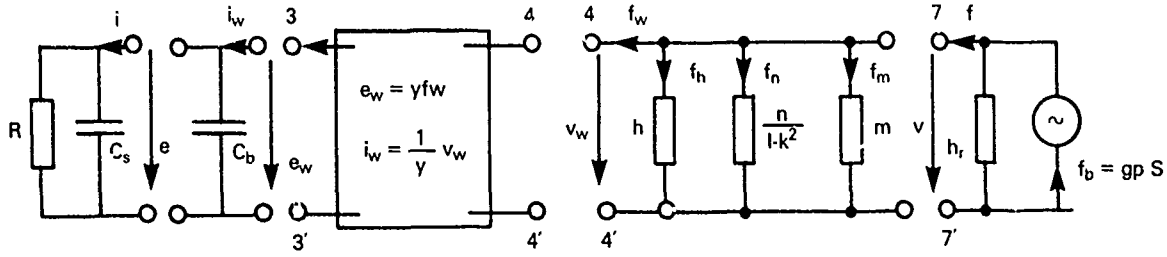


Fig. 1.24.2 — An equivalent circuit representation based on current/force analogy of Fig. 1.24.1 in which the mechanical branch is in VF representation

For purposes of this section we consider the secondary circuit to consist of two components: the mechanical diaphragm membrane and the acoustic impedance. We start the cascade at terminals 7-7'. The driving source is a force generator F_b created by incident pressures acting over area S, in parallel with the radiation admittance h_r, Fig. 1.13.2 and Eq. 1.14.5. The mass m, compliance n and conductance h of the secondary mechanical storage represent the diaphragm of the microphone. All have the same velocity. A notable feature of this storage matrix is that the mechanical compliance is increased by the coupling factor k^2 (for explanation see Sect. 1.37 thru 1.40). The primary storage is an electrical capacitor C_b, and the primary load is a passive impedance (generally a resistor) in parallel with the capacitance C_s of the attached lead-in wires. The transduction component 3,3' - 4,4' is taken to be a VF form of gyrator (see Eqs. 1, 2 of 1.23.2).

We desire to convert the secondary coordinates f, v into primary coordinates e, i using the methods of the previous section. First the free source F_b in parallel with the radiation admittance h_r becomes a voltage source $e = y\ F_b$ in series with an electrical impedance $Z = \frac{y^2}{h_r}$ (units of h_r: m/Ns; units of y^2: Vm/NsA; units of $Z = V/A$). Second, the parallel elements of secondary storage represented by damping h, compliance n (units: m/N), and mass m (units: Ns^2/m) become series elements of primary storage represented by resistance y^2/h (units: V/A), capacitance n/y^2 (units: AS/V), and inductance y^2m (units: Vs/A). The equivalent circuit with secondary elements transferred to primary elements thus becomes Fig. 1.24.3: Note that terminals 5,5' have replaced 4,4' and 3,3'. The electrical equivalent circuit is now complete. It is readily seen that a purely mechanical circuit is also possible and can be constructed similarly by the methods of the previous section.

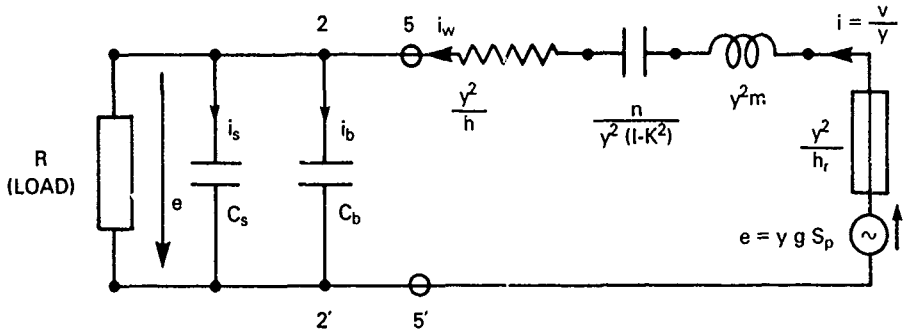


Fig. 1.24.3 — An all-electrical representation of the condenser microphone of Fig. 1.24.1

1.25 METHODS OF ANALYZING ONE-CONNECTION AND MULTIPLE-CONNECTION MECHANICAL SYSTEMS

As noted in Secs. 1.0, 1.1 a mechanical system may be defined as an assembly of mechanical elements connected to each other in series/parallel form. They may be categorized as active systems if they have energy sources, or passive systems if they do not. Each system has a minimum of two terminals (often more) which allow them to be connected to other systems, or to a rigid immovable frame, here called the "ground," in analogy to electrical systems.

Mechanical systems are conveniently divided into *one-connection systems*, or *multiple-connection systems*. Their properties are discussed next.

1.26 GENERALIZED ONE-CONNECTION SYSTEMS AND THEIR THEVENIN AND NORTON EQUIVALENTS

These systems have two terminals, Fig. 1.26.1, of which one (labelled 2) is permanently attached to ground, and the other (labelled 1) is available for external connection. Thus they have only one set of energy coordinates, F_1, V_1. In applications such systems often appear as sources or loads. The mechanical impedance Z (units: Ns/m) is the ratio of an applied force F at point 1 to the resultant velocity V_1. In complex circuits the calculation of Z is tedious. Circuit simplification is then highly advantageous. This is done by use of circuit equivalents explained next.

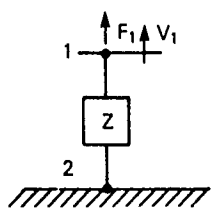


Fig. 1.26.1 — A one-connection mechanical system [16]

When the system containing Z includes sources of force and is attached to a load one may reduce it to a single constant force generator in parallel with a single impedance connected to the load. This is the Thevenin's equivalent system and is experimentally obtained by these steps:

- the load is replaced by an infinite mechanical impedance and the force exerted by the system at the point of attachment is measured as the clamped force F_c.

- the load is disconnected and the free velocity v_f is measured at the point of attachment.

Thevenin's equivalent system is then a force generator of magnitude F_c in parallel with a single impedance $Z_s = F_c/v_f$. This is shown in Fig. 1.26.2.

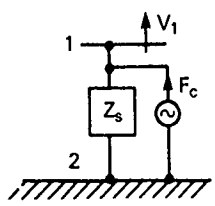


Fig. 1.26.2 — Thevenin's equivalent of Fig. 1.26.1 [16]

In a similar way a 1-connection system containing sources may be converted to a Norton's equivalent in which v_f is the equivalent velocity source in series with the internal impedance Z_s. This is shown in Fig. 1.26.3.

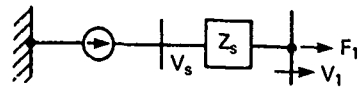


Fig. 1.26.3 — Norton's equivalent of Fig. 1.26.1 [16]

It is useful in transducer analysis based on equivalent circuits to convert a source-network-load into a Thevenin (or Norton) equivalent. The procedure is this: we suppose the equivalent circuit has several meshes, with possible active elements (= sources) in one or more of these meshes. Furthermore we suppose there is a pair of terminals on this network to which a load may be attached. We first disconnect any load, and measure the voltage V_{0c} across the (exposed) terminals due to operation of all internal active elements. Next, all the internal active elements are replaced by their internal impedance and the impedance Z_{in} looking in, as measured at the terminal pair in question, is measured. The voltage V_{oc} in *series* with the impedance Z_{in} then constitute the Thevenin form of the *equivalent source.* When connected to the load Z_L the combination *source-load* constitute the Thevenin equivalent circuit.

In a similar way one can derive the form of the Norton equivalent circuit. The two (unconnected) terminals are short-circuited and the current I_{sc} is measured. All active elements are then replaced by their internal admittances and the admittance Y_{in} of the entire network looking in from the terminals is measured. The current I_{sc} in parallel with the admittance Y_{in} constitutes the Norton form of the equivalent source. When connected to the load Z_L the combination source-load constitutes the Norton equivalent circuit.

Actually the word "terminals" in the above statement can mean any two distinct points in a network between which there are active/passive elements.

Summary: The Thevenin and Norton equivalent sources are mathematical representations which generate the same across-quantity V_t and through quantity I_t at a pair of terminals to which a load can be attached. As such they are completely interchangeable.

1.27 BOND GRAPHS OF EQUIVALENT SOURCES

Bond graphs of Thevenin and Norton equivalent source are shown in Fig. 1.27.1. In these graphs mechanical velocity is the "effort", and mechanical is the "flow."

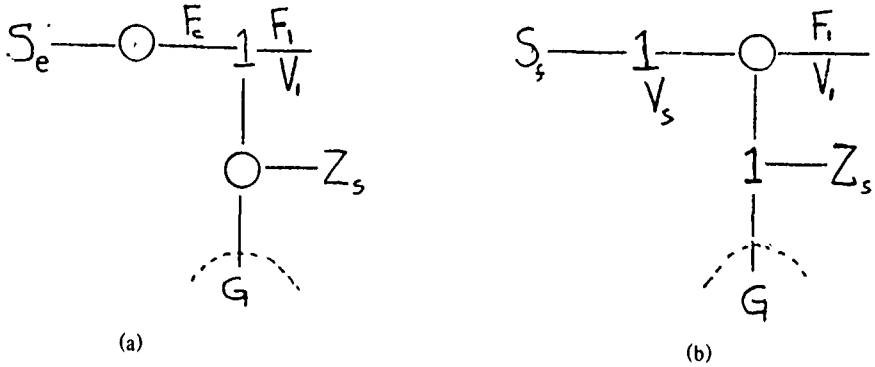


Fig. 1.27.1 — Bond graphs of (a) Thevenin and (b) Norton Equivalent Sources

1.28 ANALYSIS OF ONE-CONNECTION SYSTEMS

The generalized impedance Z of Fig. 1.26.1 is composed of chains of "black boxes" connected in series and/or in parallel. In this assembly one can identify points of common velocity among the boxes. These correspond to force nodes. Analysis of mechanical systems consists in finding these nodal velocities when the system is driven by given sources. The procedure for doing this is based on the assumption that all impedances of the component black boxes are explicitly known. The steps are:

- at each point of unknown common velocity (V_c) multiply each impedance by V_c and add them together; then multiply each of these same impedances by the velocity at its other connection point and subtract these from the sum. The algebraic result of additions and subtractions is set to zero. As an example let the following Fig. 1.28.1 be a *part* of a mechanical system under analysis:

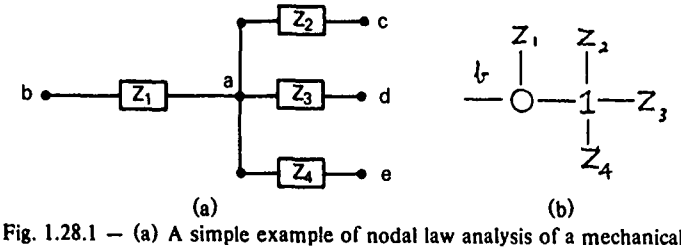


Fig. 1.28.1 — (a) A simple example of nodal law analysis of a mechanical system. This is a VF network (b) bond graph.

For velocity V_a, following the above cited rule, one obtains,

$$V_a\,[Z_1 + Z_2 + Z_3 + Z_4] - V_b\,Z_1 - V_c\,Z_2 - \dot{V}_d\,Z_3 - V_e Z_4 = 0. \qquad (1.28.1)$$

Since for the *entire* system (of which the above is a part) there are as many of these equations as unknown velocities, the latter are obtainable by solution of a set of simultaneous algebraic equations. When all velocities are so determined one may find all forces by considering each point in succession, noting that the net force at a point is equal to the algebraic sum of products of impedance and velocity for each impedance. The net force at point a in the above example is therefore $V_a[Z_1 + Z_2 + Z_3 + Z_4]$.

The *directions* of these forces may be assigned by use of the following convention: a force (at a node) pointing in an arrow direction is equal in magnitude to the product of the associated impedance and the velocity difference across it between head and tail of the arrow. Thus the force at a due to Z_1 is $Z_1(V_a - V_b)$ pointing *into a*. Similarly the forces at a due to Z_2, Z_3, Z_4 each pointing *away* from a are $Z_2(V_c - V_a)$, $Z_3(V_d - V_a)$, $Z_4(V_e - V_a)$. Using the nodal law of forces at point a one arrives again at Eq. 1.28.1.

In an alternate procedure of analysis one deals directly with unknown forces regarded as flowing around loops. The steps of analysis are:

- first, one calculates the number of independent forces in the mechanical system and assigns an arbitrary direction to each of them.

- next, a set of velocity loops, corresponding in number to these forces, is constructed. These velocities are regarded as potential drops.

- in each loop one sums velocities by multiplying each admittance encountered in the loop by the loop force flowing into it in a clockwise direction. If the loop force agrees with an assigned force direction, a plus sign is attached to this "velocity drop". Otherwise a minus sign is attached. The algebraic sum of all velocities in any one loop is set to zero.

Figure 1.28.2 is an example of loop analysis of a mechanical system driven by a velocity source V_s:

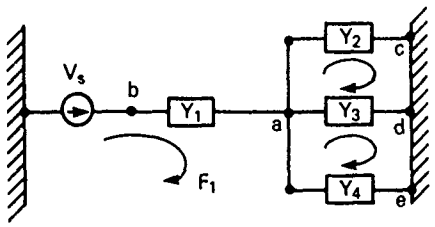


Fig. 1.28.2 — A simple example of loop analysis of a mechanical system. This is a VF network. [16]

The loop equations are,

$$\begin{aligned} Y_1 F_1 + Y_4(F_1 - F_3) &= V_s \\ Y_2 F_2 + Y_3(F_2 - F_3) &= 0 \\ Y_3(F_3 - F_2) + Y_4(F_1 - F_3) &= 0. \end{aligned} \tag{1.28.2}$$

Since there are as many unknown forces (here F_1, F_2, F_3) as loops the forces may be obtained by solution of a set of simultaneous algebraic equations. The velocities at each node (here only V_a) are then given by products of admittance and force,

$$V_a = V_s - Y_1 F_1 \tag{1.28.3}$$

An important thing to note is that in one-connection mechanical systems the element of mechanical mass must have one terminal fixed at the rigid reference frame (similar to be "grounded" in electrical circuit theory) (see Sect. 1.6).

1.29 ANALYSIS OF TWO-CONNECTION SYSTEMS BY USE OF EQUIVALENT π OR T NETWORKS

These systems feature two points of external connection: one point allows energy to be received from a source and the other point allows energy to be delivered to a load, Fig. 1.29.1. Thus they have two sets of energy coordinates, F_1, V_1 and F_2, V_2. While the system itself is fixed to "ground", its terminals are "off-ground". The source and load to which this system may be connected are considered one-connection systems.

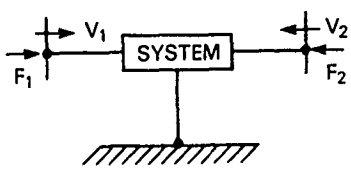


Fig. 1.29.1 — A two-connection system

If a two-connection system is composed of chains of linear bilateral (that is, reciprocal), mechanical elements in series/parallel form, it can be represented by either of two equivalent systems: the π system Fig. 1.29.2a or the T system, Fig. 1.29.2b.

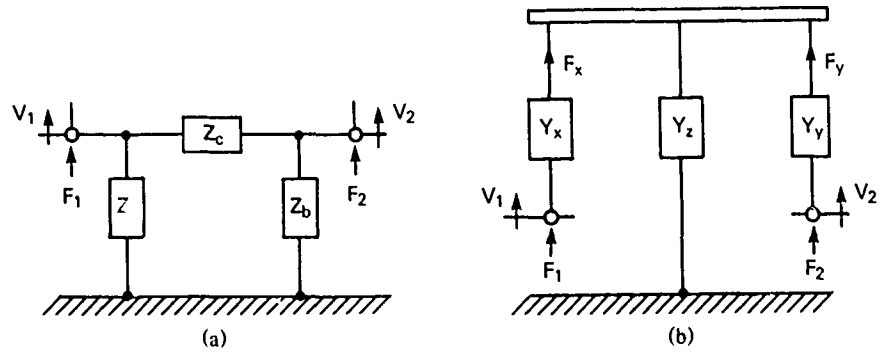


Fig. 1.29.2 — (a) A π-equivalent of Fig. 1.29.1 and (b) a T-equivalent of Fig. 1.29.1

In both figures one impedance Z_a (or admittance Y_x) is associated with F_1, V_1 and a second impedance Z_b (or admittance Y_g) is associated with F_2, V_2. A third impedance Z_c couples V_1 to V_2, and a third admittance Y_z couples the force F_x to F_y.

The π equivalent impedances (Z_a, Z_b, Z_c) are found in the following way:

- terminal 2 is first clamped ($V_2 = 0$) by being connected to a rigid reference frame, and a force F_1 is applied to terminal 1. The ratio $Z_{11} = F_1/V_1$ is then calculated or measured in an experiment. Similarly, a force F_1' is applied to terminal 1 to keep it from moving and the ratio $Z_{12} = F_1'/V_2$ is measured, or calculated.

- terminal 1 is clamped ($V_1 = 0$) and the ratio $Z_{22} = F_2/V_2$ is measured (or calculated) for any applied force F_2. Then a force F_2' is applied to terminal 2 to keep it from moving, and the ratio F_2'/V_1 is measured (or calculated).

These procedures give Z_{11}, Z_{12}, Z_{21}, Z_{22}. To relate them to Z_a, Z_b, Z_c it is noted that when V_2 is clamped, $Z_b = 0$ and Z_a, Z_c are in parallel. Hence, for mechanical circuits,

$$Z_{11} = Z_a + Z_c.$$

When V_1 is clamped, Z_b and Z_c are in parallel because $Z_a = 0$. Hence,

$$Z_{22} = Z_b + Z_c.$$

Again, when V_1 is clamped by applying F_1, the impedance Z_a is short-circuited making $Z_c = Z_{12} = F_1/V_2$. Similarly, $Z_c = Z_{21} = F_2/V_1$. Solving all equations simultaneously leads to the π system equivalents:

$$Z_a = Z_{11} - Z_{12};\ Z_b = Z_{22} - Z_{21};\ Z_c = Z_{12} = Z_{21}. \tag{1.29.1}$$

The T equivalent admittances are found in the following way:

- first, terminal 2 is made free ($F_2 = 0$), and a force F_1 is applied. The ratio $Y_{11} = V_1/F_1$ is then measured. Similarly, terminal 1 is made free ($F_1 = 0$) and a force F_2 is applied. The ratio F_2/V_2 is then measured.

- again, terminal 2 is made free and F_1 is applied. The ratio $Y_2 = V_2/F_1$ is measured. Similarly, terminal 1 is made free, and F_2 is applied. The ratio $Y_{12} = V_1/F_2$ is measured. When F_2 is zero, the admittances Y_x, Y_z are in series. Hence,

$$Y_{11} = Y_x + Y_z; \quad Y_{12} = Y_z$$

When F_1 is zero, the admittances Y_z, Y_y are in series. Hence,

$$Y_{22} = Y_z + Y_y; \quad Y_{21} = Y_z$$

Solving all equations simultaneously leads to the T system equivalents:

$$Y_x = Y_{11} - Y_{12}; \quad Y_y = Y_{22} - Y_{21}; \quad Y_{21} = Y_{12} = Y_z. \tag{1.29.2}$$

The π and T equivalent systems, when applied to systems with two connections, are accompanied with sources and loads. In the π system the source is a *force* source, and the load is a load impedance. In the T system the source is a *velocity* source, and the load is an admittance.

1.30 ANALYSIS OF TWO-CONNECTION SYSTEMS BY USE OF FOUR-POLE PARAMETERS

Let the energy coordinates (force and velocity) at terminals 1, 2 be related to each other through a 2×2 matrix of coefficients α_{ij}:

$$\begin{pmatrix} F_1 \\ V_1 \end{pmatrix} = \begin{pmatrix} \alpha_{11} & \alpha_{12} \\ \alpha_{21} & \alpha_{22} \end{pmatrix} \begin{pmatrix} F_2 \\ V_2 \end{pmatrix} \tag{1.30.1}$$

in which

$$\alpha_{11} = \left.\frac{F_1}{F_2}\right|_{V_2=0}; \quad \alpha_{12} = \left.\frac{F_1}{V_2}\right|_{F_2=0}; \quad \alpha_{21} = \left.\frac{V_1}{F_2}\right|_{V_2=0}; \quad \alpha_{22} = \left.\frac{V_1}{V_2}\right|_{F_2=0}.$$

These are the *four-pole parameters* of the two-connection system. They describe the system in the terminology of input and output, that is, if terminal 1 has a force F_1 and velocity V_1 on it, then terminal 2 has a force F_2 and velocity V_2. Here, F_2 is the *transmitted* force, and V_2 is the *transmitted* velocity.

The four-pole parameters of simple mass, spring, damper mechanical elements are:

$$\text{mass } m: \quad P_m = \begin{pmatrix} 1 & j\omega m \\ 0 & 1 \end{pmatrix}$$

$$\text{spring } k: \quad P_k = \begin{pmatrix} 1 & 0 \\ \dfrac{j\omega}{k} & 1 \end{pmatrix} \tag{1.30.2}$$

$$\text{damper } c: \quad P_c = \begin{pmatrix} 1 & 0 \\ \dfrac{1}{c} & 1 \end{pmatrix}.$$

In complex mechanical systems these simple elements are combined in series/parallel networks. If the entire system is regarded as a two-connection system, the input-output relation between F_1, V_2 and F_2, V_2 can be found by use of these rules:

- in series-connected systems where the mechanical elements form a chain of P, P', P'', ... the relation reduces to a product of matrices:

$$\begin{bmatrix} F_1 \\ V_1 \end{bmatrix} = [P][P'][P''] \ldots . [P^N] \begin{bmatrix} F_2 \\ V_2 \end{bmatrix} \tag{1.30.3}$$

A key feature in series-connected four-pole parameter treated systems is that dynamic mass can appear in series (that is, not "grounded"). This is quite different from one-connection sources and loads analyzed by impedance parameters where mass must be connected to "ground."

- in parallel-connected systems where P, P', P'' ... form parallel branches between cause F_1, V_1 and effect F_2, V_2, the relation is,

$$\begin{bmatrix} F_1 \\ V_1 \end{bmatrix} = \begin{bmatrix} \frac{A}{B} & \left(\frac{AC}{B} - B\right) \\ \frac{1}{B} & \frac{C}{B} \end{bmatrix} \begin{bmatrix} F_2 \\ V_2 \end{bmatrix} \tag{1.30.4}$$

$$A = \sum_{i=1}^{n} \frac{\alpha_{11}^{(i)}}{\alpha_{21}^{(i)}}; \quad B = \sum_{i=1}^{n} \frac{1}{\alpha_{21}^{(i)}}; \quad C = \sum_{i=1}^{n} \frac{\alpha_{22}^{(i)}}{\alpha_{21}^{(i)}}$$

Because there is no velocity difference across a mass, this formulation does not allow a mass to be in parallel with a spring or damper unless it is "grounded." When four-pole analysis is used in conjunction with sources, the coordinates F_1, V_1 can be constructed directly from the Thevenin's or Norton's equivalents, repeated for convenience as Figs. 1.26.2, 1.26.3.

In Fig. 1.26.2 one has $F_1 = F_c - Z_s\, v_1$; in Fig. 1.26.3, $F_1 = Z_s(v_c - v_1)$.

1.31 ANALYSIS OF TWO-CONNECTION MECHANICAL SYSTEMS BY IMPEDANCE AND ADMITTANCE PARAMETERS

If the mechanical elements inside the system of Fig. 1.30.1 are linear and bilateral it is often convenient to relate forces and velocities by use of impedance parameters Z_{ij}:

$$\begin{bmatrix} F_1 \\ F_2 \end{bmatrix} = \begin{bmatrix} Z_{11} & Z_{12} \\ Z_{21} & Z_{22} \end{bmatrix} \begin{bmatrix} V_1 \\ V_2 \end{bmatrix} \tag{1.31.1}$$

where,

$$Z_{11} = \left.\frac{F_1}{V_1}\right|_{V_2=0}; \quad Z_{12} = \left.\frac{F_1}{V_2}\right|_{V_1=0}; \quad Z_{21} = \left.\frac{F_2}{V_1}\right|_{V_2=0}; \quad Z_{22} = \left.\frac{F_2}{V_2}\right|_{V_1=0}$$

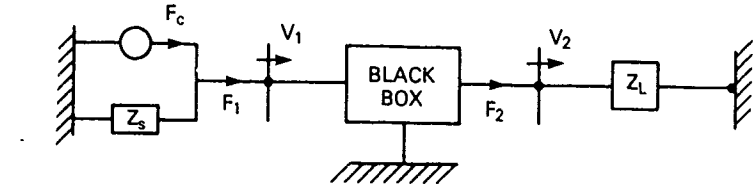
Alternatively, the relations can be written in tems of admittance parameters Y_{ij},

$$\begin{pmatrix} V_1 \\ V_2 \end{pmatrix} = \begin{pmatrix} Y_{11} & Y_{12} \\ Y_{21} & Y_{22} \end{pmatrix} \begin{pmatrix} F_1 \\ F_2 \end{pmatrix} \tag{1.31.2}$$

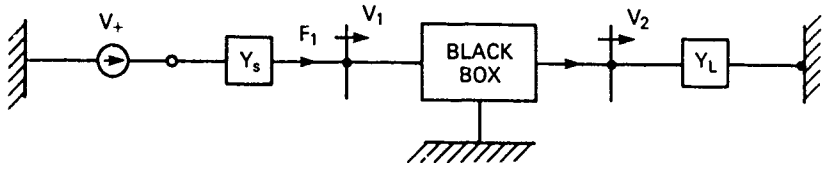
$$Y_{11} = \left.\frac{V_1}{F_1}\right|_{F_2=0}; \quad Y_{12} = \left.\frac{V_1}{F_2}\right|_{F_1=0}; \quad Y_{21} = \left.\frac{V_2}{F_1}\right|_{F_2=0}; \quad Y_{22} = \left.\frac{V_2}{F_2}\right|_{F_1=0}$$

Generalized two-connection system with source and load attached can then be represented by the much simplified diagrams, Figs. 1.31.1a, 1.31.1b.

All electromechanical energy converters connected to loads can be modeled by either of these generalized systems.



(a)



(b)

Fig. 1.31.1 — (a) A two-connection mechanical system represented as a "black-box" driven by a Thevenin's equivalent source and loaded by impedance Z_L. (b) A two-connection mechanical system represented by a "black-box" driven by a Norton's equivalent [16]

1.32 CONVERSION OF ONE-CONNECTION INTO TWO-CONNECTION SYSTEMS AND COMBINATIONS OF SIMPLE SYSTEMS

A. One-connection systems, customarily appearing as sources and loads, can be regarded also as transmission systems if simple modifications are made to the formulas describing their performance. The method can be explained by examples.

Consider first a one-connection system in series form. A series form is defined in this treatise as a mechanical system in which all elements have a common force. The appropriate equation of performance is a summation of velocities:

$$V = \sum_i V_i = F \sum_i Y_i. \tag{1.32.1}$$

To convert this expression from a one-connection to a two-connection system we replace V by $V_1 - V_2$:

$$V_1 = V_2 + F_\alpha \sum_i Y_i. \tag{1.32.2}$$

Simultaneously the *VF* representation implicit in Eq. 1.32.1 is replaced by an *FV* representation. Then Eq. 1.32.2 is recognized as a nodal equation in velocities. The subscript on F, namely α, is momentarily left undetermined.

We next consider a one-connection system in parallel form. In this treatise such a form is defined as a mechanical system in which all elements have a common velocity. Its appropriate equation of peformance is a summation of forces,

$$F = \sum_i F_i = V \sum_i Z_i. \tag{1.32.3}$$

To convert this expression from a one-connection to a two-connection system we replace F by $F_1 - F_2$:

$$F_1 = F_2 + V_\beta \sum_i Z_i. \tag{1.32.4}$$

Simultaneously the *VF* representation implicit in Eq. 1.32.4 is replaced by an *FV* representation. Then Eq. 1.32.4 is recognized as a loop equation in forces. The β subscript on V is left undetermined at this point.

B. Two equations (1.32.2 and 1.32.4) are now available as building blocks of a combined system. To couple them we must choose α, β to be either the integer 1, or integer 2. Suppose we select $\alpha = 2$ and $\beta = 1$. Then we obtained a set of *coupled* equations which describe the combined system:

$$\begin{cases} F_1 = V_1 \sum_i Z_i + F_2 & \text{(1.32.5a)} \\ V_1 = F_2 \sum_i Y_i + V_2 & \text{(1.32.5b)} \end{cases}$$

In an *FV* representation the impedances Z_i form a series-connected branch and the admittances Y_i form a parallel (or "shunt") branch. An FV (symbolic) circuit that features this set of equations is sketched in Fig. 1.32.1a. If, next, we select $\alpha = 1$, $\beta = 2$ then we obtain the set of equations:

$$F_1 = F_2 + V_2 \sum_i Z_i \tag{1.32.6a}$$

$$V_1 = V_2 + F_1 \sum_i Y_i. \tag{1.32.6b}$$

An *FV* (symbolic) circuit that features these equations is shown in Fig. 1.32.1b.

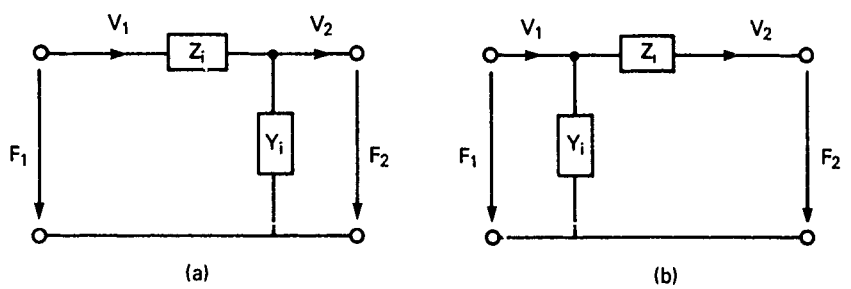


Fig. 1.32.1 — (a) FV representations of two-connection systems constructed from two one-connection systems, (a) circuit of Eqs. 1.32.5, (b) circuit of Eqs. 1.32.4

Several physical embodiments of Fig. 1.32.1 are discussed next.

C. *Example 1.* We consider the acoustic system of Fig. 1.32.2. Here a pressure differential $p_1 - p_2$ drives a volume velocity U_1 into a cavity V_1. The equations which describe this system are:

$$p_1 = p_2 + Z_A U_1$$

$$U_1 = U_2 + Y_A p_2.$$

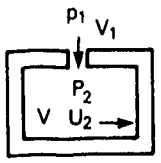


Fig. 1.32.2 — An acoustic system consisting of a hole and a cavity

These equations correspond to Eqs. 1.32.5a. At low enough frequency one may use lumped parameter representations of Z_A and Y_A. For the acoustic impedance of a hole (= orifice) we use Table 1.12.1,

$$Z_a = \mathrm{R} + j\omega\,\mathrm{M} \qquad \text{(units: Ns/m}^5\text{)} \tag{1.32.7a}$$

$$Y_A = \frac{j\omega}{\mathrm{K}_A} = \frac{j\omega \mathrm{V}}{\rho c^2} \qquad \text{(units: m}^5\text{/Ns)} \tag{1.32.7b}$$

in which

$$\mathrm{R} = \frac{\rho\omega d_v}{4\pi b^2} \ln \frac{2b}{h}$$

$$\mathrm{M} = \frac{\rho D_0}{4S_0}$$

ρ = mass density (Ns^2/m^4)
ω = radian frequency (s^{-1})
d_v = viscous boundary layer thickness (m)
b = radius of circular hole (m)
$2h$ = thickness of plate (m)
S_0 = area of orifice (m^2)
D_0 = perimeter of orifice (m)

Fig. 1.32.3 is an FV representation of Eqs. 1.32.7a, 1.32.7b.

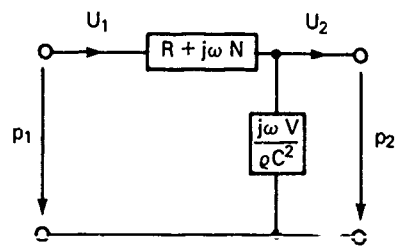


Fig. 1.32.3 — FV representation of Fig. 1.32.2

Example 2.

We consider next periodic structures of holes and cavities, shown in Fig. 1.32.4a. The corresponding circuit representation is a periodic repetition of Fig. 1.32.3 shown in Fig. 1.32.4b. Such structures contain acoustical mass in series branches and acoustical stiffness in shunt branches. They act as acoustical filters. A study of filters is made in Secs. 2.28, 2.29.

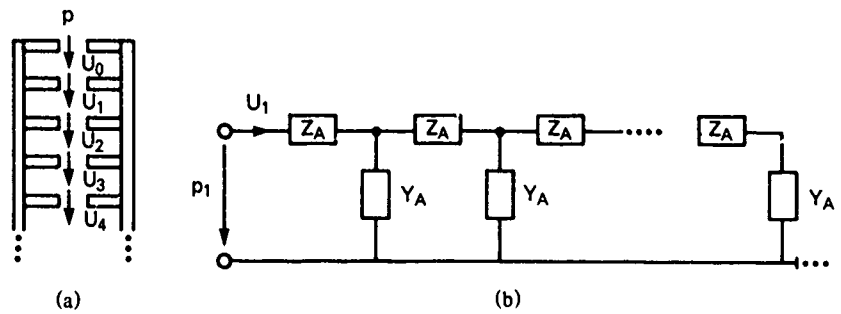


Fig. 1.32.4 — (a) Periodic structure of holes and cavities and and (b) FV representation

Example 3.

A one-connection series damper and spring together with its two-connection representation are shown in Fig. 1.32.5(a,b).

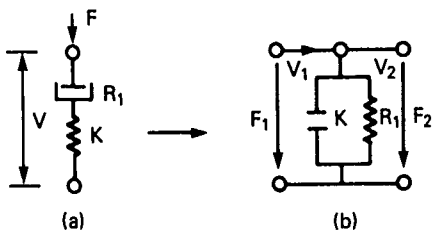


Fig. 1.32.5 — A simple spring-damper system, (a) a two-terminal VF diagram and (b) a four-terminal FV diagram

A second simple system of a damper and mass in parallel is shown in Fig. 1.32.6(a,b).

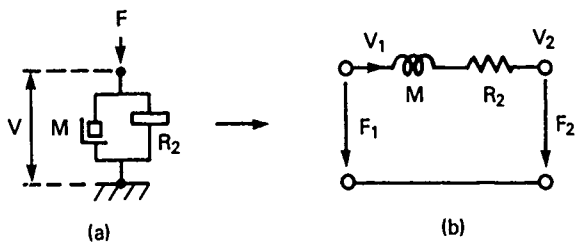


Fig. 1.32.6 — A simple parallel-connected mass-damper system, (a) its two-terminal VF diagram and (b) its four-terminal FV diagram

The separate (= uncoupled) equations describing these systems are:

series connected: $V_1 = F_\alpha\, Y + V_2$ (1.32.8a)

parallel connected: $F_1 = V_\beta\, Z + F_2$ (1.32.8b)

Let us first couple these equations through the velocity by making $V_\beta = V_2$ and $F_\alpha = F_1$. Then the branch Y directly is across F_1 and the branch Z is in series with V_2 flowing through. Figure 1.32.7a shows the circuit, while Fig. 1.32.7b shows a physical interpretation of the circuit.

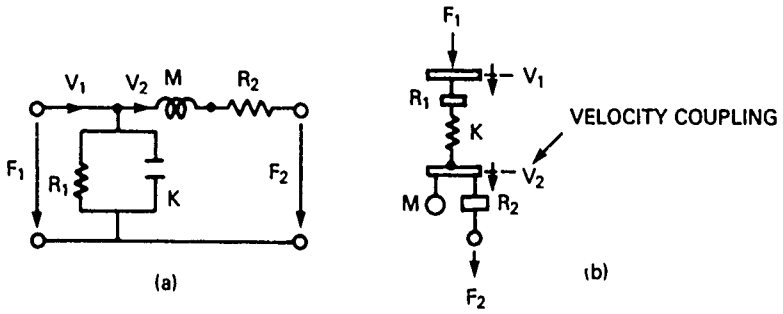


Fig. 1.32.7 — (a) FV diagram of the two systems of Figs. 1.32.5 and 1.32.6 coupled through velocity V_2, (b) a possible physical counterpart

We next couple the Eqs. 1.32.8 through the force, that is, we write $\alpha = 2$ and $\beta = 1$.

$$V_1 = F_2\, Y + V_2 \tag{1.32.9a}$$

$$F_1 = V_1 Z + F_2. \tag{1.32.9b}$$

Figures 1.32.8a, 1.32.8b give the corresponding circuit descriptions of this coupled system.

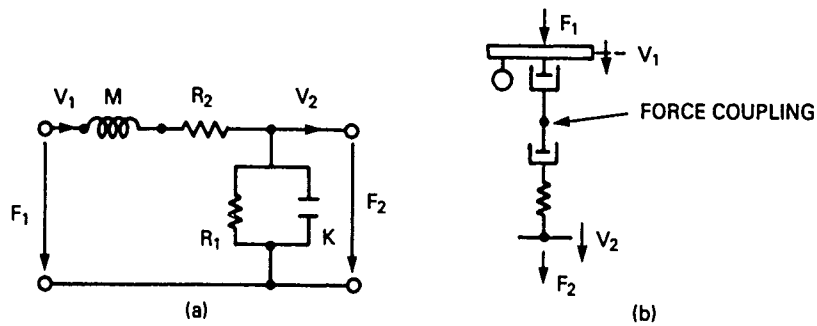


Fig. 1.32.8 — (a) FV diagram of two systems coupled through F, (b) a possible physical counterpart

1.33 BASIC THEORY OF COUPLED ELECTRICAL CIRCUITS

The theory of transduction from a primary energy form (and storage) to a secondary energy form (and storage) has been treated from earliest times as a branch of the theory of coupled electrical circuits. We consider here the basic elements of this theory. Although the symbols and concepts are electrical we can also apply the results of analysis to mechanical networks by use of a simple electromechanical analogy. The one most commonly used is $e \triangleq F$, $i \triangleq V$. Thus the following exposition applied to mechanical networks in FV form (= force across, velocity through).

1.34 BASIC FORM OF MUTUAL-INDUCTIVE COUPLED CIRCUITS; SPECIFIC CASES OF SIMPLE PRIMARIES AND SECONDARIES

Figure 1.34.1 shows two RLC circuits coupled through inductance. This simple basic elementary form reveals the underlying theory in sufficient detail to be useful in many applications.

In the general analysis let

Z_p = series impedance of the primary circuit when considered by itself

Z_s = series impedance of the secondary circuit when considered by itself.

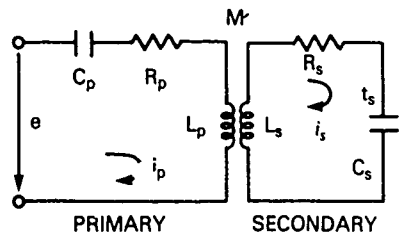


Fig. 1.34.1 — Basic form of coupled circuits. *M* is the mutual inductance.

The applied voltage e drives a current i_p around the primary circuit through the impedance Z_p. Also because of coupling, it *induces* the voltages e'_s, e_s in the primary and the secondary circuits, respectively. In turn, e_s drives the current i_s through Z_s around the secondary circuit. The loop equations describing this coupling are,

$$\begin{cases} e = i_p Z_p + T_{ps}\, i_s \\ 0 = T_{sp}\, i_p + i_s Z_s \end{cases} \tag{1.34.1a}$$

(1.34.1b)

in which,

$$T_{ps} i_s = e_s = j\omega M i_s; \quad T_{sp}\, i_p = e'_s = j\omega M i_p. \tag{1.34.1c}$$

This type of coupling makes $T_{ps} = T_{sp} = j\omega M$. Substitution of Eq. 1.34.1b into 1.34.1a leads to,

$$e = i_p \left[Z_p + \frac{\omega^2 M^2}{Z_s} \right] \tag{1.34.2}$$

This describes the equivalent primary circuit, the secondary having been eliminated. Similarly we can rewrite Eq. 1.34.1b,

$$-j\omega M i_p = i_s Z_s. \tag{1.34.3}$$

This is the equivalent secondary circuit, the primary having been eliminated. A third form of equivalent circuit may be formed by (1) opening the secondary so that $i_s \equiv 0$ and $e_{o.c.} = -\dfrac{j\omega M e}{Z_p}$ (2) shorting out e so that

$$0 = \frac{i_s Z_p}{-j\omega M} \left[Z_s + \frac{\omega^2 M^2}{Z_p} \right].$$

Thus the equivalent impedance as viewed from the open-end secondary terminals is $Z_{ss} = Z_s + (\omega M)^2/Z_p$. The open circuit voltage $e_{o.c.}$ in series with the short circuit impedance Z_{ss} constitute an alternate equivalent for the secondary circuit, the primary having been eliminated.

The three equivalent circuits are shown in Fig. 1.34.2

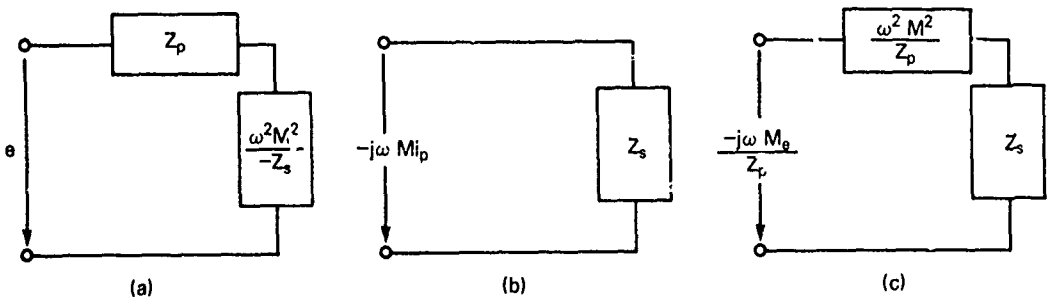


Fig. 1.34.2 — (a) Equivalent primary circuit of Fig. 1.34.1, (b) equivalent secondary circuit, and (c) equivalent secondary circuit (alternate form)

Now from Eq. 1.34.2 the voltage coupled from the secondary into the primary is $(\omega^2 M^2/Z_s) i_p$. It remains to classify simple cases by specifying Z_s.

Case 1. Assume the secondary self impedance Z_s of Fig. 1.34.1 is a pure inductance $Z_s = j\omega L_s$. Then the impedance coupled into the primary circuit is $\omega^2 M^2/j\omega L_s$. A useful parameter which expresses this impedance as an inductance in the primary circuit is the coefficient of coupling, k, defined by the relation,

$$\frac{\omega^2 M^2}{\omega L_s} = k^2 \omega L_p \text{ or } k = \frac{M}{\sqrt{L_s L_p}}. \tag{1.34.4}$$

According to the induction law of Lenz the coupled voltage must oppose the applied voltage, hence the modified primary inductance is $(1 - k^2) L_p$.

Case 2. Assume $Z_s = R_s + j\omega L_s$. Then the coupled impedance is

$$R_c + j\omega L_c = \frac{(\omega M)^2}{R_s + j\omega L_s} = \frac{(\omega M)^2}{R_s^2 + \omega^2 L_s^2} [R_s - j\omega L_s]. \tag{1.34.5}$$

As before the coupled inductance is obtained by letting $R_s = 0$. The coupled resistance is,

$$R_c = \frac{(\omega M)^2 R_s}{R_s^2 + \omega^2 L_s^2} \rightarrow \frac{k^2 L_p}{L_s} R_s = \frac{k^2 \omega L_p}{Q_s}, \quad Q_s = \frac{\omega L_s}{R_s} \tag{1.34.6}$$

provided one assumes $R_s^2 << \omega^2 L_s^2$. Thus as a result of inductive coupling the secondary circuit inserts an inductance $-k^2 L_p$ and a resistance $k^2 \omega L_p/Q_s$ in series in the primary circuit.

Case 3. Assume the secondary is tuned, $Z_s = R_s + j\omega L_s + 1/j\omega C_s$. In this case the coupled impedance is

$$R_c + j\omega L_c = \frac{(\omega M)^2\left[1 - jQ_s\left(1 - \frac{1}{\gamma^2}\right)\right]}{R_s\left[1 + Q_s^2\left(1 - \frac{1}{\gamma^2}\right)^2\right]}, \quad \gamma = \frac{\omega}{\omega_0}. \tag{1.34.7}$$

Again one may substitute $(\omega M)^2 = k^2\omega^2 L_p L_s$ and thus find the coupled resistance R_c and inductance L_c effectively inserted as series elements in the primary circuit. Of particular utility is the determination of the voltage V_C developed across the secondary capacitor at resonance $\omega_0^2 = 1/L_s C_s$. When $R_p >> L_p$ this is

$$V_C = \left\{\frac{\omega M}{R_p R_s + (\omega M)^2}\right\}\omega L_s. \tag{1.34.8}$$

In mechanical terms V_C is analogous to the force across the compliance of the mechanical circuit, here considered to be the secondary of the transducer. Since M is proportional to coupling coefficient (k) it is found that when

$$\omega M = \sqrt{R_p R_s} = k\omega\sqrt{L_p L_s}$$

the voltage V_c is maximized. The tuned secondary thus serves to amplify the force applied to the primary when the transduction is equivalent to an ideal transformer. When the transduction is equivalent to a gyrator the tuned secondary serves to amplify the velocity across the secondary spring. However the Q_{eff} of the amplification curve is less than the Q of the secondary tuned circuit

$$Q_{\text{eff}} = Q_s\left[\frac{1}{1 + \frac{(\omega M)^2}{R_s R_p}}\right] \tag{1.34.9}$$

When ωL_p is not negligible we may use the equivalent circuit shown in Fig. 1.34.1c with $Z_p = R_p + j\omega L_p$. The effect of the primary upon the secondary is displayed by the term $(\omega M)^2/Z_p$. This term increases the effective secondary resistance (thus lowering the Q of the secondary). Also, since

$$\frac{1}{Z_p} = \frac{R_p - j\omega L_p}{R_p^2 + (\omega L_p)^2}$$

the secondary inductance L_s is decreased, thus raising the resonant frequency.

Case 4. Assume both primary and secondary are tuned to the same frequency. By rearrangement of Eqs. 1.34.1a,b,c one obtains the voltage E_c across the secondary condenser:

$$E_c = e\left[\frac{-1}{\gamma^2}\sqrt{\frac{L_s}{L_p}}\,\frac{k}{\left[k^2 + \frac{1}{Q_p Q_s} - \left(1 - \frac{1}{\gamma^2}\right)^2 + j\left(1 - \frac{1}{\gamma^2}\right)\left(\frac{1}{Q_p} + \frac{1}{Q_s}\right)\right]}\right] \tag{1.34.10}$$

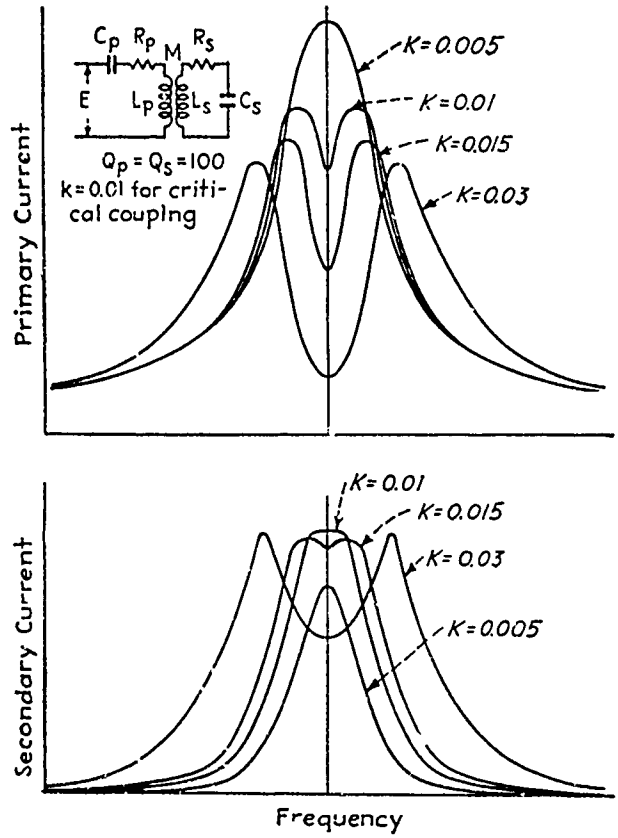


Fig. 1.34.3 — Curves showing variation of primary and secondary current with frequency for different coefficients of coupling when the primary and secondary are separately tuned to the same frequency [11]. F. E. Terman, *Radio Engineers Handbook* (1st ed) (1943), ©1943 McGraw-Hill Book Co.; by permission.

where

$$\gamma = \omega/\omega_0.$$

When the coupling is small the secondary has little effect on the primary. The primary current is then that of a series resonant circuit, Fig. 2.25.3a. The secondary current is small and shows the same single peak as the primary, Fig. 1.34.3. As the coupling increases the primary current decreases and the secondary current increases. Also both resonance curves broaden out. The maximum secondary current is reached when the coupled secondary resistance is equal to the primary resistance. The magnitude of k is then the critical coupling magnitude given by,

$$k_c = \frac{1}{\sqrt{Q_p Q_s}}, \quad \gamma = 1. \tag{1.34.11}$$

For this value of coupling both primary and secondary currents exhibit double peaks. As the coupling increases (even more) the double peaks spread out farther, Fig. 1.34.3. The condition for the existence of double peaks in the secondary is the same as the condition for two maxima in Eq. 1.34.10,

$$\frac{k}{k_c} \geq \left[\frac{1}{2}\left(\frac{Q_p}{Q_s} + \frac{Q_s}{Q_p}\right)\right]^{1/2} \tag{1.34.12}$$

The location of the peaks f_{peak} is found by further analysis to be given by,

$$f_{peak} = f_0 \left[1 \pm k \left[1 - \frac{k_c^2}{2k^2} \left(\frac{Q_p}{Q_s} + \frac{Q_s}{Q_p} \right) \right]^{1/2} \right]^{-1/2} = \gamma_p f_0. \tag{1.34.13}$$

This equation is used to find the frequency difference between peaks relative to the resonant frequency of the circuits, Fig. 1.34.4. Substituion of γ_p from Eq. 1.34.13 into Eq. 1.34.10 allows one to obtain the

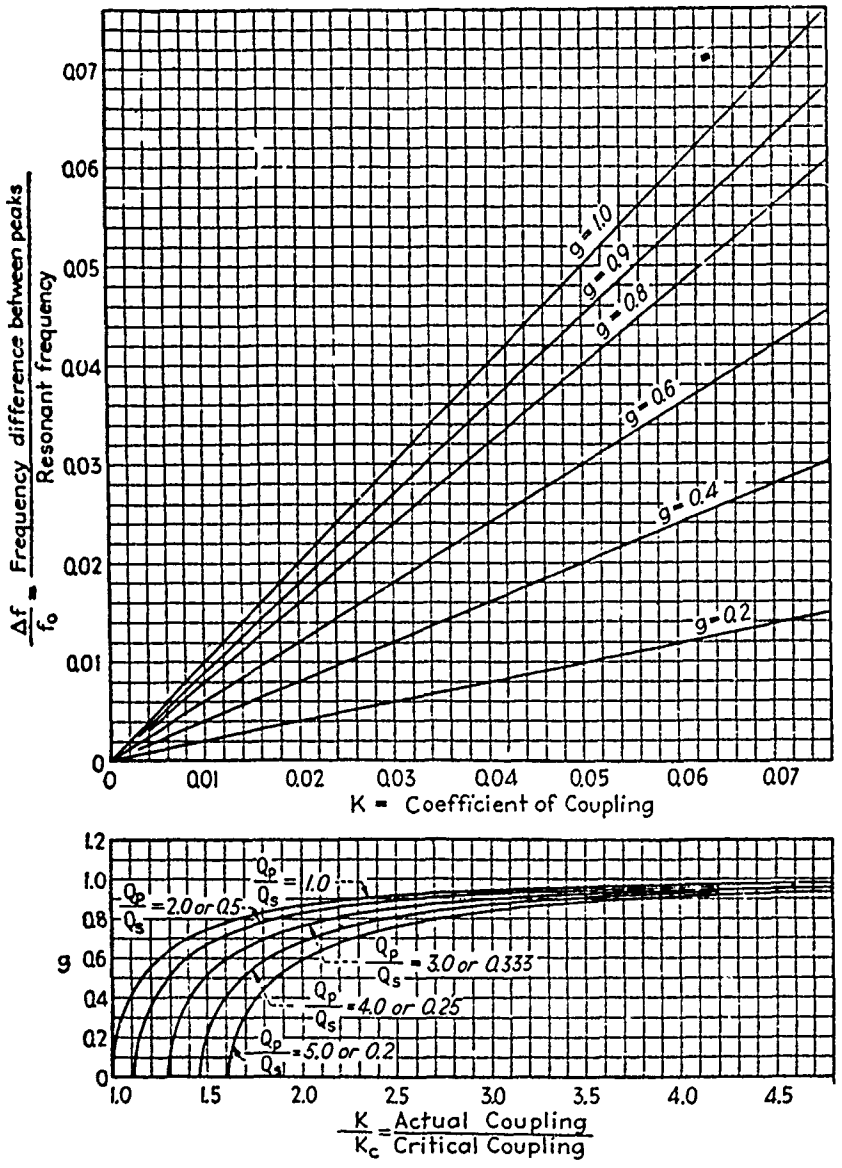


Fig. 1.34.4 — Curves from which the separation between peaks can be determined for the case of two coupled circuits resonant at the same frequency [11]. F. E. Terman, *Radio Engineers Handbook* (1st ed) (1943), ©1943 McGraw-Hill Book Co ; by permission

height of the peaks by first obtaining E_c, then calculating the secondary current through the capacitor C_s. The maximum possible voltage E_c corresponds to the maximum possible current, and is given by,

$$(E_c)_{MAX} = e\frac{1}{2k_c}\sqrt{\frac{L_s}{L_p}}. \tag{1.34.14}$$

Equations 1.34.10 and 1.34.14 can be used together to allow calculation of universal curves of the ratio $E_c/(E_c)_{MAX}$ versus the ratio of cycles off resonance to the resonant frequency. These curves are shown in Fig. 1.34.5a,b for the cases $k_c = 0$, $k_c = 0.05$, and $Q_p/Q_s = 1, 5$.

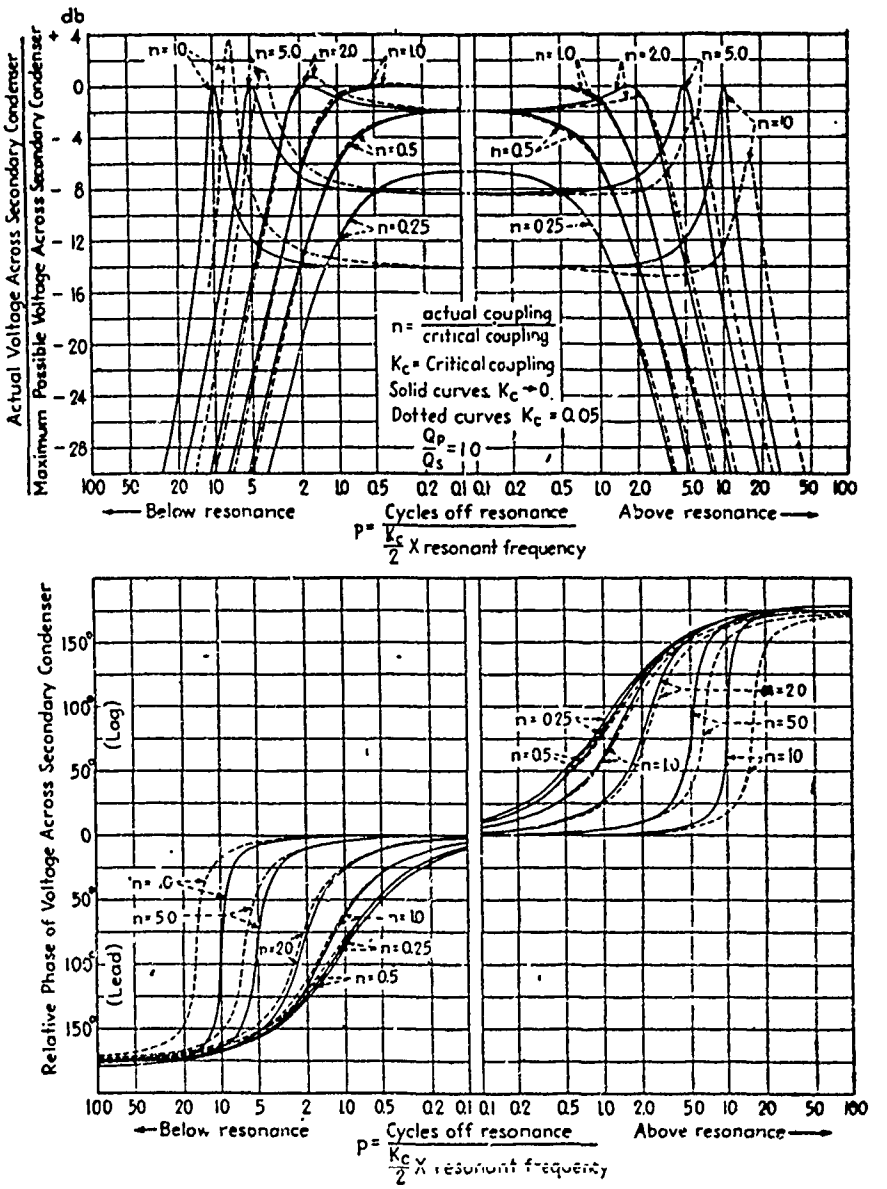


Fig. 1.34.5a — Universal curves giving phase and relative magnitude of the voltage across the secondary condenser for the case of two coupled circuits resonant at the same frequency and having a Q ratio of unity [11]. F. E. Terman, *Radio Engineers Handbook* (1st ed) (1943), ©1943 McGraw-Hill Book Co., by permission.

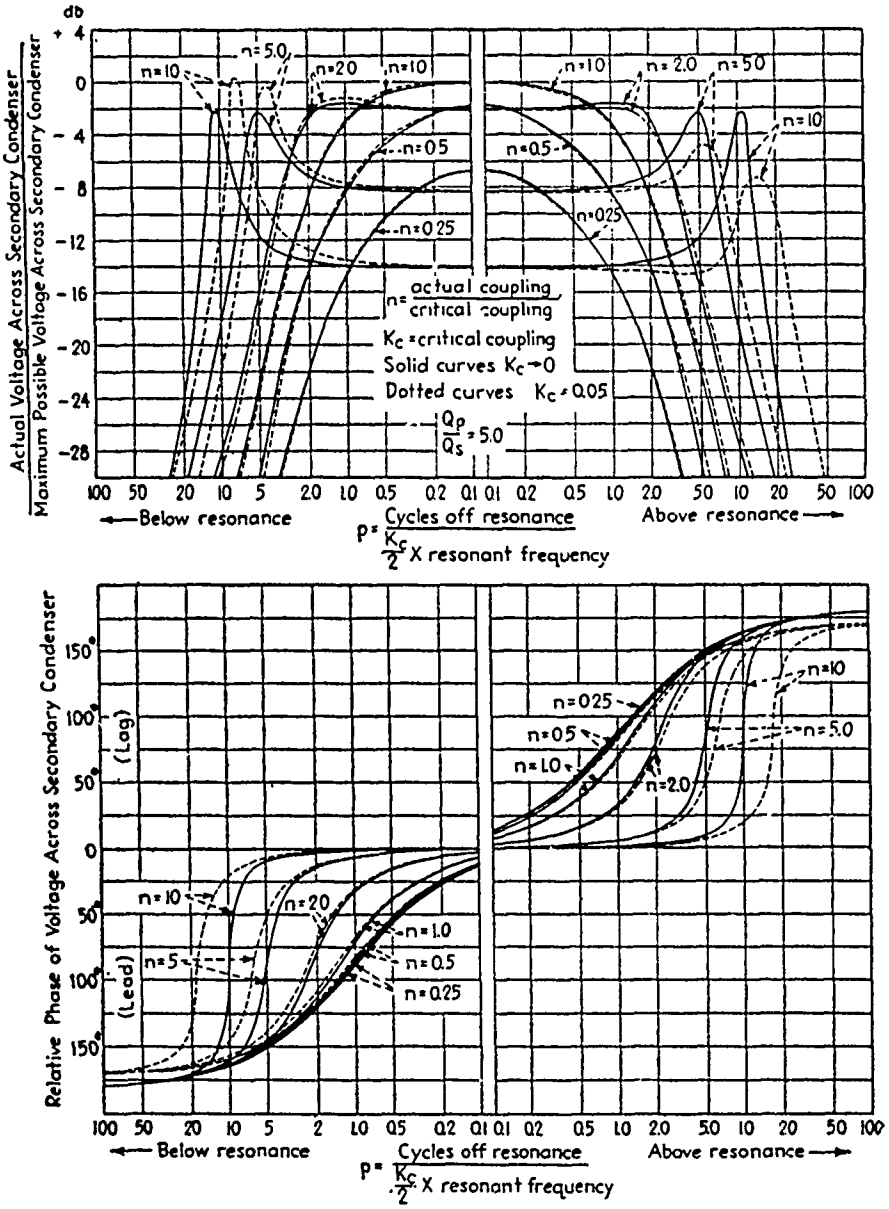


Fig. 1.34.5b — Universal curves giving the phase and relative magnitude of the voltage across the secondary condenser for the case of two coupled circuits resonant at the same frequency and having a Q ratio of 5 [11]. F. E. Terman, *Radio Engineers Handbook* (1st ed) (1943), ©1943 McGraw-Hill Book Co.; by permission.

Case 5. Assume the coupled primary and secondary circuits are tuned to different frequencies. The response of the circuits to applied voltage depends on the degree of detuning, the coupling, and the circuit Q's, Fig. 1.34.6.

a. if the detuning is slight and the Q of the primary equals the Q of the secondary then the response of the secondary is the same as if the two circuits were exactly tuned, but at a higher value of coupling and with a slightly reduced peak level.

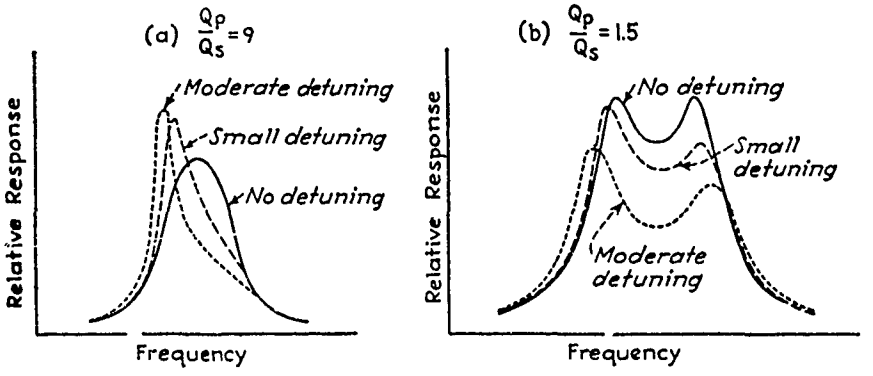


Fig. 1.34.6 — Curves illustrating the effect produced on the shape of the response curve by detuning primary and secondary circuits when the primary and secondary ciruits do not have identical Q's [17]. F. E. Terman, *Radio Engineers Handbook* (1st ed) (1943), ©1943 McGraw-Hill Book Co.; by permission.

b. if the detuning is slight and the circuit Q's are not the same the secondary response is no longer symmetrical about the mean frequency. The relative heights of the peaks are given by the rules:

$$\text{low-frequency peak depressed when } \begin{cases} f_0^{(s)} > f_0^{(p)} \\ Q_s > Q_p \end{cases} \quad \text{or} \quad \begin{matrix} f_0^{(s)} < f_0^{(p)} \\ Q_s < Q_p \end{matrix}$$

$$\text{high-frequency peak depressed} \quad \{ \text{ otherwise}$$

c. if the detuning is large and the Q's are greatly unequal the primary current curve will have only one peak even though the secondary shows two peaks.

Case 6. Assume circuit coupling is deliberately made variable with frequency, that is, the circuits are tunable over a wide frequency range. Usually the designer is required to maintain an approximately constant response over the tunable range. Several methods are available for doing this. A simple procedure is to combine capacitive and inductive coupling between primary and secondary circuits. At low frequencies the coupling is capacitive, while at high frequency it is inductive. In between, over a narrow range the coupling is zero.

Case 7. Assume the coupled circuits are to be used as bandpass filters. The design of such filters is discussed in Section 2.28. Here one has available Eqs. 1.34.10 through 1.34.14 to assist in calculation of filter parameters. In general the width of the top of the response is determined primarily by the coefficient of coupling and the flatness of the top depends on the circuit Q's. Wide top require large k's; low Q's round off tops, while high Q's give pronounced double peaks.

1.35 CAPACITIVE AND DIRECT INDUCTIVE COUPLING OF PRIMARY TO SECONDARY CIRCUITS

In Section 1.34 the theory of energy conversion from primary to secondary circuits was reviewed in the light of coupled circuit theory with mutual induction acting as the coupling agent. In this section we briefly review capacitive and direct inductive coupling.

Figure 1.35.1 shows the two types of coupling and their coupling coefficients. The analysis of these two types of coupling closely follows the analysis of coupling via mutual inductance, Section 1.34.

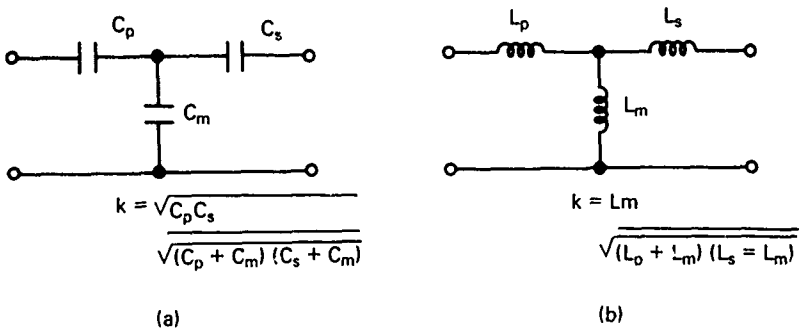


Fig. 1.35.1 — (a) Coupling via a capacitor C_M and (b) coupling via an inductor L_m

In the case of direct inductive coupling one substitutes L_m for M in all the relevant equations and applies the resultant equations without further change. In the case of capacitive coupling one substitutes $1/j\omega C_m$ for $j\omega M$ in the equations of coupling by mutual inductance and again applies them without further change. The performance of these with the values of k given in Fig. 1.35.1 is substantially the same as the performance of circuits coupled by mutual inductance: the secondary current displays two peaks if k is large, and one peak if k is small.

1.36 DUAL CIRCUITS AND SERIES-PARALLEL INVERSIONS

Let E, I be generalized across-and through-variables respectively. The relation $E(I)$, read "E is a function of I," is expressed in *impedance* form, that is,

$$E(t) = \alpha I + \beta \frac{dI}{dt} + \gamma \int I \, dt \tag{1.36.1}$$

in which α, β, and γ here the dimensions of across variable divided by through variable. In electrical systems $\alpha = R$, $\beta = L$, $\gamma = S = 1/C_e$.

The dual of Eq. 1.36.1 is obtained by replacing E by I and expressing $I(E)$ in *admittance* form, that is, by defining new coefficients δ, ϵ, and ζ:

$$I(t) = \delta E + \epsilon \frac{dE}{dt} + \zeta \int E dt \tag{1.36.2}$$

in which δ, ϵ, and ζ have the dimensions of through variable divided by across variable. In electrical systems $\delta = G$, $\epsilon = C_I$, $\zeta = \Gamma$. The descriptive words often used to identify these symbols are shown in Table 1.36.1. It is noted that while dual networks have the same mathematical form they are written with different coefficients, dependent variables and driving forces.

Table 1.36.1 — Electrical Network Duals.

RLS Network	*GC*$_I$Γ Network
resistance R	conductance G
inductance L	capacitance C_i
elastance S	reciprocal inductance Γ
voltage I	current I
open circuit condition	closed circuit condition
loop current	node-pair voltage
voltage source	current source

When Eqs. 1.36.1 and 1.36.2 refer to the same physical system they are true *duals*. Then the dual replacements of Table 1.36.1 apply. When the equations refer to different physical systems they are *analogs*. Since for a given physical system one may generate two analogs in a second physical system (namely across is the analog of across, across is the analog of through), we may apply column #1 (*RLS* Network) of Table 1.36.1 for the direct analog, and column #2 ($GC_f\Gamma$ Network) for the dual network.

In the steady state let $E(t)(= E_m \cos(\omega t + \psi))$ and $I(t)(= I_m \cos(\omega t + \phi))$ be applied quantities. Then, regarding Eq. 1.36.1 as a series circuit we solve for through-variable $I(\omega)$,

$$I(\omega) = E_m(G - jB) = E_m Y \tag{1.36.3}$$

$$G = \frac{\alpha}{\alpha^2 + \left(\omega\beta - \frac{\gamma}{\omega}\right)^2}; \quad B = \frac{\omega\beta - \frac{\gamma}{\omega}}{\alpha^2 + \left(\omega\beta - \frac{\gamma}{\omega}\right)^2}.$$

Here G is the real part of the admittance Y. In general it is not equal to α^{-1}. Also, B is the imaginary part of Y. It is not in general equal to $(\omega\beta - \gamma/\omega)^{-1}$. Eq. 1.36.3 is an *inversion* of Eq. 1.36.1. When we compare it with the (dual) Eq. 1.36.2,

$$I_m(\omega) = E\left[\delta + j\omega\epsilon + \frac{\zeta}{j\omega}\right]. \tag{1.36.4}$$

We see that, because there is no exchange of variables in the process of inversion, the dual of Eq. 1.36.1 and its inversion are completely different quantities. Thus the solution of series-parallel networks of impedance by use of inversions generates conductance functions G and susceptance functions B which are not in general reciprocals of differential coefficients in dual networks..

A similar discussion can be applied to Eq. 1.36.2 in comparison with Eq. 1.36.1, that is, comparing,

$$E = I_m(R + jX) = I_m Z$$

$$R = \frac{\delta}{\delta^2 + \left(\omega\epsilon - \frac{\zeta}{\omega}\right)^2}; \quad X = \frac{\left(\omega\epsilon - \frac{\zeta}{\omega}\right)}{\delta^2 + \left(\omega\epsilon - \frac{\zeta}{\omega}\right)^2}$$

with

$$E_m = I\left[\alpha + j\left(\omega\epsilon - \frac{\zeta}{\omega}\right)\right].$$

Again it is seen that in general α does not equal R, and $(\omega\epsilon - \zeta/\omega)$ does not equal X.

DUAL CIRCUIT ELEMENTS

In constructing duals of existing circuits one encounters the question, what is the numerical value of a dual element, and what are its units? Dual electrical circuits have simple rules in this regard: the numerical value remains unchanged while the units (in mks) conform to the units of dual exchanges. For example; a resistor of 10 ohms becomes a conductance of 10 mhos; and inductor of 1 henry becomes a capacitor of 1 farad: a capacitor of 1 farad becomes a inductor of 1 henry. A voltage sources $e(t)$ in series with an impedance Z_s becomes a current source in parallel with an admittance $Y_s = 1/Z_s$.

A second question is the inclusion of mutual inductance M as a circuit element. Figure 1.36.1 shows two loops coupled by inductance M between two inductors L_1, L_2. In the dual circuit, Fig. 1.36.2, M becomes a capacitor C_M joining the two nodes which represent the duals of these loops. Each inductance becomes changed into a capacitance $C_1 \pm C_M$, $C_2 \pm C_M$ which join these nodes to the ground node.

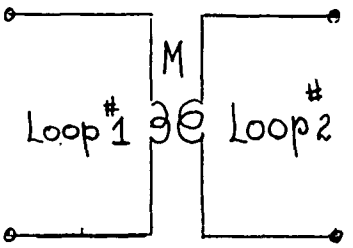


Fig. 1.36.1 — Two loops coupled by mutual inductance

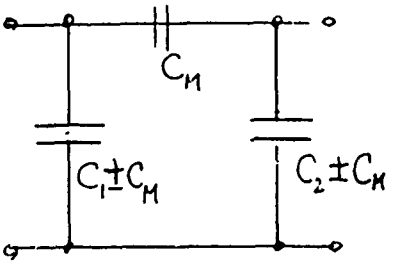


Fig. 1.36.2 — Two (dual) nodes coupled by mutual capacitance

1.37 COEFFICIENT OF ELECTROMECHANICAL COUPLING

The theory of coupled electrical circuits is extensively used in the theory of electromechanical transducers. To exemplify the latter it will be useful to employ figures and terminology appearing in Sections 1.45 and 2.29.

In the theory of a 2-mesh canonical equivalent circuit of an electromechanical transducer impedances (both electrical and mechanical) can be positioned in shunt or series position, according to the rules outlined in Section 1.44, 1.45. We consider first Fig. 1.45.2 in which the electrical impedance Z_e is in shunt position and the mechanical impedance z_m is in series position. The mechanical mesh equation corresponding to this figure is Eq. 1.45.1, which is repeated here for convenience of the reader,

$$F = \left(z_m - \frac{T_{me} T_{em}}{Z_e} \right) v + \frac{T_{me} E}{Z_e}$$

If E is set to zero,—meaning the electrical terminals are short-circuited, then

$$F = z'_m v \tag{1.37.1}$$

$$z'_m = z_m - \frac{T^2}{Z_e}; \quad T^2 = T_{me} T_{em} \tag{1.37.2}$$

Let us apply this to that of an electrostatic transducer, Fig. 2.39.1, this time using the notation of Hunt [4]. The objective will be to determine the coupling coefficient of this coupled circuit.

$$\text{(a) } T = \frac{1}{j\omega C_{em}} \quad \left[\text{units: } \frac{Vs}{m}, \text{ or } \frac{Ns}{C}\right]$$

$$\text{(b) } Z_e = \frac{1}{j\omega C_0} \quad \left[\text{units: } \frac{Vs}{C}\right]$$

$$\text{(c) } \frac{T^2}{Z_e} = \frac{1}{j\omega C^1} \tag{1.37.3}$$

$$\text{(d) } C^1 = \frac{C_{em}^2}{C_0} \quad \text{(units: } m/N\text{)}.$$

The units here require careful attention. One must choose

$$C_{em}^2 = \left[\frac{m}{V}\right]\left[\frac{C}{N}\right];\ C_0 = \frac{C}{V}$$

so that C^1 has the units of compliance ($= m/N$) as shown. Thus Eq. 1.37.3 shows that the mechanical impedance is altered by a negative compliance. The net compliance impedance is then

$$\frac{1}{j\omega C_m^1};\ C_m^1 = \frac{C_m}{1-k^2};\ k^2 = \frac{C_0 C_m}{C_{em}^2} \tag{1.37.4}$$

It is clear that k^2 must be less than, or equal to, unity for otherwise the net compliance would be negative,—meaning that an applied force would produce a displacement in a direction opposite to the force. Also, since k^2 cannot be negative its lower bound is zero.

Neglecting R and L in Fig. 2 39.1, and assuming the applied external force F is zero (= mechanical 'short circuit') the electrical equivalent circuit is given by Fig. 1.37.1.

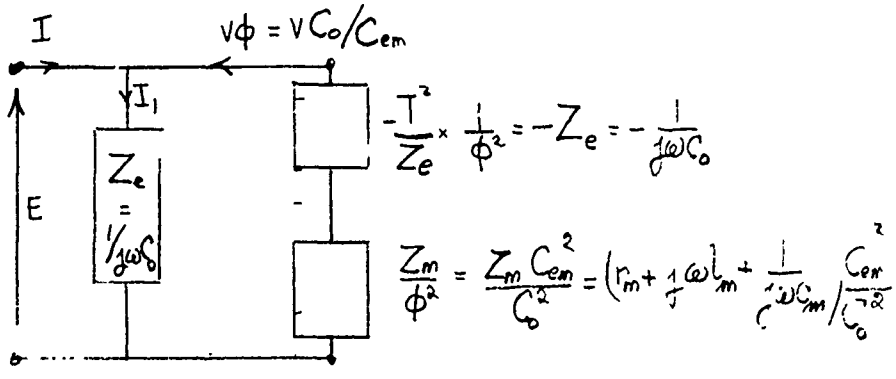


Fig. 1.37.1 — Simplified equivalent circuit of an electrostatic transducer with zero applied force, driven by an electric field E

Within the frequency limits of the velocity of this circuit we first allow the drive frequency to be 'high' enough (namely, greater then the antiresonant frequency) so that the impedance $j\omega l_m\, C_{em}^2/C_o^2$ controls the mechanical branch. The mechanical velocity v then becomes negligible—meaning the mechanical branch is 'clamped'. A measurement of capacity then yields C_0. It is given the name of *clamped capacity.* We next allow the drive frequency to be 'low' enough (namely, less than the resonant frequency) so that the impedance $(1/j\omega C_m^1)\ (C_{em}^2/C_o^2)$ controls the mechanical branch. The velocity v is then a significant quantity contributing to (mechanically derived) electrical capacity $C_m^1(C_0^2/C_{em}^{2)}$. This latter quantity is given the name *motional capacity* $(= C_{M0T})$. Since the two capacities C_0, C_{M0T} are electrically in parallel they are additive. The sum of the two is given the name 'free' capacity

$$C_{\text{free}} = C_0 + C_{M0T} = C_0 + C_m^1 \frac{C_0^2}{C_{em}^2} = C_0 \left[1 + \frac{C_m^1 C_0}{C_{em}^2}\right]. \tag{1.37.5}$$

By use of Eq. 1.37.4, one can put this expression in a more illuminating form,

$$C_{\text{free}} = C_0 \left[1 + \frac{C_m C_0}{C_{em}^2(1 - k^2)}\right] = C_0 \left[1 + \frac{k^2}{1 - k^2}\right] = \frac{C_{\text{clamped}}}{1 - k^2}. \tag{1.37.6}$$

It is thus seen that

$$1 - k^2 = \frac{C_{\text{clamped}}}{C_{\text{free}}} = \frac{C_0}{C_0 + C_{M0T}}. \tag{1.37.7}$$

From this one can derive the following list:

$$\text{(a)} \quad k^2 = \frac{C_{\text{MOT}}}{C_0 + C_{\text{MOT}}}$$

$$\text{(b)} \quad \frac{1}{1 - k^2} = \frac{C_0 + C_{\text{MOT}}}{C_0} \tag{1.37.8}$$

$$\text{(c)} \quad \frac{k^2}{1 - k^2} = \frac{C_{\text{MOT}}}{C_0}$$

$$\text{(d)} \quad \frac{1 - k^2}{k^2} = \frac{C_0}{C_{\text{MOT}}}.$$

These formulas indicate that a transducer which is designed to exhibit motion when excited, may be characterized for excellence by the magnitude of its coefficient of electromechanical coupling, since this is an indication of energy transfer.

1.38 EXPERIMENTAL DETERMINATION OF ELECTROMECHANICAL COUPLING

The dynamic response (meaning transducer displacement or velocity) of an electromechanical transducer under forced drive may be inferred by measurement of its input electrical impedance $Z_{\text{in}}(= E/I)$ or its electrical admittance, $Y_{\text{in}} = I/E$. In general a transducer with distributed parameters

shows an indefinite number of impedance (or admittance) maxima and minima. Usually the first maximum and minimum as of chief interest, and can be readily measured when the designer makes a transducer design in which these are distinctly separated (in frequency) from the next higher occurring maximum. We consider here this special case of a single *mode.*

In Section 1.37 it was shown that in the single mode case of an electrostatic transducer there are two impedance (or admittance) asymptotes. These asymptotes are properties not only of electrostatic transducers but (with change of units) appear in all types of piezoelectric transducers that effectively operate in a single mode. On a log-log plot of Z_{in} (or Yin) versus frequency (f), these asymptotes appear as straight lines. This is a mathematical result which is due to the fact that in a linear plot of impedance (or admittance) these asymptotes appear as hyperbolae [5]. Between these asymptotes, the measured input impedance in the first mode exhibits a minimum f_r(= resonant frequency) followed by a maximum f_a(= anti resonant frequency), Fig. 1.38.1. At a frequency 'far enough' below f_a (say $\frac{1}{4} f_a$) labelled here as $f_{(low)}$, one measures the capacity $C(f_{(low)})$ and inteprets it as the free capacity $(C_0 + C_{MOT})$. Similarly at a frequency "far enough" above f_a (say $2f_a$, or $4f_a$) one again measures the capacity $C(f_{(high)})$ and interprets it as the clamped capacity C_0. The ratio of these two numbers is seen from Eq. 1.37.7 to be

$$\frac{C_0}{C_0 + C_{MOT}} = 1 - k^2, \; k^2 \leqslant 1. \tag{1.38.1}$$

In this way the actual coupling k^2 may be determined.

A plot of log magnitude of admittance versus by frequency, Fig. 1.38.2, may be used in a similar way to measure k^2.

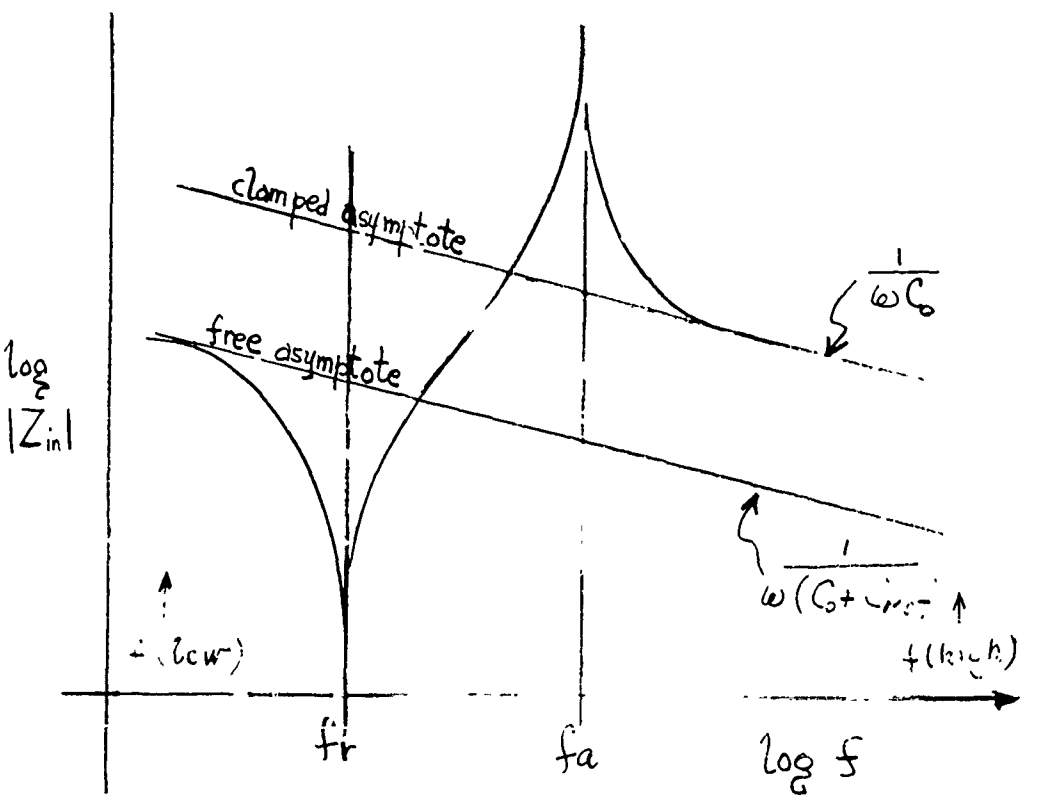


Fig. 1.38.1 — Log magnitude of input impedance versus log frequency of an electrostatic transducer in the lowest mode

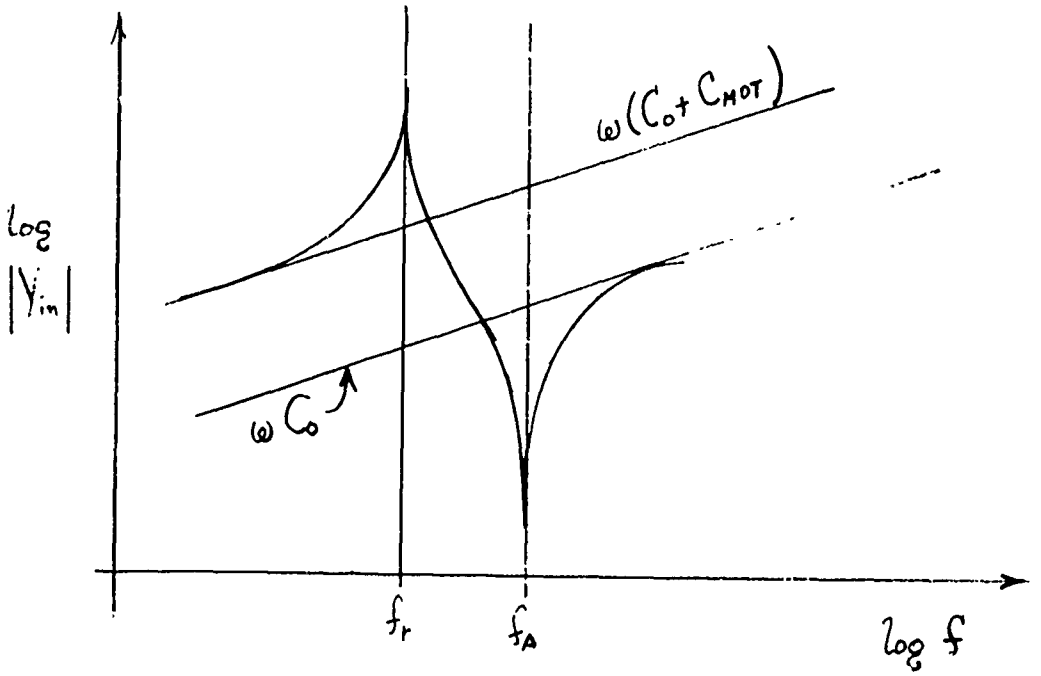


Fig. 1.38.2 — Log magnitude of input admittance versus log frequency of an electrostatic transducer in the lowest mode

In actual practices the determination of the asymptotes at the upper frequency $f_{(high)}$ is made uncertain by interference of the next succeeding mode. It is therefore desirable to determine k^2 from f_r and f_a. A simple procedure is to measure $f_a - f_r$ and make it nondimensional by writing

$$k^2 = \text{const} \times \frac{f_a - f_r}{f_a} = \text{const}\ \frac{f_a^2 - f_r^2}{f_a^2 + f_a f_r}. \tag{1.38.3}$$

Most transducers in the unloaded conditions are designed to make f_a^2 approximately equal to $f_a f_r$. Thus if the constant is chosen to be 2 one arrives at the conventional *definition* of the effective coupling coefficient of an electromechanical transducer operating in a single mode:

$$k_{\text{eff}}^2 = \frac{f_a^2 - f_r^2}{f_a^2}. \tag{1.38.4}$$

This definition implies that k^2 is a measure of transfer of energy from the electrical mesh to the mechanical mesh, as may be inferred from the electrostatic case given by Eq. 1.37.8a,

$$k^2 = \frac{C_{\text{MOT}}}{C_0 + C_{\text{MOT}}} = \frac{\frac{1}{2} E^2 C_{\text{MOT}}}{\frac{1}{2} E^2 C_0 + \frac{1}{2} E^2 C_{\text{MOT}}} = \frac{\text{mechanical energy of motion}}{\text{total energy in the mode}}. \tag{1.38.5}$$

Thus, whenever it is possible to measure (unambiguously) the resonant and antiresonant frequency of a single mode in a multi mode transducer one can determine the coefficient of electromechanical coupling for that mode.

1.39 MATERIAL COUPLING COEFFICIENTS

In a theoretical analysis of the dynamic response of a piezoelectric transducer based upon the piezoelectric equations of state (Section 2.5), the mechanical compliance s_{ij} (or stiffness c_{ij}), and the electric permittivity ϵ_{ij} (or inverse permittivity β_{ij}) are modified by the presence of piezoelectric coupling expressed in the form of a *material coupling coefficient.* Examples of these coefficients appear in Section 2.6 as k_{31}, k_{33}, k_{10}, k_{15}, etc. The theoretical value of these coefficients depends on the stress/strain distribution in the body of the active ceramic as may be inferred when the equations of state are used to formulate the dynamical equations of motion.

In many piezoelectric transducers the state of mechanical stress during motion cannot be known with sufficient accuracy to permit calculation of the material coupling coefficient. This is true when the motion is due to a mixture of modes, so that the stress distribution is not only nonuniform but cannot be known with certainty. It is then desirable to measure these coefficients by relating their values to measurements of resonant and antiresonant frequency in a dominant mode (which may have other modes within its band). Even when the stress distribution is uniform it is usual to measure these frequencies and infer from them the material coupling coefficient, a knowledge of which then permits the formulation of the dynamical equation(s) of motion.

In practice both theory and experience are required to determine the material coupling coefficient of piezoceramic transducers, particularly those constructed in odd shapes. Table 1.39.1, abstracted and codified from a report of Berlincourt [6], presents a list of coupling coefficients for shapes most often used in applications.

In all other transducer shapes and stress conditions not covered by this table it may be possible to measure the free capacity C^T and the clamped capacity C^s by techniques noted above. In these instances the material coupling coefficient k_{ij} takes on the form

$$k_{ij}^2 = 1 - \frac{C_{ij}^s}{C_{ij}^T}$$

in which ij is the mode in question.

1.40 COEFFICIENT OF ELECTROMECHANICAL COUPLING AS A MEASURE OF WORK DONE IN A WORK CYCLE

The theory of the vibration of a piezoceramic bar in forced drive is based on the theory of coupling between primary and secondary circuits of a coupled system. This coupling, expressed as a coefficient, is a measure of mechanical work done in a cycle of forced drive.

A piezoceramic bar polarized in the 3-direction and electroded on its ends, is first short circuited, Fig. 1.40.1a, while being subjected to a compressive stress increasing from 0 to T_3. The work done in generating strain $S_3^{(1)}$ is

$$W_{TOT} = T_3 S_3^{(1)} = s_{33}^E S_3^{(1)2}.$$

The electrodes are then open circuited and the stress allowed to reduce from T_3 to zero, Fig. 1.40.1b. The work done is

$$W_2 = s_{33}^D \; S_3^{(1)2}.$$

Although $D_3 = 0$ in this figure there is a charge accumulation on the electrodes.

Finally an electrical load is connected to the terminals, Fig. 1.40.1c. This completes the cycle showing that the work done in reducing $S_3^{(2)}$ to zero against a zero stress is zero mechanically but nonzero electrically.

Table 1.39.1 — Piezoelectric Material Coupling Coefficients (t = wall thickness, d = diameter, l = length, w = width, r = radius, K_p = planar material coupling coefficient, L = lateral dimension relative to axis

Shape	Conditions of Validity	Direction of Applied Electric Field	Material Coupling Coefficient
spherical shell (motion radial)	$d > 5t$	parallel with radius, (electrodes on inner and outer surfaces)	$K_p^2 = \frac{f_a^2 - f_r^2}{f_a^2}$
thin-walled ring (motion radial)	$d > 5t$ $d > 5l$	parallel to the radius (electrodes on outside and inside surfaces) or parallel to axis of ring (electrodes at ends of the length dimension)	$K_{31}^2 = \frac{f_a^2 - f_r^2}{f_a^2}$
thin-walled ring (motion radial)	$d > 5t$ $d > 5l$	tangential to axis (striped electrodes parallel to the axis)	$K_{33}^2 = \frac{f_a^2 - f_r^2}{f_a^2}$ (*in practice, measured $K_{33} < 2/3$ of the above formula particularly for walls thicker than 0.2 times distance between stripes
thin-walled ring (motion radial)	$d > 5t$ $d > 5l$	paralled to axis (striped electrodes at ends of the length dimension)	$K_{31}^2 = \frac{f_a^2 - f_r^2}{f_a^2}$ (*see note above)
bar (motion in length direction)	$l > 3t$ $l > 3w$	parallel to t or parallel to w	$\frac{K_{31}^2}{1-K_{31}^2} = \frac{\pi}{2}\frac{f_a}{f_r}\tan\left(\frac{\pi}{2}\frac{\Delta f}{f_r}\right)$ When $\frac{\Delta f}{f_r} \ll 1$, $\frac{K_{31}^2}{1-K_{31}^2} = K_c^2 \cong \frac{\pi^2}{4}\frac{\Delta f}{f_r}$ $= \frac{\pi^2}{8}\left(1 - \frac{f_r^2}{f_a}\right)$
tube (motion in length direction)	$l > 4d$ $d > 3t$	parallel to radius (electroded on inner and outer surfaces)	
segment of a tube (motion in length direction)	$l > 3w$ $l > 3t$ (curved in either length or width direction)	parallel to t (electroded on inner or outer surfaces),	
square, circular, rectangular, etc cylinder, with lateral dimension L (motion in length direction)	$l > 2.5\,L$	parallel to axis (electrodes at ends of length dimension)	$K_{33}^2 = \frac{\pi}{2}\frac{f_r}{f_a}\tan\frac{\pi}{2}\frac{\Delta f}{f_a}$

Table 1.39.1 — Piezoelectric Material Coupling Coefficients (t = wall thickness, d = diameter, l = length, w = width, r = radius, K_p = planar material coupling coefficient, L = lateral dimension relative to axis (Continued)

Shape	Conditions of Validity	Direction of Applied Electric Field	Material Coupling Coefficient
tube (motion in length direction)	$t > 4d$ $d > 5t$	tangential to axis (stripe electrodes parallel to axis)	$\frac{K_{31}^2}{1-K_{31}^2} = \frac{\pi}{2}\frac{f_a}{f_r}\tan\left[\frac{\pi}{2}\frac{\Delta f}{f_r}\right]$ (*see note above)
tube (motion in length direction)	$l > 4d$ $d > 3t$	parallel to axis stripe electrodes parallel with circumference)	$K_{33}^2 = \frac{\pi}{2}\frac{f_r}{f_a}\tan\left[\frac{\pi}{2}\frac{\Delta f}{f_a}\right]$ (*see note above)
thin wall cylinder (motions in radial and axial modes are coupled)	$\frac{d}{5} < l < 4d$ *Case I*: $l/d < 1.4$, higher frequency mode is in length *Case II*: $l/d > 1.8$, high frequency mode is radial *Case III*: $1.4 < l/d < 1.8$, two separate resonance and antiresonance frequencies	parallel to radius	When two modes are measurable $(K_d^2, K_l^{2)}$ the planar coupling is, $K_p^2 = K_l^2 + K_d^2$, where $K_d^2 = (f_a)_d^2 - (f_r)_d^2/(f_a)_d^2$ and $\frac{K_l^2}{1-K_l^2} = \frac{\pi}{2}\frac{(f_a)_l}{(f_r)_l}\tan\left[\frac{\pi}{2}\frac{(\Delta f)_l}{(f_r)_l}\right]$ For case III $K_p^2 = 1.1\,[f_a^2 - f_r^2/f_a^2]$
thin disc (f_1 = lowest mode)	Case I $d > 10t$ Case II: $t > 0.2d$	parallel to thickness (electrodes on major surfaces)	Case I (Fig. 3 of [6]) gives K_p versus $\Delta f/f$ Case II: (Fig. 4 of [6]) gives negative % correction to K_p of Case I.
square plate	Case I: $\frac{t}{d} \leqslant 0.1$ Case II: $\frac{t}{d} > 0.1$	parallel to thickness (electrodes on major surfaces)	*Case I:* Multiple K_p of Fig. (3) of [6] by 1.05 *Case II:* Use negative correction given by Fig. 4 of [6]
rectangular plate (two lowest resonances fr_1, fr_2 are available by measurement.) These are not harmonics for which $\Delta f/f$ is lower than width-controlled mode)	$\omega > 2t$ l, w arbitrary	parallel to thickness (electrodes on major surfaces)	$K_p^2 = K_1^2 + K_2^2$ $\frac{K_1^2}{1-K_1^2} = \frac{\pi}{2}\frac{(f_a)_1}{(f_r)_1}\tan\left[\frac{\pi}{2}\left[\frac{(\Delta f)_1}{(fr)_1}\right]\right.$ $\frac{K_2^2}{1-K_2^2} = \pi_2\frac{(f_a)_2}{(f_r)_2}\tan\left[\frac{\pi}{2}\frac{(\Delta f)_1}{(f_r)_2}\right]$

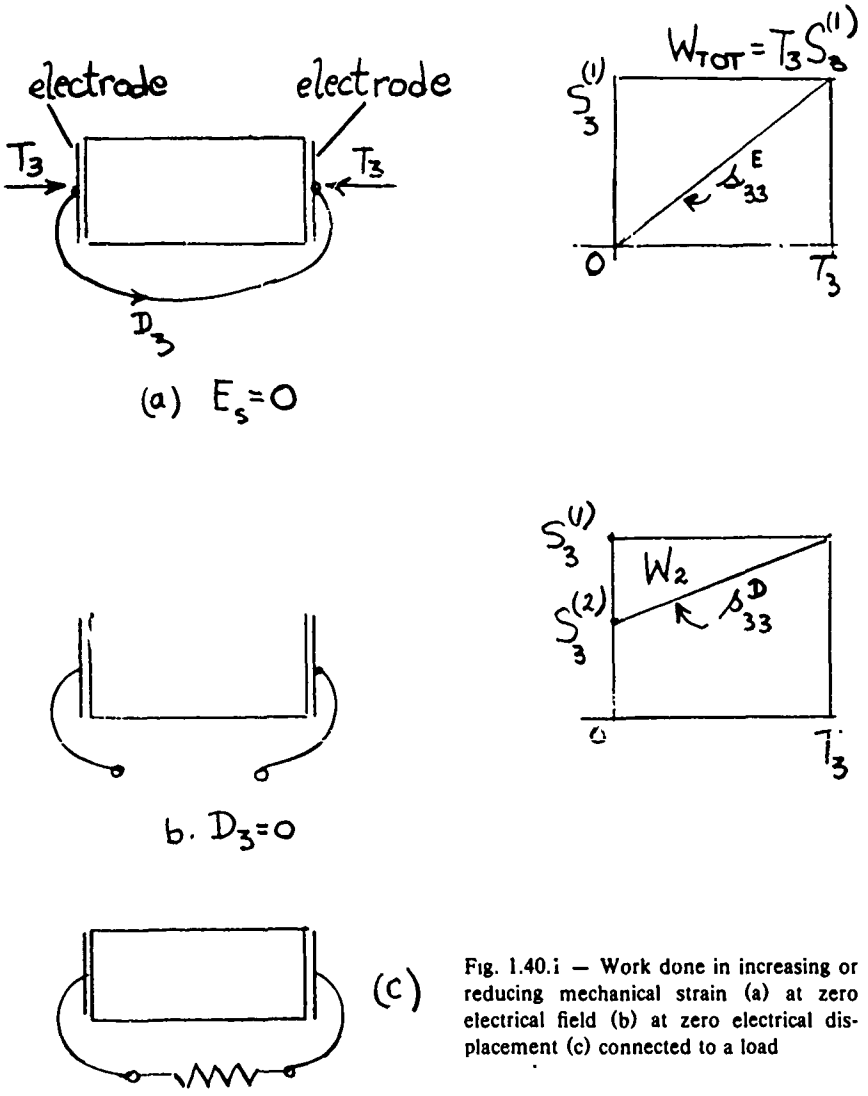


Fig. 1.40.i — Work done in increasing or reducing mechanical strain (a) at zero electrical field (b) at zero electrical displacement (c) connected to a load

The difference in work done in (a) and (b) is symbolized by the difference between s^E and s^D, where $s^D = s^E(1 - k^2)$, k = coefficient of coupling.

1.41 EFFECTIVE COEFFICIENT OF ELECTROMECHANICAL COUPLING (k_{eff})

The determination of k_{eff} by measurement is effected by use of parameters illustrated in Fig. 1.41.1.

In these illustrations the distinction between electrical and mechanical resonance must be observed. To calculate k_{eff} we use the following rules:

(a) electric field transducers: $k_{\text{eff}}^2 = 1 - \dfrac{f_{r(elec)}^2}{f_{a(elec)}^2}$ (1.41.1)

(b) magnetic field transducers: $k_{\text{eff}}^2 = 1 - \dfrac{f_{a(elec)}^2}{f_{r(elec)}^2}$

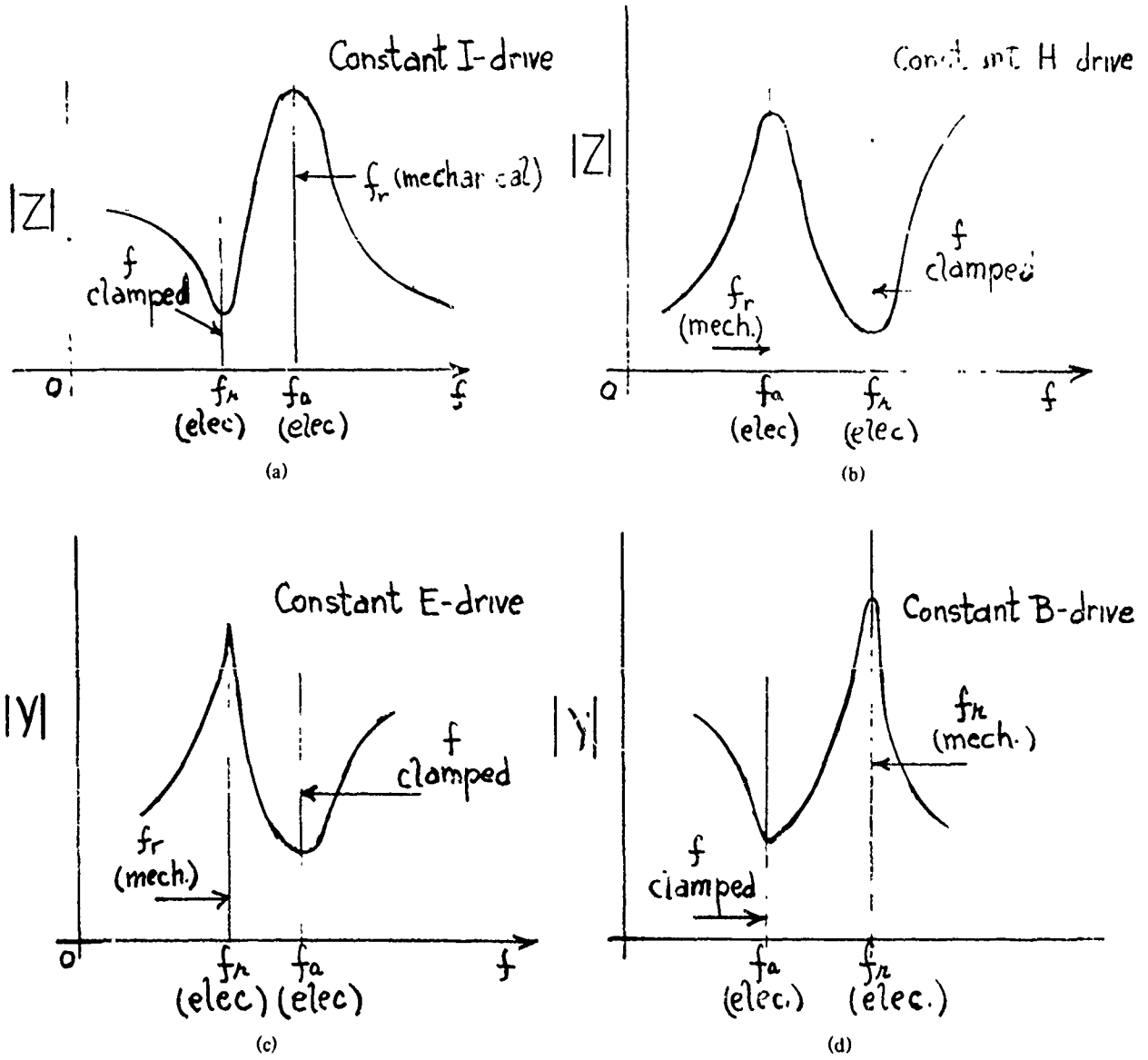


Fig. 1.41.1 — (a) Plot of $|Z|$ vs f for a piezoelectric transducer, (b) Plot of $|Z|$ vs f for a magnetic field transducer, (c) Plot of $|Y|$ vs f for a piezoelectric transducer, (d) Plot of $|Y|$ vs f for a magnetic field transducer

An important observation is the fact that the impedance plot clearly shows $f_a(elec)$ to occur at the frequency of maximum impedance, which is easily measurable, while a measurement of $f_{r(elec)}$ is more ambiguous because it is close to the clamped impedance. Similarly, $f_{r(elec)}$ is easily measured on the admittance chart while $f_{a(elec)}$ is ambiguous. Since k_{eff} is defined as frequency separation relative to $f_{r(elec)}$, it is best to use admittance data in determining k_{eff}. One can deduce that for magnetic field transducers where $f_1 f_2 \simeq f_1^2$,

$$k_{eff}^2 = \frac{f_2^2 - f_1^2}{f_2^2} \cong \frac{f_2^2 + f_1^2 - f_1 f^2}{f_2^2} \cong \frac{(f_2 - f_1)^2}{f_2^2}.$$

so that

$$k_{eff} \cong \frac{f_2 - f_1}{f_2} \tag{1.41.2}$$

and

$$f_2 = f_{r(elec)};\ f_1 = f_{a(elec)}$$

Thus k_{eff} is approximately equal to the nominal separation of frequencies divided by the *upper* frequency, $f_{r(elec)}$.

When impedance data are available the frequency $f_{a(elec)}(=f_1)$ is more easily measured. Then,

$$\frac{f_2^2-f_1^2}{f_2^2} \cong \frac{f_2^2-f_1^2}{f_1^2} \times \frac{f_1^2}{f_2^2} \cong \frac{2(f_2-f_1)}{f_1}(1-k_{eff}^2) = k_{eff}^2.$$

Hence,

$$\frac{f_2-f_1}{f_1} \cong \frac{1\ k_{eff}^2}{2(1-k_{eff}^2)} \text{ or } \frac{(f_2-f_1)^2}{f_1^2} \cong \frac{k_{eff}^2}{1-k_{eff}^2} \tag{1.41.3}$$

Thus the nominal separation of frequencies divided by the *lower* frequency is not k_{eff} but a larger number, namely $k_{eff}^2/(1-k^2eff)2$. These formulas are closely analogous to formulas for coupling of pass band filters. This is discussed next.

1.42 STATIC AND DYNAMIC ELECTROMECHANICAL COUPLING FACTORS

The relation between these coupling factors is illustrated by the behavior of a magnetostrictive toroidal ring.

The coupling of elastic (= stress/strain) fields with magnetic (= magnetic induction/magnetic intensity) fields is expressed by constitutive relations in the form of a pair of basic equations. As an example we write the following set of matrix forms for magnetic coupling:

$$T = C^B S - h_t B$$

$$H = -hS + \gamma^s B.$$

Upon elimination of B and simple rearrangement,

$$T = C^B[1 - h_t h(\gamma^s)^{-1}(C^B)^{-1}]S - h_t(\gamma^s)^{-1}H. \tag{1.42.1}$$

In the specific case of the toroidal ring in which there is simple uniform radial motion,

$$T_1 = C_{11}^B[1-k^2] - \frac{h_{11}^{(t)}H_1}{\gamma_{11}^s} \tag{1.42.2}$$

$$k^2 = \frac{h_{11}^{(t)}h_{11}}{\gamma_{11}^s C_{11}^B}. \tag{1.42.3}$$

The factor k is the static (*or material*) coefficient of electromechanical coupling, so designated because it is obtained directly from the basic set of constitutive relations for the static state.

We turn next to the dynamic relations of a toroidal ring vibrating near resonance. From Eqs. (2.10.4) and (2.10.12) it will be found that the resonant frequencies at constant B and constant H obey the relation

$$\omega_H^2 = \omega_B^2(1 - k^2)$$

or

$$k^2 = 1 - \frac{\omega_H^2}{\omega_B^2} = 1 - \frac{f_H^2}{f_B^2}. \tag{1.42.4}$$

By identifying f_H with the frequency of maximum motional impedance and f_B with the frequency of maximum motional admittance one sees directly that

$$k^2 = k_{\text{eff}}^2$$

where k_{eff} is the dynamic (= effective) coefficient of electromechanical coupling. Hence for a toroidal ring the dynamic coefficient is the same as the material coefficient. This identity of the two coefficients is due to the uniformity of elastic stress in all parts of the transducer at any instant during vibration.

In other types of transducers the elastic stress varies from point to point at any instant. The material coefficient of electromechanical coupling is then different from the effective coefficient. For a magnetic field transducer the latter is always,

$$k_{\text{eff}}^2 = 1 - \frac{f_H^2}{f_B^2} \tag{1.42.5}$$

while the former (= static case) depends on the basic set of constitutive relations. As an example of this difference we refer to the case of the longitudinal vibrator in Sections 2.19 through 2.23 of Chapter 2.

1.43. INDUCTANCE COUPLED INTO THE ELECTRICAL MESH FROM THE MECHANICAL MESH OF A TWO-MESH SYSTEM

A coupling coefficient such as discussed above in previous sections actually is the basis of the transfer of a portion of the mechanical impedance structure from the secondary to the primary. We quote here a case from Sect. 2.10 which the reader is directed to see.

From Eq. 2.10.15 it is seen that in the absence of mechanical dissipation

$$Z_{MOT} = \frac{Z_{em}^2}{j\omega M + \frac{1}{j\omega C_M}}\ ;\ Z_{em}^2 = \frac{2\pi N^2 A^2 h_{11}^2}{al(\gamma_{11}^S)^2}.$$

Thus at low frequencies for which,

$$j\omega M << \frac{1}{J\omega C_M}$$

one has,

$$Z_{MOT} \rightarrow jwL'$$

$$L' = Z_{em}^2 C_M = \frac{2\pi N^2 A^2 h_{11}^2}{a\ l(\gamma_{11}^S)^2} \times \frac{1}{\left[\text{Re}\ C_{11}^B\left(\frac{2\pi A}{a}\right) - \frac{h_{11}^2\ \text{Re}\ \gamma_{11}^S}{\left(\text{Re}\gamma_{11}^S\right)^2 + \left(C_M\gamma_{11}^S\right)^2}\ \frac{2\pi A}{a}\right]}.$$

This L' is the low frequency inductance coupled into the electrical mesh. It is a useful parameter in defining canonical circuits for magnetic field transducers. The coupling of mechanical elements into the electrical mesh gives needed flexibility to transducer design procedures.

1.44 CANONICAL CIRCUITS

Introduction

The analysis of electroacoustic transduction by use of analogous coupled electrical circuits can reveal its behavior with good accuracy over selected frequency ranges. A number of such basic (canonical) circuits form the foundations of mathematical modeling of most electroacoustic transducers. We discuss canonical circuits in the following Sections.

In the simplest case (the one most sought after by designers) the coupled circuits are two-mesh models of the set of *linear* equations,

$$E = IZ_e + T_{em}\mathrm{v} \tag{1.44.1a}$$

$$F = T_{me}I + Z_m\mathrm{v} \tag{1.44.1b}$$

The units are, T_{em}:$\frac{Vs}{m}$; T_{me}:$\frac{Ns}{C}$. The transduction coefficients are either symmetrical, $T_{em} = T_{me} = T$, or anti-symmetrical, $T_{em} = -T_{me}$. The distinction between these coefficients is significant and can be traced to physical grounds. We discuss both topics next.

1.45 TWO-MESH CIRCUITS WITH SYMMETRICAL TRANSDUCTION

Equations 1.44.1 can be represented by a two-mesh electro-mechanical network coupled by a T-network with the transduction impedance T in shunt position, Fig. 1.45.1.

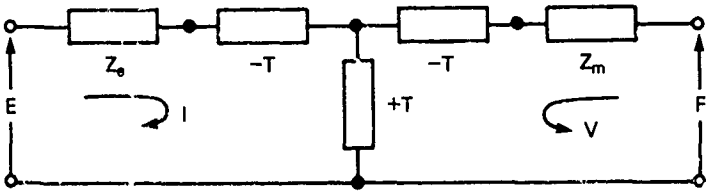


Fig. 1.45.1 — A two-mesh equivalent circuit representing Eqs. 1.44.1a,b

This circuit is advantagous because the T-network allows several convenient network transformations to be made. A simple, but very useful, transformation consists in replacing the T-network with an ideal transformer having a step up ratio of 1: ϕ^2. The applied force is then $F = \phi E$, and the current $I = \phi \mathrm{v}$. Thus the units of ϕ are N/V or C/m. Several cases occur.

Case I. Transformation of Z_e to Shunt Position.

Assume we derive Z_e to be in shunt position in the electrical mesh with no other electrical impedance present. We first solve for I in Eq. 1.44.1a and substitute into Eq. 1.44.1b,

$$F = \left(Z_m - \frac{T_{me}T_{em}}{Z_e}\right)\mathrm{v} + \frac{T_{me}}{Z_e}E \tag{1.45.1}$$

From this it is deduced that $\phi = T_{me}/Z_e = T/Z_e$. Also, since v is a through variable and E is an across variable it is seen that Z_e is in shunt position as required.

The equivalent 2-mesh circuit of Eq. 1.45.1 is sketched in Fig. 1.45.2. It shows that when Z_e is moved to the shunt position an impedance $-T^2/Z_e$ appears in series in the mechanical branch.

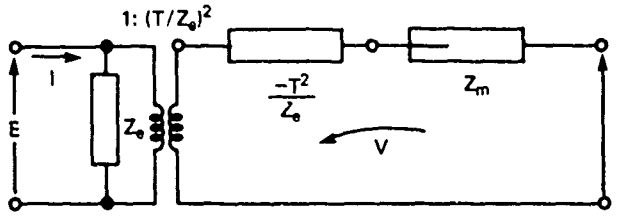


Fig. 1.45.2 — A two-mesh equivalent circuit with Z_e in shunt position, corresponding to Eqs. 1.44.1

Case II: Transformation of Z_m to Series Position

Suppose next we desire Z_m to be the (only) mechanical impedence in series position in the mechanical mesh. According to the rules of turns ratio manipulation (see below Table 1.47.1) we can transfer $-R^2/Z_e$ of Fig. 1.45.2 to the electrical mesh by noting that

$$Z_{\text{electrical}} = Z_{\text{mechanical}}/\phi^2$$

or

$$Z_{\text{electrical}} = -\frac{T^2}{Z_e} \times \frac{Z_e^2}{T^2} = -Z_e \tag{1.45.2}$$

This transfer places $-Z_e$ in series position in the electrical mesh.

The equivalent 2-mesh circuit of Eqs. 1.45.2, is shown in Fig. 1.45.3 corresponding to Eqs. 1.44.1.

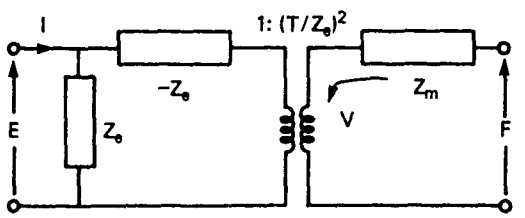


Fig. 1.45.3 — A two-mesh equivalent circuit with z_m in series position, corresponding to Eqs. 1.44.1

Case III. Transformation of Z_m to Shunt Position

A third transformation can be constructed if we specify Z_m to be the mechanical inpedence in shunt position. To accomplish this we solve Eq. 1.44.1b for v and substitute it into Eq. 1.44.1a,

$$E = \left(Z_e - \frac{T_{em}T_{me}}{z_m}\right) I + \frac{F}{(z_m/T_{em})}. \tag{1.45.3}$$

From this it is deduced that the turns-ratio is,

$$\phi = z_m / T_{em} = z_m / T. \tag{1.45.4}$$

Also, since I is a through variable and F is an across variable the mechanical impedance z_m must be in shunt position, and the impedance $-T^2/z_m$ must be in series position.

Thus the equivalent 2-mech circuit of Eqs. (1.45.3) is shown in Fig. 1.45.4. One concludes that when z_m is moved to the shunt position an electrical impedance $-T^2/z_m$ appears in series in the electrical branch. It is noted here that the turns ratio of the ideal transformer can be changed from $1 : \phi^2$ into $\mu^2 : 1$, where μ and ϕ are related by $\mu\phi = 1$. This is discussed in Section 1.47 and Table 1.47.1.

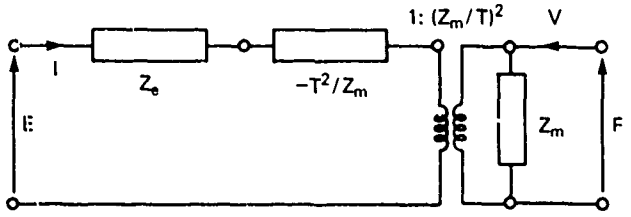


Fig. 1.45.4 — A two-mesh equivalent circuit with z_m in shunt position, corresponding to Eqs. 1.44.1

1.46 TRANSDUCTION COEFFICIENTS IN RECIPROCAL TRANSDUCTION SYSTEMS

In Eqs. 1.44.1 the coefficients T_{em}, T_{me} have the units of Vs/m and Ns/C respectively. For reciprocal systems these are equal and appear in equivalent circuits as ideal transformers with factor T^2. It is useful to define two quantities T_e', T_m' associated with electromechanical coupling such that

$$T_e' T_m' = T^2 = Z_e' Z_M' \tag{1.46.1}$$

Here Z_e' is a component electrical impedance of that part of the total electrical impedance Z_e associated with transduction, that is, associated with transducer motion. Similarly Z_M' is a component of the total mechanical impedance z_m associated with transduction, that is, with coupling to the electrical field. Those impedances of the coupled branches which are not associated with transduction are Z_e'' respectively. They are branch self-impedances. Thus, in Fig. 1.44.1 one can replace Z_e by $Z_e'' + Z_e'$, and z_m by $Z_m'' + z_m'$.

Suppose now the network transformations in Figs. 1.45.2, 3, 4 are redrawn to show ideal transformer action on Z_e', Z_M' alone. This means that in the ideal transformer ratios of Fig. 1.45.2, 3, 4, Z_e is replaced by Z_e', Z_M by Z_M' and T^2 by Eq. 1.46.1. As an example, starting with Fig. 1.44.1 we set $Z_e = Z_e''$ in the series branch and then choose the transformation, Z_e' in shunt position. According to Fig. 1.45.2 a mechanical impedance $-T^2/Z_e'$ ($= -Z_M'$ by use of Eq. 1.46.1) then appears in series position in the mechanical branch. This cancels the $+Z_M'$ already there, leaving only the uncoupled component of mechanical impedance, Z_M''. Thus the net effect of electromechanical coupling is modeled as a blocked electrical impedance (Z_e'') in series position and the coupled electrical impedance Z_e' in shunt, both in the electrical mesh of the 2-mesh equivalent circuit. The mechanical mesh consists of Z_m'' in series position plus the load impedance Z_L in shunt.

A reciprocal system can also be represented by placing the coupling impedance in the mechanical branch. Thus Z_e' is moved from shunt positon in the electrical mesh to shunt position in the mechanical mesh by use of the formula

$$Z_M' = \phi^2 Z_e' \tag{1.46.2a}$$

that is,

$$Z_M' = \frac{T^2}{Z_e'^2} \times Z_e' = \frac{T^2}{Z_e'}. \tag{1.46.2b}$$

The mechanical branch then consists of the coupling impedance T^2/Z_e' in shunt, the uncoupled mechanical impedance Z_m'' in series, and the load impedance Z_L in shunt. The electrical mesh consists of Z_e'' in series position.

In *Summary*: The cononical elementary equivalent circuit of an electromechanical device is a 2-mesh circuit, one electrical and one mechanical. If we adopt a E/F, I/V analogy, the electrical impedance Z_e is in series position, and the mechanical impedance z_m is also in series position. The meshes are then coupled by a symmetrical T-network $(-T, -T, +T)$.

If we desire Z_e to be in shunt position, the two meshes become coupled through an ideal transformer and a coupling electrical impedance-T^2/Z_e appears in series position in the mechanical branch.

If we desire the mechanical impedance z_m to be in shunt position the two meshes become coupled through an ideal transformer and a coupling mechanical impedance $-T^2/z_m$ appears in series position in the electrical branch.

If we break up Z_e into coupled part Z_e' and uncoupled part Z_e'', and break up z_m into coupled part z_m' and uncoupled part z_m'', then z_m'' can appear in series position coupled through an ideal transformer, while Z_e' and z_m' can be transformed to shunt positions as described above.

In transforming elements from series positions to shunt positions the rules to be observed are: a series electrical RLC network transformed to shunt position in the electrical branch is associated with the appearance of a parallel GCΓ network in the mechanical branch multiplied by the turns ratio (as required). A series mechanical r_m l_m c_m network transformed to shunt position in the mechanical branch is associated with the appearance of a parallel g_m c_m γ_m network in the electrical branch, multiplied by an appropriate turns ratio. When applying this rule to components Z_e', Z_e'', and z_m', z_m'' one can follow the auxiliary rules,

a. if blocked Z_e'' is in series position in the electrical branch the motional impedance due to z_m' is reflected into the electrical branch as a parallel network in series position.

b. if blocked Z_e'' is in shunt position in the electrical branch the coupled impedance Z_e' is reflected into the mechanical branch as a series network in series position.

1.47 TURNS-RATIO DISCUSSION

Electromechanical transducers modeled by the linear set of equations,

$$E = Z_e I + T_{em} \text{ v} \tag{1.47.1a}$$

$$F = z_m v + T_{me} I \qquad (1.47.1b)$$

have equivalent circuit representation as an electrical mesh coupled to a mechanical mesh through an ideal transformer or ideal gyrator. In either case the turns ratio of transformation has the representation of Fig. 1.47.1.

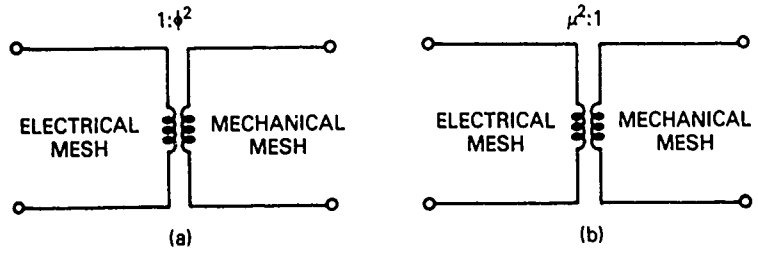


Fig. 1.47.1 — Turns ratio in two-mesh equivalent circuits

The rules governing the transfer of variables across the coupling structure are listed in Table 1.47.1.

Table 1.47.1 — Rules Concerning Turns Ratio Manipulations

	Electrical Mesh		Mechanical Mesh
Turns ratio	1	:	ϕ^2
Rules:	$\phi\times$ electrical across variable	→	= mechanical across variable
	$1/\phi \times$ electrical through variable	→	= mechanical through variable
	$\phi^2 \times$ (across/through)	→	= (across/through)
Turns ratio	μ^2	:	1
Rules:	electrical across variable =	←	$\mu \times$ mechanical across variable
	electrical through variable =	←	$\frac{1}{\mu} \times$ mechanical through variable
	(across/through) =	←	$\mu^2 \times$ (across/through)
Relation of μ, ϕ	$\mu\,\phi = 1$		

Example

A case of basic importance is the 2-mesh representation of an electromechanical system exhibiting electromagnetic coupling, Fig. 1.47.2.

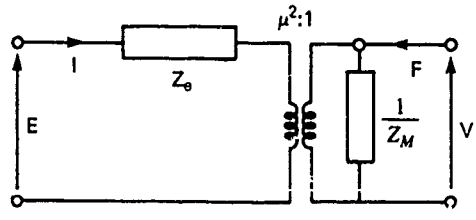


Fig. 1.47.2 — A two-mesh representation of a transducer with electromagnetic coupling

The analysis of this circuit, in which v is across and F is through, reveals important details. One has,

$$E = Z_e I + E_\alpha$$

From Table 1.47.1,

$$E_\alpha = \mathrm{v}\mu$$

Since v is an across variable we must transform it into a function of F. Now the node law for the mechanical mesh is

$$F = F_1 + F_\beta; \quad F_1 = \mathrm{v}Z_m;$$

From Table 1.47.1 $F_\beta = -I\mu$ (the negative sign means F, I are opposite in direction). Thus,

$$\mathrm{v} = \frac{F + I\mu}{z_m}$$

Hence,

$$E = \left[Z_e + \frac{\mu^2}{Z_m}\right] I + \frac{F\mu}{Z_m} \tag{1.47.2}$$

From Eq. 1.47.1a we can identify μ with T_{em}. The equations of electromagnetic coupling are therefore,

$$\begin{cases} E = \left[Z_e + \dfrac{T_{em}^2}{Z_m}\right] I + \dfrac{T_{em}}{Z_m} F \\ \mathrm{v} = \dfrac{T_{em}}{z_m} I + \dfrac{F}{z_m}. \end{cases} \tag{1.47.3}$$

Arbitrarily add and subtract $\frac{T_{em}}{Z_m}$ (without regard to dimension) in order to insert a T-circuit, Fig. 1.45.1. Then

$$E = \left(Z_e + \frac{T_{em}^2}{Z_m} - \frac{T_{em}}{Z_m} + \frac{T_{em}}{Z_m}\right) I + F \frac{T_{em}}{Z_m}$$

$$\mathrm{v} = \left(\frac{1}{Z_m} - \frac{T_{em}}{Z_m} + \frac{T_{em}}{Z_m}\right) F + \frac{T_{em}}{Z_m} I.$$

The transformation to Fig. 1.47.2 is then easily accomplished. These equations will be used in formulating models of magnetic field transducers, Sec. 1.5.1.

1.48 TRANSDUCTION COEFFICIENTS IN ANTIRECIPROCAL SYSTEMS

In antireciprocal systems the underlying transduction mechanism requires that T_{em} have the same magnitude as T_{me} but be opposite in sign. This is the case of electromagnetic transduction. When an

attempt is made to construct a 2-mesh equivalent circuit of Eqs. 1.47.1 with $T_{em} = -T_{me}$ it is found that as long as force F is an across variable the attempt fails to generate the required canonical set of equations if loop analysis is used. However when Eq. 1.47.1b is solved for velocity v in terms of electric current I and force F, thereby making F a through-variable, and when this solution for v is substituted into Eq. 1.47.1a, one obtains the set,

$$E = \left(Z_e - \frac{T_{me}T_{em}}{Z_m}\right) I + \frac{T_{em}}{Z_m} F; \quad \mathrm{v} = -\frac{T_{me}}{Z_m} I + \frac{F}{Z_m}. \tag{1.48.1}$$

Since $T_{em} = -T_{me}$ it is found that an equivalent 2-mesh circuit can be constructed which yields the required canonical set Eqs. 1.47.1. The mechanical branch however must appear in mobility form (that is, one in which force is the through-variable and velocity is the across-variable. The equivalent circuit for this case is reviewed in Sect. 1.47. There it is noted that in the case of electromagnetic coupling the physical relations of voltage, velocity, force and current are,

$$\begin{aligned} E_\alpha &= \mu \mathrm{v} \\ F_\alpha &= -I\mu \end{aligned} \tag{1.48.2}$$

in which the negative sign, arising from assignment of directions of current and force in the equivalent circuit, is purely conventional. The symbol μ is the transduction coefficient. Its explicit value depends on the nature of the transduction. Several forms of μ will be discussed in later chapters of this treatise.

1.49 INTRODUCTION TO ANALYSES OF TRANSDUCERS BY VARIATIONAL METHODS

The analysis of energy-conversion systems containing many components is laborious. One procedure for reducing the labor is to employ variational calculus of Lagrange and Hamilton. Its use has the additional advantage of defining the natural boundary conditions of such multifield components. We review the chief elements of this procedure.

1.50 GENERALIZED COORDINATES, GENERALIZED FORCES, VARIATIONAL PRINCIPLE

When an operating dynamical system (electrical, mechanical, hydraulic, etc) is momentarily frozen in time its state can be specified by a set of coordinates which define its configuration relative to a reference frame. Examples of this configuration are spatial points, angles, electric charge, flux, thermodynamic pressure, entropy, etc. These coordinates are selected to conform to admissible changes in configuration in the next instant of time. A set of coordinates is *complete* when the "location" of all components in a configuration state are accounted for, and is *independent* when any one coordinate is not a function of any, or all, of the rest of the coordinates. When a configuration undergoes a physically admissible variation the coordinates undergo generalized (infinitesimal) variations. These constitute the variational variables of the system.

Generalized coordinates are related to the energy coordinates of a field. When a system undergoes an admissible variation work is done by the components of the system. We can treat the generalized coordinates as *extensive* variables of energy and associate with each an *intensive* variable such that the product of the two gives the work done. Table 1.50.1 summarizes the expressions for the work done in various systems of importance to acoustic transduction. The complementary expressions for work done (column #2) are based on a simple change of variables. The energy associated with each entry of column #2 is called *coenergy* and is written with an asterisk (W^*) in contrast to the energy W each entry of each entry of column #1. In using variational methods it is necessary to express the vari-

Table 1.50.1 — Formulas for Work Done in Energy Systems

System	Extensive Coordinate	Intensive Variable	(#1) Variational Work Done	(#2) Complementary Work Done
mechanical	**R** (displacement (m))	**F** (force (*N*))	$\mathbf{F} \cdot \delta\mathbf{R}$	$\mathbf{R} \cdot d\mathbf{F}$
electrical	q (charge (C))	E (electric potential difference (units (V))	$E\delta q$	qdE
magnetic	λ (magnetic flux linkage (Vs))	I (electric current $\left(\frac{C}{s}\right)$)	$I\delta\lambda$	λdI
fluid flow	V (flow volume (m^3))	P (fluid pressure $\frac{N}{m^2}$)	$P\delta V$	Vdp
(acoustical) elastic	ϵ_{ij} (strain)	σ_{ij} (stress N/m^2)	$\sigma_{ij}\delta\epsilon_{ij}$ (units: Nm/m^3)	$\epsilon_{ij}d\sigma_{ij}$

ational principle in selected choices of energy or coenergy of the system in question. This is best seen in the electrical case. Suppose one chooses electrical charge q, $\dot{q}$ as the generalized coordinate. The energies are then $\int edq$ (= intensive × differential of extensive), and $\int \lambda\, d\dot{q}$ (= extensive × differential of intensive). Thus the energy of the magnetic field is expressed in coenergy form. Similarly if one choose λ, $\dot{\lambda}$ as the generalized coordinate, the energies are $\int qd\dot{\lambda}$ (= extensive × differential of intensive) and $\int id\lambda$ (intensive × differential of extensive). The electric field is then in coenergy form.

The expression for the work done allows one to construct a variational principle: When a system changes from configuration at time t_1 to another configuration at time t_2 it traces out a history of energy content $\mathscr{W}$ at every instant such that

$$\delta I = \int_{t_1}^{t_2} \delta\, \mathscr{W}\, dt = 0 \tag{1.50.1}$$

provided every variation of coordinates is "geometrically permissible," that is, the system does not violate the constraints built into it.

The usefulness of this principle for each system in Table 1.50.1 is discussed in the following cases.

A. *Variational Principle for Mechanical Systems*

The admissible change in the configuration of a mechanical system from time t_1 to time t_2 acting under external and internal forces **F** is such that the integral

$$\delta I = \int_{t_1}^{t_2} \mathbf{F} \cdot d\mathbf{R}\, dt \tag{1.50.2}$$

vanishes. The forces **F** are characterized as:

- inertial forces acting on masses (F_m), which in time $t_2 - t_1$ contribute to the energy integral I in the amount,

$$\int_{t_1}^{t_2} F_m \cdot \delta R\, dt = \int_{t_1}^{t_2} \delta\, T^* dt$$

in which T^* is the coenergy,

$$T^* = \int_0^v p dv \qquad \text{(units: Nm)}.$$

Here p is the momentum (units: Ns) of the mass, and v is the velocity.

- conservative forces, or forces F_k exerted on masses by ideal springs. They have the characteristic feature of being derivable from a potential energy U. When work is done by such springs the potential energy decreases. Hence the variation of the work of these conservative forces contributes to I in the amount,

$$\int_{t_1}^{t_2} \mathbf{F}_k \cdot \delta \mathbf{R}\, dt = \int_{t_1}^{t_2} -\delta U\, dt \qquad \text{(units: Nm)}$$

- nonconservative forces $\mathbf{f}_i$ acting through displacements ξ_i. They contribute to I in the amount,

$$\int_{t_1}^{t_2} \sum_1^n \mathbf{f}_i \cdot \delta \xi_i\, dt$$

Accordingly, the variational principle states that allowable changes in configuration of the mechanical system require that,

$$\delta \mathrm{I} = \int_{t_1}^{t_2} (\delta T^* - \delta U + \sum_1^n \mathbf{f}_i \cdot \delta \xi_i)\, dt = 0. \tag{1.50.3}$$

Here T^* is the sum of all the kinetic energies of the masses of the system, and U is the sum of all the potential energies of the system. The forces $\mathbf{f}_i$ are called *generalized forces* of the system. Equation 1.50.2 is the formulation of Hamilton's variational principle for a lumped-parameter mechanical system. Noting that T^*, U are functions of generalized coordinates ξ_i, $\dot{\xi}_i$ one can apply the method of the calculus of variations to obtain Lagrange's equations for n coordinate displacements,

$$\frac{d}{dt}\left(\frac{\partial \mathrm{L}}{\partial \dot{\xi}_j}\right) - \frac{\partial \mathrm{L}}{\partial \xi_j} = f_j,\ j = 1, 2 \ldots n \tag{1.50.4a}$$

$$\mathrm{L}(\dot{\xi}_j, \xi) = T^*(\dot{\xi}_j, \xi_j) - U(\dot{\xi}_j, \xi_j). \tag{1.50.4b}$$

Forces f_j are of two types: *internal* forces, corresponding to friction, viscosity, mechanical hysteresis etc. These are given a negative sign; *external* forces, corresponding to applied forces. These are given a positive sign.

In continuous mechanical systems both T^* and U may be integrals over spatial and temporal coordinates. Since the variation operation (δ) commutes with both space and time differentiation,

$$\delta\left(\frac{\delta \xi}{\partial t}\right) = \frac{\partial(\delta \xi)}{\partial t};\ \delta\left(\frac{\partial \xi}{\partial x}\right) = \frac{\partial(\delta \xi)}{\partial x} \tag{1.50.5}$$

one may eliminate these quantities by integrating by parts over the domain of the spatial and temporal variables. By Hamilton's principle the variational quantity δI vanishes at the end points of integration

while the spatial integral sets boundary conditions to the problem at the end points of the spatial domain. These are the natural boundary conditions.

B. *Variational Principle for Electrical Systems*

Table 1.50.1 shows that one may choose charge variables q_l (units: C) or flux-linkage variables λ_j (units: Vs) as generalized coordinates of an electric system. Suppose first we choose q_l. Then, by definition the Lagrangian function is,

$$L(\dot{q}, q) = W_m^* - W_e \tag{1.50.6a}$$

in which,

$$\text{magnetic coenergy:} \quad W_m^* = \sum_j \frac{1}{2} L_j i_j^2 = \sum_j \frac{1}{2} L_j \dot{q}_j^2 = \int_0^i \lambda \, di \tag{1.50.6b}$$

$$\text{electrical energy:} \quad W_e = \sum_j \frac{1}{2} \frac{q_j^2}{C_j} = \int_0^q e \, dq \tag{1.50.6c}$$

Here the summation sign is over all inductances L_j and all capacitors C_j of the system. Also, since we have chosen q, $\dot{q}$ as the generalized variables, the magnetic energy must be expressed in coenergy form Eq. 1.50.6b. The variational principle then takes the form,

$$\delta I = \int_{t_1}^{t_2} \left\{ \delta [W_m^* - W_e] + \sum_j e_j \delta q_j \right\} dt = 0. \tag{1.50.7}$$

The symbol e_j represents the generalized voltages corresponding to the generalized coordinate δq_l. They consist of internal voltage drops due to resistance (hence have a negative sign) and external applied voltages (hence have a positive sign). Lagrange's equations corresponding to Eq. 1.50.7 are the set,

$$\frac{d}{dt} \left(\frac{\partial L}{\partial \dot{q}_k} \right) - \frac{\partial L}{\partial q_k} = E_k \quad k = 1, 2, \ldots . m \tag{1.50.8}$$

where E_k contributes to the work term as,

$$\sum_k E_k \, \delta q_k = \text{Sum of external work minus internal work.} \tag{1.50.9}$$

When flux-linkage variables are employed the Lagrangian function is

$$L(\dot{\lambda}, \lambda) = W_e^* - W_m \tag{1.50.10}$$

$$\text{electrical coenergy} \quad W_e^* = \int_0^e q \, de = \frac{1}{2} C e^2 = \frac{1}{2} C \dot{\lambda}^2 \tag{1.50.11}$$

$$\text{magnetic energy} \quad W_m = \frac{\lambda^2}{2L} = \int_0^\lambda i \, d\lambda, \; i = \frac{\lambda}{L}. \tag{1.50.12}$$

The variational principle is then,

$$\delta I = \int_{t_1}^{t_2} \{\delta[W_e^* - W_m] + \sum_i i_j d\lambda_j\} dt = 0. \tag{1.50.13}$$

For n independent flux-linkage coordinates λ_k, Lagrange's equations become,

$$\frac{d}{dt}\left(\frac{\partial L}{\partial \dot{\lambda}_k}\right) - \frac{\partial L}{\partial \lambda_k} = I_k, \quad k = 1, 2, \ldots n \tag{1.50.14}$$

where I_k are the generalized currents, which contribute to 'work done' as,

$$\sum_k I_k \delta\lambda_k. \tag{1.50.15}$$

The generalized currents may have two forms: internal currents $I_i = \dot{\lambda}_i / R_i$, and external (applied) currents I_s.

Constitutive Relations In Electrical Systems

In electrical systems the generalized coordinate (charge q, or flux-linkage λ) is related to potential difference e, and current i. For the case of charge variables. One has,

$$i(q_j) = dq_j/dt \quad j = 1, 2 \ldots \tag{1.50.16a}$$

$$e(q_j) = e(q_1, q_2 \ldots) \tag{1.50.16b}$$

while for the case of flux-linkage variables,

$$e(\lambda_j) = \frac{d\lambda_j}{dt} \quad j = 1, 2 \ldots \tag{1.50.17a}$$

$$\dot{\lambda}(i_j) = (i_1, i_2, \ldots). \tag{1.50.17b}$$

Electrical passive elements for which these constitutive relations are linear in a single variable are the simplest to consider. Their energies are tabulated here:

linear capacitor: $e = q/C$; $W_e = \frac{q^2}{2C}$; $W_e^* = \frac{1}{2} Ce^2$ (1.50.18a)

linear inductor: $\lambda = Li$; $W_m = \frac{\lambda^2}{2L}$; $W_m^* = \frac{1}{2} Li^2$. (1.50.18b)

Next in order of complexity are passive elements for which the constitutive relations are linear in two variables, typified by mutual-inductance between two coils in which the flux-linkages are λ_1, λ_2 and the currents i_1, i_2. Here, Eq. 1.50.17 reduces to a matrix relation of column vectors { } and square matrices [ ],

$$\begin{Bmatrix}\lambda_1 \\ \lambda_2\end{Bmatrix} = [L]\begin{Bmatrix}i_1 \\ i_2\end{Bmatrix}, \quad [L] = \begin{bmatrix}L_{11} & L_{12} \\ L_{21} & L_{22}\end{bmatrix} \tag{1.50.19a}$$

with its inverse,

$$\begin{Bmatrix} i_1 \\ i_2 \end{Bmatrix} = [\Gamma] \begin{Bmatrix} \lambda_1 \\ \lambda_2 \end{Bmatrix}, \quad [\Gamma] = \begin{bmatrix} \Gamma_{11} & \Gamma_{12} \\ \Gamma_{21} & \Gamma_{22} \end{bmatrix}. \tag{1.50.19b}$$

The energies associated with mutual inductance are formulated as products of a matrix by a row vector and a column vector,

$$W_m(\lambda_1, \lambda_2) = \frac{1}{2} \{\lambda_1, \lambda_2\} [\Gamma] \begin{Bmatrix} \lambda_1 \\ \lambda_2 \end{Bmatrix} \tag{1.50.20a}$$

$$W_m^*(i_1, i_2) = \frac{1}{2} \{i_1, i_2\} [L] \begin{Bmatrix} i_1 \\ i_2 \end{Bmatrix}. \tag{1.50.20b}$$

In a similar way one can construct constitutive equations for linear mutual capacitance,

$$\begin{Bmatrix} q_1 \\ q_2 \end{Bmatrix} = [C] \begin{Bmatrix} e_1 \\ e_2 \end{Bmatrix} \qquad [C] = \begin{bmatrix} C_{11} & C_{12} \\ C_{21} & C_{22} \end{bmatrix} \tag{1.50.21a}$$

$$\begin{Bmatrix} e_1 \\ e_2 \end{Bmatrix} = [D] \begin{Bmatrix} q_1 \\ q_2 \end{Bmatrix} \qquad [D] = [C]^{-1} = \begin{bmatrix} D_{11} & D_{12} \\ D_{21} & D_{22} \end{bmatrix}. \tag{1.50.21b}$$

The energies associated with mutual capacitance are also products of row vectors column vectors and a square matrix,

$$W_e(q_1, q_2) = \frac{1}{2} (q_1, q_2) [D] \begin{Bmatrix} q_1 \\ q_2 \end{Bmatrix} \tag{1.50.22a}$$

$$W_e^*(e_1, e_2) = \frac{1}{2} (e_1, e_2) [C] \begin{Bmatrix} e_1 \\ e_2 \end{Bmatrix}. \tag{1.50.22b}$$

C. *Variational Principle for Electromechanical Systems*

When electrical and mechanical systems are coupled together the expression for the Lagrangian function L_{em} contains terms which exhibit coupling between the generalized coordinates of both systems. Formally, the coupling is a functional f:

$$L_{em} = L(\xi, \dot{\xi}, q, \dot{q}, f(\xi, \dot{\xi}, q, \dot{q})) \tag{1.50.23a}$$

or

$$L_{em} = L(\xi, \dot{\xi}, \lambda, \dot{\lambda} f(\xi, \dot{\xi}, \lambda, \dot{\lambda})) \tag{1.50.23b}$$

Hamilton's principle then takes on one of two forms (#1, #2) depending on the choice of generalized coordinates. These are:

Form #1 uses displacement ξ and charge q,

$$\delta I = \int_{t_1}^{t_2} [\delta(T^* - V + W_m^* - W_e) + \sum_L f_l \, \delta\xi_l + \sum_j e_j \, \delta q_j] \, dt = 0 \qquad (1.50.24a)$$

The work expression

$$\sum_l F_l \, \delta \, \xi_l + \sum_k E_k \, \delta q_k \qquad (1.50.24b)$$

defines the generalized forces F_l and generalized voltages E_k of the nonconservative elements. The corresponding equations of Lagrange are,

$$\frac{d}{dt}\left(\frac{\partial L}{\partial \dot{\xi}_l}\right) - \frac{\partial L}{\partial \xi_l} = F_l, \; l = 1, 2, \ldots \qquad (1.50.25a)$$

$$\frac{d}{dt}\left(\frac{\partial L}{\partial \dot{q}_k}\right) - \frac{\partial L}{\partial q_k} = E_k, \; k = 1, 2, \ldots \qquad (1.50.25b)$$

Because of electromechanical coupling Eq. 1.50.25a contains generalized coordinate q_k and Eq. 1.50.25b contains generalized coordinate ξ_l.

Form #2 uses displacement ξ and flux-linkage λ,

$$\delta I = \int_{t_1}^{t_2} [\delta(T^* - V + W_e^* - W_m) + \sum_l fi \, \delta\xi_l + \sum_j i_j \delta\lambda_j] dt = 0. \qquad (1.50.26a)$$

The work expression

$$\sum_l F_l \delta\xi_l + \sum_k I_k \delta\lambda_k \qquad (1.50.26b)$$

defines the generalized forces F_l and generalized currents I_k of the nonconservative elements. The corresponding equations of Lagrange are,

$$\frac{d}{dt}\left(\frac{\partial L}{\partial \dot{\xi}_l}\right) - \frac{\partial L}{\partial \xi_l} = F_l \quad i = 1, 2, \ldots \qquad (1.50.27a)$$

$$\frac{d}{dt}\left(\frac{\partial L}{\partial \dot{\lambda}_k}\right) - \frac{\partial L}{\partial \lambda_k} = I_k \quad k = 1, 2, \ldots \qquad (1.50.27b)$$

Because of electromechanical coupling the force equation 1.50.27b contains generalized coordinate λ_k, while the current equation contains generalized coordinate ξ_l.

Transduction Factors

In electromechanical systems one, several, or all of the terms in the Lagrangian L are functions of the generalized coordinates of both systems. From these coupling terms we can derive expressions for transduction factors.

a. transduction factor for capacitive coupling of a moving-plate condenser

Assume first the electrical energy $W_e = W_e(\xi, q)$. For the nonlinear case, Eq. 1.50.18 becomes,

$$W_e(\xi, q) = \frac{q^2}{2C(\xi)}. \tag{1.50.28}$$

Here the dependence of the capacity C on separation distance ξ serves to couple the electrical properties of the capacitor to its mechanical properties. Thus the incremental force f_e required to keep the plates of a movable-plate condenser separated an incremental distance $d\xi$ is,

$$f_e(\xi, q) = \frac{\partial W_e}{\partial \xi} = -\frac{q^2 (dC/\partial \xi)}{2\, C(\xi)^2}. \tag{1.50.29}$$

Similarly, the potential differences across the capacitor is,

$$e(\xi, q) = \frac{\partial W_e}{\partial q} = \frac{q}{C(\xi)}. \tag{1.50.30}$$

In an alternate formulation one can use the electrical coenergy, Eq. 1.50.10,

$$W_e^*(\xi, e) = \frac{1}{2} C(\xi) e^2$$

from which

$$-f_e(\xi, e) = \frac{\partial W_e^*}{\partial \xi} = \frac{1}{2}\left(\frac{dC}{d\xi}\right)e^2 \tag{1.50.31}$$

$$q = \frac{\partial W^*}{\partial e} = C(\xi)e \tag{1.50.32}$$

Equation 1.50.29 may be used to determine the transduction factor (sometimes called the transduction coefficient). This is defined in terms of the generalized coordinates chosen to describe the system — in this case, charge q and displacement ξ. For a movable-plate condensor area A (m^2) dielectric constant ϵ (C^2/Nm^2) and initial unbased spacing d_0 (m) one assumes

$$C(\xi) = \frac{\epsilon A}{d_0 + \xi}\ ;\ \frac{dC(\xi)}{d\xi} = -\frac{\epsilon A}{(d_0 + \xi)^2} \tag{1.50.33}$$

so that

$$f_e = \frac{q^2}{2\epsilon A} \quad \text{(units:} \quad N\text{)}$$

In MKS units we write $\epsilon = \epsilon_0 \epsilon'$ where $\epsilon_0 = 8.854 \times 10^{-12} (C^2/Nm^2)$, and ϵ' is the relative permitivity of the medium between the plates of the condenser. To obtain linear response one charges the transducer with (large) dc charge q_0 which establishes an equilibrium separation ξ_0 between the plates. In addition during dynamic motion there is a time varying charge $\xi_1(t)$ imposed by the generalized forces of the system. Thus, in biased operation,

$$q = q_0 + q_1(t) \tag{1.50.34}$$

and so,

$$f_e = \frac{1}{2\epsilon A}\,[q_0^2 + 2q_0 q_1 + q_1^2] \tag{1.50.35}$$

By making q_0 large and allowing q_1 to be small relative to q_0 it is seen that for the time varying component of force one has,

$$f_e(t) = \left\{\frac{q_0}{\epsilon A}\right\} q_1(t) = T_{me}\, q_1(t) \tag{1.50.36a}$$

$$(q_0/\epsilon A) = e_0/(d_0 + \xi_0) \quad \text{(units: V/m)} \tag{1.50.36b}$$

in which e_0 is the equilibrium potential difference corresponding to charge q_0. The symbol T_{me} (subscripts mean mechanical to electrical) is the transduction coefficient for the choice of charge as generalized coordinate. Since $i = dq/dt$, the transduction coefficient for the choice of (sinusoidal) current is,

$$T_{me} = \frac{e_0}{j\omega(d_0 + \xi_0)} \quad \text{(units: Vs/m)}. \tag{1.50.36c}$$

It will be noted later by examination of Lagrange's equations of dynamic motion of an electromechanical transducer with electrostatic coupling that the transduction coefficient T_{em} (electrical to mechanical) is the same as T_{me}.

b. transduction factor for inductive coupling of an electrodynamic coil

A coil of differential length $d\mathbf{l}$ ($\mathbf{l}$ is positive in the direction of current flow) moves with velocity $\mathbf{v}$ through a magnetic field with flux density $\mathbf{B}$. The increment of voltage de in the direction of current flow is

$$de = \mathbf{v} \times \mathbf{B} \cdot d\mathbf{l}.$$

If vector $\mathbf{V}$, $\mathbf{B}$ and $\mathbf{l}$ are at right-angles to each other and obey Fleming's right-hand rule then de represents a *drop* in potential difference,

$$de = -vBdl.$$

At the terminals there is therefore a *rise* in potential of amount

$$e = T_{em}v,\ T_{em} = Bl \quad \text{(units: Vs/m)}. \tag{1.50.37}$$

Again, a coil carrying a current i in a magnetic field with flux density B (units: Vs/m^2) has acting on it a differential force of amount,

$$d\mathbf{f} = id\mathbf{l} \times \mathbf{B} \quad \text{(units: } N\text{)}.$$

The coil in turn acts upon an external constraint with a force of opposite sign. The total constraint force over length l is,

$$\mathbf{f} = -i\,\mathbf{l} \times \mathbf{B}.$$

If vector **l**, **B** are at right angles to each other then the direction of f is determined by Fleming's left-hand rule •

$$f = -\mathrm{T}_{me} i \qquad \mathrm{T}_{me} = Bl \tag{1.50.38}$$

Eqs. 1.50.37, 1.50.38 constitute the transduction relations for an electrodynamic transducer. The quantity $\mathrm{T} = Bl$ is the transduction coefficient. It can be used in determining the magnetic field coenergy W_m^*: from Eq. 1.50.37 one has,

$$e = \frac{d\lambda}{dt} = \mathrm{T}_{em} \frac{d\xi}{dt}.$$

Upon integration over ξ,

$$\lambda = \mathrm{T}_{em}(\xi - \xi_0).$$

Since $\partial W_m^*/\partial i = \lambda$, it is seen that,

$$W_m^* = \mathrm{T}_{em} i(\xi - \xi_0). \tag{1.50.39}$$

One should compare this with Eq. 1.50.18b where $W_m^* = \frac{1}{2} L(\xi) i^2$. In conventional theory of moving-coil transducers $\mathrm{T}_{me} = -\mathrm{T}_{em}$. The negative sign is traceable to customary assignments of directions of the vector quantities involved in the analysis. Several proposals have been made to remove it. They will be discussed in Section 1.44.

c. transduction factor for a moving armature (magnetic) transducer.

A coil of N turns with cross-sectional area S is threaded by a time-varying flux-density $\dot{B}$. The induced *emf* in the coil is

$$E = N\,\mathrm{S}\,\dot{B} = N\dot{\lambda} = N\frac{\partial \lambda}{\partial \xi}\,\mathrm{v}, \qquad \mathrm{v} = d\xi/dt \tag{1.50.40}$$

in which the direction of E is determined by Fleming's right-hand rule. We apply this formula to the interactions of a magnetic pole-piece, area S_g and an armature, the two separated by an air gap d. The magnetic flux density B_g in the gap is assumed normal to the pole-piece (no leakage). The flux $\lambda (= BS_g)$ depends on the ratio of magnetomotive force $\mathscr{F}$ (units: ampere turns) to reluctance $\mathscr{R}$ (units: ampere turns/weber), where

$$\mathscr{F} = \int \mathbf{H} \cdot d\mathbf{l}, \qquad \text{(units: C/s)} \tag{1.50.41a}$$

$$\mathrm{H} = Ni/l \qquad \text{(units: C/sm)} \tag{1.50.41b}$$

and

$$\mathscr{R} = l/\mu_0 S_g, \qquad \text{(units: } \mathrm{C/Vs^2}) \tag{1.50.41c}$$

l = length of fluxpath (m^2); $\mu_0 = 4\pi \times 10^{-7}$ (units: $\mathrm{Ns^2/C^2}$).

Since the force acting on the armature is proportional to the square of the flux, the response of the moving-armature transducer is seen to be nonlinear. In order to linearize it one applies a large bias flux linkage λ_0, which is added to the useful flux λ_1 of the magnetomotive force in the exciting coil due to the applied current i. In a first approximation to calculating a total λ the dominant path reluctance is assumed resident in the air gap, with a small correction factor δ_m to account for remainder of the iron-core path. Thus, for a small displacement ξ of the armature,

$$\lambda = \lambda_0 + \lambda_1;\ \lambda_0 = \frac{\mathscr{F}_0 \mu_0 S_g}{(d_0 + \xi)\ (1 + \delta_m)};\ \lambda_1 = \frac{Ni\mu_0 S_g}{(d_0 + \xi)\ (1 + \delta_m)} \quad \text{(units: Vs)}. \quad (1.50.42)$$

Now from Eq. 1.50.40 it is seen we require $\partial\lambda/\partial\xi$ to relate E to v. The displacement ξ introduces hysteresis in the magnetic circuit, which is accounted for by multiplying μ_0 by the nondimensional complex hysteresis factor $\bar{\chi}$. Furthermore, since the transduction coefficient can be evaluated for any flux excitation of the core, we set $i = 0$ and write,

$$\frac{\partial\lambda_0}{\partial\xi} = -\frac{\mathscr{F}_0 \mu_0 \bar{\chi} S_g}{(d_0 + \xi)^2} = -\frac{\lambda_0}{d_0 + \xi}$$

(in which δ_m is neglected). Thus,

$$E = T_{em}v;\ T_{em} = -\frac{N\lambda_0\bar{\chi}}{d_0 + \xi} \quad \text{(units of } T_{em}\text{: Vs/m)}. \quad (1.50.43)$$

In the conventional theory of moving-armature transducers $T_{me} = -T_{em}$. The reason for the negative sign, and proposals made by several authors to remove it will be discussed in Sect. 1.44.

1.51 EXAMPLES OF ANALYSIS OF TRANSDUCERS BY USE OF THE VARIATIONAL PRINCIPLE

Electromechanical transducers in current use are complicated structures. Analysis of them requires much skill. Experience has shown that the use of a variational principle can serve to illuminate the physical aspects of transduction, as well as to lighten labor. We consider here two examples of electroacoustic transduction. Since the purpose is to illustrate procedure, the examples are much simplified.

A. Dynamical Equations of a Condenser Microphone

This transducer is modeled as a moving-plate condenser. Its configuration is specified by a single generalized coordinate in space, ξ, and a single generalized coordinate of the electrical field, charge q. Mechanically, the (electroded) moving plate is a diaphragm modeled as mass m, spring k, and damper b which are idealized to have the same velocity. The (electroded) fixed plate is charged with electric voltage e_0 through a resistor R.

The analysis begins with the variational principle Eq. 1.50.24a, in which the Lagrangian L (of conservative press) is written with W_m^* omitted and the electromechanical coupling term is given by Eq. 1.50.28,

$$L = T^* - V - W_e = \frac{1}{2}m\left(\frac{d\zeta}{dt}\right)^2 - \frac{1}{2}k\xi^2 - \frac{q^2}{2C(\xi)} \quad (1.51.1)$$

The expression for work is formulated by use of Eq. 1.50.24b. We recognize two nonconservative generalized forces: the exterior excitation by the acoustic field, $F(t)$ and the interior damper force $-b(d\xi/dt)$. In addition there are two generalized voltages: the external bias field e_0 and the internal voltage drop, $-R(dq/dt)$. Thus, the work expression is,

$$\left[F(t) - b\frac{d\xi}{dt}\right]\delta\xi + \left[C_o - R\frac{dq}{dt}\right]\delta q \tag{1.51.2}$$

Upon application of Eq. 1.51.1 and 1.51.2 to Lagrange's equations, 1.50.25, one obtains

$$\frac{d}{dt}(m\dot{\xi}) + k\xi - \frac{q^2(dC/dxi)}{2C^2(\xi)} = F(t) - b\frac{d}{dt} \tag{1.51.3a}$$

$$0 - \frac{q}{C(J\xi)} = e_o - R\frac{dq}{dt} \tag{1.51.3b}$$

The terms here which couple ξ and q are clearly in evidence.

Further progress in the analysis can be made if one assumes $C(\xi)$ to be given by Eq. 1.50.33. By rearrangement of terms the last two equations then reduce to,

$$m\dot{\xi} + bd\xi + k\xi + \frac{q^2}{2C_o d_o} = F(t) \tag{1.51.4a}$$

$$R\frac{dq}{dt} + \frac{(d_o + \xi)}{C_o d_o}q = e_o \tag{1.51.4b}$$

This coupled set is the goal of the variational analysis. Both of these coupled equations are seen to be nonlinear in the terms, q^2 and ξq The procedure for linearization, together with a more realistic analysis, is presented in Sect. 2.38.

B. Dynamical Equations of a Moving Coil Loudspeaker

The loudspeaker is modeled as a diaphragm, mass m, spring content k, damper b assumed to be ideally moving with the same velocity ξ. It is driven by the force of a voice coil generated by an applied voltage $E(t)$ acting through a resistance R and an inductance L. Its configuration is given by generalized coordinates of displacement and charge ξ, q.

The analysis begins with the variational principle Eq. 1.50.24a and the work expression 1.50.24b. Since the transduction does not involve the electric field the term We in the Lagrangian is omitted. The term which couples q and ξ is W_m^*, given by Eq. 1.50.39. Thus the Lagrangian of conservative press is

$$L = \frac{1}{2}m\dot{\xi}^2 - \frac{1}{2}k\xi^2 + L\dot{q}^2 + Bl\dot{q}(\xi - \xi_o) \tag{1.51.5a}$$

In the work expression we recognize two nonconservative mechanical forces namely the internal damping force $-bd\xi/dt$ and the reactive force $(-p_A S')$ of the acoustic pressure p_A over area S. There are in addition two nonconservative electromotive forces, the external applied voltage $E(t)$, and the internal voltage drop due to resistance R. For arbitrary variations δq and $\delta\xi$ one has:

$$(E(t) - R\dot{q})\delta q + [-b\dot{\xi} - paS]\,\delta\xi \tag{1.51.5b}$$

Application of Eqs. 1.51.5 to Lagrange's Eqs. 1.50.25, leads to the coupled set,

$$m\dot{\xi} + k\xi - Bl\dot{q} = -b\dot{\xi} - p_A S \tag{1.51.6a}$$

$$L\dot{q} + Bl\dot{\xi} = E(t) - R\dot{q} \tag{1.51.6b}$$

This coupled set is the goal of the variational analyses. It is a pair of ordinary differential equations with constant coefficients. In the steady state (time given by the real part of exp jωt) they can be reduced to the set,

$$-p_A S = Z_m \mathrm{v} - Bli \tag{1.51.7a}$$

$$E = Bl\mathrm{v} + Z_e i \tag{1.51.7b}$$

in which

$$Z_m = j\omega m + \frac{K}{j}\omega + b$$

$$Z_e = R + j\omega L$$

The reactive force of the medium is proportional to the diaphragm velocity,

$$p_A S = Z_A \mathrm{v} \tag{1.51.8}$$

Z_A = mechanical impedance (units: NS/m)

The electrical inpedence E/i obtained by eliminating v from Eqs. 1.51.7, shows the effect of the electromechanical coupling,

$$\frac{E}{i} = Ze + \frac{B^2 l^2}{Z_m + Z_A} (\text{units: } V/A) \tag{1.51.9}$$

A more realistic analysis of moving-coil transducers will be presented in Sect. 2.35.

To summarize: variational methods constitute powerful tools for extracting sets of dynamical equations that describe (coupled) transducer systems. Although applied to lumped parameter systems above; they are equally valid for distributed systems. Their use materially reduces the labor of analysis.

1.52 TRANSDUCER ANALYSIS VIA SIGNAL FLOW GRAPHS AND BLOCK DIAGRAMS

In previous sections of this treatise the representation of transducers by equivalent circuits was expressed by electric circuit analogies in which mass, spring, resistance-wave symbolized by conventional circuit symbols. Such methods are highly useful whenever the actual forces and velocities of internal components are needed in explicit form. The transducer designer may however want to focus his attention on overall output as a function of input. While it is true that an initial *formulation* of this goal may require knowledge of all intermediate forces and velocities, this requirement is dispensed with by reduction methods inherent in the technique of block diagrams and signal flow graphs.

Since all circuit representations are equivalent to relations between integral-differential equations it is useful to formulate the ***function*** of elements in a given circuit as an input-output statement. For conventional circuits the following rules apply:

1. in a series branch between two points 1, 0 the output is a current $i_1\ (t)$ and the input is a potential difference $\dot{e}_1(t) - e_0(t)$. For an RLC series branch,

$$i_1(t) = \frac{e_1(t) - e_0(t)}{R + L\frac{d}{dt} + \frac{1}{C}\int dt} \tag{1.52.1}$$

in which the circuit parameters are in operational form.

2. in a shunt branch (to ground) the output is the voltage to ground and the input is the net current. For an RLC shunt branch:

$$e_0(t) = \left[i_1(t) - i_2(t)\right]\left[R + L\,\frac{d}{dt} + \frac{1}{C}\int dt\right]$$

while for a $GC\Gamma$ parallel (shunt) system:

$$e_0(t) = \frac{i_1(t) - i_2(t)}{G + C\,\frac{d}{dt} + \Gamma\int dt}. \tag{1.52.2}$$

Figure 1.52.1 shows the two rules in schematic form:

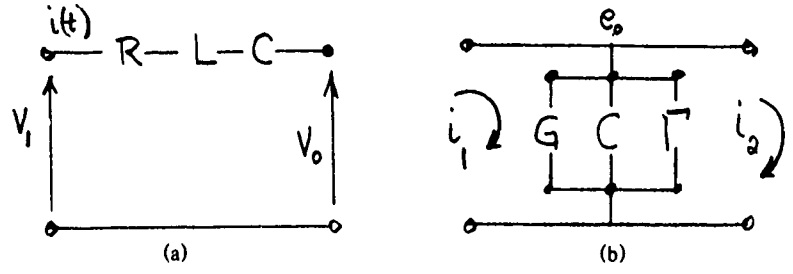


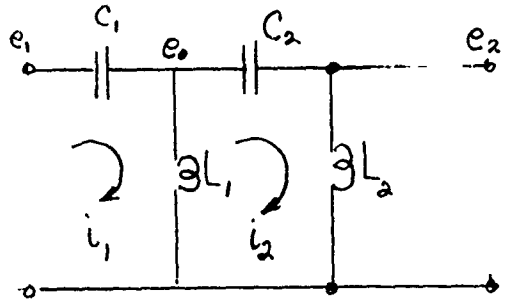
Fig. 1.52.1 — Illustration of input-output formulation of a circuit component, (a) series circuit, (b) parallel circuit

Eqs. 1.52.1 and 1.52.2 have the general form,

$$i_j = \sum_i T_{ji}\, e_i,\quad T_{ji} = \frac{1}{z_{ji}},\quad z_{ji} = R_{ji} + L_{ji}\,\frac{d}{dt} + \frac{1}{C_{ji}}\int dt$$

$$e_j = \sum_i U_{ji}\, i_i,\quad U_{ji} = \frac{1}{Y_{ji}},\quad Y_{ji} = G_{ji} + C_{ji}\,\frac{d}{dt} + \Gamma_{ji}\int dt. \tag{1.52.3}$$

From these equations one may construct a block diagram or a signal flow graph. A specific example illustrates the method. Figure 1.52.2 is a simple conventional 2-mesh electrical circuit. Applying the rules noted above one derives the equations in the figure.



$$i_1 = sC_1e_1 - sC_1e_0$$

$$e_0 = \frac{s}{\Gamma} i_1 - \frac{s}{\Gamma} i_2$$

$$i_2 = sC_2e_0 - sC_2e_2$$

$$e_2 = sL_2i_2.$$

Fig. 1.52.2 — A two-mesh network and its associated equations in which $s = j\omega$

A block diagram of this structure in which the operation of addition or subtraction is indicated by a circle (summing) symbol, and operation of multiplication is indicated by a rectangular box, is shown in Fig. 1.52.3.

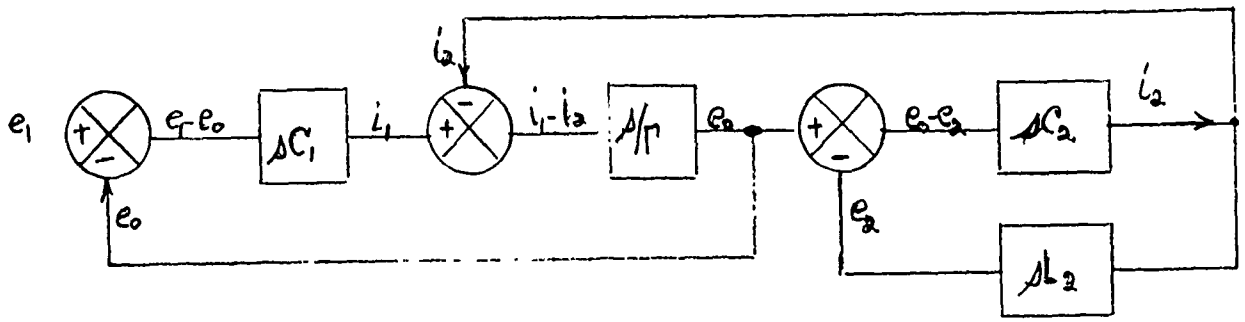


Fig. 1.52.3 — A block diagram of Fig. 1.52.2 in which operations called for by the associated equations are represented by circles and squares

A further simplification, derived again from Eqs. 1.52.3 is the signal flow graph. In this construction the symbols e_1, i_1, e_0, i_2, e_2 are interpreted as nodes and the symbols sC_1, s/Γ, sC_2, sL_2 are interpreted as directed lines or branches connecting the nodes. A straight line is first drawn and provided with nodes and branches, Fig. 1.52.4. On the branches are placed the branch *transmittance* symbols, sC_1, s/Γ, etc.

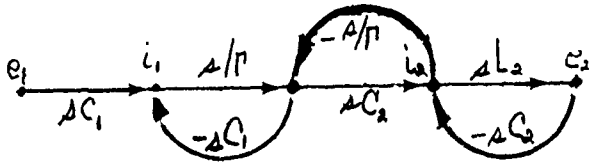


Fig. 1.52.4 — Signal flow graph of Fig. 1.52.2

The graph is read as follows: each node symbol multiplied by the directed branch symbol (= the branch *transmittance*) contributes to the node symbol in the arrow direction. *Only contributions entering a node are listed.*

The great advantage of the this representation is the ease with which the transfer function from input to output is obtained. This is done by a process of reduction of the flow graph. To illustrate the

method we sketch first a fictitious flow graph which features two distinct signal paths from input to output, Fig. 1.52.5.

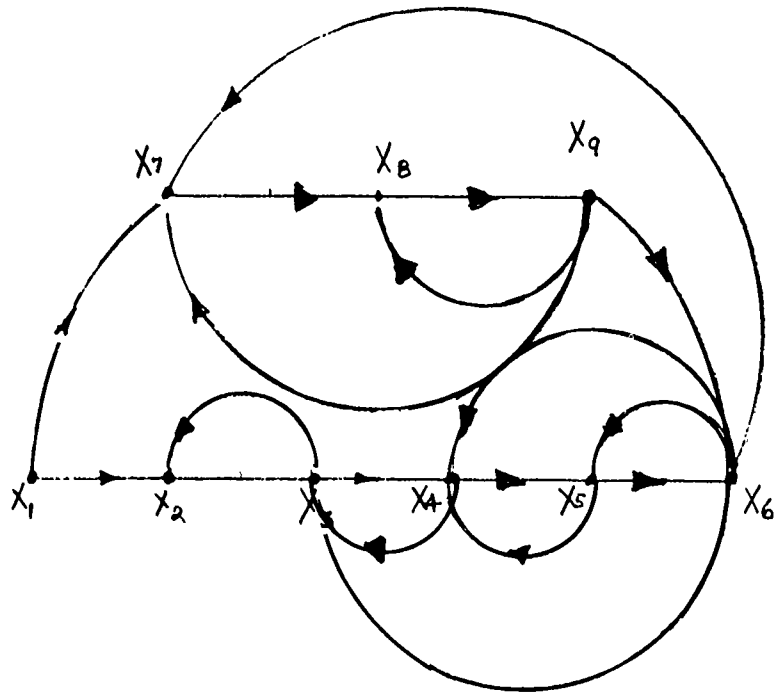


Fig. 1.52.5 – A signal flow graph which features two paths from input to output

The following steps will be needed to accomplish a reduction:

1. there are two signal paths ($j = 1, 2$) from input to output.

$j = 1$: $X_1 \rightarrow X_2 \rightarrow X_3 \rightarrow X_4 \rightarrow X_5 \rightarrow X_6$
$j = 2$: $X_1 \rightarrow X_7 \rightarrow X_8 \rightarrow X_9 \rightarrow X_6$

To each path assign a symbol of products:

$T_j = T_1\ T_2\ T_3\ T_4\ T_5$. For $j = 1$, $T_1 = T_{12}$; $T_2 = T_{23}$; $T_3 = T_{34}$; $T_4 = T_{45}$; $T_5 = T_{56}$.
$T_j = T_\alpha\ T_\beta\ T_\gamma\ T_\delta$. For $j = 2$, $T_\alpha = T_{17}$; $T_\beta = T_{78}$; $T_\gamma = T_{89}$; $T_\delta = T_{96}$.

2. in each path count the number of feedback loops:

in path $j = 1$ there are 6 feedback loops, hence 6 products of feedback transmittances:

loop 1. $X_2 \rightarrow X_3 \rightarrow X_2$, $T_6 = T_{23}\ T_{32}$

loop 2: $X_3 \rightarrow X_4 \rightarrow X_3$; $T_7 = T_{34}\ T_{43}$

loop 3: $X_3 \rightarrow X_4 \rightarrow X_5 \rightarrow X_6 \rightarrow X_3$; $T_8 = T_{34}\ T_{45}\ T_{56}\ T_{63}$

loop 4: $X_4 \rightarrow X_5 \rightarrow X_4$; $T_9 = T_{45}\ T_{54}$

loop 5: $X_5 \rightarrow X_6 \rightarrow X_5$; $T_{10} = T_{56}\ T_{65}$

loop 6: $X_4 \rightarrow X_5 \rightarrow X_6 \rightarrow X_4$; $T_{11} = T_{45}\ T_{56}\ T_{64}$.

A similar listing can be made for signal path 2.

loop 7: $X_7 \rightarrow X_8 \rightarrow X_9 \rightarrow X_7$; $T_{12} = T_{78}\ T_{89}\ T_{97}$
loop 8: $X_8 \rightarrow X_9 \rightarrow X_8$; $T_{13} = T_{89}\ T_{98}$
loop 9: $X_7 \rightarrow X_8 \rightarrow X_9 \rightarrow X_6 \rightarrow X_7$; $T_{14} = T_{78}\ T_{96}\ T_{67}$.

3. Count the number of nontouching feedback loops taken 2 at a time. These are,

in path 1: loops		; in path 2, loops 8,9
1, 4	2, 5	
1, 5	3, 4	
1, 6		

For the pair 1,4 one has the products $T_6\ T_9$

For the pair 1,5 one has the products $T_6\ T_{10}$

etc.

A similar listing can be made for signal path 2.

4. Count the number of nontouching feedback loops taken 3 at a time. In paths 1, 2 there are no groups of three which are nontouching.

5. Calculate Δg the graph determinant. This is defined as

$\Delta g = 1 -$ Sum of all independent feedback loop transmittances taken one at a time
$+$ Sum of all products of feedback *nontouching* loop transmittances taken two at a time
$-$ Sum of all products of feedback nontouching loops taken three at a time.

Here the words "feedback loop transmittance" means a product of the loop transmittances e.g., $T_{32}\ T_{23}$. Thus,

$$\Delta g = 1 - [\underbrace{T_6 + T_7 + T_8 + T_9 + T_{10} + T_{11} + T_{12}}_{\text{Path 1}} + \underbrace{T_{13} + T_{14}}_{\text{Path 2}}]$$

$$+ [\underbrace{T_6\ T_9 + T_6\ T_{10} + T_6\ T_{11} + T_7\ T_{10} + T_8\ T_9}_{\text{Path 1}} + \underbrace{T_{13}\ T_{14}}_{\text{Path 2}}]$$

6. Calculate Δj, $j = 1, 2$. By definition Δ_j is obtained by deleting all transmittances of feedback loops from Δg which "touch" path j. Thus,

$$\Delta_1 = 1 - [T_{12} + T_{13} + T_{14}] + [T_{13}\ T_{14}]$$

$$\Delta_2 = 1 - [T_6 + T_7 + T_8 + T_9 + T_{10} + T_{11}] + [T_6\ T_9 + T_6\ T_{10} + T_6\ T_{11} + T_7\ T_{10}].$$

The overall transfer function $G(s)$ defined as the ratio of output to intput (X_6/X_1) is found from the notation,

$$G(s) = \frac{1}{\Delta_g} \sum_j T_j \Delta_j = \frac{1}{\Delta_g} [T_1 \Delta_1 + T_2 \Delta_2].$$

The example of Fig. 1.52.2 will serve to illustrate this procedure. The steps are:

1. there is one signal path $X_1 \rightarrow X_2 \rightarrow X_3 \rightarrow X_4 \rightarrow X_5$. Thus $T_1 = T_{12}\ T_{23}\ T_{34}\ T_{45}$
2. there are three independent feedback loops

   $X_3 \rightarrow X_2 \rightarrow X_3$; $T_{32}\ T_{23}$

   $X_4 \rightarrow X_3 \rightarrow X_4$; $T_{43}\ T_{34}$

   $X_5 \rightarrow X_4 \rightarrow X_5$; $T_{54}\ T_{45}$
3. there are two nontouching feedback loops

   $$X_3 \rightarrow X_2 \rightarrow X_3;\ X_5 \rightarrow X_4 \rightarrow X_5$$
4. since all 3 feedback loops touch path from output to input $\Delta_j = 1$
5. the graph determinant is

   $$\Delta_g = 1 - (T_{32}\ T_{23} + T_{43}\ T_{34} + T_{45}\ T_{54}) + (T_{32}\ T_{23}\ T_{54}\ T_{45})$$
6. the overall transfer function is

$$G(s) = \frac{X_6}{X_1} = \frac{e_2}{e_1} = \frac{T_{12}\ T_{23}\ T_{34}\ T_{45}}{1 - (T_{32}\ T_{23} + T_{43}\ T_{34} + T_{45}\ T_{54}) + (T_{32}\ T_{23}\ T_{54}\ T_{45})}.$$

This result is the same as would be obtained by solving the equations of Fig. 1.52.2 for the ratio e_2/e_1.

To summarize: signal flow graphs and block diagrams can be used in transducer analysis to express graphical representations of the differential/integral relations between the dynamic response of components. Such representations help in finding transfer functions from input to output.

1.53 DYNAMICAL EQUATIONS OF TRANSDUCER OPERATION IN ABSTRACT FORM FOR SYSTEMS EXHIBITING COUPLING BETWEEN n-MESHES

Let the configuration of a transducer (that is, its 'state' in electrical, hydraulic, mechanical, acoustical chemical, etc. coordinates) be described by the generalized coordinates q_i, $i = 1, 2, \ldots$ and for each such coordinate let the generalized force be Q_i. The relation between Q_i and q_i can be expressed as operators L_{ij}, or inverse operators L_{ij}^{-1}, describing either static or dynamic force balance:

$$\text{(a)}\quad L_{ii}\, q_i + \sum_{j \neq i} L_{ij}\, q_j = Q_i, \quad i = 1, 2, \ldots n$$

$$\text{(b)}\quad L_{ii}^{-1}\, Q_i + \sum_{j \neq i} L_{ij}^{-1} Q_{ij} = q_i, \quad i = 1, 2, \ldots n \qquad (1.53.1)$$

In these equations the operators, generalized coordinates and generalized forces are all functions of space **x** and time t.

An example of Eq. 1.53.1 is the *single-mode* (lumped parameter) electrical-mechanical-acoustical transducer. Table 1.53.1 lists the generalized forces and coordinates of this system.

Table 1.53.1 — Single Mode (Lumped Parameter) Generalized System

Energy Field	Generalized Coordinate	Generalized Force
electrical	i (ampere)	E (volt)
mechanical	v (meter/sec)	F (Newton)
acoustical	u (meter^3/sec)	P (Newton/meter^2)
Inverse Description		
electrical	e (volt)	I (ampere)
mechanical	f (Newton)	V (meter/sec)
acoustical	p (Newton/meter^2)	U (meter^3/sec)

To display Eq. 1.53.1 in simple form we take time to be given by $\exp(-i\omega t)$ and choose a 3-mesh system. Then the operators are impedances and transduction factors:

$$\begin{cases} Z_{ee} i + T_{em}\,\mathrm{v} + T_{ec}\,u = E \\ T_{me} i + Z_m\,\mathrm{v} + T_{ma}\,u = F \\ T_{ae} i + T_{am}\,\mathrm{v} + z_{aa} u = P \end{cases} \tag{1.53.2}$$

In many transducers the volume velocity and the nominal component of surface velocity v are easily related to each other. For these cases the contributions $T_{ee}u$ and $T_{ma}u$ are incorporated into the terms containing v in the E and F equations. In the acoustical the term $T_{ae}i$ is not directly coupled to P, while the term T_{am}v is left as a boundary condition. Also, because acoustic pressure p is easily measurable while acoustic velocity is difficult to measure it is customary to use the inverse discription involving the inverse operator Y_{aa}. Thus Eqs. 1.53.2 reduce to two groups of equations, one for the transducer proper, and the other for the medium:

$$\begin{aligned} &\textit{transducer}: && \begin{cases} Z_{ee} i + T_{em}\mathrm{v} &= E \\ T_{me} i + Z_m \mathrm{v} &= F \end{cases} \\ &\textit{medium}: && Y_{aa}\, p \quad = Q \end{aligned}$$

An equivalent circuit of Eqs. 1.53.2 is sketched in Fig. 1.53.1.

1.54 ANALYSIS OF A MULTIMODE — MULTIELECTRODE PIEZOACTIVE SYSTEM BY USE OF GREEN'S FUNCTIONS

We now consider a piezoactive system which is distributed in spatial coordinate and has multiple force input. For simplicity in following the analysis we consider only one component of displacement and take it to be a function of one spatial coordinate (say x), and harmonic time $\exp(-i\omega t)$. Thus in Eq. (1.53.1) we set

$$L\, q(x, \omega) = Q(x, \omega). \tag{1.54.1}$$

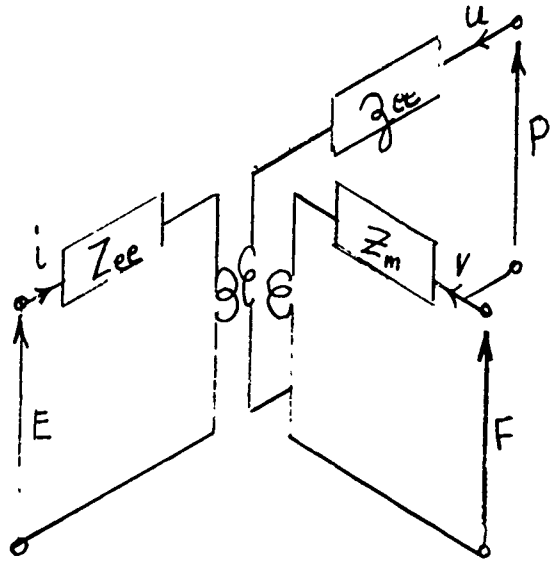


Fig. 1.53.1 — An equivalent circuit in the force/voltage/ pressure analogy of Eq. 1.53.2

To visualize a mult'force input we choose a piezoelectric bar with J electrode terminals and K mechanical terminals. A force developed by the j 'th applied voltage is designated $F_e^{(j)}$ (units: N/m^3), while the purely mechanical forces are designated $F_m^{(k)}$. Thus for displacemnt ζ (units. m)

$$\mathscr{L}\,\zeta(x,\,\omega) = \sum_{j}^{J} F_e^{(j)} + \sum_{k}^{K} F_m^{(k)} \tag{1.54.2}$$

$\mathscr{L}$ is an integro-differential operator (units: N/m^4). It is of second order involving longitudinal or torsional motion, or fourth order involving flexural motion. To keep the analysis within bounds we consider here only longitudinal motion. Equation (1.54.2) is an inhomogeneous equation which can be solved by use of the Green's function G. This is a function satisfying the boundary conditions $\zeta(x_i,\,\omega)$ (at $x = 0,\ X = l$) and the relation,

$$\mathscr{L}'\,G_\omega(x|x_0) = -\,\delta(x - x_0). \tag{1.54.3}$$

Here the operator $\mathscr{L}$ has been altered to $\mathscr{L}'$ in order to make G have the units of a displacement. Since the right hand side has the units of meter^{-1} it is (for the above reason) convenient to give force the same units. Thus we multiply both sides of Eqs. 1.51.1 or 1.51.2 by a constant α (units: m^2/N), and obtain,

$$L'\,\zeta(x,\,\omega) = \alpha[\sum_{j}^{J} F_e^{(j)} + \sum_{k}^{K} F_m^{(k)}] \tag{1.54.4}$$

in which the units of L' are m^{-2}. Thus the units of G_ω are meter, which is the same as displacement ζ. In the bounded realm $0 \leqslant x \leqslant l$, G_ω can be expanded in normalized eigenfunction ϕ_m (units: m$^{1/2}$/s) of longitudinal motion:

$$G_\omega\,(x|x_0) = \sum_{n} \frac{\phi_n\,(x)\,\phi_n\,(x_0)}{\omega_M^2 - \omega^2}. \tag{1.54.5}$$

The solution of Eq. (1.54.2) is then

$$\zeta\ (x,\ \omega) = \alpha \int\ G_\omega\ (x|x_0)\ Q\ (x_0,\ W)\ dx_0 \tag{1.54.6}$$

or

$$\zeta(x,\ \omega) = \alpha \int_0^l \sum_n^\infty \frac{\phi_n(x)\phi_n(x_0)}{\omega_m^2 - \omega^2} \left[\sum_j^J F_e^{(j)}(x_0) + \sum_k^K F_m^{(k)}(x_0)\right] dx_0. \tag{1.54.7}$$

This formula shows that the displacement at any point is a superposition of displacements due to all electrical and mechanical forces exerted over all the electrodes and at the ends.

We now specify more closely the nature of these forces as externally applied to the bar. First let us take the piezoelectric equations of state in matrix form to be:

$$\begin{aligned} &(a)\quad S = sT + dE \\ &(b)\quad D = dT + \epsilon E \end{aligned} \tag{1.54.8}$$

(see Sec. 2.5). Solving (a) for T and differentiating with respect to x one obtains

$$\frac{dT^{(j)}}{dx} = [s]^{-1}\ \frac{dS^{(j)}}{dx} - [s]^{-1}\ \frac{d}{dx}\ ([d]E^{(j)}). \tag{1.54.9}$$

Thus the external applied electrical forces are defined as

$$\frac{dT^{(j)}}{dx} = F_e^{(j)} = -[s]^{-1}\ \frac{d}{dx}\ ([d]E^{(j)}) \quad \text{(units: N/m}^3\text{)}. \tag{1.54.10}$$

It is noted that the force involving the strain is an *internal* force. In a similar way we can represent the applied mechanical forces. For simplicity let us take these forces to be,

$$F_m^{(k)} = -F_0\ \delta(x_0 - 0) + F_l\ \delta\ (x_0 - l). \tag{1.54.11}$$

(The minus sign in $-F_0$ is a convention).

With these expressions for the applied forces it is seen that the displacement at any point in the bar can be expressed as a sum of characteristic modes:

$$\begin{aligned} \zeta(x,\ \omega) = \alpha \int_0^l \sum_n^\infty \frac{\phi_n(x)\ \phi_n(x_0)}{\omega_n^2 - \omega^2} \left[\sum_{j=1}^J [-s]^{-1}\ \frac{d}{dx}\ ([d]\ E^{(j)}(x_0))\right] dx_0 \\ + \sum_n^\infty \{F_l\ \phi_n\ (l) - F_0\phi_n(0)\}\ \frac{\phi_n(x)}{\omega_n - \omega^2}. \end{aligned} \tag{1.54.12}$$

(We omit here all motion of center of mass.)

The electric current I_p in the p'th electrode is found by integrating the time-derivative of the electric displacement over the area of the p'th electrode,

$$I_p = -i\omega \oint D^{(p)}(x)\, dA(x).$$

From Eq. (1.54.8),

$$D = s^{-1}dS + (\epsilon - s^{-1}dd)E.$$

By definition

$$S = \frac{1}{2}\left[\frac{\partial \zeta_i}{\partial x_j} + \frac{\partial \zeta_j}{\partial x_i}\right] = \frac{d\zeta}{dx}.$$

Thus,

$$I_p = -i\omega \oint \left\{ s^{-1}\,[d]\,\frac{d\zeta_1^{(p)}(x)}{dx} + (\epsilon - s^{-1}\,[d][d])E^{(p)}(x) \right\} dA. \tag{1.54.13}$$

Here $\zeta^{(p)}(x)$ is obtained by differentiation of Eq. (1.54.12), and by restricting x to lie in the p'th electrode. Since the displacement over the coordinate x of the p'th electrode is due to *all* J voltages coupling to *all* n modes it is seen that one can define coupling factors A, B, C by performing the integrations called for in Eqs. (1.54.13) and (1.54.12). Then,

$$I_p = \sum_{n}^{\infty} \sum_{q=1}^{J} A_{pn}\, A_{nq}\, E^{(q)} + B_{pp}\, E^{(p)} + \sum_{n}^{\infty} (C_{pn}^{(1)}\, F_0 + C_{pn}^{(2)}\, Fl). \tag{1.54.14}$$

In this equation the terms on the right hand side are verbally interpreted to mean:

(a) ... the voltage $E^{(q)}$ on the qth electrode couples into the n'th mode which then develops a current in the p'th electrode. Summation overall modes gives the total contribution due to $E^{(q)}$. Summation over all electrodes gives the current due to electromechanical coupling ... ,

(b) ... the voltage $E^{(p)}$ develops a self current in the p'th electrode ... .

(c) ... the force F_0 couples into the nth mode which develops a current in the p'th electrode. Summation over all modes gives the total contribution due to F_0 ... .

In application to electroacoustic transduction it is a usual practice for one of the mechanical forces (say F_0) to be designed to be zero. The second mechanical force F_l is the acoustic reaction force and as such is absorbed into the first term. The electrical admittance Y_{pq} of the pth electrode due to the voltage $E^{(q)}$ on the q'th electrode is then derived to be:

$$\frac{\partial I_p}{\partial E^{(q)}} = Y_{pq} = \sum_{n}^{\infty} A_{pn}\, A_{nq} + B^{pp}\, \delta_{pq}. \tag{1.54.15}$$

The above scheme of analysis may be generalized. For example, if the displacement is a vector $\mathbf{q}$ (x, ω) with 3 components, all functions of one space coordinate, then we again use a constant α to modify the equations of motion so that

$$\mathscr{L}' \mathbf{q}(x, \omega) = \alpha \mathbf{Q}(x_0, \omega).$$

The solution can then be written in terms of a Green's dyadic G which satisfies the boundary conditions and the relation,

$$\mathscr{L}' G_w = -\mathscr{I}\delta(x - x_0), \quad \mathscr{I} = \text{idemfactor}.$$

The vector displacement solution is then

$$\mathbf{q}(x, \omega) = \alpha \int \mathscr{G}_\omega(x|x_0) \cdot Q(x_0)\, dx_0.$$

Similarly, if the displacement is a single component of flexure of a plate one uses a constant β (units: m/N) so that:

$$\mathscr{L}' q(x, y, \omega) = \beta\, Q(x_0, y_0, \omega)$$

$$\mathscr{L}' G_\omega(x, y|x_0, y_0) = -\delta(x - x_0)\delta(y - y_0)$$

$$q(x, y, \omega) = \beta \int\int G_\omega(x, y|x_0, y_0)\, Q(x_0, y_0, \omega)\, dx_0 dy_0.$$

In addition to (normal) forces Q there will possibly be bending moments $M(x,y)$ distributed over the plate, or along the edges. In many cases these are applied at points. For each, one has,

$$M(x, y) = M\delta(x - x_0)\,\delta(y - y_0).$$

The Green's function G_ω, or Green's dyadic G are expanded in orthornormal sets, chosen to be in conformity with the boundary conditions, and the expansions are used to construct the displacements, as already indicated in the method above.

STATE MODELS OF DISCRETE SYSTEMS

1.55 LOW FREQUENCY ACOUSTIC TRANSDUCTION

The generation of long wavelength sound for underwater applications in the frequency range below 200 Hz at other than trivial acoustic power requires large particle velocity in the medium and hence large displacements of the radiating surface of the generator. A survey of devices that can be efficiently driven to large displacements rules out the use of unmodified electroacoustic converters of the electrostrictive or magnetostrictive type such as are prevalent in high frequency generators. This is because of their inherent stiffness in the usual geometric form and sizes available (bars, rings, cylinders, etc.), resulting in unreasonable-size structures to supply the large energy storage needed. Often convenient modifications are devised to reduce stiffness reactance, such as sandwiching the piezoactive material between masses supplying inertial reactance, or using piezoactive material to drive plates or diaphragms in flexture. While feasible these structures generally are stress or electric field limited hence (may) generate inadequate power in reasonable-size packages.

Instead of these applications of high frequency technology to the alien demands of low frequency sound generation it has been a well justified practice for the designer of low frequency generators to

resort to discrete physical systems made up of an assembly of interconnected electrical, mechanical or hydraulic components that deliver the required large displacements at sufficient force to radiate long wavelength sound efficiently. Low frequency generators of sound therefore generally take on the appearance of electrical/mechanical/hydraulic *networks*.

Networks designed for transmission of high power are complicated multiloops, Fig. 1.2.1. The analysis of such systems for purposes of component optimization, prediction of performance, and interpretation of field experiment require the application of powerful tools of network theory. Often the networks can be simulated on an analog computer and all response characteristics of the original system studied in real time for selected choices of component parameters. Analog simulation of major components may however be difficult in cases where component performance is nonlinear, or exhibits negative resistance, or where the interconnection of components leads to mutual coupling, with coupling parameters that are frequency dependent. When networks have large numbers of components connected into many loops, it is more advantageous to employ the resources of digital computers to analyze their behaviour. The discipline of formulating a mathematical model of these networks is contained in the *Theory of Discrete Physical Systems*. The purpose of the following Sections is to outline the major concepts of this theory and show how they can be used to erect a mathematical model of a given system that can be submitted to efficient numerical calculation on a digital computer.

1.56 MEASUREMENT DIAGRAMS

A physical system (or network) can be considered an assembly of interconnected subsystems that, in turn, are assemblies (ultimately) of elementary components. To characterize components with a minimum number of mathematical symbols we consider the following procedure. When a subsystem is removed from a system there is laid bare all of its points of interconnection. These are the *vertices* of the subsystem (or component). A component that has n vertices is designated an n-terminal component. Each pair of terminals on an n-terminal component serves as a *port* through which power flows: one says that between the two vertices of a passive port there is resident at any time t an instantaneous power if a "driver" (actual or conceptual) is connected between them. Drivers are of two sorts: (1) the across-variable or e-driver, which maintains a specified time varying physical variable $E(t)$ across the two vertices of a port, or (2) a through-variable (or i-driver) which maintains a specified physical variable $I(t)$ flowing from one vertex to the second of the port. If a e-driver is connected across a port, it will cause the flow $i(t)$ of the through variable between the vertices. The instantaneous power in the port is then the product $W(t) = E(t)\ i\ (t)$. Since E or i may be negative this power $W(t)$ may be negative part of the time. If an i-driver is connected into (not across!) the vertices of a port it will induce an across-variable $e(t)$ across the vertices. The instantaneous power in the port is then $W(t) = e(t)\ I\ (t)$. Thus a port of a disconnected component can be characterized by the pair of numbers $E(t)$, $i(t)$, or (alternatively) $I(t)\ e(t)$, obtained by connecting a e-driver or an i-driver and measuring the variable that is complementary to the driver selected.

The measurement of $i(t)$ when $E(t)$ is specified, or $e(t)$ when $I(t)$ is specified is done by an *i-meter* or a e-meter respectively. Such meters are two-terminal devices that can give either positive or negative readings depending on how the terminals are connected to the vertices. Since a e-driver itself is a two terminal device, it is required that when $E(t)$ is specified to be positive at one of its terminals the e-meter connected to it must read positive. To insure this, manufacturers place a polarity sign (i.e., + sign) on one terminal of the e-meter which if connected to a e-driver at a time of positive $E(t)$ will read positive, or at the time $E(t)$ is negative, will read negative. Switching terminals will give a negative reading when $E(t)$ is positive, and a positive reading when $E(t)$ is negative. Similarly manufacturers fix the polarity of i-meters, generally by an arrow, such that when the through-variable is specified to flow in the direction of the arrow, the meter will read positive, whereas if it flows in the contrary direction, it will read negative.

Now when an *i*-driver with specified $I(t)$ is placed inbetween two vertices of a component and an associated *i*-meter reads positive at the time $I(t)$ is positive, the polarity sign of the *i*-meter can be inserted as an arrow connecting the two vertices and pointing in the direction of positive flow. Naturally when the flow reverses, the *i*-meter so connected is in correct orientation to give a negative reading. Furthermore, when the $I(t)$ is positive, a e-meter connected across the vertices should read positive induced $e(t)$ if its + terminal is connected to that vertex which is at the tail of the arrow already oriented to show positive flow. Thus a complete description of a terminal pair driven by an *i*-driver is an arrow stretching between the terminals, and a + sign at the tail of the arrow. (It is important to note this arrow is a *measurement sign of a single port:* it is not a system sign indicating flow in the connected network). Similarly when this same terminal-pair is driven by a e-driver having a specified $E(t)$ at one of its own terminals, *a* + sign is placed on that terminal of the terminal-pair connected to $E(t)$, and an arrow is stretched from this + sign polarized vertex to the other vertex to indicate that an *i*-meter will read positive when the induced $i(t)$ is positive, and negative when the induced $i(t)$ is negative.

Thus each terminal-pair of a component can be represented as an *oriented line* called an edge between two vertices, and a + sign, Fig. 1.56.1. Associated with this edge is a e-number $e(t)$ indicating the magnitude of the induced across-variable resulting from an applied *i*-driver, $I(t)$; and an *i*-number, $i(t)$, indicating the magnitude of the induced through-variable resulting from an applied e-driver, $E(t)$. Figure 1.56.1 represents any terminal pair of an *n*-terminal component. In particular, it represents a 2-terminal component of a network. It is called a measurement diagram of a terminal-pair of one edge and two vertices.

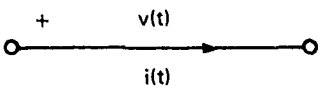


Fig. 1.56.1 — A terminal pair represented by an oriented line

The measurement diagram forms the basis for construction of a mathematical model of the terminal pair. This is done by plotting the *measured* induced $i(t)$ versus the driver $E(t)$, for the range of t under consideration; or plotting the measured induced $e(t)$ versus the driver $I(t)$, for the range of t under consideration. The plots thus obtained can generally be cast in the idealized mathematical form,

$$e(t) = Z\{I(t)\};\ i(t) = Y\{E(t)\}$$

in which Z and Y are integro-differential operators. These equations constitute the mathematical model of the terminal-pair, with Z, Y fully known by experiment.

From the method of constructing Fig. 1.56.1 we can infer that a component with *n*-terminal pairs can be represented by a connected graph of $n - 1$ oriented lines. Figure 1.56.2 shows a measurement diagram of a 4-terminal graph. There are three terminal-pairs (or oriented lines), three induced e-variables, e_1, e_2, e_3 and three induced *i*-variables i_1, i_2, i_3. The mathematical model for such an *n*-terminal component relates a column vector of applied e-drivers $\mathbf{E}(t)$ with a column vector $\mathbf{i}(t)$ of induced *i*-variables; or alternatively, a column vector of applied *i*-drivers $\mathbf{I}(t)$ with a column vector of induced v-variables. The model becomes,

$$\mathbf{i}(t) = \mathrm{Y}\,\mathbf{E}(t);\ \mathbf{e}(t) = \mathrm{Z}\,\mathbf{I}(t).$$

The symbols Z, Y are now a matrix of integral-differential operators with elements Z_{pg}, Y_{pg} respectively. These are determined (as before) by measurement. First each terminal-pair of the component

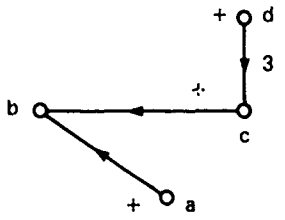


Fig. 1.56.2 — A measurement diagram of a 4-terminal graph

is provided with its own *i*-driver (I_1, I_2, ... I_n). To measure Z_{p1}, $p = 1, 2 \ldots n$, all the I_q are set to zero (that is, the *i*-drivers are *open-circuited*) except $I_1(t)$, and the plots of $e_1(t)$, $e_2(t) \ldots e_n(t)$ versus $I_1(t)$ are made. The slopes of these plots at specific time t_1 are the values of $Z_{11}(t)$, $Z_{21}(t_1)$, etc. The process is then repeated for each I_q until all Z_{pq} are obtained. These values of Z_{pq} are called the *open-circuit parameters* of the component equations. Secondly, each terminal-pair of the component is provided with its own e-driver (E_1, $E_2 \ldots$, E_n). To measure Y_{p1}, $p = 1, 2 \ldots n$, all E_q are set to zero (that is, the e-drivers are *short-circuited*) except E_1, and plots of $i_1(t)$, $i_2(t) \ldots . i_n(t)$ versus $E_1(t)$ are made. The slopes of these plots at specific time t_1 are the values of $Y_{11}(t_1)$, $Y_{21}(t_1) \ldots Y_{n1}(t_1)$. The process is then repeated for each E_q until all Y_{pg} are obtained. These values of Y_{pg} are called the *short-circuit parameters* of the component equations. Figures 1.56.3(a)-3(c) illustrate the method.

In summary we see that the mathematical model of each terminal-pair is constructed by exciting with *i*– (or *e*–) drivers and measuring the induced $e(t)$ or $i(t)$ variables as functions of time. Since this procedure can always be carried out it is a well-justified assumption in network analysis that the mathematical model of each terminal-pair is known.

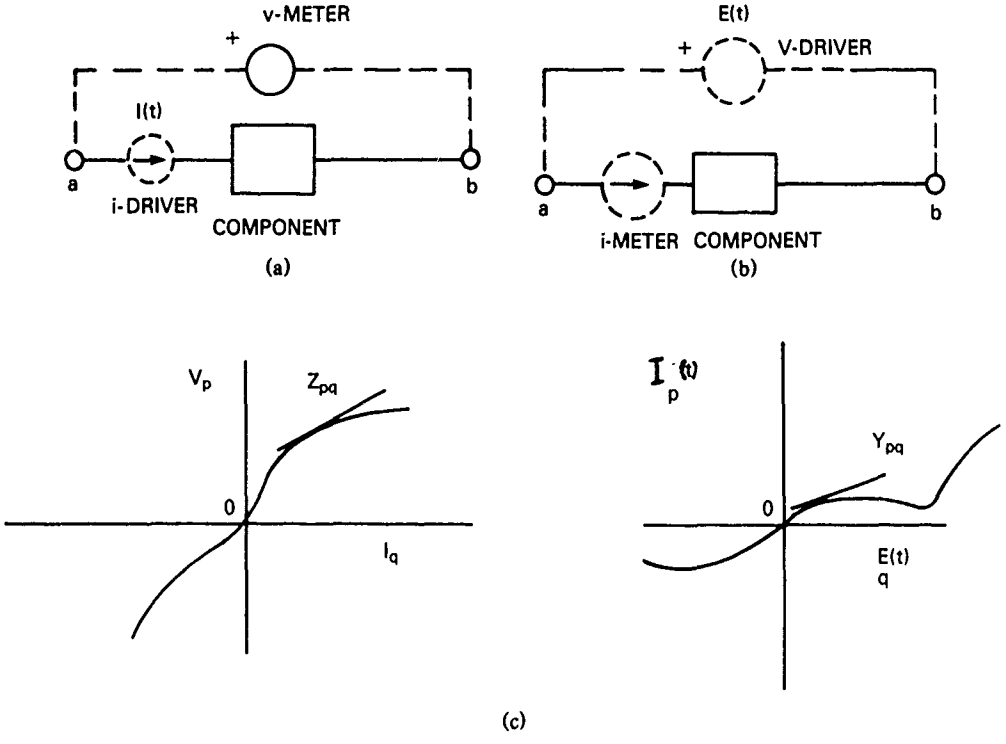


Fig. 1.56.3 — Procedure for obtaining measurement graphs (a) open circuit parameters (b) short circuit parameters (c) measurement of slopes

1.57 IDEALIZED TERMINAL-PAIRS AND THEIR COMPONENT-EQUATIONS

The graphical plots of $i(t)$ versus $E(t)$, and $e(t)$ versus $I(t)$ that constitute the model of the terminal pairs can be approximated by algebraic, differential or integral equations. With sufficient idealization it is found that three distinct types of terminal pairs can be described. In the first, or *dissipator* type, the slope of measured $i(t)$ versus $E(t)$ is a constant over an extended range of time, making this a G-terminal pair with an algebraic component equation. The dissipator also has a constant slope of $e(t)$ versus $I(t)$, and is then called an algebraic R-terminal pair. In the second, or *C-storage type*, the slope of $i(t)$ versus $dE(t)/dt$ is a constant, C (alternatively $\int_{t_1}^{t_2} idt$ versus $[E(t_2) - E(t_1)]$ is a constant C). In the third, or *L-storage type*, the slope of $e(t)$ versus dI/dt is a constant L (alternatively, the slope $\int_{t_1}^{t_2} edt$ versus $[I(t_2) - I(t_1)]$ is a constant L). While a terminal-pair is idealized as an R (or G), C, or L type, it generally partakes in real fact of a mixture of types. When a combination of these three types in a terminal-pair cannot be neglected, its mathematical model is a sum of them, as for example, in the presence of a e-driver, the induced i-variable of a combined type is given by,

$$i(t) = (G + C\frac{d}{dt})E(t)$$

Similarly in the presence of an i-driver the induced v-variable of a combined type is given by,

$$e(t) = (R + L\frac{d}{dt})I(t)$$

Although components may have n-terminals, the 2-terminal component has served as building blocks for analysts of discrete systems. Table 1.57.1 lists the building blocks of 2-terminal hydraulic, electric and mechanical system modeling that are of focal interest here:

Table 1.57.1 — Two-Terminal Components

System	e-variable	i-variable	K-Component	L-Component	C-Component
Hydraulic	p	$\dot{g}$	$p = R_h\dot{g}(t)$	$p = H\frac{d\dot{g}}{dt}$	$\dot{g} = C_h\frac{dp}{dt}$
Electric	e	i	$\mathrm{v} = R_m i$	$\mathrm{v} = L\frac{di}{dt}$	$i = C\frac{d\mathrm{v}}{dt}$
Translational Mechanical	$\dot{\delta}$	f	$\dot{\delta} = \frac{1}{B_f} f$	$\dot{\delta} = \frac{1}{k}\frac{df}{dt}$	$f = M\frac{d\dot{\delta}}{dt}$
Rotational Mechanical	$\dot{\theta}$	T	$\dot{\theta} = \frac{1}{B_T} T$	$\dot{\theta} = \frac{1}{k}\frac{dT}{dt}$	$T = J\frac{d\dot{\theta}}{dt}$

p = pressure (Newton/meter^2)
$\dot{g}$ = volume flow (meter^3/sec)
$\dot{\delta}$ = mechanical velocity (meter/sec)
f = mechanical force (Newtons)
e = electric potential (volts)
i = electric current (ampere)
$\dot{\theta}$ = anguiar velocity (radians/sec)
T = torque (Newton-meter)

The symbols R_h, H, B_f, B_T are defined by the equations in which they appear. These building blocks are clearly descriptive of linear small amplitude models, suitable in modeling small departures of the variables from an *operating point* on a e-variable versus i-variable plot. They are helpful in constructing

first models of large systems-models that can later be modified to include large amplitude effects. It is noted that the building blocks are couched in differential form only. This is done with the object of constructing models that can be numerically evaluated on digital computers which can execute numerical differentiation faster, with less error in given time then numerical integration. Thus in an n-terminal component those terminal-pairs that are L-component are written with open circuit parameters Z_{pq}, and those that are C-component are written with short circuit parameters Y_{pq}. This method of writing the component equations has additional advantages to be discussed in the following sections.

1.58 MIXED (OR HYBRID) COMPONENT EQUATIONS

The generic form of the equations of a multiterminal component derived earlier had the form,

$$\mathbf{e}(t) = \mathrm{Z}\{\mathbf{I}(t)\};\ \mathbf{i}(t) = \mathrm{Y}\{E(t)\}.$$

We assume now that the vector $\mathbf{e}$ can be partitioned into e-variables that pertain only to types R, L terminal pairs, forming subvector $\mathbf{e}_2$, and the remainder forming $\mathbf{e}_1$. Similarly we assume the vector $\mathbf{i}$ can be partitioned into a subvector $\mathbf{e}_1$ whose elements pertain only to types G, C terminal pairs, and the remainder $\mathbf{i}_2$. Thus, in accordance with this partition, the model is written,

$$\begin{bmatrix}\mathbf{e}_1\\ \mathbf{e}_2\end{bmatrix} = \begin{bmatrix}\mathrm{Z}_{11} & \mathrm{Z}_{12}\\ \mathrm{Z}_{21} & \mathrm{Z}_{22}\end{bmatrix}\begin{bmatrix}\mathbf{I}_1\\ \mathbf{I}_2\end{bmatrix};\quad \begin{bmatrix}\mathbf{i}_1\\ \mathbf{i}_2\end{bmatrix} = \begin{bmatrix}\mathrm{Y}_{11} & \mathrm{Y}_{12}\\ \mathrm{Y}_{21} & \mathrm{Y}_{22}\end{bmatrix}\begin{bmatrix}\mathbf{E}_1\\ \mathbf{E}_2\end{bmatrix}.$$

The $\mathrm{e} - I$ set constitutes the open-circuit model, and the $i - E$ set constitutes the short-circuit model. We first solve for $\mathbf{I}_1$ in terms of $\mathbf{e}_1$ and $\mathbf{I}_2$, then substitute the result into the equation for $\mathbf{e}_2$ to obtain,

$$\begin{bmatrix}\mathbf{I}_1\\ \mathbf{e}_2\end{bmatrix} = \begin{bmatrix}\mathrm{H}_{11} & \mathrm{H}_{12}\\ \mathrm{H}_{21} & \mathrm{H}_{22}\end{bmatrix}\begin{bmatrix}\mathbf{e}_1\\ \mathbf{I}_2\end{bmatrix};\ \begin{matrix}\mathrm{H}_{11} = Z_{11}^{-1};\quad \mathrm{H}_{12} = \mathbf{Z}_{11}^{-1}\mathbf{Z}_{12}\\ \mathrm{H}_{21} = \mathbf{Z}_{21}Z_{11}^{-1};\ H_{22} = -Z_{21}Z_{11}^{-1}Z_{13} + Z_{22}\end{matrix}.$$

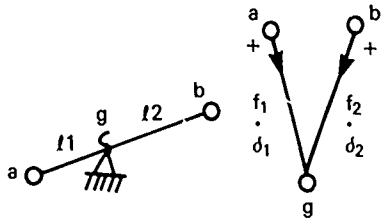
This is an intermediate set of equations and has the drawback that applied and induced variables appear together on the left hand side. However we apply a *reciprocity theorem* for power flow in a physical system which states that the roles of driver variables and induced variables can be interchanged in a linear passive system. Leaving the discussion of reciprocity for Sects. 1.46 and 1.48, we proceed to rewrite the above set of equations, replacing $\mathbf{I}_1$ by $\mathbf{i}_1$ and $\mathbf{e}_1$ by $\mathbf{E}_1$:

$$\begin{bmatrix}\mathbf{i}_1\\ \mathbf{e}_2\end{bmatrix} = \begin{bmatrix}\mathrm{H}_{11} & \mathrm{H}_{12}\\ \mathrm{H}_{21} & \mathrm{H}_{22}\end{bmatrix}\begin{bmatrix}\mathbf{E}_1\\ \mathbf{I}_1\end{bmatrix}.$$

By comparison of this set with the $\mathbf{i} - \mathbf{E}$ set of component equations it is seen that some elements of the H matrix have open-circuit parameters (e.g., H_{22}), and others have short-circuit parameters (e.g. H_{11}). This set is therefore called the mixed (or hybrid) component equations.

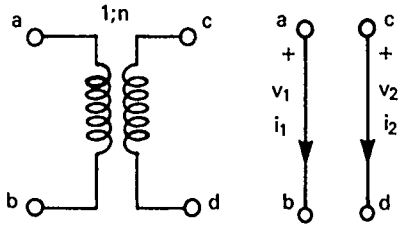
Several forms of hybrid equations play an important role in the modeling of multiterminal components. For example, setting $\mathrm{H}_{11} = 0 = \mathrm{H}_{22}$ and $\mathrm{H}_{21} = -H_{12}^{T}$ (T = symbol of transpose) leads to a mathematical model of a *linear perfect coupler*, exemplified by the common lever in mechanical systems and the transformer in electrical systems. Figure 1.58.1 shows the lever modeled as a 3-terminal coupler, and Fig. 1.58.2 shows the transformer as a 4-terminal coupler.

Note that in Fig. 1.58.2 if the measurement diagram with vertices c, d had been modeled with reversed polarity, the negative sign in the matrix of the component equations would have been changed to a positive sign, indicating a flow of the through variable toward vertex c on the assumption that the through variable is flowing away from a. In perfect couplers the H (or "coefficient") matrix is skew-



$$\begin{bmatrix} f_1 \\ \dot{d}_2 \end{bmatrix} = \begin{bmatrix} 0 & \frac{\ell_2}{\ell_1} \\ -\frac{\ell_2}{\ell_1} & 0 \end{bmatrix} \begin{bmatrix} \dot{d}_1 \\ f_2 \end{bmatrix}$$

Fig. 1.58.1 — Lever modeled as a 3-terminal coupler



$$\begin{bmatrix} v_2 \\ i_1 \end{bmatrix} = \begin{bmatrix} 0 & n \\ -n & 0 \end{bmatrix} \begin{bmatrix} i_2 \\ v_1 \end{bmatrix}$$

Fig. 1.58.2 — Transformer modeled as a 4-terminal coupler

symmetric (i.e., the diagonal elements are zero and the off-diagonal elements have opposite signs). From this it is concluded that the net power input to the component vanishes, at least in the ideal models of Figs. 1.58.1 and 1.58.2. In more realistic models mechanical friction and mass (or electrical friction and energy storage) make the diagonal elements nonzero and therefore make the power input finite.

We return now to the $i - \mathcal{E}$ (i.e., short-circuit) model and make the Y matrix skew-symmetric,

$$\begin{bmatrix} \mathbf{i}_1 \\ \mathbf{i}_2 \end{bmatrix} = \begin{bmatrix} 0 & Y_{12} \\ -Y_{12}^T & 0 \end{bmatrix} \begin{bmatrix} \mathbf{E}_1 \\ \mathbf{E}_2 \end{bmatrix}$$

Contrary to ideal transformers the i-variable here transforms to a e-variable, i.e., there is a variable switch. This set of equations describes the *ideal-gyrator* model, ideal because the net power input to the model vanishes, and gyrator because the equations (by switching its variables) closely resemble those of a mechanical gyroscope under simplifying comditions. By making the drivers E_1, E_2 belong to *different physical systems* the designer can adopt the gyrator to serve as a model of transduction devices. For example [7] a hydraulic ram converts fluid pressure into mechanical force. Figure 1.58.3 shows a schematic diagram of the ram driven by an incompressible fluid and loaded by a restraining spring, together with its associated measurement diagram. By choosing the hydraulic v-driver as the pressure $P_2(t)$ and the mechanical v-driver as the velocity $\dot{\Delta}_1(t)$, an elementary gyrator model can be written in the form,

$$\begin{bmatrix} f_1 \\ \dot{g}_2 \end{bmatrix} = \begin{bmatrix} 0 & A \\ -A & 0 \end{bmatrix} \begin{bmatrix} \dot{\Delta}_1 \\ P_2 \end{bmatrix}$$

in which A is the area of the piston subject to pressure P_2. In this model the mechanical force flows from the piston plunger A to ground B while the hydraulic fluid flows from inlet C to outlet D. The negative sign in the coefficient matrix Y is explained in this way: if terminal-pair *cd* is made part of a closed loop, the flow of $\dot{g}$ (as drawn) is clockwise, while the flow in a closed loop constructed on terminal-pair *ab* would be counterclockwise. Thus the mechanical displacement is made to be opposite in sign to the hydraulic flow.

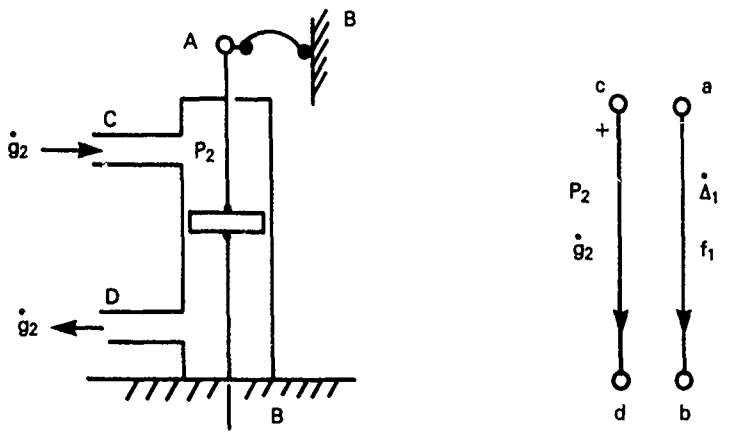


Fig. 1.58.3 — Hydraulic ram illustrating construction of a measurement diagram

1.59 ENERGY-CONVERSION TRANSDUCERS AS TWO-PORT COMPONENTS

Energy conversion transducers may be modeled as a $e - I$ (i.e., open-circuit parameter) two-port set. Taking variables with subscript 1 to refer to the first physical system and subscript 2 to refer to the second physical system, we write the component equations in the general form

$$e_1 = V_1(I_1, I_2)$$

$$e_2 = V_2(I_1, I_2).$$

Here, as before, e_1, e_2 are induced variables, and I_1, I_2 are driver variables. In most physical systems the driver variables operate in the vicinity of an *operating point.* We designate these points with subscript 0. Near the operating point the component equations may be formulated as expansions in Taylor series, viz., for

$$e_1 = V_1(I_{01}, I_{02}) + \frac{\partial V_1}{\partial I_1}(I_{01}, I_{02})(I_1 - I_{01}) + \frac{\partial V_1}{\partial I_2}(I_{01}, I_{02})(I_2 - I_{02})$$

$$+ \frac{1}{2}\frac{\partial^2 V_1}{\partial I_1^2}(I_{01}, I_{02})(I_1 - I_{01})^2 + \frac{1}{2}\frac{\partial^2 V_1}{\partial I_2^2}(I_{01}, I_{02})(I_2 - I_{02})^2$$

$$+ \frac{1}{2}\frac{\partial^2 V_1}{\partial I_1 \partial I_2}(I_{01}, I_{02})(I_1 - I_{01})(I_2 - I_{02}) + \ldots.$$

plus a similar expansion for e_2. Since most transducers are required to be linear, these Taylor series must be terminated with the linear terms. Considering *incremental* values only we formulate the two-port component equations as the set,

$$e_1 = \frac{\partial V_1}{\partial I_1} I_1 + \frac{\partial V_1}{\partial I_2} I_2$$

$$e_2 = \frac{\partial V_2}{\partial I_1} I_1 + \frac{\partial V_2}{\partial I_2} I_2.$$

This general set of coupled equations is very nearly universally used to describe two-port energy-conversion transducers.

As an application we review the construction of the measurement diagram for an electromechanical transducer. The *i*-drivers (called I_1, I_2 above) are taken to be the applied electric current I and the applied mechanical force F. The induce variables are taken to be the terminal voltage e, and the mechanical velocity $\dot{\delta}$. From standard theory [8] the e – *I* set in *linear steady-state approximation* of an electromechanical transducer is written as,

$$\begin{bmatrix} e \\ \dot{\delta} \end{bmatrix} = \begin{bmatrix} Z_e - \dfrac{T_{em}}{Z_m} & \dfrac{T_{em}}{Z_m} \\ -\dfrac{T_{me}}{Z_m} & \dfrac{1}{Z_m} \end{bmatrix} \begin{bmatrix} \mathrm{I} \\ \mathrm{F} \end{bmatrix}.$$

T_{em} = transduction coefficient, electrical-to-mechanical

T_{me} = transduction coefficient, mechanical-to-electrical

Z_m = mechanical impedance.

To study this set further we neglect the main diagonal terms and write the component equations in the very simplified form,

$$(1)\ e = \frac{T_{em}}{Z_m}\,\mathrm{F} \qquad (2)\ \dot{\delta} = -\frac{T_{me}}{Z_m}\,\mathrm{I}.$$

If $T_{me} = T_{em}$ (as in electrostatic and piezoelectric transducers), the coefficients on the right hand side of these equations have opposite signs, making the original coefficient matrix from which they are drawn antisymmetrical. If $T_{me} = -T_{em}$ (as in moving-conductor, moving armature, and magnetostrictive), the coefficients have the same sign, making the original coefficient matrix symmetrical. The measurement diagram for both symmetrical and antisymmetrical cases is the same, Fig. 1.59.1. Here vertex *b* is the electrical ground (or reference) and vertex *d* is the physical ground (or reference). According to definition the e – *I* set of equations in antisymmetrical form describes a gyrator. Thus *electrostatic and piezoelectric transducers are gyrators* when modeled by e – *I equations that use mechanical force and electrical current as through variables.*

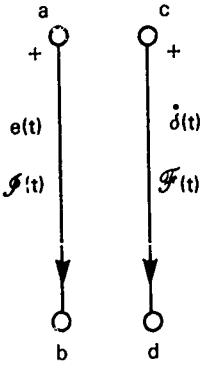


Fig. 1.59.1 — Gyrator modelled as a 2-port

Electromechanical transducers can also be modeled by e − *I* equations that use applied electrical current I and applied mechanical velocity $\dot{\Delta}$ as through variables. In this case the simplified component equations (obtained by neglecting the main diagonal of the coefficient matrix) are,

$$(1)\ e = T_{em}\dot{\Delta};\ (2)\ f = T_{me}\mathrm{I}.$$

If $T_{em} = T_{me}$ (as in electrostatic or piezoelectric transducers), the coefficients have the same sign, making the original coefficient matrix symmetrical. If $T_{em} = -T_{me}$ (as in moving conductor, moving armature, or magnetostrictive transducers) the original coefficient matrix is unsymmetrical. Thus with the choice $\dot{\Delta}$ and I as through variables the mathematical models of the latter type of transducers describe gyrators.

When a gyrator is energized by an energy input to port *ab* (Fig. 1.59.1) part of this remains resident in *ab*, and part is coupled to port *cd*. The ratio of energy instantaneously stored in *cd* to that stored in *ab* is a number equal to or less than unity. Of course the total energy in the system is always equal to the energy input. At unity ratio the coupling coefficient is said to be 1 00. If no energy of *ab* is coupled into *cd*, this coefficient is zero. The phenomenon of coupling on gyrators is analogous (*but not identical!*) to the coupling of two coils of an electrical transformer. If all the flux of one coil threads all the turns of the second coil the coupling coefficient is 1.00. If on the other hand the flux of one coil completely bypasses the second coil the coupling coefficient is zero. In gyrators the partition of energy between *ab* and *cd* is more than geometrical (as in electrical transformers). It is *physical* in the sense that energy partition depends on the physical properties of the component ports of the system. Coupling phenomena are discussed in Sects. 1.33, 1.34, 1.35, 1.37 through 1.42.

In sum: energy converting two-ports (i.e., transducers) that are modeled with unsymmetric coefficient matrices are gyrators. By interchanging the mechanical through-variable with the mechanical across-variable the model is given a symmetric matrix, and loses its gyrator character. The chief advantage in constructing models with symmetric coefficient matrices is the knowledge that it will always be possible to find electric network representations of these two-port energy converters that are reciprocal, and hence physically realizable. However, for machine computation of component equations (say on digital computers) the electrical network equivalent is an unnecessary step in making an analysis. A discussion of this assertion is taken up in the next sequence of Sections.

1.60 STATE SYSTEMS, SYSTEM GRAPHS, TREES AND COTREES

In the previous section components have been modeled as collections of terminal pairs, some of which are connected with common vertices (such as couplers) and others are uncoupled, i.e., they exist as separate parts (such as gyrators or transducers). Components modeled with separate parts are typically different physical systems that are coupled by fields (gravitational, electromagnetic, chemical, etc.), such as the transducers discussed above. A collection of components connected among themselves at some, but not necessary all, common vertices form a system. In general such a system will have *P* parts, that is, *P* subsystems, that are related to each other not by common vertices but only by physical fields. A system of *P* parts will have *N* vertices and *E* edges, the latter corresponding to the edges of the individual components. Since each edge is associated with an unknown *i*-variable and an unknown e-variable it is seen that there are a total of 2 *E* variables to be solved for in the analysis of the system The component equations that relate each e to each *i* of a terminal pair clearly provide *E* equations towards the required solution. The basic problem in analysis of discrete systems is to generate an additional set of *E* equations to complete the solution. Although several techniques have been used by analysts of discrete systems, we will employ here the method of *linear graphs*. While a full account of the system of linear graphs is a vast undertaking, we can with great profit consider certain key features that are suitable to the formulation of system equations, delaying the problem of solving them to later discussions.

We consider then a general discrete physical system of E edges, N vertices and P parts. Some of the edges taken together form closed loops, while the remaining ones do not. If a path of edges is sequentially traced through every vertex of a selected part in such a way that no closed loops are formed, the path so obtained is a *tree* of that part. Its edges are labeled *branches.* The edges not included in the tree form together the cotree. Its edges are labeled *chords.* In contrast to trees, cotrees may have closed loops. A system of P parts has a forest of trees, and a coforest of cotrees. It is important to note that the formation of trees and cotrees is not a unique process. In large systems the number of possible trees is very great. However there is an *optimum tree* (and cotree) whose choice simplifies the analysis of the system. Optimum tree selection will be discussed later in the presentation of examples and in Sect. 1.64

The formation of trees and cotrees enables the analyst to combine pertinent features of each and form from them E *equations of constraint* (or E *system Equations*). Of these a number are constructed from closed loops of banches and chords. They are the *circuit equations.* The remainder are constructed from conditions of vertices. They are the "*supernode*" (or "cutset") equations. The E system equations complement the E component equations. Together they provide the 2E equations needed to solve for the E unknown induced e-variables and the E unknown induced f-variables of the edges of the system.

1.61 CIRCUIT EQUATIONS ON THE ACROSS-VARIABLES

Figure 1.61.1a shows a system of $P = 2$ parts, $E = 10$ edges, and $N = 8$ vertices. One forest (not necessarily optimum) of this system may be constructed by deleting branches 2, 7, 8 of part $P = 1$, and branch 10 of $P = 2$. The forest then has one tree Fig. 1.61.1b made up of branches 3, 4, 5, 6, 1 and a second tree made up of branch 9. The total number of branches is $N - P = 6$. The coforest of this system is shown in Fig. 1.61c. One cotree is constructed of chords 2, 7, 8 and the second cotree is constructed of chord 10. The total number of chords of the coforest is $E - (N - P) = 4$ chords.

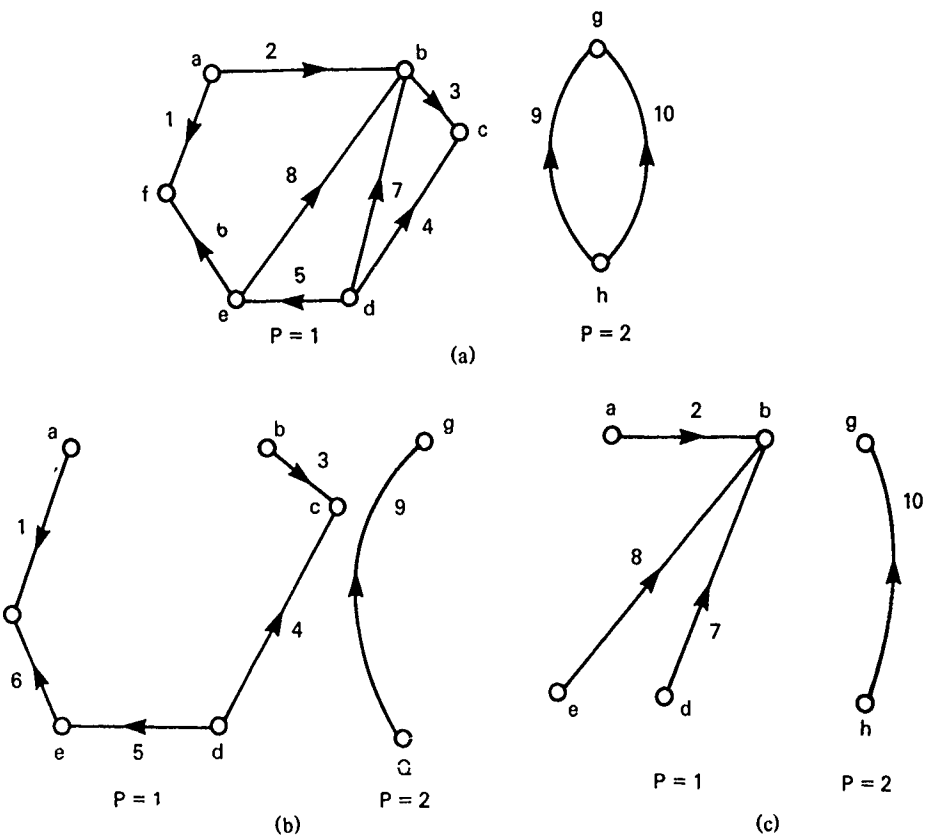


Fig. 1.61.1 — (a) A system of components (b) one tree of (a) (c) coforest of (b).

The system graph thus depicted with its associated forest and coforest are now in a form to permit construction of the circuit equations The procedure is this. to form a circuit equation one takes a single chord from the coforest and restores it to its correct position in the associated tree. This restoration creates a closed loop, from which one circuit equation can be constructed. For example, if chord 2 is restored to part 1, a closed loop of edges 2, 3, 4, 5, 6, 1 is formed. We call this (arbitrarily) circuit 1. Similarly the restoration of chord 10 to the original tree makes up closed loop 10, 9 which is called circuit 2. Chord 8 generates closed loop 8, 3, 4, 5 on the original tree which is circuit 3. Finally, chord 7 generates circuit 7, 3, 4. The circuits formed in this way are called *fundamental circuits.* Their total number is equal to the number of chords in the coforest, viz. $E - (N - P) = 4$.

Every circuit must be assigned be a *loop orientation*, clockwise or counterclockwise. A convenient convention is to assign the orientation of the chord that closes the loop. Thus circuit 1 is oriented clockwise, circuit 2 is counterclockwise, circuit 3 and 4 are both clockwise. Since the edges in a circuit are themselves oriented, the directions of some will agree, and others disagree, with the polarity assigned to the loop. A useful label of agreement or disagreement of edge j of circuit i is the symbol β_{ij}. It is assigned a value of $+1$ if there is agreement, -1 if there is disagreement, and 0 if the edge j is not in circuit i. For the four circuits of the selected forest (and coforest) the *circuit row vectors* may be displayed as a *circuit matrix* B:

							(branches)			
	$j =$ 3,	4,	5,	6,	1,	9	2,	10,	8,	7
circuit 1 = 2, 3, 4, 5, 6, 1: $\beta_{1j} =$	[1	−1	1	1	−1	0	1	0	0	0]
circuit 2 = 10, 9: $\beta_{2j} =$	[0	0	0	0	0	−1	0	1	0	0]
circuit 3 = 8, 3, 4, 5: $\beta_{3j} =$	[1	−1	1	0	0	0	0	0	0	0]
circuit 4 = 7, 3, 4: $\beta_{4j} =$	[1	−1	0	0	0	0	0	0	0	1]

This display has the following (useful) but not obligatory characteristics: (1) the circuits begin with their generating chord, (2) the components of vector $\boldsymbol{\beta}$ begin with a list of branches and end with a list of chords, (3) the listing of the chords is in the same order as the corresponding chords in the list of circuits, (4) all branches and all chords of the selected forest are listed.

The construction of the circuit row matrix B enables the analyst to formulate $E - (N - P)$ circuit equations on the across-variable vector $\mathbf{e} = (e_1, e_2 \ldots e_{10})$. They obey Kirchoff's loop law which states that,

$$\mathbf{Be} = 0; \text{ or } \sum_{j=1}^{10} \beta_{ij}\, e_j = 0,\ i = 1,\ 2,\ 3,\ 4.$$

Since B is a 4 row × 10 column matrix, it is seen that this set of equations supplies only 4 independent relations among the across-variables e. Noting that the matrix B is partitioned into branch and chord sections B_b, B_c it is useful to partition the across-variable vector into $\mathbf{e}_b$ and $\mathbf{e}_c$ respectively. The circuit equations in matrix form then read,

$$[B_b,\ B_c] \begin{bmatrix} \mathbf{e}_b \\ \mathbf{e}_c \end{bmatrix} = 0$$

or

$$\mathbf{e}_c = -(B_c^{-1} B_b)\mathbf{e}_b.$$

The matrix formulation of the circuit equations thus leads to the very important conclusion that the across-variables of the cotree are uniquely related to the across-variables of the tree.

In sum: Selecting a forest (and coforest) from the system graph and construction of all the circuit equations from it generates $E - (N - P)$ equations of the total number of E equations required to analyze the system. There still remain $N - P$ equations of constraint to be constructed. These constitute the "cutset" or "supernode" equations which are now to be discussed.

1.62 SUPERNODE (OR CUT SET) EQUATIONS ON THE THROUGH-VARIABLES

We return to the system graph Fig. 1.61.1a and select the forest shown in Fig. 1.61.1b. It will be advantageous to consider one tree of this forest at a time. Let this be the tree of part P1. In general this tree will have J vertices and $J - 1$ branches. Here $J - 1 = 5$ branches. The procedure for forming a "supernode" equation on a selected tree is as follows: first, one *edge* of the tree (but not its associated vertices), is deleted, leaving the tree in two pieces (note: one of the pieces can be an isolated vertex). In each piece all the vertices are collapsed to form one "supernode." The result is then two "supernodes" which are identified by the labels of the collapsed (original system) vertices. For example, in Fig. 1.61.1b deletion of edge 6 results in two pieces that when collapsed yield the two supernodes *af* and *bcde*. Second, the two supernodes are connected by all the edges in the *original* system graph that run from any vertex labeled in one supernode to a vertex labeled in the second supernode. Examination of Fig. 1.61.1a shows two such edges, namely 6, 2. This set of edges is called a "cutset" and is labeled (arbitrarily say) "cutset" 5, and written as (6, 2). After formation of a cutset the deleted edge is restored. The process is then repeated by selecting a second edge of the tree, and proceeding in the same manner to form a second cutset. In this way, for the tree shown in Fig. 1.61.1b, Part 1, the cutsets are determined to be:

Cutset 1, on edge 1: (1, 2)
Cutset 2, on edge 3: (3, 2, 7, 8)
Cutset 3, on edge 4: (4, 2, 7, 8)
Cutset 4, on edge 5: (5, 2, 8)
Cutset 5, on edge 6: (6, 2)

All cutsets must be assigned a *supernode orientation*, that is, a positive direction pictured as an arrow running from one supernode to the second. A convenient convention is to assign the direction of the generating edge of the selected tree to be the orientation of the cutset. For example the cutset formed on edge 1 is oriented positive in the direction of the arrow of edge 1. If this cutset is depicted as in Fig. 1.62.1, the positive direction is as shown. This assigned orientation of the cutset to be with the same as the generating edge of the set causes the remaining edges of the set to agree with, or disagree with that orientation. To record this condition one constructs a cutset matrix A with row vector α [9] in the following manner. Let the particular cutset be labeled subscript i where $i = 1, 2, \ldots (N - P)$ (i.e., N = number of vertices of the system graph and P = the number of parts), and let the edges of the cutset be labeled subscript $j (j = 1, 2 \ldots E)$. Assign to each edge the number $\alpha_{ij} = 1$ if the edge j is in the cutset i and its direction agrees with the assigned orientation; and $\alpha_{ij} = -1$, if this edge disagrees with the assigned orientation. If edge j is not in cutset i, assign the number $\alpha_{ij} = 0$. Using these rules one finds the cutset matrix A to be:

		(branches)						(chords)			
	j	= 1,	3,	4,	5,	6,	9	2,	7,	8,	10
Cutset 1 (6, 2):	α_{ij}	= 1	0	0	0	0	0	1	0	0	0
Cutset 2 (3, 2, 7, 8):	α_{2j}	= 0	1	0	0	0	0	−1	−1	−1	0
Cutset 3 (4, 2, 7, 8):	α_{3j}	= 0	0	1	0	0	0	1	1	1	0
Cutset 4 (5, 2, 8):	α_{4j}	= 0	0	0	1	0	0	−1	0	−1	0
Cutset 5 (6, 2):	α_{5j}	= 0	0	0	0	1	0	1	0	0	0
Cutset 6 (9, 10):	α_{6j}	= 0	0	0	0	0	1	0	0	0	1

The mode of display of the cutset matrix A has the same characteristics of matrix partitioning as that of the circuit matrix B. It is seen to be an $N - P$ row by an E column matrix.

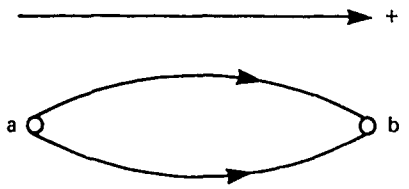


Fig. 1.62.1 — Assignment of orientation of a cutset

The construction of the cutset matrix A allows one to form the cutset (or supernode) equations of the system through-variables $\mathbf{i} = (i_1, i_2, \ldots i_E)$. They are analogs of Kirchoff's node laws,

$$\mathrm{A}\mathbf{i} = 0, \text{ or } \sum_{j=1}^{E} \alpha_{ij} i_j = 0, \; i = 1, 2, \ldots (N - P).$$

Partitioning A into branch matrix A_b and chord matrix A_c, and (similarly) partitioning $\mathbf{i}$ into branch $\mathbf{i}_b$, and chord $\mathbf{i}_c$, one can restate the cutset equations in the form,

$$\mathbf{i}_b = -\mathrm{A}_b^{-1}\mathrm{A}_c i_c \text{ or } (i_b)_p = \sum_{q=1} \sum_{r=1} (A_b^{-1})_{pq} (A_c)_{qr} (i_c)_r.$$

From this matrix formulation comes the very important conclusion that the through-variables of the cotree uniquely determine the through-variables of the tree. It is seen from them that a total of $N - P$ cutset equations can be made available for a system of N vertices and P parts.

The construction of the cutset equations completes the formulation of the problem of analyzing a system of E edges. On hand are 2 E equations for determing the E unknown e-variables, and the E unknown i-variables of the system. In the formulation the following point is to be emphasized:

The component equations that constitute half of the total number of equations needed are mathematical models of the components *as they exist in unconnected form.* The models are determined by connecting ideal e or i-drivers to their terminal pairs and *measuring* the induced variables. When these components are connected into a system, each terminal pair is excited by its mating pair: the induced variables then depend on each other. This dependence, or interconnection, of the system variables is accounted for by the circuit and cutset equations.

1.63 THE PRIMARY MATHEMATICAL MODEL

We gather together the results of the previous sections to present the *Primary Mathematical Model* of a discrete physical system represented by a system graph of E edges, N vertices and P parts. First we list the equations of the components into which the system can be broken down. As discussed we can write them in open-circuit or short-ciruit form. For passive components these are:

open circuit: $\mathbf{e} = (\mathrm{R} + \mathrm{L}\frac{d}{dt} + \mathrm{C}^{-1}\int dt)\mathbf{i}$

$$\mathbf{e} = (e_1, e_2 \ldots e_E); \; i = (i_1, i_2, \ldots i_E)$$

short circuit:

$$\mathbf{i} = (G + \mathrm{C}\frac{d}{dt} + \mathrm{L}^{-1}\int dt)\mathbf{v}.$$

Here R, L, C^{-1}, G and L^{-1} are matrices. Other components of the system may be active. They are represented by a set of equations of the form:

$$\text{e-sources} \quad \mathbf{e}_d = E$$
$$\text{i-sources} \quad \mathbf{i}_d = \mathbf{J}$$

The quantities **E** and **J** are specified (i.e., known apriori). The total number of passive and active component equations is equal to the number of edges E.

In addition there are E system equations. As discussed, these are obtained by selecting a forest of trees of the system graph (plus an associated coforest) and constructing $E - (N - P)$ circuit equations,

$$\mathbf{e}_c = -(\mathbf{B}_c^{-1}\mathbf{B}_b)\mathbf{e}_b$$

and $N - P$ cutset equations,

$$\mathbf{i}_b = -\mathbf{A}_b^{-1}\mathbf{A}_c i_c$$

These together with the component equations form the 2 E equations of the primary model. From them all of the system variables can be found.

1.64 THE STATE MODEL

The E component equations of the Primary Mathematical Model have been formulated as integro-differential equations in time. In combination with the E system equations they pose a severe problem of solution to the numerical analyst. Modern numerical analysis seeks (wherever possible) to exploit the tremendous resources of the digital computer to make the handling of large system possible. With the aim of adapting the $2E$ equations of the Primary Mathematical Model to digital computer routines it has been a widespread practice to write these equations in differential (or algebraic) form only. The primary model is thus modified, and the derived (or secondary) model is called the *State Model* of the System.

To begin the construction of the state model we first seek to reduce the 2E equations to a minimal set, the solution of which determines all the remaining variables of the system. To accomplish this end we begin by selecting from the system graph a special tree called the *maximally selected tree* [10] whose definition and properties we discuss below. Associated with this tree is the maximally selected cotree. We next chose a special set of variables, called the *primary variables*, consisting of the $N - 1$ across-variables ($= \mathbf{e}_b$) of this tree and the $E - N + 1$ through-variables ($= \mathbf{i}_c$) of the associated cotree, to form a total of E unknown variables. The primary variables can be considered the components of a vector Ψ, e.g.,

$$\Psi = (\mathbf{e}_b, \mathbf{i}_c).$$

This defines the *state vector* of the system variables. The complementary set of variables ($\mathbf{e}_c$, $\mathbf{i}_b$) constitute the *secondary variables* of the system. The state vector contains the unknown variables to be solved for. Since the branch variables $\mathbf{e}_b$ uniquely determine the chord variables $\mathbf{i}_c$ through the circuit equations, and the chord variables $\mathbf{i}_c$ uniquely determine the branch variables $\mathbf{i}_b$ through the cutset equations it is seen that the determination of the state vector leads directly to the determination of all the unknown variables of the system. The state vector obeys a first order ordinary differential equation;

$$\frac{d}{dt}\Psi = \mathrm{P}\Psi + \mathrm{Q}\Psi_0$$

in which P, Q are matrices, and Ψ_0 is a vector whose components are sources (active drivers, and/or initial conditions). This equation is the *state model* corresponding to the selected maximal tree.

A tree is said to be maximally selected if (1) in the algebraic component equations (i.e. the *R*-component equations) the primary variables are explicit functions of the secondary variables, $\mathbf{v}_b = \mathbf{R}\mathbf{i}_b$ (2) in the differential component equations the time derivatives of the primary variables are explicit functions of the secondary variables, $d\mathbf{e}_b/dt = C^{-1}i_b$ (3) the number of differential equations is optimally maximum. A practical application of these rules leads to the requirement that the tree is maximally selected if all the *C*-component edges and e-drivers are in the tree, all the *L*-component edges and *i*-drivers are in the cotree, all the algebraic equations in the tree are of the form $\mathbf{e}_b = \mathbf{R}\mathbf{i}_b$, and all the algebraic equations of the cotree are in the form $\mathbf{i}_c = \mathbf{G}\mathbf{e}_c$. The maximum number of state equations is then equal to the number of storage components in the system graph.

Assuming the tree of the system graph is maximally selected we may construct the state model in the following steps. First, the state vector Ψ is formulated to contain as many vector components (say n of them) as there are energy-storage terminal pairs in the system graph. Of these there will be group of m across-variables $(\mathrm{e}_1, \mathrm{e}_2 \ldots \mathrm{e}_m)$, followed by a group of n-m through-variables $(i_{m+1}, i_{m+2} \cdots i_n)$, so that the vector appears as,

$$\Psi = (\mathrm{e}_1, \mathrm{e}_2, \ldots \mathrm{e}_m \mid i_{m+1}, i_{m+2} \ldots i_n).$$

Second we select the storage-component equation in the across-variable e_1, namely $d\mathrm{e}_1/dt = C^{-1}i_1$, and modify it by expressing i_1, in terms of $(i_{m+1}, i_{m+2}, \ldots i_n)$, *using the cutset equations*, in the process. The result is

$$\frac{d\mathrm{e}_1}{dt} = C^{-1}f(i_{m+1}, i_{m+2}, \ldots i_n).$$

Upon assuming the function f is linear in the first power of the i's we arrive *by this equation at* the required state model for the terminal pair corresponding to edge No. 1. In a similar manner all of the time derivatives of the edge across-variables e, subscripted 2 to m can be expressed in terms of the through variables i_{m+1} up to i_n.

Following the completion of the state models in the across variables we take up the storage-component equations in the through variables $(i_{m+1}, i_{m+2} \ldots i_n)$, the first being $di_{m+1}/dt = L^{-1}\mathrm{e}_{m+1}$. This is modified by expressing e_{m+1} in terms of $(\mathrm{e}_1, \mathrm{e}_2, \ldots \mathrm{e}_m)$ by *use of the circuit equations*—a procedure that leads to the equation,

$$\frac{di_{m+1}}{dt} = L^{-1}g(\mathrm{e}_1, \mathrm{e}_2, \ldots \mathrm{e}_m).$$

Again, by assuming the function g to be linear in the first power of the e's we arrive (by this equation) at the state model equation for i_{m+1}. By repetition of the process all of the time derivatives of the primary variables in i can be expressed in terms of the primary variables in e.

Upon assembly of all of the modified equations derived above the complete state model is formed and appears as the ordinary vector differential equation:

$$\frac{d}{dt}\begin{bmatrix} e_1 \\ e_2 \\ \vdots \\ e_m \\ \hline i_{m+1} \\ i_{m+2} \\ \vdots \\ i_n \end{bmatrix} = \begin{bmatrix} p_{11} & p_{12} & \cdots & p_{1m} \\ & & & \\ p_{m1} & p_{m2} & \cdots & p_{mm} \\ \hline p_{m+1} & p_{m+1,2} & \cdots & p_{m+1,n} \\ & & & \\ p_{n1} & p_{n2} & \cdots & p_{nn} \end{bmatrix} \begin{bmatrix} e_1 \\ e_2 \\ \vdots \\ e_m \\ \hline i_{m+1} \\ i_{m+2} \\ \vdots \\ i_n \end{bmatrix} + \begin{bmatrix} \cdot \\ \mathscr{I}_2 \\ \vdots \\ \mathscr{I}_m \\ \hline \mathscr{V}_{m+1} \\ \mathscr{V}_{m+2} \\ \vdots \\ \mathscr{V}_n \end{bmatrix}$$

or

$$\frac{d}{dt}\Psi = P\Psi + D, \quad D = Q\,\Psi_0.$$

Here we have added to the state model a vector **D** whose elements consist of the i-drivers $I_1, I_2 \ldots$, assigned by the analyst to be in the cotree, and the e-drivers, V, assigned to be in the tree. The elements p_{ij} of the matrix P are two-terminal or multiterminal R, L, C, G parameters. Although initially the tree variables $\mathbf{e}_b$ and cotree variables $\mathbf{i}_c$ were selected to be the primary variables of the system graph it is seen that the employment of the circuit equations and the cutset equations incorporates the R and G parameters of the algebraic equations into the component differential equations. It is the latter set that constitutes the state model. Thus the state model contains only the primary variables $(\mathbf{e}_b)_C$ of the energy-storage components of the tree and the primary variables $(\mathbf{i}_c)_L$ of the energy-storage components of the cotree. The primary variables $(\mathbf{e}_b)_R$ associated with R-components of the tree, and the primary variables $(i_c)_G$ of the cotree are not in the state model explicitly. However, though not in the state model, $(\mathbf{e}_b)_R$ and $(i_c)_G$ are determined when $(\mathbf{e}_b)_C$ and $(i_c)_L$ of the state model are successfully solved for.

In a system that is simultaneously driven by both i-drivers and e-drivers it is possible to obtain a solution by superposition, provided the system is linear. In this case the e-drivers are first short-circuited and a solution is obtained with all i-drivers in place. Then the i-drivers are open-circuited and a solution is obtained with all the e-drivers in place. The two solutions are then added to obtain the same result as would have been obtained if a solution was sought with both types of drivers acting simultaneously.

Whenever it is not possible to incorporate all the e-drivers and all the C-components in a single tree, or all the i-drivers and L-components in the corresponding cotree, the state model will not contain the maximum number of e-elements of the tree and i-elements of the cotree in the state vector. In that case one selects at least one C-component (say $\mathbf{e}_q$) in the tree (with all e-drivers) and one L-component (say i_n) in the cotree (with all i-drivers), and from these one constructs a 2-component state vector $\Psi = (e_q, i_r)$. This is the minimum-dimension state vector, leading to a state model made up of two (energy-storage) dynamic equations, together with a sufficient number of system equations to provide a complete solution by repeated substitutions. Often the state vector can be enlarged to contain as many C-components as possible in the tree, leaving the remaining C-components aside to serve as constraints: plus as many L-components as possible in the cotree, leaving the remaining L-components to also serve as constraints. While not maximally selected the tree will nevertheless provide a basis of solution.

In addition it is important to note that in constructing the state model one must not use those circuit equations that contain the e-variables corresponding to i-drivers, nor the cutset equations that contain the i-variables corresponding to the e-drivers. These omitted equations are accounted for by the presence of the constraint equations of the e-drivers and i-drivers.

1.65 EXAMPLES OF CONSTRUCTION OF STATE MODELS

The construction of state models is illustrated in the following examples. It will be clear from them that the selection of the "maximum" tree is simple in many cases. It should be recognized however that counter-examples can be forwarded in which it is not possible to make this selection. For these cases the analysis though possible is not optimally executed.

Example 1.65.1

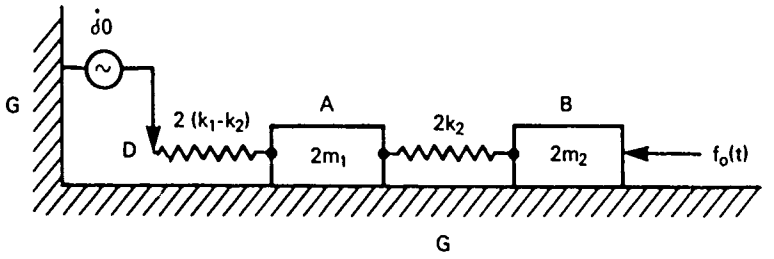


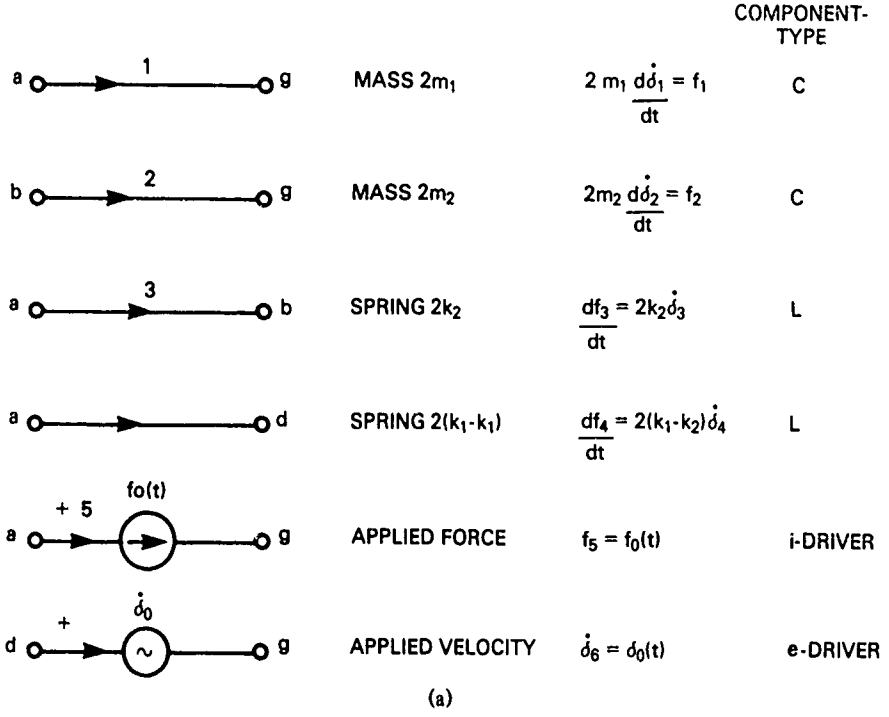
Fig. 1 65.1 — Translational mechanical system to illustrate construction of a state model

Figure 1.65.1 shows a translational mechanical system consisting of two masses connected by a spring, one of the masses ($2m_1$) being itself elastically restrained by a second spring attached to a moving foundation. We neglect the effects of friction and acoustic radiation in this model. The device is driven by an external force $f_0(t)$ acting on mass $2m_2$, and an external driver of displacement $\delta_0(t)$ acting on spring 2 $(k_1 - k_2)$. To construct the system graph we proceed formally by listing the measurement diagram and associated equation of each component. The latter by definition, is disconnected from the system. This listing is shown in Fig. 1.65.2a. The vertices of the diagrams are a, b, g, d with g being "ground." In Fig. 1.65.2b the components are shown assembled by coalescing corresponding vertices. Note that in this diagram we trace the "velocity drops" in the system. From this connection diagram the system graph is then constructed (Fig. 1.65.2c). In this system there are two C-components (edges 1, 2), two L-components (edges 3, 4), a e-driver (edge 6) and an i-driver (edge 5). To form the state model we select the tree 6, 1, 2 (i.e., a e-driver and two C-components), shown in Fig. 1.65.2d. The corresponding cotree with edges 4, 3, 5 is shown in Fig. 1.65.2e. The primary variables are $\dot{\delta}_1$, $\dot{\delta}_2$ of the tree and f_3, f_4 of the cotree. We first construct the circuit equations and the cutset equations of the system:

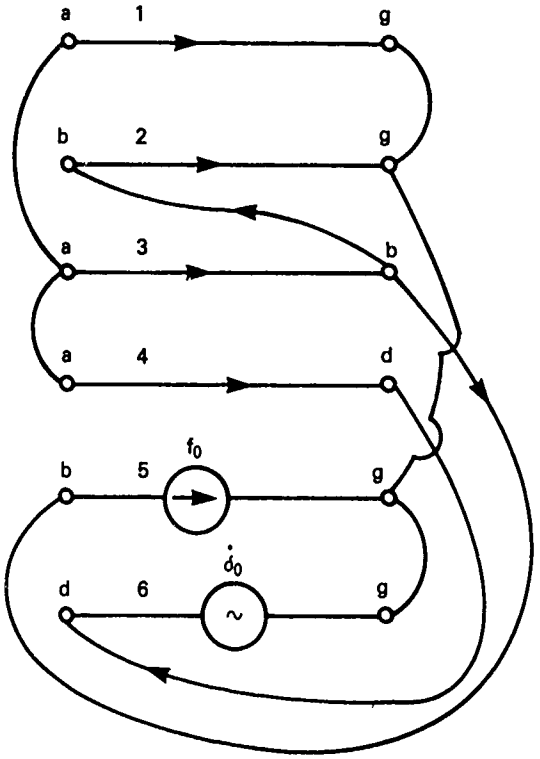
$$\begin{array}{ll} \text{circuit (4, 6, 1):} \quad \dot{\delta}_4 + \dot{\delta}_6 - \dot{\delta}_1 = 0 & \text{cutset (6, 4):} \quad f_6 = f_4 = 0 \\ \text{circuit (3, 2, 1):} \quad \dot{\delta}_3 + \dot{\delta}_2 - \dot{\delta}_1 = 0 & \text{cutset (1, 3, 4):} \quad f_1 + f_3 + f_4 = 0 \\ \text{circuit (5, 2):} \quad \dot{\delta}_5 - \dot{\delta}_2 = 0 & \text{cutset (2, 5 3):} \quad f_2 - f_3 + f_5 = 0 \end{array}$$

Since $\dot{\delta}_5$ is the across variable of a *specified* f_5, the circuit (5, 2) cannot be used as a constraint. Also since f_6 is the through variable of a *specified* across-variable, the cutset (6, 4) cannot be used as a constraint. There remain therefore four equations of constraint plus two equations of specified drivers. The state model, directly obtainable by substituting the equations of constraint into the components equations, reduces to the form:

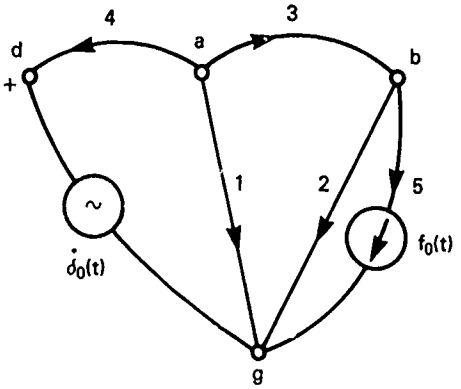
$$\frac{d}{dt}\begin{vmatrix} \dot{\delta}_1 \\ \dot{\delta}_2 \\ f_3 \\ f_4 \end{vmatrix} = \begin{vmatrix} 0 & 0 & -\frac{1}{2M_1} & -\frac{1}{2M_2} \\ 0 & 0 & \frac{1}{2M_1} & 0 \\ 2k_2 & -2k_2 & 0 & 0 \\ 2(k_1 - k_2) & 0 & 0 & 0 \end{vmatrix} \begin{vmatrix} \dot{\delta}_1 \\ \dot{\delta}_2 \\ f_3 \\ f_4 \end{vmatrix} + \begin{vmatrix} 0 \\ -f_0(t)/2M_2 \\ 0 \\ -2(k_1 - k_2)\dot{\delta}_0 \end{vmatrix}$$



(a)



(b)



(c)

Fig. 1.65.2 — Construction of system graph (a) listing if components (b) assembly of components (c) system graph. Note: these are *VF* charts.

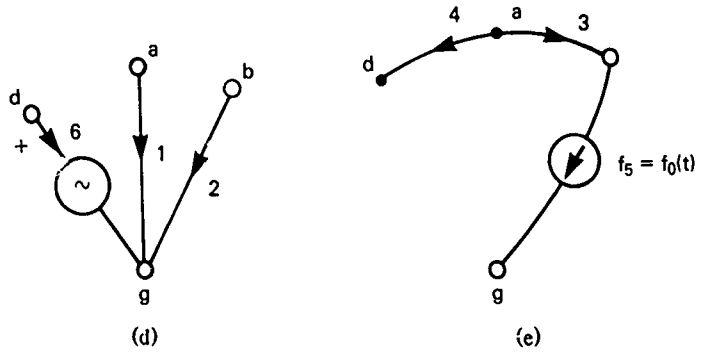


Fig. 1.65.2 — (d) tree of (c) (e) cotree of (c)

This model is suitable for machine computation. The equations of motion of the two masses (edges 1, 2) can easily be constructed from the state model by writing the component equations of the springs in the form.

$$f_3 = 2k_3\delta_3; \quad f_4 = 2(k_1 - k_2)\delta_4$$

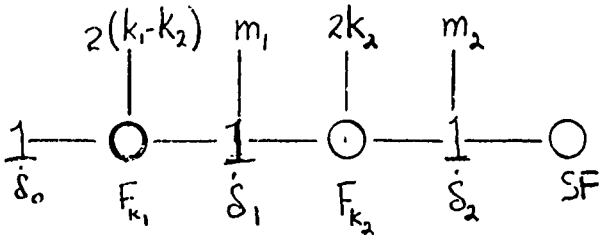
The result is:

$$m_1\frac{d\dot{\delta}_1}{dt} + k_1\delta_1 - k_2\delta_2 = (k_1 - k_2)\delta_0(t)$$

$$m_2\frac{d\dot{\delta}_2}{dt} + k_2\delta_2 - k_2\delta_1 = -f_0(t)$$

It is clear that the equations of motion are not suitable to machine computation because velocities and displacements appear together, and the across-driver is a specified displacement rather than a specified velocity.

An alternate approach based on bond graph theory (Sect. 1.68) is shown in Fig. 1.65.2f, together with the appropriate dynamical equations. It is inserted here to indicate the relative ease of obtaining the basic relations between components of the system.



$$(j\omega K_1^{-1})F_{K_1} + \dot{\delta}_1 = \dot{\delta}_0$$

$$j\omega m_1\dot{\delta}_1 + F_{K_2} = F_{K_1}$$

$$(j\omega K_2^{-1})F_{K_2} + \dot{\delta}_2 = \dot{\delta}_1$$

$$j\omega m_2\dot{\delta}_2 + SF = F_{K_2}$$

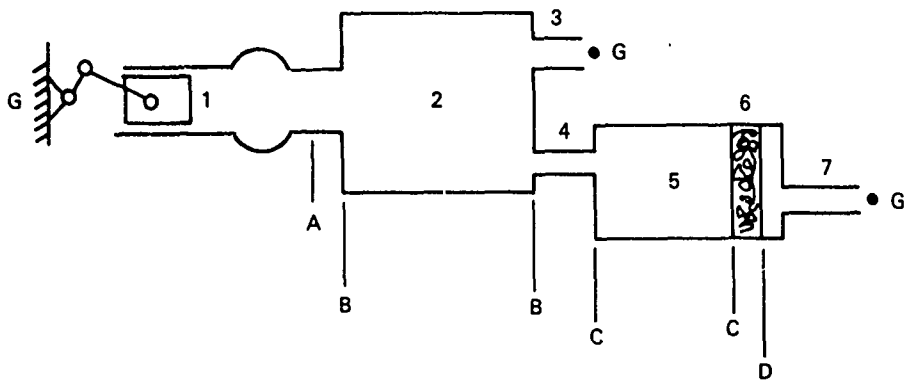
(f)

Fig. 1 65.2f — Bond graph of Fig. 1.65.1.
Note: this represents an *FV* chart.

Example 1.65.2. An Acoustical Circuit

Figure 1.65.3a shows an acoustical network of aerial acoustic waves in duct work generated by a e-driver in the form of a reciprocating piston and accumulator. A model of this network is begun by identifying the acoustic components that make up the edges of the system graph. There are eight components· one driver (labeled edge 0) and seven passive components (edges 1 through 7). This identification is equivalent to the selection of vertices *A, B, C, D, G* of the graph. The "ground" or reference vertex is *G.* Secondly, the component equation of each edge is formulated by choosing a model to represent its physical behaviour. For simplicity the model is often an approximation to reality. For example, edge 1 is approximated as an acoustic mass H_1 in which friction of the walls and compressibility (or stiffness) of the volume are neglected. Similarly, we approximate component 2 as an acoustic spring having volume compliance C_2; components 3, 4 as acoustic mass H_3, H_4; component 5 as spring C_5; component 6 as a resistance R_6, and component 7 as a mass H_7. By such approximations the acoustical network is reduced to a *discrete system.*

Figure 1.65.3a is analyzed in the following figures (b) through (f).



(a)

Fig. 1.65.3a — Acoustic network

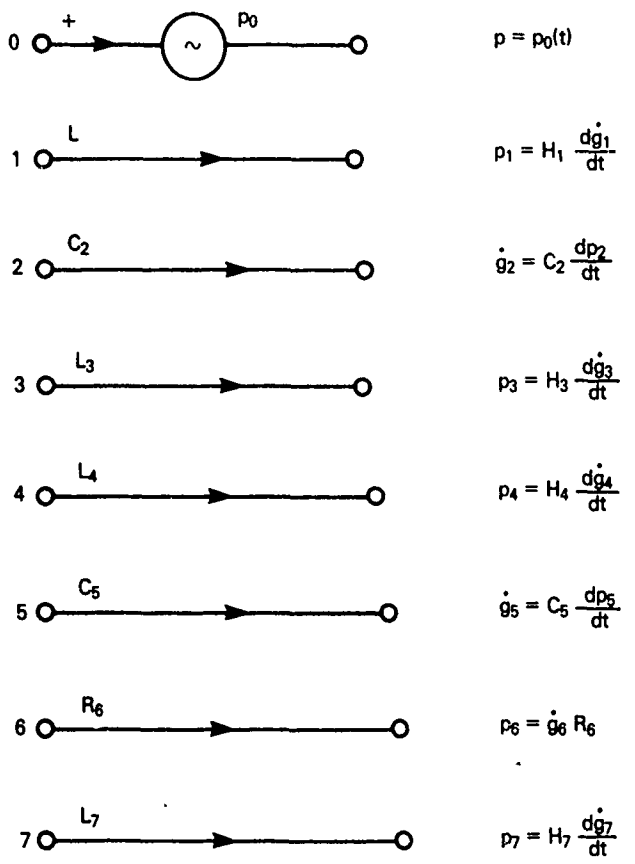
Figure 1.65.3b shows a list of measurement diagrams of this system and their associated component equations. Figure 1.65.3c shows the connection lines by which the components are assembled into the system. These lines trace the "pressure drops" in the system. Note that in acoustical circuits compliances in stiff walled cavities have one vertex at "ground." We redraw Fig. 1.65.3c into the system graph shown below in Fig. 1.65.3d.

Since our goal is to form a state model of this system we seek first a "maximally selected" tree that has all the e-sources and *C*-components in it. This is not possible because vertex *d* (which must be included in the tree) has no *C*-component incident to it. However we note that vertex *d* can be eliminated by combining edges 6 and 7 into one edge with the component equation;

$$p_6 = R_6\dot{g}_6 + H_7 \frac{d\dot{g}_6}{dt}.$$

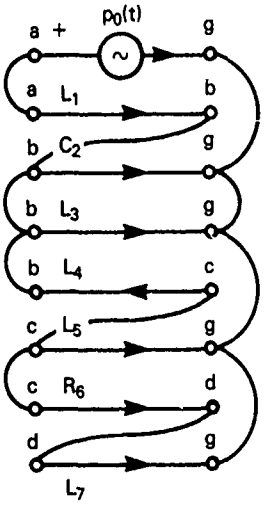
With this change we can construct the "maximally selected" tree shown in Fig. 1.65.3e, and its associated cotree, Fig. 1.65.3f. The circuit equations are obtained directly by the procedures discussed Section 1.60.

$$\begin{aligned}
&\text{circuit } (1, 2, 0): && p_1 + p_2 - p_0 = 0\\
&\text{circuit } (4, 5, 2): && p_4 + p_5 - p_2 = 0\\
&\text{circuit } (3, 2): && p_3 - p_2 = 0\\
&\text{circuit } (6, 5): && p_6 - p_5 = 0.
\end{aligned}$$



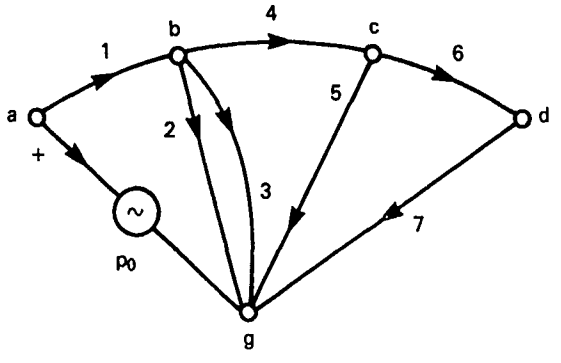
(b)

Fig. 1.65.3b — Listing of measurement diagrams of Fig. 1.65.3a



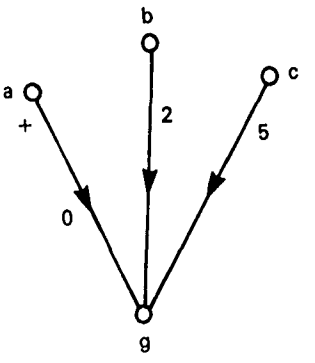
(c)

Fig. 1.65.3c — Assembly of diagrams of Fig. 1.65.3b



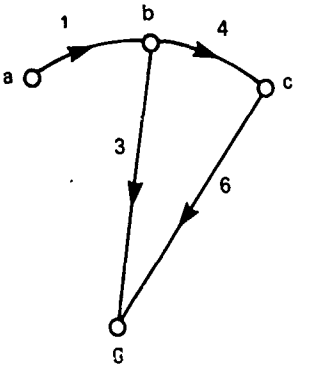
(d)

Fig. 1.65.3d — System graph of Fig. 1.65.3c



(e)

Fig. 1.65.3e — Maximally selected tree of Fig. 1.65.3d



(f)

Fig. 1.65.3f — Cotree of Fig. 1 65 3d

Using the rules of Section 1.61 we construct the cutset equations.

$$\begin{aligned} &\text{cutset } (0,\ 1): && \dot{g}_0 + \dot{g}_1 = 0 \\ &\text{cutset } (2,\ 3,\ 1): && \dot{g}_2 + \dot{g}_3 - \dot{g}_1 = 0 \\ &\text{cutset } (5,\ 4,\ 6) && \dot{g}_5 + \dot{g}_6 - \dot{g}_4 = 0. \end{aligned}$$

Note that cutset (0,1) cannot be used because p_0 is specified. The primary variables are the e-variables of the tree (namely p_2, p_5) and the i-variables of the cotree ($\dot{g}_1$, $\dot{g}_3$, $\dot{g}_4$, $\dot{g}_6$). By use of the circuit and cutset equations the state model is easily constructed to be:

$$\frac{d}{dt}\begin{bmatrix} p_2 \\ p_5 \\ \dot{g}_1 \\ \dot{g}_3 \\ \dot{g}_4 \\ \dot{g}_6 \end{bmatrix} = \begin{bmatrix} 0 & 0 & \frac{1}{C_2} - \frac{1}{C_2} & 0 & 0 \\ 0 & 0 & 0 & 0 & \frac{1}{C_5} - \frac{1}{C_5} \\ -\frac{1}{H_1} & 0 & 0 & 0 & 0 & 0 \\ \frac{1}{H_3} & 0 & 0 & 0 & 0 & 0 \\ \frac{1}{H_4} & -\frac{1}{H_2} & 0 & 0 & 0 & 0 \\ 0 & \frac{1}{H_5\frac{d}{dt} + R_6} & 0 & 0 & 0 & 0 \end{bmatrix} \begin{bmatrix} p_2 \\ p_5 \\ \dot{g}_1 \\ \dot{g}_3 \\ \dot{g}_4 \\ \dot{g}_6 \end{bmatrix} + \begin{bmatrix} 0 \\ 0 \\ \frac{p_0}{H_1} \\ 0 \\ 0 \\ 0 \end{bmatrix}$$

Simultaneous solution of this set of equations (preferably by machine computation) determines the state vector, which in turn, determines all the remaining edge variables in the system.

Example 1.65.3. A Mechanical Network Whose Tree is not Maximally Selectable

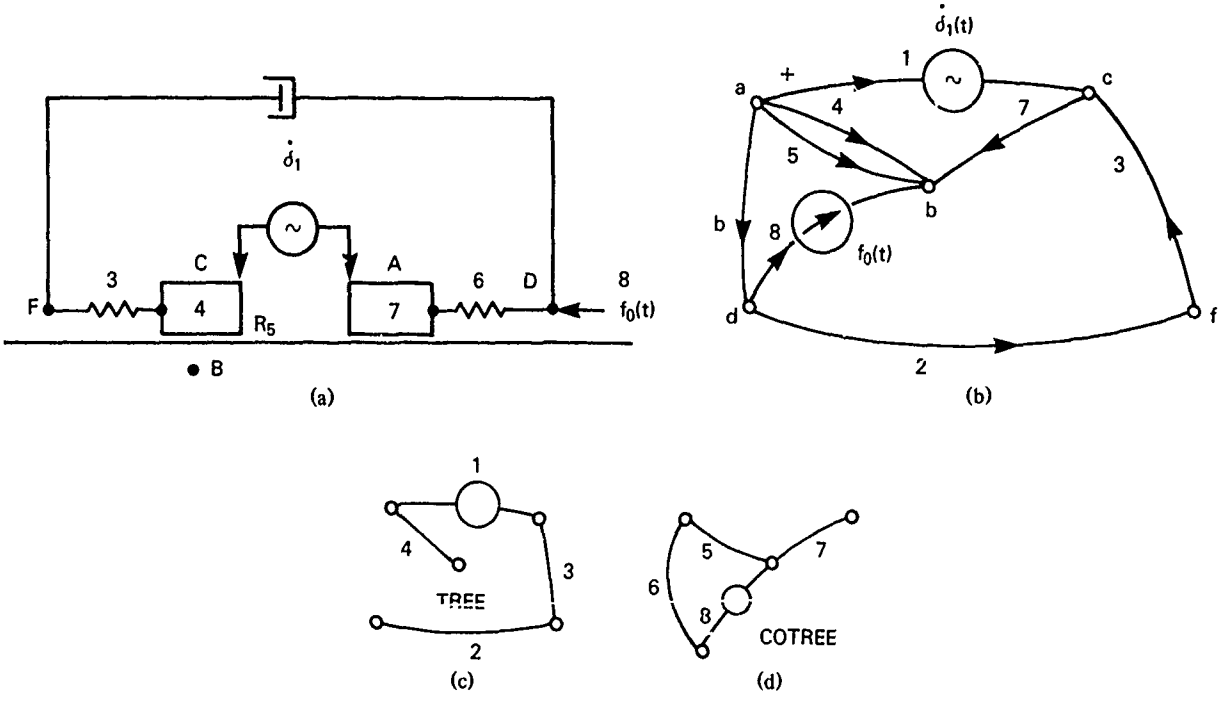


Fig. 1.65.4 — (a) Mechanical network, (b) system graph, (c) a "not-maximal" tree, (d) associated cotree

Figure 1.65.4a shows a mechanical circuit consisting of two masses driven by a e-driver (i.e. a velocity driver $\dot{\delta}_1(t)$), two springs (L_3, L_6), damper R_2, friction R_5, and an *i*-driver (namely the force $f_0(t)$) at vertex *D*. The system graph is shown in Fig. 1.65.4b.

It is noticed immediately the the *C*-components (= masses 4, 7) and the e-driver form a closed loop. Thus it is not possible to place all the *C*-components in the same maximally selected tree. The procedure to circumvent this difficulty is to select a tree (not maximal) to contain as many *C*-components as are permitted. Here this is one mass (say 4) plus the e-driver (= edge 1). This tree is 4, 1, 3, 2. The state variables are then taken to be $\dot{\delta}_4$ from the tree, and f_6 from the cotree. Since edges 1, 8 are (specified) drivers, this leaves edges 2, 3, 5, 7 as an additional set of component equations which must participate in the process of solution, *but are not primary variables.* The component equations are:

$$\begin{aligned}
&(1)\ \frac{d\dot{\delta}_4}{dt} = \frac{i_4}{M_4} && (5)\ \dot{\delta}_5 = f_5 R_5,\quad f_5 = G_5 \dot{\delta}_5\\
&(2)\ \frac{df_6}{dt} = \frac{\dot{\delta}_6}{K_6} && (6)\ m_7 \frac{d\dot{\delta}_7}{dt} = f_7\\
&(3)\ \dot{\delta}_2 = f_2 R_2 && (7)\ \dot{\delta}_1 = \dot{\delta}_0(t)\\
&(4)\ K_3 \frac{df_3}{dt} = \dot{\delta}_3 && (8)\ f_8 = f_0(t)
\end{aligned}$$

The equations of constraint are:

circuit on (5, 4): $\dot{\delta}_5 - \dot{\delta}_4 = 0$
circuit on (6, 1, 3, 2): $\dot{\delta}_6 + \dot{\delta}_1 - \dot{\delta}_3 - \dot{\delta}_2 = 0$
circuit on (8, 4, 1, 3): not useful
circuit on (7, 1, 4): $\dot{\delta}_7 - \dot{\delta}_1 + \dot{\delta}_4 = 0$.

cutset on (3, 8, 6): $f_3 + f_8 + f_6 = 0$
cutset on (2, 8, 6): $f_2 + f_8 + f_6 = 0$

Making all substitutions, and using conventional matrix inversion one arrives finally at the state model in the reduced state vector $[\dot{\delta}_4,\ f_6]$:

$$\frac{d}{dt}\begin{bmatrix}\dot{\delta}_4\\ f_6\end{bmatrix} = \begin{bmatrix}-G_5/(M_4+M_7) & 0\\ 0 & -R_2/(K_3+K_6)\end{bmatrix}\begin{bmatrix}\dot{\delta}_4\\ f_6\end{bmatrix}$$

$$+\begin{bmatrix}0 & (M_4+M_7)^{-1}\\ -(K_3+K_6)^{-1} & -R_2(K_3+K_6)\end{bmatrix}\begin{bmatrix}\dot{\delta}_0\\ f_0\end{bmatrix}$$

$$+\begin{bmatrix}M_7(M_4+M_7)^{-1} & 0\\ 0 & -K_3(K_3+K^6)^{-1}\end{bmatrix}\frac{d}{dt}\begin{bmatrix}\dot{\delta}_0\\ f_0\end{bmatrix}$$

Thus, although, the mechanical network contains four energy-storage components, the state model is constructed on only two of them, the other two being eliminated by the system equations of constraint.

Example: 1.65.4

Figure 1.65.5a shows a mechanical translation system driven by a e-source ($=\dot{\delta}_0(t)$). The system graph is constructed by noting (1) that masses M_1,M_2 (edges 2, 5) are connected to "ground" (2) that they are connected to each other by spring K_2 (edge 3) and damper B (edge 4); (3) that mass M_1 is driven through a spring K_1 (edge 1) by a e-driver $\dot{\delta}_0(t)$ (edge 0). Figure 1.65.5b shows the system graph.

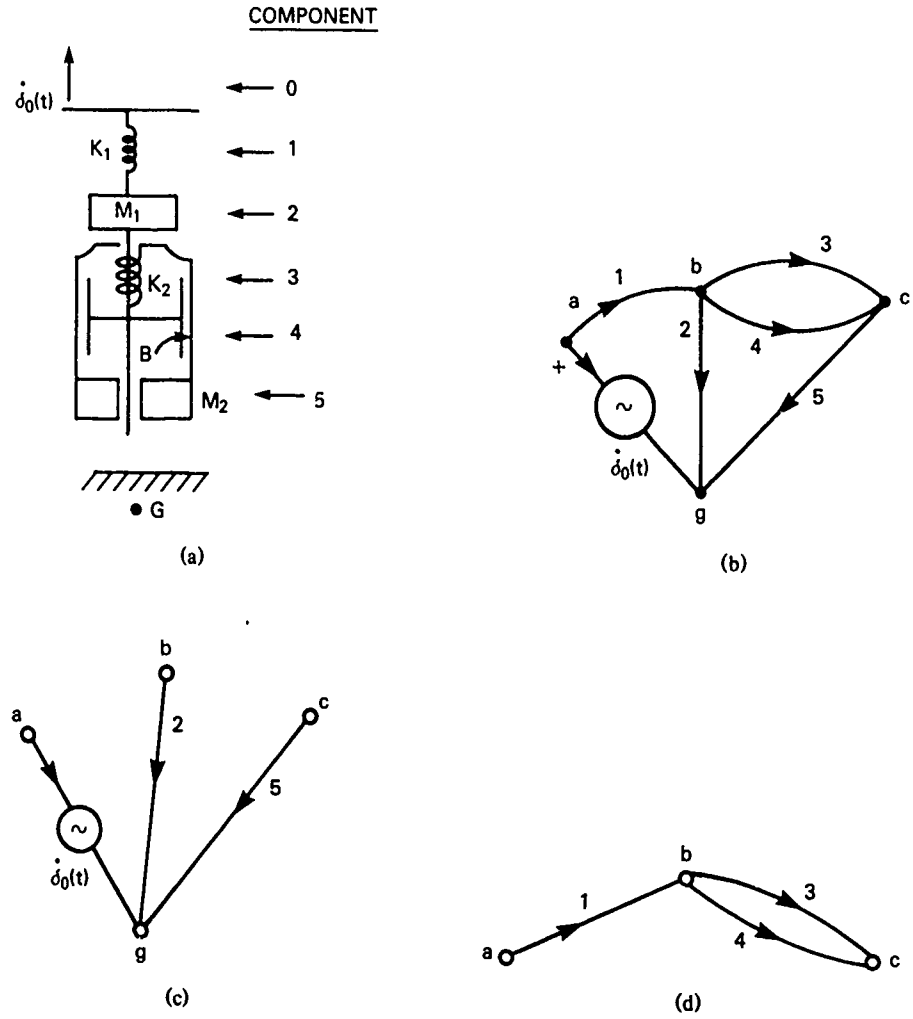


Fig. 1.65.5 — (a) Mechanical translation system (b) system graph (c) selected tree (d) associated cotree

To analyze the system we choose a tree of 2 *C*-components (masses M_1, M_2) and the e-driver (Fig. 1.65.5c). The cotree is shown in Fig. 1.65.5d.

The component equations are listed as follows:

edge 0: $\dot{\delta} = \dot{\delta}_0(t)$

$$1: \frac{df_1}{dt} = K_1 \dot{\delta}_1(t)$$

$$2: \frac{d\dot{\delta}_2}{dt} = \frac{1}{M_1} f_2$$

$$3: \frac{df_3}{dt} = K_2 \dot{\delta}_2(t)$$

$$4: B\,\dot{\delta}_4(t) = f_4$$

$$5: \frac{d\,\dot{\delta}_5(t)}{dt} = \frac{1}{M_2} f_5$$

The cotree shows there are three circuit equations to be constructed on chords 1, 3, 4: these are,

$$\text{circuit } (1,\ 2,\ 0): \dot{\delta}_1 + \dot{\delta}_2 - \dot{\delta}_0 = 0$$

$$\text{circuit } (3,\ 5,\ 2): \dot{\delta}_3 + \dot{\delta}_5 - \dot{\delta}_2 = 0$$

$$\text{circuit } (4,\ 5,\ 2): \dot{\delta}_4 + \dot{\delta}_5 - \dot{\delta}_2 = 0$$

The selected tree shows there are three cut-set equations,

$$\text{cutset } (a,\ bcg): f_0 + f_1 = 0$$

$$\text{cutset } (b,\ aqc): -f_1 + f_2 + f_3 + f_4 = 0$$

$$\text{cutset } (c,abg): f_5 - f_4 - f_3 = 0$$

Note that cutset $(a,\ bcg)$ is not independent since f_0 corresponds to an *assigned* velocity $\delta_0'(t)$. Thus there are five independent equations of constraint.

The state variables are $\dot{\delta}_2$, $\dot{\delta}_5$ associated with the tree, and f_1, f_2, f_3 associated with the cotree. The state equations are obtained by using the equations of constraint:

$$(1)\quad \frac{d\dot{\delta}_2}{dt} = \frac{1}{M_1}\,[f_1 - f_3 - f_4] \qquad (2)\quad \frac{d\dot{\delta}_5}{dt} = \frac{1}{M_2}\,[f_3 + f_4]$$

$$(3)\quad \frac{df_1}{dt} = K\quad [\dot{\delta}_0 - \dot{\delta}_2] \qquad (4)\quad \frac{df_3}{dt} = K_2\quad \dot{\delta}_2$$

$$(5)\quad f_4 = B\quad [\dot{\delta}_2 - \dot{\delta}_5]$$

or

$$\frac{d}{dt}\begin{bmatrix}\dot{\delta}_2\\ \dot{\delta}_5\\ f_1\\ f_2\end{bmatrix} = \begin{bmatrix} -\frac{B}{M_1} & \frac{B}{M_1} & -\frac{1}{M_1} & -\frac{1}{M_1}\\ \frac{B}{M_2} & \frac{-B}{M_2} & 0 & \frac{1}{M_2}\\ -K_1 & 0 & 0 & 0\\ K_2 & 0 & 0 & 0\end{bmatrix}\begin{bmatrix}\dot{\delta}_2\\ \dot{\delta}_5\\ f_1\\ f_3\end{bmatrix} + \begin{bmatrix}0\\ 0\\ K_1\dot{\delta}_0\\ 0\end{bmatrix}$$

To obtain the equations of motion we substitute for f_1, f_3 by writing

$$f_1 = K_1[\delta_0 - \delta_1],\ f_3 = K_2\delta_2,\ \delta_0 = \int_0^t \delta_0'(\tau)\,dt\tau$$

Thus,

$$(1)\ \frac{d\dot{\delta}_2}{dt} = \frac{1}{M_1}\{K_1(\delta_0 - \delta_2) - K_2\delta_2 - B\dot{\delta}_2 + B\delta_5\},$$

or

$$M_1 \frac{d\dot{\delta}_2}{dt} + B\,\dot{\delta}_2 + (K_1 + K_2)\,\delta_2 = K_1\delta_0 + B\,\dot{\delta}_5$$

$$(2)\ \frac{d\dot{\delta}_5}{dt} = \frac{1}{M_2}[K_2\delta_2 + B(\dot{\delta}_2 - \dot{\delta}_5)]$$

or

$$M_2 \frac{d\dot{\delta}_5}{dt} + B\,\dot{\delta}_5 = \frac{K_2}{M_2}\,\delta_2 + B\,\dot{\delta}_2$$

This completes the dynamic analysis of the system shown in Fig. 1.65.5a. Note that the principle result is the state model involving first order differential equations. The equations of motion in contrast are secondary results.

1.66 ACOUSTIC PORTS IN STATE MODEL THEORY

The acoustic load on a radiating surface of a sound source can be modeled in several ways. In the first, it is a mechanical load in a mechanical network in which velocity is the across-variable and force is the through-variable. The acoustic inertia is then that of a frequency dependent *C*-component (or mass) representable in a measurement diagram as a single edge with two vertices, one of which is at "ground." Similarly the accustic resistance is modeled as a (frequency dependent) frictional resistance (or *R*-component) between this mass and ground. The combined model consists of two edges "in parallel" Fig. 1.66.1a. In the second model the acoustic inertia is that of a hydraulic *L*-component, and the acoustic resistance is modeled as a hydraulic resistance. The combined measurement diagram is modeled as two edges "in series" (Fig. 1.66.1b). In the third model the acoustic load is a mechanical component in which force is the across-variable and velocity the through-variable. This model is the same as the hydraulic model if we take force to equal pressure times radiating area, and velocity to equal volume velocity times radiating area (Fig. 1.66.1c). Figures 1.66.1a and 1.66.1c are clearly duals of each other: given either representation, one can find it due by conventional electrical circuit theorems.

An example of a hydraulic (or series) representation of the acoustic field is a cavity driven by a pressure drive, radiating acoustic waves through an elastic membrane (Fig. 1.66.2a). There are four components in this system: a e-driver, edge 0, a *C*-component, edge 1; a *C*-component edge 2; an acoustic component, edge 3; Fig. 1.66.2b. The connection diagram in Fig. 1.66.2b traces the "pressure drops" in the system. Note that the acoustic edge 3 is in series with edge 2. The system graph Fig. 1.66.2c is simply the connection diagram of Fig. 1.66.2b redrawn. Although three vertices are shown, the system is essentially a 2-vertex (or 1-port) system.

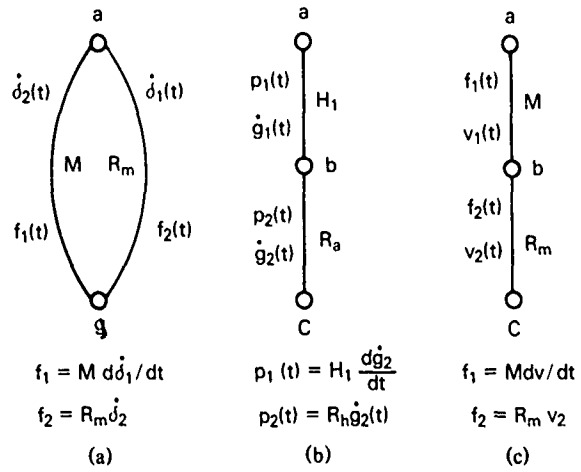


Fig. 1.66.1 — Acoustical port (a) modeled as a frequency dependent C-component and R-component (b) modeled as a hydraulic L-component and hydraulic resistance (c) modeled as mechanical force (across variable) and mechanical velocity (through variable).

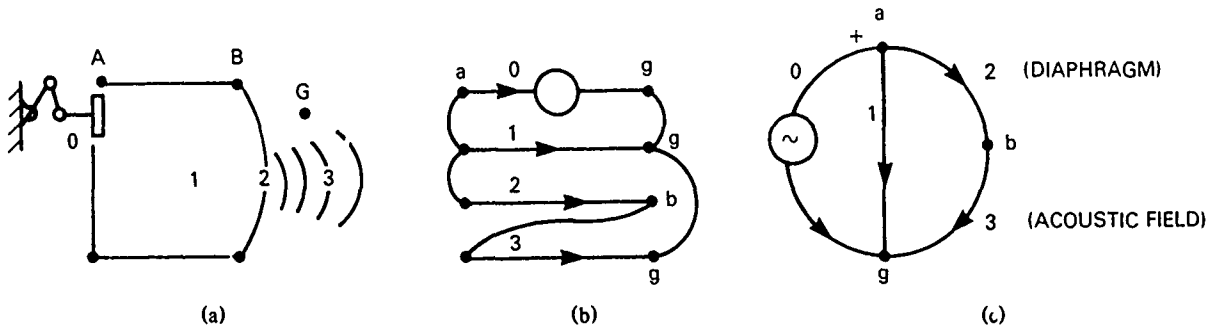


Fig. 1.66.2 — (a) Cavity radiating acoustic waves (b) components of this system (c) redrawn connection diagram of (b)

An example of a parallel representation of the acoustic field is a bilateral cam-driven source of two C-components (masses m_1, m_2), one L-components (spring R_3) and a e-driver ($\dot{\delta}_0(t)$, Fig. 1.66.3a. The acoustic radiation loads mass m_1. The system graph of this acoustic source is drawn in Fig. 1.66.3b. Here g is "ground." The acoustic resistance R_A and acoustic inertia (or mass) M_A are in parallel with mass 1 (i.e., they have the same "velocity drop" from a to g).

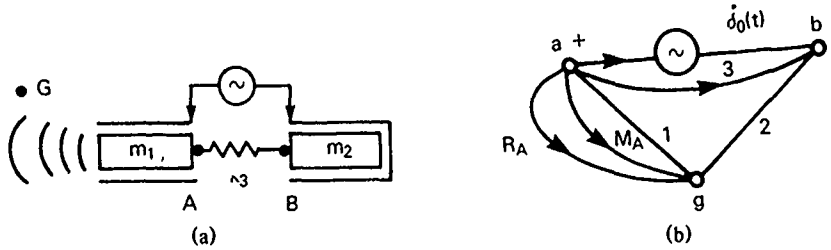


Fig. 1.66.3 — (a) Bilateral cam-driven source (b) system graph

To summarize: The analysis of multicomponent transducer systems by use of state systems models is ideally suited to calculation on digital computers. Such computation leads to explicit values of state model variables. In this method first order equations replace second order equations. Greater insight into physical theory is thereby revealed because geometric constraints on the variables are always in evidence.

1.67 ANALYSIS BY USE OF EQUATIONS OF MOTION AND EQUIVALENT CIRCUITS

A mechanical-acoustical system in which force and velocity (or pressure and volume velocity) are the energy coordinates, is assumed to have m degrees of freedom, $\dot{x}_i$, $i = 1, 2 \ldots m$. In the ith degree we have an applied force F_i which excited $\dot{x}_i$ and all other coupled velocities $\dot{x}_j$, $j \neq i$.

$$\sum_{j=1}^{m} L_{ij}\,\dot{x}_j = F_i \qquad i = 1,\ 2\ \ldots\ . \tag{1.67.1}$$

Here L_{ij} is an integro-differential operator. It is illuminating to rewrite this in the form,

$$F_i - L_{ii}\,\dot{x}_i = \sum_{j} L_{ij}\dot{x}_j = \sum_{j\neq i} \mathrm{F}_{ij} \qquad i = 1,\ 2\ \ldots\ .\ m,\ j \neq i. \tag{1.67.2}$$

The symbol F_{ij} identifies an interior *coupling force* which couples the ith and jth degrees of freedom.

The set of equations 1.67.2 define a network of interacting elements. We consider first an *FV* network (F is across variable, V is the through variable). In such a network all self operators L_{ii} are in *series* position and all forces F_i, F_{ij} are in *parallel* position. For example, in a system with two degrees of freedom,

$$\begin{cases} F_1 - L_{11}\dot{x}_1 = \mathrm{F}_{12}, & \mathrm{F}_{12} = L_{12}\dot{x}_2 \\ F_2 - L_{22}\dot{x}_2 = \mathrm{F}_{21}, & \mathrm{F}_{21} = L_{1.67}\dot{x}_1 \end{cases} \tag{1.67.3}$$

F_1, F_{12} are in parallel position and L_{11}, L_{22} are in series position. In a linear reciprocal system (as assumed here) one has,

$$\mathrm{F}_{12} = \mathrm{F}_{21} = \mathrm{F}_c \tag{1.67.4}$$

This assumption simplifies the circuit representation. Further simplification is obtained by noting that since there is generally only one mechanical driving force, we set $F_2 = 0$. Then

$$\begin{cases} F_1 - L_{11}\dot{x}_1 = \mathrm{F}_c \\ \quad - L_{22}\dot{x}_2 = \mathrm{F}_c \end{cases} \tag{1.67.5}$$

The *FV* diagram corresponding to Eq. 1.67.5 is shown in Fig. 1.67.1. Here the statement $F_2 = 0$ means a short circuit.

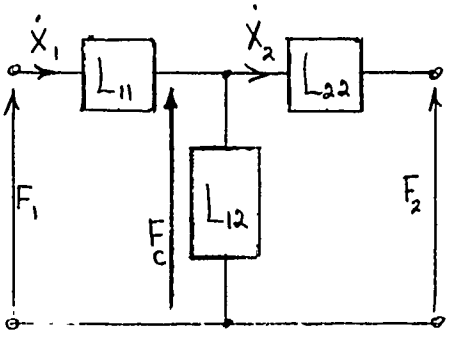


Fig. 1.67.1 — FV diagram of a system with two degrees of freedom

Equation 1.67.2 can also signify the nodal equations of a *VF* network (V across, F through). In the example of Eq. 1.67.5,

$$\begin{cases} F_1 = L_n\dot{x}_1 + \mathrm{F}_c \\ 0 \ = L_{22}\dot{x}_2 + \mathrm{F}_c \end{cases} \tag{1.67.6}$$

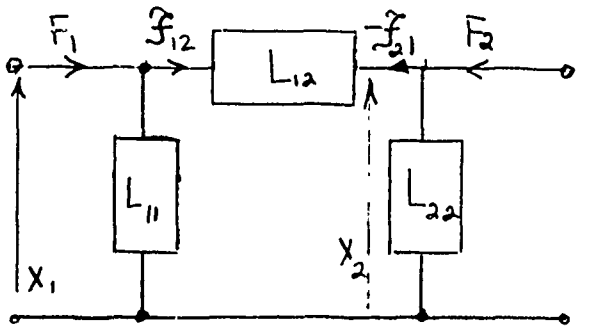


Fig. 1.67.2 – VF diagram of Fig. 1.67.1

In such a *VF* diagram the self operators L_{ii} are in parallel position (in analogy to the electrical equation $I = EY$) and the forces F, F are in series position. The equivalent circuit is shown in Fig. 1.67.2. Here the statement $F_2 = 0$ means open circuit.

To summarize: In an *FV* equivalent circuit (force "across," velocity "through") force is transmitted from node to node. Two elements are said to be in series position if they have a common velocity, and in parallel position if they have a common force. A branch of elements placed between two force nodes, one at force F and the second at force F_α is said to be in series position in the network if there is a finite residual velocity F_α of magnitude

$$F - z_m v = F_\alpha$$

in which z_m is the impedance (force/velocity ratio) and v is the branch velocity. The branch is said to be in shunt position if $F_\alpha = 0$, that is, if

$$F = z_m v$$

The second node is then at "ground" position.

In a *VF* equivalent circuit (velocity "across" force "through") velocity is transmitted from node to node. Two elements are said to be in series if they have a common force, and in parallel if they have a common velocity. A branch of elements placed between two velocity nodes, one at velocity v and the second at velocity v_α, is said to be in *series* position in the network if there is a residual velocity v_α, of magnitude

$$v - y_m F = v_\alpha$$

in which y_m is the mobility (= velocity/force ratio) and F is the branch force. The branch is said to be in shunt position if $v_\alpha = 0$, that is, if

$$v = y_m F.$$

The second node is then at "ground" position.

1.68 THEORY AND APPLICATION OF BOND GRAPHS [11]

INTRODUCTION

Since transducers are structures which interconnect physical components, often in a complex way, it is necessary for the designer to have before him a symbolic model of the structure which accounts for

interconnections in terms of convenient descriptors. Three descriptors suffice to allow an understanding of power flow in the transducer to be formed: (1) energy supply (2) energy storage (3) energy dissipation. The model is therefore a visual compendium of interconnected subsystems exchanging power and energy.

While modeling of subsystems can be done one subsystem at a time, in unconnected form, the act of connecting two such subsystems introduced *back effects* which must be accounted for in explicit ways. A modeling procedure which allows the designer to take care of back effects in a direct manner is a true advantage. The method to be described below does just that.

In common with all physical systems transducers are set in motion by known input quantities. Analysis of a physical model then gives a prediction of the output quantities. This distinction between input and output quantities serves as a definition of *causality*. Assignment of causality to components of physical models is an essential step in arriving at realistic predictions of transducer behavior. Such assignment can be in the general case quite complicated.

Physical modeling based on devising equivalent electical circuits is the first choice of transducer designers (See Sections 1.0 and 1.1). Such circuits are visual summaries of differential equations governing the operation of components which make up the model. Other techniques for generating these equations are linear graphs, block diagrams, signal flow graphs and transfer functions discussed in previous sections of this chapter.

A new *notation* which also permits direct generation of the applicable differential equations governing the exchange of power and energy in interconnected physical systems and which permits simple modeling of physical components not modelable by linear equivalent circuits is called the *bond graph*. The theory and application of bond graphs are discussed in this section. In the process of elaborating its methodology the advantage of use of bond graphs will become apparent.

1.68.1 Elements of Bond Graph Theory-Notation of N-Ports, Power Flow Conventions, Causality

In common with the methods of block diagrams and equivalent circuits discussed in previous sections of this treatise the method of bond graphs is based on a set of definitions of terms. Some of these are pecular to it and some overlap other definitions already discussed. For completeness we review all terms needed to explain the method fully. As noted, the designer of complex physical systems imagines them to be made up of interconnecting components. Each component exchanges power and energy with its neighbors. Power is described as the product of two time-varying quantities 1) *effort* $e(t)$ (2) flow $f(t)$. A component exchanging power with $i = 1, 2, \ldots$ neighbors will have i powers, $e_i(t)f_i(t)$ associated with it. Each such power (in exchange) is called a *port*, identifable by the subscript i. In bond graph notation a port is a simple short line which is provided (when needed) with an explicit statement of the power variable: effort on one side of the line and flow on the other side. Figure 1.68.1 shows a component with four ports: electrical (e, i), hydraulic (P, Q), translational mechanical (F,V), rotational mechanical (τ, ω). The power varibles are explicitly noted. In words, this multiport component α exchanges powers with four neighbors: pressure P and flow Q, with component β; force F and velocity V, with component γ; torque τ and angular velocity ω, with component δ; voltage e and current i, with component η.

The direction of flow of power going *from* multiport α *into* multiport β is indicated by a half arrowhead at β. The power is positive and flows from left to right when effort and flow are positive functions of time. Figure 1.68.1 shows only one power flow assignment. Three additional assignments can be made. The making of power flow assignments is arbitrary, with the sole caution that it must be consistent.

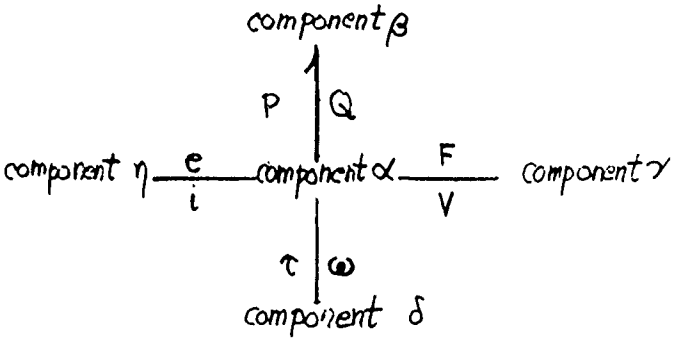


Fig. 1.68.1 — Illustration of a component with four power exchanging ports

The assignment of power flow between multiports shows *internal* exchanges between them regarded as one system. It does not indicate which power variables are inputs (or "causes") and which are outputs (or "effects"). The indication of input/output, that is, of causality, is shown by the *stroke convention*, Fig. 1.68.2. This convention is read as follows: effort $e(t)$ is determined by multiport α and impressed on multiport β; and flow $f(t)$ is determined by multiport β and impressed on multiport α. Note the important rule:

- *effort and flow on a single bond are always oppositely directed.*

It will be readily appreciated that power flow and causality are independent assignments. Figure 1,68.3 shows two examples of this double assignment. In (a) effort is determined by β and impressed on α while the flow variable oppositely directed. The power flow is from β into α. In (b) the causality is the same as in (a) but the power flow is *into* β.

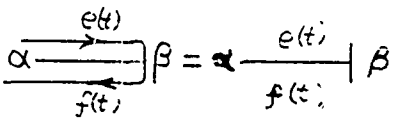


Fig. 1.68.2 — Illustration of assignment of causality

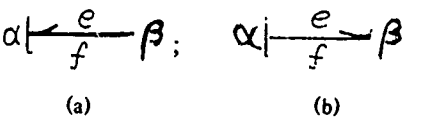


Fig. 1.68.3 — Illustration of independent assignments of power and causality

1.68.2 Description of Multiports

In the majority a physical systems a complete physical model can be constructed of three types of multiports: (1) 1-ports (2) 2-ports (3) 3-ports. Additional N-ports, if needed, can be put together by addition of these basic types.

1-Port Elements

These elements exchange power with their neighbors on a single bond.

Five elementary 1-ports are directly definable in terms of the functional relation Φ (or Φ^{-1}) between e and f:

1. *Resistance 1-Port*, defined as a port which has a power bond in which the effort is a function of flow, $e(t) = \Phi_R(f(t))$. Its symbol is $-R$.

2. *Capacitance 1-Port*, defined as a port which has a power bond in which the effort is a function of flow impulse (or generalized displacement) $e(t) = \Phi_c^{-1}(f(t)\Delta t)$. Its symbols is $-C$.

3. *Inertance 1-Port*, defined as port which has a power bond in which the flow is a function of effort impulse (or generalized momentum) $f(t) = \Phi_I^{-1}(e(t)\Delta t)$ Its symbol is $-I$.

4. *Effort Source 1-Port*, defined as port which has a power bond in which the effort is a fixed known applied quantity, $e = E(t)$. Its symbols is S_E-

5. *Flow Source 1-Port*, defined as port which has a power band in which the flow is a fixed known applied quantity, $f = F(t)$. Its symbol is S_f-.

In these definitions the incremental time Δt is a very small quantity. Over finite time the flow impulse is $q(t) = \int f(t)\,dt$, and the effort impulse is $p(t) = \int e(t)\,dt$. The use of inverse notations Φ^{-1} in these definitions has the advantage that it allows one to immediately invert functional dependence between power variables.

2-Port Elements

These elements exchange power with their neighbors on two bonds.

By definition a 2-Port has two power bonds e_1, f_1; e_2, f_2. Two special 2-ports are of use in transducer physical modeling:

1. *Transformer 2-Port*, defined by the relations $e_1 = me_2$, $mf_1 = f_2$. Its symbol is,

$$\xrightarrow[f_1]{e_1} TF \xrightarrow[f_2]{e_2}.$$

2. *Gyrator 2-Port*, defined by the relations, $e_1 = rf_2$, $rf_1 = e_2$. Its symbol is,

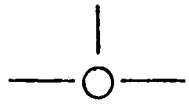
$$\xrightarrow[f_1]{e_1} GY \xrightarrow[f_2]{e}.$$

Besides these special 2-Ports there are a great variety of general-type 2-Ports in which the relations between e_1, f_1, e_2, f_2 are more complex functions than the ones cited above.

3-Port Elements

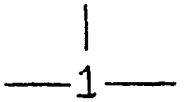
By definition a 3-Port has three power bonds: e_1, f_1; e_2, f_2; e_3, f_3. Two basic 3-Ports are all that are needed to define a large number of physical systems. These are,

1. *Common effort junction, or 0-junction*, defined by the relations, $e_1(t) = e_2(t) = e_3(t)$, $f_1(t) + f_2(t) + f_3(t) = 0$. It symbol is,



In electric circuits the 0-junction 3-Port defines circuit elements in parallel. A greater appreciation of the nature of a 3-Port is had if the bond graph itself is verbalized to read: "the 0-junction 3-Port *feeds* (or *absorbs*) power to (or from) external devices at three ports under the condition that all efforts are common." Later it will be seen that one may define a 0-junction 2-Port for a device which feeds (or absorbs) power to (from) external devices at two ports in which the two efforts are common.

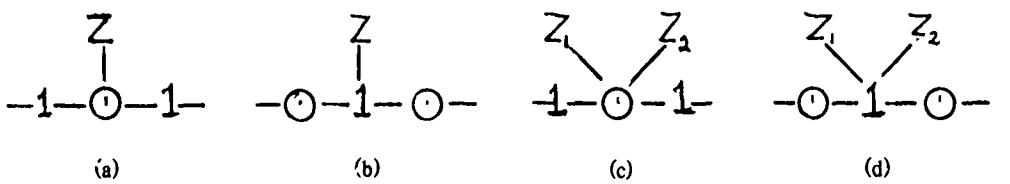
2. *Common flow junction, or 1-junction,* defined by the realtions $f_1(t) = f_2(t) = f_3(t)$, $e_1(t) + e_2(t) + e_3(t) = 0$. Its symbol is,



In electric circuits the 1-junction 3-Port defines circuit elements in series. It is verbalized to read: "the 1-junction feeds (or absorbs) power to (from) external devices at three ports under the conditon that all flows are common." One may define as well a 1-junction 2-Port in which only two pairs of power variables are involved under the condition that their flows are common.

Combination of N-Ports

The following symbols often appear in bond graph analysis:



(a) (b) (c) (d)

In (a) and (c) the 0-junction establishes the effort in Z_i by application of flow difference; in (b) and (d) the 1-junction establishes the flow in Z_i by application of effort differences. Such symbols are helpful in the initial constructions of bond graphs.

C-Fields, I-Fields, IC-Fields

The energy storage component of an acoustic transducer may have n ports. It may thus be described as a capacitive, or C-field; an inertial, or I-field; or a mixed capacitive-inertial IC-field.

An elastic cantilever beam with negligible mass response, exchanging power at n points with the environment is an example of a C-field. This field expresses the relation between an n-vector effort $e = (e_1, e_2 \ldots e_n)$ and the corresponding n-vector displacement $q = (q_1, q_2, \ldots q_n)$, $q = \int f dt$. The energy stored in this field is

$$E = \int \sum_{i=1}^{n} e_i(q)\, dq_i.$$

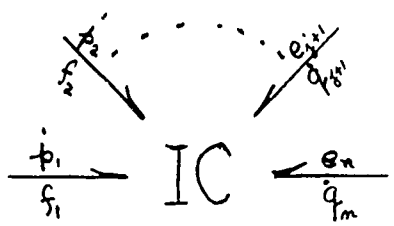
A rigid bar of given mass exchanging power with the environment at n points is an example of an I-field. This field expresses the relation between an n-vector flow $f = (f_1, f_2, \ldots f_n)$ and an n-vector momentum $p = (p_1, p_2 \ldots p_n)$, $p = \int \mathbf{e}\mathbf{d}t$. The energy stored in this field is,

$$E = \int \sum_{i=1}^{n} f(\mathbf{p})\, d\mathbf{p}.$$

An electromagnetic transducer operating below mechanical resonance is an example of a mixed IC-fixed. Here the electrical circuit is inertial (that is, inductive) while the mechanical circuit is capacitive (that is, compliant). If the electrical circuit has j ports and the mechanical circuit has $n - j$ ports the stored energy is

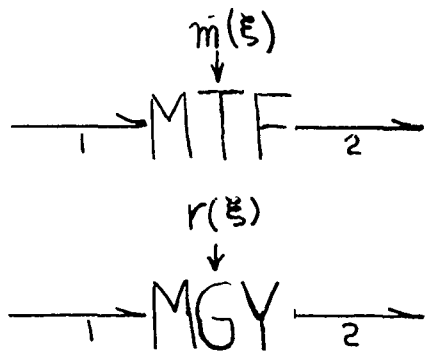
$$E = \int \sum_{i=1}^{j} f_i\, dp_i + \int \sum_{h=j+1}^{n} e_k dq_k.$$

The bond graph symbol for the mixed energy *IC*-field is,



Modulated 2-Ports

Power conserving transformers and gyrators may be 'modulated'. The symbols and constitutive laws for these modulated elements define their meanings:



$$m(\xi)e_1 = e_2 \quad e_1 = r(\xi)f_2$$
$$f_1 = m(\xi)f_2 \quad r(\xi)f_1 = e_2.$$

The modulation parameters m, r do not exchange power with the transformer or gyrator.

A rigid pivoted bar which exchanges power at two ports with its environment, namely a τ, ω port delivering power to a F_y, V_y port, is an example of a MTF since the y-component of force (F_y) delivered depends on the angle ξ of the bar. Similarly, an electric generator in which a copper wire moves through a magnetic field created by an inductance coil, thereby producing a voltage is an example of a *MGY* since the magnetic field is a function of a current through the inductance coil.

1.68.3 Assignment of Causality to 1-Ports

The bonds of the multiports discussed above are identified by the power variable e, f. They are *bilateral*, meaning that one can find (by analysis) $e = \Phi(f)$ or $f = \Phi^{-1}(e)$. To use such a representation in interconnected graphs one must assign causality.

Causality, as noted above, is a statement of input/output,-or alternatively a statement of which variables on a bond are independent and which are dependent. In this regard a convention is needed on the reading of equations. In this section the causal equations,

$$(1)\ \mathcal{L}\{X\} = Y \qquad (2)\ \mathcal{L}^{-1}\{Y\} = X$$

mean the following: (1) a cause (or input) Y produces an effect (or output) X through the action of an operator $\mathcal{L}$; (2) a cause (or input) X produces an effect (or output) Y through the action of an inverse operator $\mathcal{L}^{-1}$. Thus the right hand side is always a cause, and the left-hand side an effect. The convention will be used to assign causality in bond graphs.

Figure 1.68.2 illustrates the assignment of causality. In using it the following rules hold:

- a cause, whether effort or flow, *enters* the port; an effect *leaves* the port.
- in assigning the *causal stroke* the direction of effort circulates into the direction of flow. A causal stroke at the opposite end of the multipole bond indicates flow causality (i.e. flow into the port determines effort out of the port). A causal stroke adjacent to the multiport indicates effort causality (that is, effort into the port determines flow out of it)

An example will serve to elucidate these rules. We are given the two possible equations of a resistance 1-Port and we assign the causality stroke. Figure 1.68.4 shows the procedure. In (a) the independent variable of power into R is effort e, while in (b) it is flow f. It is important to note that the power flow (indicated by a half arrow) is always into the resistance element regardless of which variable is an input.

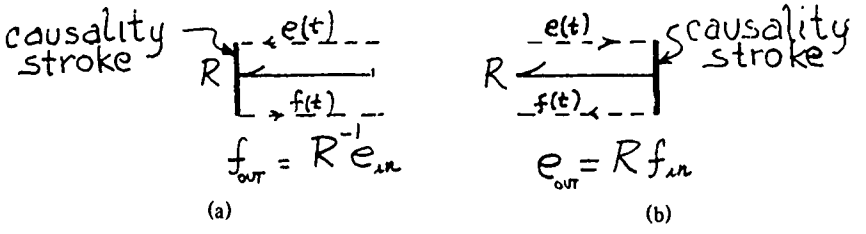
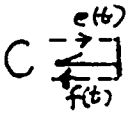


Fig. 1.68.4 — Assignment of causality to a resistance 1-port

In a similar way one can assign causality to the remaining 1-Ports cited above:

Capacitance 1-Port

integral form: $e_{out} = \mathscr{L}_C^{-1} \left\{ \int f_{in}\, dt \right\}$

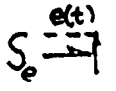


differential form: $f_{out} = \mathscr{L}_c \dfrac{de_{in}}{dt}$

...

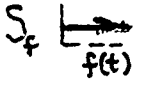
Inertance 1-Port

integral form: $f_{out} = \mathscr{L}_I^{-1} \left\{ \int e_{in}\, dt \right\}$



differential form: $e_{out} = L_I \dfrac{df_{in}}{dt}$

Effort Source 1-*Port*: $e(t) = E(t)$

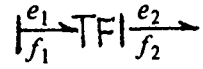


Flow Source 1-*Port*: $f(t) = F(t)$

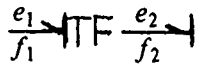
Assignment of Causality to 2-Ports

For the case of a transform 2-Port the causality assignment can take only two forms. Observing again the convention that the left hand side of the defining equations is output and the right hand side is input, one has:

$$(1)\begin{cases} e_1 = me_2 \\ f_2 = mf_1 \end{cases}$$

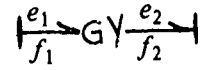


$$(2)\begin{cases} f_1 = f_2/m \\ e_2 = e_1/m \end{cases}$$

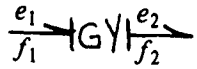


For the case of a gyrator 2-Port one can make similar assignments,

$$(1)\begin{cases} e_1 = f_2 r \\ e_2 = f_1 r \end{cases}$$



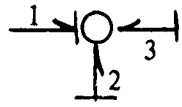
$$(2)\begin{cases} f_1 = e_2/r \\ f_2 = e_1/r \end{cases}$$



Assignment of Causality to 3-Ports

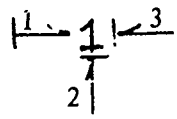
In the case an 0-junction (junction of common effort), assignment again is direct: assuming e_1 is an input, one writes a list of rules:

$$\text{Rules}\begin{cases} (1)\ \sum_i W_i = 0, \text{ i.e. } W_1 = -W_2 - W_3 \\ (2)\ e_1 f_1 = -e_2 f_2 - e_3 f_3 \\ (3)\ e_2 = e_1,\ e_3 = e_1 \\ (4)\ f_1 = -(f_2 + f_3) \end{cases}$$



The rules begin with a power statement: since an 0-junctions transmits power, but does not store or dissipate it, the power "in" must be balanced by the power "out". From the (arbitrary) assignment of power flow one balances powers as shown in step (1). Since all efforts are common they cancel out leaving the flow variable relation shown in step (4). By a permutation of subscripts one sees that there are three different permissible causalities for an 0-junction. Thus one causal stroke must be adjacent and two must be opposite in any arrangement. This means that if one effort is an input the other two efforts must be outputs. Similarly, for a 1-junction (common flow junction) assuming f_1 is an input, the remaining two flows must be outputs: the rules are,

$$\text{Rules}\begin{cases} (1)\ W_1 = -W_2 - W_3 \\ (2)\ e_1 f_1 = -e_2 f_2 - e_3 f_3 \\ (3)\ f_2 = f_1,\ f_3 = f_1 \\ (4)\ e_1 = -(e_2 + e_3) \end{cases}$$



The rules begin with a power balance (step (1)) based on the (arbitrary) assignment of power flow. Since the flows are common (step (3)) the efforts are determined, as shown in step (4).

Again, a permutation of subscripts shows there are three different permissible causalities for a 1-junction. In these one causality stroke must be opposite and two causality strokes must be adjacent.

Storage elements with differentiation causality do not contribute state variables. In a typical case the elimination of these elements leads to a state equation in which derivatives appear on both sides,

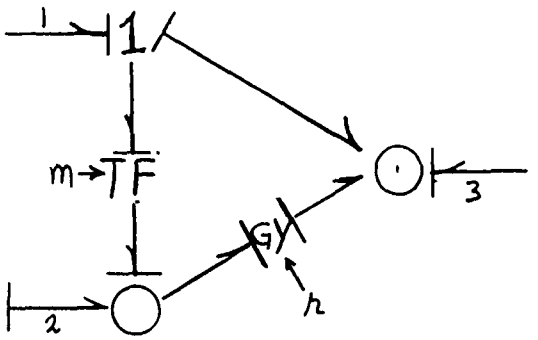
$$\dot{\mathbf{q}}(t) = \mathbf{F}\,q(t) + \mathbf{G}\,\mathbf{S}(t) + \mathbf{H}\dot{\mathbf{q}}(t).$$

Thus a single component can have the form,

$$\dot{q}_i = \frac{F_i q_i + G_i S_i}{1 - H_i}.$$

Junction Structure

A junction structure is essentially a complex n-port switch box consisting of 0- and 1-junctions, transformers, and gyrators, in which no power is generated, stored, or dissipated. It is a structure which compels the input power variables of any port to be related to the output power variables of the other ports, the relation being an $n \times n$ antisymmetric matrix (diagonal terms all zero). An example from [11] is shown below:



This is a 3-port junction structure with power variables f_1, e_1, f_2, e_e, f_3, e_3. The relation matrix is constructed from the power relations at the junctions:

at the junction with bond #1: $$e_1 - \frac{e_2}{m} - e_3 = 0$$

at the junction with bond #2: $$\frac{f_1}{m} + f_2 - \frac{e_3}{r} = 0$$

at the junction with bond #3: $$f_3 + \frac{me_1}{r} + f_1 = 0$$

Thus the power variables are related through the matrix equation:

$$\begin{bmatrix} f_1 \\ e_2 \\ f_3 \end{bmatrix} = \begin{bmatrix} 0 & -m & m/r \\ m & 0 & -m \\ -m/r & m & 0 \end{bmatrix} \begin{bmatrix} e_1 \\ f_2 \\ e_3 \end{bmatrix}.$$

1.68.4 Bond Graphs for Interconnected Systems

The formulation of rules for the interconnection of multiports is not without ambiguities. This is because the procedures, no matter how formalized, are partly art. To clarify the steps we repeat again the definitions of 0-junction and 1-junction. In this regard let $\mathscr{X}$, $\mathscr{Y}$ be two integral-differential operators, the first operating on the flow variable and the second on the effort variable. Then, for nonconnected multiports,

$\mathscr{X}\{f\} = e$ defines a 1-junction
$\mathscr{Y}\{e\} = f$ defines a 0-junction

When multiports are connected it is a prerequisite that each is required to have an input and an output. Thus we broaden the definition to read,

$$\mathscr{X}^{(j)}\{f\} + e_0^{(j)} = e_i^{(j)},\ j = 1, 2 \ldots \quad \text{defines the } j\text{th connected 1-}junction$$

$$\mathscr{Y}^{(j)}\{e\} + f_0^{(j)} = f_i^{(j)},\ j = 1, 2 \ldots \quad \text{defines the } j\text{th connected 0-}junction$$

Since each effort (or flow) symbol represents a bond it is seen from the three terms in each equation that there are at least three bonds for a fully connected multiport. Clearly the operators $\mathscr{X}$, $\mathscr{Y}$ have at least one bond, but may have many more. When there is no output bond (meaning e_0 or f_0 is zero) the mulitport can be interpreted either as a 0-junction or a 1-junction by simply writing $\mathscr{X} = \mathscr{Y}^{-1}$ or $\mathscr{X}^{-1} = \mathscr{Y}$.

In laying out bond graphs one may encounter a *free bond* (for example, an open circuit voltage in electric circuits). The system is then undefined. To complete the bond graph one must connect this free bond to a source—say a flow source with zero flow. Similarly a free bond which is equivalent to a short circuit must be connected to an effort source with zero effort.

Bond graphs may also contain *active bonds*, symbolized by a full arrow with an e(= effort) or a f(= flow) on it:

$$\xrightarrow[(a)]{e} \qquad \xrightarrow[(b)]{f}.$$

Bond (a) transmits only an effort but no flow. Bond (b) transmits only a flow but no effort. These are *singal* bonds. An example of (a) is the voltage-controlled current source:

$$\xrightarrow{e} S_i \longrightarrow.$$

Here, $S_i = S_i(e)$, that is, the magnitude of current (and its phase) is a function of the applied voltage.

With these definitions in mind we proceed with developing a technique for interconnecting multiports. This is best done by means of examples.

1.69 EXAMPLES OF INTERCONNECTED BOND GRAPHS [1]

Example #1 Lumped Parameter Mechanical System

An electrodynamic shaker in simplified representation is shown in Fig. 1.69.1. To contruct a bond graph we follow these steps.

A. choose the flow variables (or 'degrees of freedom') which define the state of the connected system at any instant.

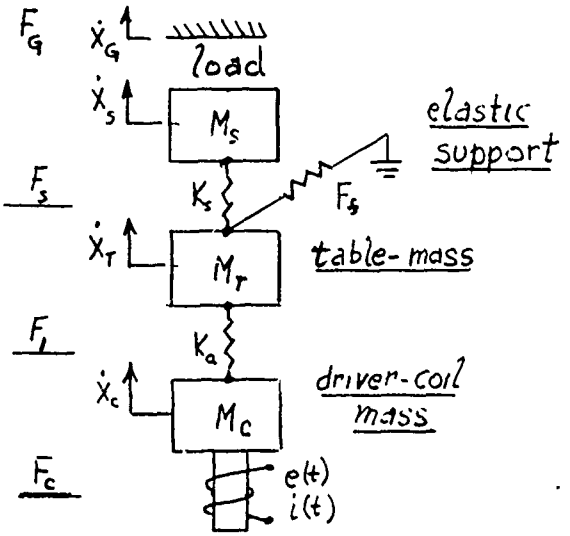


Fig. 1.69 1 — Schematic representation of an electrodynamic shaker [11]

In this example these are $i(t)$, $X_c(t)$, $X_T(t)$, $X_s(t)$.

B. write the input-output relations for each identifiable multiport, and, using the definitions noted above, assign a 0-junction or 1-junction as required for each multiport.

In this example the relations are listed below: on the left side of each entry is the relation, while on the right side is the bond graph fragment:

(1)	$Z_e i + E_0 = E_i$	Z_e | $-0-1-0-$
(2)	$i = \alpha F$	Gyrator
(3)	$Z_c \dot{X}_c + F_1 = F_c$	Z_c | $0-1-0-$
(4)	$Y_T F_1 + \dot{X}_T = \dot{X}_c$	$-1-0-1-$ | Y_T
(5)	$Z_T \dot{X}_T + F_2 = F_1$	$-0-1-0-$ | Z_T
(6)	$F_2 = F_s + F_f$	
(7)	$Y_s^{(1)} F_s + \dot{X}_s = \dot{X}_T$	Y_s | $-1-0-1-$
(8)	$Y_f F_f = \dot{X}_T - \dot{X}_G$	Y_s | $-1-0-1-$ (Note: $X_G = 0$)
or	$Z_f \dot{x}_T = F_f - F_G$	Z_f | $-0-1-0-$ (Note: $F_G =$ ground potential $= 0$)
(9)	$Z_s^{(2)} X_s^a = F_s - F_G$	Z_s | $-0-1-0-$ (Note: $F_F = 0$)
or	$Y_s(2) F_s = \dot{x}_s - \dot{x}_G$	Y_s | $-1-0-1-$ (Note: $\dot{x}_G = 0$).

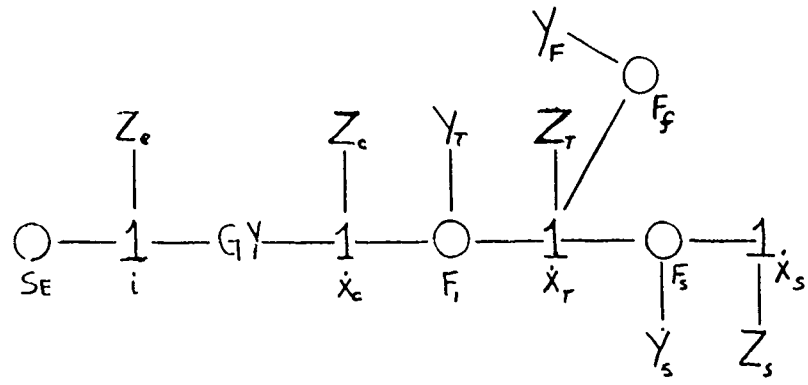


Fig. 1.69.2 — Bond graph of Fig. 1.69.1

C. With these relations established interconnect all multiports in cascade as shown in Fig. 1.69.2.

It is noted that

- two free bonds are completed with a grounded 1-junction and a grounded 0-junction respectively,
- since $Y_f = Z_F^{-1}$ the spring k_f can be represented as a 1-junction and joined to Z_T,
- since $Z_s^{(2)} = (Y_s^{(2)})^{-1}$ the terminal 1-junction can be represented as a 0-junction and joined to $Y_s^{(1)}$.

Figure 1.69.3 shows the revised bond graph with explicit Z and Y operators.

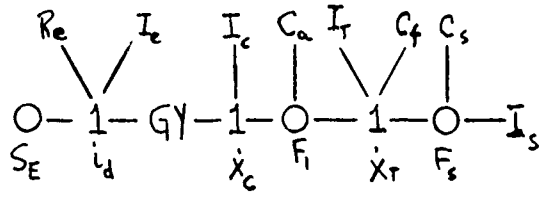


Fig. 1.69.3 — Revised bond graph of Fig. 1.69.1

Actually the bond graph can be constructed without the use of equations. The bonds simply follow this verbalization:

- electric current $i(t)$ provides force F_c.
- F_c accelerates mass M_c generating velocity $\dot{x}_c$.
- $\dot{x}_c$ generates force F_1 in spring k_a.
- F_1 accelerates mass M_T generating velocity $\dot{x}_T$.
- $\dot{x}_T$ generates force F_s in k_s and force F_f in k_f.
- F_s accelerates mass M_s generating velocity $\dot{x}_s$.

For each velocity we use a 1-junction, and for each force we use a 0-junction.

This example illustrates the rule applicable to mechanical networks: spring (and dampers) develop a force when ever there is a relative velocity difference impressed on their ends. Masses develop a velocity when ever there is a force difference impressed across them.

It is illuminating to construct an equivalent electrical circuit from this bond graph. To do this we must select which variables are 'across' and which are 'through'. In the electrical branch we choose E

to be 'across' and i to be 'through'. A 0-unction therefore shows elements that are electrically in parallel, and a 1-junction represents elements that are electrically in series. In the mechanical branch the gyrator represents a current/force analogy, hence force is the 'through' (or flow) quantity. Thus a 1-junction that comes after a gyrator signifies elements electrically in parallel, and a 0-junction after a gyrator represents elements electrically in series. Thus the translation of the bond graph into an equivalent electrical circuit takes the form shown in Fig. 1.69.4.

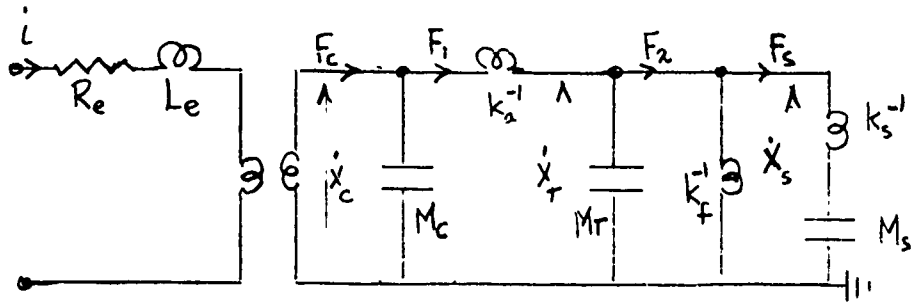


Fig. 1.69.4 — Equivalent circuit constructed from the bond graph shown in Fig. 1.69.3

Example #2 An Electric Circuit

An electric circuit with mutual inductance is shown in Fig. 1.69.5. It is analyzed as a 3-Port, identifiable by the variables,

$$e_1,\ i_1;\ e_2,\ i_2;\ e_3,\ i_3$$

The signs to be associated with the mutual impedances depend on the relative sign orientation of the three coils and upon the (assumed) directions of currents. In the practice of electrical engineering orientation is specied by ± signs, or by a convention in which dots, squares, triangles etc. placed at the ends of a coil indicate direction of potential rise or potential fall. We assume here that the signs have been established. In the associated bond graph, constructible according to the rules noted above, the junction B, C, E is recognized as an 0-junction (that is, a junction common voltage). It is bonded to three 1-junctions (that is, junctions of common flow). Figure 1.69.6 a shows the bond graph. Simplification is achieved by writing all inertances (both self and mutual) in the matrix form $Ii = p$ (p is the force impulse $\int e\ dt$), and by choosing the D node as grounded potential, Fig. 1.69.6b. When a 3-Port 0-junction or 1-junction has one bond to "ground," defined as a bond with zero effort, it is contracted to a 2-Port 0-junction, or a 2-Port 1-junction. As such *it is equivalent to a single bond.* Thus if $R_2 = 0$ the resultant 2-Port 1-junction (to which it was attached) becomes a single bond between effort B, C, E and the matrix I.

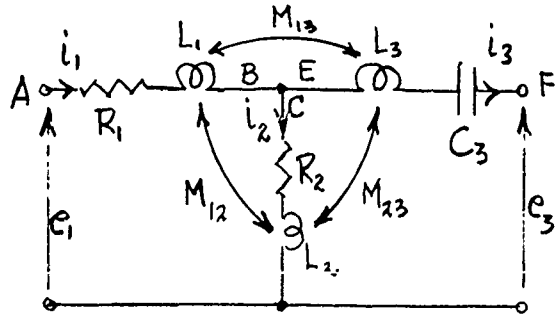


Fig. 1.69.5 — An electric circuit with mutual inductance [11]

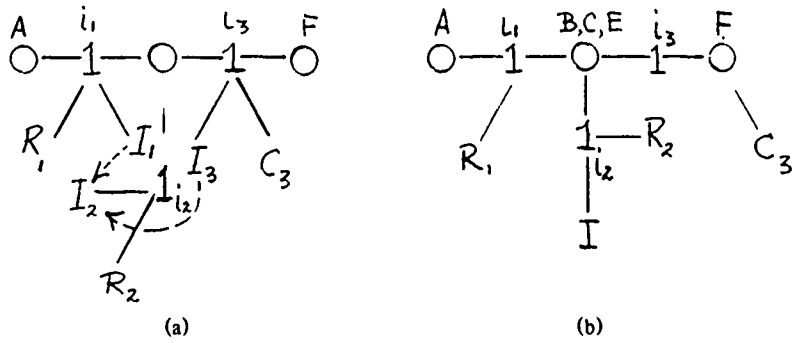


Fig. 1.69.6 — Bond graph of Fig. 1.69.5 (b) simplified bond graph

Example #3 An Electromechanical Transducer

A movable plate capacitor is idealized into the simple representation of Fig. 1.69.7. At equilibrium the deplacement distance between diaphragm and fixed plate is X_0 and the capacitance, carrying a charge q_0 at potential E_0, is

$$C_0 = \frac{\epsilon\epsilon_0 A}{X_0}, \quad q_0 = E_0\, C_0.$$

For an incremental displacement $X(t)$, the capacitance becomes

$$C(t) = \frac{\epsilon\epsilon_0 A}{X_0 - X(t)} \cong C_0 \left[1 + \frac{X(t)}{X_0}\right]$$

and the incremental charge becomes $q(t)$. The total stored potential energy under quasi-static conditions is then

$$W(t) = \frac{1}{2}\,\frac{[q_0 + q(t)]^2}{C(t)} + \frac{1}{2}\,kX^2(t)$$

in which k is the mechanical stiffness of the diaphragm.

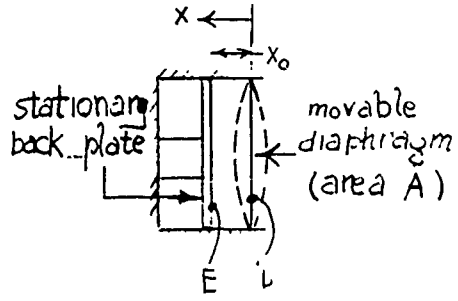


Fig. 1.69.7 — Idealized moving plate capacitor transducer

We desire to model this system as a 2-Port transducer in which the power variables are E, i for the electric field, and F, V for the mechanical field. We choose the degrees of freedom to be incremental variable of charge and displacement $q(t)$, $X(t)$ correspoding to the incremental voltage $e(t)$ and incremental force $\Delta F(t)$. Since analysis consists in finding the relation between effort variables and flow variables we look for the form,

$$\begin{bmatrix}\Delta F(t)\\ e(t)\end{bmatrix} = \begin{bmatrix}\dfrac{\partial W}{\partial X}\\ \dfrac{\partial W}{\partial q}\end{bmatrix} = \begin{bmatrix}2\times 2\\ \text{matrix}\end{bmatrix}\begin{bmatrix}X(t)\\ q(t)\end{bmatrix}.$$

Now using the approximation for $C(t)$ noted above one obtains,

$$\frac{\partial W(t)}{\partial X} = -\frac{q_0^2}{2C_0X_0} - \frac{q_0 q}{C_0X_0} + kX = f_0 + \Delta F(t).$$

It is directly seen that

$$f_0 = -\frac{q_0^2}{2C_0X_0}.$$

Also,

$$\frac{\partial W}{\partial q} = \frac{(q_0+q)}{C_0}\left[1 - \frac{X}{X_0}\right] = \frac{q_0}{C_0} + \frac{q(t)}{C_0} - \frac{q_0\,X(t)}{C_0X_0} - \frac{q(t)\,X(t)}{C_0X_0} = E_0 + e(t).$$

We neglect the term qX as being of second order and cancel $E_0 = q_0/C_0$. The equations of the 2-Port then reduce to the matrix form.

$$\begin{bmatrix}\Delta F(t)\\ e(t)\end{bmatrix} = \begin{bmatrix}k & -\dfrac{q_0}{C_0X_0}\\ \dfrac{-q_0}{C_0X_0} & \dfrac{1}{C_0}\end{bmatrix}\begin{bmatrix}X(t)\\ q(t)\end{bmatrix}.$$

These equations show that the effort variable is related to flow unpulse ($= \int i dt$) and hence that the 2-Port is a capacitance. The bond graph is

$$\frac{e}{q}\ C\ \frac{f}{X} \text{ or } \frac{e}{i}\ C\ \frac{f}{\dot{X}}.$$

Example #4 A Linear Distributed System

A linear distributed system is exemplified by a finite elastic beam of mass density ρ per unit of length (units: Ns^2/m^2) supported in some prescribed way at its ends and driven into transverse flexure by a distributed force $F(X, t)$ (units: N/m), Fig. 1.69.8. The transverse displacement $w(X, t)$ at any instant of time is governed by a dynamic equation of the form,

$$\mathscr{K}\{w(X, t)\} + \rho\ddot{w}(X, t) = F(X, t)$$

in which $\mathscr{K}$ (units: N/m^2) is a differential integral operator in both the spatial and temporal variables. At time $t = 0$ assume the transverse displacement is $w(X, 0)$, and the transverse velocity is $\dot{w}(X, 0)$.

The classical solution to this problem begins with the Laplace transformation of the time variable in both the dynamic equation and the initial conditions. The result is,

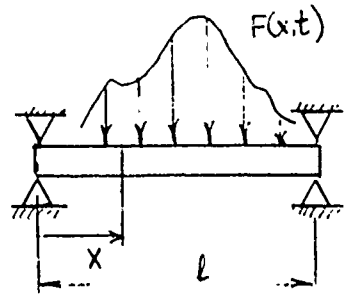


Fig. 1.69.8 — An elastic beam simply supported and driven by a force $F(x, t)$

$$(1)\quad \mathscr{K}\{\bar{w}(X, s)\} + \rho s^2\, \bar{w}(X, s) = \bar{F}(X, s) + g(X, s) + h(X)$$

$$(2)\quad g(X, s) = \rho s\, w(X, 0);\ h(X) = \rho\, w(X, 0)$$

(Here an overbar means a transformed quantity). To solve this equation in the variable X it is conventional to algebraicize the operation of $\mathscr{K}$ by writing $w(X, t) = w(X) \exp(-i\omega t)$ and setting $F(X, t) = 0$. Then

$$(\mathscr{K} - \rho\omega^2)\ W(X) = 0.$$

This equation is true only for discrete eigenvalues ω_n of ω, and special eigenfunctions W_n of w, that is,

$$(\mathscr{K}_n - \rho\omega_n^2)\ W_n = 0,\ \text{i.e.}\ \mathscr{K}_n = \rho\omega_n^2.$$

Here W_n satisfies the boundary conditions of mechanical constraint of the beam.

Since the set of W_n constitute (by construction) a complete orthonormal system, one can expand all flow and effort functions in them:

$$\bar{w}(X, s) = \sum_n \alpha_n(s)\ W_n(X)$$

$$\bar{X}(x, s) = \sum_n \beta_n(s)\ W_n(x)$$

$$g(x, s) = \sum_n \gamma_n(s)\ W_n(x)$$

$$h(x) = \sum_n \delta_n\ W_n(x).$$

Upon substitution into the equation for $\bar{w}(x, s)$, one immediately finds that

$$\alpha_n(s) = \frac{1}{\mathscr{K}_n + \rho_s^2} \left\{\beta_n + \gamma_n + \delta_n\right\}.$$

Hence,

$$\bar{w}(x, s) = \sum_n W_n(x)\ Y_n(s)\ G_n(s)$$

where,

$$Y_n(s) = \frac{1}{\mathscr{K}_n + \rho s^2};\ G_n(s) = \int_0^l \overline{F}(x,\ s) + g(x,\ s) + h(x))\ W_n(x)\ dx.$$

Using the convolution theorem for taking inverse Laplace transforms one arrives at,

$$\sum_n \alpha_n(t)\ W_n(x) = w(x,\ t)$$

where,

$$\alpha_n(t) = \mathscr{Y}_n(s) * G_n(s)$$

Now $\overline{w}(x,\ s)$ can be rewritten in the form,

$$\mathscr{Z}_n(s)\ \overline{w}(x,\ s) = \sum_n W_n\ G_n(s),\ Z_n(s) = \mathscr{K}_n + \rho s^2$$

from which it is seen that for each mode n,

$$\mathscr{Z}_n(s) * \alpha_n(s) = G_n(t).$$

The equation for $w(x,\ t)$ is interpreted as a 0-junction multiport since the right hand side can be considered to be an input flow function and the left hand side can be considered to be an output of common forces (through $G_n(s)$) in each mode. The equation for $G_n(t)$ is interpreted as a 1-junction multiport in each mode since $G_n(t)$ is a model "effort" function and $\alpha_n(s)$ is interpreted as a flow function. Figure 1.69.9 shows the bond graph. It is seen that the eigenfunction W_n in each mode play the role of a transformer (= *TF*). Since *TF* stores no energy all forces are instantaneously communicated throughout the system. This example shows how model analysis converts distributed systems into lumped parameter systems making it ideally suited to the construction of physical models.

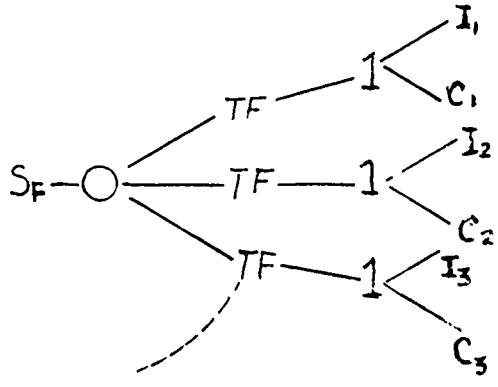


Fig. 1.69.9 — Bond graph of Fig. 1.69.8 analyzed in modes

Example #5 Word Bond Graphs

An advantage of bond graphs rests in dispensing with equations during their construction. Instead of equations one can begin analysis of a multiport with *word bond graphs.* This is illustrated by the example of a pressure controlled valve, Fig. 1.69.10 [12]. The word bond graph is constructed by

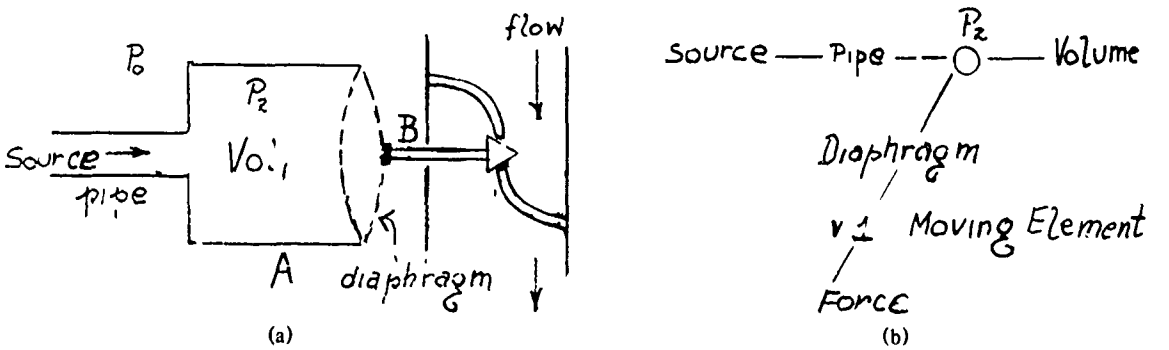


Fig. 1.69.10 — (a) Pressure controlled value, (b) word bond graph [11]

inspection. First, the container A interacts with its environment at 3 ports (1) it receives flow from the pipe (2) it is a rigid wall between pressure P_2 and outside pressure P_0, and (3) it actuates the diaphragm. Since the 3-part is a junction of efforts (= pressure) it appears as an 0-junction in the word bond graph. Second, the moving element B interacts with the environment at several ports (1) it is attached to the diaphragm which is bonded to the 0-junction (2) it experiences inertance, capacitance and resistance to its motion, and (3) it delivers a force. Since these interactions feature a common velocity the moving element B is modeled as a 1-junction. Third, the pipe itself is a 2-port. It can be described as a common flow 1-junction with flow resistance R_p. The word-bond graph in Fig. 1.69.10(b) lends itself directly to the construction of the bond graphs, Fig. 1.69.11. The symbols mean: C_1 is the capacitance of volume 1; TF is the transformer of area from diaphragm to moving element B; C_2 is the capacitance of the diaphragm; R_V is the viscous friction of B; R_C is the Coulomb friction of B; I is the inertance of B; S_F is the source force B of the flow medium.

The bond graph, thus completed without equations, serves as a basis for formation of equations or block diagrams or signal flow graphs. Analysis by system of equations is discussed in the next example.

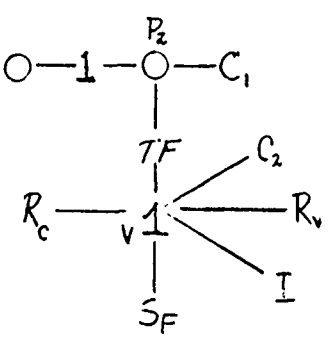
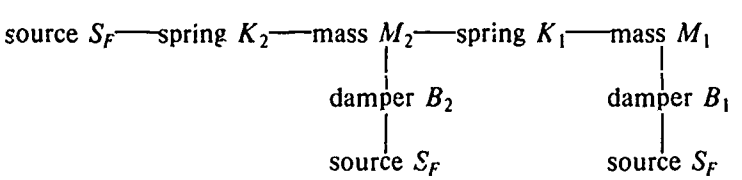


Fig. 1.69.11 — Bond graph of Fig. 1.69.10

Example #6

Figure 1.69.12 illustrates a translational system in one dimension. The platform P acts as a velocity source which drives two masses, (M_1, M_2) two springs (K_1, K_2) and two dampers (B_1 and B_2).

The word-bond graph is construed as follows:



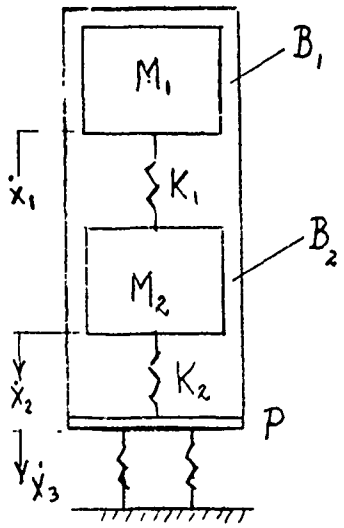


Fig. 1.69.12 — A translational system driven by a velocity source

The bond graph itself is constructed according to the rules noted above:

- springs and dampers are common effort 0-junction
- masses are common flow 1-junctions.

Figure 1.69.13 shows the augmented bond graph in which C and I are given integration casuality.

Taking C_2, I_2, C_1, I_1, B_2, and B_1 as integral-differential operators we can derive the equation of this system in a simple way: (1) $C_2F_2 + \dot{x}_2 = \dot{x}_3$ (2) $B_2^{-1}F_{B2} + \dot{x}_2 = \dot{x}_3$ (3) $I_2\dot{x}_2 + F_1 = F_2 + F_{B2}$ (4) $C_1F_1 + \dot{x}_1 = \dot{x}_2$ (5) $I_1\dot{x}_1 + F_{B1} = F_1$, and (6) $B_1^{-1}F_{B1} + \dot{x}_3 = \dot{x}_1$.

The assignment of casuality begins with (known) S_F represented by an adjacent bond stroke. All other casuality strokes follow the rules explained in Sec. 1.68.3.

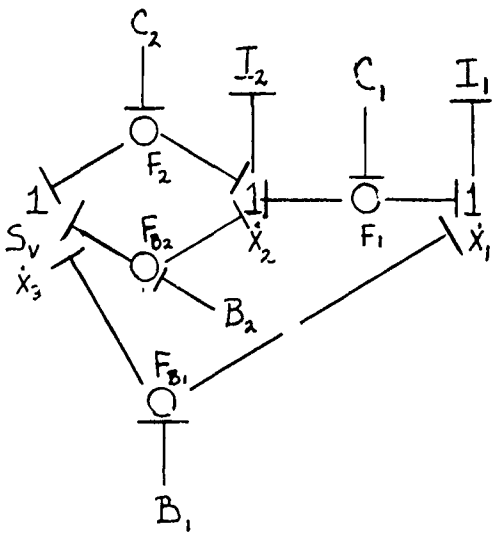


Fig 1.69.13 — Bond graph of Fig 1.69.12

Example #7 Another Example of Assignment of Causality is Shown in Fig. 1.69.14 and Fig. 1.69.15.

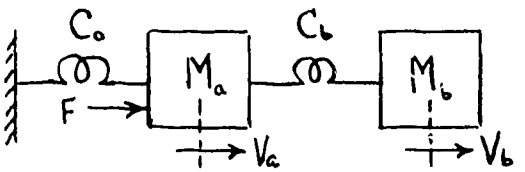


Fig. 1.69.14 — Mechanical translational system consisting of two masses and two springs

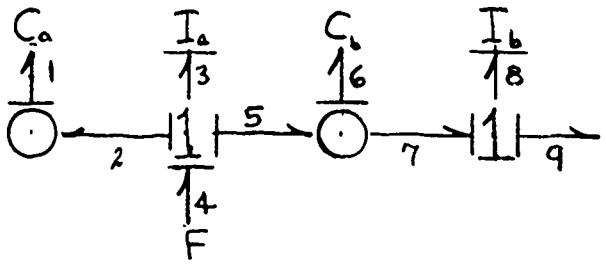


Fig. 1.69.15 — Bond graph of Fig. 1.69.14

The bond graph of this mechanical translational system based on integral causality is:

From this graph one easily constructs the dynamic relations among the various bonds:

at 0-junction of bonds 1,2: $-V_1 + V_2 = 0;\ V_2 = V_a$

or $j\omega C_a F_1 = V_a$

at 1-junction of bonds 2,3,4,5: $-F_2 - F_3 - F_5 + F = 0;\ F_2 = F_1$

or $\dfrac{V_a}{j\omega C_1} + j\omega M_1 V_a + F_5 = F$

at 0-junction of bonds 5,6,7: $-V_7 - V_6 + V_5 = 0;$ $\begin{cases} V_5 = V_a;\ V_7 = V_b \\ F_6 = F_5;\ F_6 = F_7 \end{cases}$

or $j\omega C_b F_6 + V_b = V_a$

at 1-junction: $-F_9 - F_8 + F_7 = 0$

or $j\omega M_b V_b + F_9 = F_7 = F_6 = F_5.$

From these relations one can obtain V_a, V_b and all forces.

SUMMARY

These seven examples, chosen primarily for their simplicity, are an indication of the method of bond graphs. Since other methods serve equally well. The full advantage of bond graphs is not visible. This will come with application to structure of great complexity.

1.70 ANALYSIS OF MULTIPORT SYSTEMS USING INTEGRAL CAUSALITY

It is useful to formalize a procedure for analyzing physical systems by use of bond graphs. Formal rules serve to guide the analysis in all but pathological cases. An example illustrates the method.

Example of Analysis

Assume first a given physical system has been described by a word bond graph from which the bond graph Fig. 1.70.1(a) is drawn.

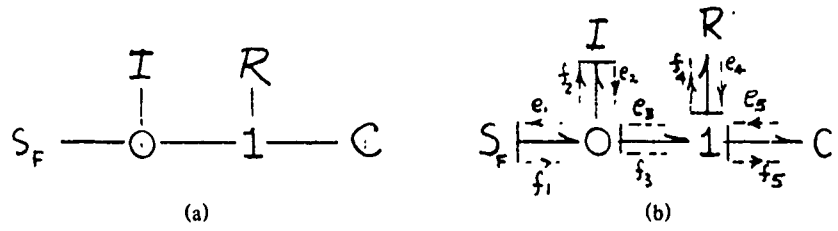


Fig 1.70.1 – (a) Bond graph, (b) causality and power assignment

We begin the analysis by augmenting the bond graph with (1) casual strokes (2) power flow. The rules for augmentation are:

- Assign effort or flow causality to all sources.

In Fig. 1.70.1b a causal stroke is placed adjacent to the flow source F(F ⊢——) to indicate that the source supplies a flow independent of the elements in the remainder of the graph. (Other sources, if present, are similarly treated: flow sources having causal strokes at the near end of the bond and effort sources at the far end).

- For each storage element (C or I) assign causality in integral form. This means the assignment of C, I in Fig. 1.70.1b as follows:

$$C \text{ ——⊣, meaning } e_{out} = L_c^{-1} \int f_{in} dt$$

$$I \text{ ⊢——, meaning } f_{out} = L_I^{-1} \int e_{in} dt.$$

The use of the integral form is convenient because it lends itself to optimal choices of state variables. However, the choice of differential form is also a valid procedure.

- for each 0-junction extend causality by allowing one adjacent casual stroke and two opposite strokes. This may mean the assignment of arbitrary causality to R-fields.

- for each 1-junction allow two adjacent causel strokes and one opposite stroke. This also may mean the assignment of arbitrary causality to R-fields.

• if above steps do not complete causality assign causal strokes to R-ports arbitrarily, but not to conflict with established causality.

• assign power flow by inspection observing the caution that sources deliver power and resistance absorb power. Experience has shown that the following rules on power flow lead to minimum ambiguity:

(1) power should be directed *into* all I, C and R 1-ports.

(2) power should be directed *into* and through all transformer and transducer 2-ports.

(3) the assignment of power flow direction in 0-functions and 1 junctions is arbitrary.

• choose *output* variables from each bond.

In Fig. 1.70.1(b) these are given as f_1, f_2, e_4, e_5, e_3. Special names are given to these variables:

f_1: *source* variables. These are generically called the $\{U\}$ set.

f_2, e_5: *state* variables (because C, I determine the state of the physical system). These are generically called the $\{X\}$ set.

e_4: *temporary* variable (because while they help in formation of the system equations they eventually are eliminated in the final solution). These are generically called the $\{T\}$ set.

e_3: *auxilary* variables (because they are associated with 0 or 1− junctions). These are generically called the $\{H\}$ set.

The total set $\{X, U, T, H\}$ is written $\{V\}$. In this example

$$\{V\} = \{f_1, f_2, e_4, e_5, e_3\} \ldots$$

Figure 1.70.1(b) shows the completed augmented graph.

From this point on the goal of analysis is to derive a set of equations which express the output of the storage elements I,C in terms of the sources. The steps in the procedure are:

(1) $f_2 = \mathscr{L}_I^{-1} \left[\int e_2 \, dt + p(0)\right]$

(2) $e_5 = \mathscr{L}_c^{-1}\left[\int f_5 dt + q(0)\right]$

(3) $e_4 = Rf_4$

(4) at the 0-juntion $f_3 = f_1 - f_2$ (See Sec. 1.68.3)

(5) at the 1-junction $f_4 = f_3$, $f_5 = f_3$

*(6) $\therefore e_5 = \mathscr{L}_c^{-1}\left[\int (f_1 - f_2)\, dt + q(0)\right]$

(7) at the 0-junction $e_2 = e_3$

(8) at the 1-junction $e_3 = e_4 + e_5 = Rf_4 + e_5$ (See Sect. 1.68.3)

*(9) $\therefore f_2 = \mathscr{L}_I^{-1}\left[R(f_1 - f_2) + e_5\right] dt + p(0)]$.

The steps with * indicate the final results. They appear as a pair of integral equations in the state variables f_2, e_5.

When a bond graph contains one or more inertance or capacitances which cannot be assigned integration causality in the completion of the augmentation of the graph, special care must be taken. Figure 1.70.2 shows just such a case. In (a) the acausal graph is laid out. In (b) inertances I_1 and I_2 are given integration causality. Upon completing graph augmentation it is found that I_3 has been assumed differential causality. The physical meaning is this: f_3 is statically determined by f_1 and f_2; that is, the relation between f_1, f_2 and f_3 is,

$$0 = Df_1 + Df_2 + Df_3,\ D = \text{operator},$$

One concludes that f_3 cannot be a state variable; it is a temporary variable, and can be eliminated from the state equations. Similarly, the appearance of capacitances in differential form leads to a static relation between it and the other capacitances which are properly assigned integration forms. The power variables of capacitances assigned differential forms become temporary variables which are finally eliminated from the state equations.

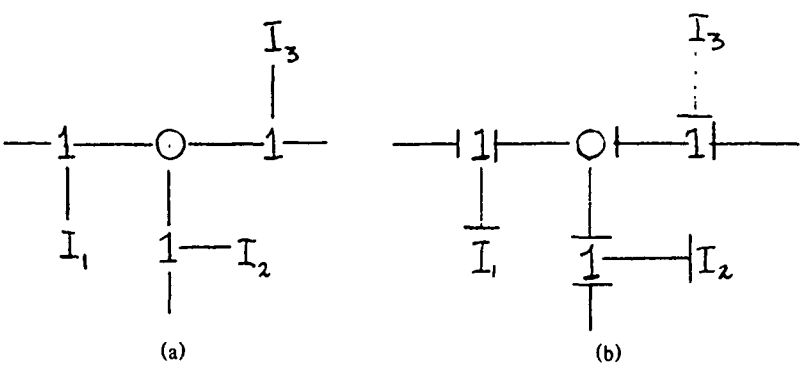


Fig 1.70.2 — (a) Bond graph featuring three inertances, (b) causality assignment

1.70.1 Formulation of Dynamic Equations From a Bond Graph

We summarize all previous exposition by a set of rules.

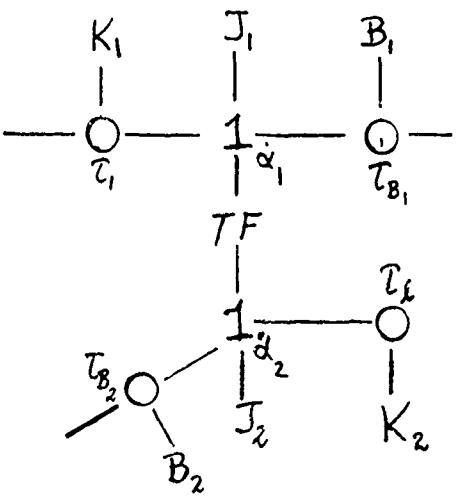
A bond graph is a chain of 0-junctions and 1-junctions with added sources and loads. It allows a rapid determination of the equations governing the dependent and independent variables. Several simple rules in formulation of these equations are helpful:

• A 1-junction bonded directly to n different 0-junctions and in different 1-ports establishes the relation of efforts,

$$\sum_{j=1}^{m} Z_j f_j + \sum_{i=2}^{n} e_i = e_1$$

in which e_1 is any choice, and f_1 is the flow variable specifying the 1-junction.

Example



A portion of a bond graph featuring a transformer is shown. Here the effort τ_1 is related to *all* the efforts bonded to the 1-junction including the transformed 1-junction:

$$j\omega J_2 \dot{\alpha}_2 + j\omega J_1 \dot{\alpha}_1 + \tau_1 + \tau_{B_2} + \tau_{B_1} = \tau_1.$$

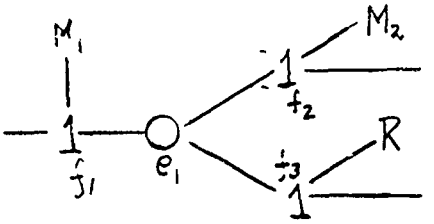
It is noted that when the effort at a junction is explicitly stated, the flow at that junction does not appear in the equation.

• A 0-junction bonded directly to n different 1-junctions and m different 1-ports establishes the relation of flows,

$$\sum_{n=1}^{n} Y_j e_j + \sum_{i=2}^{n} f_i = f_1$$

in which f_1 is any choice, and e_1 is the effort variable specifying the 0-junction.

Example

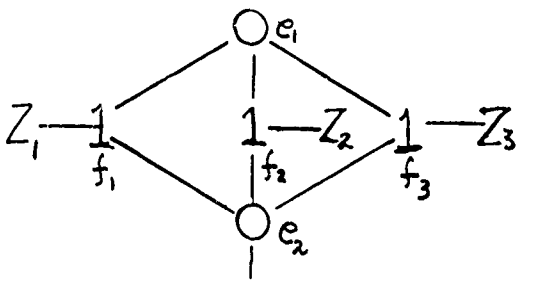


In the bond graph shown the rule states that

$$Ye_1 + f_3 + f_2 = f_1.$$

Again, it is noted that when the flow at a junction is explicitly stated, the effort at that junction does not appear in the equation.

- Two 1-junctions bonded to n 0-junctions establish a relation of flows

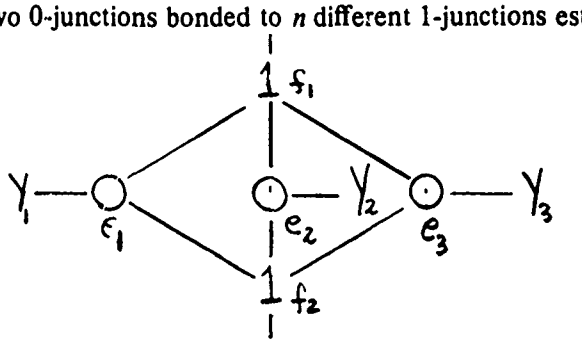


$$Y_1 e_1 + f_2 = f_1$$

$$Y_2 e_2 + f_2 = f_1$$

$$Y_n e_n + f_2 = f_1$$

Similarly, two 0-junctions bonded to n different 1-junctions establish the relations of efforts,



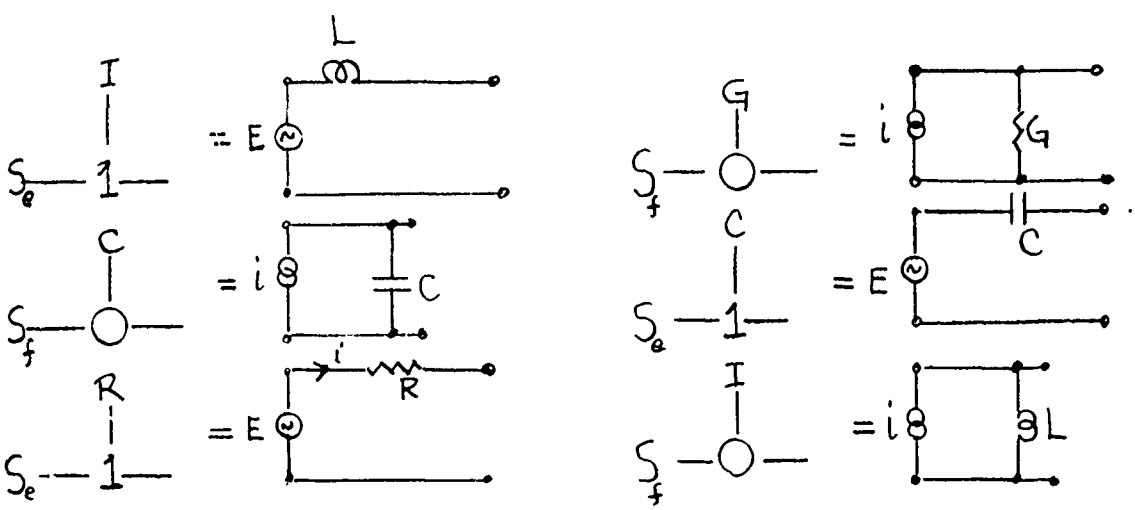
$$Z_1 f_1 + e_2 = e_1$$

$$Z_2 f_2 + e_2 = e_1$$

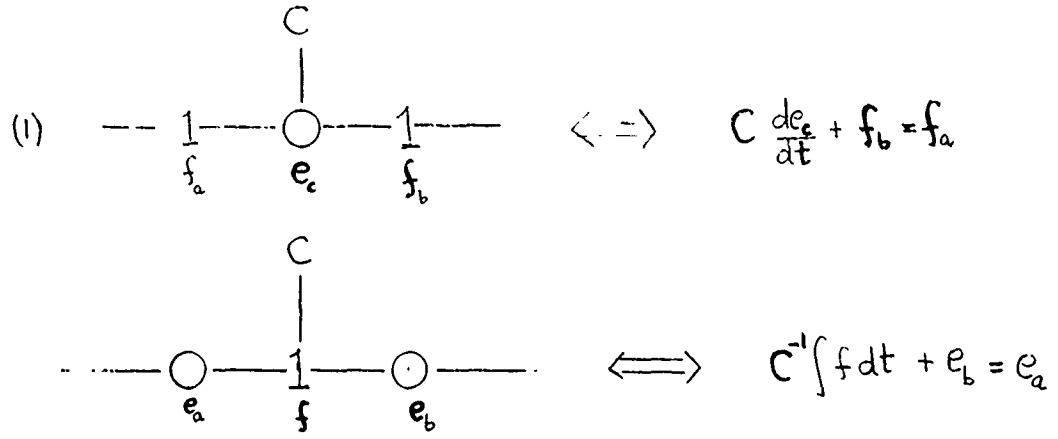
$$Z_n f_n + e_2 = e$$

- A flow source can be bonded to an 0-junction (parallel arrangement) or to a 1-junction (series arrangement).

An effort source can be bonded to an 0-junction (parallel arrangement) or to a 1-junction (series arrangement). Examples of these rules and their electrical circuit equivalents are listed below:

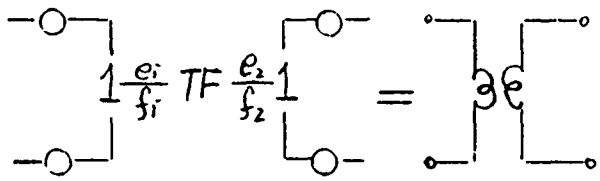


- An elementary 1-port is bonded to its neighbors in the network in one of two ways: either it is connected to a common force junction (0-junction) or to a common velocity junction (1-junction). In the former case the 0-junction is sandwiched between two 1-junctions, while in the latter case the 1-junction is sandwiched between two 0-junctions. The physical difference between these cases is made evident by the mathematical formula which express the relation between effort and flow. For example, the two possible bonding arrangements of the generalized capacitance C are:

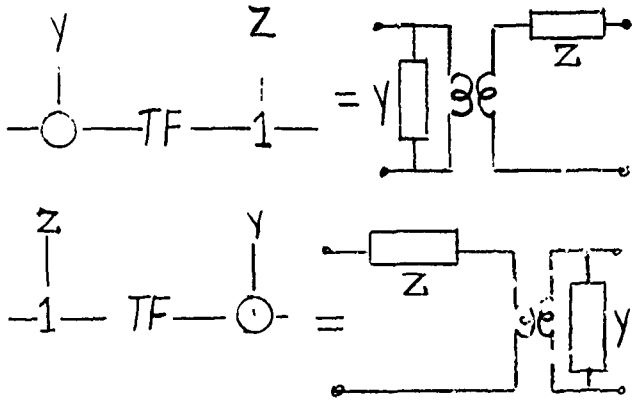


Let these represent mechanical elements. In (1) a force is transmitted through an 0-junction accompanied by a velocity difference. This is the case of a linear spring. In (2) force difference develops a velocity. This is the case of an elastic diaphragm.

- A pure transformer is bonded between two 1-junctions.



However, by simplification,



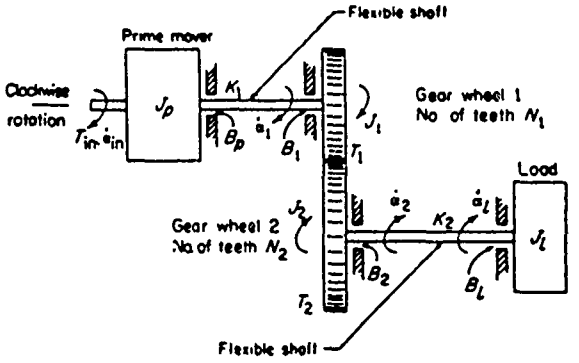
- A pure gyrator obeys the same rule as a pure transformer with the exception that

$$rf_2 = e_1$$

$$\frac{1}{r}e_2 = f_1 \ldots\ldots$$

We illustrate these rules by a step-by-step construction of the bond graph of the following rotational-mechanical system:

Example



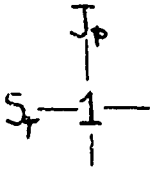
A rotational mechanical system with gears between prime mover and load.

1. the degrees of freedom are $\dot{\alpha}_{in}$, $\dot{\alpha}_1$, $\dot{\alpha}_2$, $\dot{\alpha}_l$, $\dot{\alpha}_B$. α_G is the 'ground' angular velocity, here taken to be zero.

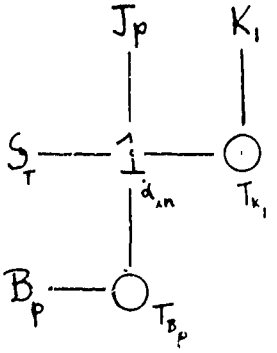
2. the torque T_{in} is an effort source represented by $S_e = S_T$. The graph is,



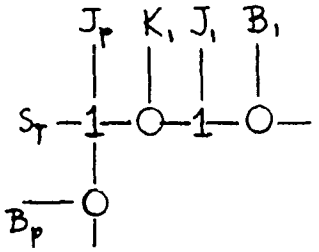
3. T_{in} drives the rotary mass J_p. Since the rule requires mass to be bonded to a 1-junction, we bond S_T directly to this 1-junction which represents $\dot{\alpha}_{in}$. The graph is



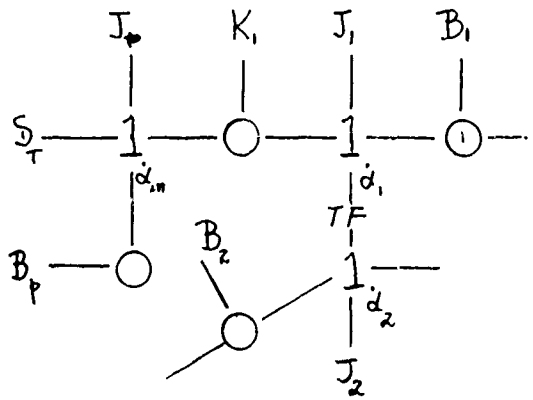
4. the 1-junction ($\dot{\alpha}_{in}$) is bonded to the capacitance (compliance) of the flexible shaft and the resistance (friction) B_p. The rule requires capacitance to be bonded to an 0-junction, and resistance to an 0-junction or 1-junction (choose the 0-junction). The graph is now,



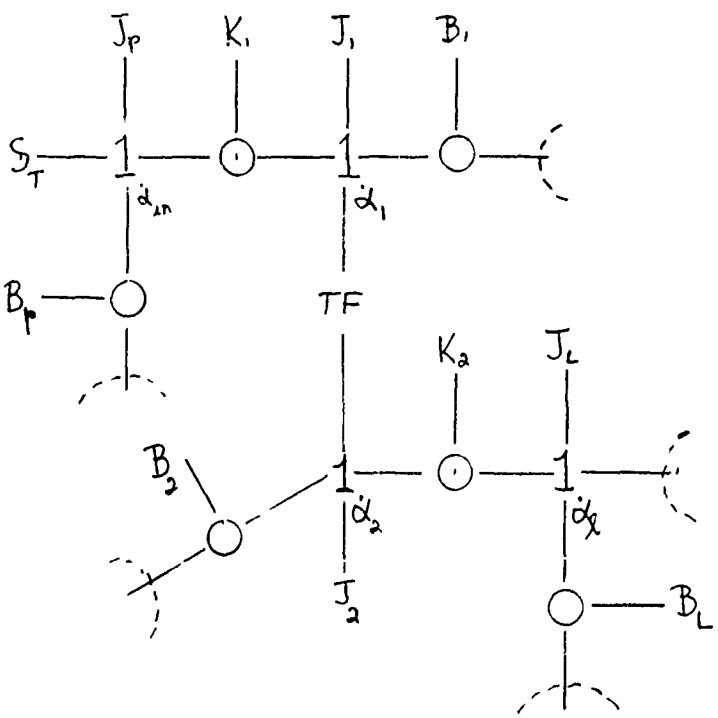
5. Since the torque T_{k_1} in Shaft #1 depends on the difference in angular velocities α_{in} and $\dot{\alpha}_1$, its 0-junction is bonded to a 1-junction representing $\dot{\alpha}_1$. The rule requires J_1 to be bonded to this 1-junction. Resistance B_1 is also bonded to this 1-junction. The graph is now,



6. the two gears constitute a transformer, that is $\dot{\alpha}_2 = (N_1/N_2)\ \dot{\alpha}_1$; $T_2 = (N_2/N_1)T_1$. We therefore bond the 1-junction representing $\dot{\alpha}_1$ to a TF 2-port, which in turn is bonded to a 1-junction representing $\dot{\alpha}_2$. The rule requires J_2 to be bonded to this ($\dot{\alpha}_2$) 1-junction, together with resistance B_2. The graph is now,



7. the rules require Shaft #2 to be bonded to an 0-junction between the 1-junction representing $\dot{\alpha}_2$ and the 1-junction representing $\dot{\alpha}_1$, and the rotary mass J_L to be bonded to the latter. In addition resistance B_L is bonded to junction α_1, and since all resistances are to 'ground' they are bonded to sources of zero angular velocity. The completed bond graph is finally,



The dynamic equations of this graph are found by inspection:

$$(1) \quad j\omega J_p\dot{\alpha}_{in} + T_{B_p} + T_{k_1} = S_T$$

$$(2) \quad j\omega K_1^{-1}T_{k_1} + \dot{\alpha}_1 = \dot{\alpha}_{in}$$

$$(3) \quad j\omega J_2\dot{\alpha}_2 + j\omega J_1\dot{\alpha}_1 + T_{k_2} + T_{B_2} + T_{B_1} = T_{k1}$$

$$(4) \quad j\omega K_2^{-1}T_{k_2} + \dot{\alpha}_l = \dot{\alpha}_2$$

$$(5) \quad j\omega J_L\dot{\alpha}_l + T_{B_L} + S_{T_G} = T_{K_2}$$

$$(6) \quad B_2^{-1}T_{B_2} + \dot{\alpha}_G = \dot{\alpha}_2$$

$$(7) \quad B_p^{-1}T_{B_p} + \dot{\alpha}_G = \dot{\alpha}_{in}$$

$$(8) \quad B_L^{-1}T_{B_L} + \dot{\alpha}_G = \dot{\alpha}_l$$

$$(9) \quad \frac{N_2}{N_1}\dot{\alpha}_2 = \dot{\alpha}_1$$

1.71 ANALYSIS OF MULTIPORT SYSTEMS BY FIRST-ORDER DIFFERENTIAL EQUATIONS [11]

In the previous Section 1.70.1 the power variables of a physical system were classified as **X**, **T**, **H**, and **U** (that is, the state, temporary, auxiliary, and source vectors). Various interrelations can be constructed between these vectors. However, for purposes of numerical computation and analog simulation it is advantageous to interrelate all these vectors through first order ordinary differential equations called the state system equations. Thus the goal of this type of analysis is to derive the set

$$\text{(a)} \quad \frac{d}{dt}\mathbf{X} = \mathbf{A}\cdot\mathbf{X} + \mathbf{B}\cdot\mathbf{U}$$

$$\text{(b)} \quad \mathbf{Y} = \mathbf{C}\cdot\mathbf{X} + \mathbf{D}\cdot\mathbf{U} \qquad (1.71.1)$$

As before, the vector **X** has a mixture of effort and flow component variables associated with the energy storage 1-ports *C*, *I*; **U** is a vector of sources; **A**, **B**, **C**, **D** are arrays whose elements contain the parameters of the physical system. The vector **Y** has all the outputs of the systems multiports which can be observed (i.e., measured). It is called the *vector of observables.*

The procedure is summarized as follows:

- choose the system vectors and assign explicit component variables to represent outputs. In the example of Fig. 1.70.1b, we select

$$\mathbf{X} = (f_2, e_5);\ T = (e_4);\ H = (f_3);\ U = (f_1)$$

Note that f_3 is an output flow of the 0-junction whereas e_3 is an output effort of the 1-junction

- for each storage multiport *C* write an equation of the form

$$C\cdot\frac{de_{out}}{dt} = f_{in} \qquad (1.71.2)$$

In the example,

$$C_5\frac{de_5}{dt} = f_5$$

• for each storage multiport I write an equation of the form

$$I\frac{df_{\text{out}}}{dt} = e_{\text{in}}$$

In the example,

$$I_2\frac{df_2}{dt} = e_2$$

• for each temporary variable express the relation between e and f to be in accord with the assumed causality.

In the example e_4 is the output of R for the input f_4. Thus

$$e_4 = R_4 f_4$$

• for each auxiliary variable write the relation of efforts or flows conformable to 0-junction or 1-junction power flow.

In the example,

for the 0-junction: $f_3 = f_1 - f_2$, $e_1 = e_2 = e_3$ (See Sect. 1.68.3)
for the 1-junction: $e_3 = e_4 + e_5$, $f_3 = f_4 = f_5$ (See Sect. 1.68.3)

• eliminate the temporary and auxiliary variables. In the example this leads to

$$I_2\frac{df_2}{dt} = R(f_1 - f_2) + e_5$$

$$C_5\frac{de_5}{dt} = f_1 - f_2.$$

From this result the matrices **A**, **B** are seen to be

$$\mathbf{A} = \begin{bmatrix} 0 & -R \\ -1 & 0 \end{bmatrix}; \mathbf{B} = \begin{bmatrix} R & 0 \\ 1 & 0 \end{bmatrix}.$$

This completes the derivation of Eq. 1.71.1(a). The construction of the components of the vector **Y** of observables is performed in a similar way. As an example we choose the observable q_4. By definition

$$\int f_4 dt = q_4(t) - q(0).$$

Since

$$f_4 = \frac{e_4}{R_4} = \frac{e_3 - e_5}{R_4} = \frac{e_2 - e_5}{R_4} = \frac{I_2}{R_4}\frac{df_2}{dt} - \frac{e_5}{R_4}$$

it is seen that q_4 may be expressed in terms of the state variables f_2, e_5:

$$\frac{I_2}{R_4} f_2 - \frac{\int e_5(t)\,dt}{R_4} = q_4(t) - q(0).$$

The example discussed, though trivially simple, embodies the complete procedure for constructing equations of state for the physical system from bond graphs.

1.72 BOND GRAPHS AND IMPEDANCE METHODS FOR 2-PORTS

A powerful method of analysis of transducer models is based on transmission of energy through a cascade of 2-Ports, each of which is defined by an impedance (or admittance) matrix. Disussion of this method has already been presented in Sections 1.0 and 1.1. The mathematical model of the transducer is then contained in a large transfer matrix which relates power coordinates at the input of the first 2-Port to power coordinates at the output of the last 2-Port. While transfer matrices can be constructed in various ways we seek in this section to elucidate the construction of the transfer matrix from the bond graph.

Let S represent a 2-Port defined by the power variables e_1, f_1 and e_2, f_2. Four possible assignments of causality are available to relate these variables. This means we can specify which of two of them are inputs (right side of the dynamical equations) and which are outputs (left side of the dynamical equations). Guidance in this choice is based on physical fact or convenience in analysis. Table 1.72.1 lists the possible combinations. When there is no assignment of causality the power variables at one port of a 2-Port system are related to the power variables at the second port through a simple matrix:

$$\begin{bmatrix} e_1 \\ f \end{bmatrix} = \begin{bmatrix} AB \\ CD \end{bmatrix} \begin{bmatrix} e \\ f_2 \end{bmatrix}$$

This is called the *acausal form.* In it no commitment is made relative to input/output variables.

The symbol S in the above table can be interpreted as a 0-junction 2-Port or a 1-junction 2-Port. These are sketched in Fig. 1.72.1(a)(b)(c). The *acausal* form of the system equations for the 0-junction 2-Port, Fig. 1.72.1b is,

$$\begin{aligned} e_1 &= e_2 \\ f_1 &= Ye_2 + f_2 \end{aligned} \quad \text{or} \quad \begin{bmatrix} e_1 \\ f_1 \end{bmatrix} = \begin{bmatrix} 1 & 0 \\ Y & 1 \end{bmatrix} \begin{bmatrix} e_2 \\ f_2 \end{bmatrix} = M_{12}^{(0)} \begin{bmatrix} e_2 \\ f_2 \end{bmatrix}$$

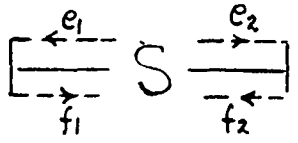
where $Y = Z^{-1}$ and $M_{12}^{(0)}$ is the 2-Port matrix for a 0-junction. For the 1-junction 2-Port (1c) the acausal form is

$$\begin{aligned} f_1 &= f_2 \\ e_1 &= Zf_2 + e_2 \end{aligned} \qquad \begin{bmatrix} e_1 \\ f_1 \end{bmatrix} = \begin{bmatrix} 1 & Z \\ 0 & 1 \end{bmatrix} \begin{bmatrix} e_2 \\ f_2 \end{bmatrix} = M_{12}^{(1)} \begin{bmatrix} e_2 \\ f_2 \end{bmatrix}$$

where $M_{12}^{(1)}$ is the 2-Port matrix for a 1 junction. The *causal* form of the system equations for the 0-junction 2-Port is different. Let the assignment of causality be Fig. 1.72.2. It is verbalized as follows: an external port (= device) J_1 accepts an effort e_1 from the 0-junction and delivers flow f_1 back to it; a second external device J_2 accepts effort e_2 from the 0-junction and delivers flow F_2 back to it; an impedance Z accepts a flow f_3 from the 0-junction and delivers an effort e_3 back to it.

Table 1.72.1 — Impedance Forms of 2-Ports

inputs: f_1, f_2
outputs: e_1, e_2



$$\begin{bmatrix} e_1 \\ e_2 \end{bmatrix} = \begin{bmatrix} Z_{11} & Z_{12} \\ Z_{21} & Z_{22} \end{bmatrix} \begin{bmatrix} f_1 \\ f_2 \end{bmatrix}$$

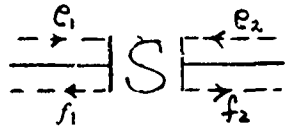
Impedance (or Z) Form

GY: $Z_{11} = 0 = Z_{22}$; $Z_{12} = Z_{21} = \text{const} = r$

$e_1 = rf_2$

$e_2 = rf_1$

inputs: e_1, e_2
outputs: f_1, f_2



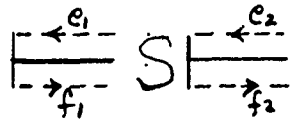
$$\begin{bmatrix} f_1 \\ f_2 \end{bmatrix} = \begin{bmatrix} Y_{11} & Y_{12} \\ Y_{21} & Y_{22} \end{bmatrix} \begin{bmatrix} e_1 \\ e_2 \end{bmatrix}$$

Admittance (or Y) Form

$GY = Y_{11} = 0 = Y_{22}$; $Y_{12} = Y_{21} = \text{const.} = r$

$f_1 = e_2 r$; $f_2 = e_1 r$

inputs: f_1, e_2
outputs. e_1, f_2



$$\begin{bmatrix} e_1 \\ f_2 \end{bmatrix} = \begin{bmatrix} Z_{11} & \eta_{12} \\ \eta_{21} & Y_{22} \end{bmatrix} \begin{bmatrix} f_1 \\ e_2 \end{bmatrix}$$

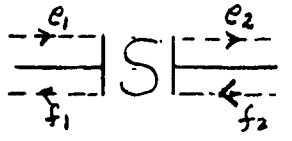
Im-mittance (or H) Form

TF: $Z_{11} = 0 = Y_{22}$

$\eta_{12} = \eta_{21} = \text{const.} = m$

$e_1 = me_2$; $f_2 = mf_1$

inputs: e_1, f_2
outputs. f_1, e_2



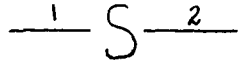
$$\begin{bmatrix} f_1 \\ e_2 \end{bmatrix} = \begin{bmatrix} Y_{11} & \eta_{12} \\ \eta_{21} & Z_{22} \end{bmatrix} \begin{bmatrix} e_1 \\ f_2 \end{bmatrix}$$

Ad-pedance (or G) Form

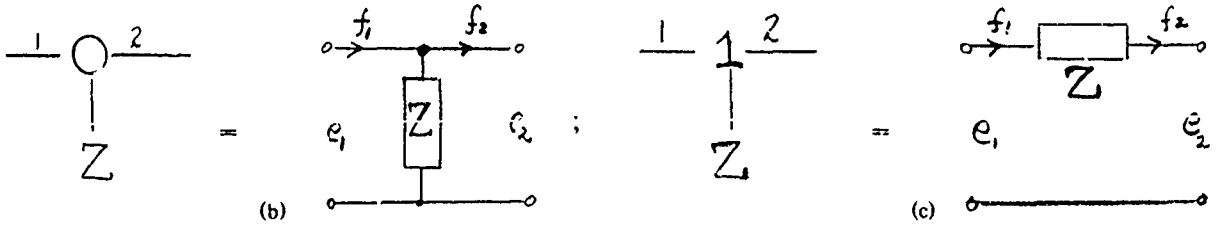
TF: $Y_{11} = 0 = Z_{22}$;

$\eta_{12} = \eta_{21} = \text{const.} = m$

$f_1 = f_2 m$; $e_2 = e_1 m$



(a)



(b) (c)

Fig 1.72.1 — (a, A generalized 2-port, (b) A 2-port 0-junction, (c) A 2-port 1-junction

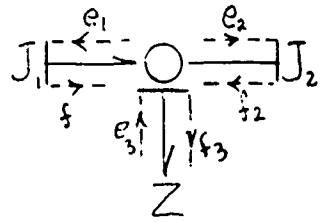


Fig. 1.72.2 — Assignment of causality to a 0-junction 2-port

From the point of view of the impedance device

$$(e_3)_{out} = (f_3)_{in} Z$$

Since $e_1 = e_3$, $e_2 = e_3$, and $(f_3)_{out} = (-f_1)_{in} - (f_2)_{in}$ the causal relations of the complete system are,

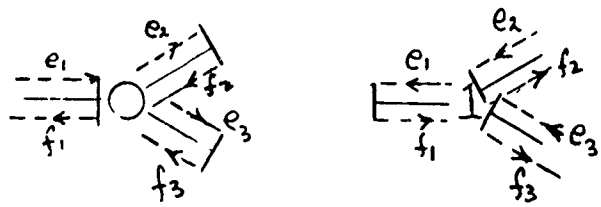
$$(e_1)_{out} = -Z(f_1 + f_2)_{in}; \quad (e_2)_{out} = -Z(f_1 + f_2)_{in}$$

The acausal form is particularly useful in the analysis of a linear cascade of 2-Ports defined by the power variables $e_1, f_1, e_2, f_2 \ldots e_n, f_n$. The (self-evident) rule is,

$$M_{1n} = M_{12} \cdot M_{23} \cdot \ldots M_{n-1n}$$

Examples of this rule are found in Sect. 1.2 of this treatise. In analyzing networks of 2-Ports which are not in cascade it is useful to recognize groups that obey simple addition of impedances. Table 1.72.2 is a list of the groups most often encountered and their flow and effort relations.

In applying causality to the 2-Ports in this table we have chosen the 0-junction and 1-junction to be represented by,

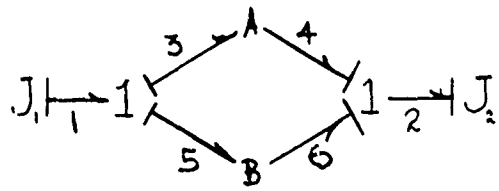
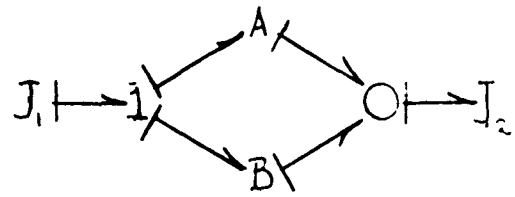
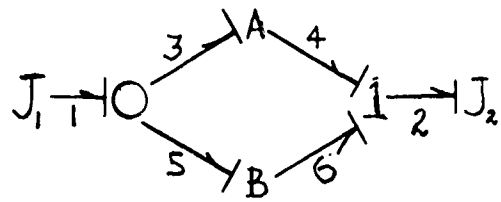
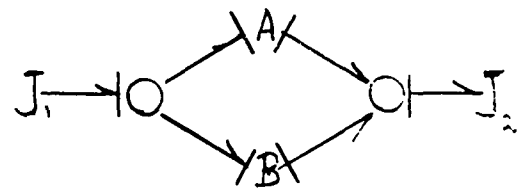


In words: For the 0-junction, Port J_1 has input e_2 and output f_2; Port J_2 has input e_3 and output f_3. For the 1-junction, port J_3 has input f_2 and output ; port J_4 has input f_3 and output e_3.

Summary

A physical system that can be modeled as an assembly of interconnected 2-Ports has an associated bond graph in the form of chains of 0-functions and 1-junctions. To each junction there are bonded 1-Ports or 2-Ports which absorb power, or store power, or transfer power. To analyze the system in terms of self and mutual impedance, or in terms of transfer functions, the bond graph is made causal by assignment of causal strokes and power flows, all in accordance with rules cited above which are designed to make the augmented graph complete and consistent. The augmented bond graph leads directly to an impedance description of the system.

Table 1.72.2 Groups of 2-Ports and Their Impedance Equivalents

Bond Graph	Impedance Relation	Block Diagrams
 Bond graph *A* is in impedance form	$Z_{12} = Z_A + Z_B$	$f_1 = f_3 = f_5$ $f_2 = f_4 = f_6$ $e_1 = -(e_3 + e_5)$ $e_2 = -(e_4 + e_6)$
 Bond graph *A* is in immittance form	$H_{12} = H_A + H_B$	$f_1 = f_3 = f_5$ $f_2 = -(f_4 + f_6)$ $e_1 = -(e_3 + e_5)$ $e_2 = e_4 = e_6$
 Bond graph *A* is in adpedance form	$G_{12} = G_A + G_B$	$f_1 = -(f_3 + f_5)$ $f_2 = f_4 = f_6$ $e_1 = e_3 = e_5$ $e_2 = -(e_4 + e_6)$
 Bond graph *A* is in admittance form	$Y_{12} = Y_A + Y_B$	$f_1 = -(f_3 + f_5)$ $f_2 = -(f_4 + f_6)$ $e_1 = e_3 = e_5$ $e_2 = e_4 = e_6$

1.72.1 An Example of the Use of Bond Graphs to Calculate Impedances in Physical Systems

Let Fig. 1.72.3a represent a portion of a bond graph in acausal form. The bonds are arbitrarily labeled. The first step in analysis is to assign direction of power flow. A convention (which is arbitrary) directs the flow *into* multiports through one bond and *out* of multiports in the remaining bond(s). All that is required in these assignments is consistency. This is shown by the half arrows in (b). A second step is to choose either e_0 or f_0 as the input quantity. This is done to establish causality among the multiports. Let us choose e_0 in this example. Since e_0 *enters* the first 0-junction (and f_0 leaves *in* the opposite direction) then the causal stroke is placed *adjacent* to the junction. The remaining two bonds also have an assignment of causal strokes. Following Sect. 1.68.1, it is seen that because $f_0 = f_1 + f_2$ (as deduced from the assumed power flow) then f_1 and f_2 must *enter* the 0-junction. The causal strokes are then placed at the ends of the bonds of the 0-junction to be in agreement with this stipulation. Such an assignment has two results: 1) the *input* to Z_1 is e_1 and the *output* is f_1. 2) as causal stroke appears adjacent t the transformer *TF*. From Table 1.72.2 the second bond of *TF* must have its causal stroke at its right end.

The assignment of causality to the 1-junction may take either of two forms as noted in Sect. 1.68.1. We choose here the one shown in (b). This makes f_4 an input to Z_4 and e_4 an output. It also places the causal stroke adjacent to *GY*. For consistency the second causal stroke must also be adjacent to *GY* (see Table 1.72.1). Hence the input to Z_6 is f_6 and the output is e_6. All these causality relations are listed in (c).

Our objective now is to find the ratio $Z_0 = e_0/f_0 (= Y_0^{-1})$. We use the causality relations to do this. Following the numbering sequence of Fig. 1.72.3(c) we have:

$$(4)\quad f_0 = f_1 + f_2 = \frac{e_1}{Z_1} + \frac{f_3}{m} = \frac{e_0}{Z_1} + \frac{e_6}{rm}$$

$$(3)\quad e_6 = Z_6 f_z = Z_6\left(\frac{e_5}{r}\right) = Z_6\left(\frac{e_3 - e_4}{r}\right) = Z_6\left(\frac{e_2}{mr} - \frac{Z_4 f_4}{r}\right)$$

$$= Z_6\left[\frac{e_0}{mr} - \frac{Z_4}{r}(mf_2)\right] = Z_6\left[\frac{e_0}{mr} - \frac{Z_4 m}{r}\left(f_0 - \frac{e_0}{Z_1}\right)\right]$$

The input impedance therefore reduces to,

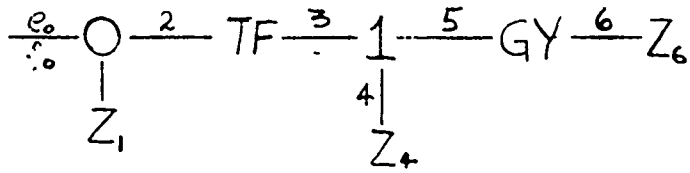
$$Z_0 = \left(\frac{r^2m^2 + Z_4Z_6m^2}{r^2m^2 + Z_4Z_6m^2 + Z_1Z_6}\right)Z_1$$

In a similar way Y_0 can be derived directly rather than first finding Z_0 and then $Y_0 = Z_0^{-1}$.

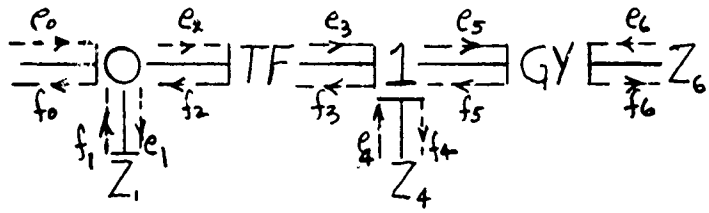
1.72.2 Conclusion to this Section on Bond Graphs

The method of bond graphs has been shown to be capable of reproducing all results that can be had in analyzing physical systems by equivalent circuits.

By extension (though not proved here) it has the same capabilities as the methods of block diagrams and signal flow graphs. The question is, what then is the advantage in its use? The answer is this: there are components of physical systems whose modeling by linear equivalent circuits is difficult, if not impossible. In such systems as long as such components can be verbalized in terms of bonds a bond graph is always available. More important, by a rigorous application of rules of causality described



(a)



(b)

Causality Relations

(1)	$f_1 = \frac{1}{Z_1} e_1$	(f_1 = output)
(2)	$e_4 = Z_4 f_4$	(e_4 = output)
(3)	$e_6 = Z_6 f_6$	(e_6 = output)
(4)	$f_0 = f_1 + f_2$ $e_2 = e_0;\ e_1 = e_0$	at 0-junction (See Sect. 1.68.3)
(5)	$f_2 = \frac{f_3}{m};\ e_3 = \frac{e_2}{m}$	at TF
(6)	$f_4 = f_5 \quad f_3 = f_5$ $e_3 = e_4 + e_5$	at 1-junction (See Sect. 1.68.3)
(7)	$f_5 = \frac{e_6}{r};\ f_6 = \frac{e_5}{r}$	at GY

(c)

Fig. 1.72.3 — (a) Bond graph, (b) augmented bond graph, (c) causality relations

in [13] and exploited above, the augmented bond graph leads directly to the equations of the system by simple steps. Impedances are found with surprising ease and system performance in both steady and transient states directly deduced. An additional bonus is the optimization of selection of state system variables in analysis of multicomponent systems: bond graphs, properly augmented with causality and power flow symbols, provide a consistent approach to this (sometimes) difficult task.

Efficient low frequency underwater sound sources generally take on the form of discrete systems which can be mathematically modeled as electric/mechanical/hydraulic networks. Although several procedures are available for constructing such networks the advantages of the *methods of linear graphs* (or alternatively the method of *bond graphs*) in regard to simplicity, universality, optimizability, and visual effectiveness, are sufficient to make it the preferred method of analysis. In particular linear graphs (or bond graphs) allow easy formulation of the *state model* of the system which is admirably suited to machine computation of digital computers. The method of system graphs replaces the method of analysis based on the construction of equivalent electrical networks. The latter are themselves system graphs of special kind, namely "coded" graphs in which the components are recognized visually as being resistances, inductances etc. However in the system graphs discussed in this chapter visual coding in omitted in favor of component equations. The analysis of discrete systems has therefore been presented as a *matrix equation formulation* aided by the toplogical concepts of trees, cotrees etc. of a linear graph.

REFERENCES

[1] "Grundlagen Der Technische Acoustik," W. Reichhardt Geest und Portig K-G Llipzig 1968.

[2] "Transients In Linear Systems," M.S. Gardner, J.L. Barnes, John Wiley, New York 1953.

[3] "Electromechanical Transducers and Wave Filters," W.P. Mason, D. Van Nostrand, New York 1942 p. 204.

[4] "Electroacoustics," F.V. Hunt, Harvard U. Press 1953 p. 180.

[5] "Handbook for the Analysis of Piezoelectric Transducers," Naval Underwater Systems Center Technical Document 6029, New London Connecticut (1978).

[6] D. Berlincourt, Engineering Memo 59-3 Clevite Corp.

[7] "Analysis of Discrete Physical Systems," H.E. Koenig et al. McGraw-Hill Book Co. New York, 1967, p. 76.

[8] Ref. 4, Chapter III.

[9] Ref. 7, p. 106.

[10] Ref. 7, p. 138.

[11] "Analysis and Simulation of Multiport Systems," D. Karnopp, R.C. Rosenberg, MIT Press 1968, Cambridge, Mass.

[12] Ref. 11, p. 69.

[13] Ref. 11, p. 39.

[14] E.E. Mott, R.C. Miner, Bell System Tech. J (1951).

[15] "Acoustical Engineering," H.F. Olson, D. Van Nostrand, Inc. 1957.

[16] "Handbook of Sound and Vibration," C. Harris ed.

[17] "Radio Engineering Handbook," F.J. Terman ed.

[18] "Theory of Vibrating Systems and Sound," I.B. Crandall, D. Van Nostand 1927, p. 145.

Chapter 2
PRINCIPLES OF DESIGN OF ACOUSTIC TRANSDUCERS

2.1 PROJECTORS AND RECEIVERS

Acoustic transducers are of two sorts:

Projectors, which convert sources of energy into sound fields, and *receivers,* which detect sound fields and convert them back into energy forms convenient for listening, display or recording. While sources of energy can take any form the ones most used are the energies resident in magnetic or electric fields. Projectors based upon them can usually serve as receivers as well, thus providing an advantage. Other sources of energy such as thermal, fluidic, or chemical are *generally* nonreciprocal, capable of producing sound fields but not detecting them in a practical way.

This chapter will discuss magnetic and electric field transducers, emphasizing the basic principle underlying their design. Only phenomena of transduction which can be described by linear differential-integral equations will receive attention. Thus a transducer structure will be regarded as an input/output device made up of input/output components. No special effort will be made to expose physical details of energy conversion except as will be needed to justify the mathematical models used.

We begin with a general discussion of magnetic and electric fields which serve as models for energy conversion in acoustic transducers.

2.2 MAGNETIC FIELDS AND DRIVES

$B-H$ Curves, Operating Points, Drive at Constant B or Constant H

The theory of magnetic field transducers requires a careful attention to units assigned to various parameters appearing in the mathematical models. It will be useful here to list the parameters and assign to them consistent MKS units.

		Units
h = piezomagnetic constant		$\frac{N}{Vs}$ or $\frac{\text{A turn}}{m}$
μ = Magnetic permeability	$\frac{\text{Weber}}{\text{amp-turn-m}}$	$\frac{Vs^2}{Cm}$ or $\frac{Ns^2}{C^2}$
$\gamma = \mu^{-1}$		$\frac{Cm}{Vs^2}$ or $\frac{Am}{Wb}$
R = reluctance	$\frac{\text{amp-turn}}{\text{weber}}$	$\frac{C}{s^2V}$
$\mathcal{F}$ = magnetomotive force	amp-turn	$\frac{C}{s}$
ϕ = magnetic flux	weber	Vs
λ = flux linkages	weber turn	Vs

PREVIOUS PAGE IS BLANK

B =	magnetic flux density, (Tesla)	weber/m^2	Vs/m^2
H =	magnetic field intensity	amp-turn/m	C/sm

It will always be useful in the following discourse to examine each field equation to insure a proper balance of units.

We begin with a discussion of B-H curves.

A ring of magnetic material (cross sectional area A) is wound with N turns of a primary coil on one segment and n turns of a secondary coil on a second segment of the circumference. The primary is connected through a set of switchable resistances to a dc battery with a dc ammeter. The secondary is connected through a standard mutual inductance (coil within coil) to a ballistic galvanometer. When the first switch is closed it connects all the resistances to the primary. A small transient current i_0 then flows through it creating an increment of flux ΔB_0 in the ring material. This flux couples with the secondary, generating in it a transient charge with deflects the galvanometer through angle by θ_0. Such a deflection is proportional to $nA\ \Delta B_0$. The proportionality factor is obtained by use of a calibrating current passed through the mutual inductance coils of the secondary circuit. Thus θ_0 corresponds to a known change in induction ($= \Delta B_0$). When the second resistance switch is closed, it short-circuits a portion of the total resistance, thereby causing a larger transient current to flow, which in turn causes a larger deflection. Hence a second increment of flux lines is added to the first. This process of closing switches is continued until further current increments do not deflect the galvanometer. The material is then in a state of magnetic *saturation*, point a in Fig. 2.2.1. When the switches are reopened in reverse order the galvanometer deflections do not retrace those obtained on closing, showing the process to be *hysteretic*. When the last switch is opened a deflection is obtained, also showing residual flux frozen in the material when there is no excitation. This is point *b* on Fig. 2.2.1 A plot of deflection vs current (or static induction B versus magnetic field intensity *H*) gives the portion *o a b* of the magnetization (or B-H) curve. Portion *bcde* is obtained by use of a commutator which causes the current to flow in the direction opposite to that first used. Similarly, portion *efa* is obtained by again reversing the commutator. Subsequent opening and closing switches causes the curve *abcdefa* to be traced out (curve oa having disappeared).

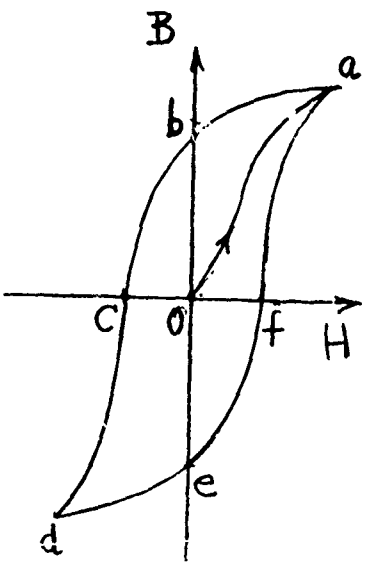


Fig. 2.2.1 — Typical B-H curve

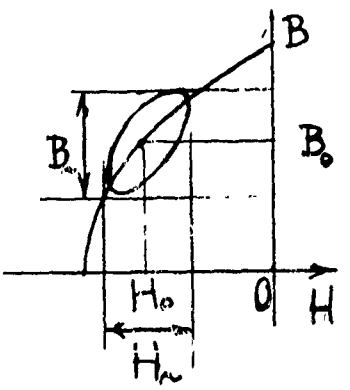


Fig. 2.2.2 — Dynamic loop on a B-H curve

In the practice of ultrasonic magnetostriction transducers a bias flux B_0 at some H_0 is permanently established at a selected point on the curve, f_a. It is chosen to give desired properties (desired permeability at $\Delta B_0/\Delta H_0$, desired magnetostriction, etc). At B_0 the transducer is excited by an ac current. The magnetization then executes a small loop, Fig. 2.2.2, at the frequency $\omega(=2\pi f)$ of the drive. The alternation $B_\sim$ of flux then induces an alternating elastic strain $S_\sim$ through the agency of magnetostriction

$$S_\sim = gB \tag{2.2.1}$$

The corresponding elastic stress is

$$T_\sim = cS_\sim = -hB_\sim. \tag{2.2.2}$$

In another description the alternating magnetic field induces a strain,

$$S_\sim = dH_\sim. \tag{2.2.3}$$

which is accompanied by a stress

$$T_\sim = -eH_\sim. \tag{2.2.4}$$

At any selected frequency these descriptions are interchangeable.

When however the frequency is changed one has the option of driving the transducer at constant $B_\sim$ or constant $H_\sim$. In the case of constant $B_\sim$, Fig. 2.2.3, the drive current varies with frequency while the drive voltage $V_\sim$ is kept constant as the frequency changes from f_1 to f_2. In the case of constant $H_\sim$, Fig. 2.2.4, the drive current remains constant while the drive voltage varies with frequency.

For drive at constant magnetization (Eq. 2.2.2), the appropriate electrical description is that of admittance because current I is varying at constant V. For drive at constant magnetic field (Eq. 2.2.4) one plots the electrical impedance because then the voltage is varying at constant current. A description of the energy resident in the magnetic field is given in Sect. 1.50. For completness the principal relations are repeated here.

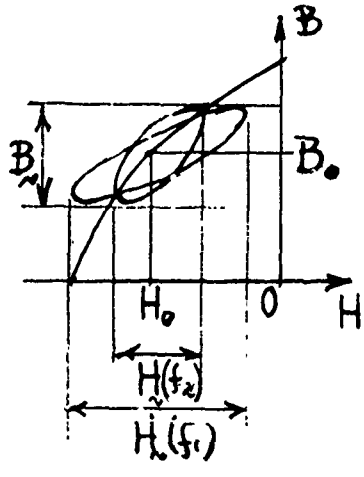


Fig. 2.2.3 — Dynamic loops at different frequencies for constant magnetization

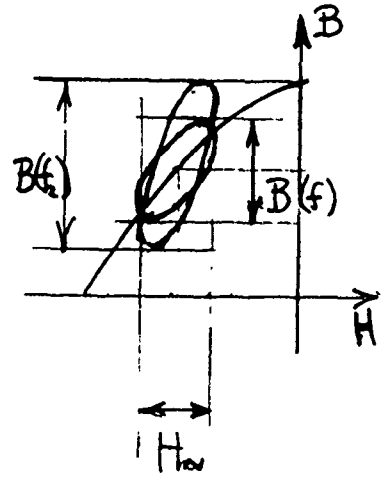


Fig. 2.2.4 — Dynamic loops at constant $H_\sim$

Magnetic Energy, Magnetic Circuits, Hysteresis Loops

Table 1.50.1 shows that the energy in magnetic fields can be expressed in terms of magnetic flux linkage (units: *Vs* turn) in the energy form $W = \int I d\lambda$, or in the form coenergy $W^* = \int \lambda dI$. We consider here the energy form and apply it to finding the energy stored in a magnetic circuit consisting of a toroidal ring of iron, radius a, cross-section A excited by a coil of N turns carrying an electric current I. Since $\lambda = N\phi$ and $I = \mathrm{F}/N$ it is seen that

$$\text{energy:} \quad W = \int I d\lambda = \int_0^{\Phi_m} \mathrm{F} d\phi \tag{2.2.5}$$

$$\text{coenergy:} \quad W^* = \int \lambda dI = \int_0^{\mathrm{F}_m} \phi d\mathrm{F}. \tag{2.2.6}$$

For each increment of length dl around the magnetic circuit the increment in magnetomotive force is

$$d\mathrm{F} = Hdl = H(l, \phi) dl. \tag{2.2.7}$$

Also the magnetic flux is expressed in terms of flux density B,

$$d\phi = BdA. \tag{2.2.8}$$

Thus the magnetic energy stored in the ring is

$$W = \int\int B(l) H(l, B) dl\, dA \tag{2.2.9}$$

From this it is seen that energy relations in magnetic circuits are made visible by plotting flux ϕ versus magnetomotive force F, Eq. 2.2.5. In contrast, energy in a magnetic material of volume $d\mathrm{V} = dl\, dA$ is made visible by plotting B vs H.

As noted in Section 1.50 the coenergy form, Eq. 2.2.6, is useful in applications of the variational principle of Hamilton to formulation of the dynamical equations of transducer operation.

We now return to the magnetic circuit of a complete toroid and use a plot of magnetic flux ϕ (units: *Vs*) as ordinate and magnetomotive force $\mathcal{F}$ (units: *C/s*) as abscissa. This has the same shape as the *B-H* curve of Fig. 2.2.1 and is reproduced here as Fig. 2.2.5a. To stabilize the circuit it is customary to partially demagnetize the material of the toroid. One therefore uses the material in a state described by some point (say 6) on the demagnetization branch (2-3) of the $\phi - \mathcal{F}$ hysteresis loop, Fig. 2.2.5b. Beginning at this point one can induce cyclical changes in flux of smaller amplitude than the remanent value ϕ_2 by creating a minor hysteresis loop. First, one reverses the demagnetization current from F_6 to $\mathrm{F}_{6'}$ to F_7, causing the ascending portion 6-6'-7 to be traced. The demagnetizing current is then increased (that is, made more negative) causing the descending portion 7-7'-6 to be traced. The flux therefore moves cyclically from ϕ_6 to ϕ_7 and back again. If the demagnetizing current is removed completely the flux in the circuit returns to ϕ_8. Thus, as long as the negative magnetomotive force does not exceed $\mathcal{F}_6$ the largest cyclical change in flux is $\phi_8 - \phi_6$. The slope of the line 6-0'-7 is given by the angle θ,

$$\tan\theta = \frac{\phi_8}{Hl_l} = \mu_l \mu_0 \frac{A}{l_l} \tag{2.2.10}$$

in which l_l is the total flux path of the magnetic circuit and μ_l is the incremental permeability.

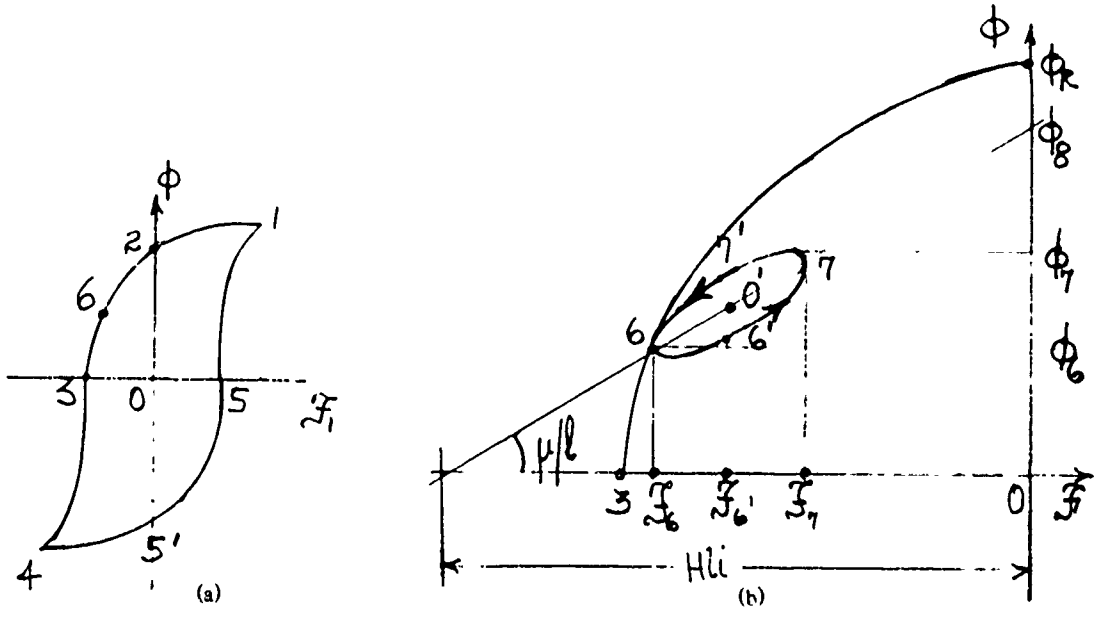


Fig. 2.2.5 — (a) Hysteresis loop of a magnetic circuit, (b) minor hysteresis loop

We next consider the case of a magnetic circuit with an air-gap Fig. 2.2.6 consisting of a yoke, a coil and a diaphragm (or armature). Assume first the magnetic material is driven into saturation (point 1 of Fig. 2.2.5), and then the magnetization current is reduced to zero. The flux in the core is then less that ϕ_R because of the presence of the air gap. Since the air-gap acts as a negative magnetomotive force the flux in the core is at some point c *on the demagnetization curve* of the iron circuit, Fig. 2.2.7. If we let l_i be the effective path length of the metal core, and l_g be the path length of the air-gap, then the magnetic field intensity H_i in the core in the absence of coil current is,

$$H_i l_i = -\mathcal{F}_y = -H_g l_g \tag{2.2.11}$$

and the flux in the air gap is

$$\phi_g = -\mu_0 H_i \frac{l_i}{l_g} A = \mu_0 H_g A \tag{2.2.12}$$

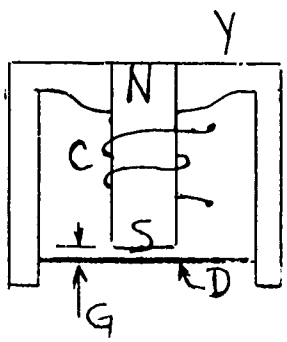


Fig. 2.2.6 — Moving-armature transducer (Y = yoke, C = coil, G = air gap, D = armature diaphragm)

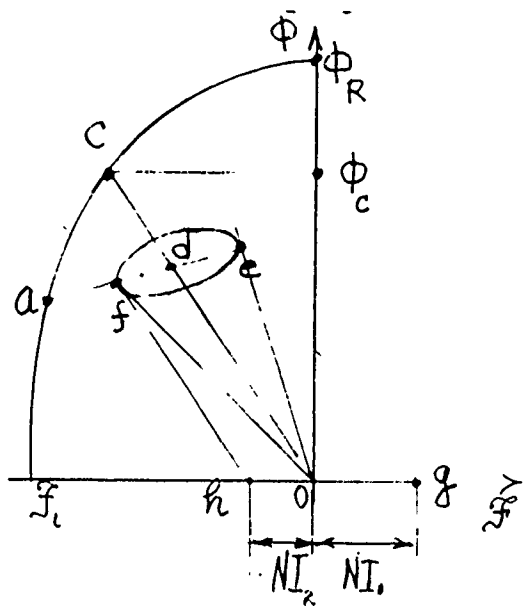


Fig. 2.2.7 — Demagnetization curve for the magnetic circuit in Fig. 2.2.5b

On the ϕ_g – F chart, this represents a straight line *OC* issuing from the origin, with a slope given by Eq. 2.2.10. It is called a *shearing line*, and its intersection with the demagnetization curve determines point C, Fig. 2 2.7. The corresponding flux in the circuit is ϕ_c. In applications, particularly where permanent magnets are used, it is often a practice to stabilize the magnetic circuit by applying a demagnetizing field to move the operating point to (say) *a*. Upon removing this field, the state in the iron-air-gap system moves to point d on the minor hysteresis loop (here represented by a straight line). This point is the intersection of the air-gap shearing line with the minor hysteresis loop. If the air-gap is increased the operating point moves to point *f* where the flux is lower, that is, closer to *a*, while if it is decreasing it moves to point e at higher flux. Thus a cyclical motion of the diaphragm-armature induces a cyclical change in the flux in the magnetic circuit corresponding to points traced out on the minor hysteresis loop *fde*. A change in flux in the circuit may also be induced by applying a (signal) current to the coil. When the current is such as to cause the magnet to draw the armature to itself the operating point moves to higher flux (point e). The magnetic field intensity required to do this is NI_1. Because of the presence of the air-gap the shearing line takes the position *ge* in Fig. 2.2.7. However, when the current is reversed and the armature moves away from the magnet the operating point moves along the hysteresis loop toward point d. The magnetic field intensity required to do this is $-NI_2$. Because of the presence of the air-gap the shearing line takes up the position *hf*. Thus a cyclic change of signal current will cause the operating point to trace out a minor hysteresis loop *fd e df*. When the signal current is zero and when no external force excites the diaphragm it occupies its equilibrium position. This corresponds to point d.

2.3 FUNDAMENTAL EQUATIONS OF PIEZOMAGNETIC ACTIVITY

The magnetic induction B (units: VS m^{-2}) induced by a magnetic field H (units: A m^{-1}) in free space is modified by the presence of a magnetic which adds magnetization **M** (units: Vs/m^2):

$$\mathbf{B} = \mu_0\mathbf{H} + \mu_0\mathbf{M} \tag{2.3.1}$$

$$\mu_0 = 4\pi \times 10^{-7} \quad \text{(units: } Ns^2C^{-2}\text{)}.$$

We note that in the MKS system of units both H and M have the same units. In linear models of piezomagnetic materials a state of magnetization can be induced by applying a magnetic field, or an elastic stres, (or both):

$$\mathbf{M} = d\mathbf{T} + \mu\mathbf{H} \tag{2.3.2}$$

in which μ is the relative permeability and d is the piezoactive coefficient relating stress and magnetization (units: VS N^{-1}). Thus the induction becomes

$$\mathbf{B} = \mu_0[1 + \mu]\mathbf{H} + d\mathbf{T} \tag{2.3.3}$$

For most magnetic materials of interest $\mu >> 1$. Hence the induction and magnetization are related as follows:

$$\mathbf{B} = \mu_0\mathbf{M} \text{ (MKS units)}; \quad \mathbf{B} \simeq \mathbf{M} \text{ (Gaussian or emu units)}. \tag{2.3.4}$$

When the magnetic material is piezoactive the coupling between elastic fields and magnetic fields is reversible: an applied magnetic field causes an elastic strain to appear in the material. This is described (in first approximation) by a linear model,

$$\underline{S} = s^H \underline{T} + d^{(t)} \underline{H}. \tag{2.3.5}$$

When the matrices are symmetrical one can use reduced indices: $\underline{S}$, $\underline{T}$ are 6-component column vectors, s^H is a 6 × 6 component matrix, $d^{(t)}$ is a transposed 6 × 3 component matrix, and $\underline{H}$ is a 3-component column vector.

Equations 2.3.2 and 2.3.5 form a basic set of constitutive relations in which M, S are the dependent variables, and T, H are the independent variables. One can construct three other sets by interchanging the roles of T, S, and M, H. However, it is useful to consider a different basic set:

$$\begin{cases} \text{(a)} \quad \underline{T} = C^M \underline{S} - h^{(t)} \underline{M} \\ \text{(b)} \quad \underline{M} = \mu_0 \mu \underline{H} + \mu_0 \mu h \underline{S}, \\ \text{(c)} \quad \underline{H} = -h \underline{S} \; \gamma^s \underline{M} \end{cases} \tag{2.3.6}$$

where $\gamma^s = (\mu_0 \mu)^{-1}$. Here both **T** and **M** are *internal* quantities while **H** is *external*. This set has been extensively used by Kikuchi [1] (who writes $\Gamma = h$ and $\mu_0 \mu = k$). By formal matrix manipulation it is seen that

$$\mathbf{T} = C^M \mathbf{S} \left[1 - \frac{\mu_0 \mu h^2}{C_M} \right] - \mu_0 \mu h^{(t)} \mathbf{H}. \tag{2.3.7}$$

Here, the units of h, C^M are:

$$h \rightarrow \frac{N}{V_S} \text{ or } \frac{A}{m}$$

$$C^M \rightarrow \frac{N}{m^2}.$$

Thus, the units of the coupling term in the brackets of Eq. 2.3.7 are,

$$\frac{\mu_0 \mu h^2}{C^M} = \frac{N s^2}{C^2} \times \frac{N}{\mathrm{Vs}} \times \frac{\mathrm{A}}{m} \times \frac{m^2}{N} \; (= \text{nondimensional})$$

as required. It is to be noted that $\gamma^s = \gamma_1^s - j \gamma_2^s$, a complex number.

Again, specific forms of coupling factors are derived for specific boundary conditions imposed on the elastic and magnetic fields. A typical example is a thin ferrite disk excited in the thickness mode and biased parallel to the thickness. Here, the 3-direction is normal to the disc. The boundary conditions are $S_1 = S_2 = 0$, $S_3 \neq 0$; $T_1 = T_2 \neq 0$, $T_3 \neq 0$. Applying a magnetic field $H_3 = H_0 e^{-i\omega t}$, it is seen that the coefficient of electromechanical coupling is

$$k_t^2 = \frac{h_{33}^2}{\gamma_{33}^s \, C_{33}^M}.$$

A sketch of the transducer is shown in Fig. 2.3.1.

On the other hand, a ferrite ring with rectangular cross section, biased tangentially (in 3-direction), and driven tangentially has an elastic state $S_1(S_{rr}) \neq 0$, $S_2(S_{zz}) \neq 0$, $S_3(S_{\theta\theta}) \neq 0$, $T_1 = T_2 = 0$, $T_3(T_{\theta\theta}) \neq 0$. The appropriate set of equations are 2.3.2 and 2.3.5. From them one finds

$$k_{33}^2 = \frac{d_{33}^2}{\mu_{33}^T s_{33}^H}; \; \mu_{33}^T = \mu_0 \mu_{33}.$$

Figure 2.3.2 shows the conditions of drive.

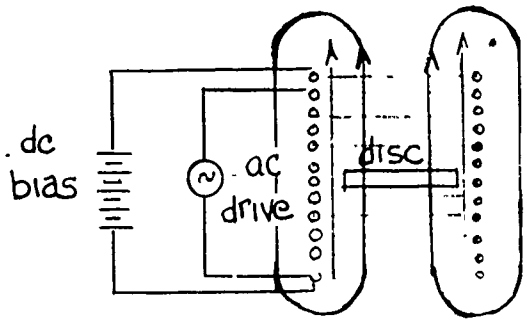


Fig. 2.3.1 — Ferrite disc excited in thickness vibration

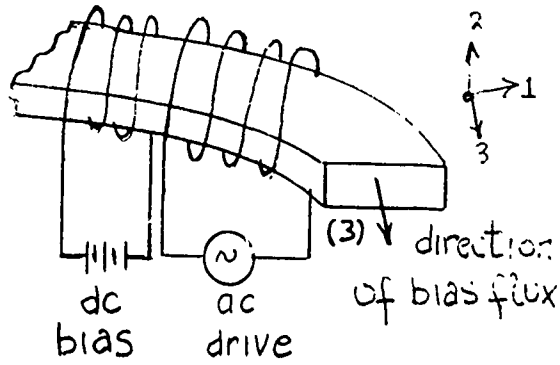


Fig. 2.3.2 — Ferrite ring excited in ring node vibration

2.4 PHYSICAL INTERPRETATION OF PIEZOMAGNETIC COUPLING

Assume an elastic piezomagnetic material is set into vibration by some external agency. At low enough frequency of forced motion the internal elastic and magnetic fields can be described by Eq. 2.3.6(c). Thus, an elementary volume of the material under strain S generates a magnetomotive force $H' = hS$. Such a force magnetizes the volume with flux $M' = H'/\gamma^s = -hS/\gamma^s$. The magnetization in turn generates an elastic stress $T'' = -h^{(t)}M' = hh^{(t)}S/\gamma^s$. The entity T'' is a complex number,

$$T'' = \left|\frac{h^2}{\gamma^s}\right| S\left[\cos \measuredangle \frac{1}{\gamma^s} + j \sin \measuredangle \frac{1}{\gamma^s}\right] = \text{Re } T'' + j \text{ Im } T''. \tag{2.4.1}$$

$$\measuredangle \frac{1}{\gamma^s} \text{ is the angle of the complex number } (\gamma^s)^{-1}.$$

The real part of $T''(= \text{Re } T'')$ corresponds to a strain in phase with the original strain and additive to it. Thus the stress field in the volume gives a larger strain than for an unpolarized (but elastically identical) material. The stress-strain modulus (and resonant frequency) are reduced by piezomagnetic activity. The imaginary part of T'' acts as a damping constant. It is in phase with the velocity of the volume, reducing its amplitude by offering resistance. It thus serves to decrease the sharpness of mechanical resonance. The physical effect of piezoactive coupling helps distinguish two types of mechanical force created by it. To elucidate this phenomenon we choose an elastic system which has effectively a single degree of freedom of vibratory motion at a low enough frequency. A typical example is a magnetostrictive ring, radius a, cross-sectional area A. A small volume of this vibrating ring has on each cross sectional face a force F of value $F = TA$. For small A the strain in the ring is $S = \xi/a$. Using 2.3.6a one finds the force in the presence of a magnetizing flux M to be,

$$F_M = C^M \frac{\xi}{a} - h^{(t)}M, \; C^M \equiv \text{Young's modulus at constant magnetization.} \tag{2.4.2}$$

Here vector M and strain ξ/a both point in the direction of F. Since the magnetization is supplied by a coil of N turns the magnetizing voltage for a drive $Me^{j\omega t}$ is,

$$V = NA\frac{dM}{dt} = j\omega NA \; Me^{j\omega t}. \tag{2.4.3}$$

Thus F_M is the force induced by magnetization on the faces of the volume element when the coil is driven at constant voltage over the whole range of frequencies in which the condition of a single degree of freedom holds.

In contrast if one chooses 2.3.6b the forces on the faces of the elementary volume in the presence of a magnetomotive force H are,

$$F_H = AC^M\left[1 - \frac{h^2}{\gamma^s C^M}\right]\frac{\xi}{a} - A\frac{h^{(t)}H}{\gamma^s}. \tag{2.4.4}$$

Here, C^M, h, γ^s, H are components of tensors which point in the direction of the tangent to the ring. Since H is generated by a current I flowing through a coil of N turns of length l, one has

$$H = \frac{NI}{l} \quad \text{(units: } Am^{-1}\text{)}.$$

Thus the force F_H is obtained when the coil is driven at constant current over the whole range of frequencies in which the condition of single degree of freedom holds.

The stress-strain modulus C^M is, in general, modeled as a complex number in order to account for internal losses caused by molecular friction,

$$C^M = C_1^M - jC_2^M. \tag{2.4.5}$$

When the ring, mass density ρ, is driven at constant voltage it reaches mechanical resonance at a frequency,

$$f_v = \frac{1}{2\pi a}\sqrt{\frac{C_1^M}{\rho}}. \tag{2.4.6}$$

The equivalent damping constant of the 1-degree of freedom system is obtained from the resonance plot of amplitude vs frequency. It is,

$$\delta_v = C_2^M/4\pi f a^2\rho \quad \text{(units: } S^{-1}\text{)}. \tag{2.4.7}$$

The same ring driven at constant current reaches mechanical resonance at a lower frequency,

$$f_I = \frac{1}{2\pi a}\sqrt{\frac{C_1^M}{\rho}\left[1 - \frac{h^2}{\gamma^s C_1^M}\right]}. \tag{2.4.8}$$

Its damping constant depends not only on C_2^M but also on piezoemagnetic coupling:

$$\delta_I = \frac{C_2^M\left[1 + \frac{h^2}{\gamma_2^s C_2^M}\right]}{4\pi f a^2\rho}. \tag{2.4.9}$$

It is seen that the resonance curve at constant voltage is much sharper than at constant current because,

$$\delta_v < \delta_I \tag{2.4.10}$$

The derivation of Eqs. 2.4.6 through 2.4.10 will be taken up in a later section.

The distinction between constant voltage and constant current drive will be discussed in greater detail in Section 2.8.

2.5 FUNDAMENTAL CONSTITUTIVE EQUATIONS OF PIEZOELECTRIC COUPLING

The charge displacement vector **D** in a dielectric material having dielectric constant ϵ (units: C/V m) is related to the applied field **E** and the polarization **P**:

$$\mathbf{D} = \epsilon_0 \mathbf{E} + \mathbf{P} \qquad \text{(rationalized MKS units)}. \tag{2.5.1}$$

in which **P** is the dipole moment per unit volume of material (units: C/m^2) and ϵ_0 is the dielectric constant of free space (units: C/Vm). In *linear* models of piezoactive materials a state of polarization can be induced by an applied electric field or by an applied elastic stress **T**. By definition of the piezoelectric coefficient d, (units: C/N) and relative dielectric constant k,

$$\mathbf{P} = d\mathbf{T} + \epsilon_0 k\, \mathbf{E}. \tag{2.5.2}$$

Thus the charge displacement can be written in the form,

$$\mathbf{D} = \epsilon_0(1 + k)\, \mathbf{E} + d\mathbf{T}. \tag{2.5.3}$$

Generally, $k \gg 1$ so that the relation between **D** and **P** is,

$$\mathbf{D} \simeq \mathbf{P} = \epsilon_0 k \mathbf{E} \text{ (MKS units)}. \tag{2.5.4}$$

More precision in definition is achieved by use of appropriate subscripts and superscripts. Thus,

$$P_i = \sum_j d_{ij}\, T_j + \epsilon_0 \sum k_{ij}^T E_j \tag{2.5.5}$$

$$\epsilon_0 = (4\pi \times 9 \times 10^9)^{-1}.$$

Often one makes the combination

$$\epsilon_0\, k_{ij}^T \rightarrow \epsilon_{ij}^T$$

where the superscript T means a condition of constant stress.

Piezoactivity is reversible. While an applied mechanical stress induces dielectric polarization it is equally true that an applied electric field induces an elastic strain S (in units of a change in length per unit length). This reversed action is approximately modeled by the linear equation of state in the elastic compliance s_{ij}:

$$S_i = \sum_j s_{ij}\, T_j + \sum_m d_{mi}^{(t)}\, E_m. \tag{2.5.6}$$

The superscript t means the 6×3 matrix d is transposed into a 3×6 matrix. From 2.5.2 and 2.5.6 the units of d are seen to be C/N or m/V.

The set of Equations 2.5.5 and 2.5.6 constitute the basic linearized model of piezoactivity of dielectric materials. They are *static* or low frequency equations because the mechanical impedance of the materials is considered to be a stiffness only. Other sets of equations are easily derived by interchanging stress and strain, or polarization and electric field. They are listed in matrix form as:

$$\begin{aligned}
&(1)\ S = sT + d^{(t)}E \\
&\quad\ P = dT + \epsilon^T E \\
&(2)\ S = sT + g^{(t)}P \\
&\quad\ E = -gT + \beta^T P \\
&(3)\ T = C^E S - e^{(t)}E \\
&\quad\ D = eS + \epsilon^S E \\
&(4)\ T = C^D S - h_t P \\
&\quad\ E = -hS + \beta^S D
\end{aligned} \tag{2.5.7}$$

in which

$$\begin{aligned}
d &= \epsilon^T g = eS^E \\
g &= \beta T d = hS^D \\
e &= \epsilon^S h = dC^E \\
h &= \beta^S e = gC^D \\
\beta &= \epsilon^{-1}
\end{aligned} \tag{2.5.8}$$

2.6 COEFFICIENTS OF ELECTROMECHANICAL COUPLING FOR DIELECTRIC-TYPE TRANSDUCERS

If set (1) of 2.5.7 is formally manipulated to allow elimination of E one obtains

$$S = s\left[1 - \frac{d^{(t)}d}{\epsilon^T s^E}\right] T + \frac{d^{(t)}}{\epsilon^T} P \tag{2.6.1}$$

in which division of matrices is understood to be multiplication by inverse. Here the entity $d^{(t)}d/\epsilon^T s^E$ is a complex matrix relation which expresses the modification of the compliance s caused by the existence of the piezoconstant d. This entity has a simple interpretation when the elastic state of the material is simplified to be approximately lumped (in contrast to distributed) and 1-dimensional. For example, consider a long bar, $0 < x < l$, of small thick t in the z-direction, and small width w in the y direction. Let x, y, z be the coordinates of directions 1, 2, 3 respectively. Assume further that electrodes are placed on the z-faces (across thickness t). Upon application of an electric field $E_3 = E_0 e^{-i\omega t}$ for the state where ω is far below frequency of mechanical resonance it is seen that the elastic response of the bar is a function of the *applied boundary conditions.* In the present case let all surfaces of the bar be free to expand. Thus all stresses in the bar vanish except the interior longitudinal stress T_1. Similar, at the boundaries, all electric fields vanish except E_3. Thus the coupling entity becomes

$$k_{31}^2 = \frac{d_{31}^2}{\epsilon_{33}^T s_{11}^E} \qquad \text{(units: none)} \tag{2.6.2}$$

The physical significance of this quantity may be understood by forming a list of the (static) energy densities in the material when elastic stress and electric fields are present:

elastic energy: $U_e = \frac{1}{2} s_{11}^E T_1^2$ (Nmm^{-3})

dielectric energy: $U_\epsilon = \frac{1}{2} \epsilon_{33}^T E_3^2$ (VCm^{-3})

coupled energy: $U_{e_\epsilon} = \frac{1}{2} d_{31} T_1 E_3 + \frac{1}{2} E_3 T_1 d_{31}$ (units: VCm^{-3}) $= 2U_m$.

The two terms in the coupled (or mutual) energy are due to coupling from fields in direction 1 to fields in direction 3, and from coupling of fields in 3 to fields in 1. Since $d_{31} = d_{13}$ the terms are equal. With these definitions it is seen directly from Eq. 2.6.2 that

$$k_{31}^2 = \frac{U_m^2}{U_G U_e}.$$

This is the ratio of the mutual energy ($= U_m$ term) squared to the product of the elastic energy and the dielectric energy. Thus the coefficient of electromechanical coupling ($= k$) is the ratio of mutual energy to the geometric mean of the self dielectric energy and the self elastic energy. These energies are calculated under static or quasi-static, conditions in which *all* the elastic energy (contained in the fields *T,S*) are coupled to all the dielectric energy (contained in fields *P,E*). In dynamic systems where the elastic stress is distributed nonuniformly throughout the material the mutual energy must be *averaged* over space. Hence the coupling coefficient is generally less than that of the same material under static condition of uniform stress.

To Summarize: When elastic stress is coupled to a dielectric through piezoactivity the strength of the coupling may be measured by stipulating the value of a coupling coefficient, which is the ratio of the mutual energy of the elastic and dielectric fields to the geometric mean of these energies separately. In practical cases the coefficient may easily be calculated for specific, generally 1-dimensional, boundary conditions of the stress (or strain) field, and of the electric (or polarization) field. This is true for static, or low frequency, operation. Operation near or at mechanical resonance, and operation in 2- or 3-dimensional stress regimes, both introduce other phenomena which add complexity to the simple picture outlined here. This topic is discussed next.

2.7 ELASTIC STRUCTURES WHICH EXHIBIT MULTIPLE VELOCITY RESONANCES

In the theory of electroacoustic transduction velocity resonance plays an important role. Designers of acoustic transducers consciously include it in narrow band transmitters, and seek by various means to avoid its presence in broadband receivers. When acoustic transducers contain elastic structures the possibility of occurrence of multiple resonances is substantial even though a single resonance is the goal of design. A theory of multiple resonances is described next.

Let there be an elastic structure which exhibits a periodic forced and free vibration in one dimension (say x). The displacement $w(x, t)$ is then a function of the applied force $F(x, t)$,

$$\mathscr{L}(x, t)\{w\} = F(x, t) \quad (\text{units: } N/m) \tag{2.7.1}$$

The linear operator L is assumed to be a sum of a differential space operator $S(x)$ and a differential time operator $T(t)$. The latter may be explicitly written in most cases as the sum of resistance and inertance;

$$T(t) = D\,\frac{\partial}{\partial t} + \rho\,\frac{\partial^2}{\partial t^2} \quad \left(\text{units: } \frac{N}{m^2}\right). \tag{2.7.2}$$

Taking the Laplace transform of $w(x,\ t)$ and $F(x,\ t)$ with respect to time,

$$\mathbf{w}(x,\ p) = \int_0^\infty w(x,\ t)e^{-pt}\,dt;\ \mathbf{F}(x,\ p) = \int_0^\infty F(x,\ t)\ e^{-pt}dt$$

one obtains

$$\left[\frac{S(x)}{\rho} + p\,\frac{D}{\rho} + p^2\right]\mathbf{w}\ (x,\ p) = \frac{\mathbf{G}}{\rho}\ (x,\ p) \tag{2.7.3}$$

in which $\mathbf{G}\ (x,\ p)$ includes terms in initial displacement and initial velocity.

In most applications the space operator satisfies an eigenvalue equation of the type,

$$S(x)\ \{W_n^{(x)}\} = \lambda_n^2\ W_n(x),\ n = 1,\ 2\ \ldots. \tag{2.7.4}$$

in which $W_n(x)$ are eigenfunctions of the (bounded) elastic system and λ_n are its eigenvalues. Effectively, this step in the analysis converts the differential operator into an algebraic operator. We assume the elements of the set $W_n(x)$ are orthogonal and normalized over the space interval l, and may thus expand both $\mathbf{w}(x,\ p)$ and $\mathbf{G}(x,\ p)$ in them:

$$\mathbf{w}(x,\ p) = \sum_{n=1}^{\infty} A^*_n(p)\ W_n(x);\ \mathbf{G}(x,\ p) = \sum G^*_n(p)\ \mathbf{W}(x) \tag{2.7.5}$$

$$A^*_{n(p)} = \int_l \mathbf{n}(x)\ dx;\ \mathbf{G}^*_n(p) = \int_l \mathbf{G}(x,\ p)\ W_n(x)dx.$$

Substitution of these expansions into Eq. 2.7.3 leads to the result,

$$A^*_n(p) = \frac{\mathbf{G}^*_n(p)/\rho}{\left[\dfrac{\lambda_n^2}{\rho} + p\,\dfrac{D_n}{\rho} + p^2\right]} \tag{2.7.6}$$

The damping resistance D_n has been assigned for each value of n, that is, for each mode. It is noted from Eqs. 2.7.5 that $\mathbf{G}^*_n$ is an integral over the interval l. Hence,

$$\mathbf{w}(x,\ p) = \sum_{n=1}^{\infty} \frac{W_n(x)}{\left[\dfrac{\lambda_n^2}{\rho} + p\,\dfrac{D_n}{\rho} + p^2\right]} \int_l \frac{\mathbf{G}}{\rho}\ (u,\ p)\ W_n(u)\ du. \tag{2.7.7}$$

We choose now to consider forced drive and set $p = i\,\omega,\ i = \sqrt{-1}$. Then

$$w(x,\ \omega) = \sum_{n=1}^{\infty} \frac{W_n(x)}{(\omega_n^2 - \omega^2 + i\omega\dfrac{D_n}{\rho})} \int_l \frac{G}{\rho}\ (u,\ \omega)\ W_n(u)du \tag{2.7.8}$$

where

$$\omega_n^2 = \frac{\lambda_n^2}{\rho}.$$

In words: the total displacement w is an infinite sum of modal displacements ($n = 1, 2, \ldots$) whose amplitudes are functions of the forcing function and of frequency ω forced drive. These amplitudes reach successive maxima whenever $\omega = \omega_n$. When all modes are lossless (that is, $D_n = 0$ for each n), the amplitudes are infinite in magnitude. The system then as exhibits an infinite sequence of displacement resonances. For forced drive at frequency ω this is also an infinite sequence of velocity resonances. In practical applications the damping D_n is significant, thus making the amplitudes finite over some bandwidth. A measure of bandwidth in each mode is the mechanical Q_M defined as,

$$Q_M = \frac{\omega_n}{D_n/\rho}, \quad n = 1, 2 \ldots \tag{2.7.9}$$

In acoustic applications the damping D_n includes the resistive part of the acoustic radiation, see Sect. 1.66 and Sect. 1.7.

2.8 VELOCITY RESONANCE IN ELECTROACOUSTIC TRANSDUCTION

The electromechanical interaction in an electroacoustic transducer is represented by the coupled set of canonical equations,

$$E = Z_e I + T_{em} \mathrm{v} \tag{2.8.1}$$

$$F = T_{me} I + (Z_m + Z_a) \mathrm{v}. \tag{2.8.2}$$

The terms here have been defined in Sect. 1.44. In the conventional electroacoustic transducer the applied (external) force F is zero, the acoustic load having been accounted for by impedance Z_a. Thus, the mechanical velocity is

$$\mathrm{v} = \frac{-T_{me}}{(Z_m + Z_a)} I \tag{2.8.3}$$

or

$$\mathrm{v} = \frac{-T_{me}}{\left[Z_m + Z_a - \dfrac{T_{em} T_{me}}{Z_e}\right] Z_e} E. \tag{2.8.4}$$

We distinguish two types of velocity maxima: in the first, the velocity is maximized by driving the transducer through a sequence of frequencies at constant electrical current until a frequency ω_A is reached at which the velocity amplitude is largest. In the second, the transducer is driven through a sequence of frequencies at constant voltage until a frequency ω_B is reached at which the velocity amplitude is largest. Equations 2.8.3, 2.8.4 show that these two frequencies are different: in the case of constant current resonance, the quantity $Z_m + Z_a$ is minimized, in the case of constant voltage resonance, the quantity $Z_m + Z_a - (T_{em} T_{me}/Z_e)$ is minimized.

The distinction between the types of drive is preserved in the respective forms of electrical driving point impedance Z_{ee}, and electrical driving point admittance, Y_{ee}. These are defined as,

$$Z_{ee} = \left.\frac{E}{I}\right|_{F=0} = Z_e + Z_{\mathrm{MOT}}; \quad Z_{\mathrm{MOT}} = \frac{-T_{em} T_{me}}{(Z_m + Z_a)} \tag{2.8.5}$$

$$Y_{ee} = \left.\frac{I}{E}\right|_{F=0} = Y_e + Y_{\text{MOT}}; \quad Y_{\text{MOT}} = \frac{T_{em}T_{me}}{Z_e^2\left[Z_m + Z_a - \dfrac{T_{em}T_{me}}{Z_e}\right]}. \tag{2.8.6}$$

Since T_{em}, T_{me}, Z_m, Z_a, Z_e are complex numbers it is convenient to define angles β, and θ such that

$$\left.\begin{aligned} -T_{em}T_{me} &= A^2e^{-j2\beta} \\ Z_m + Z_a &= |Z_m + Z_a|e^{j\theta} \end{aligned}\right\}; \quad Z_e = |Z_e|e^{-j\epsilon}. \tag{2.8.7}$$

Then

$$Z_{\text{MOT}} = \frac{A^2}{|Z_m + Z_a|}\, e^{-j[2\beta+\theta]} \tag{2.8.8}$$

$$Y_{\text{MOT}} = \frac{-A^2}{|Z_e|^2}\,\frac{e^{-j[2\beta-2\epsilon]}}{Z_a + Z_B} = |Y_{\text{MOT}}|e^{-j\xi}. \tag{2.8.9}$$

$$Z_B = Z_m + \frac{A^2e^{-j[2\beta-\epsilon]}}{|Z_e|}.$$

For the condition of velocity resonance at constant current drive it is seen that the imaginary part of $Z_m + Z_a$ must vanish

$$Im[Z_m + Z_a] = 0 \quad [\text{at } f_A]. \tag{2.8.10}$$

Thus θ must be zero, which means that the mechanical impedance of transducer and load must be purely real. For the condition of velocity resonance at constant voltage drive,

$$Im\left\{Z_m + Z_a + \frac{A^2e^{-j[2\beta-\epsilon]}}{|Z_e|}\right\} = 0 \quad [\text{at } f_B]. \tag{2.8.11}$$

To see the import of these conditions better it is useful to consider the special case of magnetic coupling in which the acoustic load is purely real ($Z_a = r_a$). We also take the blocked electrical impedance to be purely imaginary ($Z_e = j\omega L_e$). Then approximately,

$$\left.\begin{aligned} \beta &= \epsilon \\ \frac{T_{me}}{Z_e} &= \frac{A}{|Z_e|} \end{aligned}\right. \tag{2.8.12}$$

and the condition for maximization of the velocity at constant voltage is the frequency ω_B at which

$$v_{\max} = \frac{A}{|Z_e|}\,\frac{1}{r_a + r_B}E. \tag{2.8.13}$$

Thus ω_B is also the frequency at which the motional admittance is a maximum. The angle ξ of this admittance is zero. Similarly the condition for maximization of the velocity at constant current is the frequency ω_A at which,

$$v_{max} = \frac{A}{r_m + r_a} \cdot I \quad \text{(at angle } -\beta \text{ on an impedance plot).} \tag{2.8.14}$$

This is the same frequency at which the motional impedance Eq. 2.8.5 is a maximum. The angle of this impedance is -2β.

An additional discussion of different types of drive as applied to magnetic transducers is undertaken in Sect. 2.10.

2.9 DISTINCTION BETWEEN ELECTRICAL AND MECHANICAL RESONANCE

'Resonant' transducers are defined in several ways. We review them here.

In the following definitions we assume that electrical impedances are purely reactive and electrical admittances are purely susceptive.

Definition: An electromechanical transducer is electrically resonant at frequency f_r(electrical) when the reactive part of the motional electrical impedance measured at its input terminals vanishes (alternatively the input admittance is infinite). It is electrically antiresonant at frequency f_a (electrical) when the reactive part of the motional impedance at its input terminals is infinite (alternatively, the input admittance vanishes).

Definition: An electromechanical transducer is mechanically resonant at frequency f_r (mech) when the reactive part of its mechanical impedance at forced electrical drive vanishes. It is mechanically clamped at frequency f_a (clamped) when there is no motion at forced electrical drive.

The coincidence of frequencies of electrical resonance and mechanical resonance, or electrical antiresonance and mechanical clamping resonance, depends on the mode of coupling (31, 33, etc) and on the nature of forced drive (open circuit, or short circuit) The following Table 2.9.1 summarizes important coincidences of frequency.

It is noted that for

(1) electric field transducers: f_a (elec.) > f_r (elec.)
(2) magnetic field transducers: f_r (elec.) > f_a (elec.).

The mechanical resonant frequencies listed are defined in terms of the following elastic wave speeds:

short circuit bar wavespeed: $v_b^E = (\rho s_{11}^E)^{-1/2}$
open circuit bar wavespeed: $v_b^D = (\rho s_{33}^D)^{-1/2}$
short circuit plate thickness wavespeed: $v^E = (C_{33}^E/\rho)^{1/2}$
open circuit plate thickness wavespeed: $v^D = (C_{33}^D/\rho)^{1/2}$
constant H bar wavespeed: $v_b^H = \left(\frac{C_{33}^H}{\rho}\right)^{1/2}$
constant B bar wavespeed: $v_b^\beta = \left(\frac{C_{33}^\beta}{\rho}\right)^{1/2}$

Table 2.9.1 — Relation of Frequencies of Electrical Drive to Frequencies of Mechanical Resonance and Antiresonance

Transducer Type	Mode of Coupling	Type of Forced Drive	Impedance or Admittance	Coincidence of Frequencies (see definitions noted above)
length expander	31	E = const.	$Y = \infty$	f_r(elec.) coincident with f_r(mech)
$f_r(\text{mech}) = \frac{v_b^E}{2l}$		(short circuit)	$Y = 0$	f_a(elec.) coincident with f_a(clamped)
length expander	33	D = const.	$Z = \infty$	f_a(elec.) coincident with f_r(mech)
$f_r(\text{mech}) = \frac{v_b^D}{2l}$		(open circuit)	$Z = 0$	f_r(elec.) coincident with f_a(clamped)
thickness	33	E = const.	$Y = 0$	f_a(elec.) coincidence with f_a(clamped)
$f_r(\text{mech}) = \frac{v^E}{2t}$		(short circuit)	$Y = \infty$	f_r(elec.) coincident with f_r(mech)
thickness	33	D = const.	$Z = \infty$	f_a(elec.) coincident with f_r(mech)
$f_r(\text{mech}) = \frac{v^D}{2t}$		(open circuit)	$Z = 0$	f_r(elec.) coincident with f_r(clamped)
Magnetic Field Transducer				
length expander	33	H = const.	$Z = \infty$	f_a(elec.) coincident with f_r(mech)
$f_r(\text{mech}) = \frac{v^H}{2l}$		(open circuit)	$Z = 0$	f_r(elec.) coincident with f_a(clamped)
length expander	33	B = const.	$Y = 0$	f_a(elec.) coincident with f_a(clamped)
$f_r(\text{mech}) = \frac{v^B}{2l}$		(short circuit)	$Y = \infty$	f_r(elec.) coincident with f_r(mech)

2.10 DISTINCTION BETWEEN CONSTANT-*B* AND CONSTANT-*H* DRIVE OF A MAGNETOSTRICTIVE TRANSDUCER

This subject, briefly mentioned in Sect. 2.2, is treated in greater detail here.

A. CONSTANT-*B* DRIVE

We consider a magnetostrictive ring vibrator, Fig. 2.10.1, having N turns of coil wound over length l. Here a segment of mass $\rho(a\delta\theta)$ A is accelerated in positive direction v by the negative of the net forces given by,

$$F_{\text{net}} = -2\frac{F_1}{2}\sin\delta\theta \rightarrow -F_1\delta\theta.$$

Thus the dynamic relation is

$$(\rho a\ A)(j\omega v) = -F_1.$$

The internal stress T_1 at any cross-sectional area A is

$$T_1 = c_{11}^B\ S - h_1 B_1 \qquad (2.10.1)$$

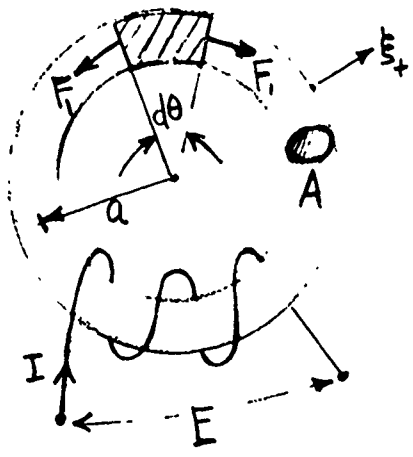


Fig. 2.10.1 — Magnetostrictive ring vibrator

For a thin ring whose radial displacement is ξ, one has

$$S = \frac{\xi}{a} = \frac{v}{j\omega a}.$$

Thus the equation of motion for the entire ring ($\theta = 0$ to $\theta = 2\pi$) reduces to

$$j\omega M v + \frac{2\pi C_{11}^{B} A}{j\omega a} v = 2\pi h_{11}^{(1)} B_1 A = \frac{2\pi h_{11}^{(1)} V}{j\omega N} \quad (2.10.2)$$

$$M = 2\pi a A \rho.$$

$$V = N \frac{d\phi}{dt} = j\omega NB_1 A.$$

In the presence of mechanical losses we write

$$C_{11}^{B} = Re\ C_{11}^{B} + j\mathrm{Im}\, C_{11}^{B}.$$

Here the plus sign is selected to insure that the mechanical resistance will be a position number. Equation 2.10.2 then becomes

$$v\left[\frac{2\pi(\mathrm{Im}\, C_{11}^{B})A}{\omega a} + j\omega M - j\frac{\mathrm{Re}\, C_{11}^{B} A}{\omega a}\right] = \frac{2\pi h_{11}^{(1)} V}{j\omega N}. \quad (2.10.3)$$

By definition, mechanical resonance occurs at the frequency ω_0 such that

$$j\omega_0 M - j\frac{(\mathrm{Re}\, C_{11}^{B})A}{\omega_0 a} = 0$$

or

$$\omega_0^2 = \frac{(\mathrm{Re}\, C_{11}^{B})}{a^2\rho},\ f_0 = \frac{1}{2\pi a}\frac{\sqrt{(\mathrm{Re}\, C_{11}^{B})}}{\rho},\ \omega_0 = 2\pi f_0. \quad (2.10.4)$$

The mechanical Q_M at constant-B resonance is

$$Q_M = \frac{\omega_0 M}{R(\omega_0)} = \frac{\omega_0 2\pi a A \rho\, \omega_0 a}{2\pi(\mathrm{Im}\, C_{11}^{B})A} = \frac{\omega_0^2 a^2 \rho}{(\mathrm{Im}\, C_{11}^{B})} = \frac{(\mathrm{Re}\, C_{11}^{B})}{(\mathrm{Im}\, C_{11}^{B})}. \quad (2.10.5)$$

The ratio of current I to voltage V is found from

$$H_1 = -h_{11}\frac{\xi}{a} + \gamma_{11}^{s} B_1 = \frac{NI}{l} \quad (2.10.6)$$

or

$$I = \frac{-h_{11} l}{j\omega N} v + \frac{\gamma_{11}^{s} Vl}{j\omega N^2 A} \quad \text{(units: } Vs/A\text{)}$$

in which l is the length of coil.

Solving Eq. 2.10.3 for v and substituting in the above equation lead to the ratio

$$\frac{I}{V} = \frac{2\pi h_{11}^2 l}{\omega^2 a N^2} \frac{1}{z_m} + \frac{1}{j\omega L} = Y_{\text{MOT}} + Y_{b_{\text{blocked}}} \tag{2.10.7}$$

$$L = \frac{N^2 A}{\gamma_{11}^{s} l} \text{ (units: } Vs/A\text{)}; \; z_m = r_m + j\omega M + \frac{K}{j\omega} \quad \text{(units: Ns/m)}$$

$$K = \frac{(\text{Re}\, C_{11}^{B}) A}{a} \quad \text{units: N/m).}$$

In the absence of any mechanical losses the electrical admittance becomes infinite at the frequency ω_0 of mechanical resonance at constant-B drive.

B. Constant-H Drive

By substituting Eq. 2.10.6 into Eq. 2.10.1 the force acting on an elementary mass of the ring is,

$$F_1 = \left[C_{11}^{B} - \frac{h_{11}^2}{\gamma_{11}^{s}} \right] \frac{\xi A}{a} - \frac{h_{11}^{(1)} H_1 A}{\gamma_{11}^{s}}. \tag{2.10.8}$$

Thus the equation of motion for the ring driven by constant H is

$$v\left\{ j\omega M + \left[C_{11}^{B} - \frac{h_{11}^2}{\gamma_{11}^{s}} \right] \frac{2\pi A}{j\omega A} \right\} = \frac{2\pi h_{11}^{(1)} H_1 A}{\gamma_{11}^{s}}. \tag{2.10.9}$$

In this type of drive the losses are both mechanical and magnetic (hysteresis and eddy currents):

$$C_{11}^{B} = \text{Re}\, C_{11}^{B} + j\, \text{Im}\, C_{11}^{B} \tag{2.10.10}$$

$$\gamma_{11}^{s} = \text{Re}\, \gamma_{11}^{s} + j\, \text{Im}\, \gamma_{11}^{s}.$$

Here the signs have been chosen to ensure positive values for mechanical resistance. Substitution of Eq. 2.10.10 into Eq. 2.10.9, leads to the dynamic equation,

(*a*) $$v\left\{ (\text{Im}\, C_{11}^{B}) \frac{2\pi A}{\omega a} + \right.$$

$$\frac{h_{11}^2\,(\mathrm{Im}\,\gamma_{11}^S)\,2\pi A}{\omega a[(\mathrm{Re}\,\gamma_{11}^S)^2+(\mathrm{Im}\,\gamma_{11}^S)^2]}+j\omega M+\frac{1}{j\omega}\left[\frac{(\mathrm{Re}\,C_{11}^B)2\pi A}{a}-\frac{h_{11}^2\,(\mathrm{Re}\,\gamma_{11}^S)}{[(\mathrm{Re}\,\gamma_{11}^S)^2+(\mathrm{Im}\,\gamma_{11}^S)^2]}\,\frac{2\pi A}{a}\right]\Bigg\}$$

$$=\frac{2\pi\,h_{11}^{(t)}\,H_1 A}{\gamma_{11}^S} \tag{2.10.11}$$

For simplicity this is written as

$$(b)\qquad \mathrm{v}z_m=\frac{2\pi h_{11}^{(t)}\,H_1 A}{\gamma_{11}^S}$$

where z_m is the mechanical impedance (units: *Ns/m*) given by quantity in braces.

By definition the frequency of mechanical resonance occurs at,

$$\omega_0^2=\frac{1}{a^2\rho}\left\{\mathrm{Re}\,C_{11}^B-\frac{h_{11}^2\,(\mathrm{Re}\,\gamma_{11}^S)}{[(\mathrm{Re}\,\gamma_{11}^S)^2+(\mathrm{Im}\,\gamma_{11}^S)^2]}\right\} \tag{2.10.12}$$

By comparing Eq. 2.10.12 with Eq. 2.10.4 one concludes:

The mechanical resonant frequency at constant-H drive is lower than that at constant-B drive. This is so even in the case of zero mechanical losses. The mechanical Q_M at constant-H resonance is easily obtained from Eq. 2.10.11 for the frequency $\omega=\omega_0$:

$$Q_M=\frac{\omega_0 M}{r_m}=\left\{\frac{\mathrm{Re}\,C_{11}^B-\dfrac{h_{11}^2\,(\mathrm{Re}\,\gamma_{11}^S)}{[(\mathrm{Re}\,\gamma_{11}^S)^2+\mathrm{Im}(\gamma_{11}^S)^2]}}{\mathrm{Im}\,C_{11}^B+\dfrac{h_{11}^2\,(\mathrm{Im}\,\gamma_{11}^S)}{[(\mathrm{Re}\,\gamma_{11}^S)^2+\mathrm{Im}(\gamma_{11}^S)^2]}}\right\} \tag{2.10.13}$$

One concludes:

The mechanical Q_M at mechanical resonance for constant-H drive is smaller (meaning the bandwidth is larger) than the mechanical Q_M at mechanical resonance for constant-B drive for two reasons: (1) the resonant frequency is lower; (2) the total losses are larger because they include magnetic field losses.

The ratio of voltage V to current I for constant-H drive is directly found from

$$B_1=\frac{H_1}{\gamma_{11}^S}+\frac{h_{11}}{j\omega a\gamma_{11}^S}\,[\mathrm{v}] \tag{2.10.14}$$

in which

$$\gamma_{11}^S=\mathrm{Re}\,\gamma_{11}^S+\mathrm{Im}\,\gamma_{11}^S$$

By using Eq. 2.10.11 to obtain v one derives the result,

$$Z_{ee} = \frac{V}{I} = \frac{j\omega N^2 A}{l\gamma_{11}^S} + \frac{2\pi N^2 A^2 h_{11}^2}{al(\gamma_{11}^S)^2} \times \frac{1}{z_m} = Z_{\text{blocked}} + Z_{MOT}. \tag{2.10.15}$$

Here the mechanical losses in the first instance are contained solely in the mechanical impedance z_m. One can include if desired, the losses in the magnetic circuit by making γ_{11}^S complex:

$$\gamma_{11}^S = |\gamma_{11}^S| e^{+j\beta}. \tag{2.10.16}$$

Since the locus of z_m^{-1} ($= g_m - jb_m$) on a b_m vs g_m plot is a circle with horizontal diameter, the factor $(\gamma_{11}^S)^2$ causes this diameter to rotate clockwise through an angle 2β on an electrical impedance plot of X_{MOT} vs R_{MOT}. Thus the inclination 2β of the motional circle is a measure of losses (eddy-currents and hysteresis) of the magnetic circuit. It is thus seen that in the absence of mechanical losses the electrical impedance becomes infinite at the mechanical resonant frequency for constant-H drive.

Vector Force Factor, Turns Ratio, Mechanical Q

The form of Eq. 2.10.15 allows one to obtain a *vector force factor*, Z_{em} defined by the relation $+T^2 = -Z_{em}^2$, and the magnitude squared of equivalent transformer ratio, ϕ^2. In general ϕ^2 differs from Z_{em}^2.

First we note that

$$Z_{ee} = Z_e + Z_{MOT};\ Z_{MOT} = -\frac{T_{me}T_{em}}{z_m} = \frac{-T^2}{z_m}.$$

Now, assuming length of coil $l = 2\pi a$, it is seen that

$$T_{em} = T = Z_{em} = \left[\left[\frac{NAh_{11}}{a\gamma_{11}^S}\right]^2\right]^{1/2}.$$

This is the vector force factor explicitly written in terms of properties of the toroid and coil. To find the turns ratio ϕ of the equivalent circuit we must restore symmetry to the canonical equations (1.44.1). Several procedures have been forwarded to do this.

(1) Symmetry may be restored by rotating F, v by 90°, setting

$$F = jF',\ \text{v} = j\text{v}'.$$

The resultant canonical set is transformed in Eqs. 1.45.1. The equivalent circuit is then Fig. 1.45.2. In this figure the equivalent mechanical impedance coupled into the mechanical mesh is

$$Z_m' = -\frac{T^2}{Z_e} = \left(-\frac{Z_{em}}{Z_e}\right)^2 Z_e.$$

According to Table 1.47.1 the appropriate turns ratio is then,

$$\phi = \sqrt{\left[-\frac{Z_{em}}{Z_e}\right]^2} = \frac{j\,Z_{em}}{Z_e} = \frac{jNAh_{11}}{a\gamma_{11}^S} \frac{2\pi a\gamma_{11}^S}{j\omega N^2 A} = \frac{h_{11}}{fN}.$$

Also,

$$Z_m' = \frac{k^2 K_0}{j\omega};\ K_0 = \frac{AY_M}{a};\ Y_M = \text{Young's modulus.}$$

(2) Symmetry can also be restored by transposing the canonical set so that velocity appears as an across quantity in the mechanical mesh see Eq. (1.47.3). The equivalent circuit is then Fig. 1.47.2, where the turns ratio is

$$T_{em} = \frac{NAh_{11}}{a\gamma_{11}^{s}} = \alpha_{em} = \alpha_{me}; \begin{cases} \text{units of } \alpha_{em}\text{: } Vs/m \\ \text{units of } \alpha_{me}\text{: } Ns/c \end{cases}$$

Since the mechanical admittance y_m appears in shunt position the transfer to the electrical mesh is

$$T_{em}^2\, y_m = Z_{\text{electrical}}.$$

Thus T_{em}^2 converts mechanical mobility into electrical *impedance*. The circuit thus describes a gyrator (see Sect. 1.47 for discussion).

Thus,

$$V = \alpha_{em} v; \quad F = \alpha_{me} I \tag{2.10.17}$$

The mechanical Q_M (Eqs. 2.10.33 or 2.10.41) can be determined by measurement of two frequencies, ω' and ω'', derived as follows. Let the mechanical impedance be written in the form,

$$Z_m = r_m + jx_m; \quad x_m = \omega M - \frac{1}{\omega C_m}$$

whose phase angle is

$$\tan\theta = \frac{x_m}{r_m}.$$

At $\theta = +45°$, one sets $\omega = \omega''$ so that

$$r_m = \omega'' M - \frac{1}{\omega'' C_m} = \omega'' M \left[1 - \frac{\omega_0^2}{\omega''^2}\right]. \tag{2.10.18}$$

At $\theta = -45°$, on sets $\omega = \omega'$, which gives,

$$r_m = -\omega' M + \frac{1}{\omega' C_m} = \omega' M \left[1 - \frac{\omega_0^2}{\omega'^2}\right]. \tag{2.10.46}$$

By subtracting Eqs. 2.10.18 and Eq. 2.10.19 it is determined that

$$\omega'\omega'' = \omega_0^2$$

and by adding the two equations it is determined that

$$\frac{r_m}{M} = \omega'' - \omega'.$$

Thus, the mechanical Q_M is

$$Q_M = \frac{\omega_0 M}{r_m} = \frac{\omega_0}{\omega'' - \omega'}. \tag{2.10.20}$$

Now,

$$Z_{MOT} \propto \frac{1}{z_m} = y_m$$

Since

$$\text{phase angle of } y_m = -\text{phase angle of } z_m$$

it is seen that in the electrical impedance circle of $X_{\text{electrical}}$ vs $R_{\text{electrical}}$ the conditions (for zero magnetic losses) hold:

$$\begin{cases} \omega' \text{ occurs at } +45° \\ \omega'' \text{ occurs at } -45° \end{cases}$$

These are then the *quadrantal* frequencies of the electrical impedance circle. Similarly when the presence of magnetic field losses causes the circle diameter to dip clockwise at angle 2β, the quadrantal frequencies remain at $\pm 45°$ relative to this diameter. In all cases it is seen that measurement of ω', ω'' on an electrical impedance plot determines the Q_M, and thus determines the bandwidth of the resonant mechanical circuit.

2.11 SUMMARY OF NOMENCLATURE USED BY VARIOUS AUTHORS TO DESCRIBE RESONANCE IN ELECTROMECHANICAL TRANSDUCERS

The word "resonance" in electromechanical systems has a variety of different symbols and meanings. Table 2.11.1 presents a summary of the most often encountered usages.

Table 2.11.1

Electric Field Transducers: C_0 = static capacitance; C = electrical equivalent mechanical capacitance

Symbol	Nomenclature	Meaning	Table References
ω_r	resonance frequency	frequency at which total electrical impedance vanishes, or resonance frequency of the mechanical series branch ($\omega_r = K/M$)	[1]
ω_a	antiresonance frequency	frequency at which total electrical admittance vanishes $\left(\omega_a = \sqrt{\frac{K}{M} + \frac{4\alpha^2}{C_0 M}}\right)$.	[1]
ω_{r0}, ω_{a0}		undamped values of ω_r, ω_a	
k_c	electromechanical coupling factor	$k_c^2 \sim \frac{\pi^2}{4}\left[\frac{f_a - f_r}{f_r}\right]$	[2]
$\omega_v =$	$(1/LC)^{1/2}$	frequency of maximum power output at constant voltage drive	[3]
$\omega_I =$	$\left\{\left[1 + \frac{C}{C_0}\right]/LC\right\}^{1/2}$	frequency of maximum power output at constant current drive	[3]

f_s	motional (series) resonance frequency	$f_s = \frac{1}{2\pi}\left(\frac{1}{LC}\right)^{1/2}$, or frequency of maximum motional admittance	[4]
f_p	parallel resonance frequency	$f_p = \frac{1}{2\pi}\left\{\frac{(1 + C/C_0)}{LC}\right\}^{1/2}$	[4]
f_r	resonance frequency	Electrical susceptance = 0, at G_r	[4]
f_a	antiresonance frequency	Electrical susceptance = 0, at G_a	[4]
f_m		frequency at which the total electrical admittance is a maximum	[4]
f_n		frequency at which the total electrical admittance is a minimum	[4]
$C/C_0 =$	$(f_p^2 - f_s^2)/f_s^2$		
k	dynamic electromechanical coupling factor	$k^2 = \frac{f_p^2 - f_s^2}{f_p^2}$	[5]
k_{eff}	effective coefficient of electromechanical coupling	$k_{eff} = 1 - \left(\frac{f_v}{f_R}\right)^2$	[6]
f_R	resonance frequency	frequency at which the motional impedance is a maximum, $X_m(f_R) + X_L(f_R) = 0$	[7]
f_Y		frequency at which the motional admittance is a maximum, $X_m(f_y) + X_L(f_y) = \mathrm{Im}\left[-\frac{Z_{em}^2}{Z_e}\right]$	[7]

Magnetic Field Transducers

k_{eff}	effective coefficient of electromechanical coupling	$k_{eff} = 1 - \left(\frac{f_R}{f_Y}\right)^2$	[6]
ω_A	A-type resonance	frequency at which the motional impedance is a maximum, or at which the velocity becomes a maximum at constant voltage	[8]
ω_B	B-type resonance	frequency at which the motional admittance is a maximum, or at which the velocity becomes a maximum at constant current	[8]

Table References

[1] "Sonics" T.F. Hueter, R.H. Bolt, p. 110.

[2] Ibid [1], p. 119.

[3] Ibid [1], p. 116.

[4] "Physical Acoustics" Vol. I. Part A, p. 244, Academic Press, W. Mason Ed.

[5] Ibid [4], p. 245.

[6] "Electroacoustics" F.V. Hunt, p. 140, Harvard Press.

[7] Ibid [6], p. 137.

[8] "Ultrasonic Transducers" Y. Kikuchi, Ed. p. 271, Corona Press.

2.12 MECHANICAL AND ELECTRICAL BOUNDARY CONDITIONS IN PIEZOELECTRIC TRANSDUCERS

Piezoelectric materials exhibiting electromechanical transduction are described by thermodynamic equations of state. In the first approximation temperature and entropy are neglected and the description is reduced to use of four variables: two mechanical variables, namely, stress (T) and strain (S); and two electrical variables, namely, the electric field intensity E and the electric displacement D. T and E can be regarded as *intensive* variables, and S D as *extensive* variables. In application, most transducers of this type are characterized by *linearized* equations of state in which one mechanical variable is a function of the second mechanical variable and an electrical variable; and one electrical variable is a function of the second electrical variable and a mechanical variable. Four variables thus generate four pairs of equations in which the dependent pairs are S,D; S,E; T,D; T,E. Customarily the sets of equations are written in Cartesian tensor form whenever the tensor aspect connecting dependent and independent variables is essential, and written in matrix form whenever simplified notation is serviceable. For convenience the matrix form is repeated here.

$$\begin{array}{ll} S = s^E T + d_t E & T = C^E S - e_t E \\ (1)\ D = dT + \epsilon^T E & (2)\ D = eS + \epsilon^S E \end{array} \qquad (2.12.1)$$

$$\begin{array}{ll} S = s^D T + g_t D & T = C^D S - h_t D \\ (3)\ E = -gT + \beta^T D & (4)\ E = -hS + \beta^S D \end{array}$$

$$S = S_i, i = 1,2 \ldots 6; \quad T = T_i, i = 1,2 \ldots 6; \quad s = s_{ij}, d = d_{ij}, g = g_{ij}\ h = h_{ij},$$

$$C = C_{ij}, e = e_{ij}, i,j = 1,2 \ldots .6.$$

$$E = E_i, i = 1,2,3; \ D = D_i, i = 1,2,3; \ \epsilon = \epsilon_{ij}, i,j = 1,2,3; \ \beta = \beta_{ij}, i,j = 1,2,3.$$

Subscript t means 'transpose.' Convention assigns the subscripts as follows:

$$T_1 = T_{xx}, T_2 = T_{yy}, T_3 = T_{zz}; T_4 = T_{yz}; T_5 = T_{xz}; T_6 = T_{xy}$$

$$S_1 = S_{xy}, S_2 = S_{zy}, S_3 = S_{zz}; S_4 = S_{yz}; S_5 = S_{yz}; S_6 = S_{xy}.$$

In general then, equations featuring S,T as dependent (left-hand side) variables are six in number, while equations in dependent variables D,E are three in number. There are thus for any selected set (say 1 above) nine equations in nine unknown (= independent) variables.

In application the number of unknowns is greatly reduced. The transducer designer usually chooses to restrict wave propagation to a few dimensions, or one dimension, or equivalently, to select a few or one mode of vibration. This is accomplished by fabricating the piezoelectric material in a shape which emphasizes the (say) single dimension of motion (rod, disk, cylinder, etc.), and placing the necessary electrodes on strategic surfaces to gather charge, or apply electric fields generating or resulting from this motion. The nature of the fabricated shape determines the appropriate mechanical boundary conditions, and the placing of the electrodes determines the appropriate electrical boundary conditions.

We consider first the mechanical boundary conditions and take the example of a long bar of rectangular cross-section, length l, width w, thickness t. By making w,t very small compared to a wavelength of compressional waves in the length direction, one permits the lateral surfaces to be free to accommodate any stress condition. This is the constant-T case. In the most useful applications the lateral surfaces are free of stress ($T = 0$), hence the stresses in the plane of the cross section are also zero. Only the longitudinal stress normal to the cross-section is significant. This simplification makes it advantageous to adopt stress T as the *independent* variable.

The same stress condition applies to a thin ceramic ring in the radial mode of vibration in which all stresses are negligible except the circumferential hoop (tensile) stress.

We next consider the second type of mechanical boundary condition which occurs when the lateral dimensions of the transducer's active material are much larger than the dimension in the direction of elastic wave propagation. An example is the piezoelectric plate vibrating in the thickness mode where the thickness is much smaller than the plates length or width. Since there is very little motion in the plane of the plate normal to its thickness it is useful to assume the elastic strain is everywhere negligible except in the direction of the thickness. The plate is said then to be laterally clamped. The boundary condition is called constant-S. This simplification makes it advantageous to adopt strain S as the independent variable since then there is only one strain component to consider.

The two elastic (that is mechanical) boundary conditions of constant-T or constant-S, are easily selectable because most piezoactive materials are deliberately designed to exhibit a single direction of propagation, or operate in a single mode.

Similar rules can be adopted for the electrical boundary conditions. Here, two factors must be considered: (1) the direction of the electric field, and (2) the direction of wave propagation. In the first type of boundary conditions the electric field is applied in the designer-selected direction of wave propagation by the simple means of electroding the end surfaces of the piezoelectric vibrator so that they are normal to the direction of wave propagation. The dielectric displacement D (that is, the electric charge collector) is then assumed to be zero everywhere except in these surfaces, an assumption which is valid when the piezoactive material is an insulating dielectric with no fringing flux leakage. Since there is only one component of D to consider it is advantageous to adopt this constant-D boundary condition by selecting D to be the independent variable. The electric field E, in contrast, is a function of position along the direction of elastic wave propagation.

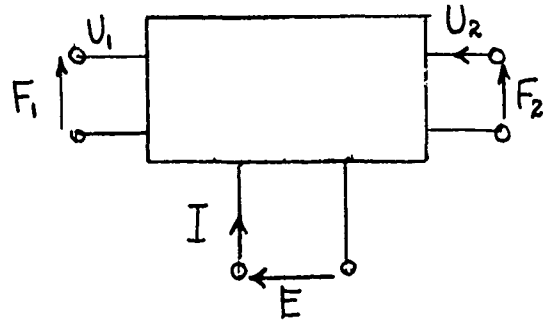
In the second type of boundary conditions the electric field is applied normal to the direction of wave propagation by sandwiching the piezoelectric vibrator between electrodes which provide equipotential surfaces in that direction. Here there is only one component of electric field, constant along the vibrating direction. This is the constant-E boundary condition in which E is the independent variable.

The electrical boundary conditions just described, as well as the mechanical boundary condition noted above, form an indispensable adjunct to solution of the equations of motion. It is through their use that electric field and magnetic field transducers are designed to generate elastic motion in preferred directions. Commonly used designs are discussed next.

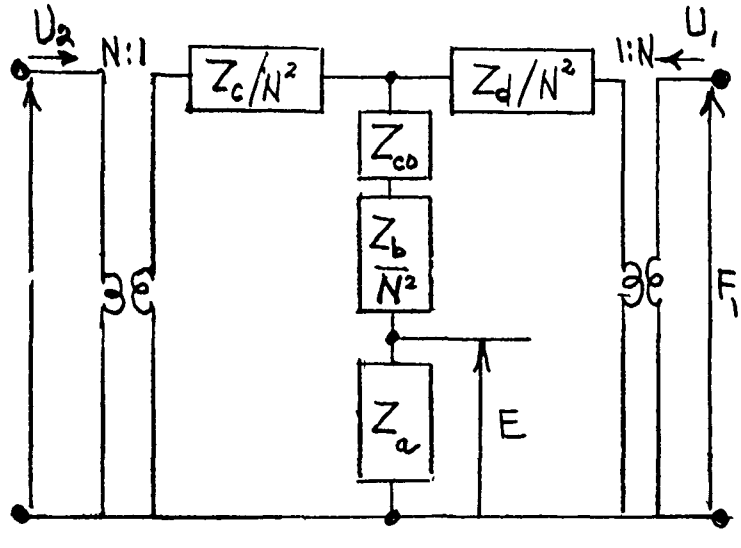
2.13 LIST OF COMMONLY USED MODES OF VIBRATION OF PIEZOELECTRIC TRANSDUCERS AND THEIR EQUIVALENT CIRCUITS

Generalized equivalent circuits underlie current applications of most transducers in use. The Mason equivalent circuit, discussed in greater detail in Section 2.21 below, is the prototype equivalent circuit for all piezoelectric transducers. For a transducer of length l in the direction of wave propagation and lengths w,t transverse to l, its generalized form is shown here in Fig. 2.13.1a,b.

The analogy used is voltage (V)/force (F), current (I)/mechanical velocity (v). All mechanical impedances have been transferred to the electrical side of the ideal transformer of turns-ratio N. For piezoelectric coupling one has:



(a)



(b)

Fig. 2.13.1 — (a) Generalized form of a three-port transducer represented as a 6-terminal "black-box," (b) generalized equivalent circuit of a piezoelectric transducer

piezoelectric coupling one has:

$$(a)\ Z_a = \frac{1}{j\omega C_0} \quad (b)\ Z_{C_0} = -\frac{1}{j\omega C_0} \quad (c)\ Z_b = \frac{Z_0}{j\sin\left(\frac{\omega l}{v_b^D}\right)}$$

$$(d) Z_c = Z_d = jZ_0 \tan \frac{\omega l}{2v_b^D}$$

in which

$$v_b^D = \sqrt{\frac{1}{\rho s_{33}^D}}\ ; Z_0 = \rho v_b^D A, \qquad A = \text{area transverse to direction of propagation.}$$

This circuit network may be analyzed as three electrical meshes: loops 1, 2, 3; and two mechanical meshes, loops 4,5. In loop 1 current I_1 flows through impedances Z_c, Z_b, Z_{c0}, Z_a; current I_2 flows through Z_b, Z_{c0}, Z_a; current I flows through Z_a. In loop 2, current I_2 flows through Z_d, Z_b, Z_{c0}, Z_a; current I_1 flows through Z_b, Z_{c0}, Z_a; and current I flows through Z_a. In loop 3 currents I, I_1, I_2 flow through Z_a. In loop 4, $NV_1 = F_1$ and $I_1/N = U_1$. In loop 5, $NV_2 = F_2$ and $I_2/N = U_2$.

It is to be noted that Z_{c0} appears in the electrical mesh, just as required by the canonical circuit Fig. 1.45.3. Its appearance is associated with the superscript D of s_{33}^D. It is exemplified in the thickness expander mode of a piezoelectric plate, cited here as the first case of our list.

Case I. Thickness expander mode of a piezoelectric plate with 3-3 coupling, Fig. 2.13.2. This figure conforms to the canonical equivalent circuit, Fig. 1.45.3, which features the electrical impedance in shunt position, the mechanical impedance in series position, and the coupled impedance $-T^2/Ze$ transferred to the electrical mesh where it appears in series position as $-1/j\omega C_0$. The mechanical boundary condition is constant S, while the electrical boundary condition is constant D.

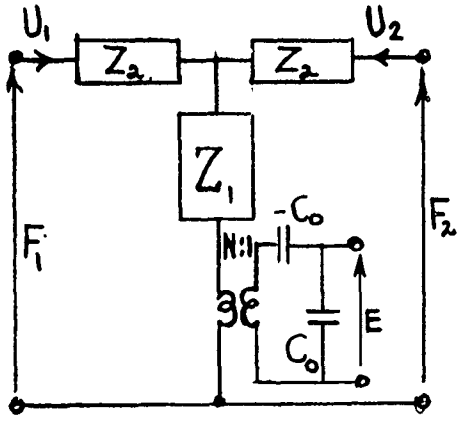
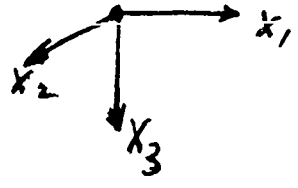


Fig. 2.13.2 — Equivalent circuit of a thickness expander piezoelectric plate

Case II. Thickness shear mode of a piezoelectric plate with 15 coupling. In this case the equivalent circuit is Fig. 2.13.2 modified as follows:



(a) the orientation of axes is changed as shown to the right:
(b) v_b^D is replaced by v_s^D (defined below).
(c) all other parameter are given by

$$C_0 = \frac{lw}{\beta_{11}^S t}, \quad v_s^D = \left(\frac{c_{55}^D}{\rho}\right)^{\frac{1}{2}},$$

$$Z_0 = \rho l w v_s^D, \quad N = C_0 h_{15} = \frac{lw}{t}\left(\frac{C_{55}^D}{\beta_{11} s}\right)^{\frac{1}{2}} k_{15}.$$

Case III. Length expander with 31 coupling, Fig. 2.13.3. In this case the coupling capacitance,

$$Z_e' = \frac{1}{j\omega C_1}$$

is in parallel with C_0. Hence the electrical capacitance C_0 is reduced by a factor $1 - k_{31}^2$, where

$$k_{31}^2 = \frac{d_{31}^2}{s_{11}^E \epsilon_{33}^T}.$$

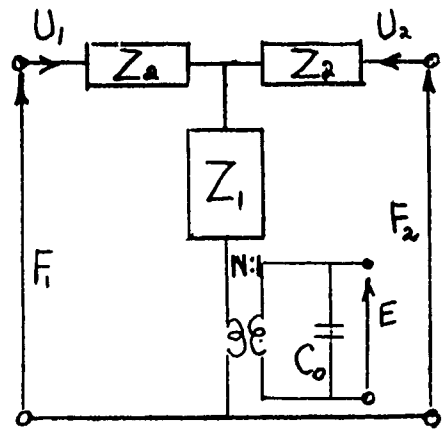


Fig. 2.13.3 — Equivalent circuit of a thickness shear mode in a piezoelectric plate

This figure conforms to the canonical equivalent circuit, Fig. 1.45.2, with the coupling between meshes accounted for by k_{31}^2.

Case IV. Length expander with 33 coupling, Fig. 2.13.2 modified. This figure conforms to the canonical circuit Fig. 1.45.2 in which

$$S_3 = s_{33}^D T_3 + g_{33} D$$

$$E_3 = -g_{33} T_3 + \beta_{33}^T D_3$$

$$k_{33}^2 = \frac{g_{33}^2}{\beta_{33}^T s_{33}^D}.$$

To summarize: the design of piezoelectric (and piezoceramic) transducers is greatly facilitated by use of the basic Mason equivalent circuit displayed in several forms. Other standard equivalent circuits are discussed next.

2.14 STANDARD EQUIVALENT CIRCUITS

The representation of transducers by equivalent electrical circuits has been standardized into simple diagrams. These are listed below.

I. Electric Field Transducers

The canonical equivalent circuit is Fig. 1.45.2. The transformer ratio ϕ has the units of C/m or N/V. Fig. 2.14.1 shows the conventional circuit. In it, all shunt branches are in admittance form and all series branches are in impedance form. Because the direction of v is reversed, the direction of F is also reversed. The analogy used is e/F, i/v.

$$\left[\text{units of } \phi^2 : \frac{CN}{mV}\right].$$

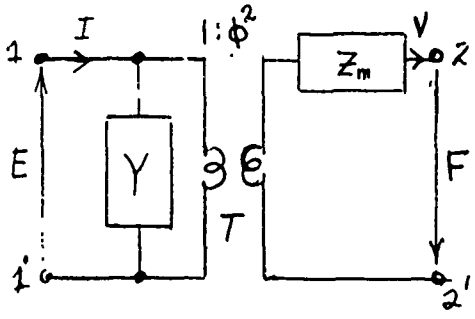


Fig. 2.14.1 — Standard simplified equivalent electrical circuit of an electrostatic transducer

When this transducer acts as a sound radiator it is convenient to convert Fig. 2.14.1 into an all electrical circuit. To do this we use the rules of Table 1.47.1. Figure 2.14.2 shows the result. Here Y represents the shunt portion of the purely electrical admittance; L_m, R_m, C_m represent the (transformed) mechanical, and R_a, X_a represents the (transformed) acoustic load, the latter written here as mechanical impedance $r_a + jx_a$ (see Fig. 1.7.7a).

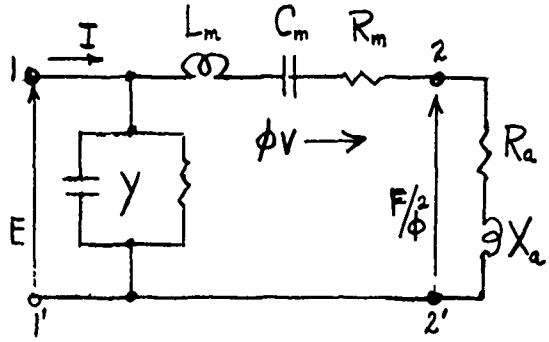


Fig. 2.14.2 — All electrical equivalent circuit of an electrostatic sound radiator

$$L_m = m/\phi^2;\ C_m = \frac{\phi^2}{C_m};\ R_m = \frac{r_m}{\phi^2}$$

$$R_a = \frac{r_a}{\phi^2};\ X_a = \frac{x_a}{\phi^2}. \tag{2.14.1}$$

When the electrostatic transducer is used as a sound receiver it is convenient to convert Fig. 2.14.1 into an all mechanical equivalent circuit, again using the rules of Table 1.47.1. The result is Fig. 2.14.3. Here, F_a is the equivalent acoustic (force) generator, Y_0 is the electrical load admittance and Y is the purely electrical portion of the electromechanical transducer.

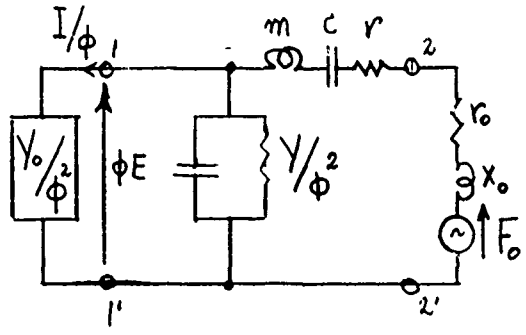


Fig. 2.14.3 — All mechanical equivalent circuit of an electrostatic sound receiver

II. Magnetic Field Transducers

The canonical equivalent circuit is Fig. 1.47.2, shown here as Fig. 2.14.4, in which

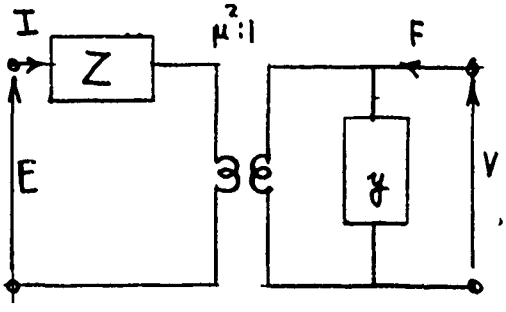


Fig. 2.14.4 — Standard simplified equivalent of a magnetostrictive transducer

$$\mu = \frac{\phi N \chi}{d_0 + \xi},$$

as obtained from Eq. 2.36.4. Here, $y(=Z_m^{-1})$ is the mechanical admittance (or mobility). Note that,

$$\text{units of } \mu^2\text{: } \frac{Ns}{C} \times \frac{Vs}{m}$$

When used as a sound radiator this circuit is modified by adding an acoustic load to terminals 2, 2', and then transferring all the mechanical mesh to the electrical (left) side. To do this we first note from Table 1.20.3 that a parallel mechanical network is converted into an equivalent electrical parallel VF network according to the rule:

$$F = \mathrm{v}\left[c + j\omega m + \frac{K}{j\omega}\right]$$

$$i = e\left[\frac{1}{R} + j\omega C + \frac{1}{j\omega L}\right].$$

Since velocity v is an across variable we also see from Table 1.47.1 that

for mechanical resistance c: $F = \mathrm{v}c$ transforms to $\frac{F}{\mu} = i$, $\mu\mathrm{v} = e$, so that $\frac{e}{i} = \frac{\mu^2}{c} = R_m$

for mechanical mass m: $F = j\omega m\mathrm{v}$ transforms to $\frac{e}{i} = \frac{\mu^2}{j\omega m}$ or $C_m = m/\mu^2$

for mechanical spring k: $F = \frac{K}{j\omega}\text{v}$ transforms to $\frac{e}{i} = \frac{j\omega\mu^2}{K}$, or $L_m = \frac{\mu^2}{K}$.

The parallel form of the acoustical loading in VF form is shown in Fig. 1.7.7b. Again one sees from Table 1.47.1 that the following transformations occur:

for acoustical resistance: $\text{v} = F_R/R_{\text{RAD}}$ transforms to $\frac{e}{i} = \frac{\mu^2}{R_{\text{RAD}}}$, or $G_a = \frac{R_{\text{RAD}}}{\mu^2}$

for acoustical reactance: $\text{v} = F_x/j\omega M_{\text{RAD}}$ transforms to $\frac{e}{i} = \frac{\mu^2}{j\omega M_{\text{RAD}}}$ or $C_{\text{RAD}} = \frac{M_{\text{RAD}}}{\mu^2}$.

The equivalent circuit of the magnetic field sound radiator, in which all the mechanical mesh has been transformed to the electrical side, is shown in Fig. 2.14.5. Here, Z_0 is the internal impedance of the voltage generator. When the magnetic field transducer, Fig. 2.14.4, is used as a sound receiver its equivalent circuit is modified by inserting a force source F_0 in shunt across terminals 2, 2′ and placing an electrical load Z_0 across terminals 1, 1′. Again, according to the rules of Table 1.47.1 the electrical equivalent of the force source acting as a through variable is F_0/μ, and the electrical equivalent of the velocity (acting as an across quantity is μv. The equivalent circuit is then given by Fig. 2.14.6.

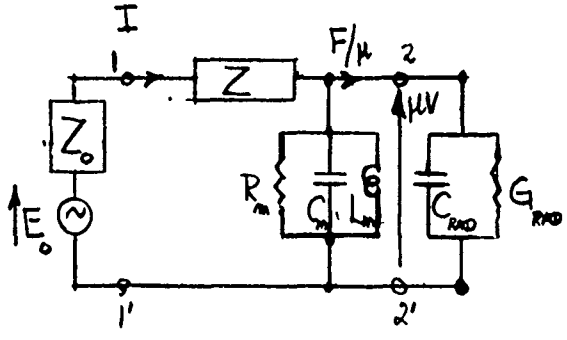


Fig. 2.14.5 — Equivalent circuit of a magnetostrictive sound radiator

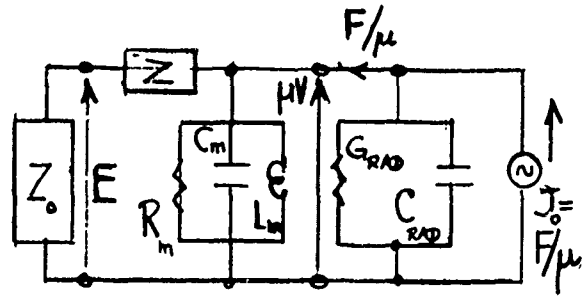


Fig. 2.14.6 — Equivalent circuit of a magnetostrictive sound receiver

We consider next the case where the core loss is a prominent feature of transduction. In Fig. 2.36.1 (see below) the core is represented by R_e', L_e' in shunt position. We may write it in complex form:

$$Z_e' = jX_e'e^{-j\theta} = R_e' + j\omega L_e' \tag{2.14.2}$$

Now let us consider this shunt impedance together with the *transformed* mechanical impedance $(=Z_m)$ and acoustic impedance Z_a. This is the impedance involved in electromechanical coupling,

$$Z_{\text{coupled}} = Z_e' + \frac{-T_{me}T_{em}}{\bar{Z}_m + \bar{Z}_a} = Z_e' + \frac{T^2}{\bar{Z}_m + \bar{Z}_a}. \quad T = \mu. \tag{2.14.3}$$

Since we take T to be lossy we can also write it in complex form, $Te^{-j\theta}$. We now wish to write mechanical elements as equivalent electrical elements. Calling these Z_M, Z_A, we can find explicit formulas for them by assuming $Z_M + Z_A$ are in parallel with Z_e'.

$$Z_{\text{coupled}} = \frac{1}{\frac{1}{Z_e'} + \frac{1}{Z_M + Z_A}} = \frac{Z_e'(Z_M + Z_A)}{Z_e' + Z_M + Z_A} = Z_e' - \frac{Z_e'^2}{Z_e' + Z_M + Z_A}$$

$$Z_{\text{coupled}} = Z_e' + \frac{|X_e'|^2 e^{-j2\theta}}{Z_e' + Z_M + Z_A}. \tag{2.14.4}$$

Equating corresponding terms in Eqs. 2.14.3 and 2.14.4 one obtains

$$\frac{|T|^2 e^{-j2\theta}}{Z_m + Z_A} = \frac{|X_e'|^2 e^{-j2\theta}}{Z_e' + Z_M + Z_A}$$

or

$$R_M = r_m \left|\frac{X_e'}{T}\right|^2 - R_e' \qquad R_A = \left|\frac{X_e'}{T}\right|^2 r_a$$

$$L_M = m\left|\frac{X_e'}{T}\right|^2 - L_e' \qquad X_A = \left|\frac{X_e'}{T}\right| x_a$$

$$C_M = \frac{1}{K}\left|\frac{T}{X_e'}\right|^2.$$

The turns-ratio corresponding to these equivalent circuit elements is

$$\phi^2 \equiv \left|\frac{X_e'}{T}\right|^2 = \left(j\frac{X_e'}{T}\right)\left(j\frac{X_e'}{T}\right)^*, \text{ or } \phi = +j\left|\frac{X_e'}{T}\right|, \ \mu = -j\left|\frac{T'}{X_e'}\right|.$$

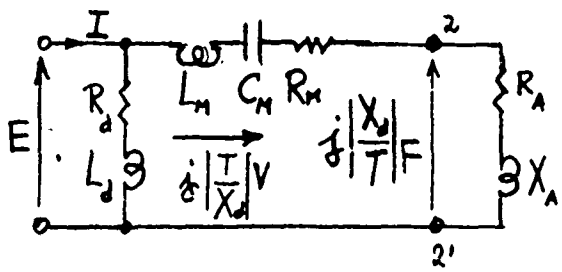
We use ϕ in transforming all mechanical parameters to the electrical side, and μ in transforming all electrical parameters to the mechanical side. Hence velocity and force are transformed according to the rules of Table 1.47.1:

$$i \rightarrow j\left|\frac{T}{X_e'}\right| \text{v} \qquad \text{v} \rightarrow -j\left|\frac{X_e'}{T}\right| i$$

$$e \rightarrow j\left|\frac{X_e'}{T}\right| F \qquad F \rightarrow -j\left|\frac{T}{X_e'}\right| e$$

The equivalent circuit of the magnetic field transducer (acting as a sound radiator) reduced to the electrical side is shown in Fig. 2.14.7. When acting as a sound receiver we transform all electrical parameters to the mechanical side and obtain Fig. 2.14.8.

To summarize: standard transducer circuits based on canonical models provide the transducer designer with easy means to make initial designs and estimates of performance. Other design aids are considered next.



14.7 — Equivalent circuit of a magnetostrictive transducer reduced to the electric side

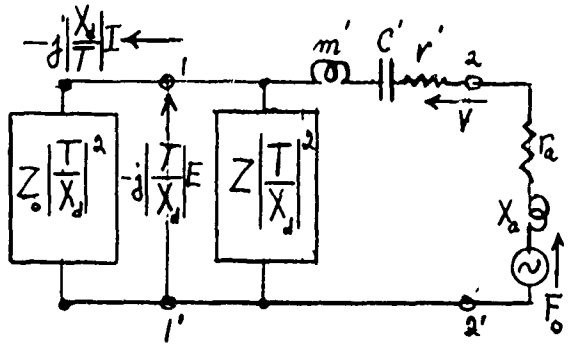


Fig. 2.14.8 — Equivalent circuit of a magnetostrictive sound receiver reduced to the mechanical side

2.15 INTRODUCTION TO DESIGN AIDS

In Chapter 1 the structure of an acoustic transducer was presented as a cascade of component parts whose interaction with themselves and with the environment was described by a set of matrix equations relating input and output through integral differential equation in space and time or through impedance. These relations were interpreted as electrical circuits with lumped parameters, or with distributed parameters, in conformity with historical precedent and convention. Newer methods of analysis such as signal flow graphs and bond graphs were shown also to be capable of displaying and analyzing the complex matrix equations of relations between components, sometimes with advantage.

A *rational* design of acoustic transducers is itself based on the formulation of dynamical description of elements in the matrices, including numerical values to be assigned to material parameters. In the course of the historical development of the art of transducer design, procedures have been developed to aid rational design, and models have been created to provide insight and guidance. The following Sections are a list of procedures, models and design aids which will prove helpful in constructing explicit forms of the elements of input/output matrices. The full appreciation of these Sections can be achieved by frequent reference back to the pertinent parts of Chapter 1.

Since the driver/load structure of a transducer is complicated it will be useful to define the most important impedances which describe the transfer of energy from input to load.

Transducer Impedances

A simple, but quite general, acoustic transducer structure is shown in Fig. 2.15.1. The representation of the transduction block as a *T*-network is discussed in Sect. 1.29 of Chapt. 1.

Each pair of terminals of this equivalent diagram is characterized by a voltage "across" and a current "through." The corresponding electrical impedances relating voltages and currents (not necessarily at the same terminals) are several in number. They constitute a group of important diagnostic and performance parameters. A list of terminal voltages, currents and impedances is presented in Table 2.15.1.

The words "available power" appearing in this table refer to a condition in which a source with impedance Z_s is connected to a load with conjugate impedance Z_L. For simplicity this is shown in Fig. 2.15.1 with the transductions block omitted. By definition "conjugate" means $R_{4-4'} = R_s$ and $X_{4-4'} = -X_s$. Since the load power is

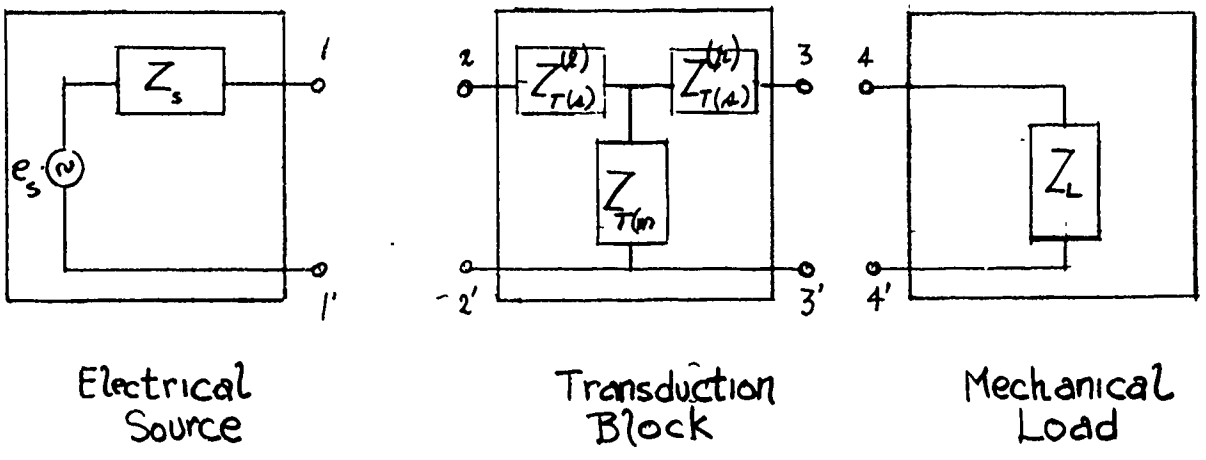
$$W_{4-4'} = e_s^2 \frac{R_{4-4'}}{|Z_s + Z_{4-4'}|^2}$$

it is seen by denominator that the load power is a maximum if $Z_{4-4'}$ is the conjugate of Z_s,

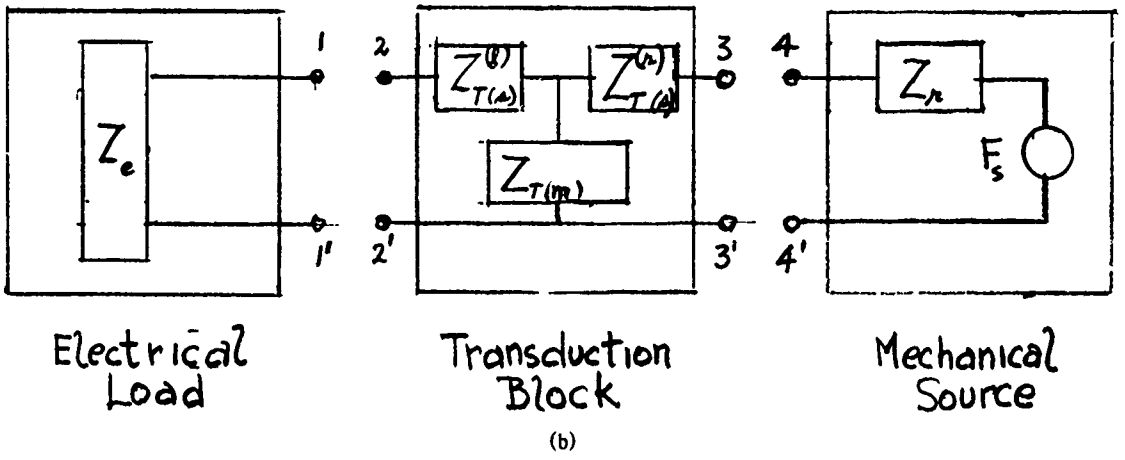
$$W_{4-4'} = \frac{e_s^2}{4R_{4-4'}}.$$

Similarly, the available power of a source is,

$$W_s = \frac{e_s^2}{4R_s}.$$



(a)



(b)

Fig. 2.15.1 — Generalized block diagram of acoustic transducers, (a) projector, (b) receiver

Table 2.15.1 — Voltages, Currents, Impedances of Acoustic Transducers [after [9]]

Symbol	Definition	Conditions of Measurement
e_s	source voltage	terminals 1-1 opend-circuited
I_s	source current	terminals 1-1 short-circuited
Z_s	source impedance at terminals 1-1	(1) no load at terminals 1-1 (2) $e_s = 0$
W_s	available power at terminals 1-1	impedance of load at source impedance
e_{2-2}	input voltage of T-network	both source and load are connected to the T-network
i_2	input current of T-network	both source and load are connected to the T-network
$W_{2-2'}$	input power to the T-network	both source and load are connected to T-network
$Z_{2-2'}$	input impedance loading forward into the T-network from terminals 2-2'	(a) load connected to T-network (b) terminals 2-2' open circuited
$e_{3-3'}$	output voltage at terminals 3-3'	(a) source connected to T-network (b) terminals 3-3' open-circuited
i_3	out current at terminals 3-3'	(a) source connected to T-network (b) terminals 3-3' short circuited
$Z_{3-3'}$	output impedance at terminals 3-3' looking toward the source	(a) terminals 3-3' open-circuited (b) source voltage $e_s = 0$
$W_{3-3'}$	output available power of transduction block at terminals 3-3'	source connected to T-network (load has conjugate impedance)
$(Z_{2-2'})_b$	blocked (input) impedance at terminals 2-2'	load terminals 3-3' are open-circuited
$(Z_{2-2'})_f$	free (input) impedance at terminals 2-2'	load terminals 3-3' are short-circuited
$(Z_{3-3'})_b$	reverse blocked output impedance looking toward source	terminals 1-1' open-circuited
$(Z_{3-3'})_f$	reverse free output impedance looking toward source	terminals 1-1' short-circuited
$Z_{T(m)}$	mutual impedance of the T-network,	$Z_{T(m)} = e_{2-2'}/i_3$ where $e_{2-2'}$ is open-circuited
Z_{tfr}	transfer impedance of transducer	(a) both source and load connected (b) $Z_{tfr} = e_s/i_f$
i_4	load current	source is connected to T-network
$Z_{4-4'}$	load impedance	terminals 4-4' open-circuited
$W_{4-4'}$	power delivered to the load at terminals 4-4'	source is connected to T-network

Relations Between Impedances

(1) In the *T*-network representation of the transduction block it is seen from the definitions given in Table 2.15.1 that

$$(Z_{2-2'})_b = Z_{T(s)}^{(l)} + Z_{T(m)}$$

$$(Z_{3-3'})_b = Z_{T(s)}^{(r)} + Z_{T(m)}.$$

(2) By inspection of Fig. 2.15.1 it can be deduced that

$$Z_{T(m)} = \{(Z_{3-3'})_b[(Z_{2-2'})_b - (Z_{2-2'})_f]\}^{1/2}$$

$$= \{(Z_{2-2'})_b[(Z_{3-3'})_b - (Z_{3-3'})_f]\}^{1/2}$$

$$= \{[(Z_{2-2'})_b - Z_{2-2'}][Z_{3-3'} + Z_{4-4'}]\}^{1/2}$$

$$= \{[(Z_{3-3'})_b - Z_{3-3'}][Z_s + (Z_{2-2'})_b]\}^{1/2}.$$

(3) By definition of the transfer impedance

$$Z_{tfr} = \frac{e_s}{i_4} = \frac{|Z_s + Z_{2-2'}||(Z_{3-3'})_b + Z_{4-4'}|}{Z_{T(m)}}$$

$$= |Z_{3-3'} + Z_{4-4'}| \left\{ \frac{|Z_s + (Z_{2-2'})_b|}{|(Z_{3-3'})_b - Z_{3-3'}|} \right\}^{1/2}.$$

(4) Using simple algebra one finds

$$Z_{2-2'} = (Z_{2-2'})_b - \frac{Z_{T(m)}^2}{(Z_{3-3'})_b + Z_{4-4'}}$$

$$Z_{3-3'} = (Z_{3-3'})_b - \frac{Z_{T(m)}^2}{(Z_{2-2'})_b + Z_s}.$$

(5) Knowing $Z_{T(m)}$, $Z_{2-2'}$, and $Z_{3-3'}$ one can deduce source and load impedances,

$$Z_s = \frac{Z_{T(m)}^2}{(Z_{3-3'})_b - Z_{3-3'}} - (Z_{2-2'})_b$$

$$Z_{4-4'} = \frac{Z_{T(m)}^2}{(Z_{2-2'})_b - (Z_{2-2'})} - (Z_{3-3'})_b.$$

Other impedance relations can easily be inferred by use of this table in conjunction with Fig. 2.15.1.

Transmission Losses

The two output powers, $W_s (= W_{1-1'})$ and $W_{3-3'}$ of Fig. 2.15.1 are regarded as *available powers,* meaning the impedance of the block following each of them is the conjugate impedance. The two input powers, $W_{2-2'}$ and W_{4-4} are regarded as powers derived to nonconjugate impedances.

Because of internal resistivity and impedance mismatch at junctions between components, the power transfer from terminal to terminal is accomplished by losses. Such losses can be expressed as ratios of powers between selected terminals. Table 2.15.2 contains a list of six possible ratios of powers formulated in terms of impedance ratios derives from the definition given in Table 2.15.1.

Table 2.15.2 — Transmission Power Ratios [after [9]]

Power Ratio	Impedance Formulation	Description as $10 \log_{10} \times$ Ratio
$\frac{W_s}{W_{2-2'}}$	$\frac{Z_s + Z_{2-2'}}{4R_s R_{2-2'}}$	dB power loss between electrical source output and transducer input caused by mismatch
$\frac{W_{2-2'}}{W_{3-3'}}$	$\frac{4R_{2-2'}R_{3-3'}\lvert Z_s + (Z_{2-2})_b\rvert^2}{\lvert Z_s + Z_{2-2'}\rvert^2 \lvert Z_{3-3'} + Z_{4-4'}\rvert^2}$	dB power loss between input and output terminals of the transducer due to internal resistance
$\frac{W_{3-3'}}{W_{4-4'}}$	$\frac{\lvert Z_{3-3'} + Z_{4-4'}\rvert^2}{4R_{3-3'}R_{4-4'}}$	dB power loss between transducer and load due to mismatch
$\frac{W_s}{W_{3-3'}}$	$\frac{R_{3-3'}}{R_s} \frac{\lvert Z_s + (Z_{2-2'})_b\rvert^2}{\lvert Z_{t(m)}\rvert^2}$	dB available power loss from electrical power output and transducer output
$\frac{W_s}{W_{4-4'}}$	$\frac{\lvert Z_{3-3'} + Z_{4-4'}\rvert^2 \lvert Z_s + (Z_{2-2})_b\rvert^2}{4R_s R_{4-4} \lvert Z_{T(m)}\rvert^2}$	dB power loss between electrical source output and load
$\frac{W_{2-2'}}{W_{4-4'}}$	$\frac{R_{2-2'}}{R_{4-4'}} \frac{\lvert (Z_{3-3'})_b + Z_{4-4'}\rvert^2}{\lvert Z_{T(m)}\rvert^2}$	dB power loss between input to transducer and input to the load

The subject of design aids is continued next with a discussion of impedance and admittance diagrams.

2.16 FREQUENCY OF MAXIMUM MOTIONAL IMPEDANCE AND FREQUENCY OF MAXIMUM MOTIONAL ADMITTANCE

In Eqs. 2.8.10, 2.8.11 the symbol Z_m must be properly interpreted to contain electrical terms coupled into the mechanical mesh. We consider first the moving armature transducer which is an example of magnetic coupling shown in Fig. 2.36.1 in which the coupling terms are $Z_e' = R_e' + j\omega L_e'$. Upon transferring these to the mechanical mesh according to Table 1.47.1 one sketches the equivalent circuit to be that of Fig. 2.16.1. Here, Z_m'' is the intrinsic (= uncoupled) mechanical impedance, and $Z_m' = T^2/Z_e'$ is the equivalent mechanical impedance coupled from the electrical mesh into the mechanical mesh. The frequency ω_A at which the motional impedance is a maximum is then

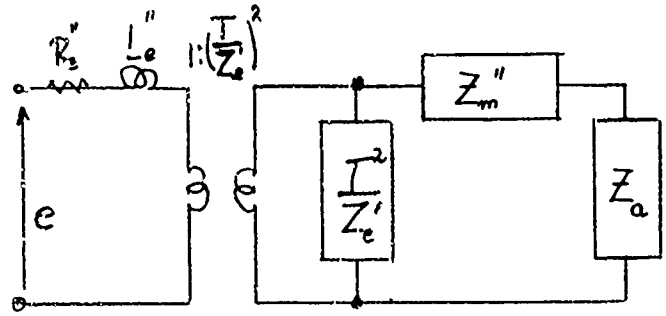


Fig. 2.16.1 — Equivalent circuit of the moving armature transducer

$$\mathrm{Im}\left\{\frac{T^2}{Z_e'} + Z_m'' + Z_a\right\} = 0 \quad [\text{at } \omega_A\ (\simeq \omega_R)]$$

in which

$$\frac{T^2}{Z_e'} = \frac{1}{j\omega}\,\frac{\phi^2 x}{(d_0 + \xi)\mu_0 S_g} \quad \left[\text{units: } \frac{Ns}{m}\right].$$

From Eq. 2.8.3 this is the condition for maximum velocity at constant current drive. Similarly the frequency at which the motional admittance is a maximum corresponds to the condition,

$$\mathrm{Im}\left\{\frac{T^2}{Z_e'} + Z_m'' + Z_a\right\} = \mathrm{Im}\left\{-\frac{A^2 e^{-j[2\beta - \epsilon]}}{|Z_e|}\right\} \quad [\text{at } \omega_B (= \omega_Y)].$$

From Eq. 2.8.4 this is the condition for maximum velocity at constant voltage drive.

The case of electrostatic coupling in the form of an electrostatic transducer is illustrated by Fig. 2.39.1. Here the symbol Z_m must be interpreted to contain both the coupled compliance C_n and the self compliance C_m,

$$Z_m = r_m + j\omega m + \frac{1}{j\omega C_m^*},\ C_m^* = \frac{C_m}{1 - k^2}.$$

The transferred impedance is obtained from Eq. 2.39.2,

$$-\frac{T^2}{Z_e'} = \frac{-C_0}{j\omega\left(\dfrac{\epsilon_0 S}{q_0}\right)^2}.$$

2.17 GEOMETRICAL CONSIDERATIONS OF MOTIONAL IMPEDANCE AND MOTIONAL ADMITTANCE CIRCLES

A. Case of Magnetic Field Coupling

The motional impedance, Eq. 2.8.5, features the reciprocal of the mechanical impedance (self plus loading impedance), $Z_M = Z_m + Z_a = R_m + jX_M(\omega)$. Since a plot of Z_M, for R_M constant, versus ω is a straight line, a plot of Z_M^{-1} is a circle. Hence a plot of the motional impedance is a circle tilted down from the horizontal by the angle of $-T_{me}T_{em}$, which is 2β. The origin O′ of Z_{MOT} is at the blocked

electrical impedance $R_e + jX_e$. Figure 2.17.1 shows the geometry of this circle. Point A obtained by drawing a diameter D from O' inclined at angle 2β is the resonance frequency f_R, defined as the frequency at which the motional impedance is a maximum. Point B, obtained by drawing a chord O'B at angle β with the horizontal, is the point of maximum resistance,

$$R_{MAX} = R_e + D \cos^2 \beta. \tag{2.17.1}$$

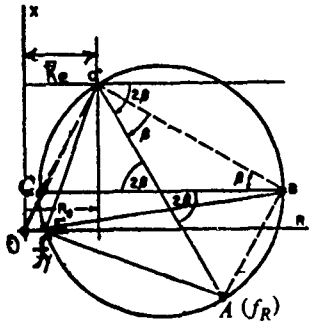


Fig. 2.17.1 – Geometric relations in the motional-impedance circle for the case of magnetic coupling

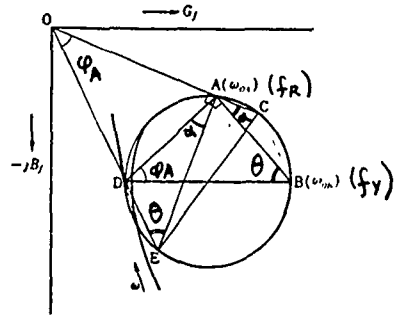


Fig. 2.17.2 – Geometric relations of a motional admittance circle anchored to the clar,ped admittance at D, for the case of magnetic coupling

Point C, the terminus of the diameter through B, locates the minimum resistance,

$$R_{\min} = R_e - D \sin^2 \beta. \tag{2.17.2}$$

Point E, which is the intersection of line OB with the circle, locates the frequency f_Y at which the motional admittance is a maximum. A proof of this construction is discussed below. In the case of magnetic coupling (shown in Fig. 2.17.1) one has $f_Y > f_R$. Hence, the effective coupling coefficient is;

$$k^2_{\text{eff}} = \frac{f_Y^2 - f_R^2}{f_Y^2}. \tag{2.17.3}$$

The geometric basis for finding f_R (= A-type resonance) given f_Y (= B-type resonance) is shown in Fig. 2.17.2 for the case of magnetic coupling. The following steps explain the rationale and illustrate the procedure

1. assume radiation loading is purely real.

2. locate point A (as defined above) on the circle at some arbitrary point ($\omega_A < \omega_B$), later to be determined with certainty by a geometric construction.

3. line OD is the clamped admittance and line OA is the admittance at resonance f_R. The angle between them is ϕ_A.

4. line DB is the motional admittance at resonance f_Y (= ω_B). Line DA is the motional admittance at resonance f_R (=ω_a). The angle between them is also ϕ_A.

5. lines BA and BD subtend chord DA at angle θ. lines ED and EA also subtend this chord. Therefore angle DEA equals θ.

6. Triangle OEA is congruent to triangle DBA. Therefore angle OAE is a right angle.

7. Draw diameter EC. Triangle O″ED = triangle O″BC. Therefore chord CB equals chord DE.

8. lines AC and AB subtend chord CB at angle α. lines AD, AE subtend chord DE. Since DE equals CB, the angle DAE = α. Therefore line OAC is a straight line.

Hence, to find point A, draw line ODE, connect E to C through a diameter, then draw straight line OC. The intersection A locates point f_R given point f_Y.

The construction becomes approximate when the radiation impedance is not purely real, and when the admittance circle is small.

The procedure for finding point f_Y on the impedance circle given point f_R follows similar lines, Fig. 2.17.3.

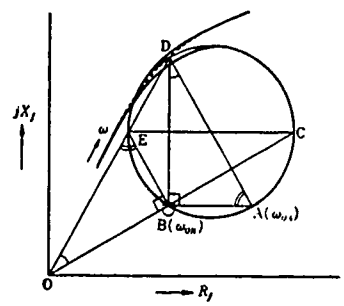


Fig. 2.17.3 — Geometric construction for finding f_y ($=\omega_{0B}$) given f_R ($=\omega_{0A}$) for the case of magnetic coupling

1. draw line OD intersecting the circle at E.

2. draw diameter EC.

3. draw OC, intersecting circle at point B where $f = f_y = \omega_{OB}$.

B. Case of Electric Field Coupling Transducers

These are analyzed by use of motional admittance diagrams with a simple transfer of symbols from the case of magnetic field transducers. Thus the parameters and constructions of electric field transducers can be said to be governed by rules very analogous to magnetic field transducers provided a substitution of notation is used. Table 2.17.1 is a list of changes needed.

Table 2.17.1 — Interchange of Notation Which Allows Electric Field and Magnetic Field Transducers to be Governed by Analogous Rules in Geometrical Relations of Impedance and Admittance Charts

Magnetic Field	Electric Field
current I	voltage V
electric impedance Z	admittance Y
electric resistance R	conductance G
electric reactance X	suceptance B
magnetization M	electric polarization P
magnetic field H	electric field intensity E
magnetic permeability μ	electric permittivity ϵ
inductance L	capacitance C

With this table in mind we examine the admittance diagram of an electric field transducer (in this case, a piezoelectric resonator), Fig. 2.17.4. The frequency f_s corresponds to the condition of maximum motional admittance (that is, maximum electric current for constant voltage drive): f_p corresponds to the condition of parallel resonance, or minimum current for constant voltage drive. The frequencies f_r, f_a mark the transitions from capacitive to inductive reactance.

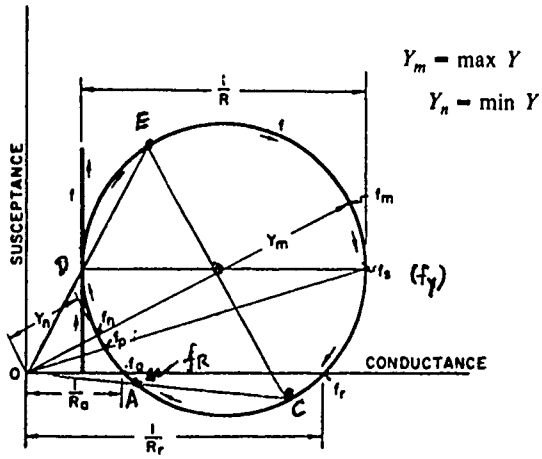


Fig. 2.17.4 — Vector admittance diagram of a piezoelectric resonator

If we use the construction procedure outlined above we can find the *approximate* location of the frequency of maximum motional impedance f_R. We draw lines ODE, EC and CO. The intersection A locates f_R. It is seen to fall close to the antiresonant frequency f_a (where the electric current is a minimum).

In practice, measurements on ordinary loaded piezoelectric resonators show f_m, f_s and f_r differ very little from each other. Similarly, f_m, f_p, f_a, f_R are all nearly the same point.

We continue the subject of design aids with a discussion of turns-ratio.

2.18 TURNS-RATIO IN EQUIVALENT CIRCUITS OF PIEZOELECTRIC TRANSDUCERS

In this application one defines the turns-ratio N as the magnitude of the ratio of force to voltage under static clamped conditions. Thus for each of the four sets Eq. 2.12.1, assumed to be reduced to single components of dependent and independent variables, one sets the strain component to zero. Noting that $E = V/t$ and $T = F/A$, and eliminating D as an independent variable, one can solve for the ratio $N = F/V$, and thereby obtain the turns-ratio. A possible negative sign is disregarded since we are considering here the transduction to be described as an ideal transformer with transformation $1{:}N^2$.

As an example we consider the pair,

$$S_1 = s_{11}^E \; T_1 + d_{31} \; E_3 \tag{2.18.1}$$

$$D_3 = d_{31} \; T_1 + \epsilon_{33}^T \; E_3 \tag{2.18.2}$$

Since T and E are already independent variables only one equation (namely 2.18.1) is needed. Then at constant (= zero) strain:,

$$0 = s_{11}^E \frac{F}{A} + d_{31} \frac{V}{t}, \; A = wt$$

leads to the ratio,

$$\frac{V}{t} = -\frac{s_{11}^E \; F}{d_{31} \; A}$$

or

$$N = \frac{wd_{31}}{s_{11}^E} \qquad (\text{units:} \frac{N}{V}). \tag{2.18.3}$$

A second example involves the pair

$$T_5 = C_{55}^D \; S_5 - h_{15} \; D_1$$

$$E_1 = h_{15} S_5 + \beta_{11}^S \; D_1 \tag{2.18.4}$$

Then,

$$T_5 = - \; h_{15} \left[\frac{E_1}{\beta_{11}^S} \right].$$

For $A = wl$,

$$N = \frac{wl}{t\beta_{11}^S} \; h_{15} \qquad (\text{units:} N/V). \tag{2.18.5}$$

In view of the definitions:

$$d_{31} = k_{31} \sqrt{s_{11}^E \; \epsilon_{33}^T} \quad ; h_{15} = k_{15} \sqrt{\beta_{11}^S C_{55}^D}$$

both Eq. 2.18.3 and 2.18.5 can be interpreted in terms of material coupling coefficients k_{31} and k_{35}. It is thus seen that the turns-ratio in every case can be written in terms of the coefficient of electromechanical coupling.

2.19 RESONANT FREQUENCIES AT CONSTANT CURRENT AND CONSTANT VOLTAGE DRIVE

This topic, discussed earlier in Sect. 2.10, is further developed here in connection with impedance and admittance plots.

We return to Eq. 2.10.15 and write the electrical impedance for constant-H drive:

$$Z_e = Z_e + Z_{MOT}; \; Z_{MOT} = \frac{Z_{em}^2}{Z_m} = -\frac{Z_{em}^2}{r_m + jX_m}$$

Let Z_m include a load impedance $r_L + X_L$. It is seen immediately that Z_{MOT} is a maximum at frequency $\omega = \omega_r$ such that,

$$X_m = \omega_1 M - \frac{1}{\omega_1 C_m} + X_L(\omega_1) = 0, \tag{2.19.1}$$

that is

$$\omega = 2\pi f_r(mech)$$

This condition, shown in Fig. 1.41.1b, is one where the total electrical impedance is a maximum.

We now invert Z_{ee} to obtain the total admittance, also at constant -H drive,

$$Y_{ee} = Y_e + Y_{MOT}$$

$$Y_{MOT} = \frac{-Z_{em}^2/Z_e}{r_m + jx_m + (Z_{em}^2/Z_e)}. \tag{2.19.2}$$

This is a maximum at a frequency ω_2 such that,

$$X_m(\omega_2) = \text{Imaginery part of}(-Z_{em}^2/Z_e).$$

Since

$$\frac{Z_{em}^2}{Z_e} = \frac{2\pi}{a^l}\,\frac{N^2A^2h_{11}^2}{(\gamma_{11}^2)^2} \times \frac{l\gamma_{11}^S}{j\omega N^2A}.$$

$$\frac{Z_{em}^2}{Z_e} = \frac{2\pi}{a}\,\frac{Ah_{11}^2}{j\omega}\,\frac{\mathrm{Re}(\gamma_{11}^S) - j\mathrm{Im}(\gamma_{11}^S)}{(Re\gamma_{11}^S)^2 + \mathrm{Im}(\gamma_{11}^S)^2}.$$

This leads to the condition:

$$\omega_2 M - \frac{1}{W_2C_m} + X_L(\omega_2) = \frac{2\pi A}{a}\,\frac{h_{11}^2}{W_2}\,\frac{\mathrm{Re}\gamma_{11}^S}{(Re\gamma_{11}^S)^2 + (\mathrm{Im}\gamma_{11}^S)^2}. \tag{2.19.3}$$

It is to be noted that the imaginary part of $-Z_{em}^2/Z_e$ is a positive number. Hence the net mechanical impedance at ω_2 is positive. This means that in a plot of X_{mech} *vs* ω for a magnetic field transducer the frequency ω_2 will be greater than the frequency ω_1. Thus the frequency separation $\omega_2 - \omega_1$ depends specifically on the right hand side of Eq. 2.19.3, that is, on Z_{em}^2/Z_e. This latter quantity is proportional to h_{11}^2, hence proportional to the coefficient of electromechanical coupling. One then *defines* (as earlier) the,

$$k_{eff}^2 = 1 - \frac{f_1^2}{f_2^2}$$

In practice f_2 is measured from the admittance plot and f_1 from the impedance. The above formula then gives k_{eff}^2. Alternatively, one measures on the impedance plot of Fig. 1.41.1b, the quantities $f_{r(mech)}$ at maximum impedance and $f_{(damped)}$ at minimum impedance. Then one set f (damped $= f_2$ and $f_{r(mech)} = f_1$ by observing the coincidences between Fig. 1.41.1d and 1.41.1b. This latter procedure for funding k_{eff} is called the *resonance method* and is often used.

2.20 QUARTER-WAVE AND HALF-WAVE LONGITUDINAL VIBRATORS

Longitudinal vibrators under forced harmonic drive are often used at frequencies of mechanical resonance. The number of such resonances in distributed systems is infinite. Two cases of resonant operation of widespread applications are presented here.

Case I. Quarter-wave Resonance

Assume a bar, mass M, length l, is rigidly fixed into a wall at end b and is force driven into *quarter-wave* resonance. This means driving it at a frequency $\omega_0(=\pi c(2n-1)/2l,\ n=1, 2\ldots)$ at which the length of the bar is a multiple $(2n-1)$, $n=1, 2\ldots$ of a fourth of a wavelength, $\lambda/4$. Effectively the wall represents infinite mass (namely the earth) and its velocity v_b is always zero. At each length $l=\lambda/4$, $l=3\lambda/4$, $l=5\lambda/4\ldots$ the terminal velocity v_a is a maximum.

Thus, at quarter-wave resonance, for every pair of consecutive masses the one at v_b must be short-circuited. Then the mass m_{a_1} is in parallel (= has the same velocity difference) with the spring n_1, the mass ma_2, is in parallel with n_2, etc. The *VF* mechanical circuit then appears as Fig. 2.20.1 with short circuits introduced:

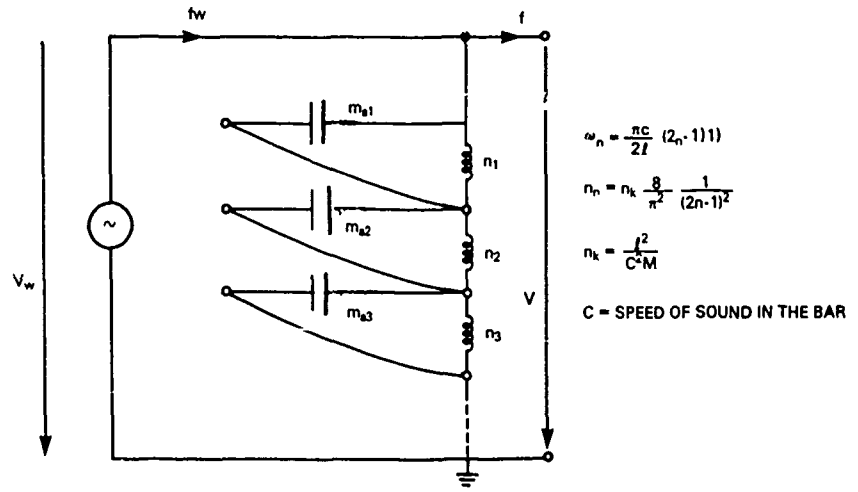


Fig. 2.20.1 — Lumped parameter approximation to a quarter-wave longitudinal vibrator in VF form

The meaning of this figure is: at the first quarter wave resonance $l=\lambda/4$, $\omega_1=\pi c/2l$, $m_1=M/2$, $n_1=n_k 8/\pi^2$.* *Where $n_k=n_l/1-k^2$, n_l being the low frequency compliance of the bar, and k^2 a coefficient of electromechanical coupling when such coupling exists. All remaining masses and springs are short circuited. Similarly at the second quarter-wave resonance, $l=3\lambda/4$, $\omega_2=3\pi c/2l$, $n_2=8n_k/9\pi^2$, and again all other masses and springs are short circuited, etc.

Case II. Half-wave Resonance

Let a bar be driven at a frequency $\omega_n=\pi c/l_{eff}$, where l_{eff} is the fraction $1/(2n-1)$ of the actual length of the bar. Thus at $\omega_1=\pi cl$ the length is $\pi c/\omega_1=\pi/(2\pi/\lambda)=\lambda/2_g$ i.e., it is exactly one half-wavelength long. The equivalent circuits for equal loads at a, b is the same as two quarter-wave resonators Fig. 1.22.5. It is customary however to design half-wave resonators to be free at one end and loaded at the other end. Assume, for example, end a of Fig. 1.22.5 is unloaded, so that $f_a\equiv 0$. The output terminals a, c are then opened and Y_2 is directly connected to terminal C, Fig. 2.20.2.

The mechanical admittances Y_1, Y_2 are the same as Fig. 1.22.5. Note that Y_2 belonging to the unloaded part of the resonator now appears in series position. Since velocity v_w is across the ends a and b it is desirable to derive a circuit for the loaded end b alone. This is accomplished by introducing a velocity transformer which steps the velocity v_w down by 1/2 to give v_w'. Also the π-network (right hand side of Fig. 2.20.2) being such that the series branch is equal to one parallel branch is reducible to a half-tee by standard transformation. Thus the equivalent circuit becomes Fig. 2.20.3.

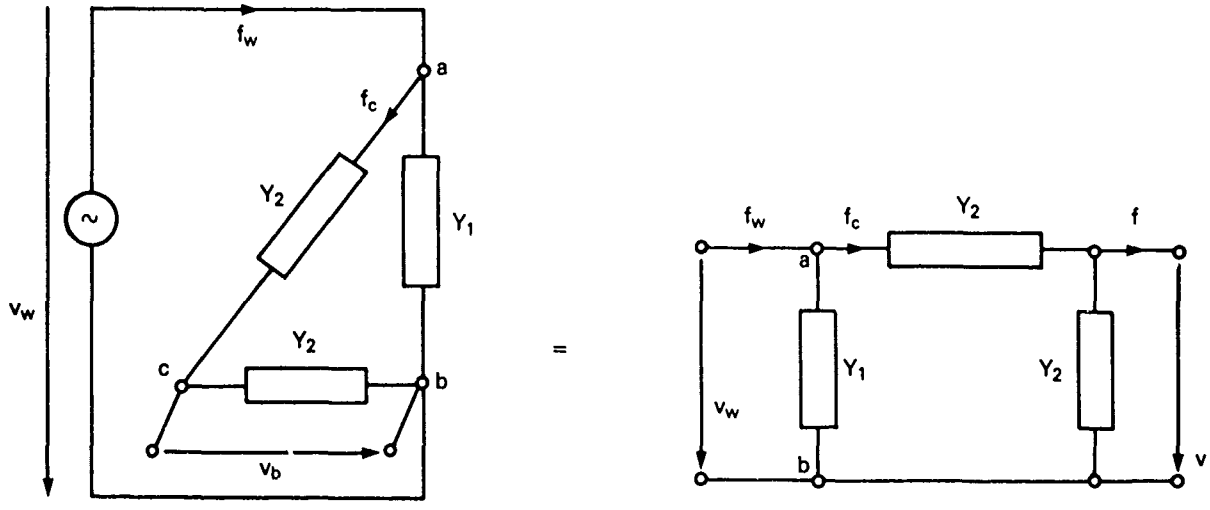


Fig. 2.20.2 — A VF mechanical equivalent circuit of a one-side-loaded half wave longitudinal vibrator. Y_1, Y_2 are defined in Fig. 1.22.5.

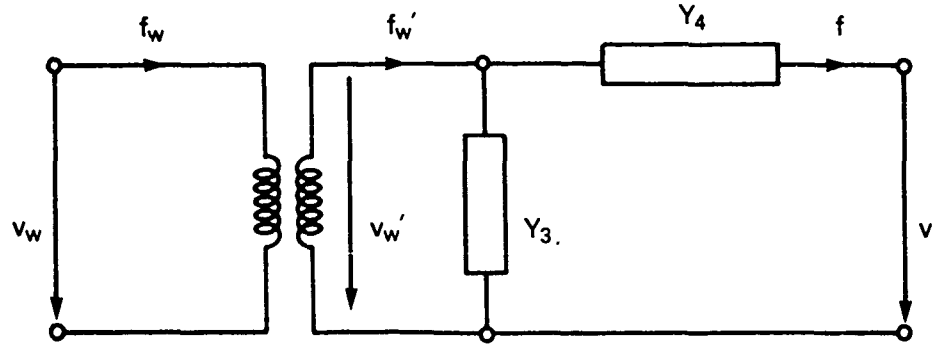
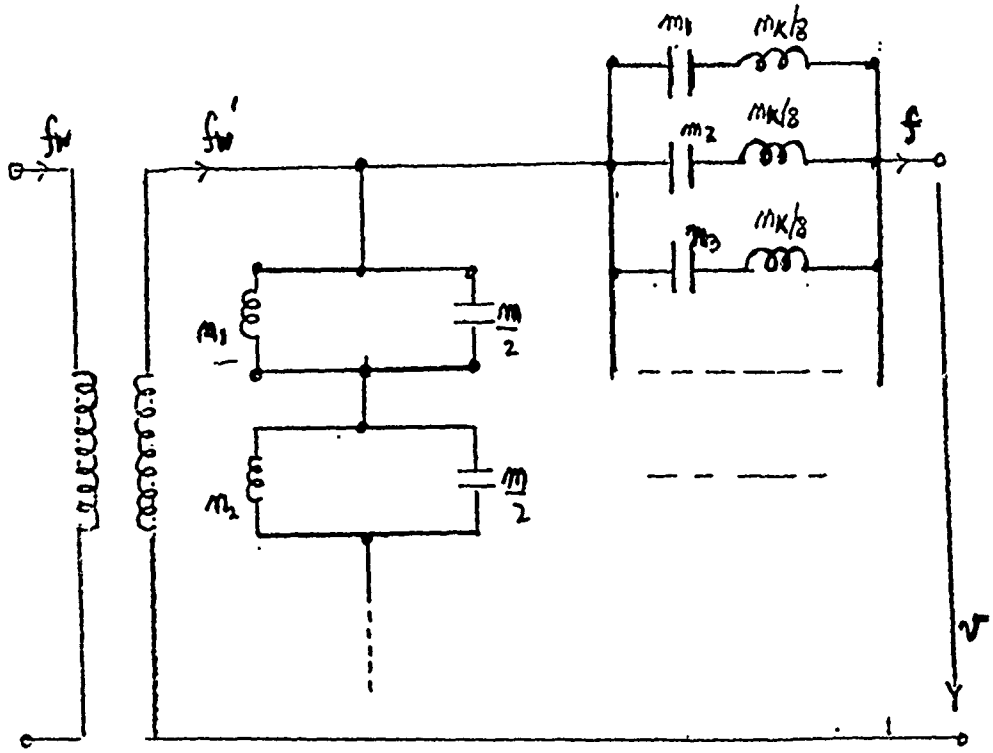


Fig. 2.20.3 — A VF mechanical equivalent circuit of a half wave longitudinal vibrator with one end loaded and the other end free

At very low frequencies $\tan \omega l/2c \rightarrow \omega l/2c$. Hence the Y_3 branch (which represents the free half of the resonator) can be approximated by a series grouping of parallel LC circuits designed to represent velocity resonances, similar to Fig. 2.20.1. However the compliances n_n will be different (see Fig. 2.20.4 below). Similarly the series branch Y_4, which represents the loaded half of the resonator, can be approximated by a parallel echelon of series connected LC circuits calculated to represent force resonances. The approximate equivalent circuit in the *i-f* analogy is Fig. 2.20.4.

2.21 THE MASON EQUIVALENT CIRCUIT OF THE LONGITUDINAL TRANSDUCER

This circuit, discussed earlier in Sect. 2.13 as a design aid, is analyzed here in greater detail. A bar of rectangular cross-section, length L_y, width L_w, and thickness L_t made of piezoactive material is electroded on the faces P, Q normal to the 3-direction, Fig. 2.21.1. It is loaded on both faces in the 1-direction. Upon being excited by a voltage $\bar{E}(y, t) = \bar{E}(y) \times e^{j\omega t} = \bar{E}_0 e^{-j\omega t}$, it vibrates in a complex pattern of modes. In order to grasp the fundamentals of the analysis it will be useful to consider only motion in the 1-direction. The analysis which follows will lead directly to the Mason equivalent circuit [2].



$$m_K = \frac{l^2}{C^2 M}$$

$$\dot{M} = l w \, dp$$

$$\omega_n = \frac{\pi c}{l}(2n-1)$$

$$m_n = \frac{2}{\pi^2} m_K \frac{1}{(2n-1)^2}$$

$$m_n = \frac{8}{\pi^2} M \frac{1}{(2n-1)^2}$$

Fig. 2.20.4 — An approximation to Fig. 2.20.3

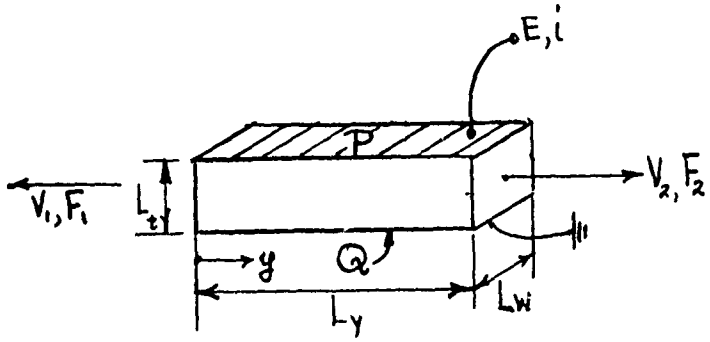


Fig. 2.21.1 — A longitudinal vibrator

I. *The Constitutive Equations of the Piezoelectric Material*

Because of its widespread use the material of the bar is assumed to be polarized electrostrictive ceramic, U.S. Navy Type I or Type III (formerly designated as PZT-4 or PZT-8). The piezoactivity of this material for the case of dc polarization in the 3-direction and motion only in the 1-direction is described by constitutive equations,

$$T_1 = h_{31}D_3 - C_{11}^D S_1 \tag{2.21.1a}$$

$$E_3 = \beta_{33}^S D_3 - h_{31}' S_1 \tag{2.21.1b}$$

T_1 = mechanical stress on cross section $L_w L_t$ at any position y (Nm^{-2})
h_{31} = mechanical stress-electric displacement piezo constant (NC^{-1})
C_{11}^D = mechanical stress-strain (stiffness) coefficient measured at zero electric displacement (= circuit) (Nm^{-2})
S_1 = longitudinal strain (mm^{-1})
β_{33}^S = inverse electrical permittivity (VmC^{-1})
h_{31} = (same as h_{31}, but with units Vm^{-1})
D_3 = electric displacement (Cm^{-2}) .

Solving (1b) for D_3,

$$D_3 = \frac{E_3 + h_{31}S_1}{\beta_{33}^S} \tag{2.21.1c}$$

and substituting the result in (1a) leads to the relation,

$$T_1 = \frac{E_3 h_{31}}{\beta_{33}^S} - [1 - k^2]C_{11}^D S_1 \tag{2.21.2}$$

$$k^2 = \frac{h_{31}h_{31}'}{\beta_{33}^S C_{11}^D}. \tag{2.21.3}$$

The symbol k^2 is the coefficient squared of electromechanical coupling. Its appearance in (2) shows that the stiffness coefficient C_{11}^D is reduced by the piezoactivity of the material. The reduced coefficient may be written as an open circuit parameter (that is, $E = 0$),

$$C_{11}^E = (1 - k^2)C_{11}^D \tag{2.21.4}$$

Eq. (2) is a statement that the force F_c at any cross section is the sum of an elastic reaction F_M and an applied electrically induced force F_E,

$$F_c = F_M - F_E \tag{2.21.5a}$$

$$F_E = \frac{L_w L_t h_{31} E_3}{\beta_{33}^S} \qquad \text{(units: N)} \tag{2.21.5b}$$

$$F_M = L_w L_t C_{11}^E \frac{\partial \xi}{\partial y} \qquad (\textit{units}: \text{N}). \tag{2.21.5c}$$

II. *One Dimensional Equation of Motion*

The longitudinal vibrator is first modeled as an infinitely long piezoactive rod along which is propagating an elastic stress. The force accelerating a unit volume of material at any cross section in the 1-direction giving it a displacement $\xi\ (y,\ t)$ (units: m) is given by the dynamical equation,

$$C_{11}^E \frac{\partial^2 \xi}{\partial y^2} = \rho \frac{\partial^2 \xi}{\partial t^2} \qquad \text{(units of each term: Nm}^{-3}\text{)}. \tag{2.21.6}$$

Since only the steady state is considered, $\xi(y,\ t) = \xi(y)e^{-i\omega t}$, so that (6) reduces to,

$$\frac{\partial^2 \xi}{\partial y^2} + k^2 \xi = 0, \tag{2.21.7a}$$

$$k^2 = \frac{\omega^2}{v_c^2}, \qquad k = \frac{2\pi}{\lambda} \tag{2.21.7b}$$

$$v_c^2 = \frac{C_{11}^E}{\rho}. \tag{2.21.7c}$$

Here v_c (units: m/s) is the speed of sound in the elastic rod, and k is the wavenumber at frequency ω.

The solution of (7a) may be couched in the form

$$\xi(y) = G \cos ky + H \sin ky \tag{2.21.8}$$

in which G, H are to be determined by application of boundary conditions. To this purpose the rod is made finite (length L_y) and two boundary conditions are imposed at the left end, namely the force applied is F_1, and the velocity applied is ξ_1.

F_1 is considered first. The mechanical force at any cross section is .Eq (2.21.5c)

$$F_M = L_w L_t C_{11}^E [-Gk \sin ky + Hk \cos ky] \tag{2.21.5d}$$

At $y = 0$, $F_M = F_1$. Hence,

$$H = \frac{F_1}{\omega L_w L_t \rho v_c} \tag{2.21.8a}$$

Next $\dot{\xi}_1$ is considered. Then $y = 0$, $\dot{\xi} = \dot{\xi}_1 = -i\omega\xi_1 = G$. Hence,

$$G = \frac{\dot{\xi}_1}{-i\omega}. \tag{2.21.8b}$$

Thus the mechanical displacement due to the *mechanical forces* (action and reaction) only is,

$$\xi(y,\ t) = \left\{ \frac{\dot{\xi}_1}{-i\omega} \cos ky + \frac{F_1}{\omega L_w L_t \rho v_c} \sin ky \right\} e^{-i\omega t}. \tag{2.21.8c}$$

The total force at any cross section also includes the mechanical force due to the applied electric field. The mechanical velocity at any cross section is therefore,

$$\dot{\xi}(y,\ t) = \left\{ \dot{\xi}_1 \cos ky - i \frac{\left[F_1 + \dfrac{L_w L_t h_{31} E_3}{\beta_{33}^S} \right]}{L_w L_t \rho v_c} \sin ky \right\} e^{-i\omega t}. \tag{2.21.9}$$

This is the velocity equation. In a similar way the force equation can be constructed. Substituting (2.21.8a, 8b) into (2.21.5d) and simplifying terms lead to the explicit form,

$$F_M = F_1 \cos ky - i\dot{\xi}_1 L_w L_t v_c \rho \sin ky. \tag{2.21.10a}$$

Here the first term represents an applied force while the second term is a reactive force. Since the mechanical force due to the applied field is an *applied* force, it can be grouped with F_1. Thus the total force at any cross section is

$$F + \frac{L_w L_t h_{31} E_3}{\beta_{33}^S} = \left(F_1 + \frac{L_w L_t h_{31} E_3}{\beta_{33}^S} \right) \cos ky - i\dot{\xi}_1 L_w L_t \rho v_c \sin ky. \tag{2.21.10b}$$

III. *The Electrical Equation*

Equation (2.21.1c) for the electric displacement with help of Eq. (2.21.8) may now be written,

$$D_3(y,\ t) = \left\{ \frac{E_3}{\beta_{33}^S} + \frac{h_{31}}{\beta_{33}^S} [-Gk \sin ky + Hk \cos ky] \right\} e^{-i\omega t} \tag{2.21.11a}$$

Since the electric current is

$$i = \frac{d}{dt} \int_0^{L_y} D_3 L_w dy \qquad \text{(units: } Cs^{-1} = A\text{)} \tag{2.21.11b}$$

the required integration along y leads to

$$i = \frac{-i\omega L_w L_y E_3}{\beta_{33}^S} + \frac{n_{31} L_w}{\beta_{33}^S} [\dot{\xi}_2 - \dot{\xi}_1]. \tag{2.21.11c}$$

IV. *The Electromechanical Transformer Ratio*

Examination of Eq. (2.21.11c) shows that electric current and mechanical velocity are related through a constant ϕ,

$$i = \phi \dot{\xi} \tag{2.21.12a}$$

$$\phi = \frac{L_w h_{31}}{\beta_{33}^S} \qquad \text{(units: N/V)}. \tag{2.21.12b}$$

Similarly, examination of Eq. (2.21.10b) shows that mechanical force and electrical voltage are related,

$$F = \phi E \tag{2.21.12c}$$

$$E = E_3 L_t \qquad \text{(units: V)}. \tag{2.21.12d}$$

Since (12a) and (12c) combined give,

$$\frac{F}{\dot{\xi}} = \phi_2 \frac{E}{i}$$

it is concluded that in the conversion of electrical power to mechanical power the conversion may be described as that of a transformer with ratio 1 to ϕ^2:

$$\phi^2 Z_E = Z_M. \tag{2.21.13}$$

This conclusion is based on the analogy $F \rightarrow E$, $\dot{\xi} \rightarrow i$.

V. *The Equivalent Circuit*

The longitudinal vibrator is modeled as a short transmission line. By analogy with the theory of electric transmission lines the assumption is first made that the longitudinal vibrator has distributed mass, stiffness and mechanical resistance. The analysis then follows electric circuit theory closely. These are the steps.

Let R, L, C be the electrical resistance, inductance and capacitance *per unit length* of an electrical transmission line, and let G be the leakance to ground. The voltage drop per unit of length is then

$$dE = -\, i(j\omega L + R)\, dx$$

and the current branching is

$$di = -\, E(G + j\omega C)\, dx.$$

These equations describe a set of propagating waves (for time $e^{+j\omega t}$) traveling to the right and to the left. (For a discussion of transmission line theory see Sections 2.29, 2.30, 2.31 below). The sum constitutes a *standing wave* with complex propagation constant θ:

$$i = Ae^{\theta y} + Be^{-\theta y}, \qquad \theta = \sqrt{(R + j\omega L)\,(G + j\omega C)} \quad \text{(units: } \mathrm{m}^{-1}\text{)}$$

where A, B are constants to be determined from boundary conditions at $y = 0$. In terms of applied current i_0 and applied voltage E_0, both at $y = 0$, it can directly be deduced that at any point y of the transmission line the values of A, B lead to the equations,

$$E = E_0 \cosh \theta y - i_0 Z_0 \sinh \theta y \tag{2.21.14a}$$

$$i = i_0 \cosh \theta y - \frac{E_0}{Z_0} \sinh \theta y \tag{2.21.14b}$$

$$Z_0 = \sqrt{\frac{R + j\omega L}{G + j\omega C}}. \tag{2.21.14c}$$

[3].

These are the exact equations for a very long transmission line. When the line is made "short enough" its filtering action may be approximated by a *T*-network, Fig. 2.21.2, for which,

$$E_2 = -E_1\left(\frac{Z_1 + 2Z_2}{2Z_2}\right) + i_1\,\frac{Z_1(Z_1 + 4Z_2)}{4Z_2} \tag{2.21.15a}$$

$$i_2 = i_1\left(\frac{Z_1 + 2Z_2}{2Z_2}\right) - \frac{E_1}{Z_2}. \tag{2.21.15b}$$

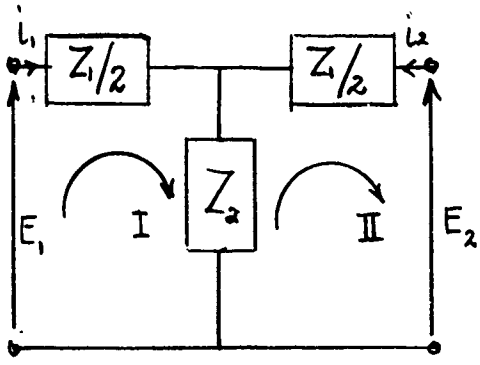


Fig. 2.21.2 — T-network representation of a short transmission line

The sign associated with E_2 comes from the loop equation for mesh II in which E_2 is regarded as a *rise* in potential. On comparing 2.21.15a, b with 2.21.14a, b it is deduced that by making

$$\frac{Z_1}{2} = Z_0 \tanh\left(\frac{\theta y}{2}\right); \quad Z_2 = \frac{Z_0}{\sinh \theta y} \tag{2.21.16}$$

the two sets of equations will be *formally* the same, provided E is opposite in sign to E_2.

To this point θ is complex with both real and imaginary parts. It is useful to consider the resistance R and leakance G to be very small so that θ becomes purely imaginary. Then, for time given by exp $j\omega t$,

$$\frac{Z_1}{2} = jZ_0 \tan\left(\frac{\omega\sqrt{LC}}{2}\right); \quad Z_2 = \frac{-jZ_0}{\sin \omega\sqrt{LC}}. \tag{2.21.17}$$

These are the parameters associated with the *T*-network representation of a short transmission line described by the equations

$$E = E_0 \cos(y\omega\sqrt{LC}) - i_0 Z_0 \sin(y\omega\sqrt{LC}) \tag{2.21.18a}$$

$$i = i_0 \cos(y\omega\sqrt{LC}) - \frac{E_0}{Z_0} \sin(y\omega\sqrt{LC}). \tag{2.21.18b}$$

A *formal* comparison of 18a, b with Eqs. 2.21.10b and 2.21.9 shows that if one makes the correspondences

$$E \rightarrow F + \frac{L_w L_l h_{31} E_3}{\beta_{33}^S}$$

$$i \rightarrow \dot{\xi}$$

$$Z_0 \rightarrow L_w L_l \rho v_c = Z_0'$$

$$y\omega\sqrt{LC} \rightarrow \frac{\omega y}{v_c}$$

then the *mechanical* equations can be represented by an equivalent circuit in the form of a *T*-network, Fig. 2.21.3. This network equivalent is valid for all frequency ranges provided the vibrator is "short-enough" (generally a fraction of a wavelength).

Several cases of Fig. 2.21.3 are now considered.

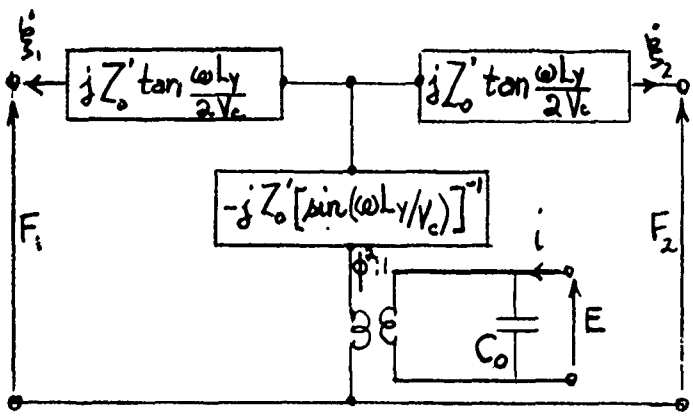


Fig. 2.21.3 — T-network representation of the piezoelectric longitudinal vibrator in Fig. 2.21.1

2.22 LONGITUDINAL BAR TRANSDUCER CLAMPED AT ONE END

In this case $\dot{\xi}_1 = 0$, and

$$\frac{-j\,Z_0'}{\sin\left[\frac{\omega L_y}{v_c}\right]} + j\,Z_0' \tan\frac{\omega L_y}{2v_2} = -\,j\,Z_0' \cot\left[\frac{\omega L_y}{v_c}\right] \qquad (2.22.1)$$

Hence the equivalent circuit reduces to Fig. 2.22.1.

In many important applications the vibrator is operated at (or near) a frequency ω_R such that the impedance of the series branch vanishes. Setting $\omega = \omega_R + \Delta\omega$, $\Delta\omega \ll \omega_R$, it is found that,

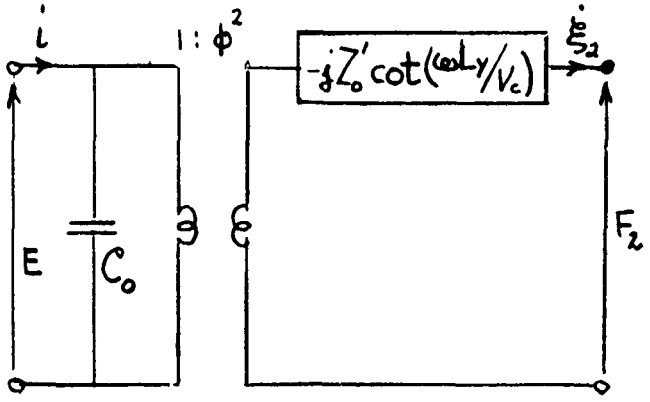


Fig. 2.22.1 — Equivalent circuit based on electric current/mechanical velocity analogy of a longitudinal vibrator clamped at one end

$$-j\ Z_0'\ \cot\left(\frac{\omega L_y}{v_c}\right) \rightarrow j\ Z_0'\left(\frac{\pi}{2}\ \frac{\Delta\omega}{\omega_R}\right). \tag{2.22.2}$$

This form suggests a representation of Fig. 2.22.1 by a coil L_M and condenser C_M in series. Formally, one has for them,

$$Z = -\ j\left[\frac{1}{\omega C_M} - \omega L_M\right] = \frac{-j}{\omega C_M}\left[1 - \frac{\omega^2}{\omega_R^2}\right]. \tag{2.22.3}$$

For $\omega = \omega_R + \Delta\omega$,

$$Z = \frac{-j}{\omega_R C}\left[1 - \frac{(\omega_R + \Delta\omega)^2}{\omega_R^2}\right] \simeq j\ \frac{2\Delta\omega}{\omega_R^2 C_M}. \tag{2.22.4}$$

On comparing 20b with 19b it is seen that the equivalent compliance of the vibrator near $\omega = \omega_R$ is

$$C_M = \frac{4}{\pi\omega_R Z_0'}. \tag{2.22.5}$$

The equivalent mass M which resonates with this compliance is

$$MC_M = \frac{1}{\omega_R^2} \quad \text{or} \quad M = \frac{1}{\omega_R^2 C_M} \tag{2.22.6}$$

$$\omega_R = \frac{\pi}{2}\ \frac{v_c}{L_y}, \qquad v_c = \sqrt{\frac{C_{11}^E}{\rho}}.$$

Thus, near $\omega = \omega_R$ the longitudinal vibrator clamped at one end is represented by Fig. 2.22.2.

2.23 A LONGITUDINAL BAR TRANSDUCER WITH ONE END FREE AND ONE END DRIVING A LOAD

In this case $F_1 = 0$, meaning the left terminal of Fig. 2.21.3 is short-circuited. The equivalent circuit then takes on the appearance of Fig. 2.23.1.

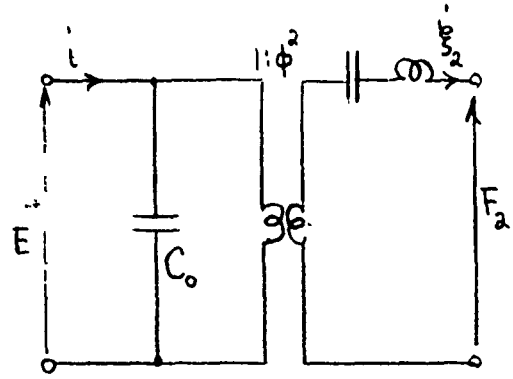


Fig. 2.22.2 — Approximation of Fig. 2.22.1 near $\omega = \omega_R$

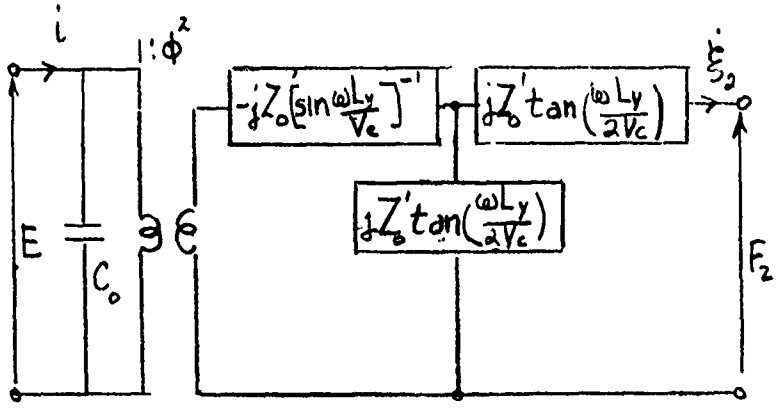


Fig. 2.23.1 — Equivalent electrical circuit of a longitudinal vibrator free at one end and driving a load at the other end

The right end of this circuit is a left L-network with two equal branches ($Z_1 = Z_2$). According to Norton [4] it is equivalent to a right L-network ($Z_x = Z_y$) as seen through a transformer of turns ratio Φ. Since

$$Z_y = Z_x = 2jZ_0' \tan \frac{\omega L_y}{2v_C} = Z_1 + Z_2 \tag{2.23.1}$$

and $\Phi = 2$, the right side of Fig. 2.23.1 reduces to Fig. 2.23.2.

Thus, Fig. 2.23.1 simplifies to Fig. 2.23.3.

According to this equivalent circuit the longitudinal vibrator exhibits a frequency dependence of both a series branch and a shunt branch. Near the resonant frequency ω_R of the series branch

The series branches are combined through the transformer (turns ratio $\Phi = 2$),

$$\frac{-j4Z_0'}{\sin\left(\frac{\omega L_y}{v_c}\right)} + 2j\ Z_0' \tan \frac{\omega L_y}{2v_c} = -\ j2\ Z_0' \cot \frac{\omega L_y}{2v_c} \tag{2.23.2}$$

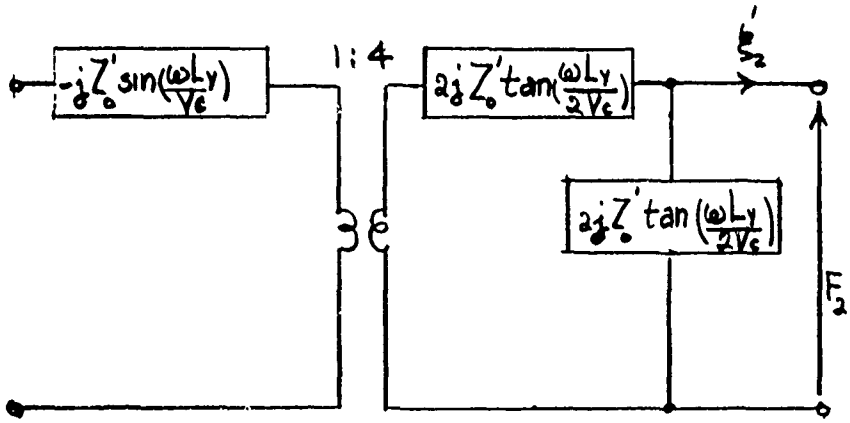


Fig. 2.23.2 — Right side of Fig. 2.23.1 after conversion from a left L-network to a right L-network

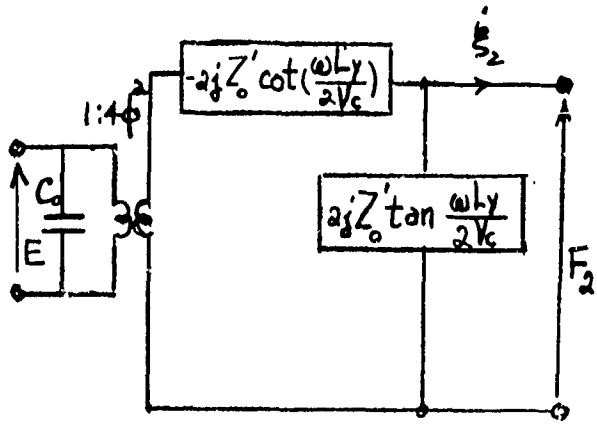


Fig. 2.23.3 — A simplified circuit which contains all the features of Fig. 2.23.1

$$-2j\ Z_0' \cot\left(\frac{\omega L_y}{2v_c}\right) \rightarrow -2j\ Z_0' \left(\frac{\pi}{2}\ \frac{\Delta\omega}{\omega_{R_v}}\right) \tag{2.23.3}$$

$$C_1 = \frac{2}{\pi\omega_R Z_0'}, \quad M_1 = \frac{1}{\omega_R^2 C_1}. \tag{2.23.4}$$

As for the shunt branch one seeks a parallel combination of C_2, M_2 which represents its frequency dependence near the anti-resonant frequency ω_A. From electrical circuit theory, for $\omega = \omega_A + \Delta\omega$,

$$Y = j\omega C + \frac{1}{j\omega L} = \frac{j}{\omega L}\left[\frac{\omega^2}{\omega_A^2} - 1\right] \tag{2.23.5}$$

$$Z = \frac{1}{Y} = \frac{\omega L}{j\left[\frac{\omega^2}{\omega_A^2} - 1\right]} = \frac{-j\omega_A^2 L}{2\Delta\omega}. \tag{2.23.6}$$

Since

$$2j\,Z_0'\tan\frac{\omega L_y}{2v_c} \rightarrow -j\,\frac{4}{\pi}\,\frac{Z_0'\omega_A}{\Delta\omega} \tag{2.23.7}$$

it is seen by comparing .Eq (2.23.27) with .Eq (2.23.6) that the equivalent mass M_2 is

$$M_2 = \frac{8}{\pi}\,\frac{Z_0'}{\omega_A} \qquad \text{(units: Ns}^2\text{/m)} \tag{2.23.8}$$

and the resonating stiffness is

$$C_2 = \frac{1}{\omega_A^2 M_2} \qquad \text{(units: m/n).} \tag{2.23.9}$$

With these approximations Fig. 2.23.3 reduces to Fig. 2.23.4. Its frequency dependence is discussed in the next section under the title of bandwidth properties of transducers.

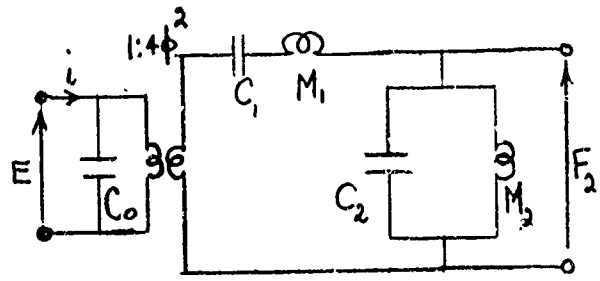


Fig. 2.23.4 — Equivalent electrical circuit near the resonant and antiresonant frequencies of a longitudinal vibrator loaded at one end and free at the other end

2.24 INTRODUCTION TO BANDPASS AND BANDREJECT PROPERTIES OF TRANSDUCERS

In the theory reviewed in Secs. 1.0, 1.1 transducers were modeled as simple, or complex, cascades of series/parallel components. These components were classified as resonant or nonresonant. We treat in the next sections components which are series resonant, or parallel resonant to show their bandpass properties.

2.25 PARALLEL RESONANT MECHANICAL CIRCUITS

By definition in this treatise, a mechanical network whose elements are in parallel relative to force is one in which the force divides among the elements. Alternatively, it is a network whose elements possess a common velocity. We consider first a network of mass m_p, compliance n_p, and damping R_p in parallel, Fig. 2.25.1a. The appropriate equation of motion in the steady state involves a sum of mechanical impedances:

$$F = V\sum_i Z_i = V\left[j\omega m_p + c_p + \frac{1}{j\omega n_p}\right] = VZ. \tag{2.25.1}$$

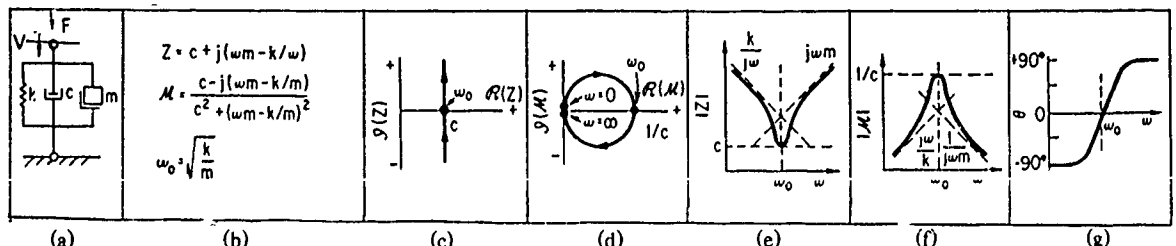


Fig. 2.25.1 — (a) A parallel mechanical network, (b) formulas for impedance and mobility, (c) plot of its complex impedance, (d) plot of its complex mobility, (e) plot of magnitude of total mechanical impedance vs frequency, (f) plot of magnitude of total mobility vs frequency (g) phase angle of velocity vs force [16]. C. M. Harris and C. E. Crede, *Shock and Vibration Handbook*, **1** (1961), ©1961 McGraw-Hill Book Co.; by permission.

The magnitude of impedance ($= |F/V|$) and angle of impedance (θ) is shown in (b) and (d) of this figure. Here $\omega_0^2 = (m_p n_p)^{-1}$. The magnitude of mobility ($= |V/F|$) is also given in (c).

When the mechanical circuit forms the secondary of a transduction chain it is convenient (as noted earlier in Sec. 1.23) to transform secondary parameters into primary parameters with the aid of the law of transduction. To simplify this transformation one adopts a suitable analogy. For example, let us assume the parallel mechanical circuit of Fig. 2.25.1 forms the secondary of an electromechanical transducer whose transduction is that of a *gyrator.* A simple VF form of gyrator satisfies the formulas,

$$\text{gyrator transduction:} \quad V = iy; \quad F = \frac{e}{y} \quad \begin{bmatrix} V \text{ is the across-variable} \\ \text{and } F \text{ is the through-variable} \end{bmatrix}. \tag{2.25.2}$$

in which y is a simple scale factor. Substitution in Eq. 2.25.1 gives the electrical equivalent network

$$\frac{F}{V} \rightarrow \frac{e}{y}\,\frac{1}{iy} \rightarrow \frac{e}{i}\,\frac{1}{y^2}$$

or

$$\frac{e}{i} = y^2 \left[j\omega m_p + c_p + \frac{1}{j\omega n_p} \right]. \tag{2.25.3}$$

This is the equation of an electrical *series* circuit in which

$$y^2 m_p = L_m; \quad y^2 c_p = R_c; \quad n_p/y^2 = C_p \quad i = \frac{V}{y}; \quad e = yF. \tag{2.25.4}$$

In this circuit the electrical current i is the through-quantity and the electrical voltage e is the across-quantity. Figure 2.25.2 shows the electrical equivalent circuit of this parallel mechanical circuit, as transduced by a gyrator:

A universal curve of the velocity response of a parallel resonant circuit for fixed applied force is shown in Fig. 2.25.3. The parameter a used in this figure is defined as,

$$a = Q \left(\frac{\text{cycles off resonance}}{\text{resonant frequency}} \right) = Q\Omega$$

$$Q = \omega_0 L/R$$

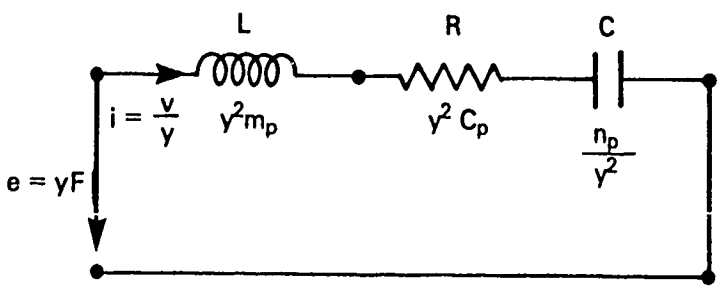


Fig. 2.25.2 — An electrical equivalent circuit of a secondary parallel mechanical circuit transduced to the primary by agency of a gyrator

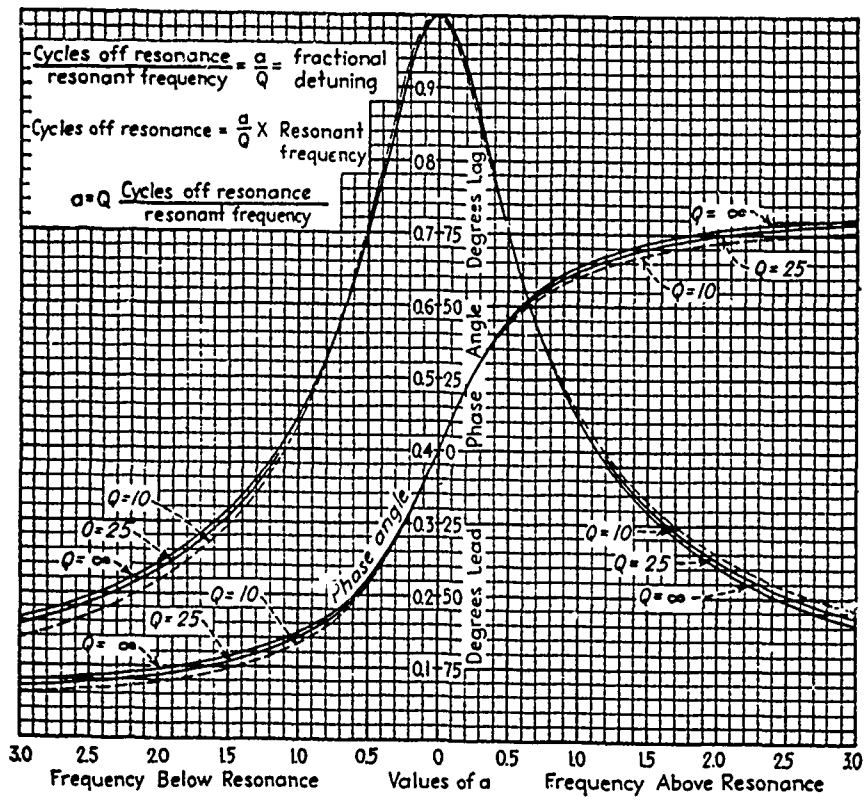


Fig. 2.25.3 — Velocity response, or current response, of Fig. 2.25.2 normalized to response at resonance. A = magnitude, B = phase relative to phase of applied force [11]. F. E. Terman, *Radio Engineers Handbook* (1st ed) (1943), ©1943 McGraw-Hill Book Co.; by permission.

It is noted that because Fig 2.25.2 is a FV diagram and Fig. 2.25.1 is a VF diagram the phase angle θ opposite in sign (that is, lead and lag are interchanged). Table 2.25.1 gives several responses for rapid estimation of this curve.

Table 2.25.1

$\Omega = \frac{\text{cycles off resonances}}{\text{resonant frequency}}$	a	$V/V_{\text{resonance}}$	Phase θ (average)
$\frac{1}{6Q}$	1/6	0.95	18° lag
$\frac{1}{4Q}$	1/4	0.90	26° lag
$\frac{1}{2Q}$	1/2	0.707	45° lag
$1/Q$	1	0.447	63° lag
$2/Q$	2	0.242	75° lag
$4/Q$	4	0.124	83° lag

When Ω is greater than $3/Q$ a good working rule is

$$V/V_{\text{resonance}} = \left[Q\gamma\left(1 - \frac{1}{\gamma^2}\right)\right]^{-1}$$

$$\gamma = \frac{\text{actual frequency}}{\text{resonant frequency}}.$$

The force through the mass (or spring) at resonance for applied force F_0 is,

$$F_L \cong F_C = F_0 Q.$$

Far below resonance (i.e., where $\gamma > 3/Q$) one has

$$F_L \simeq \left[Q\left(1 - \frac{1}{\gamma^2}\right)\right]^{-1}; \quad F_C \simeq [Q(\gamma^2 - 1)]^{-1}.$$

The magnitude and phase of impedance corresponding to are shown in Figs. 2.25.4a and 2.25.4b.

It is often useful to represent the secondary mechanical circuit by analogous primary circuit forms (in this case, electrical forms). For example, the parallel mechanical network of Fig. 2.25.1 can be described in terms of the forces F_n, F_m, and F_c flowing through the spring, mass and damper:

$$= j\omega n_p F_n = \frac{1}{j\omega m_p} F_m = \frac{1}{C} F_c \tag{2.25.5}$$

Since is it always convenient to represent parallel mechanical elements by parallel-type electrical symbols, we *choose* the analogy $i \triangleq F$; $e \triangleq V$, thus making force the through-quantity and velocity the across-quantity. Then n_p appears as an inductance, m_p as a capacitor, and $\frac{1}{c}$ $(= h)$ as an admittance. Fig. 2.25.5 shows this representation of the secondary:

To summarize the salient features of Figs. 2.25.1, 2.25.2, and 2.25.5. Figure 2.25.1 gives the response of a parallel mechanical circuit in the form of impedance, mobility, and phase plots. Figure 2.25.5 gives an electrical symbol representation of the circuit as it would appear in the secondary of an electromechanical transformer. Figure 2.25.2 gives the electrical symbol representation of the circuit as it would appear transduced by a gyrator into the primary of an electromechanical transducer.

It remains now to consider the parallel mechanical circuit of Fig. 2.25.1 to be the secondary of an electromechanical transducer in which the transduction is that of an *ideal transformer* in VF form:

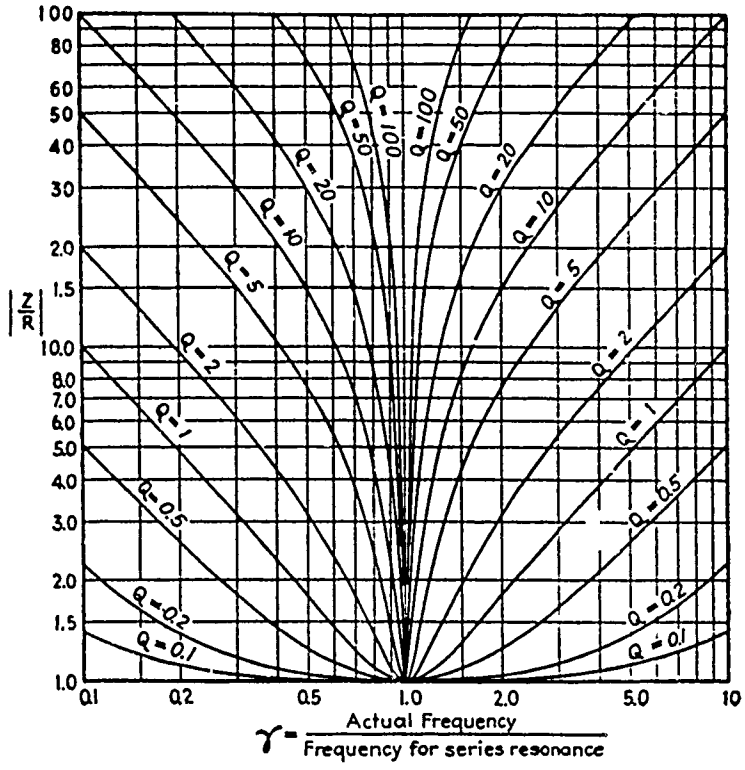
$$VF \text{ form of ideal transformer transduction: } e = \frac{V}{x}; \; i = xF \quad \begin{pmatrix} V \text{ is across-variable} \\ F \text{ is through-variable} \end{pmatrix}. \tag{2.25.6}$$

Here, x is a scale factor. Substitution into Eq. 2.25.1 leads to the relation,

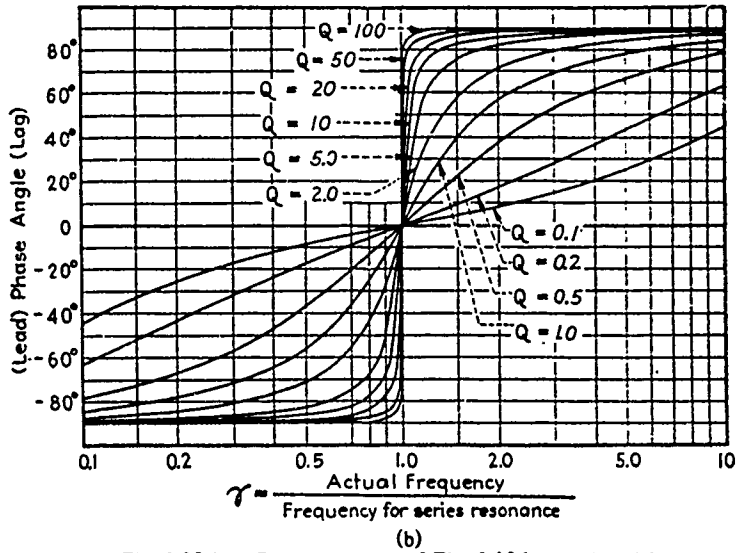
$$\frac{i}{e} = X^2 \left[j\omega m_p + c_p + \frac{1}{j\omega n_p}\right] = X^2 \left[\frac{F}{V}\right]. \tag{2.25.7}$$

This is the equation of an electrical parallel circuit in which,

$$X^2 m_p = C_p; \quad X^2 c_p = h; \quad \frac{X^2}{n_p} = L_p. \tag{2.25.8}$$



(a)



(b)

Fig. 2.25.4 — Representation of Fig. 2.25.1 transduced by an ideal transformer from the secondary into the primary of an electromechanical transducer, (a) magnitude of Z/R versus γ, (b) phase of versus $Z\gamma$ [11]. F. E. Terman, *Radio Engineers Handbook* (1st ed) (1943), ©1943 McGraw-Hill Book Co.; by permission.

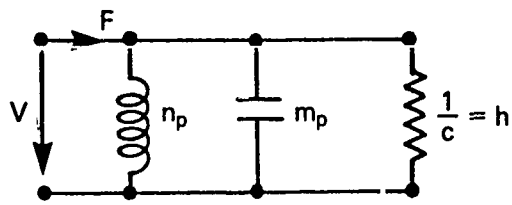


Fig. 2.25.5 — A VF representation of Fig. 2.25.1 expressed in electrical symbols, as it appears in the secondary of an electromechanical transducer [11]. F. E. Terman, *Radio Engineers Handbook* (1st ed) (1943), ©1943 McGraw-Hill Book Co.; by permission.

Figure 2.25.6 shows the parallel primary circuit equivalent of the parallel secondary circuit, when the latter is transduced through an ideal transformer:

The effect of type of transduction on the dynamic behavior of a parallel mechanical circuit is very significant. Transduction by the VF form of gyrator action converts this circuit into a series-connected electrical equivalent circuit, with the current i being the analog of the velocity. Transduction by ideal transformer action converts this circuit into a parallel-connected electrical equivalent circuit, with the current i being the analog of the force.

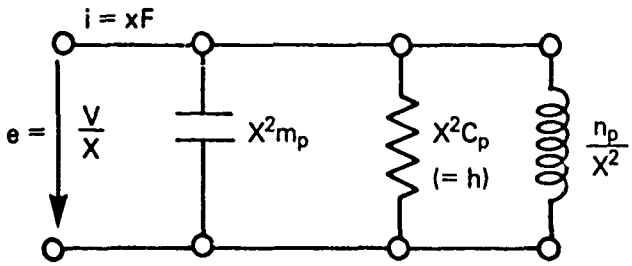


Fig. 2.25.6 — Parallel primary-circuit equivalent of the parallel secondary-circuit

2.26 SERIES-CONNECTED RESONANT MECHANICAL CIRCUITS

By definition in this treatise, a mechanical network whose elements are in series relative to force is one in which the force is common to all elements. Alternatively, it is a network in which the input velocity is divided among the elements. We consider here a network of mass m_s, damping c_s, and compliance n_s connected in series, Fig. 2.26.1.

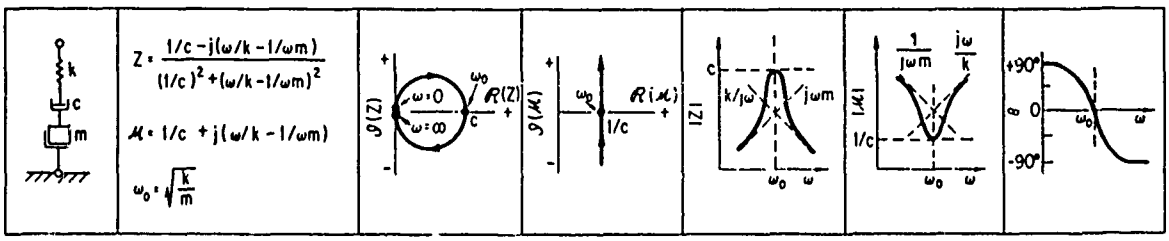


Fig. 2.26.1 — (a) A spring dashpot, mass series-connected mechanical network (b) impedance and mobility equations (c) Plot of ImZ vs ReZ (d) Plot Im M vs ReM (e) Plot $|Z|$ vs ω (f) Plot $|M|$ vs ω (g) Plot of θ vs ω [16]. C. M. Harris and C. E. Crede, *Shock and Vibration Handbook*, 1 (1961), ©1961 McGraw-Hill Book Co.; by permission.

The appropriate equation of motion in the steady state involves a sum of mobilities:

$$V = F\sum_l M_l = F\left[\frac{1}{c_s} + j\omega n_s + \frac{1}{y}j\omega m_s\right] = FM \tag{2.26.1}$$

where

$$\omega_0^2 = (m_s n_s)^{-1}.$$

We now let this circuit be the secondary of an electromechanical transducer. To display a convenient *representation* for it we choose the analogy $i \mathrel{\hat{=}} F$, $e \mathrel{\hat{=}} V$, and compare Eq. 2.26.1 with the form,

$$e = i\left[j\omega L_s + \frac{1}{j\omega C_s} + R_s\right].$$

Thus it is concluded that

$$L_s \rightarrow n_s;\ C_s \rightarrow m_s;\ R_s \rightarrow 1/c_s \tag{2.26.2}$$

Figure 2.26.2 shows this representation.

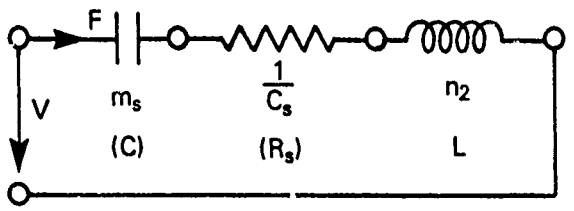


Fig. 2.26.2 — Equivalent circuit representation of Fig. 2.26.1a as a secondary circuit of a transducer

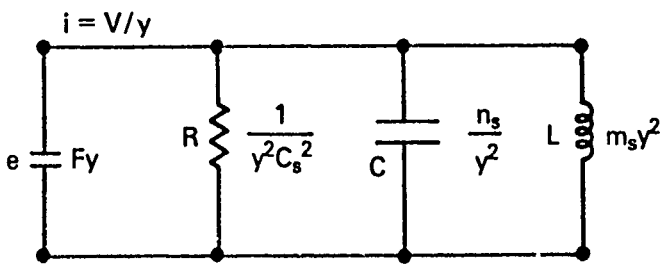
A first step in analysis of a transducer is to convert secondary circuits into equivalent primary circuits, or vice versa, through use of the transduction circuit. We consider here transduction via gyrator, or via ideal transformer.

gyrator transduction: $V = iy;\ F = \frac{e}{y}$.

Substitution into Eq. 2.26.1 leads to the result that,

$$\frac{i}{e} = \frac{U}{y^2} = \frac{1}{y^2 c} + \frac{y\omega n_s}{y^2} + \frac{1}{j\omega m_s y^2}. \tag{2.26.3a}$$

This formula corresponds to the parallel electrical circuit shown in Fig. 2.26.3a.



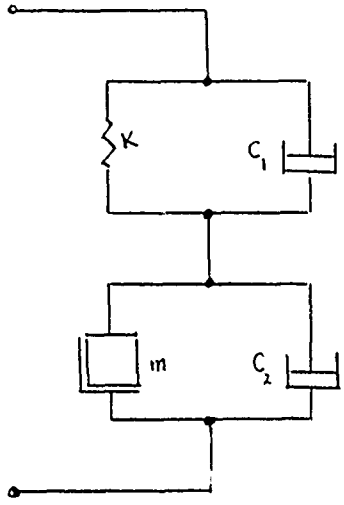
(a)

Fig. 2.26.3a — Equivalent circuit obtained by transferring the secondary circuit of Fig. 2.26.2 into a primary representation via a gyrator

A mechanical series network more commonly encountered consists of a lossy spring in series with a "lossy" mass, Fig. 2.26.3b. Its *FV* diagram is shown in Fig. 2.26.3c.

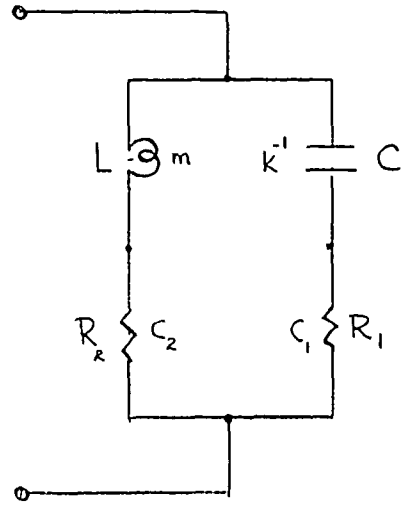
The electrical circuit consists of $Z_c (= R_1 + 1/j\omega C)$ and $Z_L (= R_2 + j\omega L)$ in parallel. The total impedance Z, the electrical Q, and resonant frequency ω_0, are

$$Z = \frac{Z_c Z_L}{Z_c + Z_L};\ Q = \frac{\omega L}{R_s};\ R_s = R_1 + R_2;\ \omega_0^2 = 1/LC. \tag{2.26.3b}$$



(b)

Fig. 2.26.3b — A mechanical series network consisting of a lossy spring and a damped mass

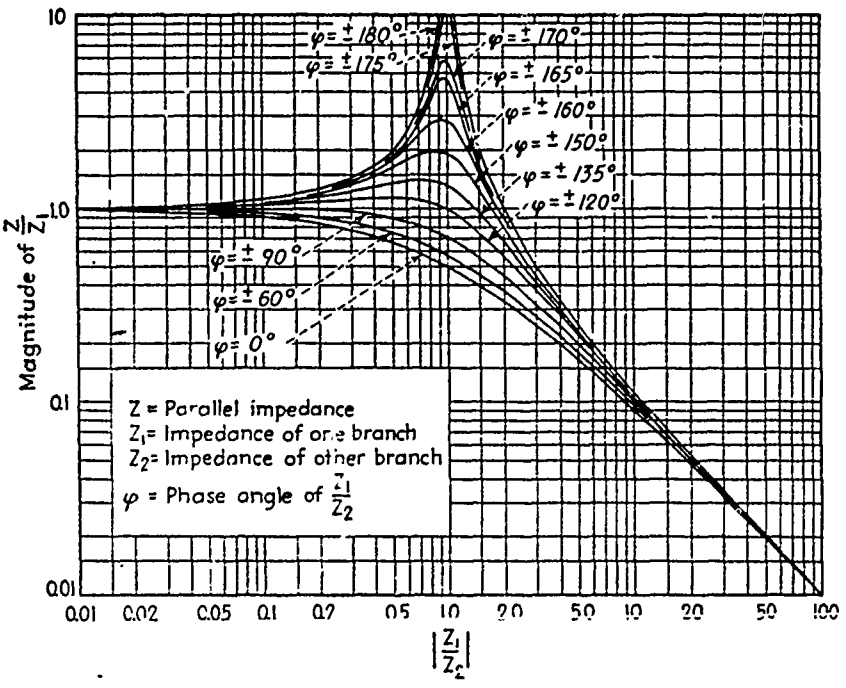


(c)

Fig. 2.26.3c — Electrical equivalent circuit of Fig. 2.26.3b

The magnitude of Z varies with frequency as shown in Fig. 2.26.1e. It phase is given by Fig. 2.26.1g with the sign reversed (because of change from a *VF* to a *FV* diagram). A plot of the magnitude Z/Z_1 versus Z_1/Z_2 (Z_1, Z_2 being Z_C or Z_L) is shown in Fig. 2.26.3d. For each value of frequency one determines Z_1, Z_2, and phases ϕ_1, ϕ_2. Then the chart is consulted for the value of $|Z/Z_1|$. A second chart, Fig. 2.26.3e, shows the phase angle of Z/Z_1.

When the electrical Q, defined by Eq. 2.26.3a is greater than 10 the resistance and reactance components have the shape shown in Fig. 2.26.3.f.



(d)

Fig. 2.26.3d — Magnitude of Z/Z_1 vs Z_1/Z_2 where Z_1, Z_2 can be Z_c or Z_L [11]. F. E. Terman, *Radio Engineers Handbook* (1st ed) (1943), ©1943 McGraw-Hill Book Co.; by permission.

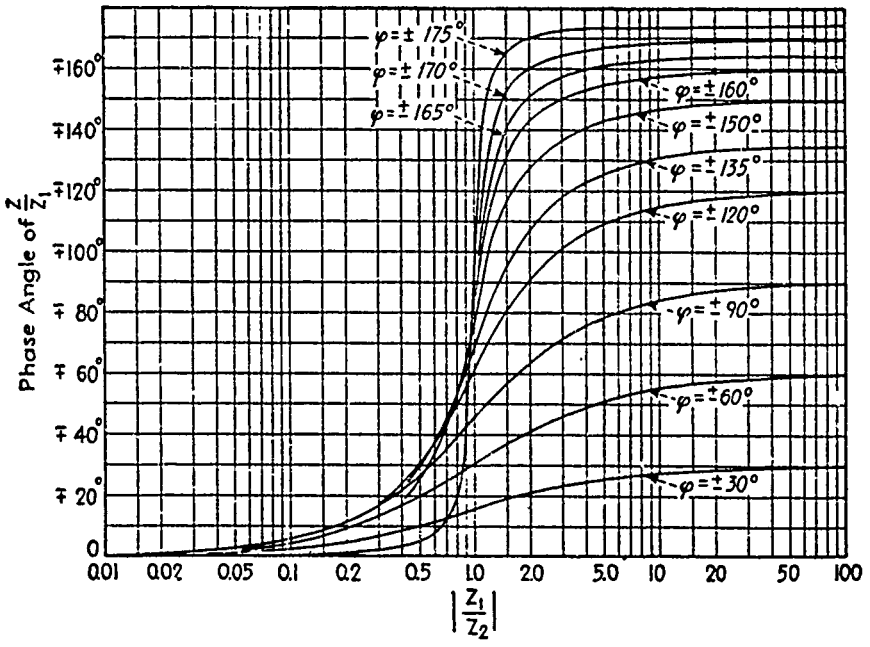


Fig. 2.26.3e — Phase of Z/Z_1 vs Z_1/Z_2 where Z_1, Z_2 can be Z_c or Z_L [11]. F. E. Terman, *Radio Engineers Handbook* (1st ed) (1943), ©1943 McGraw-Hill Book Co.; by permission.

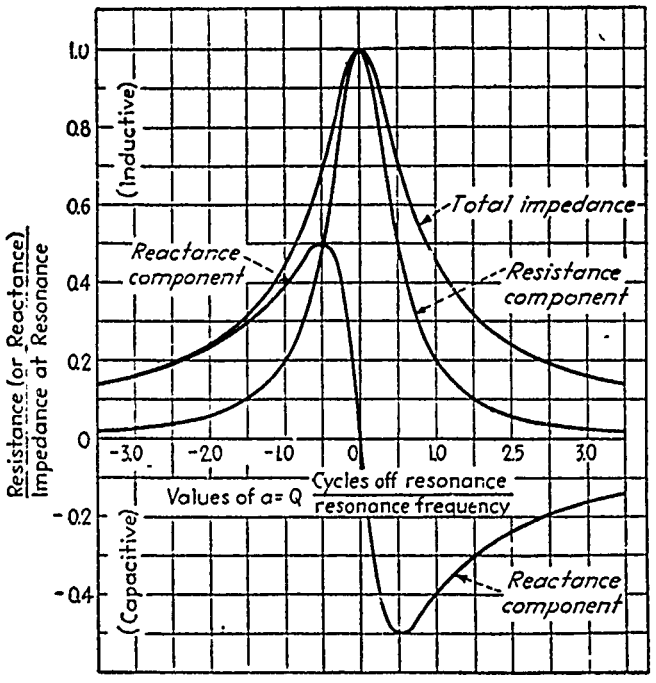


Fig. 2.26.3f — Resistance and reactance components of Eq. 2.26.3b for $Q > 10$ [11]. F. E. Terman, *Radio Engineers Handbook* (1st ed) (1943), ©1943 McGraw-Hill Book Co.; by permission.

As for transduction via ideal transformer, one has:

$$e = \frac{V}{x};\ i = xF.$$

Substitution into Eq. 2.26.1 leads to the result that,

$$\frac{e}{i} = \frac{U}{x^2} = \frac{1}{y^2x^2} + \frac{j\omega n_s}{x^2} + \frac{1}{j\omega m_s x^2}. \tag{2.26.4}$$

This formula corresponds to the series electrical circuit shown in Fig. 2.26.4.

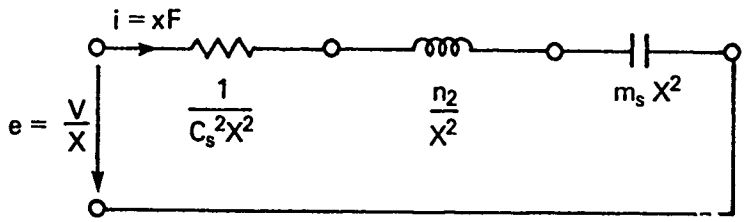


Fig. 2.26.4 — Representation of Fig. 2.26.1a as a primary equivalent circuit transduced from the secondary via an ideal transformer

2.27 SERIES/PARALLEL-CONNECTED MECHANICAL CIRCUIT

The series-parallel mechanical circuit shown in Fig. 2.27.1 may be analyzed conveniently as a parallel circuit with one series branch. The appropriate equation of motion is

$$\text{(a) } F = F_1 + F_2 = V(Z_1 + Z_2) \tag{2.27.1}$$

$$\text{(b) } Z_2 = \frac{k_2}{j\omega};\ Z_1 = \frac{1}{Y_1} = \frac{1}{\frac{j\omega}{k_1} + \frac{1}{j\omega m}} = \frac{1}{j\left[\frac{\omega}{k_1} - \frac{1}{\omega m}\right]}$$

$$\text{(c) } Z_{\text{total}} = Z_1 + Z_2 = \frac{-j\left[\frac{k_2 + k_1}{k_1} - \frac{k_2}{\omega^2 m}\right]}{\frac{\omega}{k_1} - \frac{1}{\omega m}}$$

$$\text{(d) } \omega_1 = \sqrt{\frac{1}{m}\left[\frac{k_1k_2}{k_1 + k_2}\right]},\ \omega_2 = \sqrt{k_1/m}.$$

We now let this circuit be the secondary of an electromechanical transducer and choose the $i \triangleq F$, $e \triangleq v$ analogy to display it. In this analogy one sets spring compliance → inductor, mechanical damper → inverse resistor, mechanical mass → capacitor. Figure 2.27.2 shows the representation.

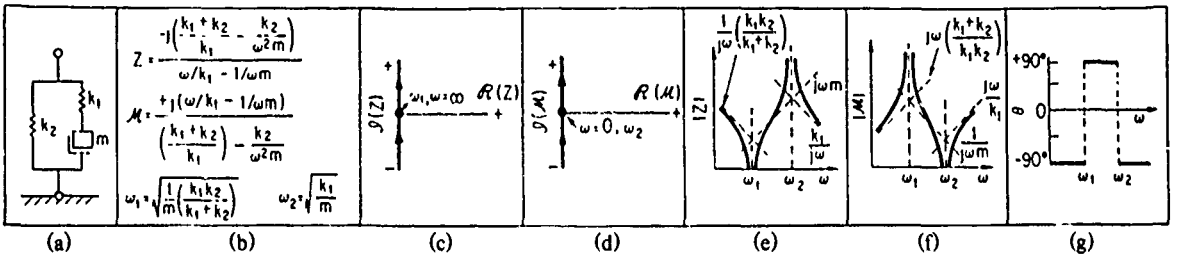


Fig. 2.27.1 — (a) Series/parallel circuit (b) Impedance and mobility equations (c) plot of ImZ vs ReZ (d) plot ImM vs ReM (e) plot of $|Z|$ vs ω (f) plot of $|M$ vs $\omega|$ (g) plot of θ vs ω [16]. C. M. Harris and C. E. Crede, *Shock and Vibration Handbook*, 1 (1961), ©1961 McGraw-Hill Book Co.; by permission.

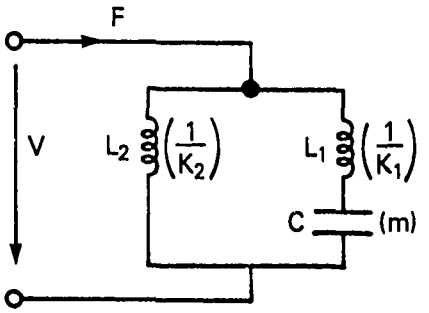


Fig. 2.27.2 — Representation of Fig. 2.27.1a by an equivalent circuit in the i/F analogy

The transfer of this secondary circuit to the primary side of the transducer make use of the transduction block (see Fig. 1.2.1 of Chapter 1). As before, two simple transductions are the VF form of gyrator and ideal transformer. When we substitute the gyrator transduction $v = iy$, $F = e/y$ into Eqs. 2.27.1a and 2.27.1c, we find that

$$\frac{e}{i} = y^2\left(\frac{F}{V}\right) = y^2 Z_{\text{mech}} = \frac{y^2 k_2}{j\omega} + \frac{1}{\dfrac{j\omega}{k_1 y^2} + \dfrac{1}{j\omega m y^2}}. \tag{2.27.2}$$

This equation corresponds to a series-connected electrical circuit in which each element is multiplied by y^2. Figure 2.27.3 shows the result.

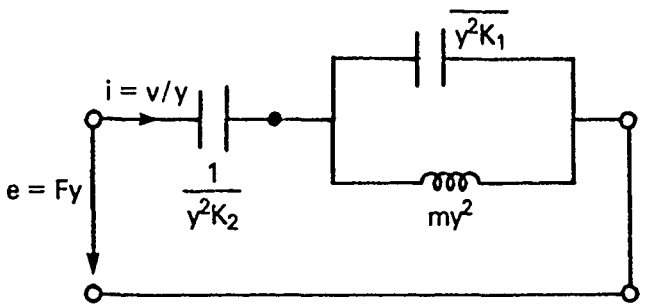


Fig. 2.27.3 — Transfer of Fig. 2.27.2 to the primary side via a gyrator

An important observation here is that transfer from secondary to primary (and vice versa) through a gyrator converts parallel-connected elements into series-connected elements (and vice-versa).

When the transduction is through an ideal transformer ($e = V/x$; $i = xF$) the result is quite different:

$$\frac{i}{e} = x^2\left(\frac{F}{V}\right) = x^2 Z_{mech} = \frac{x^2 k_2}{j\omega} + \frac{1}{\frac{j\omega}{k_1 x^2} + \frac{1}{j\omega m x^2}}. \tag{2.27.3}$$

This equation corresponds to a parallel-connected electrical circuit in which each element is multiplied by x^2. The result is shown in Fig. 2.27.4

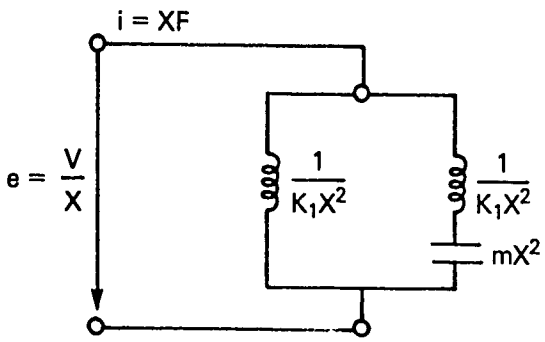


Fig. 2.27.4 — Transfer of Fig. 2.27.3 to the primary side via an ideal transformer

One notes that, except for a scale factor, the analogy $i \triangleq \dot{F}$, $e \triangleq V$ allows the preservation of series (or parallel) form from secondary to primary, provided the transduction is through an ideal transformer.

2.28 MECHANICAL AND ACOUSTICAL WAVE FILTERS

In Secs. 1.0, 1.1 it was seen that periodic repetition of a combination of simple series parallel circuits in the form of a "ladder" constitutes a wave filter structure. The filter building blocks discussed there were configured as left-, or right-, *L*-sections in which acoustical mass appeared in the series branch and acoustical stiffness in the parallel branch. Repetition of such *L*-branches in a ladder leads naturally to an echelon of *T* networks. Since any 4-terminal (= two-connection) system can be represented by an equivalent *T* network it is seen that mechanical (acoustical) wave filters can be constructed by repetition of a basic single two-connection system. In the discussion now to be presented the *T*-section comprising the filter can thus be any suitable network.

A. Theory of a T-Section Filter

We consider a chain of identical *T*-sections driven by a force source, and model it by use of an *FV* diagram, Fig. 2.28.1. For mathematical convenience the first and last series branch are made $Z/2$.

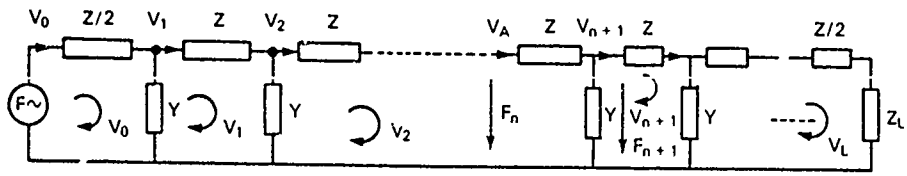


Fig. 2.28.1 — A T-section mechanical wave filter in the form of a FV network

At the nth T-section the node-equation connecting velocities and the loop equation connecting forces have the forms:

$$V_n = V_{n+1} + F_{n+1}\, Y_n \tag{2.28.1a}$$

$$F_n = F_{n+1} + V_n Z_n. \tag{2.28.1b}$$

We now assume that the nth T-section attenuates the (sinusoidal) wave and changes its phase, by amounts e^{Φ}, where Φ is a complex quantity. Thus,

$$V_{n+1} = e^{\Phi}\, V_n; \quad F_{n+1} = e^{\Phi} F_n. \tag{2.28.2}$$

Substitution of Eq. 2.28.2 into 2.28.1 leads to the relation

$$e^{\pm\Phi} = 1 + \frac{Z_n Y_n}{2} \pm \sqrt{\left(1 + \frac{Z_n Y_n}{2}\right)^2 - 1} = q \pm \sqrt{q^2 - 1} \tag{2.28.3}$$

$$q = 1 + \frac{Z_n Y_n}{2}.$$

Let

$$q = \cosh \Phi$$

then

$$q + \sqrt{q^2 - 1} = e^{\Phi}; \qquad q - \sqrt{q^2 - 1} = e^{-\Phi} \tag{2.28.4a}$$

and

$$\Phi = \ln\left[1 + \frac{Z_n Y_n}{2} + \sqrt{\left(1 + \frac{Z_n Y_n}{2}\right)^2 - 1}\right]. \tag{2.28.4b}$$

The term $Z_n Y_n/2$ is complex in the general case. By choosing $Z_n Y_n$ to have purely reactive components $\cosh \Phi$ can be made into a real number. If the magnitudes are adjusted such that,

$$-2 < \frac{Z_n Y_n}{2} < 0 \tag{2.28.5}$$

then Φ is purely imaginary (i.e., $\cosh i\,\Phi = \cos \Phi$). Since Z_n, Y_n are functions of frequency there is evidently a band of frequencies $\Delta\omega$ over which the condition posed by Eq. 2.28.5 holds.

The filtering properties of the structure in Fig. 2.28.1 are described by the ratio of output force (across the load impedance Z_L) to input force $F_{in} = F_{\sim}$. This ratio may be obtained by solving the network for the loop velocities $v_1, v_2, \ldots v_N$ of an N section filter. First, for any two adjacent sections it is seen that by the loop law:

$$\frac{-v_{n-1}}{Y} + v_n \left[Z + \frac{2}{Y}\right] - \frac{1}{Y} v_{n+1} = 0. \tag{2.28.6}$$

This is a difference equation in loop velocities, which has, by analogy with differential equations the solution

$$v_n = c_1 e^{n\Phi} + c_2 e^{-n\Phi}, \qquad (\Phi = \text{complex function}) \tag{2.28.7}$$

where Φ is defined by Eqs. 2.28.4a,b. Application of this solution to the first and last loop of Fig. 2.28.1 leads to the set of equations,

$$\begin{cases} \frac{1}{Y}\left[-c_1 \sinh \Phi + c_2 \sinh \Phi\right] = F_{in} \\ c_1 e^{N\Phi}(Z_L Y + \sinh \Phi) + c_2 e^{-N\Phi}(Z_L Y - \sinh \Phi) = 0 \end{cases} \tag{2.28.8}$$

Upon easy solution for constants c_1, c_2, and upon substitution into Eq. 2.28.7, one finds (for the case of N sections) that the velocity of the rth loop is

$$v_r = FY \frac{\sinh \Phi \cosh(N-r)\Phi + Z_L Y \sinh(N-r)\Phi}{\sinh \Phi[\sinh N\Phi + Z_L Y \cosh(N\Phi)]}.$$

In particular when $r = N$,

$$v_N = \frac{F_{in} Y}{\sinh N\Phi \sinh \Phi + Z_L Y \cosh N\Phi} \tag{2.28.9a}$$

and when $r = 0$,

$$v_0 = FY \frac{\sinh \Phi \cosh N\Phi + Z_L Y \sinh N\Phi}{\sinh \Phi[\sinh N\Phi \sinh \Phi + Z_L Y \cosh N\Phi]}. \tag{2.28.9b}$$

Thus, the output/input ratio becomes

$$\frac{F_{out}}{F_{in}} = \frac{Z_L V_N}{F} \frac{1}{\cosh N\Phi + \frac{1}{Z_L Y} \sinh \Phi \sinh N\Phi}. \tag{2.28.10}$$

The filtering properties described by this ratio can be summarized here: in general $\Phi = \alpha + j\beta$, and

$$\cosh(\alpha + j\beta) = 1 + \frac{ZY}{2}. \tag{2.28.11}$$

For a "pass-band" of frequencies such that (a) $Z(\omega)$, $Y(\omega)$ are purely imaginary (and the product therefore being purely real), and for (b) the condition of Eq. 2.28.5, one has $\alpha = 0$ and

$$\cos \beta = 1 + \frac{ZY}{2}, \qquad -2 < 1 + \frac{ZY}{2} < 0. \tag{2.28.12}$$

All hyperbolic functions in Eq. 2.28.10 become trigonometric functions. There is then no *attenuation* between sections: that is, Eq. 2.28.2 takes on the form

$$V_{n+1} = e^{i\beta} V_n; \qquad F_{n+1} = e^{i\beta} F_n. \tag{2.28.13}$$

Thus each T-section introduces only a phase change, or alternatively, introduces only an (apparent) time delay in traveling wave signals.

Outside of this "pass-band" of frequencies α is no longer zero. In this "stop-band" of frequencies the attenuation is given by

$$\begin{cases} \cosh \alpha = \left| 1 + \dfrac{ZY}{2} \right|, & \left| 1 + \dfrac{ZY}{2} \right| > 0 \text{ or } < -2 \\ \beta = \pm \pi, \text{ or } \beta = 0. \end{cases} \tag{2.28.14}$$

If a single *T*-section is connected to a source of internal impedance Z_S and a load of impedane Z_L, then the *image impedance* of the *T*-section "looking in" from the source is just the impedance of the source; and the image impedance "looking back" from the load is again just the impedance of the load. The image impedances of the *T*-sections discussed here is

$$Z_T = \sqrt{\frac{Z}{Y} + \frac{Z^2}{4}} \tag{2.28.15}$$

In the pass-band both $Z(\omega)$, $Y(\omega)$ are imaginary; hence, Z_T is (ideally) real, that is, it is a pure resistance. In the stop-band the ideal image impedance is a pure reactance.

B. Input-Output Relations of One T-Section

In Eq. 2.28.10 we take $N = 1$. Then the output force is related to the input force via the equation:

$$F_1 = A\mathbf{F}$$

$$A = \left[\cosh \Phi + \frac{1}{Z_L Y} \sinh^2 \Phi \right]^{-1}. \tag{2.28.16}$$

Also, from Eq. 2.28.9b, for the case of $N = 1$ section

$$v_0 = \mathbf{F} Y \frac{(\cosh \Phi + Z_L Y)}{[\sinh^2 \Phi + Z_L Y \cosh \Phi]}$$

$$v_1 = \frac{FY}{[\sinh^2 \Phi + Z_L Y \cosh \Phi]} = v_0 B \tag{2.28.17}$$

$$B = \frac{1}{\cosh \Phi + Z_L Y}.$$

The input-output relation for one T-section terminated in load Z_L can therefore be written as a simple matrix equation:

$$\begin{bmatrix} F_1 \\ v_1 \end{bmatrix} = \begin{bmatrix} A & 0 \\ 0 & B \end{bmatrix} \begin{bmatrix} F \\ v_0 \end{bmatrix} \tag{2.28.18}$$

C. *Qualitative Description of Low-Pass, High-Pass, Band-Pass Filters*

Mechanical-acoustical wave filters can be designed to exhibit low-pass, high-pass, or band-pass frequency regimes. The basic T-structures are shown in Fig. 2.28.2.

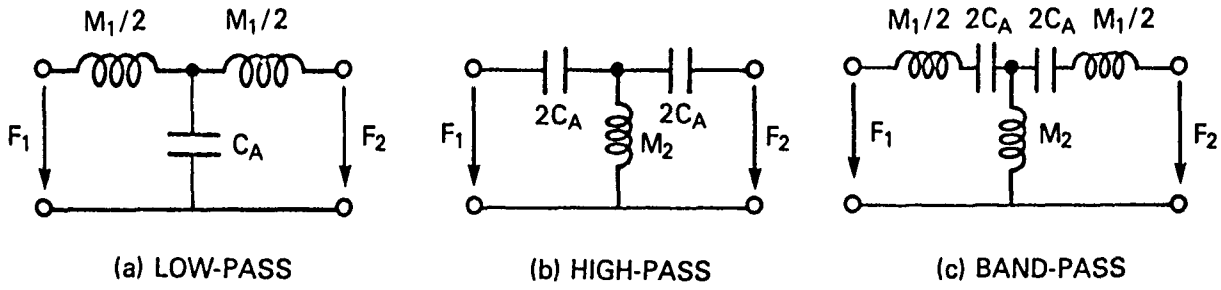


Fig. 2.28.2 — Simple T-section filters (a) low pass, (b) high pass, (c) band pass

In a low-pass filter the mass impedance is small at low frequency while the compliance impedance is large. Hence the transmitted force (F_2) is nearly that across the shunt branch and is nearly the applied force ($=F_1$) itself. As the frequency increases, the mass impedance increases. This results in a substantial diminution of force across the compliance, which tends to reduce the force still further because of its own lowered impedance. Thus at high frequencies the output force F_2 is considerably attenuated.

In a high-pass filter the force at low frequencies across the shunt mass M_2 is much smaller than the applied force both because the series compliance impedance is very high and the shunt impedance is very low. As the frequency increases, the force across M_2 increases because the series impedance is diminishing and the shunt impedance is increasing. Finally at very high frequencies the force across M_2 is nearly the applied force and the output force F_2 is nearly the force across the mass M_2.

In a band-pass filter the attenuation at low frequencies is very great because of the presence of the open-circuited compliance impedance. The force across M_2 is therefore much smaller than the applied force. As the frequency increases, the series mass and compliance tend to cancel each other and the force across M_2 tends to be equal to the applied force. This condition endures over the pass-band of the filter. Beyond the pass-band the impedance of the series branch again increases due to the mass M_1. Again the force across M_2 diminishes, and hence the output force F_2 becomes greatly attenuated.

D. Design of Mechanical-Acoustical Filters

The nomenclature of filter design has been standardized by electrical engineers. Figure 2.28.3 shows the attenuation diagram of a very general case of a band-pass filter. We use it here to define the quantities needed in designing filters.

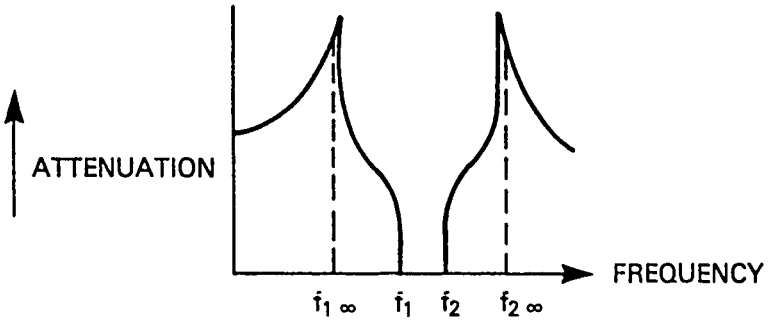


Fig. 2.28.3 — Standard nomenclature of filter design

The parameters are:

f_1 = low frequency limit of pass band
f_2 = higher frequency limit of pass band
$f_{1\infty}$ = a frequency of very high attenuation in the low-frequency attenuating band
$f_{2\infty}$ = a frequency of very high attenuation in the high frequency attenuating band
R = load resistance, i.e., ideal real image impedance of a T-section filter
L = mechanical or acoustical, mass
C = mechanical or acoustical, compliance
m = $\left[1-\left(\frac{f\infty}{f_\alpha}\right)^2\right]^{1/2}$; , $\alpha = 1$ or 2

Table of Parameters [11]. F. E. Terman, *Radio Engineers Handbook* (1st ed) (1943), ©1943 McGraw-Hill Book Co.; by permission.

These formulas apply for both end and Type I sections

$$g=\sqrt{\left(1-\frac{f_1^2}{f_{1\infty}^2}\right)\left(1-\frac{f_1^2}{f_{2\infty}^2}\right)}$$

$$h=\sqrt{\left(1-\frac{f_1^2}{f_{2\infty}^2}\right)\left(1-\frac{f_2^2}{f_{2\infty}^2}\right)}$$

$$m_1=\frac{\frac{f_1f_2}{f_{2\infty}^2}g+h}{1-\frac{f_1^2}{f_{2\infty}^2}} \qquad m_2=\frac{g+\frac{f_{1\infty}^2}{f_1f_2}h}{1-\frac{f_{1\infty}^2}{f_{2\infty}^2}}$$

$$a=\frac{(1-m_1^2)f_{2\infty}^2}{4gf_1f_2}\left(1-\frac{f_{1\infty}^2}{f_{2\infty}^2}\right)=\frac{(1-m_2^2)f_1f_2}{4gf_{1\infty}^2}\left(1-\frac{f_{1\infty}^2}{f_{2\infty}^2}\right)$$

$$b=\frac{(1-m_2^2)}{4g}\left(1-\frac{f_{1\infty}^2}{f_{2\infty}^2}\right) \qquad c=\frac{(1-m_1^2)}{4h}\left(1-\frac{f_{1\infty}^2}{f_{2\infty}^2}\right)$$

$$d=\frac{(1-m_1^2)f_{2\infty}^2}{4hf_1f_2}\left(1-\frac{f_{1\infty}^2}{f_{2\infty}^2}\right)=\frac{(1-m_2^2)f_1f_2}{4hf_{1\infty}^2}\left(1-\frac{f_{1\infty}^2}{f_{2\infty}^2}\right)$$

when $(m_1 = m_2)$,

$$g=h,\ a=d,\ b=c,\ f_{1\infty}=\frac{f_1f_2}{f_{2\infty}},\ m_1=m_2=\frac{h}{1-\frac{f_1f_2}{f_{2\infty}^2}}$$

and

$$f_{2\infty}^2=\frac{f_1^2+f_2^2-2m^2f_1f_2}{2(1-m^2)}+\left[\left(\frac{f_1^2+f_2^2-2m^2f_1f_2}{2(1-m^2)}\right)^2-f_1^2f_2^2\right]^{1/2}$$

D 1. Design of Low-Pass Mechanical-Acoustical Filters

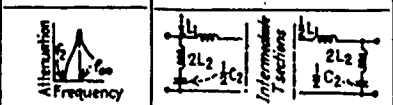
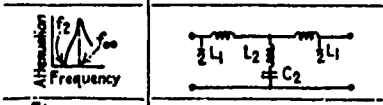
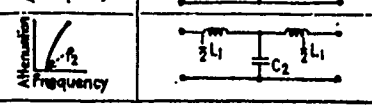
The following Table 2.28.1 gives the essential formulas for the design of low-pass mechanical-acoustical filters:

Table 2.28.1 [11]. F. E. Terman, *Radio Engineers Handbook* (1st ed) (1943), ©1943 McGraw-Hill Book Co.; by permission.

R = load resistance f_2 = cut-off frequency (highest frequency transmitted) f_∞ = a frequency of very high attenuation

$$L_k = \frac{R}{\pi f_2} \qquad C_k = \frac{1}{\pi f_2 R} \qquad m = \sqrt{1 - \left(\frac{f_2}{f_\infty}\right)^2}$$

Design of Sections

Type	Attenuation characteristic	A. Filters having T intermediate sections	
		Configuration	Formulas
End (m of approximately 0.6)			$L_1 = mL_k$ $L_2 = \frac{1 - m^2}{4m} L_k$ $C_2 = mC_k$
I			$L_1 = mL_k$ $L_2 = \frac{1 - m^2}{4m} L_k$ $C_2 = mC_k$
II ($U_\infty = \infty$)			$L_1 = L_k$ $C_2 = C_k$

The calculation procedure is illustrated by the following example.

Example 1.

Design a single T-section low-pass acoustical wave filter with a cut-off frequency of 50 Hz for a design (image) impedance of 10^4 MKS acoustic ohms.

We begin by noting that since $R = \pi f_2 L_K$ and $C_K = \frac{1}{\pi f_2 R}$ one has,

$$f_2 = \frac{1}{\pi \sqrt{C_K L_K}}$$

and

$$R = \sqrt{\frac{L_K}{C_K}}; \; L_K = C_K R^2.$$

Thus,

$$C_K = \frac{1}{\pi f_2 R} = \frac{1}{\pi \times 50 \times 10^4} = 6.37 \times 10^{-7} \quad \text{(units: } \mathrm{m^5/N)}$$

$$L_K = C_K R^2 = 6.37 \times 10^{-7} \times (10^4)^2 = 63.7 \quad \text{(units: } \mathrm{Ns^2/m^5} = \frac{\mathrm{kg}}{\mathrm{m^4}}).$$

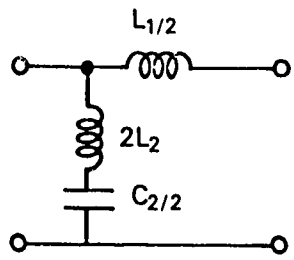
Assume $m \sim 0.6$, that is, assume

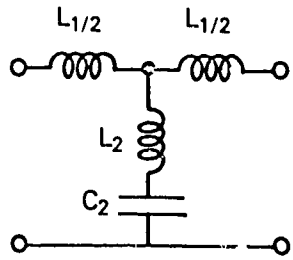
$$1 - \left(\frac{f_\infty}{f_2}\right)^2 = m^2 = 0.36$$

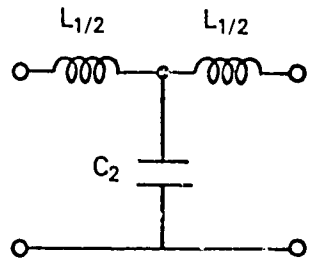
so that,

$$\frac{f_\infty}{f_2} = \sqrt{1 - 0.36} = 0.8.$$

Using Table 2.28.1 we summarize the circuit parameters needed for each type:







$L_1 = 0.6 \times 73.7 = 38.2 \frac{\text{kg}}{\text{m}^4}$

$L_2 = \frac{1 - .6^2}{4 \times .6} \times 63.7 = 16.98 \frac{\text{kg}}{\text{m}^4}$

$C_2 = 0.6 \times 63.7 \times 10^{-7} = 38.2 \times 10^{-7} \frac{\text{m}^5}{\text{N}}$

$L_1 = 0.6 \times 63.7 = 38.2 \frac{\text{kg}}{\text{m}^4}$

$L_2 = \frac{1 - .6^2}{4 \times 0.6} 63.7 = 17.0 \frac{\text{kg}}{\text{m}^4}$

$C_2 = 0.6 \times 63.7 \times 10^{-7} = 38.2 \times 10^{-7}\ \text{m}^5/\text{N}$

$L_1 = 63.7\ (\text{kg/m}^4)$

$C_2 = 63.7 \times 10^{-7}\ (\text{m}^5/\text{N})$

A physical embodiment of a low-pass acoustical filter consists of a hollow vessel with a circular hole. The acoustic mass M_A is the small volume (of air) that moves into and out of the hole when the cavity is excited to vibrate at a specific frequency. Its magnitude is given by

$$M_A = \frac{\rho_0 [l' + l'']}{\pi a^2} \quad (\text{units: } \text{Ns}^2/\text{m}^5)$$

l' = actual depth of hole

l'' = end correction of hole

a = radius of hole.

In the present case we choose $l' = 0$ and $l'' = 0.85a$ [5]. Then

$$63.7 = 1.18 \frac{\text{kg}}{\text{m}^3} \times \frac{0.85}{\pi\ a} \frac{1}{(\text{m})} = \frac{0.319}{a}$$

or $a = 5 \times 10^{-3}$ meter.

The volume of the cavity is determined from the bulk modules K.

$$C_A = \frac{\text{V}}{k} = \frac{\text{V}}{\gamma P_0}$$

$$\text{or } V = 63.7 \times 10^{-7} \left(\frac{\text{m}^5}{\text{N}}\right) \times 1.4 \times 10^5 \frac{\text{N}}{\text{m}^2} = 0.89 \text{ m}^3.$$

A possible filter structure embodying these parameters is shown in Fig. 2.28.4.

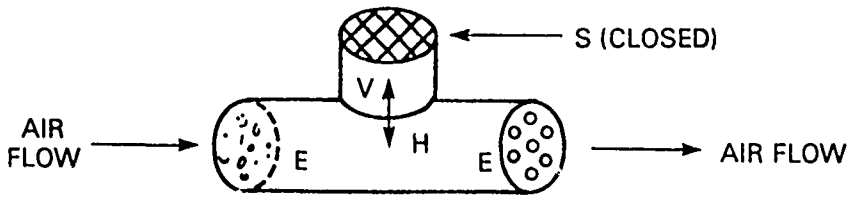


Fig. 2 28.4 — A low pass acoustical filter (type II) [5]

In this figure the mass component of the filter resides in the hole at H and at the holes at E, while the compliance component resides in closed volume V. The image impedance (resistance) resides in the holes E.

A Type I low-pass filter may be constructed along similar lines. The holes E in this case are relocated in hole H. This places acoustic mass in the shunt branch.

D 2. Design of High-Pass Mechanical-Acoustic Filters

Table 2.28.2 gives the essential formulas for the design of high-pass acoustical filters. We illustrate its use with an example:

Table 2.28.2 [after 11]. F. E. Terman, *Radio Engineers Handbook* (1st ed) (1943), ©1943 McGraw-Hill Book Co.; by permission.

Fundamental Relations

R_L = load resistance f_1 = cut-off frequency (lowest frequency transmitted) f_∞ = a frequency of very high attenuation

$$L_k = \frac{R}{4\pi f_1} \qquad C_k = \frac{1}{4\pi f_1 R} \qquad m = \sqrt{1 - \left(\frac{f_\infty}{f_1}\right)^2}$$

Design of Sections

Type	Attenuation characteristic	A. Filters having T intermediate sections	
		Configuration	Formulas
End (m of approximately 0.6)	Attenuation, f_∞, f_1, Frequency	$2C_1$, $2L_2$, $\frac{1}{2}C_2$, Intermediate T sections, $2C_1$, $2L_2$, $\frac{1}{2}C_2$	$C_1 = \frac{C_k}{m}$; $C_2 = \frac{4m}{1-m^2}C_k$; $L_1 = \frac{L_k}{m}$
I	Attenuation, f_∞, f_1, Frequency	$2C_1$, $2C_1$, L_2, C_2	$C_1 = \frac{C_k}{m}$; $C_2 = \frac{4m}{1-m^2}C_k$; $L_1 = \frac{L_k}{m}$
II $f_\infty = 0$	Attenuation, f_1, Frequency	$2C_1$, L_2, $2C_1$	$C_1 = C_k$; $L_1 = L_k$

Example 2.

Design a high-pass T-section acoustical filter to cut off at $f_1 = 150$ Hz and to be heavily attenuated at $f_\infty = 0.8(150) = 120$ Hz. The image impedance should be $R = 10^3$ MKS ohms.

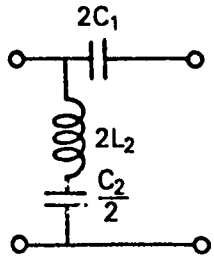
The calculated parameters are:

$$C_K = \frac{1}{4\pi f_1 R} = \frac{1}{4\pi \times 150 \times 10^3} = 5.3 \times 10^{-7}\ \text{m}^5/\text{N}.$$

$$L_K = \frac{R}{4\pi f_1} = \frac{10^3(\text{Ns/m}^5)}{4\pi\ 150\left(\frac{1}{5}\right)} = 0.53\ \frac{\text{NS}^2}{\text{m}^5}$$

$$m = 0.6.$$

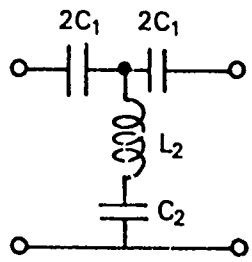
The parameters for each type are:



$C_1 = 8.83 \times 10^{-7}\ \text{m}^5/\text{N}$

$C_2 = \frac{4 \times .6}{1 - .6^2} \times 5.3 \times 10^{-7}$
$= 1.99 \times 10^{-7}\ \text{m}^5/\text{N}$

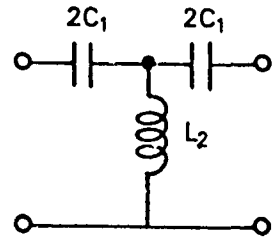
$L_2 = \frac{0.53}{.6} = 0.88\ \frac{\text{Ns}^2}{\text{m}^5}$



$C_1 = \frac{5.3 \times 10^{-7}}{0.6} = 8.83 \times 10^{-7}\ \text{m}^5/\text{N}$

$C_2 = \frac{4 \times .6}{1 - .6^2} \times 5.3 \times 10^{-7}$
$= 1.99 \times 10^{-7}\ \text{m}^5/\text{N}$

$L_2 = \frac{0.53}{.6} = 0.88\ \frac{\text{Ns}^2}{\text{m}^5}$



$C_1 = 5.3 \times 10^{-7}\ \text{m}^5/\text{N}$

$L_2 = 0.53\ \frac{\text{Ns}^2}{\text{m}^5}$

Figure 2.28.4 may also serve as a high-pass acoustic filter (Type II) by opening the side-branch (= area S).

D 3. Design of Band-Pass Mechanical Acoustical Filters

Table 2.28.3 gives the essential formulas for the design of band-pass acoustical filters. We illustrate its use with an example:

Example 3.

Design a Type II band-pass T-section acoustical filter to pass all frequencies from $f_1 = 100$ Hz to $f_2 = 300$ Hz. Let the image impedance $(R) = 10^4$ MKS ohms. The calculated parameters are:

$$L_1 = \frac{f_1 R}{\pi f_2 (f_2 - f_1)} = \frac{100 \times 10^4}{\pi\ 200(100)} = 15.9\ \frac{\text{NS}^2}{\text{m}^5}$$

$$L_2 = \frac{(f_1 + f_2)R}{4\pi f_1 f_2} = \frac{300 \times 10^4}{4\pi 100 \times 200} = 11.93\ \frac{\text{Ns}^2}{\text{m}^5}$$

$$C_1 = \frac{f_2 - f_1}{4\pi f_1 f_2 R} = \frac{200 - 100}{4\pi 100 \times 200 \times 10^4} = 3.98 \times 10^{-8}\ \text{m}^5/\text{N}.$$

Table 2.28.3 [after 11]. F. E. Terman, *Radio Engineers Handbook* (1st ed) (1943), ©1943 McGraw-Hill Book Co.

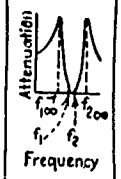
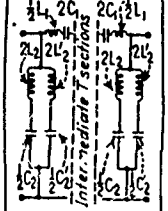
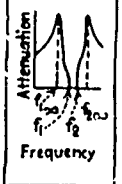
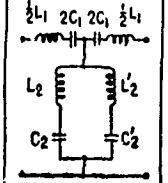
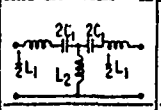
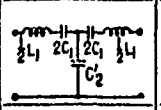
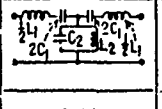
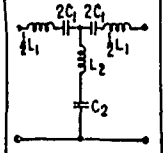
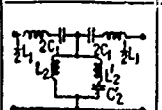
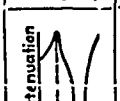
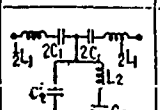
Fundamental Relations

R = load resistance f_1 = lower frequency limit of pass band f_2 = higher frequency limit of pass band

$f_{1\infty}$ = a frequency of very high attenuation in low-frequency attenuating band $f_{2\infty}$ = a frequency of very high attenuation in high-frequency attenuating band

$$L_{1k} = \frac{R}{\pi(f_2 - f_1)} \qquad L_{2k} = \frac{(f_2 - f_1)R}{4\pi f_1 f_2} \qquad C_{1k} = \frac{f_2 - f_1}{4\pi f_1 f_2 R} \qquad C_{2k} = \frac{1}{\pi(f_2 - f_1)R}$$

Design of Sections

Type	Attenuation characteristic	A Filters having T intermediate sections: Configuration	Formulas	
End ($m_1 = m_2$ = approximately 0.6)			$L_1 = m_1 L_{1k}$ $L_2 = aL_{1k}$ $L_2' = eL_{1k}$ $C_1 = \frac{C_{1k}}{m_2}$ $C_2 = \frac{C_{1k}}{b}$ $C_2' = \frac{C_{1k}}{d}$	
I			$L_1 = m_1 L_{1k}$ $L_2 = aL_{1k}$ $L_2' = eL_{1k}$ $C_1 = \frac{C_{1k}}{m_2}$ $C_2 = \frac{C_{1k}}{b}$ $C_2' = \frac{C_{1k}}{d}$	
II $f_{1\infty} = 0$ $f_{2\infty} = f_2$			$L_1 = \frac{f_1 R}{\pi f_2(f_2 - f_1)}$ $L_2 = \frac{(f_1 + f_2)R}{4\pi f_1 f_2}$ $C_1 = C_{1k}$	
III $f_{1\infty} = f_1$ $f_{2\infty} = \infty$			$L_1 = L_{1k}$ $C_2' = \frac{1}{\pi(f_1 + f_2)R}$ $C_1 = \frac{f_2 - f_1}{4\pi f_1 f_2 R}$	
IV $f_{1\infty} = 0$ $f_{2\infty} = \infty$			$L_1 = L_{1k}$ $L_2 = L_{1k}$ $C_1 = C_{1k}$ $C_2 = C_{1k}$	
V $f_{1\infty} = f_1$			$L_1 = m_1 L_{1k}$ $L_2 = \frac{(1 - m_1^2)}{4m_1} L_{1k}$ $C_1 = \frac{C_{1k}}{m_2}$ $C_2 = \frac{4m_2}{1 - m_2^2} C_{1k}$ See notation for m_1 and m_2	$m_1 = \frac{f_1}{f_2} m_2$ $m_2 = \sqrt{\frac{1 - \frac{f_1^2}{f_{1\infty}^2}}{1 - \frac{f_1^2}{f_2^2}}}$
VI $f_{1\infty} = f_1$		Same circuit as above for Type V	Same formulas as above for Type V. See notation for m_1 and m_2	$m_1 = \sqrt{\frac{1 - \frac{f_2^2}{f_{2\infty}^2}}{1 - \frac{f_1^2}{f_{2\infty}^2}}}$ $m_2 = \frac{f_1}{f_2} m_1$
VII $f_{1\infty} = 0$			$L_1 = m_1 L_{1k}$ $L_2 = aL_{1k}$ $L_2' = \frac{(1 - m_1^2)}{4h} L_{1k}$ $C_1 = C_{1k}$ $C_2' = \frac{h}{a} C_{1k}$	$h = \sqrt{\left(1 - \frac{f_1^2}{f_{1\infty}^2}\right)\left(1 - \frac{f_2^2}{f_{2\infty}^2}\right)}$ $m_1 = \frac{f_1 f_2}{f_{2\infty}^2} + h$ $a = \frac{(1 - m_1^2) f_{2\infty}^2}{4 f_1 f_2}$
VIII $f_{2\infty} = \infty$			$L_1 = L_{1k}$ $L_2 = \frac{d}{g} L_{1k}$ $C_1 = \frac{C_{1k}}{m_2}$ $C_2 = \frac{4g}{1 - m_2^2} C_{1k}$ $C_2' = \frac{C_{1k}}{g}$	$g = \sqrt{\left(1 - \frac{f_1^2}{f_{1\infty}^2}\right)\left(1 - \frac{f_1^2}{f_2^2}\right)}$ $m_2 = g + \frac{f_1^2}{f_1 f_2}$ $d = \frac{(1 - m_2^2) f_1 f_2}{2 f_{1\infty}^2}$

A physical embodiment of this filter is shown in Fig. 2.28.5.

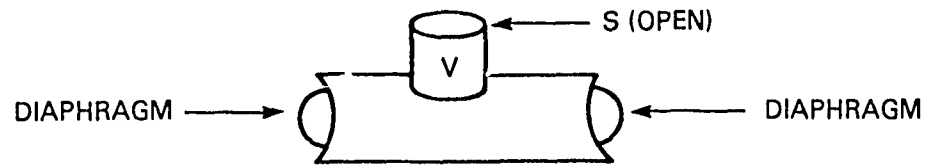


Fig. 2.28.5 — A band pass acoustic filter

Acoustic Filters and Bond Graphs

Acoustic filters which consist of cascades of tubes and cavities are customarily designed by use of lumped parameter equivalent circuits in which the relations between pressure and flow are assumed linear. Such models are valid for low flow rates and small pressure differentials. High flow rates and high pressure levels require nonlinear theory for accurate prediction of filtering capability. Nonlinear theory is difficult to apply in practice, and one is reduced to making modifications to linear theory by use of a simple perturbation of the formulas, often leading to numerical and graphical procedures for obtaining results.

The extension of lumped parameter (linear) theory to distributed parameter (linear theory) increases the validity of analysis in frequency ranges where lumped parameter theory fails. The extension is carried out by use of normal modes. In applications where one-dimensional analysis is satisfactory, and where only a few normal modes are adequate to extend the frequency range as needed, a representation of the filter by bond graphis should prove useful. The theory of these filters of extended frequency range has been developed by Karnopp [13] and is presented now.

Assume a pipe flow in which the pressure distribution $p(x, t)$ and the acceleration of flow $Q(x, t)$ per unit of length is adequately described by the set of second-order integral-differential equations.

$$\text{(a)}\ \rho_0 C^2 \frac{\partial^2 Q}{\partial x^2} - \rho_0 \frac{\partial^2 Q}{\partial t^2} = -\frac{\partial f(x, t)}{\partial t} + \rho_0 C^2 \frac{\partial q}{\partial x} \tag{2.28.19}$$

$$\text{(b)}\ \frac{\partial^2 p}{\partial x^2} - \frac{1}{C^2}\frac{\partial^2 p}{\partial t^2} = -\frac{\rho_0}{S}\frac{\partial q}{\partial t} + \frac{\partial f}{\partial x}$$

ρ_0	=	mass density (Ns^2/m^4)
C	=	speed of sound (m/s)
Q	=	volume flow (m^3/s)
f	=	applied force per unit length (N/m)
q	=	injected volume flow per unit of length ($m^3/s \cdot m$)
p	=	fluid pressure (N/m^2)

A solution of Eq. (a) in normal modes is obtained by setting $q = 0$ and writing,

$$Q = \sum_{n=0}^{\infty} G_n(x)\, \xi_n(t)$$

in which the units of $\xi_n(t)$ are m^3/s, and the G_n is dimensionless. To determine $G_n(x)$ we make the pipe to have rigid walls and assume the pipe pressure does not fluctuate with time at the ends of the pipe. From the equation of mass continuity of flow, it is seen that $\partial Q/\partial x = 0$ at the ends. Hence

$$G_n(x) = \cos \frac{n\pi x}{l}.$$

The eigenvalue problem posed by Eq. (a) thus has the solution,

$$\frac{\partial^2 G_n(x)}{\partial x^2} = \lambda_n G_n(x)$$

$$\lambda_n = -\left(\frac{n\pi}{l}\right)^2$$

in which G_n is orthogonal over the range $x = 0$ to $x = l$, with normalization $l\epsilon_{nm}$, where

$$\begin{cases} \epsilon_{nm} = 0 \text{ if } r \neq m, \\ \epsilon_{nm} = 1 \text{ if } n = m = 0 \\ \epsilon_{nm} = \frac{1}{2} \text{ if } n \end{cases}$$

Eq. (a) therefore becomes,

$$\rho_0 C^2 \sum_{n=0}^{\infty} (-) \left(\frac{n\pi}{l}\right)^2 G_n(x)\, \xi_n(t) - \rho_0 \sum_{n=0}^{\infty} G_n(x)\, \ddot{\xi}_n(t) = -\frac{\partial f}{\partial t}.$$

Multiplying through by $G_m(x)$ and integrating over $0 \leqslant x \leqslant l$, one obtain

$$\rho_0 C^2 \left(\frac{n\pi}{l}\right)^2 l\epsilon_{mn}\, \xi_n(t) + \rho_0\, l_{\epsilon mn} \ddot{\xi}_n(t) = \int_0^l \frac{\partial f}{\partial t} \cos \frac{n\pi x}{l}\, dx.$$

Choose the forcing function to be

$$f = S\,\{p_0 \delta(x) - p_l\, \delta(x - l)\}$$

in which S is the cross-sectional area of the pipe. Performing the integration over x, then integrating the entire expression over time lead to the set of formulas,

$$\text{for } n = m = 0: \quad \frac{\rho_0 l}{S} \dot{\xi}_0(t) = p_0 - p_l$$

$$\text{for } n > 0: \quad \rho_0 C^2 \frac{n^2\pi^2}{2lS} \int^t \xi_n(t)\, dt + \frac{\rho_0 l}{2S} \dot{\xi}_n(t) = p_0 \delta(x) - p_l(-1)^n. \tag{2.28.20}$$

The coefficients multiplying $\dot{\xi}_n$ are *acoustic* masses (units: Ns^2/m^5) and the coefficient multiplying ξ_n are *acoustic* capacitances (units: m^5/N). It is seen that for the zeroth-order mode the pipe acts as a pure inertance while for modes 1, 2 .... the pipe acts as a combined inertance and capacitance.

The bond graph corresponding to these equations is shown in Fig. 2.28.6.

In sum: solution of the equation in flow Q when driven by forces has led to the existence of modes in a long pipe, characterized by inertance of mass flow accompanied by capacitance in the higher order modes.

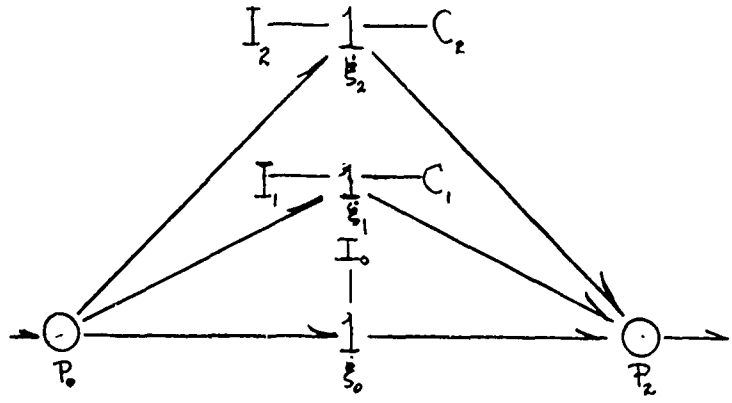


Fig. 2.28.6 — Bond graph of a pipe flow with normal modes

$TF_1 = \cos \frac{\pi x_1}{l}$; $TF_2 = \cos \frac{\pi x_2}{l}$

$TF_3 = \cos \frac{2\pi x_1}{l}$; $TF_4 = \cos \frac{2\pi x_2}{l}$

One turns now to a solution of Eq. 2.28.19 (b) in the pressure distribution $p(x, t)$ of a long cavity. For simplicity assume $\partial f/\partial x = 0$, and let the flow injection between $x = x_1$, and $x = x_2$ be

$$q = Q_1 \delta(x - x_1) - Q_2 \delta(x - x_2).$$

At the ends of the cavity let the flow vanish. Then $\partial p/\partial x = 0$ at the ends. Assume a solution in modes,

$$p = \sum_{n=0}^{\infty} H_n(x)\eta_n(t)$$

in which the mode shapes satisfy the boundary conditions

$$H_n(x) = \cos \frac{n\pi x}{x}.$$

The eigenvalue problem is again,

$$\frac{\partial^2 H_n(x)}{\partial x^2} = \lambda_n H_n(x) = -\left(\frac{n\pi}{l}\right)^2.$$

As before, $H_n(x)$ is orthogonal in the interval $0 \leqslant x \leqslant l$ with normalization $l\epsilon_{mn}$. For each mode Eq. (b) reduces to,

$$\left(\frac{n\pi}{l}\right)^2 l\epsilon_{mn}\,\eta_n(t) + \frac{1}{C^2}\, l\epsilon_{mn}\ddot{\eta}_n(t) = \int_0^l [\dot{Q}_1\delta(x - x_1) - \dot{Q}_2\delta(x - x_2)] \cos \frac{n\pi x}{l}.$$

Performing the integration over x, then integrating the entire result over t one obtains:

$$\text{for } n = m = 0: \quad \frac{S}{\rho_0}\,\frac{l}{C^2}\,\dot{\eta}_n(t) = Q_1 - Q_2 \tag{2.28.21}$$

$$\text{for } n = m \neq 0: \quad \frac{Sl}{2\rho_0 C^2}\,\dot{\eta}_n(t) + \frac{n^2\pi^2}{2l}\,S\int^t \eta_n(t)\,dt = Q_1 \cos \frac{n\pi x_1}{l} - Q_2 \cos \frac{n\pi x_2}{l}.$$

Thus the pressure distribution in the long cavity, when driven by injection of massflow, is described by modes characterized in the lowest order by capacitance $C = Sl/\rho_0 C^2$ (units: m^5/N), and by capacitance $2Sl/\rho_0 C^2$ accompanied by inertance $I = 2\rho_0 l/n^2\pi S$ (units: Ns^2/m^5) in the higher order modes. The bond graph corresponding to these equations is formed by writing them in the form,

$$\left(C\frac{d}{dt} + \frac{1}{I}\int \ldots dt\right)\eta_n^{(t)} + Q_2 \cos\frac{n\pi x_2}{l} = Q_1 \cos\frac{n\pi x_1}{l}. \qquad (2.28.22)$$

In electrical terms, using the current/fluid flow analogy this is seen to be a modal equation in which Q is in series position and pressure (i.e., η) is in shunt position. The bond graph reduces to the following structure, Fig. 2.28.7.

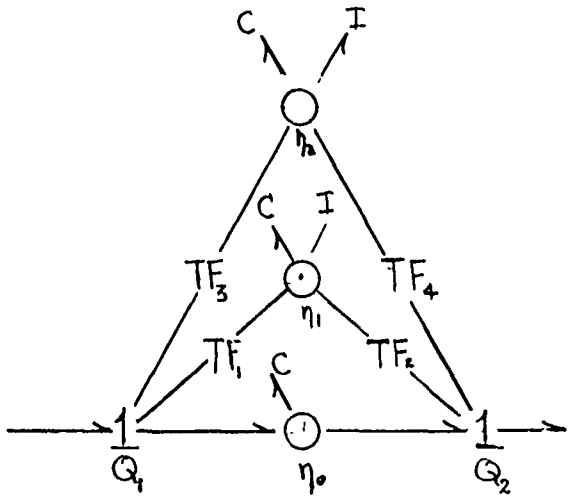
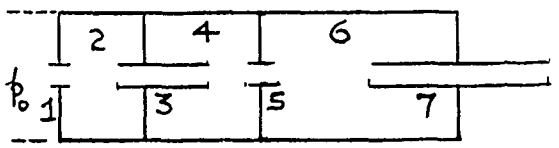


Fig. 2.28.7 — Bond graph of pressure/flow in a long cavity

Figures in combination allow to construct lumped parameter models of acoustic filters using normal modes. An example illustrates the procedure.

Example: Figure 2.28.8 shows an acoustic filter with three cavities and four tubes. Cavity 2 and pipes 1 and 5 are 'short,' while cavities 4, 6 and tubes 3, 7 are 'long.' The corresponding bond graph is shown in Fig. 2.28.9.

Fig. 2.28.8 — A fluid filter



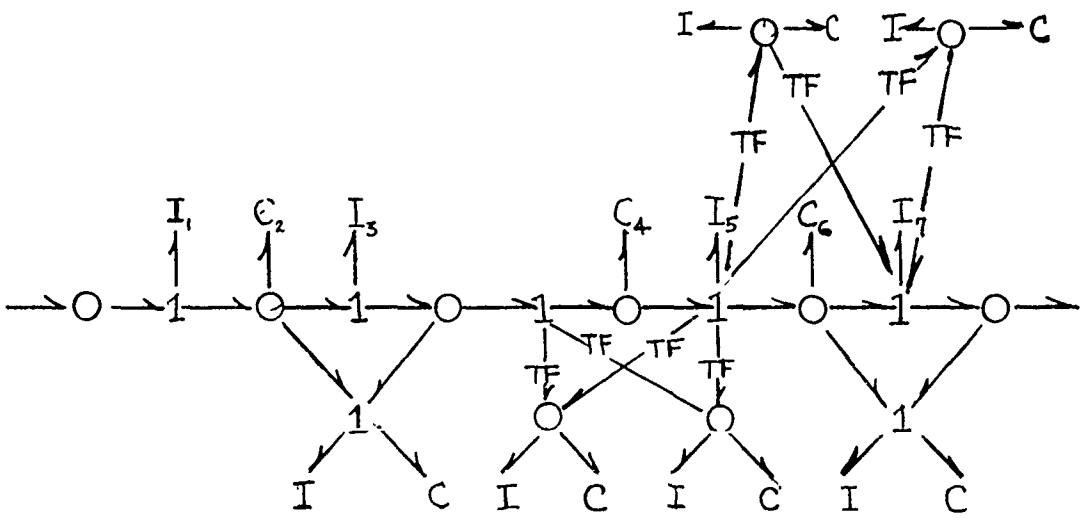


Fig 2.28.9 — Bond graph of Fig. 2.28.8

It is noted that the sequence $q_3 - p_4 - q_3 - p_4$ is used to simplify the readibility of the graph. Since the second q_3 has no multiport attached to it directly, it is a redundant dummy, inserted for pure convenience.

2.29 THEORY OF ACOUSTICAL AND MECHANICAL TRANSMISSION LINES

The design of acoustic transducers is often facilitated by use of analysis based on transmission line theory. This design aid is treated below.

Case I. Lumped Parameter Transmission Lines

In Sect. 2.28 the characteristics of acoustic wave filters were discussed in detail. Key points in the discussion are reviewed here to provide an introduction to mechanical transmission lines.

Figure 2.29.1 shows a section of a transmission line with an opening A, a construction B, and a shunt volume D. Its equivalent circuit is based on a FV analogy—that is, pressure p is chosen to be the across variable and volume velocity u the through variable. In accordance with procedures already elucidated the equivalent circuit is constructed in these steps:

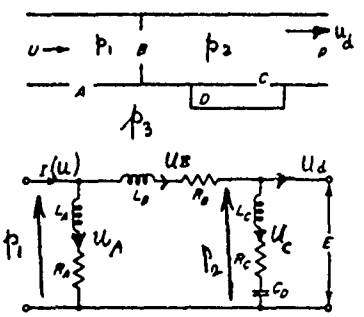


Fig. 2.29.1 — Lumped parameter representation of elements of acoustic transmission lines

(1) the degrees of freedom to be used in analysis are first determined. Here there are three, namely volume velocities u_A, u_B, u_C. A fourth u_d is used below, but it is set to zero upon allowing the equivalent circuit to be open-circuited.

(2) the number of acoustic pressures to be used is determined. Here there are three, p_1, p_2, $p_3 = p_G$.

(3) the acoustic pressures are related to the volume velocities through acoustical impedances:

$$p_1 - p_3 = Z_A u_A \tag{2.29.1}$$

$$p_1 - p_2 = Z_B u_B \tag{2.29.2}$$

$$p_2 - p_3 = Z_C u_C \tag{2.29.3}$$

(4) the acoustic volume velocities are related to the acoustic pressures through acoustical admittances:

$$u_A - u_B = Y_A(p_1 - p_3) \tag{2.29.4}$$

$$u_B - u_d = Y_C(p_2 - p_3) \tag{2.29.5}$$

$$u_B = Y_B(p_1 - p_2). \tag{2.29.6}$$

To illustrate the method of obtaining the equivalent circuit let us assume p_3 is a reference pressure, taken here to be zero and let us set $u_d = 0$, as before . Then

$$p_1 = Z_A u_A \tag{2.29.7}$$

$$p_1 - p_2 = Z_B u_B \tag{2.29.8}$$

$$p_2 = Z_c u_c \tag{2.29.9}$$

$$u_A - u_B = Y_A p_1 \tag{2.29.10}$$

$$u_c = Y_c p_2 \tag{2.29.11}$$

$$u_B = u_c = Y_B(p_1 - p_2). \tag{2.29.12}$$

An interpretation of these equations on the basis of an *FV* analogy leads directly to the equivalent circuit. For example, Eqs. 2.29.7, 2.29.9 are statements of *single* pressures p_1, p_2. These are construed as branches acting as across-variables, hence are placed in shunt position. In contrast Eq. 2.29.8 is a statement involving *two* pressures. It is therefore a coupling (that is, a series) branch. This series branch and the parallel branches are inserted in their proper places, leading to the circuit constructed in the manner shown in Fig. 2.29.1. In a second example a simple periodic acoustic transmission line is shown in Fig. 2.29.2. Following the previously outlined procedure one finds the pressures and volume velocities to be:

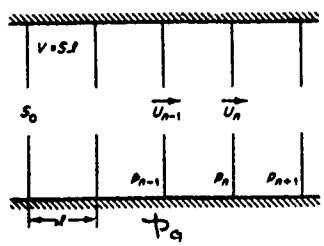


Fig. 2.29.2 — Illustrative sketch of a periodic acoustic transmission line

$$p_{n-1} - p_n = Z_{n-1}\, u_{n-1} \tag{2.29.13}$$

$$p_n - p_{n+1} = Z_n\, u_n \tag{2.29.14}$$

.

.

.

$$u_{n-1} - u_n = Y_n(p_n - p_G) \tag{2.29.15}$$

$$u_n - u_{n+1} = Y_{n+1}(p_{n+1} - p_G) \tag{2.29.16}$$

In the E/p, I/u analogy an FV equivalent circuit, Fig. 2.29.3a,b, is easily constructed. In it we take $p_G = 0$.

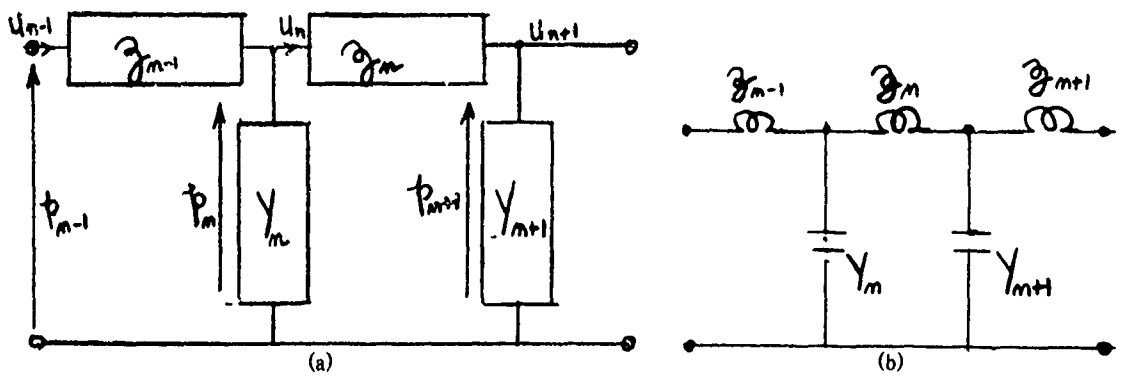


Fig. 2.29.3 — A section of the FV equivalent circuit of Fig. 2.29.2, (a) black-box description, (b) electrical equivalents based on mass/inductance, spring/capacitance analogies

These examples, though simple, show the desirability of using the FV analogy in modeling lumped-parameter *acoustic* transmission lines.

We next turn to a mechanical lumped parameter transmission line, Fig. 2.29.4. Here k_n is a spring constant, M_n is a mass and b_n is a damping coefficient. As before, we analyze this line by first selecting the degrees of freedom x_0, x_1, x_2 .... The equations of force and velocity are:

$$\begin{aligned} \dot{x}_0 - \dot{x}_1 &= y_1 F_1 \\ \dot{x}_1 - x_2 &= y_2 F_2 \\ &\cdot \\ &\cdot \\ &\cdot \end{aligned} \tag{2.29.17}$$

$$\begin{aligned} F_1 - F_2 &= z_1(x_1 - \dot{x}_G) \\ F_2 - F_3 &= Z_2(\dot{x}_2 - \dot{x}_G) \\ &\cdot \\ &\cdot \\ &\cdot \end{aligned} \tag{2.29.18}$$

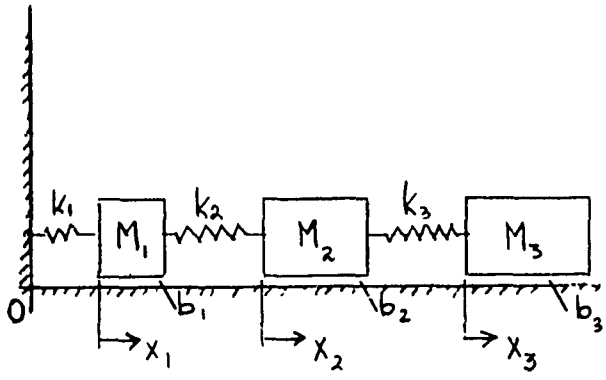


Fig. 2.29.4 — Illustrate sketch of a short mechanical transmission line

To interpret these relations as describing an equivalent circuit we consider first the *arbitrary* choice of analogy. We let velocity be the across-variable and force the through-variable (= *VF* anology). Then Eqs. 2.29.17 are each interpreted as voltage = impedance × current. Thus the mechanical admittances y_1, y_2 ... are seen to be all in series position on this *VF* chart, Fig. 2.29.5. In contrast Eqs. 2.29.18 are each interpreted as current = admittance × voltage. Thus the mechanical impedances z_1, z_2 ... are all in shunt position on this *VF* chart, as shown in Fig. 2.29.5.

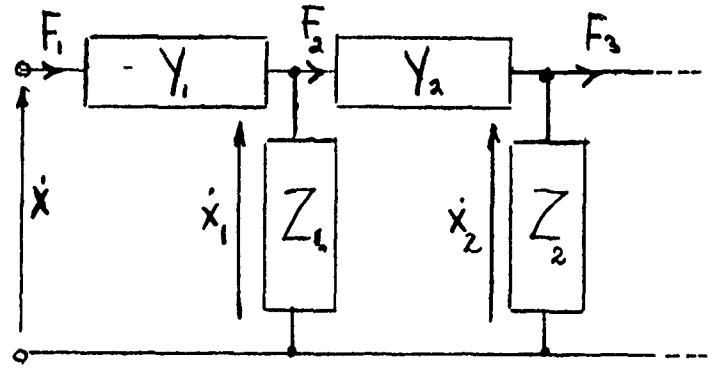


Fig. 2.29.5 — A VF black-box description of the mechanical transmission line in Fig. 2.29.4

The admittances y and impedances z can be assigned specific electrical symbols. Noting that

$$y_1 = \frac{-i\omega}{k_1};\ y_2 = \frac{-i\omega}{k_2} \ldots . \tag{2.29.19}$$

one can interpret these as electrical inductances

$$L_1 = k_1^{-1};\ L_2 = K_2^{-1},\ \ldots . \tag{2.29.20}$$

Also, since

$$Z_1 = i\omega M_1 + b_1;\ z_2 = -i\omega M_2 + b_2;\ \ldots . \tag{2.29.21}$$

one can interpret these symbols as electrical admittance in which mass is capacitance, and damping is conductance:

$$M_1 = C_1 b_1 = G_1;\ M_2 = C_2, b_2 = G_2 \ldots . \tag{2.29.22}$$

Thus the electric circuit equivalent of Fig. 2.29.5 with these explicit electrical symbols can be displayed as Fig. 2.29.6.

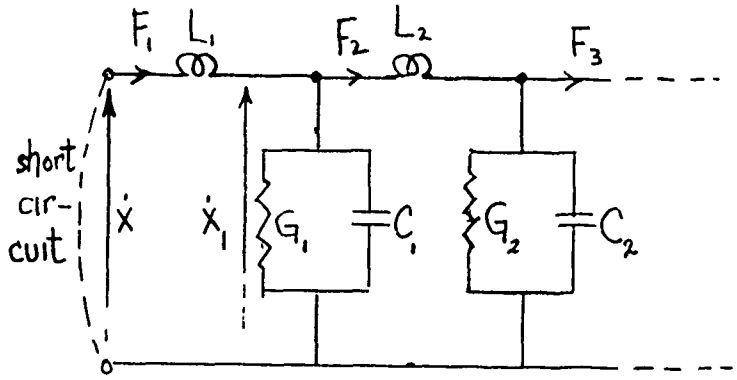


Fig. 2.29.6 — An electrical equivalent circuit of the mechanical transmission line, Fig. 2.29.4, in VF form (velocity across, force through)

The dual of this circuit is constructed by changing the interpretation of the basic equations. We first make the choice that force is the across-variable and velocity is the through-variable in a *FV* chart. Equations 2.29.18 are the interpreted as voltage = impedance × current. This places all the mechanical impedances z in series position on the *FV* chart, Fig. 2.29.7. Similarly, Eqs. 2.29.17 can be interpreted as current = admittance × voltage. This places all the mechanical admittances y in shunt position on the *FV* chart. The equivalent electrical symbols in such a construction are:

$$\frac{1}{K_1} = C_1;\ \frac{1}{K_2} = C_2 \ldots.$$

$$M_1 = L_1,\ b_1 = R_1;\ M_2 = L_2, b_2 = R_2 \ldots.$$

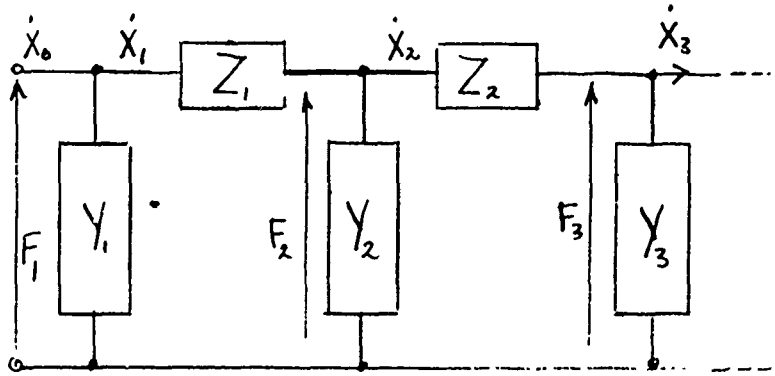


Fig. 2.29.7 — FV black-box description of Fig. 2.29.4

Using them one arrives at the electrical equivalent circuit in *VF* form, Fig. 2.29.8.

Case II: Travelling Wave Transmission Line [6a]

The importance of transmission line theory in the design of acoustic transducers leads one to expand the theory to include fluid transmission lines a they appear in hydraulic circuits. The following is a discussion of the chief concepts of this theory.

The transmission of power in a 1-dimensional transmission line can be modeled as a pair of first-order partial differential equations. While the exact form of these equations depends on the choice of power variables the derivation and final results of these equations follow a general pattern which is independent of which variable are chosen.

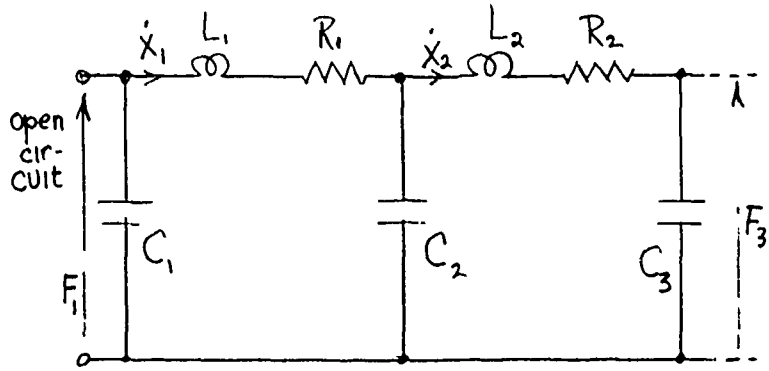


Fig. 2.29.8 — An electrical equivalent circuit in FV form of Fig. 2.29.4 based on mass/inductance, spring/capacitance analogy

To illustrate the method we consider the flow of fluid in a long, uniform diameter, frictionless pipe. The power variable in this case are total fluid pressure P (units: N/m^2) and fluid flow $\mathscr{V}(m^3/s)$. For a fluid in motion $P = p + wz + \rho V^2/2$ which is Bernoulli's equation), in which p is the thermodynamic pressure, w the weight density, z is the elevation above a datum plane, ρ the mass density and V the magnitude of the fluid velocity vector **V**. Similarly, in a pipe of cross-sectional area A the flow $Q \triangleq AV$

Assuming unsteady conservative fluid motion in which nonpotential body forces viscous forces are negligible one can reduce Navier-Stokes equation to the form

$$\frac{D\mathbf{V}}{Dt} = -\frac{1}{\rho}\nabla p; \quad \frac{D}{DT} = \frac{\partial}{\partial t} + \mathbf{V}\cdot\nabla \tag{2.29.23}$$

Similarly the equation of continuity of mass becomes,

$$\frac{D\rho}{DT} = -\nabla\cdot\mathbf{V} \tag{2.29.24}$$

Since the pressure and velocity are functions of distance and of time, it is natural to consider the unsteady motion to take the form of propagating waves. One then introduces the *celerity* C (units: m/s) of these waves, and, for compressible motion, obtains,

$$\left[C(\rho)\right]^2 = \frac{\partial p}{\partial \rho} \tag{2.29.25}$$

In addition, from the nature of the dynamic equation and the need to track pressure in relation to fluid velocity it is useful to scale the pressure so that it is represented by an entity which has the units of velocity. A model of such scaling can be deduced from the case of plane waves,

$$U = \frac{p}{\rho C}$$

Introducing C in the conservation laws one obtains

(a) $\frac{D\mathbf{V}}{Dt} + C\nabla U = 0$ (conservation of momentum)

(b) $\frac{DU}{Dt} + C\nabla\cdot\mathbf{V} = 0$ conservation of mass)

This set of coupled equations, one scalar and one vector, reduces to two scalar equations if one takes the case of 1-dimensional flow, say in the s-direction:

$$\frac{\partial \mathrm{V}}{\partial t} + \mathrm{V}\frac{\partial \mathrm{V}}{\partial s} + C\frac{\partial U}{\partial s} = 0 \tag{2.29.26}$$

$$\frac{\partial U}{\partial t} + \mathrm{V}\frac{\partial U}{\partial s} + C\frac{\partial \mathrm{V}}{\partial s} = 0$$

By addition and subtraction it is readily seen that

$$\text{(a)}\ \ \frac{\partial J}{\partial t} + (\mathrm{V} + C)\frac{\partial J}{\partial s} = 0,\ J = \mathrm{V} + U \tag{2.29.27}$$

$$\text{(b)}\ \ \frac{\partial K}{\partial t} + (\mathrm{V} + C)\frac{\partial K}{\partial s} = 0,\ K = \mathrm{V} - U$$

These equations (first derived by Riemann) can be interpreted in a physical sense: the quantities J, K are characteristics of the partial differential equations of conservation noted above: J = const. travels along the path $ds = (\mathrm{V} + C)\,dt$ *downstream;* K = const. travels along the path $ds = (\mathrm{V} - C)\,dt$ *upstream.* Thus, for an-upstream point $s = a$, and a downstream point $s = b$, and for travel time T, the propagation of J, K is governed by the relations:

$$J_b(t) = J_a(t - T) = \Delta\, J_a$$

$$K_a(t) = K_b(t - T) = \Delta\, K_b \tag{2.29.28}$$

where

$$\Delta = e^{-TD},\ D = \frac{d}{dt}$$

Here Δ is a time translation operator defined by the relation $\Delta X(t) = X(t - T)$. Returning now to the equations of pipe flow one can immediately deduce from the J, K characteristics that

$$\Delta\, U_a + \Delta\, \mathrm{V}_a = U_b + \mathrm{V}_b$$

$$\Delta\, U_a - \Delta\, \mathrm{V}_a = \Delta^2 U_b - \Delta^2 \mathrm{V}_b \tag{2.29.29}$$

and hence that,

$$\begin{bmatrix} U_a \\ \mathrm{V}_a \end{bmatrix} = \begin{bmatrix} AB \\ CD \end{bmatrix} \begin{bmatrix} U_b \\ \mathrm{V}_b \end{bmatrix},$$

$$A = D = \frac{1 + \Delta^2}{2\Delta};\ C = B = \frac{1 \quad \Delta^2}{2D}. \tag{2.29.30}$$

In terms of hyperbolic function,

$$\begin{bmatrix} U_a \\ V_a \end{bmatrix} = \begin{bmatrix} \cosh TD & \sinh TD \\ \sin TD & \cosh TD \end{bmatrix} \begin{bmatrix} U_b \\ V_b \end{bmatrix}$$

where

$$\cosh TD = \frac{e^{TD} + e^{-TD}}{2} = \frac{1 + \Delta^2}{2\Delta} \tag{2.29.31}$$

$$\sinh TD = \frac{e^{TD} - e^{-TD}}{2} = \frac{1 - \Delta^2}{2\Delta}$$

By simple inversion,

$$U_b = (\cosh TD)\, U_a - (\sinh TD) V_a$$

$$V_b = -\sinh TD\ U_a + (\cosh TD) V_a \tag{2.29.32}$$

These are canonical forms of transmission line equations, more easily recognized when in steady state, for then $D = j\omega$.

We consider next 1-dimensional flow of a liquid in a pipe which is surrounded by air. Because the pipe is elastic the speed of propagation of waves ($=a$) inside must be less than the celerity C waves in an unbounded medium. For the important case where $V << a < C$ (called the subsonic case) we may set $D/Dt \simeq \frac{\partial}{\partial t}$, thereby neglecting the convection term. Replacing C by a, and s by x one can reformulate the conservation equations to read,

$$\text{(a)}\ \ I \frac{\partial Q}{\partial t} = -\frac{\partial P}{\partial x};\ I = \rho/A \left[\text{units: } Ns^2/m^6\right]$$

$$\text{(b)}\ \ C \frac{\partial P}{\partial t} = -\frac{\partial Q}{\partial x};\ C = \frac{A}{\rho a^2} \left[\textit{units: } \frac{m^4}{N}\right] \tag{2.29.33}$$

Here I can be interpreted as the inertance (units: Ns^2/m^5) per unit of length, and C can be interpreted as the capacitance C (units: m^5/N) per unit of length. These partial differential equations are given a physical interpretation by use of finite differences over distance $\Delta x = x_{n+1} - x_n$:

$$\frac{\partial P}{\partial x} \to \frac{P_{n+1} - P_n}{\Delta x};\ \frac{\partial Q}{\partial x} \to \frac{Q_{n+1} - Q_n}{\Delta x}$$

The interpretation is:

$$\text{(a)}\ \ P_n = P_{n+1} + \left[I\Delta x \frac{\partial}{\partial t}\right] Q_n$$

$$\text{(b)}\ \ Q_n = Q_{n+1} + \left[C\Delta x \frac{\partial}{\partial t}\right] P_n \tag{2.29.34}$$

An equivalent electric circuit based on a pressure/voltage analogy shows these equations to represent the n'th segment of an inductance coil in series (Eq. (a)) and a capacitance condenser is parallel (Eq. (b)). This is a classical result.

Since the pair of equations in P, Q have been derived from the pair in U, V it is useful to relate the four variables P, Q, U, V. A simple way to do this is to write the plane wave relations:

$$U\rho a = P$$

$$VA = Q$$

and divide the two to arrive at,

$$\frac{U}{P} = \frac{\mathrm{V}}{Z_0 Q}, \text{ where } Z_0 = \frac{\rho a}{A} \tag{2.29.35}$$

Thus in formulas involving U, V we may replace U by P provided we replace V by $Z_0 Q$. Similarly

$$\frac{\mathrm{V}}{Q} = \frac{U}{P/Z_0} \tag{2.29.36}$$

which shows that we may replace V by Q provided we replace U by P/Z_0.

The quantity Z_0 appearing in these *scaling laws* has a special meaning. By direct calculation of units:

$$Z_0 = \sqrt{\frac{\mathrm{I}}{\mathrm{C}}} \rightarrow \sqrt{\frac{\rho\rho a^2}{AA}} = \frac{\rho a}{A} \text{ (units: Ns/m}^5\text{)} \tag{2.29.37}$$

Z_0 is seen to be the *characteristic impedance* of the transmission line model of the pipe. It is a fundamental parameter of the equation governing the propagation of pressure waves in the pipe.

A second transmission line parameter which is important in unsteady flow is the *characteristic time* T, defined relative to a pipe length L. A meaningful selection of this parameter is

$$T = L\sqrt{\mathrm{IC}} = L/a \quad \text{(units: s)} \tag{2.29.38}$$

This T appeared earlier in the transmission line equations derived above, as the delay operator $\Delta = e^{-TD}$. It is a fundamental parameter of a pipe line in the transient state of fluid flow.

We now make use of the scaling laws in the equations of U, V in order to convert them to expressions in P, Q. Replacing U by P and V by $Z_0 Q$ one obtains,

$$P_b = (\cosh TD)\, P_a - (\sinh TD) Z_0 Q_a$$

$$Q_b = -(\sinh TD)\frac{P_a}{Z_0} + (\cosh TD) Q_a \tag{2.29.39}$$

This pair of equations has an analog in electric transmission line theory. Customarily the input to the line is taken to be sinusoidal in time ($\exp j\omega t$) and the field variable E, i express the frequency response of the line as a function of distance x. For a line with inductance L and associated resistance R, together with capacitance C to ground and associated conductance G, all per unit length, and with input voltage E_0, and input current i_0, the electrical transmission line equations become,

$$\text{(a)}\quad E = E_0 \cosh Bx - i_0 Z_0 \sinh Bx$$

$$\text{(b)}\quad i = i_0 \cosh Bx - \frac{E_0}{Z_0} \sinh Bx \tag{2.29.40}$$

$$\text{(c)}\quad K = \sqrt{(R + j\omega L)(G + j\omega C)} \rightarrow \frac{\omega}{a} \text{ (when } R,\ G \text{ are both very small).}$$

$$\text{(d)}\quad Z_0 = \sqrt{\frac{R + j\omega L}{G + j\omega C}}$$

It is seen that in going from the transient state to the steady state the parameter TD is replaced by the parameter Kx

A similar analog exists for elastic fields in isotropic solids [6b]. To develop this model we consider only those fields that can be described by the simple constitutive equation relating stress **T**, strain **S**, stiffness matrix C, viscosity η:

$$\mathbf{T} = \mathbf{C} : \mathbf{S} + \eta : \frac{\partial \mathbf{S}}{\partial t}$$

that is stress is proportional to strain and strain rate. For body forces **F** the equation of motion in the particle displacement **u** reduces to

$$\rho \frac{\partial^2}{\partial t^2} \mathbf{u} = \nabla \cdot \mathbf{T} + \mathbf{F}$$

and the strain rate reduces to

$$\frac{\partial S}{\partial t} = \frac{\partial}{\partial t} \nabla \mathbf{u} = \nabla \mathbf{u},\ \mathbf{V} = \frac{\partial u}{\partial t}$$

Since it is advantageous to consider stress as the independent variable one multiplies T by the compliance tensor **s** and rearranges terms:

$$\mathbf{S} = \mathbf{s} : \mathbf{T} - \tau : \nabla_s \mathbf{V},\ \tau = \mathbf{s} \cdot \eta$$

(Note that all terms of this equation are second-order tensors (dyadics)). The basic equations of conservation of momentum and mass of the elastic field then become,

$$\text{(a)}\quad \rho \frac{\partial \mathbf{V}}{\partial t} = \nabla \cdot \mathbf{T} + \mathbf{F}$$

$$\text{(b)}\quad \left(1 + \tau : \frac{\partial}{\partial t}\right) \nabla \mathbf{V} = \mathbf{s} : \frac{\partial \mathbf{T}}{\partial t} \tag{2.29.41}$$

A more manageable form for (b) is obtained by multiplying each term with the stiffness isotropic tensor **C**,

$$\text{(c)}\quad \mathbf{C} : \left(1 + \tau : \frac{\partial}{\partial t}\right) \nabla \mathbf{V} = \frac{\partial \mathbf{T}}{\partial t}$$

A simple example will illustrate the formation of a transmission line model. First the divergence and gradient operations are explicity listed in rectangular coordinates:

$$\nabla \cdot \mathbf{T} = \left(\hat{i}\,\frac{\partial}{\partial x} + \hat{j}\,\frac{\partial}{\partial g} + \hat{k}\,\frac{\partial}{\partial z}\right) \cdot \begin{bmatrix} \hat{i}\hat{i}T_{xx} & \hat{i}\hat{j}T_{xy} & \hat{i}\hat{k}T_{xz} \\ \hat{j}\hat{i}T_{yx} & \hat{j}\hat{j}T_{yy} & \hat{j}\hat{k}T_{yz} \\ \hat{k}\hat{i}T_{zx} & \hat{k}\hat{j}T_{zy} & \hat{k}\hat{k}T_{zz} \end{bmatrix}$$

$$\nabla \mathbf{V} = \left(\hat{i}\frac{\partial}{\partial x} + \hat{j}\,\frac{\partial}{\partial y} + \hat{k}\frac{\partial}{\partial t}\right)[\hat{i}v_x\ \hat{j}\mathrm{V}_y\ \hat{k}\mathrm{V}_z]$$

Now let the propagation be only along the z-axis by setting $\partial/\partial x = 0 = \partial/\partial y$. Then both $\nabla \cdot T$ and $\nabla \mathbf{V}$ have only three rectangular components:

$$\nabla \cdot \mathbf{T} = \mathbf{i}\,\frac{\partial Tzx}{\partial z},\ \mathbf{j}\ \frac{\partial Tzy}{\partial z},\ \mathbf{k}\,\frac{\partial Tzz}{\partial z}$$

$$\nabla \mathbf{B} = \mathbf{ki}\,\frac{\partial \mathrm{V}_x}{\partial z},\ \mathbf{kj}\,\frac{\partial \mathrm{V}_y}{\partial z},\ \mathbf{kk}\,\frac{\partial \mathrm{V}z}{\partial z}$$

For simplicity let $\tau = 0$.

The conservation equations then reduce to the 3 sets:

Component	Conservation Relations
i	$\rho\,\dfrac{\partial \mathrm{V}_x}{\partial t} = \dfrac{\partial T_{zx}}{\partial z} + F_x$
ki	$C_{44}\,\dfrac{\partial \mathrm{V}_x}{\partial z} = \dfrac{\partial T_{zx}}{\partial t}$

Component	Conservation Relations
j	$\rho\,\dfrac{\partial \mathrm{V}_y}{\partial t} = \dfrac{\partial T_{zy}}{\partial z} + F_y$
kj	$C_{44}\,\dfrac{\partial \mathrm{V}_y}{\partial z} = \dfrac{\partial T_{zy}}{\partial t}$

Component	Conservation Relations
k	$\rho \dfrac{\partial V_z}{\partial t} = \dfrac{\partial T_{zz}}{\partial z} + F_z$
KK	$C_{11} \dfrac{\partial V_z}{\partial z} = \dfrac{\partial T_{zz}}{\partial z}$

When F_x, F_y, F_z are all zero each pair describes a (traveling) wave motion in which we can identify inertance and capacitance. For example, in set (a) the inertance $I = -\rho$, and capacitance $C = -1/C_{44}$. The characteristic impedance and characteristic time are then,

$$Z_0 = \sqrt{\frac{I}{C}} = \sqrt{\rho C_{44}} \quad \text{(units: } NS/m^3\text{)}$$

$$\frac{T}{L} = \sqrt{IC} = \sqrt{\frac{\rho}{C_{44}}} = \frac{1}{c} \quad \left(\text{units: } \frac{s}{m}\right)$$

The corresponding transmission line equations become

$$(T_{zx})_b = (\cosh TD)(T_{zy})_a - (\sinh TD) Z_0 (V_x)_a \tag{2.29.42}$$

$$(V_x)_b = (-\sinh TD)\left(\frac{T_{zx}}{Z_0}\right)_a + (\cosh TD)(V_x)_c$$

in which

$$D = \frac{d}{dt}$$

$$T = \frac{L}{c};\ c = \text{celerity of the elastic wave}$$

It is important to note that wave motion exists only when *both* conservation of momentum and conservation of mass participate in the stress-strain relation.

The transmission line model just derived describes transient propagation. When the input is sinusoidal in time and the line is finite in length a standing wave model can be defined in a similar manner. Such models are discussed in Sects. 2.31, 2.32, 2.33.

2.30 DISTRIBUTED PARAMETER TRANSMISSION LINES

In a 1-dimensional transmission line with continuously x-distributed inertance, compliance and resistance, a standing wave, composed of interfering plane waves at frequency $\omega = kc/2\pi$, has the form

$$p = A \cosh (ikx + \Phi_0) = A_+ e^{ikx} + A_- e^{-ikx} \tag{2.30.1}$$

$$A_+ = \frac{A}{2}e^{\Phi_0};\ A_- = \frac{A}{2}\ e^{-\Phi_0}.$$

Here x is measured from the point ($x = 0$) launching the waves to the observation point. The symbol Φ_0 is a complex phase whose form depends on the acoustic-impedance of the termination of the transmission line at $x = l$. The corresponding particle velocity if this transmission line is,

$$u = \frac{A}{\rho c}\sinh(ikx + \Phi_0). \tag{2.30.2}$$

Thus, the specific acoustic impedance at at x is

$$z(x) = p/u = pc\coth(ikx + \Phi_0) = \rho_c \tanh(ikx + \Phi_0 + i\pi/2). \tag{2.30.3}$$

Now, to facilitate the use of calculation charts, prepared for the purpose, it has been found convenient to express Φ_0 in terms of two parameters α_0, β_0, and an arbitrary phase of $i\pi/2$:

$$\Phi_0 \equiv \pi(\alpha_0 - i\beta_0 - i/2) \tag{2.30.4}$$

Thus,

$$z(x) = \rho c\tanh\left\{\pi\alpha_0 - i\pi\left[\beta_0 - \frac{2x}{\lambda}\right]\right\} \tag{2.30.5}$$

If it is supposed that the wave attenuates as it moves toward the termination the propagation constant becomes complex,

$$K = \frac{2\pi}{\lambda} + i\pi\eta. \tag{2.30.6}$$

At the termination there are the real and imaginary part of the termination specific acoustic impedance which one can choose to express in arbitrary units as $\pi\alpha_l$, $\pi\beta_l$ respectively. Thus, by definition

$$\alpha_0 = \alpha_l + \eta l;\ \beta_0 = \beta_l + 2\ l/\lambda. \tag{2.30.7}$$

In terms of these quantities, the specific acoustic impedance at any point x measured from $x = 0$ is,

$$Z(x) = \rho c\tanh\left\{\pi(\alpha_l + \eta(l - x) - i\pi\left[\beta_l + \frac{2l^n}{\lambda} - \frac{2x}{\lambda}\right]\right\}. \tag{2.30.8}$$

Many authors find it convenient to express x in terms of the distance d from the termination, $x = l - d$. Then,

$$Z(d) = \rho c\tanh\left\{\pi(\alpha_l + \eta d) - i\pi\left[\beta_l + \frac{2d}{\lambda}\right]\right\}. \tag{2.30.9}$$

To simplify this expression it is often assumed that there are no losses in the system, meaning $\alpha_l = 0 = \eta$. Then

$$Z(d) = \rho c\tanh\left\{-i\pi\left[\beta_l + \frac{2d}{\lambda}\right]\right\}. \tag{2.30.10}$$

in which β_l is the phase change upon reflection at the termination. Two important values of B are.

$$\text{clamped end: } \beta_l = \frac{1}{2}; \text{ free end: } \beta_l = 0 \tag{2.30.11}$$

These values are selected, for mathematical convenience, to be in accord with the reflection law at the termination,

$$P_- \exp[-i(k - i\pi\eta)l] = P_+ \exp[i(K + i\eta)l + i\pi(1 + 2\beta_l) - 2\alpha_l].$$

Now we consider an acoustic transmission line consisting of n different segments in echelon, Fig. 2.30.1. Let the first segment (at $X = l$) have a characteristic acoustic impedance $Z_0 = \rho_1 c_1$ and a cross-sectional area S_1. The characteristic impedance of the mth segment is then written in terms of the parameter,

$$q_m = \frac{\rho_m c_m S_m}{\rho_1 c_1 S_1} = \frac{Z_{0m}}{Z_0} \tag{2.30.12}$$

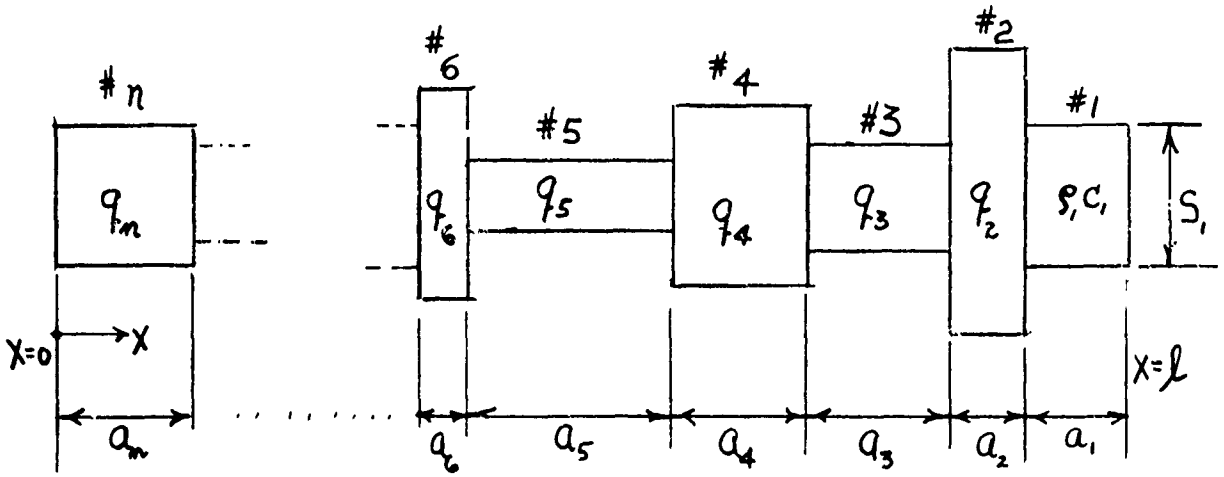


Fig. 2.30.1 — An illustrative acoustic transmission line

Suppose it is desired to find the *mechanical* impedance at the point $x = l$ looking back to the point $X = 0$ of Fig. 2.30.1. We may obtain this by repeated use of Eq. (2.30.8). Keeping in mind that the segments are in echelon, one has:

$$\frac{Z(l)}{Z_0} = T\left\{\gamma_1 a_1 + T^{-1}\left[q_2 T\left\{\gamma_2 a_2 \ldots + T^{-1}\left[q_{n-1} T\left\{\gamma_{n-1} a_{n-1} + T^{-1}\left[q_n T\left\{\pi(\alpha_n + \eta a_n) - i\pi\beta_n + \gamma_n a_n\right\}\right]\right\}\right]\right\}\right\}$$

$$T \equiv \tanh; \qquad T^{-1} \equiv \tanh^{-1}$$
$$\gamma_m = -ik_m; \qquad k_m = \frac{\omega}{C_m} = \frac{2\pi}{\lambda_m} \tag{2.30.13}$$
$$Z_0 = \rho_1 C_1 S_1$$

As before, the complex phase $\pi\alpha_n - i\pi\beta_n$ must be specified at the reference plane $X = 0$.

Let us use Eq. 2.30.13 to find the impedance at the radiating end of the composite-bar transducer shown in Fig. 2.30.2. For simplicity, let us assume the transmission line is lossless. Looking in from $X = l = b + a$ to $X = 0$, the mechanical impedance is,

$$\frac{Z(l)}{Z_0} = T\left\{\gamma_1 a + T^{-1}\left[q_2 T(\gamma_2 b - i\beta_2\pi)\right]\right\}. \tag{2.30.14}$$

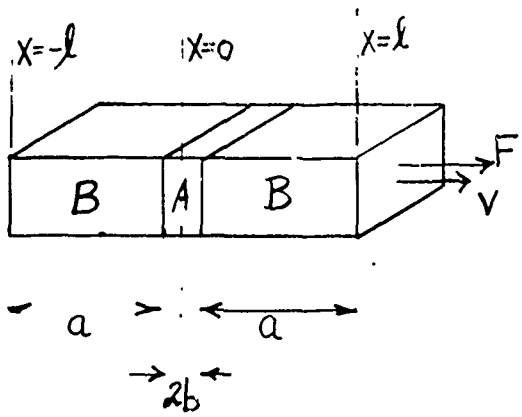


Fig. 2.30.2 — A composite-bar transducer A = piezoceramic, B = elastic layer

Since $X = 0$ is a node of motion (= clamped) its impedance is infinite. Then $\beta_2 = \frac{1}{2}$. To account for the remaining part of the symmetric bar ($X = 0$ to $X = -l$) we must double this impedance:

$$\frac{Z(l)}{Z_0} = -i2\frac{T^*(k_1 a)T^*(k_2 b) - q_2}{T^*(k_2 b) + q_2 T^*(k_1 a)}$$

where T^* now stands for 'tan.' Written in explicit form, this is:

$$Z(l) = -i2\left[\frac{\tan\frac{\omega b}{c_c}\tan\frac{\omega a}{c_s} - \frac{\rho_c c_c S_c}{\rho_s c_s S_s}}{\tan\frac{\omega_b}{c_c} + \frac{\rho_c c_c S_c}{\rho_s c_s S_s}\tan\frac{\omega a}{c_s}}\right]\rho_s c_s S_s \quad \text{(units: } Ns/m\text{)} \tag{2.30.15}$$

in which

$\rho_c c_c$ = characteristic impedance of the piezoceramic
$\rho_s c_s$ = characteristic impedance of the elastic material.

Equation 2.30.15 is the standard formula for the mechanical impedance of a symmetrically loaded composite bar.

The general Eq. 2.30.13 allows one to analyze an acoustic transmission line with any number of segments. It is seen however that a line of many segments presents a formidible task of analysis. Other cases of Eq. 2.30.13 are treated next.

2.31 DISTRIBUTED PARAMETER TRANSMISSION LINE WITH LUMPED IMPEDANCE AT ONE TERMINUS

In this case let the mth segment be terminated by a mechanical impedance Z_m. Then in Eq. (2.30.13) the mth entry is replaced by an augmented term

$$q_m T(\gamma_m A_m \rightarrow q_m T(\gamma_m A_m + T^{-1}\frac{Z_M}{Z_{0m}} \ldots . \tag{2.31.1}$$

As an example of this case suppose it is desired to find the mechanical impedance of the mass-loaded piezoceramic bar looking from $x = 0$ toward the termination $x = l$ of the piezoceramic, Fig. 2.31.1. We use Eqs. 2.30.13 and 2.31.1. Because the end is free, we set $\beta_l = 0$. We also assume the transmission and reflection are lossless so that $\eta = 0 = \alpha_n$. Since there is only one distributed system we set $q_m = 1$ and find that,

$$\frac{Z(0)}{Z_{01}} = T\left\{\gamma l + T^{-1}\frac{Z_M}{Z_{01}}\right\}$$

$$\frac{Z(0)}{Z_{01}} = \frac{T(\gamma l) + \dfrac{Z_M}{Z_{01}}}{1 + T(\gamma l)\dfrac{Z_M}{Z_{01}}} \tag{2.31.2}$$

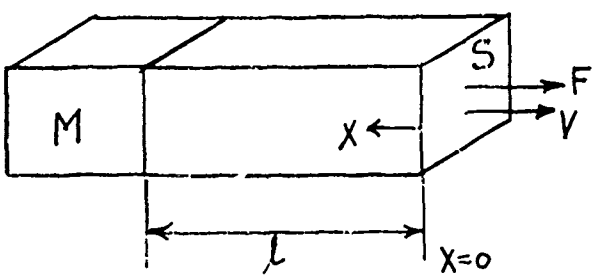


Fig. 2.31.1 — Mass-loaded piezoceramic bar, one end free

Now,

$$\frac{Z_M}{Z_{01}} = \frac{-i\omega M}{\rho CS} = -ikl\frac{M}{M_0} = -iklq \tag{2.31.3}$$

where

$$q = \frac{M}{M_0};\ M_0 = \rho Sl;\ Z_{01} = \rho CS. \tag{2.31.4}$$

Since $\gamma = -ik$, and recalling that $T \equiv \tanh$, it is directly found from 2.31.2 th..at

$$Z(0) = -i\left[\frac{\tan kl + klq}{1 - klq\ \tan kl}\right]\rho CS \tag{2.31.5}$$

When $M = 0$ one must observe a special precaution because then $X = l/2$ is a center of symmetry where the mechanical impedance is infinite. Assuming again lossless transmission we use one term of Eq. 2.30.13:

$$\frac{Z(0)}{Z_o} = 2\tanh\left\{-i\pi\left[\beta + \frac{2\ l/2}{\gamma}\right]\right\}. \tag{2.31.6}$$

The factor 2 accounts for the second half of the piezoceramic bar. Since the center is clamped we set $\beta = 1/2$ and find that,

$$\frac{Z(0)}{\rho CS} = 2i \coth \frac{kl}{2}. \tag{2.31.7}$$

This is the classical formula for the mechanical impedance of a piezoceramic bar with one free end and no mass load.

2.32 AN ELECTRICAL CIRCUIT WHICH IS THE EQUIVALENT OF A MASS-LOADED PIEZOCERAMIC BAR

The mechanical impedance of a mass-loaded piezoceramic bar Fig. 2.31.1 calculated at the force end, looking toward the mass-load, is given by Eq. 2.31.5, repeated here for convenience:

$$\frac{Z(0)}{-i\rho cS} = f(\alpha); \quad f(\alpha) = \frac{q\alpha + \tan \alpha}{1 - q\alpha \tan \alpha}; \quad \alpha = kl = \frac{2\pi}{\lambda} l = \frac{\omega l}{c}. \tag{2.32.1}$$

Since the mechanical resonant frequency ω_n occurs at values of α_n such that

$$f(\alpha_n) = 0 \tag{2.32.2}$$

where α_n are the roots of the numerator, namely

$$q\alpha + \tan \alpha = 0, \tag{2.32.3}$$

and where

$$\alpha_n = \frac{\omega_n' l}{\sqrt{\frac{Y}{\rho}}} \tag{2.32.4}$$

it is useful to write Eq. 2.32.1 in inverted form,

$$\frac{-i\rho CS}{Z(0)} = \frac{1}{f(\alpha)} = \frac{1 - q\alpha \tan \alpha}{q\alpha + \tan \alpha} = \frac{p(\alpha)}{q(\alpha)}. \tag{2.32.5}$$

Now the values α_n have two important properties:

(1) they are simple poles of the functions $1/f(\alpha)$

(2) they can be ordered as $|R_1| \leqslant |\alpha_2| \leqslant |\alpha_3| \ldots .$

Under these conditions one can expand $1/f(\alpha)$ in rational fractions of α by applying the Mittag-Leffler theorem [7]:

$$\frac{1}{f(\alpha)} = \frac{1}{f(\alpha)}\bigg|_{\alpha=0} + \sum_{n=1}^{\infty} b_n \left\{ \frac{1}{\alpha - \alpha_n} - \frac{1}{\alpha_n} \right\}. \tag{2.32.6}$$

Here b_n is the residue at the n'th pole,

$$b_n = \frac{p(\alpha_n)}{\frac{dq}{d\alpha}(\alpha_n)} = \frac{1 - q\alpha_n \tan \alpha_n}{q + \sec^2 \alpha_n}.$$

Since

$$q\alpha_n = -\tan \alpha_n$$

it is seen that

$$b_n = \frac{1}{1 + q \cos^2 \alpha_n}.$$

Thus,

$$\frac{1}{q(\alpha)} = \frac{1}{(1+q)\alpha} + \sum_{n=1}^{\infty} \frac{\alpha}{(1 + q \cos^2 \alpha_n)(\alpha\alpha_n - \alpha_n^2)}. \tag{2.32.7}$$

This form can lend itself to interpretation as a lumped-parameter network in which the equivalent masses and springs have values associated with frequencies ω near ω_n. In approximation therefore,

$$\frac{\alpha}{\alpha_n(\alpha - \alpha_n)} \times \frac{\alpha + \alpha_n}{\alpha + \alpha_n} = \frac{\alpha(\alpha + \alpha_n)}{\alpha_n(\alpha^2 - \alpha_n^2)} \to \frac{2\alpha}{\alpha^2 - \alpha_n^2}.$$

Hence,

$$\frac{1}{Z(0)} \simeq \left\{ \frac{1}{(1+q)\alpha} + \sum_{n=1}^{\infty} \frac{1}{\frac{1}{2}(1 + q \cos^2 \alpha_n)\left[\alpha - \frac{\alpha_n^2}{\alpha}\right]} \right\} \frac{1}{-i\rho CS}. \tag{2.32.8}$$

Recalling that $M_0 = \rho Sl$, $\alpha = \omega l/c$, $q = M/M_0$, one can now write,

$$\frac{V(0)}{F(0)} = \frac{1}{Z(0)} = \frac{1}{-i\omega(M_0 + M)} + \sum_{n=1}^{\infty} \frac{1}{\frac{-i\omega}{2}(1 + q \cos^2 \alpha_n)M_0 + \frac{(1 + q \cos^2 \alpha_n)\alpha_n^2}{-2i\omega} \frac{YS}{l}} \tag{2.32.9}$$

in which Y is Young's modulus for the bar. In symbolic form the velocity $V(0)$ thus consists of an infinite sum,

$$V(0) = F(0)[Y_0 + Y_1 + Y_2 \ldots .] = V_1 + V_2 + \ldots . \tag{2.32.10}$$

where

$$Y_0 = \frac{1}{-i\omega(M_0 + M)}; \quad Y_1 = \frac{1}{\frac{-i\omega}{2}(1 + q \cos^2 \alpha_n)M_0 + \frac{(1 + q \cos^2 \alpha_1)\alpha_1^2}{-2i\omega} \frac{YS}{l}}; \text{ etc.}$$

Eq. 2.32.10 can be modeled as an FV chain (F across, V through) Fig. 2.32.1, or a VF bond graph (V across, F through) Fig. 2.32.2.

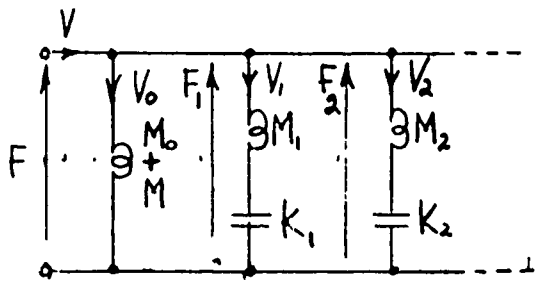


Fig. 2.32.1 — Sketches illustrating concept of work done (a), (b), (c) explained in the text

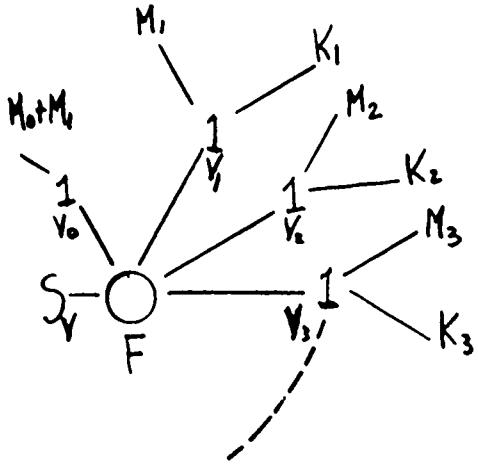


Fig. 2.32.2 — (a) FV equivalent circuit of Eq. 2.32.9, (b) VF equivalent circuiut of Eq. 2.32.9

in which

$$M_n = \frac{1}{2}(1 + q\cos^2\alpha_n)M_0;\ K_n = \frac{1}{2}(1 + q\cos^2\alpha_n)\alpha_n^2\frac{YS}{l}$$

One can see from Fig. 2.32.1 that at the n'th series resonance the velocity V_n is maximized. Similarly, from Fig. 2.32.2 it is seen that at the n'th parallel resonance the velocity again is maximized.

2.33. RESONANT TRANSDUCER INTERPRETED AS A BAND-PASS FILTER

We consider the case of a generalized transducer that can be represented by a 2-mesh equivalent circuit with the mechanical impedance in series position and the electrical (blocked) impedance in shunt position, Fig. 1.45.3. An all-electric representation is shown in Fig. 2.33.1. It can be readily applied to toroidal ring magnetostrictive transducer operating near mechanical resonance. The impedances then are in lumped form, and their values can be assigned from experimental data. A useful procedure is to use electrical admittance data for this purpose. To simplify the discussion we assume the leakage impedance to be negligible. This is the impedance due to leakage flux coupling to the core winding but not involving the core itself. The shunt impedance is then the core impedance. The measured core admittance becomes

$$Y_c = \frac{1}{Z_c} = \frac{1}{Z_c} = G_c - jB_c \qquad (2.33.1)$$

where the core susceptance is

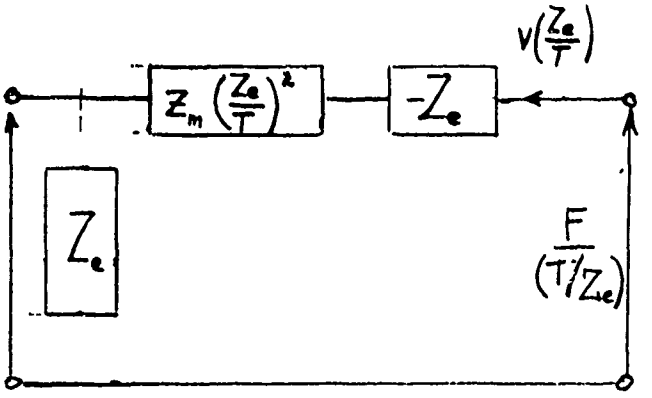


Fig. 2.33.1 — All electrical equivalent circuit obeying the canonical equations

$$B_c = \frac{1}{\omega L_2}$$

The total series branch impedance is represented by an inductance L_1, a capacitance C_1 and a load resistance R_1. At the frequency ω_y of maximum motional admittance, one measures the diameter D_y of the motional circle and the admittance Q_y obtained from the quadrantal frequencies. By definition,

$$L_1 = \frac{Q_y}{D_y \omega_y}$$

$$C_1 = \frac{D_y}{Q_y \omega_y}$$

$$R_1 = 1/D_y.$$

Suppose now the transducer is 'tuned' by adding to the terminals a shunt capacitor of special value,

$$C_2 = \frac{B_c}{\omega_y}$$

together with a generator with series resistance $R_g = 1/G_g$. The equivalent circuit of the toroidal ring is shown in Fig. 2.33.2. A significant feature of this sketch is the section between the dotted lines. It has the appearance of one section of a band-pass filter made up of two impedances:

$$Z_1 = j\omega_y L_1 + \frac{1}{j\omega_y C_1}$$

$$Z_2 = \frac{1}{j\omega_y C_2 + \frac{1}{j\omega_y L_2}}. \qquad (2.33.4)$$

Let us suppose now that C_2 is selected such that

$$L_1 C_1 = L_2 C_2. \qquad (2.33.5)$$

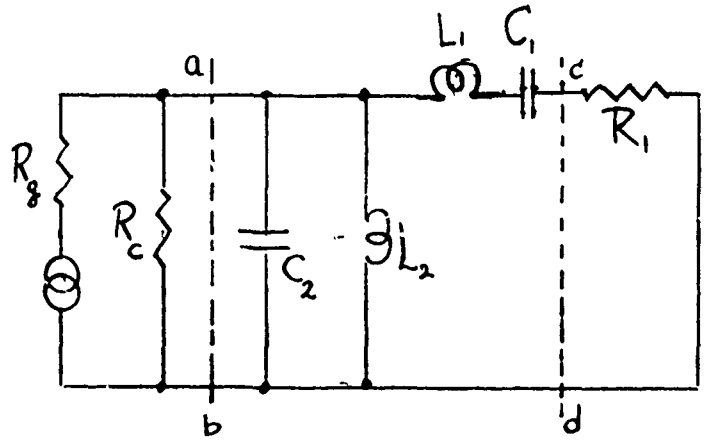


Fig. 2.33.2 — Equivalent circuit of a toroidal magnetostrictive ring transducer. Values of parameters are given in the text

Then it is seen that the zero of the series impedance Z_1 coincides with the pole of the shunt impedance Z_2. The product of these two impedances is,

$$Z_1 Z_2 = \frac{L_1}{C_2} = k^2. \tag{2.33.6}$$

Since k^2 is constant the filter is of the constant-k type. In filter theory it is useful to rescale the impedances by writing $L_1 \rightarrow L_1/2$ and $L_2 \rightarrow 2Z_2$. Such rescaling allows us to use image impedances of the symmetrical T and symmetrical π sections of a ladder filter. This is explained next.

Suppose that we can design two impedances, Z_T, Z_π such that at the terminals *ab* of Fig. 2.33.2 the impedance looking toward the right is just Z_π, and at the terminals *cd* the impedance looking toward the left is just Z_T. This is shown in Fig. 2.33.3. There are the *image impedances* of the '*L*-section' with rescaled values. By definition

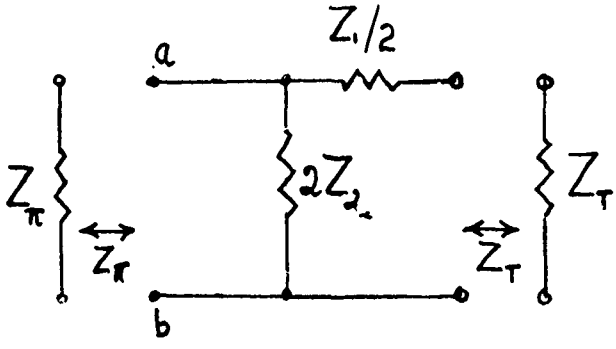


Fig. 2.33.3 — Image impedances Z_T, Z_π

$$Z_T = \sqrt{Z_0 Z_s}\Big|_{cd} = \sqrt{Z_1 Z_2}\sqrt{1 + \frac{Z_1}{4Z_2}} \tag{2.33.7}$$

in which Z_0, Z_s are the open circuit and short circuit impedances at terminals *cd* looking leftwards. Similarly,

$$Z_\pi = \sqrt{Z_0 Z_s}\Big|_{ab} = \frac{\sqrt{Z_1 Z_2}}{\left(1 + \dfrac{Z_1}{4Z_2}\right)^{1/2}} \tag{2.33.8}$$

in which Z_0, Z_s are now considered to be the relevant impedances looking rightwards.

Now at the frequency where $Z_1/4Z_2 = -1$ it is seen that $Z_T = 0$ and $Z_\pi = \infty$. No real power is then transferred to the image impedances. There are two such 'cut-off' frequencies ω_1, ω_2. The range $\omega_2 - \omega_1$ thus constitutes the pass-band of the constant-k section filter. By plotting Z_1 and $-4Z_2$ versus frequency one arrives at Fig. 2.33.4 in which the pass-band appears hatched. The frequency ω_r is identified with the frequency ω_y measured from the admittance circle at maximum admittance. In explicit terms,

$$\omega_1 = 2\pi f_1 = \sqrt{\frac{1}{L_1C_2} + \frac{1}{L_1C_1}} - \frac{1}{\sqrt{L_1C_2}}$$
$$\omega_2 = 2\pi f_2 = \sqrt{\frac{1}{L_1C_2} + \frac{1}{L_1C_1}} + \frac{1}{\sqrt{L_1C_2}}. \tag{2.33.9}$$

The width of the pass band of this L section is,

$$\omega_2 - \omega_1 = \frac{2}{\sqrt{L_1C_2}}. \tag{2.33.10}$$

Dividing this by

$$\frac{\omega_2 - \omega_1}{\omega_r} = \frac{2}{\sqrt{L_1C_2}} \frac{\sqrt{L_1C_1}}{1} = 2\sqrt{\frac{C_1}{C_2}}. \tag{2.33.11}$$

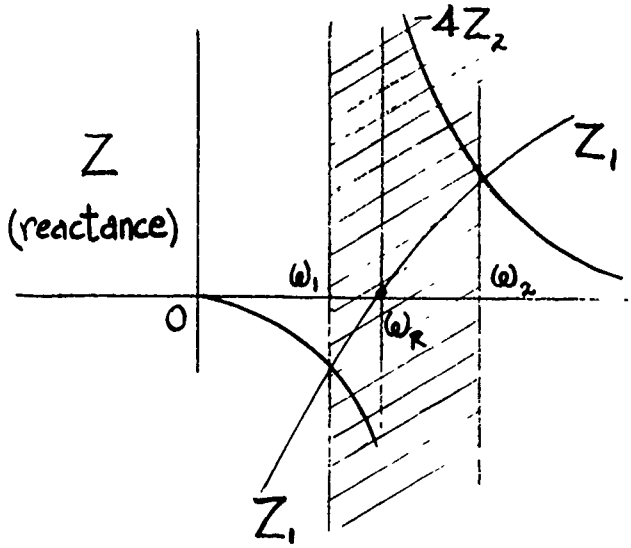


Fig. 2.33.4 — The bandpass constant-k section

The *percentage bandwidth* is defined as

$$BW' = \frac{\omega_2 - \omega_1}{\sqrt{\omega_2\omega_1}}. \tag{2.33.12}$$

By use of impedance data, this is approximated as,

$$BW' \approx \frac{f_{\min(z)} - f_{\max(z)}}{f_{\max(z)}}. \tag{2.33.13}$$

We wish to relate this BW' to the effective coefficient of electromechanical coupling. By *definition*,

$$k_{\text{eff}}^2 = \frac{f_{\min(z)}^2 - f_{\max(z)}^2}{f_{\min(z)}^2} = \frac{f_{\min(z)} - f_{\max(z)}}{f_{\min(z)}} \times \frac{f_{\min(z)} + f_{\max(z)}}{f_{\min(z)}} \tag{2.33.14}$$

or approximately, if $f_1 f_2 \simeq f_1^2$,

$$k_{\text{eff}}^2 = \frac{(f_{\min(z)} - f_{\max(z)})^2}{f_{\min(z)}^2} = \frac{(f_2 - f_1)^2}{f_2^2}. \tag{2.33.15}$$

It is important to note the difference in the denominators of BW' and K_{eff}^2, one being $f_{\max(z)}$ and one being $f_{\min(z)}$. Based on this difference it is seen that

$$BW' \approx \frac{1}{2}\left(\frac{k_{\text{eff}}^2}{1 - c_{\text{eff}}^2}\right). \tag{2.33.16}$$

If we use admittance data, BW' as defined relative to the frequency of minimum admittance while k_{eff}^2 is defined relative to the frequency of maximum admittance. When $k_{\text{eff}}^2 \ll 1$ then

$$BW' \approx \frac{1}{k_{\text{eff}}^2}$$

Reference [8] takes $\left(\frac{\omega_2 - \omega_1}{\omega_y}\right)$ for an L-section to be one half of the theoretical value. Hence it writes for a *toroid*:

$$\frac{\omega_2 - \omega_1}{\omega_y} = \sqrt{\frac{D_y}{Q_y B_c}} = k_{\text{eff}} \quad \text{(band-pass } L\text{-section)}. \tag{2.33.17}$$

This form then agrees with Eq. 2.33.15. The image impedance (defined above) at $\omega = \omega_r$ corresponds to the condition $Z_1 \equiv 0$. Thus,

$$Z_T = R = \sqrt{\frac{L_1}{C_2}} = \sqrt{\frac{Q_y}{D_y B_c}} = \frac{1}{B_c k_{\text{eff}}}. \tag{2.33.18}$$

Thus the most real power will be transferred to a load if the load is a pure resistance having a value close to R. Similarly maximum power will be delivered by the generator in Fig. 2.33.2 if its conductance G_g is chosen such that

$$B_c k_{\text{eff}} \simeq G_g + G_c \tag{2.33.19}$$

Fig. 2.33.1 is most useful in interpreting electrical admittance data because E can be held constant across impedance Z_e. In magnetostrictive transduction this corresponds to a drive at constant induction (constant-B). To obtain a drive at constant magnetic field we place Z_e in series position and Z_m in shunt position, Fig. 1.47.2. The analogy then becomes E/v, I/F and the equivalent circuit takes on the form of Fig. 2.33.5.

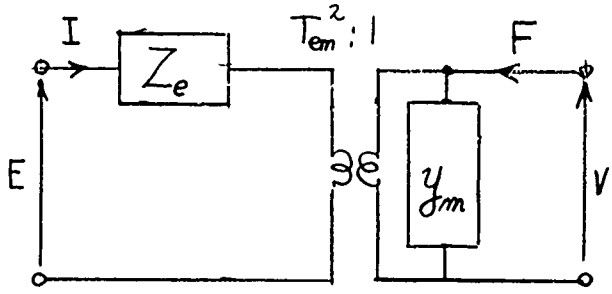


Fig. 2.33.5 — Equivalent circuit of a magnetostrictive toroid which is convenient for measurement of impedance at constant-H drive

Since Y_m ($= Z_m^{-1}$) is in shunt position its equivalent electrical impedance is

$$Y_m T_{em}^2 = Z.$$

Thus the lumped circuit mechanical admittance in parallel form will become an electrical impedance in parallel form. Adding a tuning capacitance $C_1 = (X_b \omega_R)^{-1}$ in which X_b is the sum of *both* the leakage reactance and the core reactance, and adding a generator with internal resistance R_g, one arrives at the equivalent circuit shown in Fig. 2.33.6. If we neglect R_c (which is usually small) the circuit between the dotted lines represents an L-section electrical filter. The choice of C_1 makes it a constant k bandpass filter. Following the steps outlined above, and making the same assumptions it is found that the effective electromechanical coupling factor is

$$\frac{(f_2 - f_1)^2}{f_1^2} \equiv \frac{k_{\text{eff}}^2}{1 - k_{\text{eff}}^2} \cong \frac{D_z}{Q_z X_b} \tag{2.33.20}$$

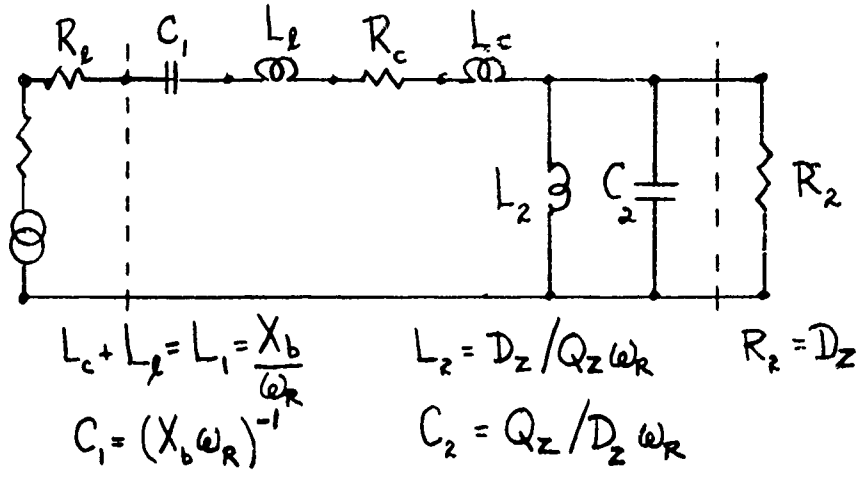


Fig. 2.33.6 — Lumped circuit equivalent corresponding to Fig. 2.33.5 with values measured on the impedance circle

and the image impedance at midband is

$$Z_T = \sqrt{\frac{D_z X_b}{Q_z}} = X_c k_{\text{eff}}. \tag{2.33.21}$$

It is emphasized that both of these formulas are valid for a *magnetostructure toroid.* The corresponding formula for a *magnetostructure bar* is different because the stress distribution in the bar is not uniform.

2.34 INTRODUCTION TO DESIGN OF RECEIVERS

The design of acoustic receiving systems based on electromagnetic transduction is well established. For completeness it will prove useful in appreciating later parts of this treatise to review the principles which guide the design of much used systems: moving-armature, electrostatic and piezoelectric.

2.35 FUNDAMENTALS OF MOVING-ARMATURE SYSTEMS

A simple moving armature system is shown in Fig. 2.35.1. A battery with voltage E_0 polarizes the magnetic circuit by supplying a polarizing magnetomotive force $\mathcal{F}_0$ corresponding to the battery dc current I_0 flowing through the coil;

$$\mathcal{F}_0 = NI_0 \qquad \left(\text{units: } \frac{C}{s} \times \text{turns}\right) \tag{2.35.1}$$

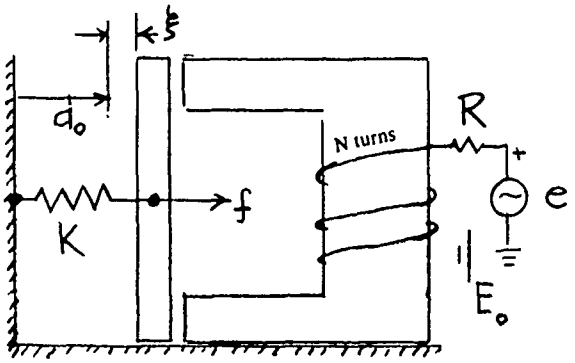


Fig. 2.35.1 — A simple moving armature system

In addition the coil is excited by a signal voltage E which drives a signal current i through the coil. The *incremental* magnetomotive force is then,

$$\mathcal{F}_i = Ni \tag{2.35.2}$$

At equilibrium (defined as the armature position d_0 when the signal current i vanishes) the magnetomotive force $\mathcal{F}_b$ drives a flux ϕ_0 around a circuit of path length l_m in the core and d_0 in the air gap. The core reluctance is then $\mathcal{R}_c$. When a signal current i is also present the air gap changes by amount ξ. The reluctance of the circuit is then the sum of core reluctance $\mathcal{R}_c$ and air gap reluctance, $\mathcal{R}_{\text{gap}}$,

$$\mathcal{R} = \mathcal{R}_c + \mathcal{R}_{\text{gap}};\ \mathcal{R}_c = \frac{l_m}{\mu\mu_0 S_m}\ ;\ \mathcal{R}_{\text{gap}} = \frac{d_0 + \xi}{\mu_0 S_g}. \tag{2.35.3}$$

Because the air gap furnishes most of the reluctance, one can write,

$$\mathcal{R} = \mathcal{R}_{\text{gap}}\,(1 + \delta_m) = \mathcal{R}^*_{\text{gap}};\ \ \delta_m = \frac{\mathcal{R}}{\mathcal{R}_{\text{gap}}} << 1. \tag{2.35.4}$$

Thus the total flux the circuit is,

$$\phi = \phi_0 + \phi_i = \frac{\mathcal{F}_0}{\mathcal{R}^*_{\text{gap}}} + \frac{N_i}{\mathcal{R}^*_{\text{gap}}}. \tag{2.35.5}$$

In moving armature systems we are interested in incremental changes in flux ϕ due to changes in armature distance ξ and signal current i. For convenience let the small number δ_m be neglected. Then,

$$\phi_0(\xi) = \frac{NI_0\mu_0 S_g}{d_0 + \xi};\ \ \phi_i(\xi, i) = \frac{Ni\mu_0 S_g}{d_0 + \xi} \quad \text{(units: } Vs\text{)} \tag{2.35.6}$$

Thus, the incremental change in flux consists of two parts:

$$d\phi_i = \left.\frac{\partial \phi_i}{\partial \xi}\right|_{i=0} d\xi + \left.\frac{\partial \phi_i}{\partial i}\right|_{\xi=0} di \tag{2.35.7}$$

$$\left.\frac{\partial \phi_i}{\partial \xi}\right|_{i=0} = 0;\ \frac{\partial \phi}{\partial i} = \left.\frac{\partial \phi_i}{\partial i}\right|_{\xi=0} = \frac{N\mu_0 S_g}{d_0 + \xi}$$

and,

$$d\phi_0 = \frac{\partial \phi_0}{\partial \xi}\, d\xi \tag{2.35.8}$$

$$\frac{\partial \phi}{\partial \xi} = \frac{\partial \phi_0}{\partial \xi} = -\frac{NI_0\mu_0 S_g}{(d_0 + \xi)^2} = -\frac{\phi_0}{d_0 + \xi}$$

Eqs. 2.35.7, 2.35.8 can be used to calculate the increment in total force exerted on the armature due to simultaneous changes in ξ and i. This force will be derived from the formula for the Maxwell stress T_{MAXWELL} associated with flux lines in the air gap where the flux density is B_g,

$$T_{\text{MAXWELL}} = -\frac{B_g^2}{2\mu_0} = \frac{F}{S_g} \qquad \text{(units: } N/m^2\text{)} \tag{2.35.9}$$

or

$$F = \frac{-B_g^2 S_g}{2\mu_0} = \frac{-\phi^2}{2\mu_0 S_g}. \tag{2.35.10}$$

Now $F = F(\xi, i)$. The increment in force is therefore

$$dF = \frac{\partial F}{\partial \phi}\,\frac{\partial \phi}{\partial \xi}\, d\xi + \frac{\partial F}{\partial \phi}\,\frac{\partial \phi}{\partial i}\, d_i.$$

Since $\phi = \phi_0 + \phi_i$, one has,

$$dF = \frac{\phi_0^2 + \phi_0\phi_i}{\mu_0 S_g(d_0 + \xi)}\, d\xi - \frac{(\phi_0 + \phi_i)N}{d_0 + \xi}\, di.$$

Now $\phi_0\,\phi_i\,d\xi << \phi_0^2\,d\xi$, and $\phi_i di << \phi_0\,di$ because ϕ_i, $d\xi$ and di are all small quantities, as assumed at the beginning of the analysis. Also, the changes in ϕ which occur when there is an increment in ξ, or i, or both, trace out a hysteresis loop on a ϕ vs F chart. Such a loop introduces a phase delay between ϕ and F, which must be accounted for by a complex hysteresis factor χ multiplying each term in the above formula. Thus dF becomes,

$$dF = \frac{\phi_0^2\chi}{\mu_0 S_g(d_0 + \xi)}\, d\xi - \frac{\phi_0 N\,\chi\, di}{d_0 + \xi} \tag{2.35.11}$$

In Words: Whereas in an ordinary spring a force must be exerted *on* its ends to extend it (or compress it) in a polarized magnetic circuit the polarizing field gives rise to the phenomenon that an increment in displacement is associated with an increment of force exerted *by* the armature acting in the same direction. The act of polarization thus introduces a *negative stiffness* into the mechanical branch of the electromechanical transducer. This stiffness is usually written as an inverse compliance C_e^{-1}. In contrast an increment of current generates a force increment orthogonal to it, in a direction obeying the Fleming left-hand (a motor) rule. This accounts for the negative sign in the above formula.

2.36 EQUIVALENT CIRCUIT OF A MOVING-ARMATURE TRANSDUCER

Let us arbitrarily choose the F/E analogy and construct a 2-mesh equivalent circuit. Beginning with Fig. 1.44.1 we break-up the electrical impedance Z_e into the blocked impedance Z_e'' and the velocity-coupled impedance Z_e'. To find an explicit expression for Z_e' we note that flux linkage λ is related to flux ϕ and inductance L by the linearized formula,

$$\lambda = N\phi = Li. \tag{2.36.1}$$

The incremental inductance is then

$$L_e' = N\,\frac{d\phi}{di} = \frac{N^2\mu_0 S_g}{d_0 + \xi}\,\chi$$

which is obtained by use of Eq. 2.35.7. Thus the electrical impedance associated with electromechanical coupling is,

$$Z_e' = j\omega L_e' = \frac{j\omega N^2\mu_0 S_g}{d_0 + \xi}\,\chi. \tag{2.36.2}$$

The corresponding mechanical impedance associated with coupling is obtained from Eq. 1.45.5

$$Z_m' = \frac{T^2}{Z_e'} \tag{2.36.3}$$

The transduction coefficient T is found from the force/current relation, Eq. 2.35.11.

$$T \equiv \frac{\phi N\chi}{d_0 + \xi} \quad \left[\text{units: } \frac{Ns}{C} \text{ or } \frac{Vs}{m}\right]. \tag{2.36.4}$$

Now let us choose (again quite arbitrarily) the 2-mesh canonical circuit in which Z_e' is in shunt position in the electrical mesh, as drawn in Fig. 1.45.5, and $-T^2/Z_e'$ is in series position in the mechanical mesh. From Eqs. 2.36.3 and 2.36.4,

$$\frac{T^2}{Z_e'} = \frac{1}{j\omega c_e}; c_e^{-1} = \frac{\phi^2 \chi}{(d_0 + \xi)\mu_0 S_g} \tag{2.36.5}$$

Thus $-T^2/Z_e'$ cancels the negative stiffness impedance $1/j\omega C_e$ in the mechanical mesh introduced by the polarization of the magnetic circuit. However the coupling impedance Z_e' (in shunt position) is a permanent feature of the electrical mesh. It contributes electromechanical coupling even when the mechanical mesh is open.

The equivalent circuit is that of Fig. 1.45.5, shown here as Fig. 2.36.1. The units of $\left(\frac{I}{Z_e'}\right)^2$ are $\frac{NC}{Vm}$. The units of the turns ratio T/Z_e' are $\frac{N}{V}$ or C/m.

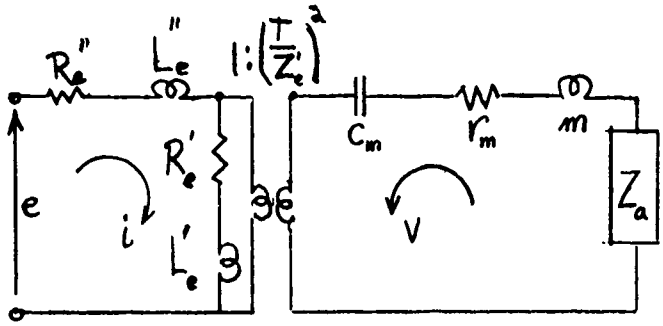


Fig. 2.36.1 — Equivalent circuit of a moving-armature transducer

2.37 THE DYNAMICS OF A LENGTH EXPANDER BAR WITH BIASING FIELD PARALLEL TO LENGTH

We consider a piezomagnetic bar, length l, mass density ρ, with rectangular cross sectional area A_b (width w, thickness t) much smaller in magnitude than l, Fig. 2.37.1. It is wrapped in a coil made up

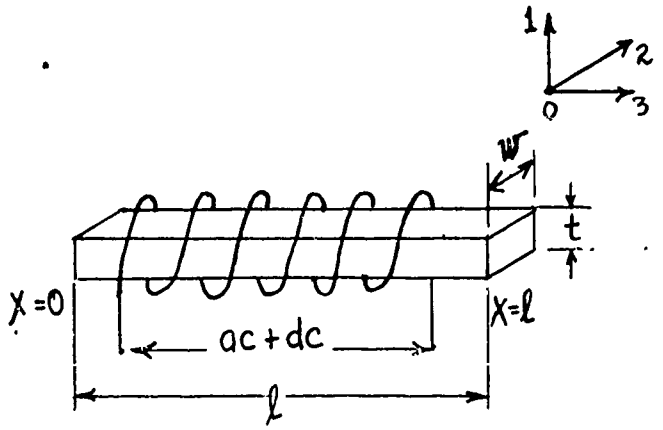


Fig. 2.37.1 — A longitudinal vibrator in the form of a magnetostrictive bar polarized by a dc current and driven by an ac current

of N turns with average cross-sectional area A_c. A dc excitation polarizes this bar at a value of B_0. At this operation-point an ac field is impressed on the coil which causes it to vibrate at the forcing frequency f. Two types of ac drive are commonly employed: one at constant voltage, and the other at constant current. Forced drive at constant voltage generates a force at each cross-sectional area of value.

$$F_M = A_b C_{33}^M \frac{d\xi_3(x_3)}{dx_3} - A_b h_{33}^{(l)} M_3(x_3). \tag{2.37.1}$$

This is a force associated with the magnetization M_3 induced in the bar by the alternating voltage through the agency of the piezoemagnetic h-constant. Similarly, forced drive at constant current generates a force at the same cross-sectional area of value,

$$F_H = A_b C_{33}^M \left[1 - \frac{h_{33}^2}{\gamma_{33}^S C_{33}^M}\right] \frac{d\rho(x_3)}{dx_3} - \frac{A_b h_{33}^{(l)} H_3(x_3)}{\gamma_{33}^S}, \text{ (units:}N\text{)} \tag{2.37.2}$$

in which H_3 is the applied magnetomotive force, and $H_1 = 0, H_2 = 0$.

Assume the coil is driven by a constant voltage ac generator. The net force accelerating an elementary volume of the bar is $dF_M(x_3)/dx_3$. Since there is no flux leakage we take $dM_3/dx_3 = 0$ everywhere. Thus, using Newton's equation of motion the displacement ρ is governed by the relation,

$$\frac{\partial^2 \xi}{\partial t^2} = \left(v_b^M\right)^2 \frac{\partial^2 \rho_3}{\partial x_3^2} \tag{2.37.3}$$

$$(v_b^M)^2 = \frac{C_{33}^M}{\rho}. \tag{2.37.4}$$

The solution of Eq. (2.37.3) for forced drive at frequency ω is,

$$\rho_3 = \left[\alpha \sin \frac{\omega x}{v_b^M} + \beta \cos \frac{\omega x}{v_b^M}\right] e^{j\omega t}. \tag{2.37.5}$$

The constants α, β are determined from the *stress* conditions at $x = 0$ and $x = l$. At $x = 0$ we set $F_M = 0$, and assume $M = M_0 e^{j\omega t}$. Then,

$$\left.\frac{d\xi_3}{dx_3}\right|_{x=0} = \frac{\alpha\omega}{v_b^M} = \frac{h_{33}^{(l)} M_0}{C_{33}^M}. \tag{2.37.6}$$

Hence

$$\alpha = \frac{v_b^M H_{33}^{(l)} M_0}{\omega C_{33}^M}. \tag{2.37.7}$$

Similarly at $x = l$, the force F_M again vanishes. Hence

$$\beta = \frac{\dfrac{h_{33}^{(l)} M_0}{C_{33}^M}\left[\cos \dfrac{\omega l}{v_b^M} - 1\right]}{\dfrac{\omega}{v_b^M} \sin \omega \dfrac{l}{v_b^M}}. \tag{2.37.8}$$

Thus, using the identity $\tan(\epsilon/2) = (1 - \cos\epsilon)/\sin\epsilon$, the displacement becomes,

$$\xi_3 = \frac{v_b^M}{\omega}\left\{\sin\frac{\omega x}{v_b^M} - \tan\frac{\omega l}{2v_b^M}\cdot\cos\frac{\omega x}{v_b^M}\right\}\frac{hs_{33}^{(l)}\,M_0}{C_{33}^M}\,e^{j\omega t} \tag{2.37.9}$$

The magnetic field is obtained from 2.3.6c

$$H_3(x_3) = \left[\gamma_{33}^S M_0 - h_{33}\cdot\frac{h_{33}^{(l)}M_0}{C_{33}^M}\left\{\cos\omega\frac{x}{v_b^M} + \tan\omega\frac{l}{2v_b^M}\sin\frac{\omega x}{v_b^M}\right\}\right]e^{j\omega t}.$$

Averaging H_3 over the length of the bar one obtains

$$\left(H_3\right)_{AV} = \frac{1}{l}\int_0^l H_3(x_3)\,dx = \gamma_{33}^T M_0\left[\left(-k_{33}^2\right) - k_{33}^2\tan\frac{\frac{\omega l}{2v_b^M}}{\frac{\omega l}{2v_b^M}}\right];\ \gamma_{33}^S = \gamma_{33}^T\left[1-k_{33}^2\right] \tag{2.37.10}$$

where

$$k_{33}^2 = h_{33}^2/C_{33}^M\gamma_{33}^T$$

The current flowing through the coil is then,

$$I = e^{j\omega t}(H_3)_{AV}\,l/N$$

The applied voltage is

$$V = NAj\omega M_0 e^{j\omega t}.$$

The electrical admittance of the coil becomes,

$$Y = \frac{I}{V} = \frac{l\gamma_{33}^T}{j\omega N^2 A}\left[\left(1-k_{33}^2\right) - k_{33}^2\,\frac{\tan\left(\omega l/2v_b^M\right)}{\left(\frac{\omega l}{2v_b^M}\right)}\right]. \tag{2.37.11}$$

The second term constitutes the motional admittance. In the absence of losses it becomes a maximum at the antiresonant (or parallel) frequency where

$$\tan\frac{\omega_a l}{2v_b^M} = \infty,\ \text{or}\ \frac{\omega_a l}{2v_b^M} = \pi/2,\ \text{or}\ f_a = \frac{v_b^M}{2al}.$$

The electrical admittance vanishes at the frequency of series of (electrical) resonance f_r, where

$$\left(1-k_{33}^2\right) - k_{33}^2\frac{\tan\frac{\pi}{2}\left(\frac{f_r}{f_a}\right)}{\frac{\pi}{2}\left(\frac{f_r}{f_a}\right)} = 0,\ \text{or}\ \frac{\tan\frac{\pi}{2}\left(\frac{f_r}{f_a}\right)}{\frac{\pi}{2}\left(\frac{f_r}{f_a}\right)} = \frac{1-k_{33}^2}{k_{33}^2}. \tag{2.37.12}$$

Thus, if the bar is driven at constant voltage as the frequency changes and if f_a, f_r are measured on a plot of electrical admittance one can find the coupling factor. Which coupling factor this is depends on the definition of Young's modulus Y_0. From 2.37.1 it is seen that when the piezomagnetic bar is observed at *constant magnetization* the effect of the coupling of the stiffness is not present. Hence we take,

$$Y_0 = C_{33}^M.$$

The coefficient of electromechanical coupling is then *defined* as

$$k_{33} = \sqrt{\frac{h_{33}^2}{C_{33}^M \gamma_{33}^T}}. \tag{2.37.13}$$

Thus,

$$\frac{h_{33}^2}{C_{33}^M \beta_{33}^S} = \frac{k_{33}^2}{1 - k_{33}^2}.$$

2.38 FUNDAMENTALS OF ELECTROSTATIC TRANSDUCERS

A charge q in an electric field $\mathbf{E}$ experiences a force $\mathbf{F} = q\mathbf{E}(q)$. In the simple cases under consideration here it is useful to assume that $\mathbf{E}(q) = q\mathbf{a}/\alpha$, in which $\mathbf{a}$ is a unit vector, α is a constant. For a parallel plate condenser, $\alpha = \epsilon_0 S$ (units: $\epsilon_0 = C/Vm$, $S = m^2$). If the charge q builds up from a datum value it is seen that the force $\mathbf{F}$ varies continuously. Thus, the final force must be the *average*,

$$\mathbf{F} = \frac{q^2}{2\alpha}\,\mathbf{a} \tag{2.38.1}$$

We consider the case of only one dimension $\mathbf{F} = F\mathbf{i}$ and note that because an increase in charge causes a parallel plate condenser to contract, we must take this force to be negative. Thus,

$$F = \frac{-q^2}{2\epsilon_0 S} \quad \text{(units: } N\text{)}. \tag{2.38.2}$$

This expression for the force coupled into the mechanical mesh by the agency of transduction appears in the equation of force for the electrostatic transducer, Eq. 1.51.4a,

$$m\ddot{\xi} + b\dot{\xi} + k\xi + \frac{q^2}{2\epsilon_0 S} = f(t) \tag{2.38.3}$$

in which ξ is the incremental distance of movement of the free plate relative to the stationary plate, and $f(t)$ is the applied external force.

Application of the variational principle (Sections 1.50, 1.51) to electrostatic transducers which are electrically excited through an RLC network by a steady voltage e_0 and a fluctuating voltage $e(t)$ also leads to the electrical equation, analogous to Eq. 1.51.4b,

$$L\ddot{q} + R\dot{q} + \frac{q(d_0 + \xi)}{\epsilon_0 S} = e_0 + e(t). \tag{2.38.4}$$

Since q is coupled to itself Eq. (2.38.3) and to the displacement ξ Eq. (2.38.4), these equations are seen to be nonlinear.

A solution of Eq. (2.38.3) which allows construction of equivalent circuits is derived by letting $f(t)$ to be

$$f(t) = F_1 \cos \omega t + F_2 \sin \omega t.$$

Since there is a dc excitation, both ξ and q have dc components:

$$\xi = \xi_0 + A_1 \cos \omega t + A_2 \sin \omega t$$

$$q = q_0 + B_1 \cos \omega t + B_2 \sin \omega t$$

$$q^2 = q_0^2 + 2q_0B_1 \cos \omega t + 2q_0B_2 \sin \omega t + \ldots.$$

$$q\xi = q_0\xi_0 + q_0A_1 \cos \omega t + q_0A_2 \sin \omega t + \xi_0B_1 \cos \omega t + \xi_0B_2 \sin \omega t + \ldots.$$

Noting that the time-varying component of displacement is

$$A_1 \cos \omega t + A_2 \sin \omega t = \left(\frac{A_1 - jA_2}{2}\right) e^{j\omega t} + \text{conjugate}$$

and the time-varying component of q^2 is

$$2q_0\left[\left(\frac{B_1 - jB_2}{2}\right) e^{j\omega t} + \text{conjugate}\right]$$

we discard the conjugate terms as being redundant. Then,

$$\xi = \xi_1 e^{j\omega t}; q = q_1 e^{j\omega t}; \quad f = f_1 e^{j\omega t}; \quad e(t) = e_1 e^{j\omega t}$$

where

$$\xi_1 = \frac{A_1 - jA_2}{2}; \quad q_1 = \frac{B_1 - jB_2}{2}; \quad f_1 = \frac{F_1 - jF_2}{2}.$$

The time-varying component of the force equation, linearized in this way, becomes

$$\left(j\omega m + \frac{k}{j\omega} + b\right)\dot{\xi}_1 + \frac{q_0}{j\omega\epsilon_0 S}\,\dot{q}_1 = f_1. \tag{2.38.5}$$

Similarly, the time-varying component of $q\xi$ is,

$$q\xi = \frac{(d_0 + \xi_0)q_1}{\epsilon_0 S} + \frac{q_0}{\epsilon_0 S}\,\xi_1.$$

Hence the time varying component of the linearized electric field equation is,

$$\left[j\omega L + R + \frac{(d_0 + \xi_0)}{j\omega\epsilon_0 S}\right] \dot{q}_1 + \frac{q_0}{j\omega\epsilon_0 S}\,\dot{\xi}_1 = e_1. \tag{2.38.6}$$

The steady (dc) components are

$$k\xi_0 + \frac{q_0^2}{2\epsilon_0 S} = 0 \tag{2.38.7}$$

$$\frac{q_0(d_0 + \xi_0)}{\epsilon_0 S} = e_0. \tag{2.38.8}$$

From Eqs. 2.38.5, 2.38.6 it is seen that the transduction coefficient is

$$T = \frac{q_0}{j\omega\epsilon_0 S} \quad (\text{units } Ns/C) \tag{2.38.9}$$

Also the static capacitance associated with the transduction is

$$C_0 = \frac{\epsilon_0 S}{d_0 + \xi_0}\left[\text{units } \frac{C}{V}\right], \quad Z_e' = \frac{1}{j\omega C_0} \tag{2.38.10}$$

2.39 EQUIVALENT CIRCUIT OF ELECTROSTATIC TRANSDUCERS

The canonical 2-mesh equivalent circuit with Ze' in shunt position Fig. 1.45.2 will be the choice to represent electrostatic tranducers. In this circuit the turns ratio is,

$$\phi = \frac{T}{Z_c'} = \frac{g_0}{j\omega\epsilon_0 S} \times \frac{j\omega\epsilon_0 S}{(d_0 + \xi_0} = \frac{q_0}{d_0 + \xi_0} \quad \left[\text{units: } \frac{C}{m} = \frac{N}{V}\right]. \tag{2.39.1}$$

In the mechanical mesh, where all elements appear in series position. there is seen to be an added impedance,

$$-\frac{T^2}{Z_e'} = \frac{1}{j\omega C_n};\ C_N = -\left[\frac{\epsilon_0 S}{q_0}\right]^2 \frac{1}{C_0} \quad \left[\text{units: } m/N\right]. \tag{2.39.2}$$

The symbol C_N is a negative compliance acting in conjunction with the positive compliance of the movable (diaphragm) plate of the condenser. Its origin is this: the force *required to compress* or expand the positive compliance is effectively *reduced* by the force of electrostatic attraction. Thus it reduces the spring constant of the diaphragm.

An equivalent circuit embodying Eqs. 2.38.5, 2.38.6, 2.39.1, and 2.39.2 is shown in Fig. 2.39.1. Upon combining stiffness in the mechanical mesh one has,

$$\frac{1}{C_m} + \frac{1}{C_N} = \frac{1 + \dfrac{C_m}{C_N}}{C_m}.$$

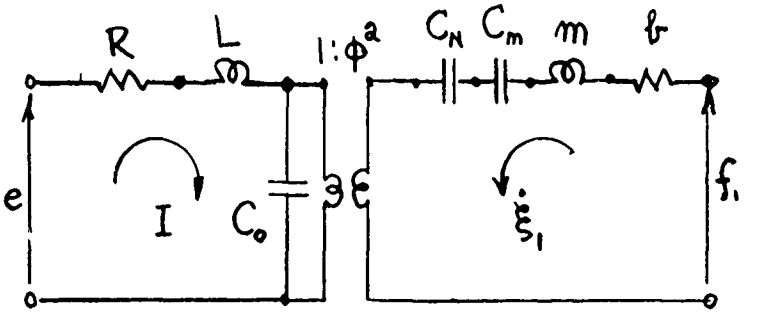


Fig. 2.39.1 — A two-mesh equivalent circuit of an electrostatic transducer; $\phi = (q_0/d_0) + \xi_0$

The combined compliance is then

$$C_m^* = \frac{C_m}{1 - k^2} \tag{2.39.3}$$

$$k^2 = \frac{C_0 C_m}{\left(\frac{\epsilon_0 S}{q_0}\right)^2} = C_0 C_m \left(\frac{e_0}{d_0 + \xi_0}\right)^2 = C_m \frac{e_0^2 \epsilon_0 S}{(d_0 + \xi_0)^3} \tag{2.39.4}$$

in which k^2 is the coefficient of electromechanical coupling; and Eq. 2.35.8 has been used to introduce the bias voltage c_0.

Equation 2.39.3 poses the question of stability. Evidently it is required that $k^2 \leqslant 1$, otherwise, upon application of the biasing dc voltage the diaphragm would collapse on the stationary electrode. The stiffness $K (= C_m^{-1})$ must obey the rule,

$$K \geqslant \frac{e_0^2 \epsilon_0 S}{(d_0 + \xi_0)^3}.$$

But, according to Eq. 2.38.8

$$K = -\frac{e_0^2 \epsilon_0 S}{2\xi_0 (d_0 + \xi_0)^2}. \tag{2.39.5}$$

Thus for stability,

$$K = \frac{-e_0^2 \epsilon_0 S}{2\xi_0 (d_0 + \xi_0)^2} \geqslant \frac{e_0^2 \epsilon S}{(d_0 + \xi_0)^3} \tag{2.39.6}$$

or

$$-\frac{\xi_0}{d_0} \leqslant \frac{1}{3}.$$

This means the bias displacement ξ_0 introduced by the dc voltage cannot be greater than 1/3 of the gap d_0 between the condenser plates in the absence of bias. This is an ideal limit. In reality the limit is less because of nonuniformity in the field structure.

Equation 2.39.5 is a cubic equation in the unknown variable ξ_0. It can be solved for a given stiffness of diaphragm by numerical (=graphical means). Once ξ_0/d_0 is determined it is directly noted from the value of K ($= C_m^{-1}$) of Eq. 2.39.5 that

$$k^2 = 2\left|\frac{-\xi_0/d_0}{1+\xi_0/d_0}\right|. \tag{2.39.7}$$

2.40 PARAMETERS OF STANDARD HYDROPHONE DESIGNS BASED ON POLARIZED PIEZOACTIVE CERAMIC MATERIALS IN CONVENTIONAL GEOMETRIES

It is common practice to design hydrophones based on sensing elements in the form of hollow piezoceramic shells. A compendium of the most useful designs is presented here.

Let the hydrophone be a simple plate or curved shell of piezoactive ceramic material, and assume its "outside" surface is exposed to a fluid pressure of magnitude P_0, while its "inside" surface is free of this pressure. In these structures the number of secondary surface exposed to P_0 depends on shape. Three simple shapes are shown in Fig. 2.40.1.

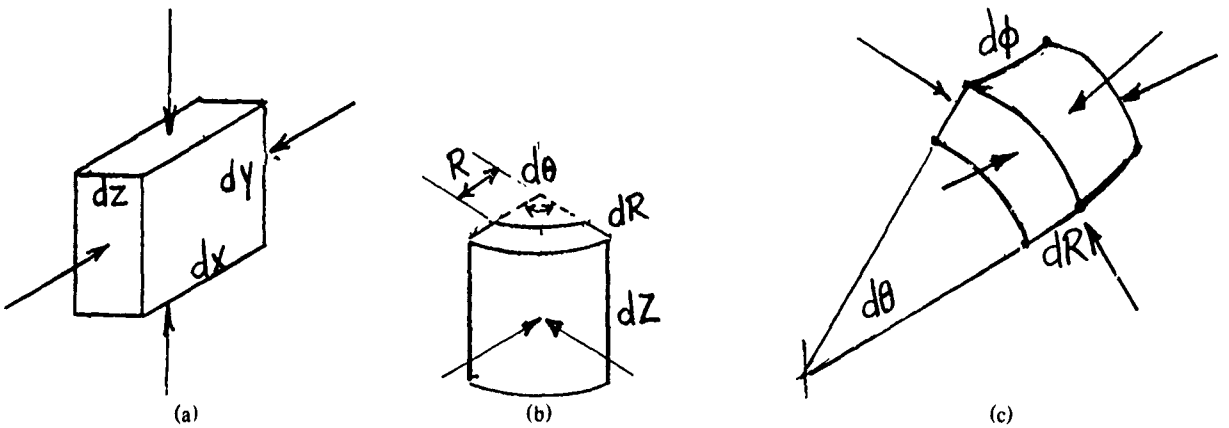


Fig. 2.40.1 — Three shapes of shells subjected to external fluid pressure, (a) rectangular, (b) cylindrical, (c) spherical

As a result of this external force the shell undergoes deformation and develops internal elastic stress. In a rectangular system of coordinates these stress are T_x, T_y, and T_z; in a cylindrical system, T_R, T_θ, and T_z; in a spherical system, T_R, T_θ, and T_ϕ. In each case the stresses vary with the thickness coordinate.

Assume next the piezoactive shells are polarized in a selected direction and are provided with electrodes to collect charge and thus develop potential difference E (units: V/m). In Fig. 2.40.1a the possible potentials are E_x, E_y, and E_z; in (b), E_R, E_θ, and E_z; and in (c), E_R, E_θ, and E_ϕ.

The induced stresses **T** generate charge (expressed as charge density **D**) or voltage (expressed as voltage gradient **E**). According to the theory of linear piezoelectricity the relations between **T**, **D**, and **E** are formulated in terms of piezoelectric stress constants d and g:

$$\text{in the absence of applied E:} \quad D_m = \sum_{i=1}^{3} d_{mi} T_i \tag{2.40.1}$$

$$\text{in the absence of applied D:} \quad E_m = -\sum_{i=1}^{3} g_{mi} T_i. \tag{2.40.2}$$

Here g is the "voltage-stress" piezoelectric constant, and d is the "charge-stress" piezoelectric constant.

Now let the subscript j indicate direction of polarization and A_j the area of the charge collecting electrodes. The charge Q_j is then given by

$$Q_j = \int\int D_j A_j = \int\int \sum_i d_{ji} T_i A_j, \quad j = 1, 2, 3. \tag{2.40.3}$$

Although "constants" d and g in curvilinear coordinates are functions of angles θ and ϕ of rotation, it is customary to use Cartesian (= unrotated) values in applications to curved shells. This practice is a source of error, but its magnitude must be ascertained in any particular case. Examples are:

$$\text{rectangular:} \quad Q_z = \int\int (d_{zx} T_x + d_{zy} T_y + d_{zz} T_z)\, dxdy$$

$$\text{cylindrical:} \quad Q_R = \int\int (d_{RR} T_R + d_{R\theta} T_\theta + d_{RZ} T_Z) R d\theta\, dz$$

$$\text{spherical:} \quad Q_R = \int\int (d_{RR} T_R + d_{R\theta} T_\theta + d_{R\phi} T_\phi) R^2 d\theta\, d\phi.$$

In a similar way the voltage developed across electrodes A_j in direction of the polarization α_g is given by

$$V_j = \int E_j d\alpha_j = \int \sum_i (-g_{ji} T_i) d\alpha_j, \quad j = 1, 2, 3. \tag{2.40.4}$$

Examples are

$$\text{rectangular:} \quad V_x = -\int (g_{xx} T_x + g_{xy} T_y + g_{xz} T_z)\, dx$$

$$\text{cylindrical:} \quad V_\theta = -\int (g_{\theta R} T_R + g_{\theta\theta} T_\theta + g_{\theta z} d_z) R d\theta$$

$$\text{spherical:} \quad V_\phi = -\int (g_{\phi R} T_R + g_{\phi\phi} T_\phi + g_{\phi\theta} T_\theta) R d\phi.$$

Equations (2.40.3) and (2.404) allow one to calculate the ratio of open circuit voltage to applied acoustic pressure in particular cases. These are discussed next.

VOLTAGE SENSITIVITY AND FIGURE-OF-MERIT OF POLARIZED PIEZOACTIVE CERAMIC SHELLS

Let the applied acoustic pressure be P_0. The internal stresses developed in the shell are taken to be negative if compressive, or positive if tensile. To avoid ambiguity when using curvilinear coordinates to describe shell geometry let the piezoelectric constants be subscript p (= parallel) when their two subscripts are identical, and subscript T (= tangential) when their subscripts are not identical. This convention assumes there is only one tangential constant, rather than two, which is true of isotropic elastic bodies in the conventional geometrical shapes of hydrophones currently in use. If there are actually two tangential constants correction to the formulas is easily made.

The mechanical constraints imposed on surfaces exposed to the incident pressure are important. The number of such surfaces is obtainable by inspection. In Fig. 2.40.1 there are 5 surfaces of concern in each case (outside surface, plus four transverse surfaces). For a cylindrical shell of resolution there are three surfaces (outside, top and bottom) while for a complete spherical shell there is only one (outside). The acoustic boundary conditions are three in nature (a) *shielded surfaces,* on which P_0 vanishes, (b) *exposed surfaces,* A_j, on which the internal developed stress is $T_j = -P_0$, (c) *capped surfaces,* A_j on which the internal developed stress $T_j = -P_{0x}MF$ (MF = *magnification factor* dependent on how the cap concentrates forces due to changes in area between cap and shell surface).

In these structures the voltage sensitivities are obtained from Eq. (2.40.4) and the charge sensitivities from Eq. (2.40.3). A figure-of-merit of the hydrophone is obtained from the discussion in Sect. 10 of Chapt. 10 centered on Eq. (10.1.8).

Table 2.40.1 gives the voltage sensitivity and figure-of-merit of piezoelectric hydrophones configures as hollow circular cylinders. Table 2.40.2 gives the same information for spheres and flexural disks. Shear-mode hydrophones are also listed.

Table 2.40.1 [12]

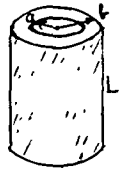
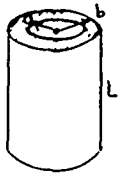
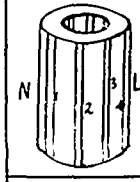
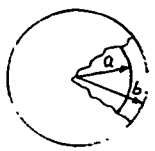
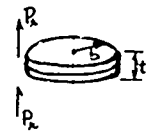
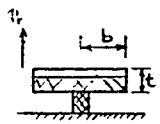
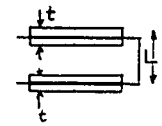
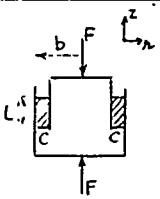
Polarization	Mechanical Constraints on Ends	Receiving Sensitivity $M_0 = V_{oc}/P_0$	Capacity C_T	Volume V_H	Figure-of-merit $= M_0^2\, C^T/V_H$ (F_M)	Geometrical Shape
Radial  $\rho = \frac{a}{b}$	Shielded	$b\left\{g_P\left(\frac{1-\rho}{1+\rho}\right)+g_T\right\}$	$\frac{2\pi\epsilon_{33}L}{\ln\frac{1}{\rho}}$	$\pi(b^2-a^2)L$	$g_T d_T \frac{2}{\ln\frac{1}{\rho}}\left\{\frac{g_P}{g_T}\frac{1-\rho}{1+\rho}+1\right\}^2\frac{1}{1-\rho^2}$	circular cylinder
	Exposed	$b\left\{g_P\frac{1-\rho}{1+\rho}+g_T(2-\rho)\right\}$ $M_0 = bg_T,\ \rho \to 1$	$\frac{2\pi\epsilon_{33}L}{\ln\frac{1}{\rho}}$	$\pi(b^2-a^2)L$	$g_T d_T \frac{1}{\ln\frac{1}{\rho}}\left\{(2-\rho)+\frac{g_P}{g_T}\frac{(1-\rho)}{(1+\rho)}\right\}^2\frac{1}{1-\rho^2}$	circular cylinder
	Capped	$b\left\{g_P\frac{1-\rho}{1+\rho}+g_T\left(\frac{2-\rho}{1+\rho}\right)\right\}$ $M_0 = \frac{3}{2}bg_T,\ \rho \to 1$	$\frac{2\pi\epsilon_{33}L}{\ln\frac{1}{\rho}}$	$\pi(b^2-a^2)L$	$g_T d_T \frac{2}{\ln\left(\frac{1}{\rho}\right)}\left\{\frac{2+\rho}{1+\rho}+\frac{g_P}{g_T}\left(\frac{1-\rho}{1+\rho}\right)\right\}^2\frac{1}{1-\rho^2}$	circular cylinder
Longitudinal 	Shielded	$\frac{2Lg_T}{1-\rho^2}$	$\frac{\pi\epsilon_{33}^T(b^2-a^2)}{L}$	$\pi(b^2-a^2)L$	$\frac{4g_T}{1-\rho^2}$	circular cylinder
	Exposed	$Lg_T\left\{\frac{2}{1-\rho^2}+\frac{g_P}{g_T}\right\}$	$\frac{\pi\epsilon_{33}^T(b^2-a^2)}{L}$	$\pi(b^2-a^2)L$	$g_T d_T\left\{\frac{1}{1-\rho^2}+\frac{g_P}{g}\right\}^2$	circular cylinder
	Capped	$Lg_T\left\{\frac{2+\frac{g_P}{g_T}}{1-\rho^2}\right\}$	$\frac{\pi\epsilon_{33}^T(b^2-a^2)}{L}$	$\pi(b^2-a^2)L$	$g_T d_T\left\{\frac{2+\frac{g_P}{g_T}}{1-\rho^2}\right\}$	circular cylinder
Tangential N = number of sections in parallel 	Shielded	For 1 section $\frac{2\pi b}{N\ln\left(\frac{1}{\rho}\right)}\cdot\left\{g_T\frac{(1-\rho)}{(1+\rho)}+g_P\right\}$	$\frac{\epsilon_{33}L}{\left(2\pi/N\ln\frac{b}{a}\right)}$	$\pi(b^2-a^2)L$	$g_P d_P \times \frac{2}{N\ln\left(\frac{1}{\rho}\right)}\frac{1}{(1-\rho^2)}\left\{\frac{g_T}{g_P}\frac{(1-\rho)}{(1+\rho)}+1\right\}^2$	circular cylinder
	Exposed	$\frac{2\pi b}{n\ln\frac{1}{\rho}}\left\{g_T\left(\frac{1-\rho}{1+\rho}\right)(2+\rho)+g_P\right\}$	$\frac{\epsilon_{33}L}{\left(2\pi/N\ln\frac{b}{a}\right)}$	$\pi(b^2-a^2)L$	$g_P d_P \frac{2}{N\ln\frac{1}{\rho}}\times\frac{1}{(1-\rho_2)}\left\{\frac{g_T}{g_P}\frac{(1-\rho)}{(1+\rho)}(2+\rho)+1\right\}^2$	circular cylinder
	Capped	$\frac{2\pi b}{n\ln\left(\frac{1}{\rho}\right)}\left\{g_T\left(\frac{2-\rho}{1+\rho}\right)+g_P\right\}$	$\frac{\epsilon_{33}L}{\left(2\pi/N\ln\frac{b}{a}\right)}$	$\pi(b^2-a^2)L$	$g_P d_P \frac{2}{N\ln\left(\frac{1}{\rho}\right)}\times\frac{1}{1-\rho^2}\left\{\frac{g_T}{g_P}\left(\frac{2-\rho}{1+\rho}\right)+1\right\}^2$	circular cylinder

Table 2.40.2 [12]

Polarization	Mechanical Constraint/ Electrical Connection	Receiving Sensitivity $M_0 = V_{oc}/P_0$	Capacity C^T	Volume V_N	Figure of Merit $f_H = M_0^2 C^T / V_N$	Geometrical Shape
RADIAL 		$bq_{31}\left\{\frac{\left[\frac{g_p}{q_T}(\rho^2+\rho+2)-(\rho^2+\rho+4\right]}{4(1+\rho+\rho^2)}\right\}$	$\frac{e\pi\epsilon_{33}b\rho}{1-\rho}$	$\frac{4}{3}\pi(b^3-a^3)$	$g_T d_T \frac{3\rho\left\{\frac{g_p}{g_T}(\rho^2+\rho-2)-(\rho^2+\rho+4)\right\}^2}{4(1+\rho+\rho^2)^2(1-\rho)}$	sphere
(see longitudinally polarized cylinders for case $\rho = 0$)						solid bodies
	(1) simply supported at edge (2) wired in parallel (3) uniform load	$\frac{3}{8}g_T\frac{b^2}{t}$	$2\left(\frac{\pi b^2\epsilon_{33}}{t/2}\right)$	$\pi b^2 t$	$g_T d_T \frac{9}{16}\left(\frac{b}{t}\right)^4$	single bilaminar disk
	(1) center support (2) one ceramic disk (3) uniform load	$\frac{3}{8}g_T\frac{b^2}{t}$	$\left(\frac{\pi b^2\epsilon_{33}}{t/2}\right)$	$\pi b^2 t$	$g_T d_T \frac{9}{32}\left(\frac{b}{t}\right)^4$	ceramic disk bonded to a second inactive disk
	(1) two belaminas disks (2) wired in parallel (3) uniform load	$\frac{3}{8}g_T\frac{b^2}{t}$	$4\left(\frac{\pi b^2\epsilon_{33}}{t/2}\right)$	$\pi b^2 L$	$g_T d_T \frac{9}{8}\frac{b^4}{t^3 L}$	trelaminar double-ended flexural disks
	same as above except wired in series	$4\left(\frac{3}{8}g_T\frac{b^2}{t}\right)$	$\left(\frac{\pi b^2\epsilon_{33}}{t/2}\right)\times\frac{1}{4}$	$\pi b^2 L$	$g_T d_T \frac{9}{8}\frac{b^4}{t^3 L}$	trelaminar double-ended flexural disks
	(1) Thin ceramic ring c in shear (2) polarized in z direction (3) dectroded in r direction	$g_s\frac{(2b)^2}{16L}(1-\rho^2)$	$\frac{\pi L\epsilon_{11}^T(1+\rho)}{1-\rho}$	$\pi b^2 L$	$g_s d_s \frac{1}{64}\left(\frac{2b}{L}\right)^2(1-\rho^2)(1+\rho)^2$	ceramic ring in shear
	(1) thin ceramic ring c in shear (2) polarized in r (3) electroded in z	$g_s\frac{b}{4}(1+\rho)$	$\frac{\pi b^2(1-\rho^2/\epsilon_{11}^T}{L}$	$\pi b^2 L$	$g_s d_s \frac{1}{64}\left(\frac{2b}{L}\right)^2(1-\rho^2)(1+\rho)^2$	ceramic ring in shear

REFERENCES

[1] "Ultrasonic Transducers," Ed. Y. Kikuchi Corona Pub. Co. Tokyo, 1969.

[2] "Electromechanical Transducers and Wave Filters," W.P. Mason, D. Van Nostrand Co. New York 1942.

[3] "Transmission Lines and Networks," W.C. Johnson, McGraw-Hall Book Co. New York, 1950.

[4] "Transmission Networks and Wave Filters," T.E. Shea D. Van Nostrand.

[5] "Acoustics," L.L. Beranek, McGraw-Hill Book Co. New York 1954.

[6a] H.M. Paynter, "Fluid Transients in Engineering Systems," Section 20 of "Handbook of Fluid Dynamics."

[6b] "Acoustic Fields and Waves In Solids," B.A. Auld Vol. 1, p. 171, J. Wiley and Sons, New York, 1973.

[7] "Modern Analysis," E.T. Whittaker, G.N. Watson, p. 134, Cambridge U. Press 1963.

[8] "Magnetostruction Transducers," National Defense Research Committee, Vol. 13 of Summary of Technical Reports, Division 6, J.T. Tate, Chief, 1946.

[9] "Fundamentals of Sonar," J.W. Horton, U.S. Naval Institute, Annapolis, 1957.

[10] Shock and Vibration Handbook, Ed. C.W. Harris, C.E. Crede, Vol. I, McGraw-Hill, 1961.

[11] "Radio Engineer's Handbook," F.E. Terman 1st Ed. 8th Impression, McGraw-Hill Book Co. 1943.

[12] "Piezoelectric Transducers," H.B. Miller NUSC Tech. Doc. 6029, NUSC New London, Conn. 1978.

[13] D. Karnopp, "Lumped Parameter Models of Acoustic Filters Using Normal Modes and Bond Graphs," J. Sound and Vib. **42** (4), 437-446 (1975).

Chapter 3
UNDERWATER HELMHOLTZ RESONATOR ACOUSTIC TRANSDUCER

3.1 INTRODUCTION

The analytic and design procedures explained in Chapters 1, 2 are exemplified in transducer practice by several modern transducers. We choose here the example of the underwater Helmholtz resonator.

The radiation of appreciable low frequency sound into a liquid medium requires large motion of substantial masses of liquid. Conventional electromechanical, or hydraulic, transducers designed for mechanical resonance tend to be large in bulk, heavy in weight, and generally too high in mechanical Q. The principle of the Helmholtz resonator offers a device that can be designed to overcome these difficulties, with the additional advantage of operating at great depths in the ocean without the need of a pressure release to avoid clamping by hydrostatic forces.

3.2 CONSTRUCTION FEATURES OF AN UNDERWATER HELMHOLTZ ACOUSTIC RADIATOR

The classical Helmholtz resonator (Fig. 3.2.1) consists of a rigid-wall cavity fitted with a short-tube neck terminated by an orifice. The compliance of the cavity volume and the inertance of the slug of fluid in the neck form a simple spring-mass system which is forced into resonance by a forcing external pressure at a specific frequency. The compliance of the equivalent spring is found as follows. For a fluid of bulk modulus $B (= \rho_0 c^2)$, the pressure increment due to volume increment is:

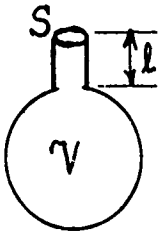


Fig. 3.2.1 — Classical Helmholtz resonator

$$dp = \left(\frac{\partial p}{\partial V}\right) dV = -\frac{B}{V}\, dV. \tag{3.2.1}$$

Since a fluid displacement ζ across the area S is equivalent to a volume change $dV = S\zeta$ and the force f on S is pS the mechanical stiffness is

$$\frac{f}{\zeta} = -\frac{\rho_0 c^2 S^2}{V} \quad \text{(units: N/m)}. \tag{3.2.2}$$

The *acoustic* compliance is then $(\zeta/f)S^2$, or,

$$C_A = \frac{V}{\rho_0 c^2} \quad \text{(units: m}^5\text{/N)}. \tag{3.2.3}$$

To find the equivalent mass we note that the mechanical mass m in the neck of length l is,

$$m = \rho_0 Sl$$

The *acoustic* mass $M = (m'/S^2)$, in which $m' = \rho_0 S l'$ and l' contains a correction to the length l due to additional fluid outside the orifice moving with the fluid in the neck,

$$l' = l + \Delta l. \tag{3.2.4}$$

For a tube of radius a of semi-infinite length the end correction is $\Delta l = 8a/3\pi \simeq 0.85a$ (unit: m) if it is terminated in an infinite rigid baffle, and $\Delta l' \simeq 0.613a$ (units: m) if there is no baffle. Thus, for these two cases,

$$M_A = \frac{\rho_0(l + 0.85a)}{S}, \text{ or } M_A = \frac{\rho_0(l + 0.613a)}{S}. \tag{3.2.5a}$$

When the tube is finite in length and forms the neck of a Helmholtz resonator, one end of which is free of baffle and the other end leads into the resonator cavity it is plausible to make the end corrections a sum of the two cases, and the corresponding acoustic mass to be,

$$M_A = \frac{\rho(l + 1.46a)}{S}. \tag{3.2.5b}$$

Helmholtz resonance (ω_r) is defined by the formula

$$\omega_r = \sqrt{\frac{1}{C_A M_A}} = \sqrt{\frac{1}{\frac{V}{\rho_0 c^2} \times \frac{\rho_0 l'}{S}}} = c\sqrt{\frac{S}{Vl'}} \quad \text{(units: } s^{-1}\text{)}. \tag{3.2.6}$$

The resonator just described can act as a receiver. It maybe converted into a projector of sound by making part (or all) of the rigid wall of the cavity into a vibrating wall. Figure 3.2.2 shows this simple modification. The wall between A and B is replaced by a diaphragm (or flexible disk) which is driven into vibration by some external agency. Both the moving wall and the neck radiate sound into the external medium.

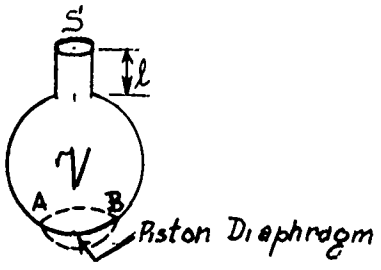


Fig. 3.2.2 — Helmholtz resonator modified to act as an acoustic source

3.3 ANALYSIS OF OPERATION OF A HELMHOLTZ RESONATOR ACTING AS A SOURCE OF SOUND

In the following exposition we take the entire wall to be the vibrator, and consider the external medium to be water and the internal medium to be oil. Since the operation of this transducer is required to be at mechanical resonance it will be useful to construct a low frequency lumped-parameter model. We consider the mechanical circuitry first and neglect the agency that supplies power which causes the diaphragm to vibrate. The steps in creating the model are as follows:

(1) we *assume* that this transducer has two degrees of freedom, $\dot{x}_1$ at the diaphragm, and $\dot{x}_2$ at the neck. Although these are, in reality, coupled to each other, the building of the equivalent circuit is rendered simpler by this assumption. The force at the diaphragm and the corresponding impedance are F_1, L_{11}; the force at the neck and the corresponding impedance are F_2, L_{22}. The coupling force in the cavity fluid is F_{21} or F_{12}, and the corresponding cavity impedance is L_{12} or L_{21}.

Corresponding to this picture the equations of motion are,

$$\begin{cases} F_1 - L_{11}\dot{x}_1 = F_{12}, & F_{12} = L_{12}\dot{x}_2 \\ F_2 - L_{22}\dot{x}_2 = F_{21}, & F_{21} = L_{21}\dot{x}_1 \end{cases} \tag{3.3.1}$$

(2) we assume further that the transducer is linear and reciprocal,

$$F_{12} = F_{21} = F_c \tag{3.3.2}$$

and permit only one applied force (at the diaphragm) by setting $F_2 = 0$. Thus, the force balance becomes,

$$\begin{cases} F_1 - L_{11}\,\dot{x}_1 = F_c \\ \quad - L_{22}\,\dot{x}_2 = F_c. \end{cases} \tag{3.3.3}$$

In words: the diaphragm generates cavity force F_c which, in turn, produces a fluid velocity in the neck.

(3) based on these formulas we construct first a *VF* mechanical circuit (V = across variable, F = through variable). In this choice of circuit Eqs. 3.3.3 are interpreted as nodal equations: F_1, F_c are flow (= through) quantities and $\dot{x}_1$, $\dot{x}_2$ are across quantities. The symbol L_{11} is an integro-differential operator which includes all impedances associated with $\dot{x}_1$ at the diaphragm: these are the impedance of the applied force driver, the external radiation load and the internal load due to the cavity fluid.

The diaphragm is taken to be a mass-spring-dashpot system having common velocity $\dot{x}_1$. To represent this in the circuit we place a capacitance C_M (= mass), an inductance L_M (= spring), and a conductance G_M (= dashpot) in *shunt position* as three elements in parallel with $\dot{x}_1$ (= the across variable).

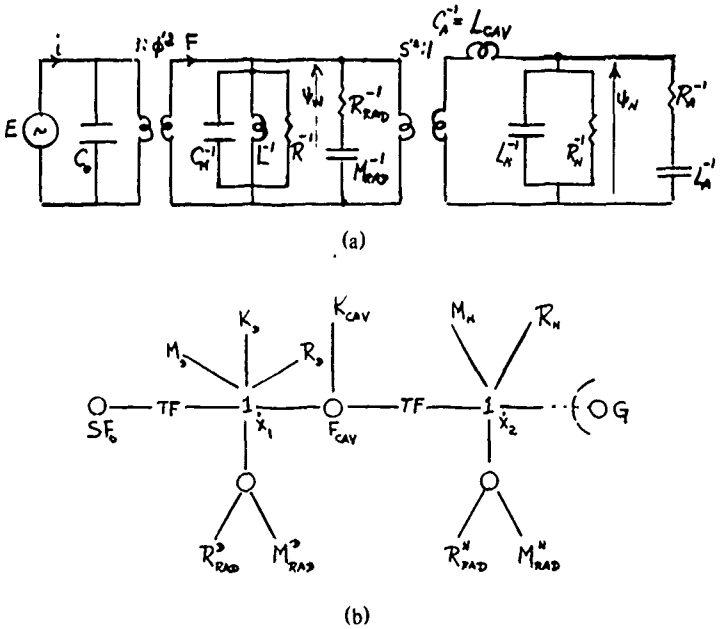
The acoustic loading of the moving spherical wall is that of a sphere radiating into a fluid medium. Its representation in the equivalent network is a matter of choice. We choose the "common force" form, Fig. 1.7.5c, in which the radiation mass M_{rad} is a capacitance and the radiation resistance is a conductance $1/R_{\text{rad}}$ (see Sec. 1.7 for explicit forms). Both of these elements are in series across the circuit—that is, also parallel with $\dot{x}_1$.

The loading on the diaphragm supplied by the cavity is considered to be a lossy spring in the low frequency range in question. As a spring it shares velocity $\dot{x}_1$ at one end and $\dot{x}_2$ at the other end. It is thus represented by an inductance L_c in series position between the two "potentials" $\dot{x}_1$, $\dot{x}_2$. In a first approximation the loss resistance of the cavity is neglected.

The cavity spring is visualized as driving the slug of fluid (capitance C_N) in the neck at velocity $\dot{x}_2$. Associated with this velocity is the viscous conductance G_N of fluid motion in the neck, in parallel with C_N.

(4) the acoustic radiation from the neck is *chosen* to be the form given by Fig. 1.7.5C (see Sec. 1.7 for the explicit values of G_{RAD}, M_{RAD}). This choice is the "common force" representation. The force driving this radiation is the remainder of the spring force after the neck forces are subtracted. The radiation velocity is the same as that of the neck mass. Hence this element is placed in parallel with the neck elements. The driver also is loaded with a mass L_{DB} on its backside (= inside the cavity).

Using steps 1 through 4 we sketch the equivalent *VF* circuit of the mechanical network, Fig. 3.3.1a. The associated bond graph is shown in the same figure as (b).



(a)

(b)

Fig. 3.3.1 — (a) A VF equivalent circuit of a spherical Helmholtz resonator sound source with all elements in mechanical impedance form (b) its bond graph

The dual, or *FV* representation of Fig. 3.3.1 is easily constructed according to the rules of Sect. 1.1.1. It will be illuminating however to retrace the derivation of the equivalent *FV* circuit by use of physical reasoning. To begin with, one first distinguishes between mechanical and acoustical components of the completed circuit.

1. On the mechanical side the driver supplies a force which becomes the across quantity of the mechanical network. This force drives the cavity wall into vibration. The wall is taken to be a mass-spring-dashpot system with common velocity. Hence its equivalent *FV* circuit representation is an inductance L_M (= mass), capacitance C_M (= spring) and resistance R_M(= dash) *in series* at common velocity flowing out of the node which represents the force of the driver. The acoustic radiation from the wall can be chosen at will from two choices, one a common velocity representation Fig. 1.7.5a and the other a common force representation, Fig. 1.7.5d. Since Fig. 3.3.1 has a common force representation we shall chose the parallel circuit oF Fig. 1.7.5d to represent radiation from the wall.

2. On the acoustic side, the cavity, neck, and neck radiation are taken to be an acoustic circuit of the same nature as that described in Sec. 1.12. Since we shall use acoustic impedances it is necessary to divide mechanical impedances by the square of the areas of the spherical surface. This is done by an ideal transformer with transformation ratios S^2 :1. The flow-quantity then becomes the volume velocity ψ and the across-quantity becomes the fluid pressure p.

The moving spherical wall generates an (interior) volume velocity ψ_ω. A portion ψ_c of this comes to rest at the wall itself. This action is represented by a capacitor "spring" to ground in the form of an acoustic compliance C_A. A second portion ψ_N flows through the neck. This is represented by an acoustic inertance (inductance) L_A and resistance R_A in *series* (= same volume velocity as the moving spherical wall). The pressure driving this volume velocity is represented by the node (across the cavity). The representation of acoustic radiation can be chosen at will. We choose here the common force representation Fig. 1.7.7d. Because the volume flow is the same as ψ_N this parallel circuit is placed in series with ψ_N and is connected to ground.

The completed electromechanical *FV* circuit (with added piezoelectric drive) is shown in Fig. 3.3.2a, together with (b) the associated bond graph. This circuit, derived by Henriquez (Ref. [1]), does not account for the mutual loading of the spherical radiating surface and the orifice as well as the mass loading inside the cavity.

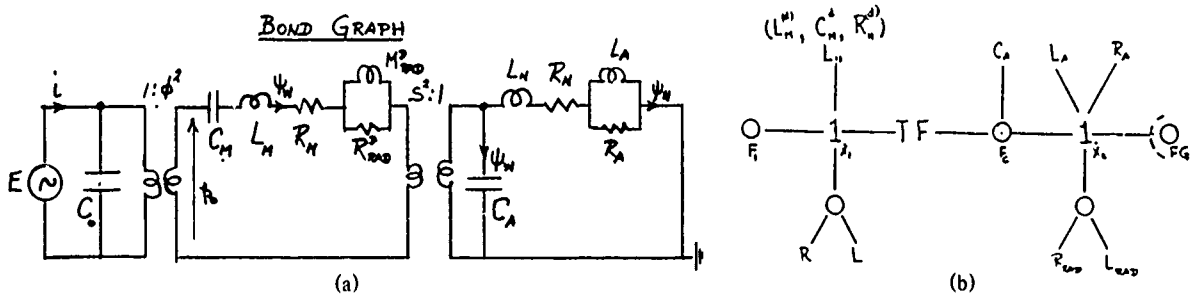


Fig. 3.3.2 — (a) A FV equivalent circuit of a spherical Helmholtz resonator sound source with added piezoceramic drive (b) its bond graph

A different approach to modeling the Helmholtz radiator is taken by Woollett [2]. Here the volume velocity ψ_w flows through the cavity compliance C_A as before, excepting that because the wall (or portion thereof) is in motion the wall velocity is terminated in a resistance which is a sum of the viscous resistance R_e of the cavity, and radiation resistance R_r of the combined driver and orifice. Thus C_A is in series with R_e and R_r and all three are in shunt position. The volume velocity ψ_N flowing through the neck is impeded by an inductance L_N which is in parallel with the cavity branch. Figure 3.3.3 shows the mechanical portion of the Helmholtz resonator in this model considered as a circuit (P = across variable and ψ through variable):

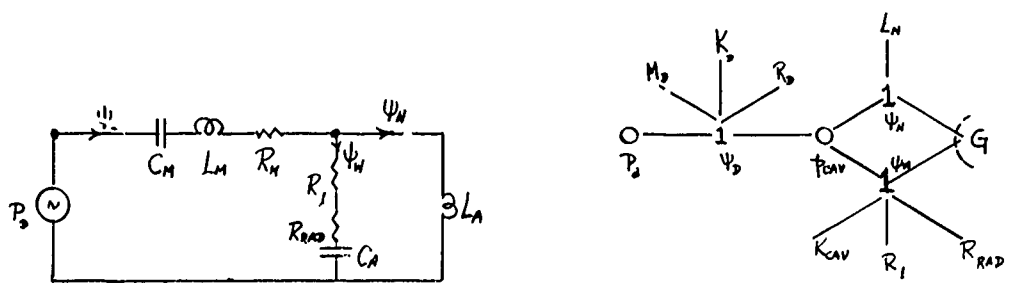


Fig. 3.3.3 — A $p\psi$ equivalent circuit of the Helmholtz resonator with moving cavity wall (after Woollett [2]) (b) its bond graph

The acoustic immittance ($= \psi_D / P_D$) of this circuit is maximized at two frequencies: (1) at mechanical resonance ω_M of the wall in which the reactance of the effective spring C_M and effective mass L_M cancel each other, $\omega_M = \frac{1}{\sqrt{L_M C_M}}$. (2) and a second resonance at mechanical resonance ω_H of the spring of the wall and the parallel circuit C_A, L_N of the cavity-neck combination. $\omega_H = \frac{1}{\sqrt{(C_M + C_A) L_N}}$.

The office-cavity resonance frequency ω_H (= Helmholtz resonance) is much lower than the elastic-radiation resonance frequency ω_M. Figure 3.3.4 shows a sketch of the transmitting (voltage) response predicted by the model.

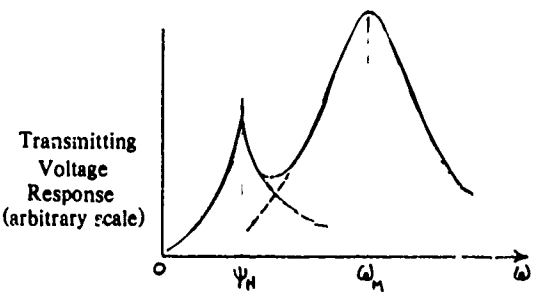


Fig. 3.3.4 — Sketch of transmitting voltage response of a Helmholtz resonator transmitter

3.4 GENERIC MODEL OF HELMHOLTZ RESONATOR SOUND SOURCE

The previous section has discussed the construction of an equivalent circuit for the spherical Helmholtz resonator sound source. Since other shapes are possible we continue with a more general approach to modeling. We adopt the FV (acoustically, $P\psi$) model of the mechanical circuit and generalize Fig. 3.3.4 as follows:

1. the electrical mesh is a voltage generator in parallel with electrical impedance Z_e. (See Sec. 1.8 for a discussion on the modeling of a source).

2. the transformer ratio is $1{:}\phi^2$ in which ϕ contains a factor $1/S_D$ where S_D is the area of the driver, inserted in order to convert equivalent mechanical impedances into acoustical impedances, that is, electrical voltage E is converted into acoustical pressure P and electrical current F into volume velocity ψ.

3. there are two "acoustical (ac) pressure nodes", p_D supplied by the electric field and p_c in the cavity. The difference between p_D and p_c drives a volume velocity ψ_D through the driver-loading impedance z_D (which includes the acoustic loading on both sides of the elastic driver surface as well as the acoustical impedance of the driver itself). The cavity pressure p_c drives a volume velocity ψ_c through the compliance z_c of the cavity, as well as a volume velocity ψ_p through the port (= Helmholtz orifice) impedance z_p and the port radiation z_R.

The mechanical-acoustical equations expressing these physical facts are:

$$(1) \quad \frac{p_D - p_c}{z_d} = \psi_D \quad or \quad p_D - z_d \psi_d = p_c \tag{3.4.1}$$

$$(2) \quad \frac{p_c}{z_c} = \psi_c \quad or \quad p_c - Z_c \psi_c = 0 \tag{3.4.2}$$

$$(3) \quad \frac{p_c}{(z_p + z_r)} = \psi_p \qquad or \; p_c - (z_p + z_R)\psi_p = 0. \tag{3.4.3}$$

From the discussion in Sec. 3.3 it will be seen that z_D is in series position, while z_c and $(z_p + z_R)$ are in shunt position.

The generalized circuit is shown in Fig. 3.4.1.

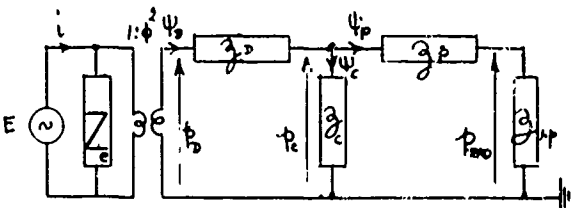


Fig. 3.4.1 — Generalized FV equivalent circuit of a Helmholtz resonant sound source

The complex acoustical pressure radiated is,

$$p_{\text{RAD}} = z_R \; \psi_p$$

while the complex acoustical power radiated is,

$$W = p_{\text{RAD}} \, \psi_p = z_R \psi_p^2. \tag{3.4.4}$$

Analysis consists in finding ψ_p for various choices of z_D, z_c, z_p, z_R.

3.5 EXPLICIT FORMS OF THE ACOUSTICAL IMPEDANCES OF THE HELMHOLTZ RADIATOR SOUND SOURCE

The driver impedance z_D contains these components:

$$z_D = z_M + z_{MR} + z_{MB} \quad (\text{units: } Hs/m^5)$$

z_M: acoustical impedance of the (elastic) driver

z_{MR}: radiation impedance into the external medium

z_{MB}: acoustical impedance of loading on backside of the driver (= interior cavity).

Explicit forms again depend on the physical character of the sound resonator.

The cavity impedance z_c contains the components:

$$z_c = R_{AB} + \frac{1}{j\omega C_{AB}}$$

R_{AB}: viscous resistance impedance in cavity

C_{AB} : acoustical compliance of cavity.

The neck impedance z_p is

$$z_p = R_p + j\omega \, M_p.$$

The neck radiation impedance is

$$z_{RP} = R_{RP} + j\omega\, M_{Mp}.$$

Explicit values to be assigned to these symbols depend on the selected physical form of the radiator. We treat here two forms:

Case I. The spherical piezoceramic Helmholtz radiator sound source

This source consists of a spherical piezoceramic shell density ρ_m, mean radius a_m, thickness t polarized through the thickness across fully electroded inner and outer spherical surfaces.

On the electrical side we take $Ze \approx 1/j\omega C_0$, where C_0 is the clamped electrical capacitance,

$$C_0 = \frac{4\pi a_m^2 \epsilon_{33}^T (1 - k_p^2)}{t}$$

k_p = planar coupling factor = $d_{31}^2/\epsilon_{33}^T s_c^E$

$$s_c^E \equiv \frac{1}{2}\,(s_{11}^E + s_{12}^E).$$

Z_e may also have a real part Re the electrical impedance determinable by measurement of the electrical Q_e at ω_r with the sphere vibrating in a vacuum.

$$\mathrm{Re} = \frac{1}{\omega_r C_0 Q_e}.$$

The transformer ratio of the equivalent circuit with a *mechanical* mesh expressed as a real number, is:

$$\phi' = \frac{4\pi a d_{31}}{s_c^E} \quad \text{(units: C/m)}.$$

When the mechanical mesh is replaced by an acoustical mesh, ϕ must be divided by $S = 4\pi a^2$. Hence

$$\phi_A = \frac{d_{31}}{s_c^E a} \quad \left[\text{units: } \frac{\text{C}}{\text{m}^3}\right].$$

On the mechanical-acoustical side of Fig. 3.4.1 we treat the vibrating shell first. The spherical shell in purely radial motion features these element values:

C_M = mechanical compliance = $s_c^E/4\pi t$ (units: m/N)

C_{MA} = acoustical compliance = $\dfrac{s_c^E 4\pi a^4}{t}$ (units: m^5/N)

M_M = mechanical mass = $4\pi a_m^2 t\rho_m$ (units: Ns^2/m)

M_{MA} = acoustical mass = $\frac{t\rho_m}{4\pi a^2}$ $\left[\text{units: } \frac{Ns^2}{m^5}\right]$

R_M = mechanical loss in material = $\frac{1}{\omega_r C_M Q_M}$ (units: Ns/m)

in which $\omega_r = 1/\sqrt{\rho_m s_c^E}$.

R_{MA} = acoustical loss in the material = $\frac{t}{\omega_r s_c^E 4\pi a^4 Q_M}$ $\left[\text{units: } \frac{Ns}{m^5}\right]$

A second component of the driver associated impedance is the acoustical radiation. We select here the common velocity form in the *FV* circuit such as that shown in Fig. 1.7.5a,

$$Z_{MR} = \frac{R_{RAD} + j\omega M_{RAD}}{S^2} = \frac{\rho c}{4\pi a^2}\left[\frac{(ka)^2}{1+(ka)^2} + j\,\frac{ka}{1+(ka)^2}\right].$$

A third component is tne acoustic impedance of the mass loading on the cavity side of the shell. This is difficult to estimate. One procedure is to assume a mass load which is the same as that of a spherical radiator at very low frequency (i.e., $ka \ll 1$). Then, from Sect. 1.7,

$$M_{AB} = \frac{1}{4}\,\frac{\rho_c}{\pi a}$$

in which ρ_c is the density of the cavity fluid.

We turn next to the cavity acoustical impedance. This compliance is simply the volume of the cavity V_c divided by the bulk modulus of the cavity fluid,

$$C_{AB} = \frac{V_c}{\rho c^2} \quad \text{(units: } m^5/N\text{)}.$$

The viscous loss in the cavity may be estimated from a measured value of the Q_c of the cavity. Approximately,

$$R_l = \frac{1}{\omega_r C_{AB} Q_c} \quad \text{(units: } N/m^5\text{)}.$$

A more accurate representation replaces C_{AB} by an effective compliance of value,

$$(1-\alpha)C_{AB};\ \alpha = \frac{C_D}{C_D + C_{AB}}.$$

As noted earlier (see Eq. 3.4.2) this compliance multiplied by the pressure p_c leaves no residual pressure. It is thus in shunt position.

The (ac, or signal) pressure also accelerates cavity fluid through the port (= orifice). This volume in motion encounters an acoustic impedance Z_p. The acoustic inertance of this impedance is associated with a mass:

$$M_p = \frac{\rho_c l' S_H}{S_H^2} = \frac{\rho_c l'}{S_H} \quad \text{(units: Ns}^2\text{/m}^5\text{)}$$

S_H = area of orifice.

The symbol l' is the length of the neck l modified by two end corrections, customarily taken as:

$$l' = l + 1.46\, a_H.$$

(See Sect. 3.2). The loss in the neck due to viscous resistance is

$$R_p = 4R_s \left[1 + 0.5\, \frac{l}{a_H}\right]; \quad R_s = \frac{1}{2}\sqrt{2\eta\rho\omega}$$

η = viscosity coefficient (units: Ns/m).

The final acoustical impedance to be accounted for is the radiation impedance of the orifice. Several models are available. Since the spherical surface provides some baffling, it is a first approximation to assume the orifice fluid acts as a piston in an infinite baffle. Then Fig. 1.7.6b applies. In this figure we assume a frequency low enough such that the impedance $1/j\omega C_{M1}$ is effectively infinite, so that,

$$R = R_{M1} + R_{M2} = (\pi + 1.386)a^2\rho c \quad \text{(units: Ns/m)}.$$

The acoustical radiation resistance is therefore,

$$R_p = \frac{R}{(\pi a_H^2)^2} = \frac{(\pi + 1.386)^2}{\pi^2 a_H^2}\,\rho c = \frac{0.459\,\rho c}{a_H^2} \quad \text{(units: Ns/m}^5\text{)}.$$

The acoustical radiation reactance is represented by an inductance of value $M_{M1} = (8/3)a^3\rho/S_H^2$, or

$$M_{M1} = \frac{8}{3\pi^2}\,\frac{\rho}{a_H} \quad \text{(units: Ns}^2\text{/m}^5\text{)}.$$

This completes the modeling of a spherical Helmholtz resonator sound source by means of an equivalent circuit. In practice the circuit parameters are determined by the transducer requirements of size, weight, frequency, power etc. and the circuit is solved for the volume velocity ψ_p flowing through the orifice. The acoustic power radiated is then given by

$$W_A = R_p \psi_p^2 = \left[\frac{0.459\,\rho c}{a_H^2}\right] \psi_p^2.$$

$$\psi_p^2 = \psi_p \psi_p^*$$

The source level p itself, expressed in maximum acoustic pressure at one meter is found from W_A by evaluating the integral,

$$W_A = \int_S \frac{p^2}{\rho c}\,(r,\theta,\phi)\; dS\;(r,\theta,\phi).$$

Customarily, the result of this evaluation is written in terms of a directivity factor R_θ:

$$p_\theta = \left.\frac{\sqrt{W_A \rho c R_\theta}}{4\pi r}\right|_{r=1 \text{ meter}}$$

$$R_\theta = \frac{\text{maximum acoustic intensity in direction of angle } \theta}{\text{average acoustic intensity over } 2\pi}.$$

In reporting measurements, θ is set to zero in the direction of maximum pressure.

A piezoceramic Helmholtz resonator sphere 4 in. in O.D. and 1/4" thick labelled USRD type F39A, was constructed by Henriquez [1]. Figure 3.5.1 compares the measured and predicted transmitting current response, and Fig. 3.5.2 compares the measured and predicted free field voltage sensitivity of this same transducer when it acts as a receiver of sound.

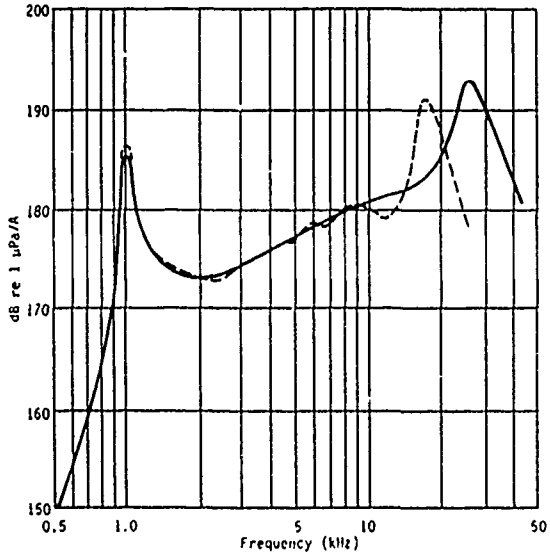


Fig. 3.5.1 — Transmitting current response of USRD type F39A transducer. Solid line: computed from circuit in Fig. 3.3.2. Dashed: measured.

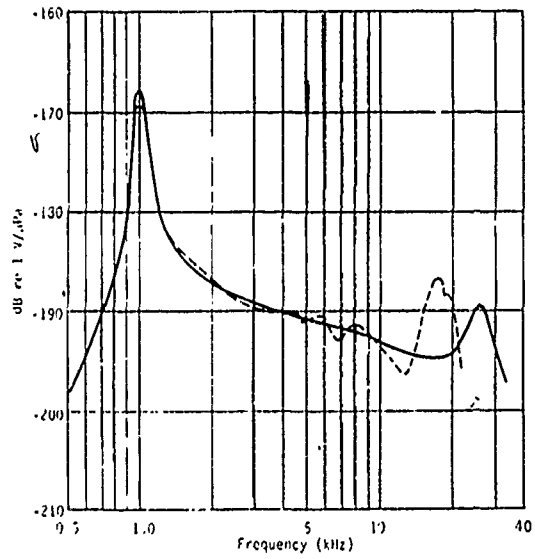


Fig. 3.5.2 — Free-field voltage sensitivity of USRD type F39A transducer. Solid line: computed from circuit in Fig. 3.3.2. Dashed line: measured.

3.6 THE CYLINDRICAL PIEZOCERAMIC HELMHOLTZ RESONATOR SOUND SOURCE

In large sizes the Helmholtz resonator is most practically made with a cylindrical body driven at its walls by piezoceramic rings, Fig. 3.6.1. Here the cylindrical walls consist of a stack of thin piezoceramic rings (6 shown), each of thickness t, height l, mean diameter D_m. The cylindrical cavity so formed provides the cavity compliance C_c (units: m^5/N) and the elastic walls provide the driver compliance C_D (units: m^5/N). A neck, area πa^2, length l_N, provides the inertance.

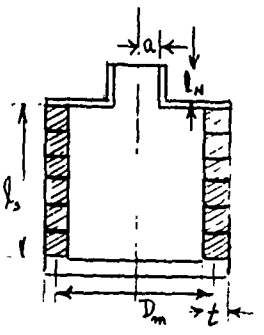


Fig. 3.6.1 — A Helmholtz resonator sound source with a cylindrical cavity

A first consideration in the operation of this transducer is the parameterization of the resonant frequency f_r. In the absence of the wall compliance the Helmholtz resonance depends on $C_c^{-1/2}$. To account for the effect of the C_D one writes,

$$f_r \propto \sqrt{\frac{1}{C_e}\left|\frac{C_e}{C_c + C_D}\right|}$$

or

$$f_r \propto \sqrt{\frac{1}{C_c}[1 - \alpha]}$$

$$\alpha = \frac{C_D}{C_c + C_D}.$$

Hence,

$$f_r^2 \propto 1 - \alpha.$$

A second consideration is the parameterization of the radiated power. In most applications (at low frequency) the sound source can be considered a point monopole with a volume source strength Q_ω (units: m^3/s). If the volume displacement of the moving walls is ΔV_f, one may assume for sinusoidal motion that,

$$Q_\omega = \omega \Delta V_f \quad \text{(peak source strength)}.$$

Thus the power radiated at resonance will be

$$W = \frac{\rho \omega^2}{2 \cdot 4\pi c} |Q_\omega|^2 = \frac{\rho (2\pi)^4 f^4}{2 \cdot 4\pi c} |\Delta V_f|^2.$$

Away from resonance the radiated power depends on the dynamic response of the cavity walls to a forcing function. Since the walls are elastic we may (in a first approximation) assume the transducer to be a simple damped harmonic oscillator, mass m, compliance $K = \omega_0^2 m$, damping $2b$, the displacement of which is,

$$|x| = \left|\frac{F/m}{\omega_r^2 - \omega^2 + j2b\omega}\right| = \frac{F/m}{\sqrt{(\omega_r^2 - \omega^2)^2 + (2b\omega)^2}} = \frac{(F/m\omega^2)}{\sqrt{\left[\left(\frac{fr}{f}\right)^2 - 1\right]^2 + \left(\frac{b}{f\pi}\right)^2}}.$$

The power in the oscillator is proportional to $|x|^2$. Thus the power radiated is modeled by the formula:

$$W = \frac{\rho(2\pi)^4 f^4 (1-\alpha)^2 |\Delta V_f|^2}{2 \cdot 4\pi c \left[\left(\frac{f_r}{f^2} - 1\right)^2 + (b/\pi f)^2\right.}.$$

Choosing $c = 1.5 \times 10^3$ m/s, $\rho = 10^3$ (Ns^2/m^4), and allowing ΔV_f to be peak value of a sinusoidal time dependence, one has

$$W = \frac{41.3\,(1-\alpha)^2 |\Delta V_f|^2 f^4}{\left[\left(\frac{fr}{f}\right)^2 - 1\right]^2 + \left(\frac{b}{f\pi}\right)^2} \quad \text{(units: Nm/s)}.$$

When $f << f_r$, W varies as f^8 so that the source level SL varies as f^4 or 24 dB/octave. When $f >> f_r$ W varies as f^4 making the SL vary as f^2 or 12 dB/octave.

The acoustic power radiated and the source levels predicted by these formulas are limited by the maximum permissible stress levels in the cavity. Letting P_{max} be this maximum stress level, it is seen that that peak volume displacement at very low frequencies is

$$\Delta V_f = C_c P_{max}.$$

The permissible (rms) radiated acoustic power is then

$$W_{\text{max stress}} = 41.3\, f^4 C_c^2 P_{\text{max stress}}^2.$$

The source level corresponding to this power is proportional to f^2. On a log-log plot the stress limited radiation is a straight line with a 12 dB/octave positive slope. A superposition of the stress limit plot on the voltage limit plot gives the operating limit of the Helmholtz radiator, Fig. 3.6.2

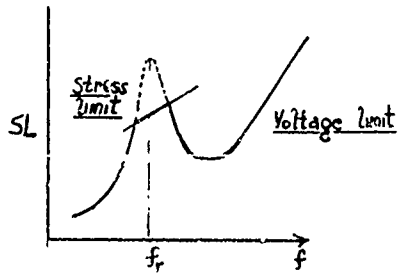


Fig. 3.6.2 — Illustration of voltage and stress limits of a Helmholtz resonator sound source

Characterization of the Driver

Since the piezoceramic driver is of barrel-stave design consisting of an assembly of n bars (length, l_c; width $w = \pi D_{\text{mean}}/n$; thickness t_c) cemented together to form a continuous cylindrical shell of mean diameter D_{mean}, each bar electroded on areas $l_c t_c$, and polarized through width w, the piezoelectric equation of state for the ring is

$$S_3 = s_{33}^E T_3 + d_{33} E$$

Here for radial displacement δ, S_3 is the hoop strain ($= \delta/a_{\text{mean}}$); T_3 is the hoop stress due to an applied force per unit angie $F/2\pi$, where

$$T_3 = \left(\frac{F}{2\pi}\right) \frac{1}{t_c l_c}$$

and E is the applied electric field,

$$E_3 = \frac{V}{w} = \frac{Vn}{\pi D_{\text{mean}}}.$$

To find the force/voltage factor we set $S_3 = 0$ and solve for

$$N = \left|\frac{F}{V}\right| = \frac{2\pi t_c l_c n d_{33}}{\pi D_{\text{mean}} s_{33}^E} \quad \text{(units: } N/V\text{)}.$$

The "free strain," (meaning the strain for $E = 0$) is

$$\frac{\delta}{a_{\text{mean}}} = \frac{s_{33}^E (F/2\pi)}{t_c l_c}$$

hence the mechanical compliance of the shell is

$$C_M = \frac{\delta}{F} = \frac{a_{\text{mean}} s_{33}^E}{2\pi t_c l_c} \quad \text{(units: m/N)}.$$

Since the mass of the shell (of density ρ_m) is,

$$M_M = \rho_m \pi D_{\text{mean}} l_c t_c$$

the frequency of radial resonance is

$$\omega_r = \frac{1}{\sqrt{M_M C_M}} = \frac{1}{a_{\text{mean}} \sqrt{s_{33}^E \rho_m}}.$$

The mechanical resistance at resonance can be obtained from a knowledge of the mechanical Q_M:

$$R_m = \frac{1}{\omega_r C_M Q_M} = \frac{a_{\text{mean}} (\rho_m s_{33}^E)^{1/2}}{C_M Q_M} \quad \left[\text{units: } \frac{\text{Ns}}{\text{m}}\right]$$

The free radial displacement δ_f generated by the applied voltage V can be deduced from the formula for C_M and N. Hence the free volume displacement is,

$$\Delta V_f = a_{\text{mean}} l_c n d_{33} V.$$

A useful modification of this formula is to use $V = E\pi D_{\text{mean}}/n$ so that,

$$\Delta V_f = 2\pi a^2 l_c d_{33} E \quad \text{(units: m}^3\text{)}.$$

This formula gives the maximum free volume displacement for a maximum applied field E (for piezoceramics this is usually taken at 4 k volt/cm).

The acoustical element parameters are derived by simple assumptions of lumped values. The compliance is

$$C_A = \frac{V}{\rho_i c_i^2} = \frac{\pi a_i^2 l_{\text{cav}}}{\rho_i c_i^2} \quad \text{(units: m}^5\text{/N)}.$$

The viscous loss in the cavity is difficult to estimate. A convenient procedure is to assume this loss is approximately that of simple time harmonic flow of a vicous fluid (dynamic viscosity η (units: Ns/m^2), density ρ, frequency f) over a large surface A. The *mechanical* resistance is then,

$$R_{\text{v}} = (\pi\eta\rho f)^{1/2} A \quad \text{(units: Ns/m)}$$

whereas the *acoustical* resistance is

$$R_{(A)\text{v}} = \frac{(\pi\eta\rho f)^{1/2}}{A} \quad \text{(units: Ns/m}^5\text{)}.$$

The form of the radiation elements of cylinder, or piston-orifice can be chosen in two ways: in the common volume velocity form, $p = \psi Z_A$, where Z_A is the acoustic radiation impedance; or in the common pressure form, $\psi = pY_A$, where Y_A is the acoustic radiation inimitance. These forms are explicitly written for the cylindrical driver on a per unit length basis,

$$Z_D = R_R + jM_R = \frac{1}{2\pi a l_c} \rho c \left\{ \frac{(2\ ka)^2}{1 + (2ka)^2} + j \frac{2ka}{1 + (2ka)^2} \right\} \left\{ \text{units: } \frac{\text{Ns}}{\text{m}^5} \right\}$$

$$Y_D = G_R - jB_R = \frac{2\pi a l_c}{\rho c} \left\{ 1 - j \frac{1}{2ka} \right\} \text{(units: m}^5\text{/Ns)}.$$

When the Z_D form is used the radiation elements are a resistance and inductance in series. When the Y_D form is used the radiation elements are a conductance and capacitance in parallel

The radiation from the orifice must be approximated: a good model is to assume the orifice to be a piston at the end of a long (rigid wall) tube. Then from Section 1.7, the FV diagram of this radiation consists of an inductance (= mass) M_{m1} and a resistance $R_{M1} + R_{M2}$:

$$Z_{RAD} = R_0 + jX_0 = (1 + 0.504)\,\pi a_i^2 \rho_0 c + j\omega\, 0.6133\,\pi a_i^3 \rho_0 \text{ (units: Ns/m)}$$

$$Z_{RAD} = \frac{1.504}{\pi a_i^2}\,\rho_0 c + j\omega\,\frac{0\,6133\,a\rho_0}{\pi a_i^2} \text{ (units: Ns/m}^5\text{)}.$$

Actually, the inertance of the orifice is that of an orifice at the end of a closed pipe of length l, radius a:

$$Z_a = -j\,\frac{\rho_0 c}{\pi a_i^2}\cot kl.$$

At low frequencies, for a stack of n rings,

$$Z_a \to j\,(\omega\, M_A - \frac{1}{n\omega C_A})$$

$$M_A \to \frac{\rho_0 l'}{3\pi a_i^2}\left\{1 + \frac{(kl')^2}{15} + \frac{(kl')^4 2}{315} + \cdots\right\}$$

in which l' is the actual length plus an orifice correction factor (see Sect. 3.2), and a_i is the orifice radius.

The equivalent circuit of the cylindrical Helmholtz resonator, sound source, based on the concepts of Sec. 1.17 through 1.22, is shown in Fig. 3.6.3. Three alternative bond graphs representing the same physical model are also displayed.

A large cylindrical Helmholtz resonator sound source was built by A. M. Young et al. [3]. Five barrel-stave piezoceramic rings, mean radius 0.267 m, wall thickness 0.025 m, each constructed of $n = 96$ segments per ring, were stacked to give a total height of 0.775 m. The cavity thus formed was completed by metal rings to a total of 0.919 m, terminating in an orifice of radius 0.210 m. The ceramic properties were

$$d_{33} = 280 \times 10^{-12} \text{ m/V}$$

$$s_{33}^E = 1.493 \times 10^{-11} \text{ m}^2/\text{N}$$

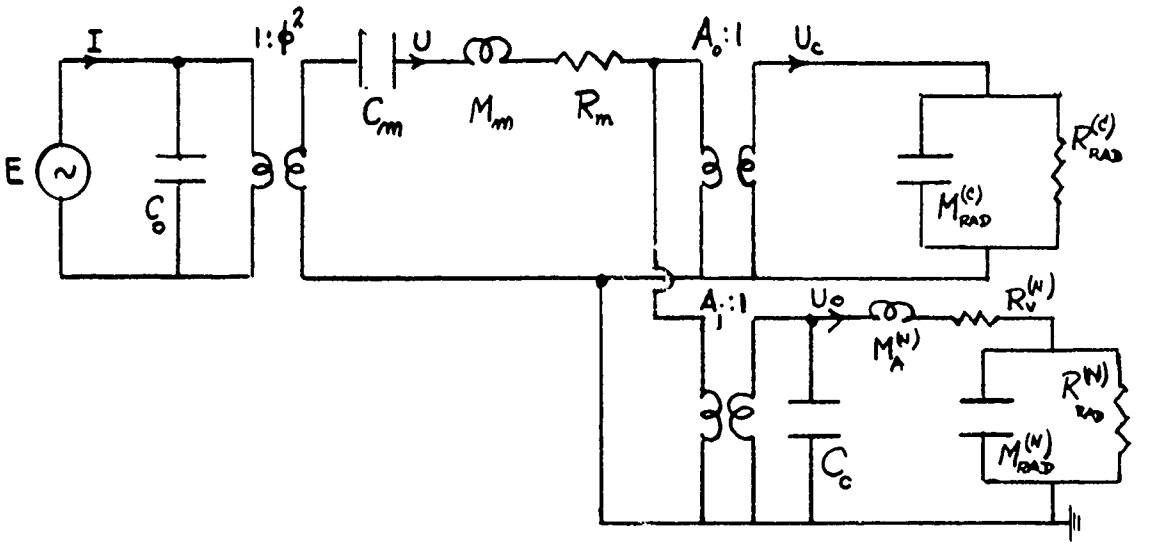
$$\rho_c = 7.55 \times 10^3 \text{ kg/m}^3.$$

The oil fill between boots was chosen to be castor oil, with properties:

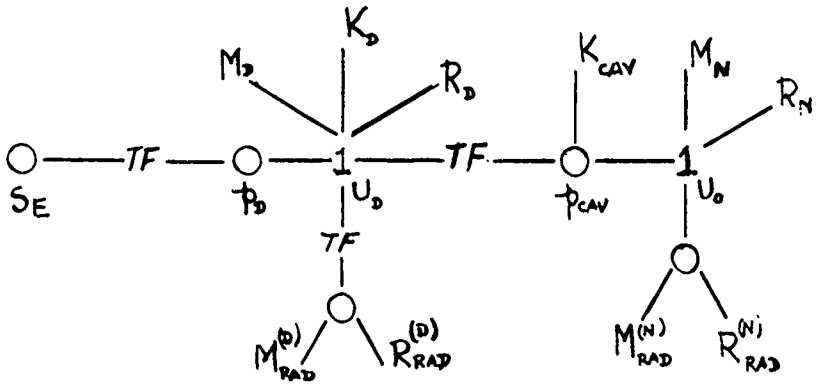
$$\rho_{oil} = 950 \text{ Kg/m}^3$$

$$c_{oil} = 1540 \text{ m/s}$$

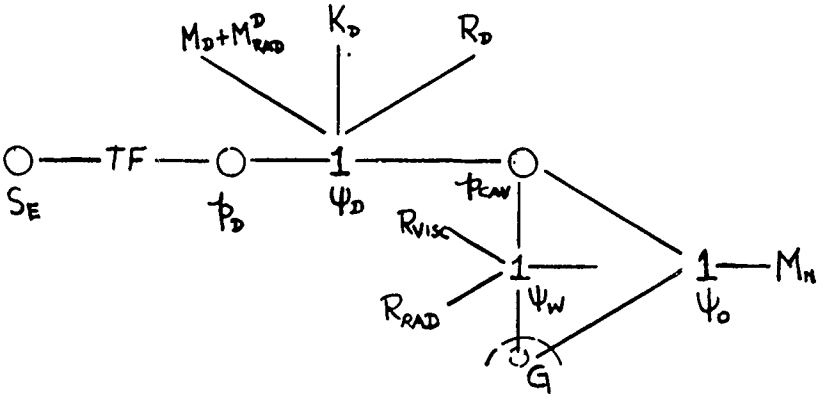
$$\eta = 0.986 \text{ Ns/m}^2.$$



(a)



(b)



(c)

Fig. 3.6.3 — (a) FV equivalent circuit of a cylindrical Helmholtz resonator sound source (b) its bond graph (c) an alternate bond graph

Figure 3.6.4 shows the conceptual design. The predicted and measured transmitting voltage response is shown in Fig. 3.6.5. The sharp peak predicted was based on under-estimating several loss mechanisms such as viscous loss in the cavity, in the oil, at the orifice, etc., as well as the modeling of the inertance of the orifice, which, because the orifice diameter is not too different from the cavity diameter, is only very approximately that of fast moving slug of water.

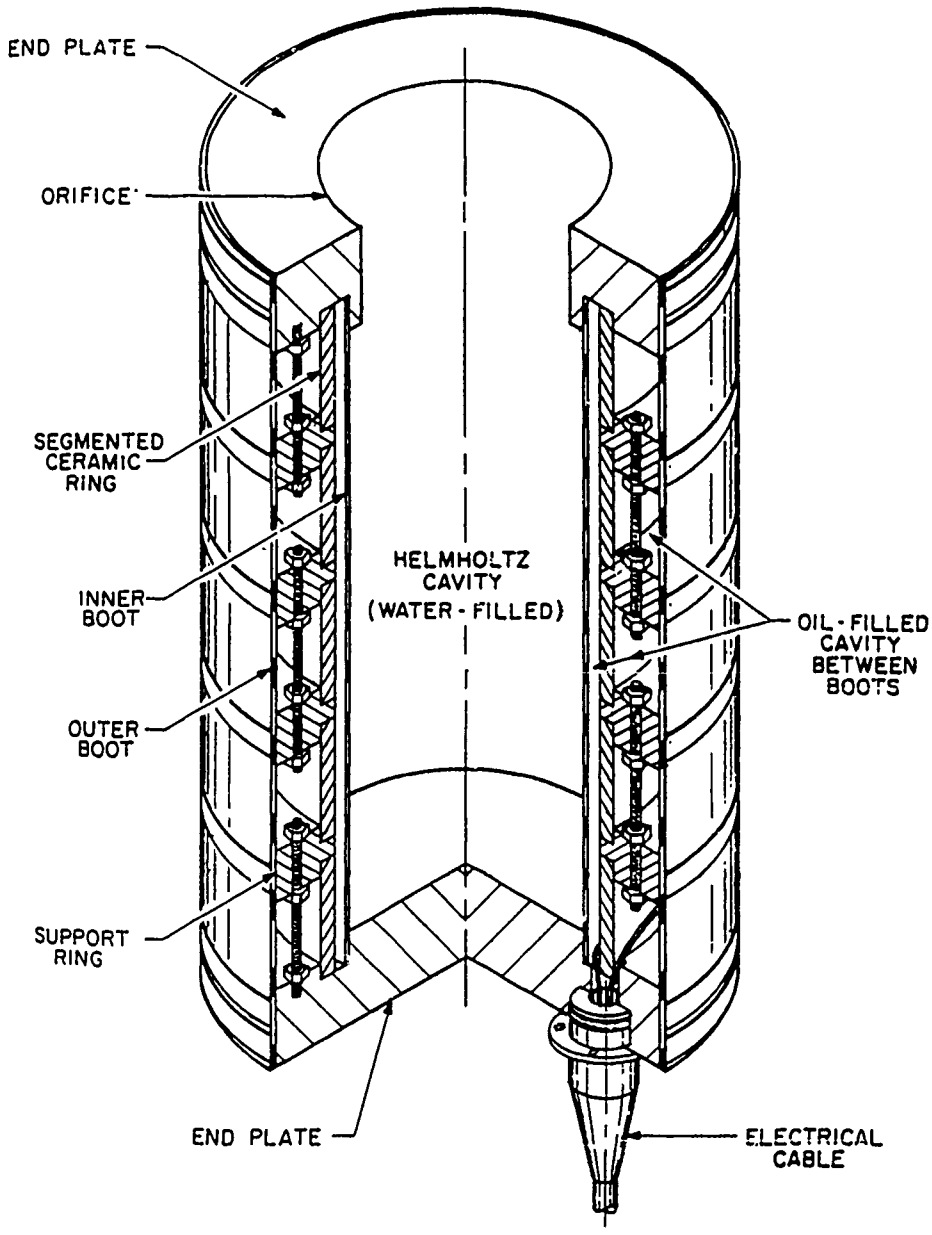


Fig. 3.6.4 — Conceptual design of a cylindrical Helmholtz resonator sound source [3]

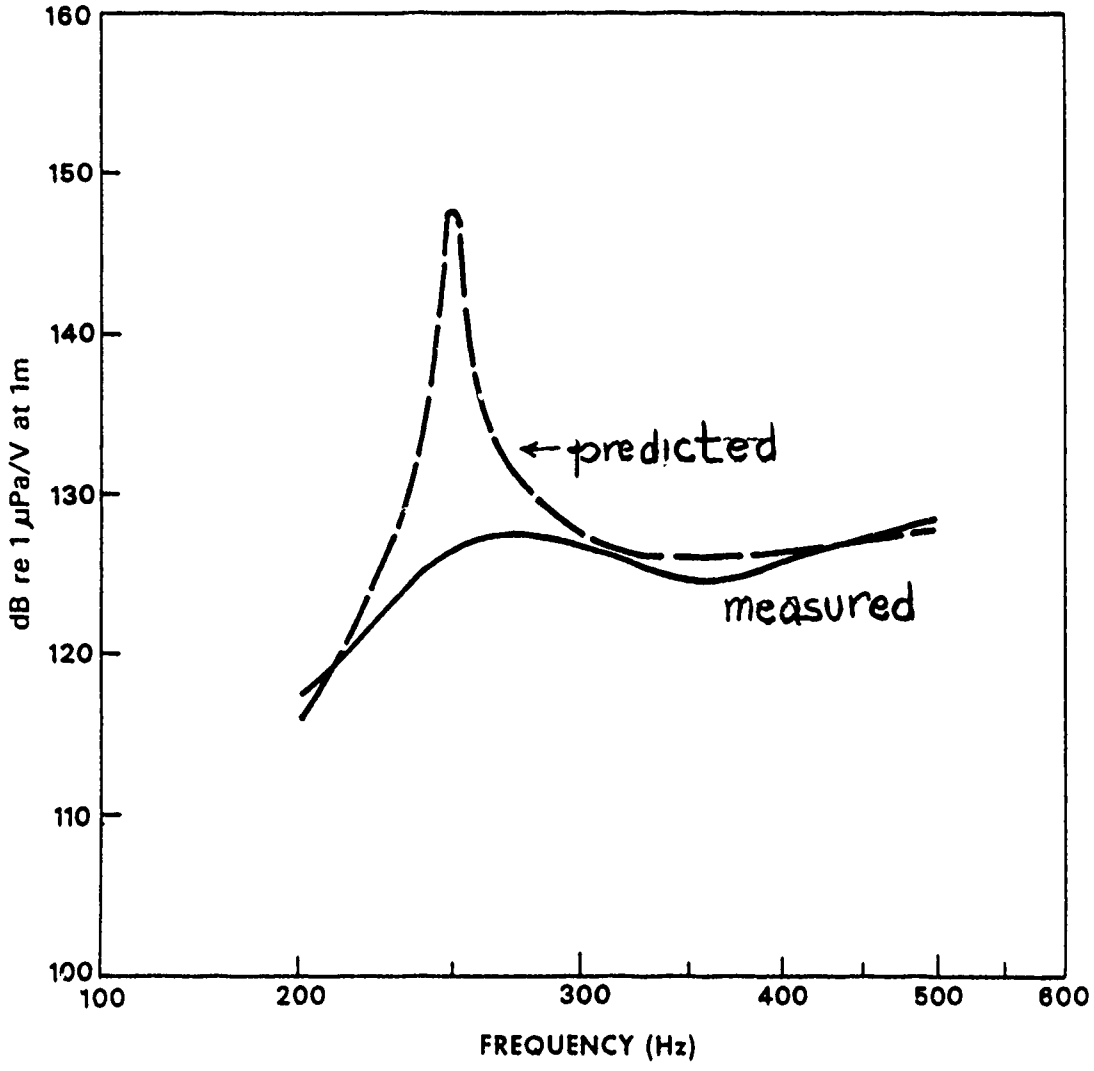


Fig. 3.6.5 — Transmitting voltage response of transducer in Fig. 3.6.4 [3]

3.7 CORRECTIONS TO CAVITY AND ORIFICE INERTANCE

The inertances of the cavity and orifice are difficult to formulate. Incorrect modeling leads to errors in predicting the frequency of Helmholtz resonance and acoustic response. To account for motion of the fluid in the cavity and orifice Alster [4] devised a formula for the resonant frequency of these resonators which includes corrections:

$$f = \frac{C}{2\pi}\left[\frac{A}{1.21\,(V + AL_N)\,L_1}\right]^{1/2}$$

$$L_1 = \left\{L_v + L_0 + (L_N + L_0)\left[1 + \frac{L_N + L_0}{2L} + \frac{A(L_N + L_0)}{2V} + \frac{A(L_N + L_0)}{3V}\,\frac{L_N + L_0}{L}\right]\right\}$$
$$\times \frac{V}{V + A(L_N + L_0)}\,\frac{L}{L + L_N + L_0}.$$

c = velocity of sound in the fluid of the cavity

A = cross-sectional area of neck

L_N = length of the neck

V = volume of the cavitry without the neck

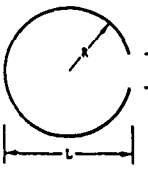
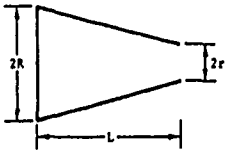
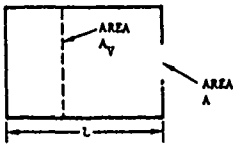
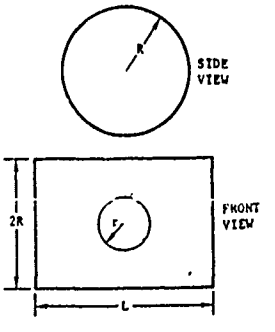
L = height of the resonator cavity, bottom to the neck

L_v = a form factor (see Table), units of length

$L_0 = 0.24\ r$, where r = radius of the neck

Table 3.7.1, reproduced from Ref. [4] provides convenient formulas for L_v. These formulas apply to simple resonators (a single cavity with a single neck). The Appendix gives formulas for the resonant frequencies of compound Helmholtz resonators.

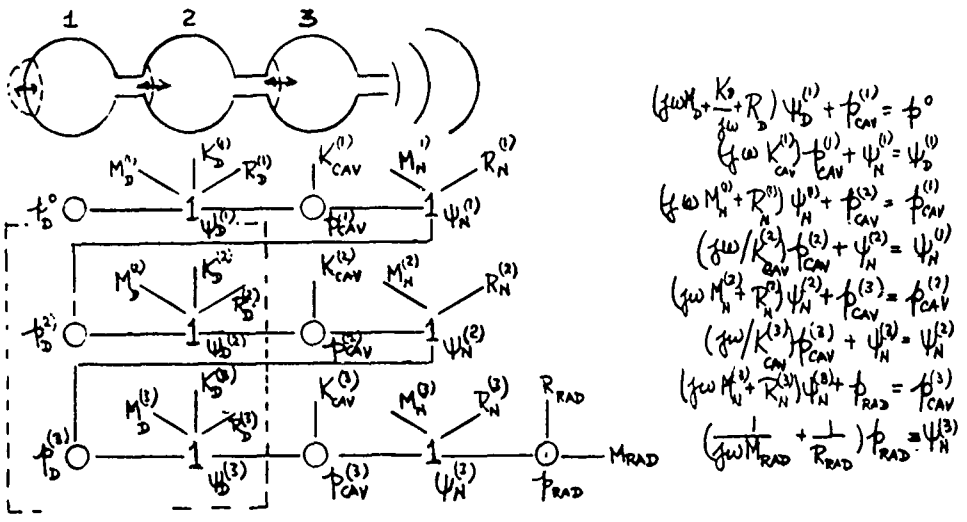
Table 3.7.1 — For Factors for Helmholtz Resonator Cavities [1]. M. Alster, *Journal Sound and Vibration*, **24** (1972), ©1972 Academic Press, Inc.; by permission.

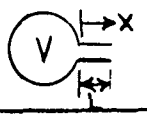
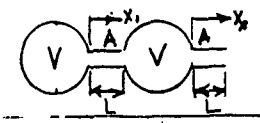
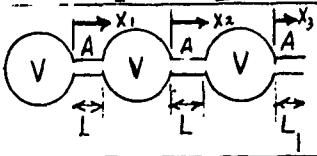
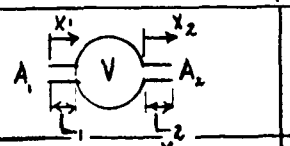
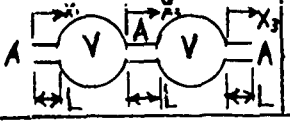
Description	Form Factor, L_V (Eq. 13-27)
1. Sphere 	$\frac{r^2}{R}\frac{1}{2-\alpha}\left[\frac{1}{3}-\frac{1}{2(\alpha+1)}-\frac{2}{(\alpha+1)^2}+\frac{4}{(\alpha+1)^3}\ln\left(\frac{2}{1-\alpha}\right)\right]$ where $\alpha=\left[1-\left(\frac{r}{R}\right)^2\right]^{1/2}$
2. Frustrum of a Cone 	$\frac{L}{\left(\frac{R}{r}\right)^2+\left(\frac{R}{r}\right)+1}\left[\frac{1}{3}-\frac{1}{2}\frac{R}{R-r}+\left(\frac{R}{R-r}\right)^3\cdot\left\{\left(\frac{R}{r}\right)-1-\ln\left(\frac{R}{r}\right)\right\}\right]$
3. Prism 	$\frac{L}{3}\frac{A}{A_V}$
4. Cylinder with Lateral Hole 	If $r \ll R$ or the resonator has a neck at the opening: $\frac{1.88r^2}{L}$

Appendix

The basic approach to modeling the performance of acoustic transducers by equivalent circuits used in this treatise is that of converting the equations of motion in all degrees of freedom of a system into loop representation or nodal representation. It is therefore useful in the design of multiple cavity Helmholtz resonators to count the degrees of freedom of particular structures, to list the associated resonant frequencies, and to show the "mode shapes". The latter term refers to the amplitude (and sign) to be associated with each degree of freedom relative to an assigned value of +1 to the first degree of freedom. Table 3A.1 gives the resonant frequency and mode shape of simple cavity and multiple cavity Helmholtz resonators [5].

Table 3.6.1 — Helmholtz Resonators



Geometry	Natural Frequency	Mode Shape
	$\Omega_r = \frac{c}{2\pi}\left(\frac{A}{VL}\right)$	
	(1) $\frac{(3-5^{1/2})^{1/2}}{2^{3/2}\pi}\Omega_R$ (2) $\frac{(3+5^{1/2})^{1/2}}{2^{3/2}\pi}\Omega_R$	$\begin{bmatrix}X_1\\X_2\end{bmatrix} = \begin{bmatrix}1\\\frac{1+5^{1/2}}{2}\end{bmatrix}, \begin{bmatrix}1\\\frac{1-5^{1/2}}{2}\end{bmatrix}$
	(1) 0.07082 Ω_r (2) 0.1985 Ω_r (3) 0.2868 Ω_r	$\begin{bmatrix}X_1\\X_2\\X_3\end{bmatrix} = \begin{bmatrix}1\\1.802\\2.247\end{bmatrix}\begin{bmatrix}1\\0.445\\-0.802\end{bmatrix}\begin{bmatrix}1\\-1.247\\0.555\end{bmatrix}$
	(1) 0 (2) $\frac{c}{2\pi}\left(\frac{A_1}{L_1V} + \frac{A_2}{L_2V}\right)$	$\begin{bmatrix}X_1\\X_2\end{bmatrix} = \begin{bmatrix}1\\-\frac{A_1}{A_2}\end{bmatrix}, \begin{bmatrix}1\\\frac{L_1}{L_2}\end{bmatrix}$
	(1) 0 (2) $\frac{c}{2\pi}\left(\frac{A}{VL}\right)^{1/2}$ (3) $\frac{c}{2\pi}\left(\frac{3A}{VL}\right)^{1/2}$	$\begin{bmatrix}X_1\\X_2\\X_3\end{bmatrix} = \begin{bmatrix}1\\1\\1\end{bmatrix}, \begin{bmatrix}1\\0\\-1\end{bmatrix}, \begin{bmatrix}1\\-2\\1\end{bmatrix}$

REFERENCES

[1] T.A. Henriquez, "The USRD Type F 39A1-kHz Underwater Helmholtz Resonator," NRL Report 7740, April 1974 (AD-778-337/HH).

[2] R.S. Woollett, "Underwater Helmholtz Resonator Transducers General Design Principles," NUSU Tech. Report 5633, July 1977, Naval Underwater Systems Center, New London, Ct.

[3] M. Young et al., NRL Report 8633.

[4] M. Alster, "Improved Calculation of Resonant Frequencies of Helmholtz Resonators," J. Sound and Vib. **24**, 64-85 (1972).

[5] "Formulas for Natural Frequency and Mode Shape," R.D. Blevin, Van Nostrand Reinhold Co. 1979, p. 375.

Chapter 4
POLYMER FILM TRANSDUCERS

4.1 INTRODUCTION

Many biological macromolecules (biopolymers) are piezoelectric: for example, it is found that films prepared of polypeptides, bone, tendon or wood develop surface charges when stressed in the film plane. The measured equivalent piezoelectric constants of these substances are comparable in magnitude to crystalline quartz, even without any previous electrical treatment. In contrast to the general run of natural crystals only shear coefficients d_{14} and d_{25} are observed in these biopolymers. Synthetic polymers (not of biologic origin) also exhibit piezoelectricity. In 1969 Kawai [1] showed that *stretched* film of (about 30-50 microns thick) polyvinylidene fluoride PVF_2 heated to 90°C and then cooled down to room temperature in a dc field ($\sim$ 0.3 MV/cm) was more strongly piezoelectric than crystalline quartz. Large piezoelectric strain coefficients d_{31} were observed in the initial (usually designated subscript 1) drawing direction. This film was however markedly anisotropic since the coefficient of electromechanical coupling is stronger in the machine direction (of stretching) than in the planar transverse direction. Electric field hysteresis, similar to that of crystalline ferroelectrics, has been observed in these polarized films. PVF_2 is also strongly pyroelectric, and does not lose its polarization after several heating cycles.

Although PVF_2 films, polarized through the thickness, have been used in applications to acoustics, electrical switching and pyrometry, a satisfactory explanation of its piezoactivity is still to be made to date (1987).

4.2 PHENOMENOLOGICAL THEORY OF PIEZOELECTRICITY IN POLYMER FILMS

A thin film of PVF_2, surface area A, thickness l, roll-drawn in the 1-direction and polarized in the 3-direction through full electrodes over both surfaces ($x = \pm l/2$), is deformed sinusoidally with time (at frequency ω). As a result of this deformation one observes an open-circuit voltage across the electrodes, or alternatively, a short-circuit current, at the same frequency ω. The deformation in question is elongational in the plane of the film, or bending of the film. In stretched PVF_2 film the anisotropy of piezoelectricity is clearly noticeable because the open circuit voltage is largest for deformation (= elongation) in the stretch direction, and is less in any other direction in the plane. The piezoelectric constant d_{31} is a complex quantity because the open-circuit voltage is not in phase with the applied strain, and the short-circuit current is not in phase with the strain rate.

A phenomenological theory of piezoelectricity in PVF_2 film is most conveniently framed in terms of the classical equations of a piezoelectric crystal in which a constant-S mechanical boundary condition, and a constant E electrical boundary condition are used:

$$\begin{cases} D = eS + \epsilon^S E \\ T = c^E S - eE \end{cases} \tag{4.2.1}$$

D is the electric displacement, e is the piezoelectric stress constant, ϵ^S is the damped dielectric constant, E is the electric field, T is the stress, c^E is the short-circuit elastic modulus and S is the elastic strain.

In the general theory both e and ϵ^s are functions of strain S or strain gradient ∇S. Expressed in Cartesian tensor form, the general theory is described by the relation,

$$D_i = e_{ik}\, S_k + e'_{ijk}\, \frac{\partial S_k}{\partial r_j} + \left[\epsilon^S_{0ij} + \frac{\partial \epsilon^S_{ij}}{\partial S_K}\, S_K\right] E_j\ ,\ i = 1,2,3 = j \tag{4.2.2}$$

where

$$r_j = (x,y,z)$$

The symbol e_{ik} when written in full tensor notation is a third-rank tensor which describes the piezoelectric property of the polymer film associated with uniform strain S_k. It vanishes when the crystalline material of the film has a center of crystalline symmetry. The symbol e_{ijk} when written in full tensor notation is a fourth-rank tensor which describes the piezoactivity of the polymer film associated with nonuniform strain $\partial S_k/\partial r_j$. It does not vanish even in the presence of a center of symmetry. The symbol $\partial \epsilon^S_{ij}/\partial S_k$ is the electrostricition constant.

In applications the deformation is specifically made along the direction, call it x, which gives the maximum piezoelectric effect. Thus only one component of the tensor of Eq. 4.2.2 is normally used,

$$D(x) = e(x)\, u(x) + \epsilon(x)\, \mathrm{E}(x) + P_0(x) \tag{4.2.3}$$

In this form, $u(x)$ is the uniform deformation strain in the x-direction and $P_0(x)$ is the polarization, excluding polarizations due to electric field and uniform (internal) strain. Figure 4.2.1 shows the film located between two electrodes. Solving for $E(x)$ and integrating it between $\pm l/2$ gives the potential difference developed across the electrodes by the strain and charge accumulation:

$$V = -\int_{-l/2}^{l/2} dx \frac{D(x) - P_0(x)}{\epsilon(x)} + \int_{-l/2}^{+l/2} \frac{e(x)u(x)}{\epsilon(x)}\, dx. \tag{4.2.4}$$

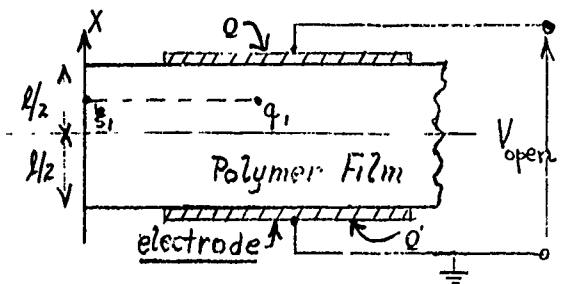


Fig. 4.2.1 — Polymer film showing two electrodes with true charges Q, Q', and a bound (interior) charge q_1 at level ξ_1

By assuming

$$\epsilon(x) = \epsilon_0 + \kappa u(x), \quad \kappa = \frac{\partial \epsilon}{\partial u} \tag{4.2.5}$$

$$e(x) = e_0 + \frac{\partial e}{\partial u}\, u(x)$$

Hayakawa and Wada [2] derived a formula for the open circuit voltage V developed across the electrodes of Fig. 4.2.1 induced by the deformation $u(x)$:

$$V_{\text{open}} = \frac{\left[1 - \dfrac{\kappa}{\epsilon_0}\right]}{\epsilon_0} \int_{-l/2}^{l/2} dx \left[u(x) - \frac{\delta l}{l}\right] \int_{-l/2}^{x} \rho(x)\, dx + \frac{e_0}{\epsilon_0}\, \delta l \tag{4.2.6}$$

in which $\rho(x)$ is the sum of the true charge density ρ_t and the polarization charge density $\rho_p = -\partial P_0(x)/\partial x$.

Discussion: Equation 4.2.6 serves as a convenient formula to describe phenomenologically the various possible origins of piezoelectricity *in polymers*. First, there is the conventional piezoactivity due to internal strain in a unit cell of polar crystals, or any asymmetric crystals. This is expressed by the term $e_0\delta l/\epsilon_0$. Polymers of biological origin exhibit this type of piezoactivity. The matrix of stress/field constants $d(=e/g)$ for them is of the face-shear form, Table 4.2.1:

Table 4.2.1

$$\begin{matrix} 0 & 0 & 0 & d_{14} & 0 & 0 \\ 0 & 0 & 0 & 0 & -d_{14} & 0 \\ 0 & 0 & 0 & 0 & 0 & 0 \end{matrix}$$

Second, there is a type of piezoelectricity which results from a combination of charge distribution $\rho(x) = [\rho_p(x) + \rho_t(x)]$ throughout a polarized amorphous material coupled to a *nonuniform* strain $\Delta u = [u(x) - \delta l/l]$. This piezoelectricity is found in synthetic polymer electrets, such as a film of PVF_2, and is attributed to the existance of polarization in the film, with an associated distribution of electric charge both in the interior and on the surface. The matrix of stress/field constants for such synthetic polymer electrets has the form:

Table 4.2.2

$$\begin{matrix} 0 & 0 & 0 & 0 & d_{15} & 0 \\ 0 & 0 & 0 & d_{15} & 0 & 0 \\ d_{31} & d_{32} & d_{33} & 0 & 0 & 0 \end{matrix}$$

Several mechanisms explaining the origin of these charges in polymer electrets have been forwarded: (1) the electrodes inject charge into the film (2) the dielectric-electrode interface exhibits breakdown with resultant injection of charge into the film (3) charge carriers migrate over macroscopic distances in the film (4) generation of dipoles caused by migration over microscopic distances. Which of these is most likely, is a matter of current dispute. A more detailed discussion is provided later in this chapter.

We choose one synthetic polymer, PVF_2, for further study.

4.3 STRUCTURE AND PROPERTIES OF PVF_2 IN 31 MODE

Polyvinylidene fluoride (PVF_2 or PVDF) is a semicriystalline polymer. It crystallizes from its melt into spherulitic structures (that is, spheres of crystalline lamina separated by amorphous components growing out of the center). The volume fraction of crystalline material is about 50%. When in liquid form, the net (charge) moment of a group of molecules is zero in absence of an applied field. In the crystal form PVF_2 exhibits two crystal phases, β and γ, which are inherently polar (that is, when they are stacked in lamellae they exhibit a net polarization). A third phase, α, although posessing a dipole moment, packs to form anti-polar cells, and hence nonpolar lamellae stacks.

PVDF is manufactured in films approximately 1 to 125 mils thick. The coordinate system used to define piezoelectric and dielectric properties of these films has been standardized, Fig. 4.3.1.

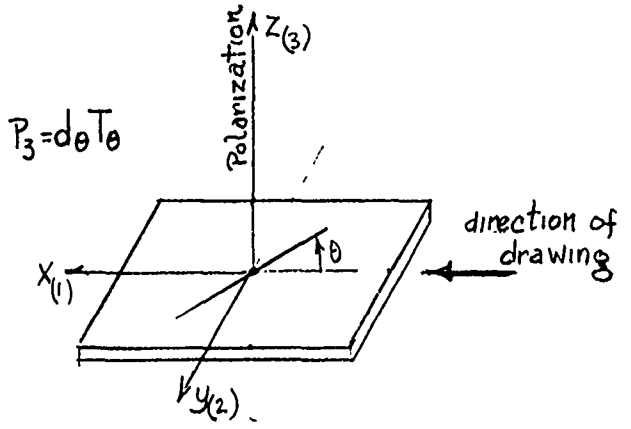


Fig. 4.3.1 — Coordinate system defining the direction of polarization of a polymer film

The orientation (or direction of drawing) in the plane of the film is labeled 1 and the direction of polarization is normal to the plane and is labelled 3. In manufacture, the film is monoaxially (= x direction) oriented. This causes piezoelectric anisotropy in the film which makes the d-constant a function of angle θ, Fig. 4.3.2. Its magnitude at $\theta = 0°$ (which is $\sim 2.3 \times 10^{-11}$ C/N for a sample specimen used in a specific test) is about 10 times that at $\theta = 90°$. Other specimens polarized under more optimum conditions of temperature, dc field, and rate of cooling show higher magnitudes ($d_{31} \sim 5 \times 10^{-11}$ C/N) for β-phase PVDF). The relative dielectric constant ϵ/ϵ_0 ranges from 8 to 14 depending on ambient temperature and applied stress.

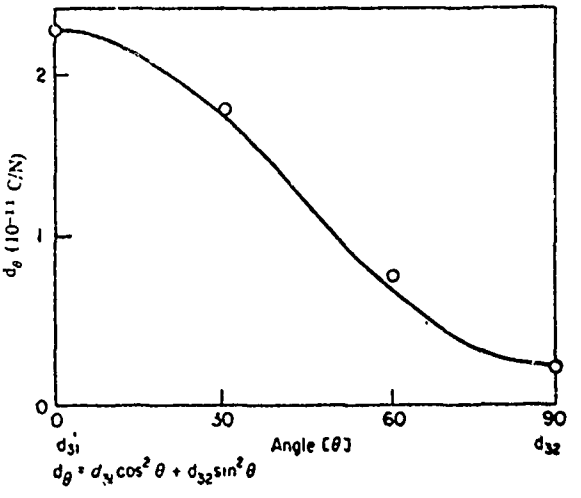


Fig 4.3.2 — Variation of d— constant of a PVDF film with angle θ as defined in Fig. 4.3.1 [3]. M. Marayama, *Ultrasonics*, 21 (1), (1976), ©1976 Butterworth & Co. (Pub) Ltd.; by permission.

The molecular structure of *PVDF* present in films depends upon conditions of film formation. The α-crystal form is found mainly in melt castings. The β-crystal form appears in oriented samples. A single crystal of β-form will naturally show a piezoelectric effect without any polarizing operations. The α-form transforms into β-form when the film is stretched at temperatures below 100°C.

Since PVDF is a synthetic structure its piezoelectric properties will vary with polarizing temperature, polarizing dc field and polarizing time. Figures 4.3.3, 4, 5 reproduced from Ref. [3] show these dependencies. Once polarized, PVDF, particularly in the β-form, is stable (in its piezoelectric properties) at room temperature. It is only when exposed to ambient temperatures that exceed 80°C that piezoactivity (as measured by the d_{31}) diminishes in the first 10 minutes of exposure to about 1/2 of its initial value and then becomes stable.

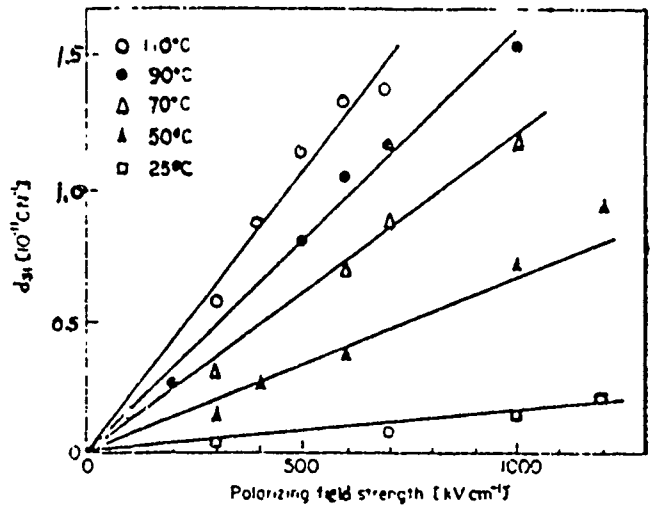


Fig. 4.3.3 — Variation of d_{31} of a PVDF film with polarizing field strength [3]. M. Marayama, *Ultrasonics*, **21**, (1) (1976), ©1976 Butterworth & Co. (Pub) Ltd.; by permission.

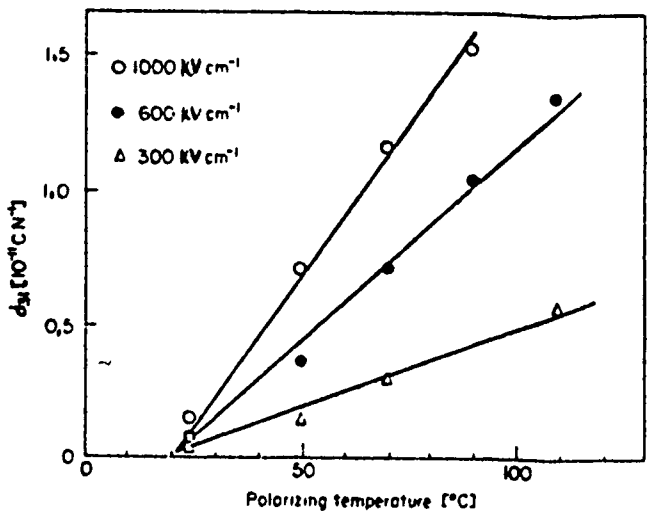


Fig. 4.3.4 — Variation of d_{31} of a PVDF film with polarizing temperature [3]. M. Marayama, *Ultrasonics*, **21** (1), (1976), ©1976 Butterworth & Co. (Pub) Ltd.; by permission.

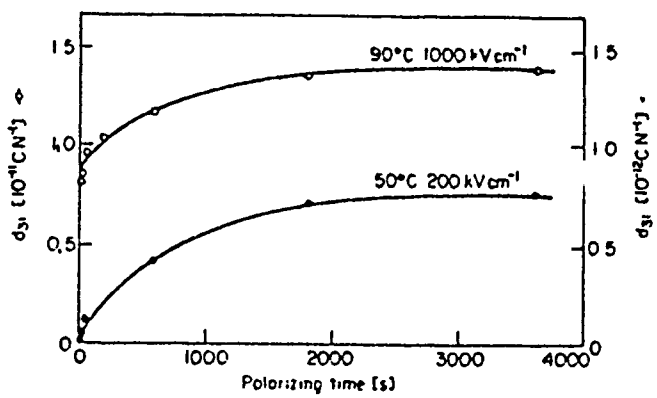


Fig. 4.3.5 — Variation of d_{31} of a PVDF film with polarizing time [3]. M. Marayama, *Ultrasonics*, **21**, (1) (1976), ©1976 Butterworth & Co. (Pub) Ltd.; by permission.

In application to electro-acoustic transducers it is useful for the designer to have a general list of elastic and piezoelectric properties with which to make initial performance estimates. Table 4.3.1 gives the range of values of currently available PVDF film.

Table 4.3.1 — General Properties of PVDF Piezoelectric Film

Property	Units	
Form		Metallic film of PVDF
Thickness	μm	9, 15, 30
Size (Tentative)	cm	(MD) 10 (TD) 10
Density	g cm^{-3}	1.78—1.79
Tensile Strength (Yield point)	10^7 Nm^{-2} kg mm^{-2}	(MD) 25-30 (TD) 5-6
Tensile Modulus	10^7Nm^{-2} kg mm^{-2}	(MD) 200-250 (TD) 240-280
Elongation (Yield Point)	%	(MD) 18-25 (TD) 4-6
Change in linear Dimension at 100°C, for 30 min	%	(MD) 4-5 (Shrinkage) (TD) 0
Volume Resistivity	10^{14} ohm-cm	8-10
Break-down Strength	kV (DC) mm^{-1}	150-200
Dielectric Constant, 1 kHz		12-13
Dissipation factor,		0.02-0.03
MD Machine direction of film TD Transverse firection of film		$d_{31} = -20$ m/V $\times 10^{-12}$ $e_{31} = -6.0$ N/Vm $g_{31} = -.174$ Vm/N $h_{31} = -53$ V/m $k_{31} \sim 0.10$

Piezoelectric PVDF is manufactured industrially by first forming a film of predominantly α-phase, then stretching the film to several times its original length at temperatures below 100°C thereby converting the dispersed crystals to β-phase. The film is then provided with metallic electrodes and polar-

ized in a high *dc* field (up to 1000 kV/cm) at 80-150°C. Most film processed in this way has values of d_{31} of about 2 to 3 $\times$ 10^{-11} C/N, and a coefficient of electromechanical coupling in the 31 mode of about 10%.

In application as a sensor of acoustic pressure a PVDF film polarized in the 3-direction and stretched (by flexure) in the 1-direction generates an open circuit voltage proportional to the piezoelectric "g" constant (see Sect. 2.1). Measurement of the g_{31} shows very high values ($\sim$ 174 $\times$ 10^{-3} Vm/N) indicating a considerable potential for use in hydrophones, microphones, pick-ups, accelerometers etc.

4.4 PIEZOELECTRIC PROPERTIES OF PVDF IN 33 MODE

A PVDF film constructed as a sandwich between metallic electrodes and backed with a rigid block, can be used in the thickness or "33mode." The piezoelectric effect will then be strongly affected by hydrostatic pressure and temperature. A study of the the electric field/stress coefficient g_{33}, the relative dielectrical constant ϵ_{33}^T and the charge/stress coefficient d_{33} as a function of hydrostatic stress σ_{33}, and temperature (°C) on samples of PVDF has been made by Berlinsky [4]. Small samples ($1.01\times$ 10^{-4}m^2 in area) cut from a 27 μm PVF_2 film, made by Kureha Chemical Industry Co. Japan, stretched, poled and electroded were cemented between stainless steels blocks with silver-filled epoxy, and the assembly encased in an alumina tube with both ends exposed to ambient pressure. The applied external pressure generated one-dimensional loading, but the fact that the lateral motion of the PVDF film was inhibited (by cementing) made the measured values "effective" ones. Figures 4.4.1, 4.4.2, 4.4.3 give the effective values of g_{33}, ϵ_{33}^T and d_{33} as a function of one-dimensional static stress ($= \sigma_{33}$) and temperature. Other samples more effectively poled and more effectively mounted in the test fixture have reported values, Table 4.4.1, about twice those shown in these figures.

Table 4.4.1

d_{33}	g_{33}	s_{33}^E	k_{33}	$\epsilon_{33}^T/\epsilon_0$
$35 \times 10^{-12} C/N$	$330 \times 10^{-3} \frac{Vm}{N}$	$320 \times 10^{-12} \frac{m^2}{N}$	0.19	12

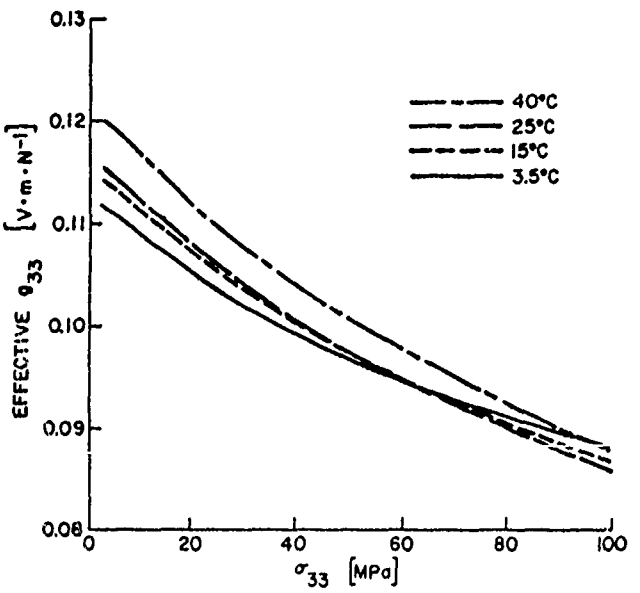


Fig. 4.4.1 — Effective piezoelectric voltage coefficient of PVDF as a function of one-dimensional static stress at 1000 Hz [4]

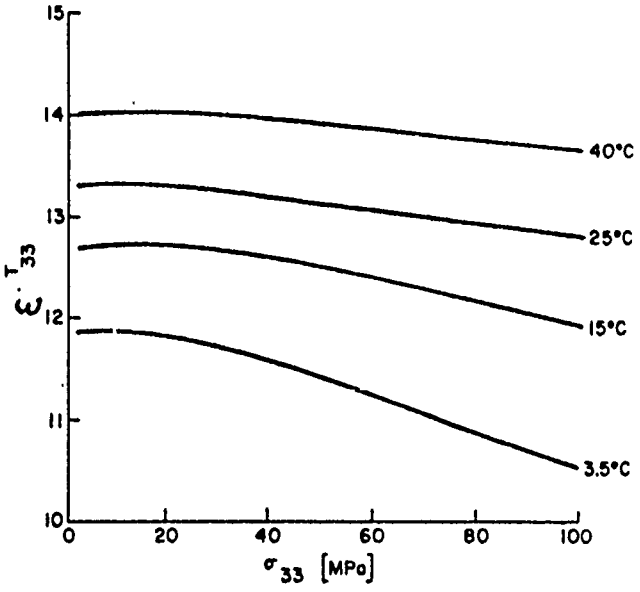


Fig. 4.4.2 — Relative dielectric constant of PVDF as a function of one dimensional static stress at 1000 Hz [4]

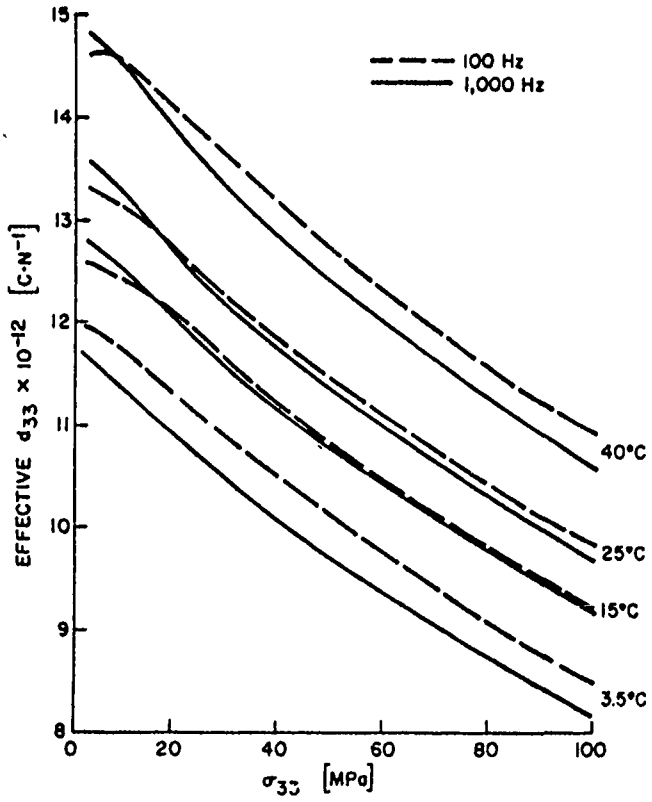


Fig. 4.4.3 — Effective piezoelectric strain coefficient of PVDF as a function of one dimensional static stress at 100 and 1000 Hz [4]

Polymer film sensors may be used in other modes of operation such as the hydrostatic mode (namely hydrostatic force applied in all directions to a sample of the film). The properties of the film in this mode are derivable from a knowledge of the full matrix of d constants, Table 4.2.2. Thus a piezoelectric material which is formed as a cube, polarized in the 3-direction and subjected to hydrostatic pressure P shows a charge accumulation per unit area on the "3" surfaces of magnitude [5],

$$D_3 = (d_{31} + d_{32} + d_{33})P$$

4.5 FURTHER DISCUSSION ON THE ORIGIN OF PIEZOELECTRICITY IN PVDF

Sussner and Dransfeld [5] have investigated various mechanisms that have been advanced to explain piezoelectricity in PVF_2 films. In one set of experiments the piezoelectric effect was detected by an optical modulation technique, Fig. 4.5.1. Here a PVF_2 film, thickness 50 μm, was supplied by Kureha Chem with no mechanical treatment (such as uniaxial drawing or rolling). After vacuum deposition of a thin aluminum layer on the surfaces of the film it was polarized at 100°C for 60 min while exposed to a dc field of 300 kV/cm. Upon application of an rf electric field (in the 10 to 60 MHz region) across the sample ($V = V_0 \sin \omega t$) the film vibrated in the thickness (=33) mode. A laser beam focused into this film was modulated by the photoelastic effect and the modulation detected by frequency analysis of the light gathered in a photoelectric cell. Fig. 4.5.1 shows that a piezoelectrically induced resonance occurs not only at the expected frequency where the thickness d equals one half a wavelength of the rf signal, but also at a thickness equal to one full wavelength. The excitation of the latter resonance is not allowed in the classical theory of piezoelectricity because of exact cancellation of positive and negative charge in a uniformly polarlized material. Resonances in such a material can occur only at thicknesses equal to an odd number of wavelengths. The appearance of this unexpected resonance is attributable only to a condition of nonuniform polarization in the bulk of the film, which manifests itself as a variation of the piezoelectric constant across the thickness of the sample.

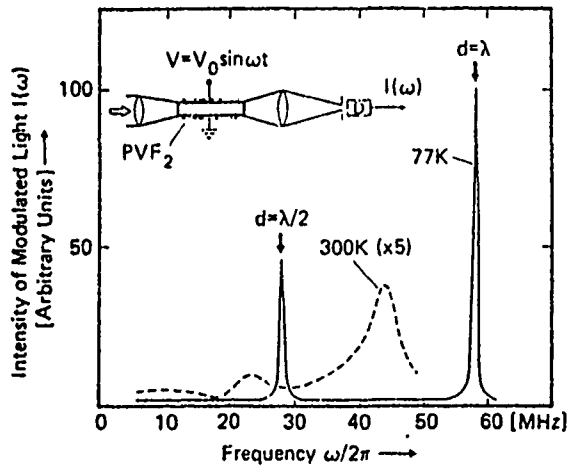


Fig. 4.5.1 — Piezoelectrically excited resonances of a freely suspended PVF_2 film (d = 50 μm) at 300 K (dashed line) and 77K (solid line) [after Ref. 5]. H. Sussner and K. Gransfeld, *Journal of Polymer Science: Polymer Chemistry Edition* (1978), ©1978 John Wiley & Sons, Inc.; by permission.

When the same experiment was performed in the 10 Hz to 10 MHz region numerous other resonances were observed, Fig. 4.5.2. These are attributable to flexural waves, similar to those excited in a thin elastic plate by bending moments and shears. Again, classical theory does not allow a homogeneously polarized piezoelectric plate subject to uniform (normal) force excitation to vibrate in flexure. A plausible explanation of Fig. 4.5.2 is then the existence of a nonuniform piezoelectric constant across the film thickness, which provides the bending moments even under uniform rf excitation. Further evidence of the importance of the interface between the *positive* electrode and the PVF_2 film was demonstrated by Sussner and Dransfield loc. cit. in the poling experiment shown in Fig. 4.5.3. In experiment (a) the PVF_2 film was sandwiched between the positive aluminum electrode and an insulator of silicon dioxide. On top of the latter was a layer of *P*-doped silcon electroded negatively with an aluminum electrode. Upon application of the poling field a strong piezoelectric effect was induced in the film. When however the polarity of poling was switched, as in (b), the poling procedure was ineffective and the PVF_2 film was not piezoelectric.

Sussner and Dransfeld conclude: a strong dependence of the piezoelectric effect on the volume fraction of β phase in PVF_2 has not been demonstrated by either their own experiments or by those of other authors. Stretching the PVF_2 film prior to poling is not a necessary condition for the occurrence

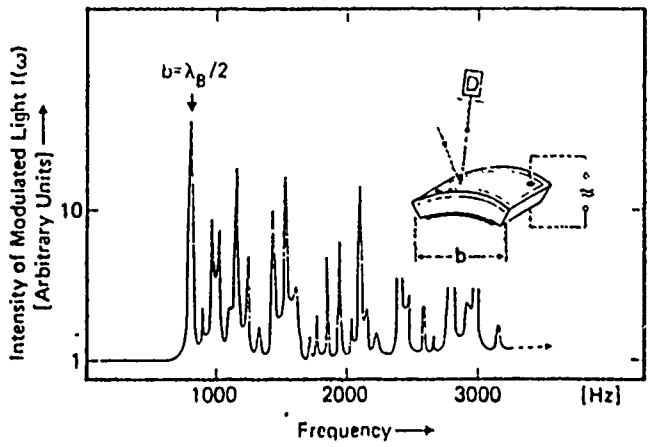


Fig. 4.5.2 — Optical observation of flexural resonances of a PVF_2 foil at 77K [after Ref. 5]. H. Sussner and K. Gransfeld, *Journal of Polymer Science: Polymer Chemistry Edition*, (1978), ©1978 John Wiley & Sons, Inc.; by permission.

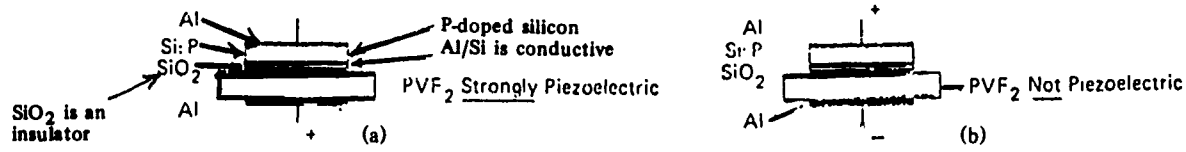


Fig. 4.5.3 — Poling PVF_2 with a "blocking" electrode. A highly P-dope. ($10^{21}/cm^3$) silicon crystal, thermally oxidized on one side with a 6000 Å thick SiO_2 layer is used as a blocking electrode. (Poling conditions: $E_p = 5 \times 10^5$ V/cm, $T_p = 100C$, $t_p = 45$ min) [6]. H. Sussner and K. Gransfeld, *Journal of Polymer Science: Polymer Chemistry Edition* (1978), ©1978 John Wiley & Sons, Inc.; by permission.

of the piezoelectric effect, but only improves the magnitude of d_{31}. A model which predicts piezoelectricity in polymer electric based on orientation of dipoles in the bulk of the polymer is insufficient to explain what is observed. A more convincing model attributes the origin of piezoelectricity in PVF_2 to physical processes occurring at the (positive) metal polymer interface. A likely mechanism is the injection of charge from the electrodes. Another mechanism is the alignment of CF_2 dipoles in the first chain layer facing the metal boundary.

4.6 PIEZOELECTRIC POLYMER HYDROPHONE

The large g_{31} constant of PVF_2 shown in Table 4.3.1 indicates that it is a suitable material for reporting an open-circuit voltage in response to an incident sound field. Since this voltage is the result of a charge accumulation on the electrodes an additional indication of its suitability as a receiver of sound is the $g_{31}d_{31}$ product, which is 3.48×10^{-12} m^2/N as compared to 1.37×10^{-12} m^2/N for PZT-4 ceramic. This favorable comparison has prompted several designers of hydrophones to conceive and build structures based on PVF_2 piezoelectricity. Figure 4.6.1 shows three designs for application to underwater environments. The measured receiving sensitivity of each of these hydrophones is shown below the corresponding figure. In Fig. (a) the liquid of submersion was at a pressure of one atmosphere. In Fig. (b) the hydrophone is filled with oil and pressure released with air-filled plastic tubes flattened to provide a compliance to the oil chamber. The stiffness of this chamber is designed to withstand hydrostatic pressures of 4 MPa. Its mechanical impedance is large, hence the motion induced by each unit of the acoustic field is smaller than the design of Fig. (a), thereby reducing the sensitivity by some 30 dB. A third method of supporting the hydrostatic pressure is to cover an air-chamber with a flexible desk of sufficient proportions to withstand deep submersion. The polymer is cemented to the surface of the disk and undergoes strain as a result of the incident time-varying acoustic field. Because of the stiffness of the disk the sensitivity was 3 dB less than Fig. (b).

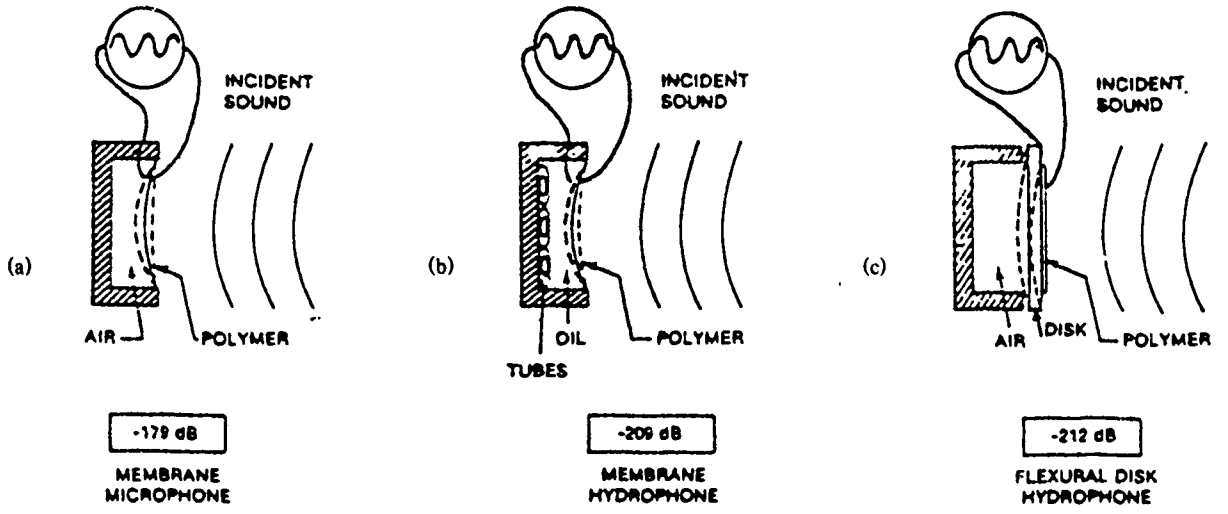


Fig. 4.6.1 — Cross sections of cylindrical piezoelectric polymer receivers. (a) membrane microphone formed by fixing a taut film over an air-filled cylindrical chamber. (b) membrane hydrophone with an oil-filled chamber containing plastic compliant tubes to provide compliance while withstanding hydrostatic pressure. (c) Flexural disk hydrophone backed by air. (Note: sensitivity is in units of dB re 1V/μPa) [after 6]. T. D. Sullivan and J. M. Powers, *J. Acous. Soc. Am.*, **63** (5), 1396 (1978), ©1978 American Institute of Physics; by permission.

In these three designs the polymer consisted of a single sheet of Kureha #9 Piezofilm, 30 mil thick, poled at 2000 V for 30 min at 80°C. To improve sensitivity a design that uses several layers of polymer film was built, Ref. [6]. Figure 4.6.2 shows this design. It is a double-disk hydrophone—four pieces of polymer on each disk were connected in series, and the two groups of 4 each were connected in parallel. The film this time was circular Kureha KF Piezofilm #30, 27.2 μm thick, radius 1.75 cm, Young's modulus 2.5×10^3 MPa, $g_{31} = -0.192$ Vm/N, $g_{32} = -0.020$ Vm/N, Poisson's ratio 0.4. The disk was acrylic plastic, thickness 0.51 cm, radius 1.75 cm, Young's modulus 3.72×10^3 MPa.

The electrical connections gave a capacitance of 1 *nF*, and a calibration test showed the sensitivity to be about −199 dB re 1/μPa. The receiving sensitivity as a function of frequency with pressure and temperature as parameters is shown in Fig. 4.6.3.

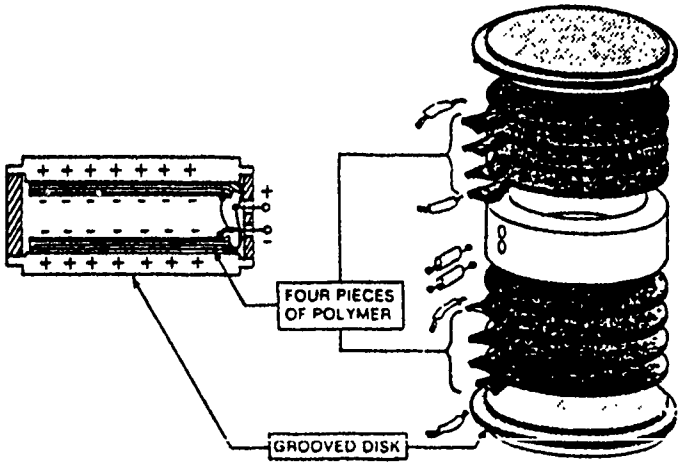


Fig. 4.6.2 — Double disk hydrophone [after Ref. 6]. T. D. Sullivan and J. M. Powers, *J. Acous. Soc. Am.*, **63** (5), 1396 (1978), ©1978 American Institute of Physics; by permission.

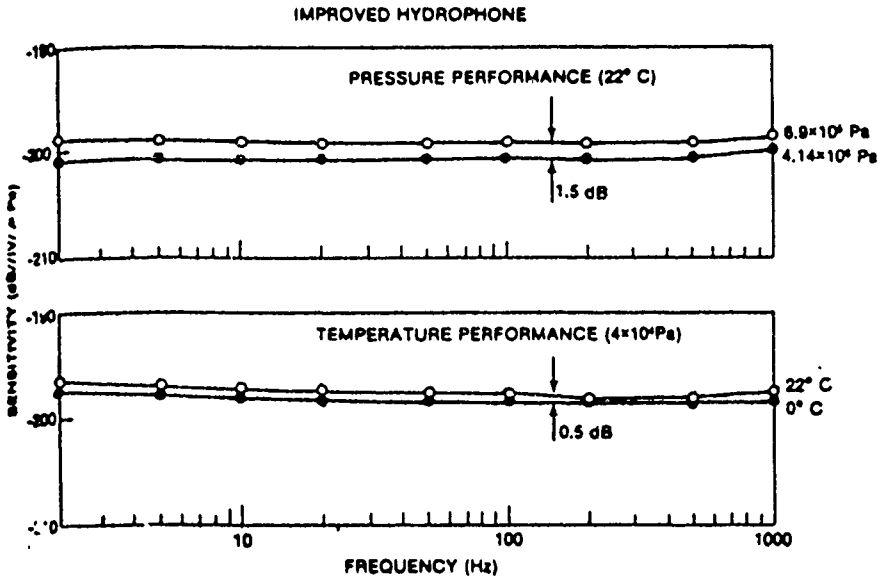


Fig. 4.6.3 — Pressure and temperature induced variations in sensitivity of the hydrophone in Fig. 4.6.2 [after Ref. 6]. T. D Sullivan, J. M. Powers, *J. Acous. Soc. Am.*, 63 (5), 1396 (1978), ©1978 American Institute of Physics; by permission.

4.7 ANALYSIS OF THE OPEN-CIRCUIT VOLTAGE OF A DISK HYDROPHONE

The choice of constitutive relocation Eqs. 2.12.1 depends on the mechanical and electrical boundary conditions. We assume the elastic disk to be simply supported, and thus adopt a constant-T mechanical boundary condition. Also, we assume the polymer surfaces to be equipotential, hence adopt a constant-$\bar{E}$ electrical boundary condition. In matrix notation the constitutive relations are,

$$\text{(a)}\quad S_i = s^E_{ij}\, T_j + d_{mi}\, E_m$$

$$\text{(b)}\quad D_m = d_{mi}\, T_i + \epsilon^T_{mk}\, E_k \tag{4.7.1}$$

$$i,\ j = 1 \text{ to } 6, \quad m,\ k = 1 \text{ to } 3.$$

The components of interest in this flexural disk are: S_1, S_2; T_1, T_2; s^E_{11}, s^E_{12}, s^E_{21}, s^E_{22}; d_{31}, d_{32}; D_3; E_3; ϵ^T_{33}. Because the polymer film is elastically and mechanically anisotropic due to mechanical stretching during the manufacture process all these quantities are functions of the polar angle θ in the plane of the film ($\theta = 0$ is the direction of stretching). The natural coordinate system is cylindrical with the axis of rotation being the z, or 3-direction. The elastic and piezoelectric constants are therefore rotated through angle θ about the z-axis. Standard formulas describing this rotation are available (Ref. [8]). Since however the elastic anisotropy is small one assumes the compliance constants s^E_{ij} are the same for both unrotated and rotated systems. In contrast the d-constants are retained as functions of θ.

We first solve Eq. 4.7.1a for stresses T and substitute in Eq. 4.7.1b

$$D_m(\theta) = d_{mj}[(S_i - d_{pi}\, E_p)(s^E_{ij})^{-1}] + \epsilon^T_{mk}\, E_k \tag{4.7.2}$$

or

$$D_m(\theta) = d_{mj}(\theta)[S_i(s_{ij}^{\epsilon})^{-1}] + \epsilon_{mk}^{T} E_k[1 - k(\theta)]$$

$$k(\theta) = \text{coupling coefficient} = d_{mj}(d_{ki})(s_{ig}^{E})^{-1}(\epsilon_{mk}^{-1})^{-1}. \tag{4.7.3}$$

Since $k(\theta)$ is only a weak function of θ it is a good approximation to use unrotated constants and arrive at $k(\theta) = k$.

When the transducer acts as a receiver of sound it is desirable to arrange the piezoelectric coefficients to display electric field generated by elastic stress. Thus, one uses the g-constant in lieu of the d-constant,

$$d_{mi} = \sum_{n} \epsilon_{nm}^{T} g_{ni}, \tag{4.7.4}$$

Eq. 4.7.2 is then rewritten in the form

$$D_m(\theta) = \epsilon_{nm}^{T} g_{ni}(\theta)[S_i(s_{ij}^{E})^{-1}] + \epsilon_{mk}^{T} E_k(1 - k) \tag{4.7.5}$$

The elastic strains in the polymer properly belong to an analysis of the flexural deformation of a two-layer disk simple supported at its edges. A good approximation is to take S_i to be the *surface* strain ϵ_i of the acrylic disk deformed in flexure by an applied acoustic pressure P_A. The stresses T in the polymer corresponding to these strains depend on the compliance coefficients s_{ij}^{E} of the polymer. Naturally these differ from the compliance coefficients (= reciprocal of the Young's modulus) of the disk. Hence $S_i(=\epsilon_i)$ and s_{ij}^{E} involve different elastic moduli.

Equation 4.7.5 is integrated over the polymer surface area A to find the charge Q_m, and through the thickness h to find the electrical potential V. Since the film is polarized and electrically driven through the 3-direction, the result of these integrations is,

$$Q_3 = \epsilon_{33}^{T} \oint g_{3j}(\theta)[S_i(r)(s_{ij}^{E})^{-1}]rdrd\theta + \epsilon_{33}^{T}\frac{VA}{h}(1 - k). \tag{4.7.6}$$

The open-circuit voltage is obtained from this formula by setting the total charge Q_3 to zero,

$$V_{oc} = -\frac{h}{A} \oint g_{3j}(\theta)\left[S_i(r)\frac{(s_{ij}^{E})^{-1}}{1 - k}\right] rdrd\theta \quad \text{(units: volts)}. \tag{4.7.7}$$

Here, as before, repeated subscripts signify summations $i, j = 1, 2, \ldots 6$. In the case of disk flexure these are only two components $j = 1, 2$, $i = 1, 2$. Thus

$$V_{oc} = -\frac{h}{A} \oint \left\{ g_{31}(\theta)\left[S_i(r)\frac{(s_{ij}^{E})_{11}^{-1}}{1-k} + \frac{S_s^{r}(s_{ij}^{E})_{12}^{-1}}{1-k}\right]\right. \tag{4.7.8}$$

$$\left. + g_{32}(\theta)\left[\frac{S_1^{(r)}(s_{ij}^{E})_{12}^{-1}}{1-k} + \frac{S_2^{(r)}(s_{ij}^{E})_{22}^{-1}}{1-k}\right]\right\} rdrd\theta$$

From Ref [5],

$$g_{31}(\theta) = g_{31}\cos^2\theta + g_{32}\sin^2\theta$$

$$g_{32}(\theta) = g_{32}\cos^2\theta + g_{31}\sin^2\theta. \tag{4.7.9}$$

Also, in Eq. 4.7.8 the first square bracket under the integral sign is T_1, and the second is T_2, where T_1, T_2 are *purely elastic*:

$$T_1 = \frac{S_1 + \sigma^E S_2}{s_{11}^E(1-k)(1-\sigma^{E2})}\ ;\ T_2 = \frac{S_2 + \sigma^E S_1}{s_{11}^E(1-k)(1-\sigma^{E2})};\ \sigma^E = -\frac{s_{12}^E}{s_{11}^E} \tag{4.7.10}$$

Since $S_1(r)$, $S_2(r)$ are surface elastic strains in a simply supported disk deformed by a uniform acoustic pressure P_i and are well-known in classical theory [8], the integration required by Eq. 4.7.8 is easily carried out. The free-field voltage sensitivity is then,

$$\frac{V_{0c}}{P_i} = -\frac{(1-\nu)}{(1-\sigma^E)}\ \frac{h}{s_{11}^E(1-k)}\ \frac{1}{Y}\ \frac{3}{8}\ \frac{a^2}{t^2}\ (g_{31}+g_{32})\left\{(3+\nu)-(1+\nu)\frac{b^2}{a^2}\right\} \tag{4.7.11}$$

in which

a = radius of disk

b = radius of polymer film

ν = Poisson's ratio of disk material

σ^E = Poisson's ratio of polymer film = $-s_{12}^E/s_{11}^E$

Y = Young's Modulus for the disk.

Sullivan and Powers [7] arrive by a different route to an equation similar to Eq. 4.7.11 but with these exceptions: in their formula σ^E appears as σ^D, and $s_{11}^E(1-k^2)$ appears as $^*E$ = Young's, Modulus) for the polymer, and the sign (of Eq. 4.7.11) appears positive. By using the values: $g_{31} = 0.192$ Vm/N; $g_{32} = 0.020$ Vm/N; $h = 27.2\ \mu$m; $a = b = 1.75$ cm; $t = 0.51$ cm; $\nu = \sigma = 0.4$; $^*E = 2.5 \times 10^3$ MPa; and $Y = 3.72 \times 10^3$ MPa, they calculated the free-field open-circuit voltage of a *single* layer polymer hydrophone to be $\frac{V_{0c}}{P_i} = -209$ *dB* re1V/μPa, at a capacitance of 3.6 nF. As noted earlier this sensitivity can be greatly improved by using multiple layers of polymer film but this is done at the expense of reducing the capacitance.

Conclusion: The use of polymer electrets as acoustic sensors is being greatly expanded at the time of writing of this memoir (1982). In spite of relatively low sensitivity the possibility of making large area sensors out of rolled film, suitable for ambient noise cancellation, is a decisive advantage. Other advantages are (1) it can be shaped to more desired geometries than piezoceramic (2) its dynamic range

is large, thus making it useful as a shock-sensor (3) it can be used in the hydrostatic mode. (4) unlike brittle piezoceramics, it is flexible and can withstand great hydrostatic pressures. (5) it has a close impedance match to water. Some disadvantages remain to be corrected. These are (1) it has pyroelectric response (2) its elastic stiffness changes with depth of submergence, thus inducing changes in sensor-response (3) its piezoelectric properties depend on stretching and poling, which are generally variable (4) it has a measurable aging.

REFERENCES

[1] H. Kawai, Japan J. Applied Phys. **8**, 975 (1969).

[2] R. Hayakawa, Y. Wada, "A general description of piezoelectricity of polymer film," Rep. Progress Polymer Phys. Japan **14**, 467 (1971).

[3] M. Murayama et al., "The strong piezoelectricity in polyvinylidene fluoride (PVDF)" Ultrasonics, Jan. 1976, p. 15.

[4] Y. Berlinsky, "Transduction With PVF_2 in the Ocean Environment," Naval Research Laboratory Report 8265, March 28, 1980.

[5] "Piezoelectricity," W.G. Cady, Vol. 1, p. 194, Dover Publications.

[6] H. Sussner, K. Dransfeld, "Importance of the Metal-Polymer Interface for the Piezoelectricity of Polyvinylidene Fluoride," J. Poly. Sci. **16**, 529-543 (1978).

[7] T.D. Sullivan, J.M. Powers, "Piezoelectric polymer flexural disc hydrophone," J. Acous. Soc. Am. **63** (5) p. 1396 (1978).

[8] "Formulas for Stress and Strain," R.J. Roark, McGraw Hill, New York, 1954, 3rd Ed., p. 194.

Chapter 5
FIBER-OPTIC TRANSDUCERS

5.1 ACOUSTO-OPTIC MATERIALS AND THEIR MODELS

A material which, in unstressed condition, is optically isotropic may become optically anisotropic when it is stressed. This phenomenon, related to the photoelastic effect, is described by changes in the dielectric constant ϵ. Since ϵ is a second-rank symmetric tensor for the general anisotropic material it will be useful to formulate the change in ϵ due to application of stress by energy methods.

The electric field energy of an anisotropic optical material is given by,

$$W_e = \frac{1}{8\pi} \sum_{kl} E_k \, \epsilon_{kl} E_l \qquad \text{(units: Gaussian (ergs))}. \tag{5.1.1}$$

[1]. This a quadratic form. In Cartesian tensor notation, noting again that ϵ_{kl} is symmetric, one has,

$$\epsilon_{xx}E_x^2 + \epsilon_{yy}E_y^2 + \epsilon_{zz}\,E_z^2 + 2\epsilon_{yz}E_yE_z + 2\epsilon_{xz}E_xE_z + 2\epsilon_{xy}E_xE_y = C, \; C = 8\pi \mathbf{E} \cdot \mathbf{D}. \tag{5.1.2}$$

Since $\mathbf{D} = \epsilon\mathbf{E}$, and since in Gaussian units, the index of refraction n is given by,

$$n^2 = \epsilon$$

Eq. 5.1.1 may be cast in the form,

$$\frac{X_1^2}{n_1^2} + \frac{X_2^2}{n_2^2} + \frac{X_3^2}{n_3^2} + \frac{2X_2X_3}{n_4^2} + \frac{2X_3X_1}{n_5^2} + \frac{2X_1X_2}{n_6^2} = 1 \tag{5.1.3}$$

$$X_1 = \frac{D_x}{\sqrt{C}} \; ; \; X_2 = \frac{D_y}{\sqrt{C}} \; ; \; X_3 = \frac{D_z}{\sqrt{C}}$$

$$n_1^2 = \epsilon_{xx}; \; n_2^2 = \epsilon_{yy}; \; n_3^2 = \epsilon_{zz}; \; n_4^2 = \epsilon_{yz}; \; n_5^2 = \epsilon_{xz}; \; n_6^2 = \epsilon_{xy}.$$

In contracted notation this equation becomes,

$$\sum_{i,j} \left(\frac{1}{n^2} \right)_{ij} X_i X_j = 1, \quad i,j = 1,2,3 \tag{5.1.4}$$

$$n_1 = \left(\frac{1}{n^2} \right)_{11} \; ; \; n_2 = \left(\frac{1}{n^2} \right)_{22} \; ; \; n_3 = \left(\frac{1}{n^2} \right)_{33} \; ; \; n_4 = \left(\frac{1}{n^2} \right)_{23} \; ; \; n_5 = \left(\frac{1}{n^2} \right)_{31} \; ; \; n_6 = \left(\frac{1}{n^2} \right)_{12}$$

Equation 5.1.4 is the *index ellipsoid* or *optical indicatrix*. A light ray *OP*, Fig. 5.1.1 propagating normal to the shaded plane of its associated plane wave front defines an ellipse of intersection. Any radius vector in this ellipse is equal to the index of refraction for light polarized in its direction.

PREVIOUS PAGE IS BLANK

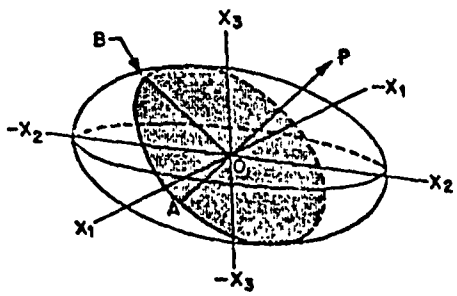


Fig. 5.1.1 — Index ellipsoid showing light propagation direction OP and ellipse perpendicular to OP having semi-major axes OA and OB

When OP coincides with the OX_3 axis, the semi-major axes OB, OA define the principal indices of refraction n_y, n_x respectively. Similarly when OP coincides with OX_2 the axis of OB defines the principal indices n_z.

In terms of these principal indices the ellipsoid is in the canonical form,

$$\sum_{i=1,2,3} X_i^2 \left(\frac{1}{n^2}\right)_{ii} = 1. \tag{5.1.5}$$

Now when some external influence, such as elastic strain distorts the index ellipsoid (strain-optic effect) these distortions can be described by phenomenological tensor quantities,

$$\Delta \left(\frac{1}{n^2}\right)_{ij}$$

in which Δ means "change," or "distortion." Thus in the presence of an elastic perturbation the distorted index ellipsoid becomes,

$$\sum_{i,j} \left[\left(\frac{1}{n^2}\right)_{ij} + \Delta\left(\frac{1}{n^2}\right)_{ij}\right] X_i X_j = 1 \tag{5.1.6}$$

In the case of distortion due to the photoelastic effect the change in the indicatrix is written in terms of a fourth-rank strain-optic tensor $p_{ij,kl}$,

$$\Delta \left(\frac{1}{n^2}\right)_{ij} = \sum_{k,l=1}^{3} p_{ij,kl} S_{kl}, \tag{5.1.7}$$

in which S_{kl} are components of the strain tensor. Since the tensors on both sides of this equation are symmetrical it is convenient to rewrite it in contracted notation,

$$\Delta \left(\frac{1}{n^2}\right)_i = \sum_{j=1}^{6} p_{ij} S_j; \quad i,j = 1,2 \ldots 6. \tag{5.1.8}$$

According to IRE Standards (1949)

$$S_{11} = S_1; \quad 2S_{23} = S_4$$
$$S_{22} = S_2; \quad 2S_{31} = S_5.$$
$$S_{33} = S_3; \quad 2S_{12} = S_6$$

It is to be noted that p_{ij} is nondimensional. In general p_{ij} is a 6 × 6 matrix with 36 components. For the particular case of isotropic materials, there are only two independent components $p_{11} = p_{22} = p_{33}$; $p_{12} = p_{21} = p_{13} = p_{23} = p_{32}$, $p_{44} = p_{55} = p_{66} = \frac{1}{2}(p_{11} - p_{12})$.

It is important to relate changes in index of refraction (due to strain) to the index n of the unstressed material. In contracted notation,

$$\Delta\left(\frac{1}{n^2}\right)_i = -\frac{2}{n^3}\Delta n \quad \text{or} \Delta n = -\frac{n^3}{2}\Delta\left(\frac{1}{n^2}\right)_i, \; i = 1,2\ldots6 \tag{5.1.9}$$

This is true because the change in n is (generally) very small relative to n. These acousto-optical material properties will be used in the following sections to describe the modulation effects of light in silica fibers when stressed by mechanical forces.

5.2 STRESS-STRAIN RELATIONS IN A LONG FUSED SILICA FIBER

An elastic fiber can be modeled as a cylinder which is perfectly symmetrical about the cylindrical axis, with cross-sectional area A very much smaller in diameter than its length L. The fiber may be stressed in several ways. We choose here three ways, Fig. 5.2.1a, b, c. In (a) a tensile force T causes the fiber to stretch by amount ΔL along the axis, and contract by amount Δu_n radially. The strain vector in Cartesian (x, y, z or 1, 2, 3) ... is then

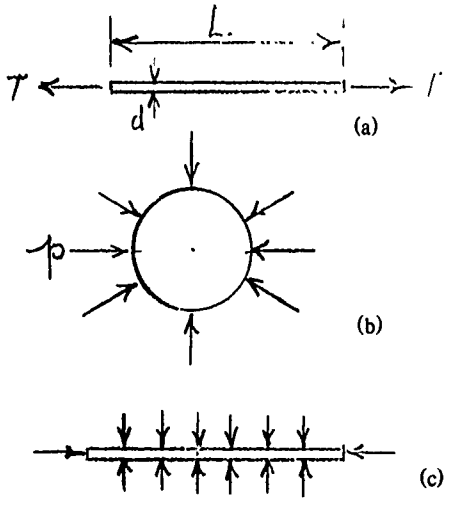


Fig. 5.2.1 — Elastic stress conditions on a long fiber, (a) extension, (b) radial tension, (c) both longitudinal and radial extension

$$S_1 = e;\; S_2 = -\nu e;\; S_3 = -\nu e;\; S_4 = S_5 = S_6 = 0$$

where

$$e = \Delta L/L = T/AE. \tag{5.2.1}$$

In (b) axisymmetric tensile forces p act uniformly around the circumference of the fiber. The strains are

$$S_1 = -\frac{2\nu p}{E};\; S_2 = \frac{du}{dr} = \frac{1-\nu}{E}p;$$

$$S_3 = \frac{u}{r} = \frac{1-\nu}{E}p;\; S_4 = S_5 = S_6 = 0 \tag{5.2.2}$$

In (c) the tensile forces p act uniformly both axially and radially. The strain vector is

$$S_1 = (1-2\nu)\frac{p}{E} = S_2 = S_3;\; S_4 = S_5 = S_6 = 0. \tag{5.2.3}$$

Numerical values of elastic properties of fused silica will be presented later in this chapter in conjunction with a discussion on the acoustic sensitivity of fused silica fibers.

5.3 PRESSURE-INDUCED PHASE CHANGES IN A BARE LIGHT-CARRYING FIBER

Let a plane-polarized monochromatic light wave (wavenumber $\mathbf{k} = k_0 n \mathbf{a}_z$) propagate in the axial (= subscript 1) direction of a bare fused-silica fiber. The phase increment in a length L for constant k_0 and n is

$$\phi = k_0 nL \qquad k_0 = \frac{\omega}{c_0},\ c_0 = \text{speed of light in a vacuum.} \tag{5.3.1}$$

Since the material is isotropic and nonmagnetic the index of refraction in Gaussian units is,

$$n = \sqrt{\mu\epsilon} = \sqrt{\epsilon}$$

where the dielectric constant is the same in all directions.

When, however, the fiber is placed under mechanical stress it becomes *optically* anisotropic, meaning that it exhibits a photoelastic effect which couples the stress-strain condition with a change in index of refraction. The phase then changes by an amount,

$$\Delta\phi = \Delta k_0 nL + k_0 \Delta nL + k_0 n \Delta L. \tag{5.3.2}$$

Since it is assumed the disturbance does not significantly change k_0 we set $\Delta k_0 = 0$. The change in index of refraction Δn given by Eq. 5.1.9 for the case L = constant, must occur only in the transverse direction (namely, in the radial (subscript 2) and tangential (subscript 3) directions). Also, since the strain in the axial direction is $S_1 = \Delta L/L$, we can rewrite Eq. 5.3.2 in the form

$$\Delta\phi = k_0 n S_i L - \frac{1}{2} k_0 L n^3 \Delta\left(\frac{1}{n^2}\right)_i. \tag{5.3.3}$$

The subscript i indicates which component of indicatrix (in the transverse direction) is in question, namely $i = 2$, or $i = 3$. The choice depends on the distribution of stress loading.

Assume now that the stress loading is always radially symmetric in the transverse plane. Then the change in Δn for $i = 2$ is the same as for $i = 3$. Choose the light to be linearly polarized in the $i = 2$ direction and apply Eq. 5.1.8, then,

$$\Delta\phi = k_0 n S_1 L - \frac{1}{2} k_0 L n^3 \sum_{j=1}^{6} p_{2j} S_j \tag{5.3.4}$$

in which p_{2j} are elements of the strain-optic tensor. For a body which is optically homogeneous and isotropic,

$$P = [P_{ij}] = \begin{bmatrix} p_{11} & p_{12} & p_{13} \\ p_{21} & p_{22} & p_{23} \\ p_{31} & p_{32} & p_{33} \end{bmatrix} = \begin{bmatrix} p_{11} & p_{12} & p_{12} \\ p_{12} & p_{11} & p_{12} \\ p_{12} & p_{12} & p_{11} \end{bmatrix}. \tag{5.3.5}$$

If one now applies Eq. 5.3.4 using the strains given by Eqs. 5.2.1, 5.2.2, 5.2.3 and the strain-optic matrix of Eq. 5.3.5, the resultant phase changes for a loading $p = eE$ (E = Young's modulus) are described to be:

$$\text{1–D longitudinal loading: (a)}\ \frac{\Delta\phi}{pL} = \frac{k_0 n}{E} - \frac{1}{2}\frac{k_0}{E} n^3\{p_{12}(1-\nu) - \nu p_{11}\}$$

$$\text{2–D transverse loading: (b)}\ \frac{\Delta\phi}{pL} = -\frac{2\nu\, k_0 n}{E} - \frac{1}{2}\frac{k_0\, n^3}{E}\{p_{11}(1-\nu) + p_{12}(1-3\nu)\} \tag{5.3.6}$$

uniform 3-D loading: (c) $\dfrac{\Delta\phi}{pL} = \dfrac{k_0 n(1-2\nu)}{E} - \dfrac{1}{2}\dfrac{k_0 n^3}{E}\{(1-2\nu)(p_{11}+2p_{12})\}$

[2]. The units of the sensitivity $\Delta\phi/pL$ are rad/(N/m^2) m. Equations are 5.3.6 are simple enough to permit numerical estimates to be made of sensitivity of a fiber to various conditions of loading. This is discussed next.

5.4 NUMERICAL ESTIMATES OF THE ACOUSTIC PRESSURE SENSITIVITY OF A BARE FUSED SILICA FIBER

The optical and strain-optic properties of fused silica are found in several publications. Since different values are given we choose here those of Pinnow [3] which are displayed in the following table.

Table 5.4.1

$$n = 1.456;\ \lambda = 0.63\ \mu\text{m};\ \nu = 0.17;\ p_{11} = 0.12;\ p_{12} = 0.27;\ E = 7.3 \times 10^{10}\ \text{N/m}^2.$$

The calculation proceeds as follows:

Case I. Longitudinal loading, Eq. 5.3.6a:

$$\frac{k_0 n}{E} = \frac{2\pi n}{\lambda E} = \frac{2\pi \times 1.456}{0.63 \times 10^{-6} \times 7.3 \times 10^{10}} = 1.99 \times 10^{-4}\ \frac{\text{radians}}{\text{Pascal} \times \text{meter}}$$

$$\frac{1}{2}\left(\frac{k_0 n}{E}\right) n^2\{p_{12}(1-\nu) - \nu p_{11}\} = \frac{1}{2}(1.99 \times 10^{-4})(1.456)^2\{(0.27)(0.83) - 0.17(0.12)\} = 4.30 \times 10^{-5}$$

$$\frac{\Delta\phi}{pL} = 1.99 \times 10^{-4} - 4.30 \times 10^{-5} = 1.56 \times 10^{-4}\ \frac{\text{rad}}{\text{Pa} \times \text{m}} = \frac{1.56 \times 10^{-10}\ \text{rad}}{\mu\text{Pa} \times \text{m}}$$

Case II. Transverse Loading, Eq. 5.3.6b:

$$\frac{-2\nu k_0 n}{E} = -2(.17)1.99 \times 10^{-4} = -6.77 \times 10^{-5}$$

$$-\frac{1}{2} \times 1.99 \times 10^{-4}(1.456)^2\{0.12(0.83) + 0.27(0.49)\} = -4.891 \times 10^{-5}$$

$$\frac{\Delta\phi}{pL} = -6.77 \times 10^{-5} - 4.891 \times 10^{-5} = -1.166 \times 10^{-4}\ \frac{\text{rad}}{\text{Pa} \times \text{m}} = -\ 1.17 \times 10^{-10}\ \frac{\text{rad}}{\mu\text{Pa} \times \text{m}}$$

Case III. Uniform 3-D loading, Eq. 5.3.6c:

$$(1-2\nu)\left(\frac{k_0 n}{E}\right) = 0.66 \times 1.99 \times 10^{-4} = 1.3134 \times 10^{-4}$$

$$-\frac{1}{2} \times 1.99 \times 10^{-2} \times (1.456)^2\{(0.66)(0.12 + 0.54)\} = -9.188 \times 10^{-5}$$

$$\frac{\Delta\phi}{pL} = 1.3134 \times 10^{-4} - 9.188 \times 10^{-5} = 3.946 \times 10^{-5} \frac{\text{rad}}{\text{Pa} \times \text{m}} = 3.946 \times 10^{-11} \frac{\text{rad}}{\mu\text{Pa} \times \text{m}}$$

These calculations show that a fiber loaded axially (that is, under longitudinal tension and compression) gives the highest response, while a fiber loaded uniformly (that is, both axially and radially) gives the lowest response (by a factor of 4). These conclusions are in agreement with those made by Cielo [2].

5.5 PRESSURE-INDUCED CHANGES IN A FIBER-OPTIC ACOUSTIC SENSOR WITH COMPOSITE STRUCTURE

The bare single-mode fiber-optic acoustic sensor discussed in the previous section has a relatively poor sensitivity because the strain induced in the fiber per unit input acoustic pressure is limited in magnitude by the very small diameter of the fiber. The sensitivity for the same input forces can be greatly improved by use of strain-enhancement techniques. Stress-optic analysis shows what improvements are to be expected, and measurements on experimental structures indicate to what extent these expectations have already been fulfilled.

One simple procedure for enhancing axial strain consists in cementing a coil of the bare fiber on the exterior wall of an elastic hollow thin-walled cylinder (mean radius R, thickness t) and closing the ends of the cylinder to retain an air cavity when the sensor is placed in water. Since, for an applied pressure p_0 the tangential stress at the surface of the cylinder is $s_\theta = pR/t$ the fiber also partakes of this increased stress which results in a strain roughly R/t larger than that generated by p on the bare fiber. The sensitivity is thus greatly increased, limited only by the breaking strength of the fiber.

A second procedure of strain-enhancement consists in encasing the bare fiber with one or more elastic jackets. If the jacket material is chosen to be more compliant than the material of the bare fiber a proportionally larger fraction of the total load is taken in the stiffer fiber, resulting in a larger axial strain per unit applied pressure. Although the radial strain is increased as well, it does do so to a lesser degree than the axial strain. Since the two strains are of opposite sign there is a substantial gain in sensitivity just due to the length effect.

These two procedures have received experimental test. A comparison of measurement with prediction requires an analysis. We begin with an analysis of a jacketed fiber.

Case I. Analysis of a composite fiber-optic sensor consisting of an inner core and one jacket

Figure 5.5.1 shows the cross-section of an optical fiber coated with an elastic jacket. Also displayed are the geometrical, elastic and optical properties of this 2-layer structure. To predict its performance as a sensor of acoustic pressure one requires explicit formulas for the radial and axial strains inside the fiber, as discussed in the previous Section 5.3. These are determined by solution of the stress-strain relations in the composite, treated as a boundary value problem of a 2-layer compound cylinder subjected to a uniform external pressure.

It is assumed first that the length L of the composite (in the z-direction) is much greater than is overall diameter $(2R_2)$. Because of the axisymmetric loading there can be no z-dependence of any stress or strain, except near the ends. In addition there is no slippage between the jacket and inner fiber. The displacement in the z-direction must furthermore be the same for each layer, and, because of the absence of shear, this displacement must be independent of both r and θ.

Two boundaries, $r = R_2$, $r = R_1$, participate in the setting of the boundary conditions. For regions 1 and 2 these conditions are:

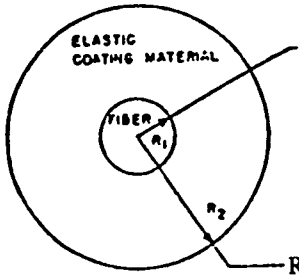


Fig. 5.5.1 — Cross section of an optical fiber (region 1) coated with an elastic medium (region 2). The fiber has Young's modulus E_1, Poisson's ratio ν_1, index of refraction n, strain-optic coefficients p_{11}, p_{12}. The coating material is specified by E_2, ν_2.

(1) the radial stress at the surface $r = R_2$ is equal to the applied acoustic pressure (the convention used is that a compressive stress is negative):

$$s_{r2}(R_2) = -P_0 \tag{5.5.1}$$

(2), (3) at the surface $r = R_1$ the radial stress s_r and the radial displacement u_r are the same for the fiber and the jacket,

$$s_{r1}(R_1) = s_{r2}(R_1) \tag{5.5.2}$$

$$u_{r1}(R_1) = u_{r2}(R_1) \tag{5.5.3}$$

(4) the axial strain is everywhere the same for both fiber and jacket

$$e_{z1} = e_{z2} \tag{5.5.4}$$

(5) since the sensitivity of the fiber depends on the axial stress, a condition on this stress at the termination of the composite must be made. A simplifying assumption is to let the external medium exert a force on the ends and to let this force be balanced by the internal axial stress induced by the acoustic pressure. Because the axial stress is uniform in each region the boundary condition on s_z is,

$$-\pi R_2^2 p_0 = s_{z1}\,\pi R_1^2 + s_{z2}\,(R_2^2 - R_1^2). \tag{5.5.5}$$

The stresses s_r, s_θ, s_z in these expressions can be explicity specified. Since the loading is assumed radially symmetric all stresses are independent of coordinate θ. In general then for each region,

$$s_i = \frac{g_i}{r^2} + h_i \qquad i = r,\ \theta \tag{5.5.6}$$

[4] in which g_i, h_i are constants. If the materials in regions 1 and 2 were identical the radial and tangential stresses would be constants because there are no boundary surfaces at $r = 0$, and at $\theta = 2\pi$, and these constants would be equal because of radial symmetry of the loading. However, when the materials of the two regions are different (as they are in this case) only the stresses in the inner fiber are constant:

$$s_{r1} = \alpha;\ s_{\theta 1} = \alpha;\ s_{z1} = \beta \qquad \text{(region 1)}. \tag{5.5.7}$$

In the jacket the stresses depend on coordinate r because there is a boundary at the surface $r = R_2$ between two different materials. Since, however, the stress in the axial direction is a constant it is required for the stresses s_r and s_θ, that the g_i have the same magnitude but be different in sign. Thus,

$$s_{r2} = \frac{\gamma}{r^2} + \delta;\ s_{\theta 2} = -\frac{\gamma}{r^2} + \delta;\ s_{z2} = \epsilon \qquad \text{(region 2)}. \tag{5.5.8}$$

Thus for the case of a 3-D uniform acoustic loading on a two layer compound cylinder there are 5 unknown constants α, β, γ, δ, ϵ. Since there are 5 boundary conditions (Eqs. 5.5.1 through 5.5.5) the stress-strain system can be solved by writing 5 simultaneous equations and solving them by matrix inversion. However, two of these conditions namely (2) and (3) require formulas for strains and displacements. In 3-D stress these are

$$e_i = \frac{1}{E}[s_i - \nu(s_j + s_k)];\ u_r = \int e_r dr \tag{5.5.9}$$

[5] in which the subscript i is one of the coordinates r, θ, z, and the subscripts j, k are the two remaining coordinates.

Substitution of Eqs. 5.5.7, 5.5.8 and 5.5.9 into Eqs. 5.5.1 through 5.5.5 and subsequent inversion of the matrix of simultaneous equations yields explicit values for the constants α, β, γ, δ, ϵ. Thus all the stresses and strains in the system become known functions of the applied pressure. For the case of 3-D loading by acoustic pressure the phase shift is given by Mahon and Cielo [7]:

$$\Delta\phi = k_0 n L p_0 \left\{ \left[1 - \frac{n^2}{2}(p_{12} - p_{11}\nu_1 - p_{12}\nu_1) \right] \left[R_2^2 \frac{(1 - 2\nu_2) + 2R_1^2(\nu_2 - n_1)}{E_2(R_2^2 - R_1^2) + E_1 R_1^2} \right] \right.$$

$$\left. - \frac{n^2}{2}(p_{11} + p_{12}) \frac{1 - \nu_1 - 2\nu_1^2}{E_1} \right\} \ldots . \tag{5.5.10a}$$

In particular one thereby determines the radial and axial strains e_{r1}, e_{z1} in the inner core fiber. With them one can calculate the sensitivity of the composite acoustic sensor.

The calculation of the sensitivity of the composite is based upon Eq. 5.3.4, modified for the present case of 3-D stress:

$$\Delta\phi = k_0 n e_{z1} L - \frac{1}{2} k_0 n^3 L[(p_{11} + p_{12})e_{r1} + p_{12} e_{z1}]. \tag{5.5.10b}$$

Figure 5.5.2 is a plot of this acoustic sensitivity as calculated by Hocker [6] for the case of a fused silica inner core and a variety of jacket materials. The optical and elastic properties of the fiber material are taken to be those of Table 5.4.1. The ordinate is the nondimensional phase shift $\Delta\phi E_1/\Delta P_0(k_0 n L)$, and the abscissa is the ratio $R = R_2/R_1$. The parameter is the ratio $E = E_1/E_2$. For the uncoated fiber this figure predicts a (nondimensional acoustic) sensitivity of -0.198. When the jacket covers the fiber the sensitivity increases quickly at each jacket size as the compliance of the material of the jacket increases. For large jacket size (say $R \sim 20$) one can predict a sensitivity increase of a factor of roughly 100 above that of a bare fiber if $E \sim 100$. For fixed values of E on the other hand the sensitivity increases with R at a slower rate and soon becomes stabilized at a value independent of R.

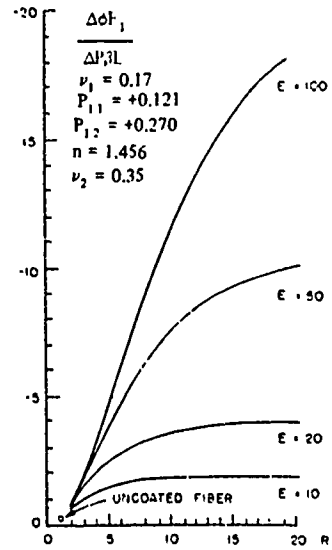


Fig. 5.5.2 — Acoustic sensitivity $[\Delta\phi/\Delta P\ E_1/\beta L$ for a coated fused silica fiber vs ratio of radii R, with ratio of elastic moduli E as a parameter [after Ref. 6]. G. B. Hocker, *Applied Optics*, **18**, 3679 (1979), ©1979 Optical Society of America; by permission.

An additional observation is this: the strain-enhancement due to jacketing occurs primarily in the axial strain and secondarily in the radial strain. Since the acoustic sensitivity increases quickly due to length change and relatively slowly due to change in radius, and since the two effects are of opposite sign, it is seen that the net phase shift increases even more quickly with increase in jacket size and jacket compliance.

The basic equations of analysis (Eqs. 5.5.1 through 5.5.9) indicate that sensitivity can be increased by reducing the Poisson's ratio of the jacket material. Figure 5.5.3 shows this effect.

It is sometimes suggested that a fiber can be embedded in a large block of elastic material and the combination be used as a sensor of acoustic pressure. In this case R_2 is taken to be infinite and the analysis is repeated. Figure 5.5.4 shows the acoustic sensitivity of this structure versus compliance parameter E of the jacket, with the Poisson's ratio of the jacket as parameter. For the choice $\nu_2 = 0.50$ (corresponding to incompressible rubber) one finds a sensitivity of $+0.32$, almost independent of E. In contrast, as ν_2 decreases the sensitivity rises rapidly when the compliance of the elastic medium is reduced.

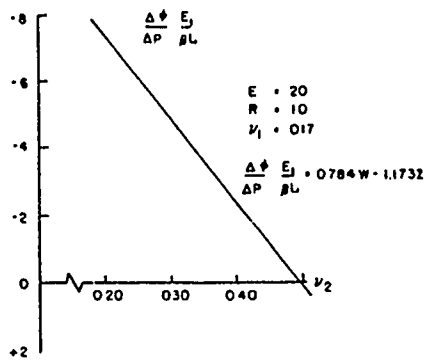


Fig. 5.5.3 Dependence of acoustic sensitivity $(\Delta\phi/\Delta P)E_1/\beta L$ for a coated fused silica fiber on Poisson's ratio in the coating material ν_2 with $E = 20$ and $R = 10$ [after Ref. 6]. G. B. Hocker, *Applied Optics*, **18**, 3679 (1979), ©1979 Optical Society of America; by permission.

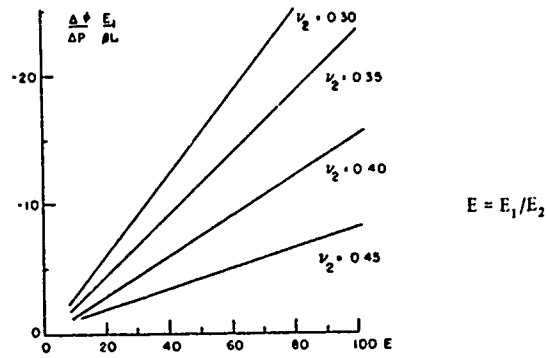


Fig. 5.5.4 — Acoustic sensitivity for fused silica fiber embedded in an elastic medium vs elastic modulus ratio E, with Poisson's ratio in embedding medium ν_2 as a parameter [after Ref. 6]. G. B. Hocker, *Applied Optics*, **18**, 3679 (1979), ©1979 Optical Society of America; by permission.

One concludes from this analysis that a composite acoustic sensor consisting of a jacket and a fiber can be designed to improve acoustic sensitivity over that of the bare fiber by some one to two orders of magnitude.

In another configuration, mentioned in the introduction to this section, the strain-enhancement is achieved by bonding a coil of the bare fiber to the exterior wall of an end-capped hollow cylinder of elastic material. When such a composite is subjected to an acoustic pressure the hoop stress s_θ of the cylinder becomes effectively the longitudinal stress of the fiber. The stress-enhancement is roughly of the order of the ratio of the mean cylinder radius to the thickness. In analyzing this structure one chooses the model of a thick-walled hollow cylinder interior radius a, exterior radius b subject to acoustic pressure p_0 in both radial and longitudinal directions. The stresses induced expressed in cylindrical coordinates r, θ, z core,

$$s_r = \frac{-b^2 p_0}{b^2 - a^2} + \frac{a^2 b^2 p_0}{(b^2 - a^2) r^2} \tag{5.5.11}$$

$$s_\theta = \frac{-b^2 p_0}{b^2 - a^2} - \frac{p_0 a^2 b^2}{(b^2 - a^2) r^2} \tag{5.5.12}$$

$$s_z = \frac{-p_0 b^2}{b^2 - a^2}. \tag{5.5.13}$$

The elastic strains associated with these stresses are those of an isotropic material given by Eq. 5.5.9. According to Eq. 5.3.4 these strains give rise to a pressure-induced phase shift of value,

$$\Delta\phi = k_0 n S_1 L - \frac{1}{2} k_0 n^3 L (p_{12} S_1 + p_{11} S_2 + p_{12} S_3). \tag{5.5.14}$$

If we choose S_1 to be the tangential strain S_θ then

$$S_\theta = \frac{1}{E}[s_\theta - \nu(s_r + s_z)], \text{ or } = \frac{1}{E}[s_\theta - \nu(s_z + s_r)] \tag{5.5.15}$$

meaning that S_2 can be S_r or S_z. Since S_r is different from S_z the sum $p_{ij} S_j$ will have a different value depending on the choice. It is simplest in this case to use an average photoelastic constant $p_{AV} = (1/2)(p_{11} + p_{12})$ for S_2 and S_3. Essentially this assumes the two polarization modes allowed by an optically anisotropic material are being excited.

From Eqs. 5.5.11, 5.5.12, 5.5.13 one can obtain the strains by use of Eq. 5.5.9 for the surface $r = b$:

$$S_\theta = -\frac{p_0}{E_2}\left[\frac{b^2 + a^2}{b^2 - a^2} - \nu_2 \frac{2b^2 - a^2}{b^2 - a^2}\right] \tag{5.5.16}$$

$$S_r + S_z = -p_0\left[\frac{2b^2 - a^2}{(b^2 - a^2)}\left[\left[\frac{1 - \nu - 2\nu^2}{E_1}\right] + \frac{2\nu_1\nu_2}{E_2}\right] - \frac{2\nu_1(b^2 + a^2)}{E_2(b^2 - a^2)}\right]. \tag{5.5.17}$$

Here subscript 1 refers to the fiber, and 2 refers to the cylinder jacket material. The phase-shift induced by the acoustic pressure is obtained by substitution of Eqs. 5.5.15, 5.5.16 and 5.5.17 into Eq. 5.5.14 using p_{AV} in the process:

$$\Delta\phi = \frac{-p_0 k_0 nL}{E_2(b^2 - a^2)}\left\{[b^2 + a^2 - \nu_2(2b^2 - a^2)]\left[1 - \frac{n^2 p_{12}}{2}\right] - \frac{n^2 p_{AV}}{2}\left[(2b^2 - a^2)\right.\right.$$

$$\left.\left. \times \left[\frac{1 - \nu_1 - 2\nu_1^2}{E_1/E_2} + 2\nu_1\nu_2\right] - 2\nu_1(b^2 + a^2)\right]\right\} \qquad (5.5.18)$$

[7]. Figure 5.5.5 shows phase sensitivity $\Delta\phi/p_0 k_0 nL$ plotted as a function of the ratio of outside radius $(r = b)$ to wall thickness $(b - a)$ for three different types of jacket cylinder material, polyethylene, Lucite and aluminum.

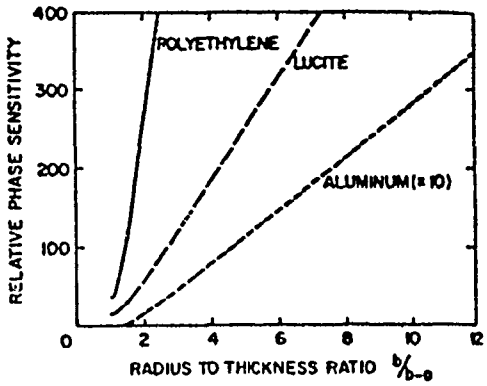


Fig. 5.5.5 — Phase sensitivities of end-capped, cylindrical fiber optic hydrophones of polyethylene, Lucite, and aluminum relative to the sensitivity of an unjacketed fiber of the same length [after Ref. 7]. G. W. McMahon and P. G. Cielo, *Applied Optics*, **18**, 3720 (1979), ©1979 Optical Society of America; by permission.

The optical and elastic properties of the structural components used in the calculation are:

bare fiber	jacket cylinder (Lucite)	polyethylene	aluminum
radius: 20 μm	$E_2 = 4 \times 10^9$ Pa	$E_2 = 0.76 \times 10^9$ Pa	$E_2 = 71 \times 10^9$ Pa
$E_1 = 73 \times 10^9$ Pa	$\nu_2 = 0.4$	$\nu_2 = 0.458$	$\nu_2 = 0.355$
$\nu_1 = 0.17$			
$p_{11} = 0.12$			
$p_{12} = 0.27$			

Again it is seen that an end-capped cylindrical fiber-optic acoustic sensor wrapped with an embedded coil of fused silica fiber can be designed to be at least two orders of magnitude greater in acoustic sensitivity than the bare fiber alone. A caution however is necessary. Experience has shown that a coated fiber wrapped on an elastic cylinder shows little improvement due to the coating but much improvement due to the cylinder deformation. While both methods of strain-enhancement predict sensitivity improvement when used separately, the effects do not appear additive.

5.6 FIBER OPTIC HYDROPHONE—THEORY AND EXPERIMENTAL RESULTS

The use of optical-fibers in hydrophone construction as the main sensing element has been reported by Bucaro et al [8]. A theoretical and experimental discussion of this type of transducer is taken up next.

In Sections 5.4, 5.5 the theoretical pressure-induced phase shift in a fiber optic sensor was derived in the form

$$\Delta\phi = p_0 L \times \text{const} \qquad (5.6.1)$$

in which the value of the constant was determined by the elastic properties of the fiber and by the distribution of mechanical stresses imposed upon it by the pressure loading.

A fiber-optic hydrophone may be constructed with this sensor in the manner shown in Fig. 5.6.1 [9]. It consists of an optical interferometer, one (signal) arm of which contains a fiber-optic coil immersed in an underwater sound field, and the other (reference) arm of which is also an optical fiber of the same manufacture placed outside the tank. The reference arm is injected with a beam of light at wavelength λ and power P_r (watts) while the signal arm is injected with the same wavelength light at power P_s. Upon passing through the sound field and being modulated by it the signal light is superimposed on the reference light in a photomultiplier. The electric current out of the photomultiplier is

$$I = \alpha\,[P_r + P_s + 2\beta(P_rP_s)^{1/2}\cos(\phi_0 - \Delta\phi)] \tag{5.6.2}$$

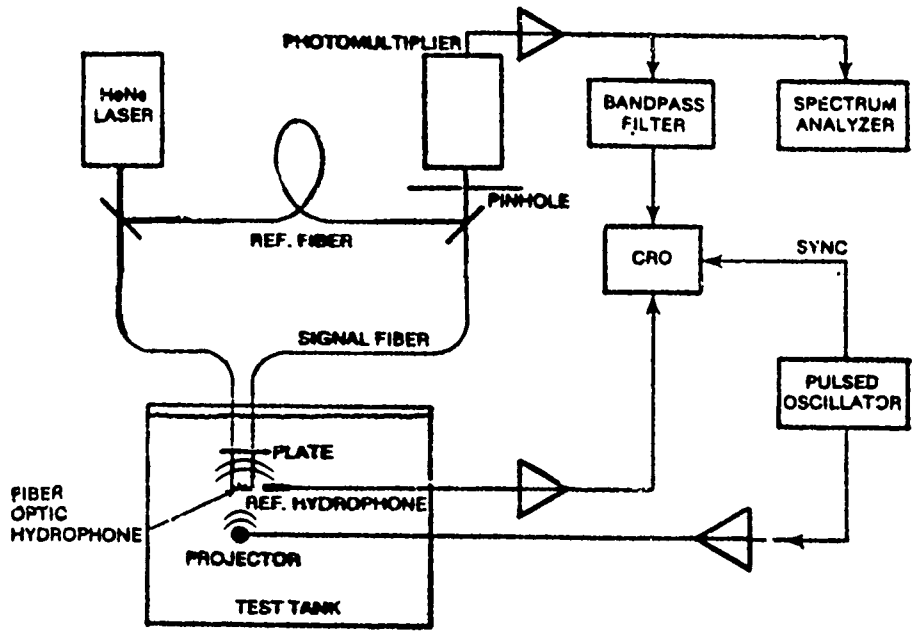


Fig. 5.6.1 — Experimental fiber-optic hydrophone tested in a laboratory tank [after Ref. 9]. P. Shajenko, J. P. Flatley and M. B. Moffett, *J. Acous. Soc. Am.*, **64**, 1286 (1978), ©1978 American Institute of Physics; by permission.

in which α is the photomultiplier response (units: A/watt), and $\beta(\leqslant 1)$ is the homodyne efficiency (see Section 5.8 for definition and discussion of this term). The phase ϕ_0 is the phase difference between signal and reference when there is no sound modulation, and the phase shift $\Delta\phi$ is the phase shift due to the sound field. Since

$$\cos(\phi_0 - \Delta\phi) = \cos\phi_0 \cos\Delta\phi + \sin\phi_0 \sin\Delta\phi$$

it is seen that for $\phi_0 = \pi/2$, $\Delta\phi << \pi/2$, the signal term

$$i_s = 2\alpha\beta(P_rP_s)^{1/2}\Delta\phi = 2\alpha\beta(P_rP_s)^{1/2}p_0L \times \text{const.} \tag{5.6.3}$$

is both linear and maximized. Across the photomultiplier load-resistance R_M the voltage per unit acoustic pressure for a 3-D uniform loading on the signal arm Eq. 5.3.6c gives the hydrophone sensitivity M,

$$M = \frac{V}{p_0} = 2\alpha\beta R_M(P_rP_s)^{1/2}k_0L\left\{\frac{n(1-2\nu)}{E} - \frac{1}{2}\,\frac{n^3}{E}\,[(1-2\nu)\,(p_{11}+2p_{12})]\right\} \tag{5.6.4}$$

Now from Sect. 5.4, Case III,

$$\frac{\Delta\phi}{p_0} = 3.946 \times 10^{-11}\,\frac{L}{k_0} = \frac{3.946 \times 10^{-11}}{9.97 \times 10^{6}}\,k_0L = 3.96 \times 10^{-18} k_0L\ \frac{rad}{\mu Pa}. \qquad (5.6.5)$$

(The contribution from the length change is $13.2 \times 10^{-18}\ k_0L$, and from the refractive index change is $-9.2 \times 10^{-18}\ k_0L$.) Thus the predicted sensitivity of this hydrophone is,

$$M = 7.92 \times 10^{-18}\alpha\beta R_M (P_r P_s)^{1/2} k_0 L \quad \text{(units: V/}\mu\text{Pa)} \qquad (5.6.6)$$

This value is in good agreement with the theoretical formula derived by [9] in which the constant for borosilicate glass turned out to be 8.1×10^{-18} as compared to 7.92×10^{-18}.

To test the accuracy of their formula an experiment, based on the construction shown in Fig. 5.6.1, was run. Two single-mode optical fibers were used, each was 4 m long, 2.5 μm in core diameter, with an attention of 0.25 dB/m. A 1 m portion in the center of the signal arm was wound in a coil 5 cm in diameter and immersed below a reflection plate in the test tank of water. The projector shown in Fig. 5.6.1 was a spherical acoustic source 3.5 cm in diameter, driven by 60 kHz pulses of length 50 μs. By use of a reference hydrophone the acoustic pressure at the fiber coil was measured to be 191 dB/1 μPa.

A He-Ne laser, driven at $P_r = P_s = 9.5$ nW, furnished both signal and reference beams. The homodyne efficiency was estimated at $\beta = 0.5$.

The photomultiplier tube (EMI 9798 B) had a 400 μm pinhole, a responsiveness of $\alpha = 2100$ A/W, and a load resistance of 50 Ω.

A calculation of Eq. 5.6.6 based on these value gives a theoretical sensitivity of −268 dB re 1 volt per micropascal. The measured value was −264 dB.

The actual sound field was monitored by a small probe acoustic hydrophone of standard construction. A comparison of the waveforms of the acoustic hydrophone and the fiber-optic hydrophone is shown in Fig. 5.6.2. The fidelity however is progressively weakened as the acoustic level is increased, or as the length of the fiber is increased [10]. The effect is due to the accession of harmonics of the acoustic signal.

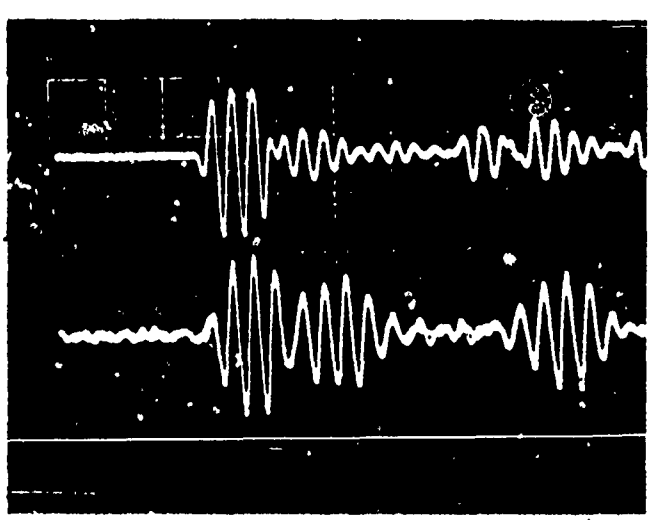


Fig. 5.6.2 — Comparison of acoustic and fiber-optic hydrophone signals. Top trace: acoustic hydrophone, 1V/div. Bottom trace: fiber-optic hydrophone, 50 mV/div. Time scale: 40 μs/div. [9]

The sensitivity just discussed must be judged relative to the detection threshold, or lowest level of detectable signal.

A second parameter of importance is the noise equivalent pressure level of the hydrophone. This is determined as follows. The signal current in the photomultiplier is approximated by the relation,

$$i_s = 2\alpha\beta(P_r P_s)^{1/2} \cos(\phi_0 - \Delta\phi) \rightarrow 2\alpha\beta(P_r P_s)^{1/2}\Delta\phi. \tag{5.6.7}$$

If we assume the noise in the photomultiplier is primarily photon shot-noise then the noise current is

$$i_N = \sqrt{2e(I_r + I_s)B}, \quad \begin{matrix} e = \text{electron charge (units: C)} \\ B = \text{bandwidth (units: Hz)} \end{matrix} \tag{5.6.8}$$

Assume now that the noise current equals the signal current:

$$\sqrt{2e(I_r + I_s)B}, = \alpha\beta(P_r P_s)^{1/2}\Delta\phi$$

or

$$\Delta\phi = \frac{1}{\beta}\left[\frac{e(P_r + P_s)B}{2\alpha P_r P_s}\right]^{1/2} \tag{5.6.9}$$

in which $I/\alpha = P$. From Eq. 5.3.6c, $\Delta\phi$ is related to the applied acoustic pressure p_1,

$$p_1 = \frac{\Delta\phi}{C_1 L}, \quad C_1 = \frac{k_0 n(1-2\nu)}{E} - \frac{1}{2}\frac{k_0 n^3}{E}\{(1-2\nu)(p_{11}+2p_{12})\}$$

or

$$p_N = \frac{1}{\beta C_1 L}\left[\frac{e(P_r + P_s)B}{2\alpha P_r P_s}\right]^{1/2} \tag{5.6.10}$$

This is the noise equivalent pressure. When other noises are present i_N is larger than Eq. 5.6.8. It is clear from this formula that the threshold of detection may be lowered by altering the following factors. (1) increasing the homodyne efficiency β (2) increasing the strain enhancement (contained in factor C_1) (3) increasing the length L (4) decreasing the bandwidth B (5) increasing the photodetector response α (6) increasing the input laser power P (7) reducing the electronic noise in the laser, detector etc.

Two experimentally determined thresholds are discussed next.

A numerical estimate will serve to indicate magnitude. Let $P_r = P_s = 9.5 \times 10^{-9}$ watt, $B = 1$ Hz, $\beta = 0.5$, $L = 1$ m, $\alpha = 2100$ A/Watt. From Sect. 5.4, Case III it is seen that $C_1 = 3.946 \times 10^{-11}$ rad/μPa $\times$ m $= 3.946 \times 10^{-5}$ rad/Pa $\times$ m. The electron charge is 1.602×10^{-19} C. Thus,

$$p_N = \frac{1}{0.5 \times 3.946 \times 10^{-5} \times 1}\left[\frac{1.602 \times 10^{-19} \times 1}{2.1 \times 10^{3} \times 9.5 \times 10^{-9}}\right]^{1/2} = 4.54 \times 10^{-3}\ \text{N/m}^2 = 4.54 \times 10^{3}\ \mu\text{Pa}$$

$20 \log p_N = 73$ dB *re*, μPa.

The internal noise *in this particular arrangement* is thus equivalent to an excitation of external acoustic pressure of the amount calculated. This is therefore the threshold of detection.

An alternate formula for the threshold corresponding to shot-noise is derived as follows. From Eq. 5.6.9 let $P_r = P_s = P_0$, then

$$\Delta\phi = \frac{1}{\beta}\left[\frac{eB}{\alpha P_0}\right]^{1/2} \tag{5.6.11}$$

If the change in phase ϕ is due *solely* to a change in index of refraction n then

$$\Delta\phi = k_0 L \Delta n$$

so that

$$\Delta n = \frac{1}{k_0 L \beta}\left[\frac{eB}{\alpha P_0}\right]^{1/2} \tag{5.6.12}$$

Now the change ϵ_1 in relative dielectric constant ϵ due to a harmonic acoustic wave propagating with wavenumber K_x and frequency Ω is given in the formula,

$$\epsilon = \epsilon_0 + \epsilon_1 \cos\,(K_x x - \Omega t)$$

in which ϵ_0 is the relative dielectric constant in the absence of the acoustic disturbance. In terms of the change in density $\Delta\rho$ one defines a constant γ such that

$$\epsilon_1 = \gamma \frac{\Delta\rho}{\rho}. \tag{5.6.13}$$

Since $\epsilon_1 = \Delta(n^2)$, $\epsilon = n^2$, then

$$\epsilon_1 = 2n\Delta n. \tag{5.6.14}$$

Mass density ρ is related to compressibility K by the formula,

$$\kappa = \frac{\Delta\rho}{\Delta p}\,\frac{1}{\rho}. \tag{5.6.15}$$

Also, under the assumption that $\epsilon_1 << \epsilon_0$ it is easy to show by use of the Lorentz-Lorenz law that

$$\gamma = \frac{1}{3}\,(\epsilon_0 - 1\,(\epsilon_0 + 2) \tag{5.6.16}$$

[11] Assembling Eqs. 5.6.11 through 5.6.16, one has finally

$$\Delta p = \frac{6n\lambda_0}{2\pi L\kappa(n^2 - 1)\,(n^2 + 2)}\left(\frac{eB}{\alpha P_0}\right)^{1/2}\frac{1}{\beta}. \tag{5.6.17}$$

Except for the factor 2β in the denominator this is the formula used by Cole et al [12]. The factor 2 arises because in expanding $\cos[\phi_0(t) - \Delta\phi(t)]$ in Bessel functions of the first kind and approximating the first side-lobe for small argument the phase change becomes $\Delta\phi/2$.

In making numerical estimates of Eq. 5.6.17 reference [10] used the values $n = 1.465$, $L = 0.254$ n, $\lambda_0 = 0.6328 \times 10^{-6}$ m, $\alpha = 0.3$ A/watt, $P_0 = 3 \times 10^{-4}$ W, $B = 1$ Hz. It is to be noted that the value of α is that of a photodetector rather than the photomultiplier used by reference [8]. We calculate here that $\beta = 0.5$, and

$$\kappa = \frac{3(1-2\nu)}{E} = \frac{3[1-2(.17)]}{7.3 \times 10^{10}} = 2.71 \times 10^{-11} \left[\frac{m^2}{N}\right]. \tag{5.6.18}$$

Substitution of these values in Eq. 5.6.17 leads to the result that for a 1 Hz band of reception,

$$\Delta p = 2.34 \times 10^{-3} \text{ Pa} = 2.34 \times 10^{3} \,\mu\text{Pa} = 67.4 \text{ dB } re \text{ } 1 \,\mu\text{Pa}.$$

Measurements made by Cole et al. (loc. cit) at laser wavelength 0.5145 μm are reproduced here as Fig. 5.6.3. Although there is considerable spread, particularly at the higher acoustic frequencies, the agreement between theory and experiment is reasonably good.

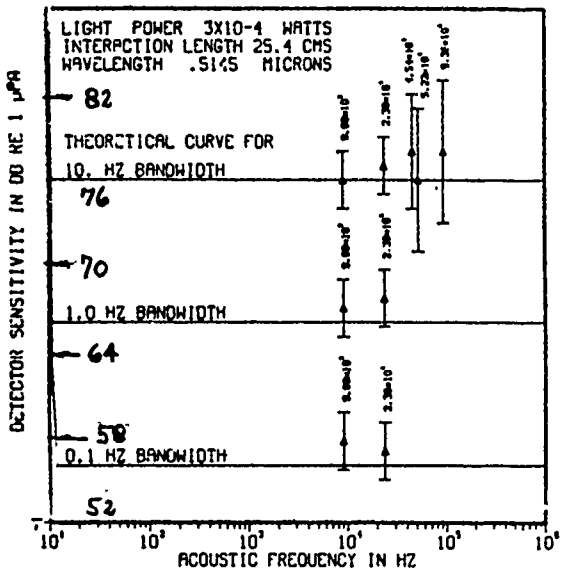


Fig. 5.6.3 — Measured thresholds of a fiber interferometer with frequencies as specified [after Ref. 12]. J. H. Cole et al., *J. Acous. Soc. Am.*, **62**, 1135 (1977), ©1977 American Institute of Physics; by permission.

Other (unpublished) results show measured thresholds of some 55 dB re 1 μPa at 0.1 kHz, to some 25 dB at 2 kHz.

5.7 FIBER-OPTIC HYDROPHONE—PROTECTION AGAINST ENVIRONMENTAL NOISE

The fiber-optic hydrophone described above consists of two laser-excited monomode fibers forming two arms of an interferometer; one a reference fiber and the other a signal fiber. Such an arrangement is prone to distortion by environmentally induced noise and vibration because the signal arm is disturbed by these agents while the reference arm is not. Since in the usual design the phase shift to be detected must be limited for linearity to $\Delta\phi \ll \pi$, and since a dynamic range of 10^4 is customarily required, optical path variations of the order of 10^{-5} μm must be detected. These small quantities are likely to be swamped out by platform vibration or ocean noise of various origins.

To overcome distortions in reception which are associated with a two-fiber design it is suggested to use a single monomode fiber. Bucaro and Carome [10] have proposed a high coherence length source E_0 injected into a single fiber with both ends cut perpendicular to the fiber axis. A first beam exiting the fiber has a magnitude TE_0, T being the transmission coefficient. It is subject to an acoustically induced phase shift due to *one* pass through the fiber. A second beam exiting the fiber has a magnitude $T\,R^2E_0$, where R is the reflection coefficient of the cut end. It is subject to an acoustically induced phase shift due to *three* passes through the fiber. The relative phase shift between the two beams is therefore twice that of a beam that makes a single pass through the fiber. This relative phase indicates the presence of the acoustic signal. The intensity of the transmitted beams is however much reduced by the absorption and reflection parameters of the fiber.

An extension of this concept was made by Cielo [13]. It is best understood by use of the classical theory of multiple beam interference, Fig. 5.7.1. A plane wave W, wavelength λ_0 is incident on a plane parallel plate, thickness h, index of refraction n'. The transmitted light consists of a number of parallel beams at angle θ' having phase difference, one beam to the following beam, of value

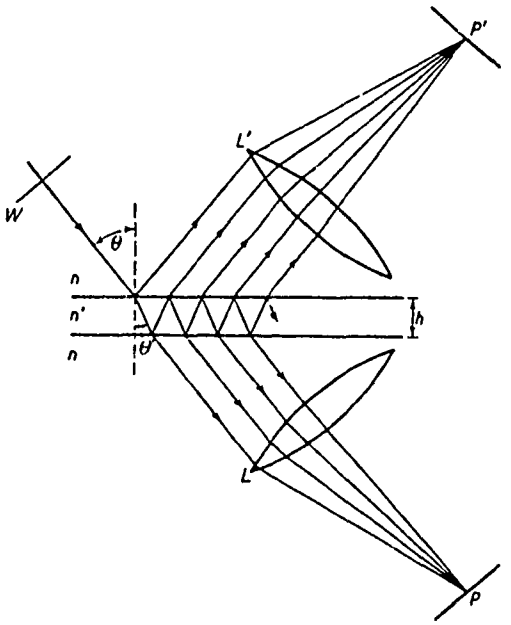


Fig. 5.7.1 — Illustrating formation of multiple beam fringes of equal inclination with a plane parallel plate

$$\delta = \frac{4\pi}{\lambda_0}\, n'h \cos\theta'. \tag{5.7.1}$$

When these beams are superimposed upon a focal plane by a convergent lens they display maxima, at orders

$$m = \frac{\delta}{2\pi} = \frac{2n'h\cos\theta'}{\lambda_0} \qquad m = 1,\ 2\ \ldots\ldots \tag{5.7.2}$$

and minima at orders,

$$m = \frac{1}{2},\ \frac{3}{2},\ \frac{5}{2}\ \ldots\ldots$$

The fringe pattern is approximately the same as for a two-beam interference, but the intensities and fringe widths are modified by the reflection properties of the plate surfaces. The theory shows that the ratio of transmitted intensity to incident intensity is

$$\frac{I^{(t)}}{I^{(i)}} = \frac{1}{1 + F\sin^2\delta/2} \tag{5.7.3}$$

$$F = \frac{4\,R}{(1-R)^2} \tag{5.7.4}$$

in which R is the reflectivity of the plate surfaces. It is seen that when $\delta/2$ is an integral multiple of 2π, the intensity of transmitted light is equal to the intensity of the incident light—that is, a maximum.

When, however, $\delta/2$ is an odd multiple of π, the transmitted light is a minimum of value given by,

$$I^{(t)} = \frac{I'}{1+F} \tag{5.7.5}$$

For $R = 0.18$,

$$I^{(t)}/I^{(i)} \sim 0.94$$

while for $R = 0.87$,

$$I^{(t)}/I^{(i)} \sim 4.8 \times 10^{-3}$$

(In these calculations the inherent absorption of the glass has been neglected.) Thus for surfaces of high reflectivity the fringe pattern in the focal plane of the lens consists of very sharp bright lines at phase differences $2m\pi$, m integer, and near total darkness in between as illustrated by Fig. 5.7.2.

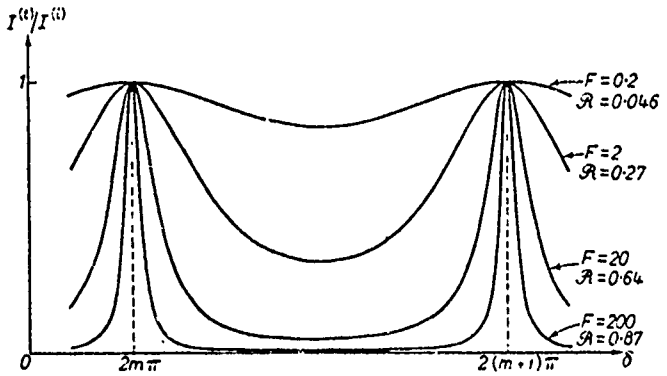


Fig. 5.7.2 — Multiple beam fringes of equal inclination in transmitted light: ratio $I^{(t)}/I^{(i)}$ of transmitted and incident intensities as a function of phase difference δ (m is an integer) [after Ref. 13]. P. G. Cielo, *Applied Optics*, **18**, 2933 (1979), ©1979 Optical Society of America; by permission.

In applying multiple beam interference Cielo replaced the plane parallel plate by a cavity between two reflectors, Fig. 5.7.3. The reflectors are analogs of the two surfaces of the plate while the cavity is a piezoelectric cyclinder wrapped with the fiber. It constitutes the analog of the thickness of the plate, made adjustable by "tuning" so that the phase delay is a function of the mean radius of the cylinder, hence of an applied voltage. In this way, once the wavelength λ_0 of the laser, and the reflectivity of the reflectors R are fixed, once can sharpen the fringe pattern of interference. This means sharpening the discrimination of phase difference by "tuning" the radius of the piezoelectric cylinder.

In operation all beams are simultaneously in the fiber. Actually, only the first transmitted beam and the beam consisting of one internal reflection between reflectors followed by transmission, effectively interfere. This is because the remaining beams are, for the usual values of reflectivity, relatively very weak.

Two such cavities are used in the Cielo concept, Fig. 5.7.3. Their intended operation is shown in Fig. 5.7.4. The first, or reference, cavity performs the function of sharpening the transmitted laser spectrum by multiple beam interference: beam 1 is transmitted directly while beam 2 undergoes reflections before transmission. They are superimposed upon exiting the cavity and together yield the spectrum shown in Fig. 5.7.2. The phase delay associated with this spectrum is $\delta_1 = \omega_0 L_1/v_1$, where L_1 is the fiber length within the cavity, v_1 is the phase velocity of light within the cavity, and ω_0 is the frequency of this light. The length L_1 is adjustable by applying a voltage to the piezoelectric cylinder causing it to expand. The second, or remote, cavity is submerged in the water and is subject to the acoustic signal. Beam 3 operates at phase shift δ_3 while beam 4 operates at phase shift $\delta_4 = \delta_3 + (N+1)\Delta\delta$ where N is the number of reflections in the cavity and $\Delta\delta$ is the phase shift due to one pass through the cavity. Because of absorption and loss at reflection the value of N is approximately 2. The difference between the two phases is $\delta_2 = \delta_4 - \delta_3$. Again it is emphasized that all beams occur simultaneously in a single fiber.

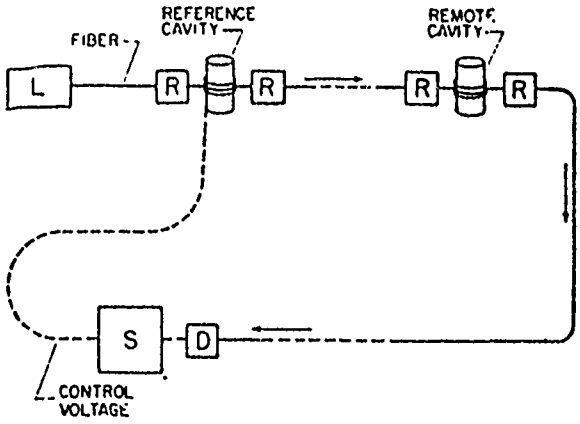


Fig. 5.7.3 — Double cavity configuration. *L*, light source coupled to the fiber; *R*; reflectors; *D*, photodetector; *S*, servo-control electronics [after Ref. 13]. P. G. Cielo, *Applied Optics*, **18**, 2933 (1979), ©1979 Optical Society of America; by permission.

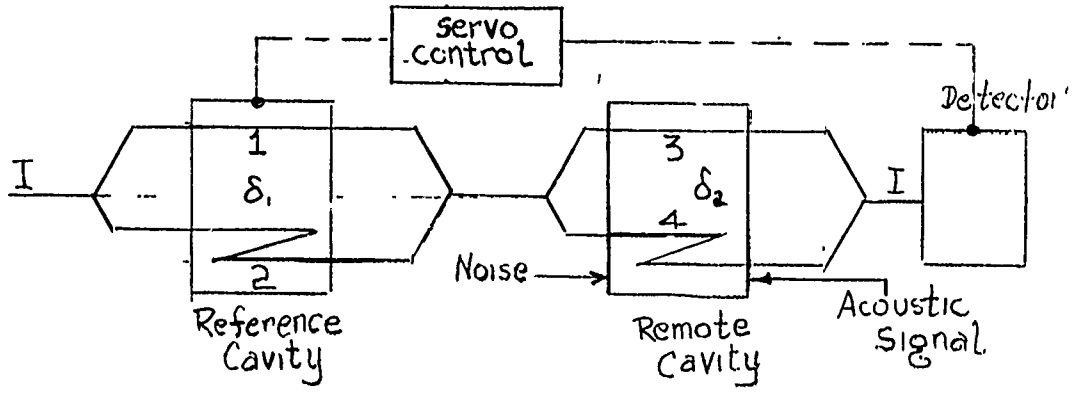


Fig. 5.7.4 — Illustration of operation of a double-cavity fiber-optic hydrophone

The responses of the two cavities are in cascade. Thus the intensity of the light entering the detector is,

$$I(\omega) = \frac{\eta^2 I^{(i)}(\omega)}{\left(1 + F \sin^2 \frac{\delta_1}{2}\right)\left(1 + F \sin^2 \frac{\delta_2}{2}\right)} \tag{5.7.6}$$

in which η is the absorption coefficient.

In operation we suppose first that the e is no acoustic signal. The reference cavity, being tunable, is tuned by an applied voltage V to some value of $\delta_1 - \delta_2$. The responses of the two cavities can thus be made to exactly superpose and generate maxima at $\delta_1 - \delta_2 = 0, 2\pi, 4\pi$ and minima between them at $\delta_1 - \delta_2 = \pi, 3\pi/2, 5\pi/2$. At high reflectivity the minima are nearly zero in intensity. The *operating point* is set at the peak of one of the maxima.

We now suppose there is an acoustic signal. The remote cavity undergoes a phase change which reduces the intensity $I(\omega)$ from its peak value. A control voltage V is applied to bring back $I(\omega)$ to its peak value once again. The fluctuations of this tuning voltage is maintained by servocontrol. It mirrors the phase fluctuations caused by the acoustic signal. It is the quantity actually to be measured and analyzed.

An experimental demonstration that a single optical fiber can serve simultaneously as reference and signal has been carried out by Bucaro and Carome [9].

A significant advantage of this concept is its insensitivity to ocean noise and platform vibration. This comes about because reference and signal, being the same fiber, are equally disturbed by such external agencies, and hence when the matching of the two cavities is performed in the detector the noise disturbancies do not affect the matching process in any way. A second advantage of the two-cavity single fiber concept is the relaxation of the need for laser light of very extended spatial coherence. Reference [13] reports that incoherent sources such as LED or tungsten lamp have proved successful in other applications of the concept of two-cavity modulation.

5.8 SIGNAL/NOISE RATIO OF FIBER-OPTIC HYDROPHONES

Heterodyne and Homodyne Detection

In discussing signal/noise ratio of optical fiber hydrophones it will be useful to distinguish between heterodyne and homodyne systems. In a heterodyne system, as applied to radar, a signal at carrier frequency f_0 is transmitted to a target where it is modulated to $f_0 \pm f_d$ and reflected back to the receiver. Inside the receiver the original carrier is mixed with a local oscillator frequency f_{if} (called the IF signal) to yield f_0, $f_0 + f_{if}$, $f_0 - f_{if}$. This is filtered to give $f_0 + f_{if}$, which is mixed with $f_0 \pm f_d$ to give $f_{if} \pm f_d$. This signal is IF amplified and then detected to give f_d, the doppler signal.

In a homodyne detection system no IF local oscillator or IF amplifier is used. Demodulation of the received signal is done directly at the laser frequency.

The same distinction between detection system appears in optical hydrophones. In heterodyne systems the laser frequency is reduced to an IF frequency by use of a Bragg cell and detection is accomplished at this lowered frequency. In homodyne systems no Bragg cell is used and detection is accomplished at carrier frequency.

Homodyne systems are much simpler than heterodyne systems. However they are less sensitive and more noisy.

Photodetector Current

In a laser heterodyne (or homodyne) detection system the superposition on the surface of the photodetector of the reference beam, with intensity I_r, and the signal beam, with intensity I_s, can be modeled as noted earlier on the theory of partially coherent light [14]. In this theory the total intensity of two superimposed beams which differ in phase by $\Delta\phi$ is

$$I_{rs} = I_r + I_s + 2|\gamma_{rs}|\sqrt{I_r I_s}\cos[\alpha_{rs}(\tau) - \Delta\phi] \quad \text{(units: V} \cdot \text{A/m}^2\text{)}, \tag{5.8.1}$$

in which γ_{rs} is the complex degree of mutual coherence, $|\gamma_{rs}|$ is its modulus, and

$$\alpha_{rs}(\tau) = \arg \gamma_{rs} + 2\pi\bar{f}\tau, \tag{5.8.2}$$

where $\bar{f}$ is the mean frequency of the laser and $\Delta\phi$ is path difference. In terms of the laser-beam wavenumber k, one can write the phase difference as a path difference Δx,

$$\Delta\phi = k\Delta x \quad \text{(units: rad)}.$$

If the laser field is represented by the analytic signal $V(t)$, then by definition

$$\gamma_{rs}(\tau) = \frac{\Gamma_{rs}(\tau)}{\sqrt{\Gamma_{rr}(0)}\sqrt{\Gamma_{ss}(0)}} = \frac{\Gamma_{rs}(\tau)}{\sqrt{I_r}\sqrt{I_s}} \tag{5.8.3}$$

and

$$\Gamma_{rs}(\tau) = \langle V_r(t+\tau)\ V^*_s(t)\rangle \quad \text{(units: } V \cdot A/m^2\text{)},$$

in which $\langle\ \rangle$ signifies statistical average in time, Γ_{rr} is the autocorrelation of the random variable $V(t)$, Γ_{rs} is the crosscorrelation of the random variables V_r and V_s, and τ is the delay time. Since $|\gamma_{rs}| \cos [\alpha_{rs}(\tau) + \Delta\phi]$ is a real number, Re γ_{rs}, it is a measurable quantity, namely,

$$\text{Re } \gamma_{rs} = \frac{I_{rs} - I_r - I_s}{2\sqrt{I_r}\sqrt{I_s}}. \tag{5.8.4}$$

The total intensity I_{rs} thus is a sum of coherent and incoherent parts. It is justifiable to assume that over sufficiently long time the random part is uniformly incident over the area of illumination of the photodetector. By integration over this area the total light power incident on the collecting surface becomes

$$P_{rs} = P_r + P_s + 2|\gamma_{rs}|\sqrt{P_r P_s}\cos[\alpha_{rs}(t) - \Delta\phi] \quad \text{(units: V} \cdot \text{A)}. \tag{5.8.5}$$

This light power generates a photodetector current of time-average value

$$\langle i\rangle = \alpha\langle P_{rs}\rangle \qquad \text{(units: A)}, \tag{5.8.6}$$

in which α is the photodetector conversion factor (units: V^{-1} or $A/V \cdot A$). To emphasize partial coherency, it is useful to write this current in the form

$$\langle i\rangle = |\gamma_{rs}|\alpha[P_r + P_s + 2\sqrt{P_r P_s}\cos(\alpha_{rs} - \Delta\phi)] + (1 - |\gamma_{rs}|)\alpha(P_r + P_s). \tag{5.8.7}$$

The first term represents the coherent superposition of two beams of powers $|\gamma_{rs}|P_r$ and $|\gamma_{rs}|P_s$, while the second term represents incoherent superposition of two beams of powers $(1 - |\gamma_{rs}|)\ P_r$ and $(1 - |\gamma_{rs}|)\ P_s$. This distinction between coherent and incoherent parts of the photodetector current will be used to advantage in further developments.

The phase $\Delta\phi$ is the sum of two terms: a nonacoustic phase $\Delta\phi_0$ and an acoustically induced phase $\Delta\phi_A$. In the absence of the latter the average photodetector current can be written just as shown above with $\Delta\phi$ replaced by $\Delta\phi_0$. It is then essentially a sum of dc terms, I_{ph} (units: A). In the presence of an acoustic signal which varies sinusoidally in time, the cosine term becomes

$$\cos(\alpha_{rs} - \Delta\phi_0 - \Delta\phi_A) = \cos(\alpha_{rs} - \Delta\phi_0)\cos\Delta\phi_A + \sin(\alpha_{rs} - \Delta\phi_0)\sin\Delta\phi_A. \tag{5.8.8}$$

If we assume that $\sin\Delta\phi_A \approx \Delta\phi_A$, then there exists a time-varying photodetector component current,

$$\langle i_{AC}\rangle \approx 2\alpha|\gamma_{rs}|\sqrt{P_r P_s}\sin[\alpha_{rs}(\tau) - \Delta\phi_0]\,\Delta\phi_A(t). \tag{5.8.9}$$

The nonacoustic phase $\Delta\phi_0$ may contain a random component of time $\Delta\phi_0(t)$ caused by environmental disturbances. In this case, when there is no useful acoustic signal,

$$\cos[\alpha_{rs} - \Delta\phi_0 - \Delta\phi_0(t)] = \cos\alpha_{rs} - \Delta\phi_0)\cos\Delta\phi_0(t) + \sin(\alpha_{rs} - \Delta\phi_0)\sin\Delta\phi_0(t).$$

When the *fixed* phase $\alpha_{rs} - \Delta\phi_0$ is adjusted to be $\pi/2$, as is customary, there remains a random component of photodetector current

$$i_{\Delta\phi_0} \approx 2\alpha|\gamma_{rs}|\sqrt{P_r P_s}\sin[\Delta\phi_0(t)]. \tag{5.8.10}$$

The probability distribution of $i_{\Delta\phi_0}$ is determined by the sine of the probability distribution of $\Delta\phi_0(t)$. $\Delta\phi_0(t)$ can be considered (for example) to be caused by random temperature fluctuations or by mechanical stress, each with its own statistics.

Coherent and Incoherent dc Photodetector Currents

The time-averaged dc photodetector currents contribute noise in the detection circuits. As noted above these currents are the sum of coherent and incoherent terms. The incoherent terms consist of three contributions:

- scattering of laser light in the fiber by Bragg reflection from thermally induced acoustic plane-wave trains (Brillouin scattering);
- scattering from mass-density fluctuations caused by random motion of the molecules of glass in the fiber whenever the wavelength of the incident laser beam is much smaller than the size of the molecules (Rayleigh scattering); and
- scattering from spherical (or irregular) inhomogenities where the characteristic dimension is larger than, or comparable with, a wavelength of the incident light (Mie scattering).

Thus, the incoherent part of the dc current may be explicitly written in the form

$$(I_{ph})_{\text{incoh}} = \alpha(1 - |\gamma_{rs}|)(P_r + P_s)$$

$$= \alpha(P_{rB} + P_{rR} + P_{rM} + P_{sB} + P_{sR} + P_{sM}) \qquad \text{(units: A)}, \tag{5.8.11}$$

where the subscripts B, R, and M refer to Brillouin, Rayleigh, and Mie scattering, respectively. The coherent part of the dc current has already been formalized above:

$$(I_{ph})_{\text{coh}} = |\gamma_{rs}|\alpha[P_r + P_s + 2\sqrt{P_r P_s}\cos(\alpha_{rs} + \Delta\phi_0)] \qquad \text{(units: A)}. \tag{5.8.12}$$

Here all terms are nontime-varying.

Noise in the Photodetector and Associated Preamplifier Circuitry

Shot Noise

Shot noise power is determined from the dc current I_{ph} of the photodetector explicitly formulated above, and two other currents: a dc current due to background light (I_{BK}) and the dc dark current which enters the detector (I_D). If the photodetector has an internal current gain G the total shot noise will be given by

$$2e[(I_{ph})_{\text{coh}} + (I_{ph})_{\text{incoh}} + I_{BK} + I_D]\langle G^2\rangle \qquad \left\{\text{units: } \frac{\text{A}^2}{\text{Hz}}\right\}, \tag{5.8.13}$$

in which e is the electronic charge and $\langle G^2\rangle = \langle G\rangle^2 F(G)$, where $F(G)$ accounts for an additional multiplication (or gain) due to the nonlinear properties of gain development inside the photodetector. The value of $F(G)$ is 0.5 to 3.0, depending on the type of detector used [15].

Thermal Noise

The load resistor R_L of the detector generates Johnson noise W_J when a thermally induced current i_T flows through it:

$$W_J = \langle i_T^2 \rangle R_L.$$

This noise power in a band δf units wide at absolute temperature Θ is

$$W_J = 4k\Theta\delta f \qquad \text{(units: V} \cdot \text{A)}, \tag{5.8.14}$$

where $k = 1.38 \times 10^{-23}$ J/K (Boltzmann's constant). The noise density is thus

$$\frac{\langle i_T^2 \rangle}{\delta f} = \frac{4k\Theta}{R_L} \qquad \left[\text{units: } \frac{\text{A}^2}{\text{Hz}}\right]. \tag{5.8.15}$$

This noise component is additive to the shot noise formulated above.

Laser Jitter Noise

Laser beams have associated with their steady intensity I a corresponding fluctuating intensity δI. This is the laser jitter. It generates in the photodetector a noise current $i_J(t)$. If a data record T seconds long of this current is Fourier analyzed it will have a power spectral density $|I_J(\omega)|^2$ and a power spectral density *factor*, defined here to be the quantity

$$\frac{2\pi}{T}|I_J(\omega)|^2,$$

in which $I_J(\omega)$ (units: A · s) is the Fourier transform $i_T(t)$ over the duration of the finite sampling time. The mean-squared value of $i_J(t)$ is then obtained by integration over the band of frequencies spanned by $I_J(\omega)$ in the power spectral density factor:

$$\langle i_J^2(\Delta\omega) \rangle = \int_{\Delta\omega} \frac{2\pi}{T} |I_J(\omega)|^2 \, d\omega \qquad \text{(units: A}^2\text{)}. \tag{5.8.16}$$

A convenient way of deriving the power spectral density factor is through use of the autocorrelation $Y_J(\tau)$ of $i_J(t)$:

$$\frac{2\pi}{T}|I_J(\omega)|^2 = \frac{1}{2\pi}\int_{-\infty}^{\infty} e^{i\omega\tau} Y(\tau) \, d\tau,$$

where

$$Y(\tau) = \frac{1}{T}\int_T i_J(t) i_J(t+\tau) dt \qquad \text{(units: A}^2\text{)}.$$

Environmental Noise

Assume that the environment generates a random thermal disturbance and a random mechanical disturbance of the fiber. Let one of these disturbances be $\delta\epsilon(\mathbf{r},t)$, meaning it is a spatial and temporal fluctuation of an environmental parameter (temperature or mechanical stress). The power spectral density factor of this random function over finite volume V and finite time T is then defined to be

$$(2\pi)^4 \left| \frac{|E(\mathbf{K},\omega)|^2}{VT},\right.$$

in which the quantity

$$E(\mathbf{K},\omega) = \int_{-\infty}^{\infty} \delta\epsilon(\mathbf{r},\ t)\, e^{i\omega t - i\mathbf{K}\cdot\mathbf{r}}\, \frac{dt}{2\pi}\, \frac{dr}{(2\pi)^3}$$

is the Fourier transform of $\delta\epsilon(\mathbf{r},t)$. The mean-square value of $\delta\epsilon$ over these intervals is

$$<\delta\epsilon^2> = \int_{VT}\int (2\pi)^4 \frac{E(\mathbf{K},\omega)|^2}{VT}\, d^3\,\mathbf{K}\, d\omega. \tag{5.8.17}$$

A convenient way of deriving the power spectral density of $\delta\epsilon$ is through use of the autocorrelation $Y_{\delta\epsilon}(\mathbf{d},\ \tau)$:

$$\frac{1}{(2\pi)^4} \int_{VT}\int\ Y_{\delta\epsilon}(\mathbf{d},\ \tau) e^{i\omega t - i\mathbf{K}\,\mathbf{d}}\, d\tau\, d\mathbf{d} = (2\pi)^4 \frac{|E(\mathbf{K},\ \omega)|^2}{VT},$$

where

$$Y_{\delta\epsilon}(\mathbf{d},\ \tau) \rightarrow \frac{1}{VT}\int_{-\infty}^{\infty} \int\ \delta\epsilon(\mathbf{r},\ t)\delta\epsilon(\mathbf{r}+\mathbf{d},\ t+\tau)\ dt\ d^3\mathbf{d}.$$

The power spectral density per unit of bandwidth can be drived from these formulas by integration over wavenumber:

$$\frac{2\pi}{T}|E(\omega)|^2 = \int_{\mathbf{K}} (2\pi)^3 \frac{|E(\mathbf{K},\omega)|^2}{V} d^3\mathbf{K}. \tag{5.8.18}$$

By a linear conversion factor the units of this parameter can be made $A^2 \cdot s$. In most applications the spatial part of the spectrum is considered essentially one-dimensional. Then the power spectral density factor of $\delta\epsilon\ (x,t)$ becomes

$$\frac{(2\pi)^2|E(\alpha,\omega)|^2}{LT}, \tag{5.8.19}$$

where

$$E(\alpha,\omega) = \int\int\ \delta\epsilon\ (x,t) e^{i\omega t\, i\alpha x} \frac{dt}{2\pi}\, \frac{dx}{2\pi}.$$

The mean-square value of $\delta\epsilon(x,t)$ is obtained from this by integration:

$$<\delta\epsilon^2> = \int_{LT}\int\ (2\pi)^2 \frac{|\tilde{\ }(\alpha,\omega)|^2}{LT} d\alpha\, d\omega. \tag{5.8.20}$$

Also one can form the power spectral density factor per unit of frequency bandwidth,

$$\frac{2\pi}{T}|E(\omega)|^2 = \int_{\Delta\alpha} (2\pi)\ \frac{E(\alpha,\omega)|^2}{L}\ d\alpha. \tag{5.8.21}$$

Again by a linear conversion factor the units of this parameter can be made $A^2 \cdot s$.

In all cases the quantity $\sqrt{<\delta\epsilon^2>}$ is the desired representation of the environmental disturbance, averaged over space and time. The root-mean-square amplitude of fluctuation in the phase of the laser signal beam is then desired to be

$$\Delta\phi_{rms} = A_\epsilon\sqrt{<\delta\epsilon^2>}, \quad A_\epsilon = \text{const.} \tag{5.8.22}$$

However, if the goal of the analysis is to estimate the noise current in the photodetector caused by environmental disturbances, the quantity actually calculated is

$$<i_\epsilon^2> = B_\epsilon <\delta\epsilon^2>, \quad B_\epsilon = \text{const.} \tag{5.8.23}$$

in units of A^2. For purposes of relating environmental noise to other noises described above, it is convenient to represent it in the form of noise per unit bandwidth:

$$\frac{<i_\epsilon^2>}{\delta\omega} = C_\epsilon <\delta\epsilon^2(\omega)>, \quad C_\epsilon = \text{const.} \tag{5.8.24}$$

Noise Sources in the Preamplifier [15]

A preamplifier can be schematically represented as a noiseless generator with gain $A(\omega)$ and input admittance $Y_A = G_A + j\omega C_A$. It has two noise sources, a voltage noise source v_A in series with the input terminals and a current noise source in parallel with the input terminals. The latter consists of a portion i_A which is uncorrelated with the noise voltage source and a second portion which is correlated with this source through an admittance $Y_c = \text{Re } Y_c + J\,\text{Ir } Y_c$. We neglect this second portion. The spectral density of noise from the voltage source is $<v_A^2>/\delta f$ in units of V^2/Hz, and that of the current source is $<i_A^2>/\delta f$ in units of A^2/Hz.

Noise Voltage at the Output of the Preamplifier

The noise currents in the photodetector and preamplifier circuits are additive. Because of different methods of derivation, some of these noise densities are on a unit bandwidth δf basis (in cycles/s), while the remainder are on a unit angular radian $\delta\omega$ basis (in rad/s). It will be convenient to keep them in separate groups. Thus, the noises $N_{\delta f}$ and $N_{\delta\omega}$ are:

On a δf basis: $N_{\delta f}$ = shot noise + amplifier noise + Johnson noise.

On a $\delta\omega$ basis: $N_{\delta\omega}$ = laser jitter noise + environmental temperature noise + environmental mechanical stress noise.

The total noise in units of V^2 at the output of the preamplifier is the sum of two terms:

$$N_{\delta f} = \int_{\Delta f}\Bigg\{2e[(I_{ph})_{coh} + (I_{ph})_{incoh} + I_{BK} + I_D]<G>^2F(G) + \frac{<i_A^2>}{\delta f}$$

$$+ \frac{<v_A^2>}{\delta f}|Y_I + Y_c|^2 + \frac{4kT}{R_L}\Bigg\}\frac{|A(\omega)|^2}{|Y_I + Y_A|^2}\,df \quad \text{(units: } V^2\text{)} \tag{5.8.25}$$

and

$$N_{\delta\omega} = \int_{\Delta\omega}\left[\frac{2\pi}{T}\,|\delta S_J(\omega)|^2 + \frac{2\pi}{T}\int\frac{2\pi}{L}\,|\delta S_{\delta\theta}(\alpha,\omega)|^2 d\alpha + \frac{2\pi}{T}\int\frac{(2\pi)^3|\delta S_M(\mu,\omega)|^2}{V_0}\,d^3\mu\right]$$

$$\times\,\frac{|A(\omega)|^2}{|Y_I + Y_A|^2}\,d\omega \qquad \text{(units: V}^2\text{)}, \tag{5.8.26}$$

where

$|\delta S_J(\omega)|^2$ is the power spectrum of laser jitter (units: $A^2 \cdot s^2$),
$|\delta S_\theta(\alpha,\omega)|^2$ is the power spectrum of random temperature effects (units: $A^2 \cdot m^2 \cdot s^2$),
$|\delta S_M(\mu,\omega)|^2$ is the power spectrum of random mechanical effects (units: $A^2 \cdot m^6 \cdot s^2$),

and

V_0 is the volume of space (units: m^3).

Signal Current and Voltage Sensitivity of the Hydrophone

In the section "Photodetector Current" it was seen that there is a time-varying component of photodetector current, which we call here the *signal*,

$$i_{\text{signal}} \approx 2\alpha|\gamma_{rs}|\sqrt{P_r P_s}\,\sin\,[\alpha_{rs}(\tau) - \Delta\phi_0]\,\Delta\phi_A(t), \tag{5.8.27}$$

where $\Delta\phi_A(t)$ is the phase generated by the acoustic signal, considered to be of small enough magnitude such that $\sin\Delta\phi_A \approx \Delta\phi_A$. An oft-used design feature is to experimentally adjust $\alpha_{rs}(\tau) - \Delta\phi_0$ to be an odd multiple of $\pi/2$. This procedure maximizes the signal. Assume that this is done.

Now assume that $\Delta\phi_A\,(t) = \Delta\Phi_A \sin\omega_s\,t$. Then the rms ac component of photodetector current is

$$(i_{\text{signal}})_{\text{rms}} = 2\alpha|\gamma_{rs}|\sqrt{P_r P_s}(\Delta\Phi_A)_{\text{rms}}. \tag{5.8.28}$$

In the photodetector procedures the signal current appears across the photodetector load resistor R_L, where it develops the signal voltage. Hence the receiving *voltage sensitivity* M for a bare fiber of length L analogous to Eqs. 5.6.4 through 5.6.6, is

$$M \equiv \frac{<(i_{\text{signal}})_{\text{rms}}>R_L}{|p|_{\text{rms}}} = 2\alpha R_L\,|\gamma_{rs}|\sqrt{P_r P_s}\left(\frac{K^{-1}}{3} - \frac{1}{n}\,\frac{\partial n}{\partial p}\right)k_0 nL \quad \text{(units: V} \cdot \text{m}^2 \cdot \text{N}^{-1}\text{)}. \tag{5.8.29}$$

This is the sensitivity without a preamplifier. The effect of the preamplifier is discussed next.

Signal Intensity at the Output of the Preamplifier

In formulating the S/N ratio of the hydrophone we have elected to write both S and N in units of V^2 which appears across the load resistor. As noted earlier the photodetector itself amplifies the current by amount $<G>$. The preamplifier also amplifies the signal by amount $A(\omega)$. Hence the signal at the output of the preamplifier has an *intensity*

$$S = \langle (i_{\text{signal}})_{\text{rms}} \rangle^2 \langle G \rangle^2 \frac{|A(\omega)|^2}{|Y_I + Y_A|^2} \quad \text{(units: V}^2\text{)}, \tag{5.8.30}$$

where Y_I and Y_A are components electrical admittances of the photodetector amplifier circuit. It is to be noted that the signal is single frequency. If the signal has the character of banded noise it can be reported on a per bandwidth basis $\langle i_s^2 \rangle / \delta f$. Then the signal intensity appears in the form

$$S = \int_{\Delta f} \frac{\langle i_s^2 \rangle}{\delta f} \langle G \rangle^2 \frac{|A(\omega)|^2}{|Y_I + Y_A|^2} \, df \quad \text{(units: V}^2\text{)}. \tag{5.8.31}$$

Explicit Form of S/N Ratio of the Fiber-Optic Hydrophone at the Output of the Preamplifier

For the convenience of the reader we repeat here the explicit form of the S/N ratio of a fiber-optic hydrophone for the general case of a banded noise signal:

$$\frac{S}{N} = \frac{\displaystyle\int_{\Delta f} \frac{\langle i_s^2 \rangle}{\delta f} \langle G \rangle^2 \frac{|A(\omega)|^2}{|Y_I + Y_A|^2} \, df}{\displaystyle\int_{\Delta f} \left\{ 2e[(I_{ph})_{\text{coh}} + (I_{ph})_{\text{incoh}} + I_{BK} + I_D] \langle G \rangle^2 F(G) + \frac{\langle i_A^2 \rangle}{\delta f} \right.}$$

$$\left. + \frac{\langle v_A^2 \rangle}{\delta f} |Y_I + Y_c|^2 + \frac{4kT}{R_L} \right\} \frac{|A(\omega)|^2}{|Y_I Y_A|^2} \, df \tag{5.8.32}$$

$$+ \int_{\Delta\omega} \left\{ \frac{2\pi}{T} |\delta S_J(\omega)|^2 + \frac{2\pi}{T} \int \frac{2\pi}{L} |\delta S_{\delta\theta}(\alpha, \omega)|^2 \, d\alpha \right.$$

$$\left. + \frac{2\pi}{T} \int \frac{(2\pi)^3}{V_0} |\delta S_M(\mu, \omega)|^2 d^3\mu \right\} \frac{|A(\omega)|^2}{|Y_I + Y_A|^2} \, d\omega.$$

The effect of environmental noise on the S/N of fiber-optic hydrophones has been theoretically calculated [16]. A bare fiber 0.01 m in length submerged to 30-60 m in the ocean is estimated to have an rms phase fluctuation of 0.29 radians over time periods associated with the temperature microstructure of the ocean. Similarly, a bare fiber 1000 m long towed at a depth of 100 m in the ocean is estimated to have an rms phase fluctuation of approximately 4 radians over time periods associated with internal waves in the ocean.

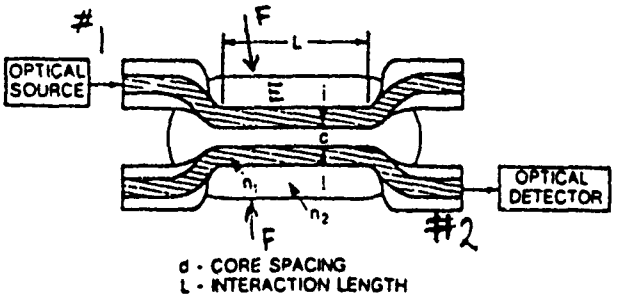
5.9 INTENSITY MODULATED FIBER OPTIC SENSORS

The fiber optic hydrophone described in Section 5.6 is of the *phase modulation* type: pressure fields sensed by the signal arm of the interferometer are read out as phase shift when compared with the reference arm.

Fiber optic sensors can also be constructed on the principle of *intensity modulation.* In this type an incoherent light-source (such as an incandescent lamp) is coupled to the optical fiber and the latter is subjected to mechanical disturbance in such a manner as to modulate the intensity of the transmitted light. The fluctuation of intensity is detected and measured by conventional means.

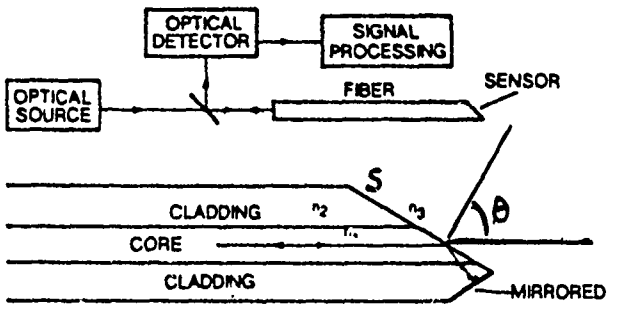
A list of four fiber optic intensity modulated sensors suitable for use as hydrophones is shown in Table 5.9.1

Table 5.9.1 — Intensity Modulated Fiber Optic Sensors [after Ref. 17]. C. M. Davis et al., *Fiber Optics Sensor Technology Handbook* (1982), ©1982 Dynamic Systems; by permission.



I. An evanescent-field intensity-type fiberoptic sensor [after Ref. 17].

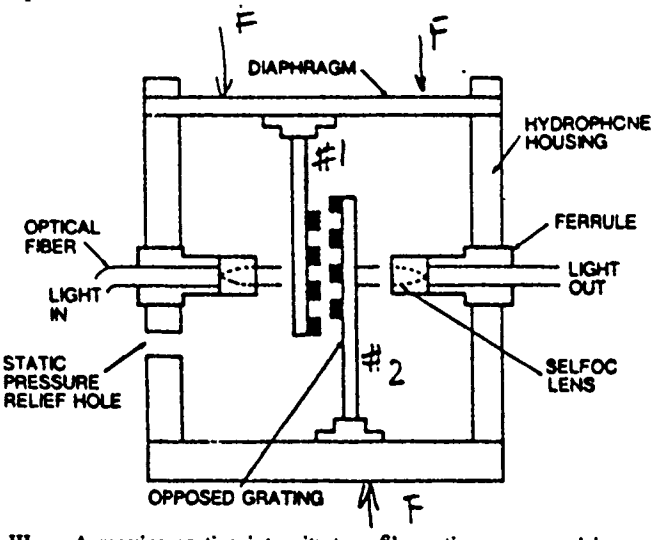
I. Two fibers (index n_1), stripped of jackets, are separated over a length L at a small distance d from each other and embedded in an elastomeric matrix E (index of refraction n_2). When excited by forces F the fibers approach each other, and in doing so the light in fiber #1 couples to fiber #2 through evanescent-field coupling. High coupling is obtained by properly choosing n_1, n_2.



II. A critical-angle intensity-type fiberoptic sensor [after Ref. 17].

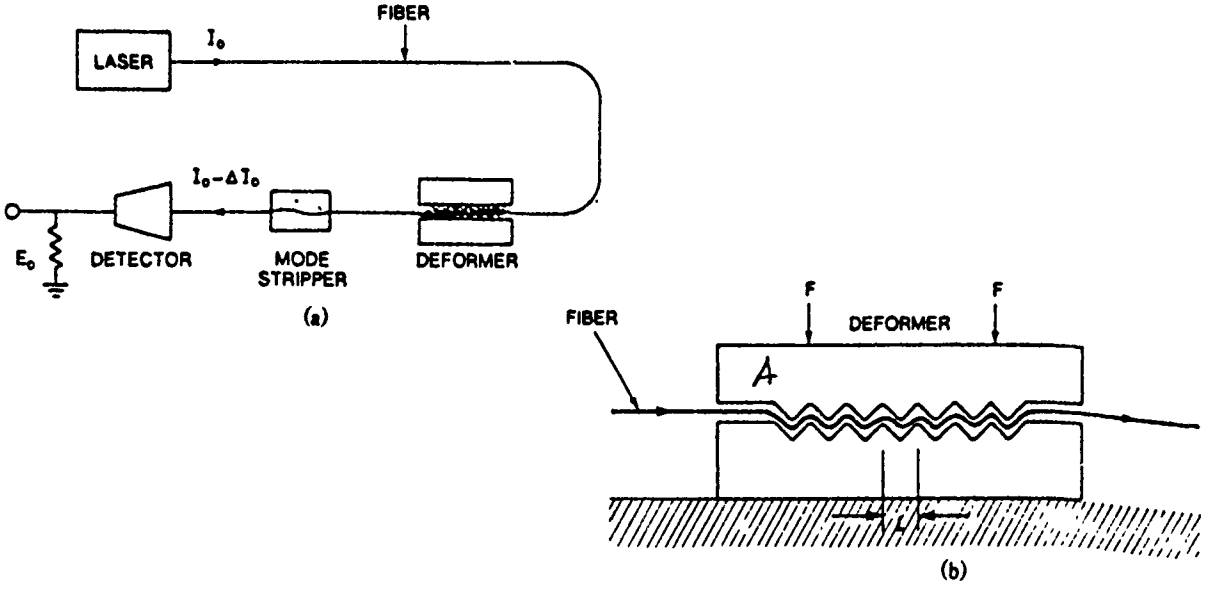
II. Surface S of an optical fiber is lapped at an angle θ (with the core axis) at slightly greater than critical angle. In absence of a pressure field the refractive indices n_1, n_2 and n_3 (in the medium) are such that incoherent light in the core is partially reflected back and partially transmitted into the medium. In the presence of a fluctuating pressure field the index n_3 changes slightly thereby altering the reflective properties of surface S, thus delivering a modulated intensity to the optical detector and signal processor. The effect is amplified by nearness of θ to the critical angle.

Table 5.9.1 (Continued) — Intensity Modulated Fiber Optic Sensors [after Ref. 17]. C. M. Davis et al., *Fiber Optics Sensor Technology Handbook* (1982), ©1982 Dynamic Systems; by permission.



III. A moving grating intensity-type fiberoptic sensor used in a hydrophone [after Ref. 17].

III. Under action of forces F the diaphragm moves optical grating #1 relative to grating #2. The intensity of light coming in from the optical fiber at the left is thereby modulated and the modulated light appears in the optical fiber at the right.



IV. (a,b) A microbend intensity-type fiberoptic sensor system developed by the Hughes Research Laboratories [after Ref. 17].

IV. Deformer A, under action of forces bends the fiber into numerous microbends. The (incoherent) light in the fiber is thereby partially ejected into the material of the deformer, becoming lost in the process. When forces F vanish the fiber recovers its unbent shape. Thus the intensity of light coming in from the left exits at the right in modulated form.

REFERENCE

[1] M. Born, E. Wolf, "Principles of Optics," 5th Ed., Pergamon press, New York, 1975, p. 665.

[2] P.G. Cielo, "Fiber Optic Hydrophone: improved stress configuration and environmental noise protection," Applied Optics **18** (2933), 1979.

[3] "Handbook of Lasers," R.T. Pressley, Ed. (CRC, Cleveland, Ohio, 1971). Section D3 "Electroptic Materials," D.A. Pinnow.

[4] S. Timoshinko, "Theory of Elasticity," McGraw-Hill Book Co. Inc., New York, 1934, p. 56.

[5] Ref. 4, p. 8.

[6] G. B. Hocker, "Fiber optic acoustic sensors with composite structure: an analysis." Applied Optics **18**, 3679 (1979).

[7] G.W. McMahon, P.G. Cielo, Applied Optics **18** (3720) (1979).

[8] J.A. Bucaro et al., Applied Optics **16**, 1761 (1977).

[9] P. Shajenko et al., "On fiber-optic hydrophone sensitivity," J. Acous. Soc. Am. **64**, 1286 (1978).

[10] J.A. Bucaro, E.F. Carome, "Single fiber interferometric acoustic sensor," Applied Optics, Vol. **17**, 330 (1978).

[11] Ref. [1], p. 596.

[12] J.H. Cole et al., "Fiber optic detection of sound," J. Acous. Soc. Am. **62**, 1136 (1977).

[13] P.G. Cielo "Fiber-optic hydrophone: improved strain configuration and environmental noise protection," Applied Optics **18**, 2933 (1979).

[14] Ref. 1, p. 497.

[15] H. Melchior, Jour of Luminescence 7, 390 (1973).

[16] S. Hanish, NRL Report 8424, Jan. 6, 1981, Naval Research Laboratory, Wash. D.C. 20375.

[17] "Fiber optic Sensor Technology Handbook," C.M. Davies et al., Dynamics Systems Inc., 8200 Greensboro Drive, Suite 500, McLean, Va. 22102.

Chapter 6
UNDERWATER LASER DOPPLER HYDROPHONE

6.1 INTRODUCTION

Coherent doppler radar is a highly developed system for detecting the range, bearing and speed of airplanes in flight by use of microwaves transmitted from stationary or moving platforms at considerable distances away. In analogy to this system it has been proposed to develop an underwater doppler system for the detection of acoustic wave fields by use of laser light projected from an underwater platform [1]. The analog of the airplane in this proposal is a volume of colloidal particles naturally occuring in the ocean and the analog of flight is the motion imparted to these particles by the presence of an acoustic field. Just as in doppler radar, the target (= colloidal particles) scatters the incident wave energy, part of which is collected by an optical receiver and analyzed for the presence of acoustic energy.

Several theoretical analyses have been made of the proposed method [1]. We shall begin here with a description of the (usually selected) procedure for detection of the presence of the acoustic signal picked up by the signal arm of an interferometer.

6.2 HOMODYNE AND HETERODYNE SYSTEMS OF DETECTION

A brief note on the use of the terms 'homodyne' and 'heterodyne' detection in optical systems is presented in Sect. 5.8.

Assume first that the laser beam injected into the optical-acoustical system is divided into a signal beam which is modulated by the acoustic field, and a reference beam which is not so modulated. The two beams, superimposed on the surface of a photo detector, can be represented as

$$E = E_S \sin(\omega_l t + \theta_S) + E_R \sin(\omega_l t + \theta_R) \tag{6.2.1}$$

E_S, E_R = amplitudes of signal beam and reference beam respectively

ω_l = optical frequency of the laser

θ_S, θ_R = phase shifts caused by time-varying modulation of the signal beam and reference beam respectively.

It is noted that while θ_S contains acoustic signal and θ_R does not, both θ_S and θ_R contain noise of various origins.

In the photodetector an electric current is developed which is proportional to E^2. Since detection will be based on the beating of signal beam and reference beam it is only the cross-product term in E^2 that is used,

$$i_{SR} = 2 E_S E_R \sin(\omega_l t + \theta_S) \sin(\omega_l t + \theta_R)$$

or

$$i_{SR} = 2 E_S E_R \left\{ \frac{1}{2} \cos(\theta_S - \theta_R) - \frac{1}{2} \cos(2\omega_l t + \theta_S + \theta_R) \right\}. \tag{6.2.2}$$

The optical term (containing ω_l) is discarded by the detector, leaving the quantity

$$i_{SR} = E_S E_R \{\cos\theta_S \cos\theta_R + \sin\theta_S \sin\theta_R\}. \tag{6.2.3}$$

Now θ_S is taken to be periodic functions of time, and so it can be expanded in a Fourier series,

$$\theta_S(t) = \sum_n m_l \sin n\,\theta_0(t), \quad \theta(t) = \omega_0 t. \tag{6.2.4}$$

Considering only the first component one can make the additional expansions,

$$\cos\theta_S = \cos(m_1 \sin\theta_0) = J_0(m_1) + 2\sum_{p=0}^{\infty} J_{2p}(m_1)\cos(2p\theta_0)$$

$$\sin\theta_S = \sin(m_1 \sin\theta_0) = 2\sum_{p=0}^{\infty} J_{2p+1}(m_1)\sin[(2p+1)\theta_0]. \tag{6.2.5}$$

Substitution of these forms into Eq. 6.2.3 and recombination into sum and difference terms lead to the expansion,

$$\begin{aligned} i_{SR} = E_S E_R \{&J_0(m_1)\cos\theta_R + J_1(m_1)[\cos(\theta_R - \theta_0) - \cos(\theta_R + \theta_0)] \\ &+ J_2(m_1)[\cos(\theta_R - \theta_0) + \cos(\theta_R + 2\theta_0)] \\ &+ \ldots.\}. \end{aligned} \tag{6.2.6}$$

Since the acoustic fields in question are quite small we require, for the application in mind, that the phase shifts due to these fields be also very small, that is,

$$m_1 \ll 1.$$

Thus, in reasonable approximation,

$$\begin{aligned} &J_0(m_1) \simeq 1 \\ &J_1(m_1) \simeq \frac{m_1}{2} \\ &J_2(m_1) \to 0, \text{ etc.} \end{aligned} \tag{6.2.7}$$

The signal current resulting from heterodyning is therefore

$$i_{SR} \simeq E_S E_R \left\{\cos\theta_R + \frac{m_1}{2}[\cos(\theta_R - \theta_0) - \cos(\theta_R + \theta_0)]\right\}. \tag{6.2.8}$$

In this expression the phases θ_R, θ_0 are functions of time. θ_R can be chosen at will. A simple procedure, which will be explained in detail in a later section, rests on letting θ_R be the phase at an *offset* frequency $\theta_R = \omega_R t$ resulting from passing the laser beam through a Bragg modulator. The phase $\theta_0(t)$ can, for illustrative purposes, be taken as that of a simple harmonic oscillation, $\theta_0 = \omega_0 t$. Thus,

$$i_{SR} \simeq E_S E_R \left\{ \cos \omega_R t + \frac{m_1}{2} [\cos(\omega_R - \omega_0) t - \cos(\omega_R + \omega_0) t] \right\}. \tag{6.2.9}$$

A spectral representation of i_{SR} is shown in Fig. 6.2.1. One concludes that the method of detection consisting in beating an acoustically modulated laser beam against a reference beam, yields the acoustic component by simple spectrum analysis.

The formulation leading to Eq. 6.2.9 can be considered an example of 2-beam Young interference in which path differences explicitly appear, Fig. 6.2.2. Here, relative to a reference distance AB a beam issuing from source S_1 undergoes a negative path difference change of amount Δr_2, and a beam issuing from source S_2 undergoes a positive path difference change of amount Δr_1. For very small angles ϕ the assumption is made that $\Delta r_2 = \Delta r_1 = \Delta r/2$, where Δr is the total change in path difference. The phases associated with these changes are those of spherical waves diverging from these sources. Assuming that the amplitudes E_S and E_R are equal to a reasonable approximation, one finds that the net phase change is

$$\exp ik\frac{\Delta r}{2} + \exp -ik\frac{\Delta r}{2} = 2\cos\left(\frac{k\Delta r}{2}\right) = 2\cos\left(\frac{\pi}{\lambda}\Delta r\right).$$

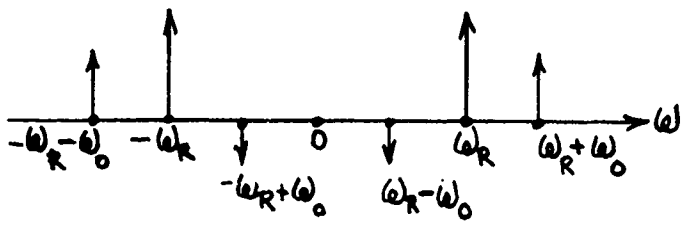


Fig. 6.2.1 — A spectral representation of Eq. 6.2.9

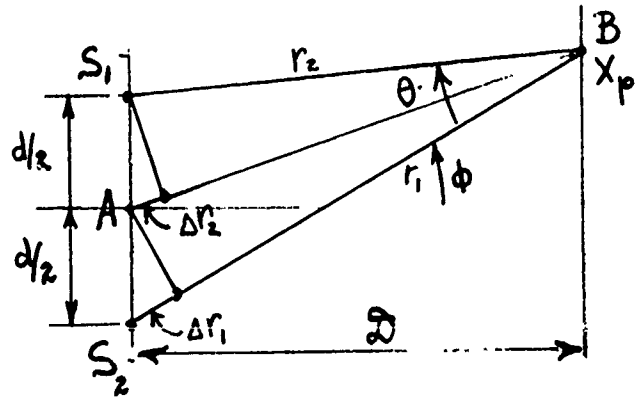


Fig. 6.2.2 — A two-beam interference experiment

Now from geometrical considerations,

$$\frac{\Delta r}{d} = \frac{X_p}{\mathscr{D}}$$

so that the phase term becomes

$$2 \cos\left[\frac{\pi}{\lambda} \frac{d}{\mathscr{D}} X_p\right].$$

Since the detector current is poportional to the square of this term,

$$i_{SR} \propto 4 \cos^2 \beta = 2(2 \cos^2 \beta) = 2[1 + \cos 2\beta]$$

$$= 2\left[1 + \cos\left[\frac{2\pi}{\lambda} \frac{d}{\mathscr{D}} X_p\right]\right].$$

It is illuminating to express this equation in terms of the angle θ between the two beams pictured in Fig. 6.2.2. From geometrical considerations, with the restriction that X_p is quite small relative to D one has,

$$\tan \frac{\theta}{2} \simeq \sin \frac{\theta}{2} = \frac{d}{2\mathscr{D}}.$$

Thus,

$$i_{SR} \propto 2\left[1 + \cos\left[\frac{4\pi}{\lambda} X_p \sin \frac{\theta}{2}\right]\right]. \tag{6.2.10}$$

Another formulation, which is applicable to heterodyne detection, begins with the superposition of two complex phasor electric fields,

$$\mathbf{E} = |\mathbf{E}_1| e^{j\phi_1} + |\mathbf{E}_2| e^{+j\phi_2}.$$

The intensity of light is proportional to E^2,

$$E^2 = E_1^2 + E_2^2 + 2|E_1||E_2| \cos(\phi_2 - \phi_1). \tag{6.2.11}$$

Assume the optical frequency of the signal beam is offset (by Bragg modulation) to an IF frequency ω_0, and assume further that the signal beam is modulated by a time harmonic acoustic signal which induces a phase change over a path length X_S of amount,

$$\Delta\phi_S = KX_S \cos \omega_S t.$$

Finally, let there also be a random noise phase $\Delta\phi_N$. The total phase change between signal beam and reference beam is then,

$$\phi_2 - \phi_1 = \omega_0 t + KX_S \cos \omega_S t + \Delta\phi_N. \tag{6.2.12}$$

From Eq. 6.2.10 it is seen that the proper interpretation of K is,

$$K \equiv \frac{4\pi}{\lambda} \sin \frac{\vartheta}{2}. \tag{6.2.13}$$

A discussion of noise modulation will be postponed to a later section. Expanding $\cos(\phi_2 - \phi_1)$ by use of formulas similar to Eq. 6.2.5 one has

$$\cos(\omega_0 t + KX_S \cos \omega_S t) = J_0(KX_S) \cos \omega_0 t + \sum_{n=1}^{\infty} J_n(KX_S) \cos [(\omega_0 + n\omega_S)t] \tag{6.2.14}$$

$$+ \sum_{n=1}^{\infty} J_n(KX_S) \cos ((\omega - n\omega_S)t).$$

Detection will be made by measurement of the electric current in the photodetector due to one sideband ($n = 1$ above). Anticipating again that the signal modulation will be very small we use the approximations given by Eq. 6.2.7, and the value of K for backscatter ($\theta = \pi$) given by Eq. 6.2.13. The current in the sideband caused by acoustic modulation is then,

$$i_{\text{sideband}} \cong \sqrt{2(I_S)_{rms}(I_{ref})_{rms}} \left[\frac{2\pi X_S}{\lambda}\right]. \tag{6.2.15}$$

Here $(I_S)_{rms}$, $(I_{ref})_{rms}$ are the currents due to the input signal and reference beams respectively.

6.3 PREDICTION OF THE LOWEST LEVEL ACOUSTIC SIGNALS THAT CAN BE DETECTED

Let the procedure for detection of an underwater laser Doppler hydrophone be based on measurement of the sideband current i_{SB} given by Eq. 6.2.15. The lowest level current to be measured is the noise current in the photodetector caused by noise modulation $\Delta\phi_N$. Sources of this noise are optical, electronic and acoustic. To establish a lower bound we select noise due to the 'shot effect' of photons impinging on the surface of the photodetector. For a photodetector circuit bandwidth $B(Hz)$, an electronic charge e (Coulombs) and signal plus reference currents $(I_s)_{rms}$, $(I_{\text{Ref}})_{rms}$, the *rms* noise current is

$$i_N = \{2e[(I_s)_{rms} + (I_{\text{Ref}})_{rms}]\, B\}^{1/2} \tag{6.3.1}$$

[2]. Assuming a laser power P_0 (watts), quantum efficiency η, and setting signal and reference currents equal one finds that

$$I_s = I_{\text{ref}} = \frac{\lambda_E \eta e P_0}{2hc_E} \quad \text{(units: } C/s\text{)} \tag{6.3.2}$$

in which h is Planck's constant, and c_E is the speed of light. The noise current is then,

$$i_N = e\{2\left(\frac{\lambda_E \eta}{hc_E}\right) P_0 B\}^{1/2}. \tag{6.3.3}$$

To estimate this current we use the following values of parameters:

$$\lambda_E = 5.145 \times 10^{-7} m, \quad h = 6.6 \times 10^{-34} \text{ joule sec}; \quad e = 1.6 \times 10^{-19} C \qquad (6.3.4)$$
$$\eta = 0.05; \quad c_E = 3 \times 10^8 \ m/s$$

Then,

$$i_N = 1.6 \times 10^{-19} \left\{ \frac{2 \times 5.145 \times 10^{-7} \times 0.05}{6.6 \times 10^{-34} \times 3 \times 10^8} P_0 B \right\}^{1/2}$$

$$i_N = 8.16 \times 10^{-11} (P_0 B)^{1/2} \quad \text{(units: } C/s\text{)}.$$

In a similar way, by use of Eq. 6.3.2 one arrives at an expression for the sideband current,

$$i_{sB} = \pi \sqrt{2} \frac{\eta e P_0}{h c_E}. \qquad (6.3.5)$$

A lower limit $(X_s)_{\min}$ on the amplitude of displacement X_s that can be detected in the presence of photon noise is obtained by setting $i_{sB} = i_N$:

$$(X_s)_{\min} = \left(\frac{\lambda_E h c_E B}{\pi^2 \eta P_0} \right)^{1/2} \quad \text{(units: } m\text{)} \qquad (6.3.6)$$

Using the numerical values cited above we arrive at the estimate,

$$(X_s)_{\min} = 4.6 \times 10^{-16} \sqrt{\frac{B}{P_0}} \quad \text{(units: m)}.$$

The choice of bandwidth (of processing) and laser power P_0 depend on the implementation of the detection process. In a laboratory experiment, to be described in greater detail in Section 6.4, the choice is made,

$$B = 20 \text{ kHz}; \ P_0 = 10^{-3} \text{ watt}.$$

The minimum detectable signal amplitude under the conditions of heterodyne detection discussed here as limited by photon noise and with choice of constants already cited is,

$$(X_s)_{\min} = 4.6 \times 10^{-16} \sqrt{\frac{20 \times 10^3}{10^{-3}}} \simeq 2.1 \times 10^{-12} \ m = 2.1 \times 10^{-2} \ A^0.$$

It is important to note that P_0 is the light power reaching the surface of the photodetector. Thus in application to detection of an acoustic signal located at a distance away it is required to account for the attenuation of the initial (= injection) laser power in going to, and coming from, the scattering volume. In media of great attenuation, such as sea water, this correction may be very substantial.

6.4 DESCRIPTION OF A LABORATORY EXPERIMENT IN THE DETECTION OF UNDERWATER ACOUSTIC SIGNALS BY USE OF A LASER HETERODYNE DETECTOR

An experimental optical-acoustical-electronic set up [3] designed for use with laboratory equipment is shown in Fig. 6.4.1. A laser (1) operating TEM_{∞} single line, single mode, generates a stable output of some 450-500 milliwatts peak power. The intensity of light in the beam cross-section varies

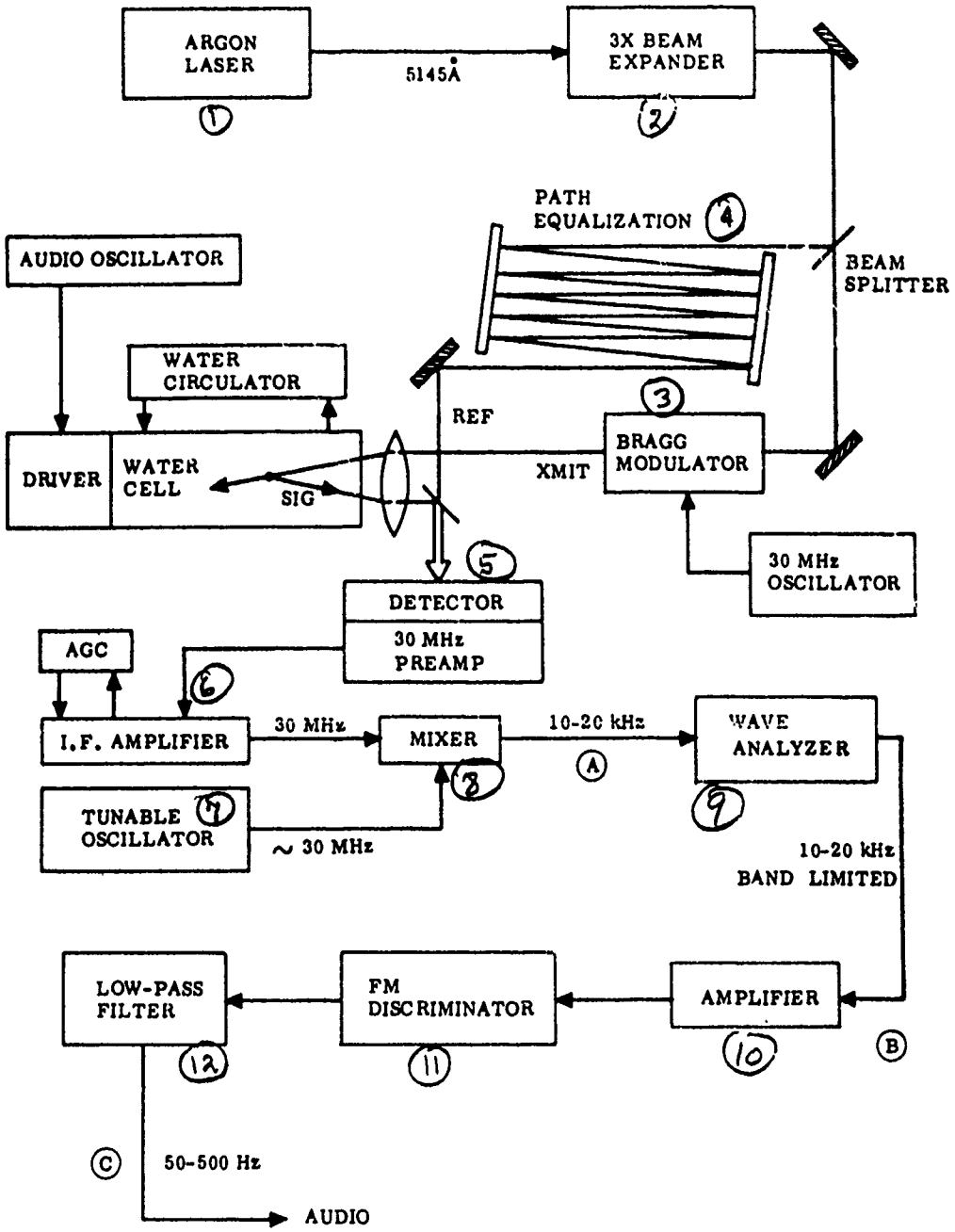


Fig. 6.4.1 — Block diagram of an experimental set-up in a laboratory water tank for detecting acoustic signals by use of a laser heterodyne system [3]

as a Gaussian curve, and is 0.40 mm in diameter at the exp (−1/2) points. In air, at the laser frequency, the wavelength is $\lambda_E = 5.145 \times 10^{-7}$ meter while in water it is 3.860×10^{-7} meter.

The laser beam is expanded by a beam expander (2) to 1.20 mm between ±1 standard deviation distances on the curve of intensity distribution in the cross-section. The divergence of the beam is simultaneously reduced to a total angle of 0.083 milliradians.

After expansion the beam is split into two equal parts. One part goes into a Bragg modulator (3) which offsets the laser frequency by an amount equal to the Bragg frequency (30 MHz in this experiment). The output beam of this modulator is the signal beam. It goes directly into converging lens which focuses it on to the test-volume in the water. The other part from the beam splitter goes into a path equalizer (4) which corrects for the phase delay caused by the Bragg modulator, and then issues as the reference beam of the heterodyne system.

The signal beam modified by the acoustic signal is scattered back from the (water) volume of interrogation and is brought to a focus on the surface of the photodetector (5) where it is superimposed on the reference beam. The current developed by the photodetector is proportional to E^2, Eq. 6.2.11 and therefore contains a term showing the acoustic modulation, Eq. 6.2.12. In the process the photodetector subtracts out the optical frequencies, leaving the Bragg (IF) offset frequency together with all sidebands. This modulation-carrying current is amplified by an IF amplifier (6) with automatic gain control (AGC) to prevent drift. The amplified signal is combined with the output of a tuneable oscillator (7) in a mixer (8) which demodulates the IF signal leaving all modulation components as output. This output of the mixer is next put through a bank of bandpass filters (or wave analyzer (9)) and the results are amplified (10). Since the frequency count is of primary interest and the waveform is of secondary interest the amplified signal is then put through a frequency discriminator (11) which hard-limits the signal amplitude and generates a pulse of fixed length and amplitude for every positive zero crossing. This train of voltage pulses is then averaged over time by use of a filter (12), which delivers an output voltage proportional to the instantaneous frequency of the signal. To help in alignment of the optical instrumentation the 30 MHz signal out of the preamplifier of the photodetector (5) is monitored by a communications receiver which is designed to give an audio output.

In actual experiment the data from points A, B, C in Fig. 6.4.1 are analyzed in a high-resolution spectrum analyzer and displayed on an oscilloscope.

6.5 DETECTION OF ACOUSTIC FIELDS IN WATER BY USE OF A LASER HETERODYNE DETECTOR-EXPERIMENTAL RESULTS

Numerous experiments using the apparatus described in Fig. 6.4.1 are reported in Ref. [1]. They show that acoustic signals of a prescribed level and frequency are detectable. To judge the potential of this achievement one must compare the levels used in the laboratory tank to levels of acoustic noise in the ocean. We take here as reference level the ambient noise in the ocean at Knudsen sea-state 1, excluding shipping noise, measured in units of plane wave equivalent in a 1 Hz band at 100 Hz. Table 6.5.1 summarizes various descriptors of the reference level adopted here.

Table 6.5.1 — Noise Levels at Sea State 1

100 Hz	Plane Wave Equivalent in a 1 Hz Band
Spectrum pressure level	−70 dB re/N/m^2
Particle Velocity	2.13×10^{-10} m/s
Particle Displacement	3.4×10^{-13} m

In the experiments noted above the acoustic transducer source in the tank was driven at a frequency of 200 Hz with a drive level adjusted to make the first order sideband equal in amplitude to the zero-order term. This corresponded to a *modulation index* m_{ID} of 1.435 radians. From Eqs. 6.2.2, 6.2.3, by definition,

$$m_{ID} = Kx_s = \frac{4\pi}{\lambda_E} x_s. \qquad (6.6.1')$$

Thus,

$$x_s = \frac{1.435 \times 5.145 \times 10^{-7}}{4\pi} = 5.88 \times 10^{-8} \quad \text{(units: m)}.$$

This particle displacement is about 5 orders of magnitude greater than the reference (sea noise) particle displacement.

The zero-order, or carrier, term corresponds to a steady Doppler shift of 12 kHz due to a deliberately inserted constant flow of tank fluid of amount 6.3 mm/sec.

During the experiment the signal at the output of the mixer (point A of Fig. 6.4.1) was spectrum analyzed in 500 adjacent frequency cells centered at 12 kHz. The average of 64 spectra with no acoustic signal present is shown in Fig. 6.5.1. The bandwidth at the −3 dB points is about 100 Hz. When the acoustic signal of 200 Hz was turned on, at the level indicated above, the spectra measured again at point A of Fig. 6.4.1 showed sidebands. An average of 64 such spectra is shown in Fig. 6.5.2. The effectiveness of the discriminator and filter in measuring the sideband frequency is shown in Fig. 6.5.3, the data being taken at point C.

It is concluded from these tests that laser doppler detection of sound is demonstrated, but at signal levels several orders of magnitude above noise at sea state #1.

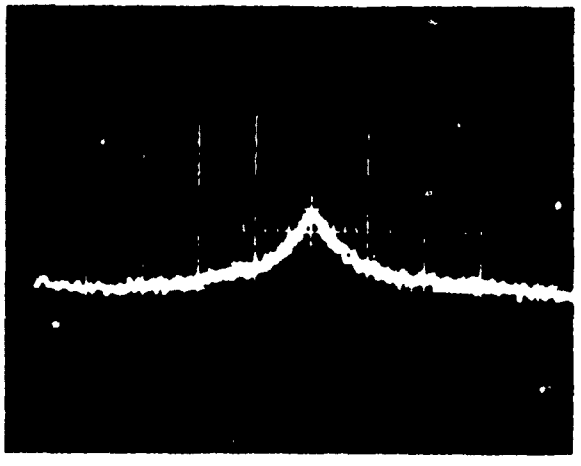


Fig. 6.5.1 — Average of 64 spectra from point A in Fig. 6.4.1 Water velocity 6.3 mm/s. Frequency range 11-13 kHz, with scale of 200 Hz/cm. Vertical scale 10 dB/cm. No acoustic signal. [1]

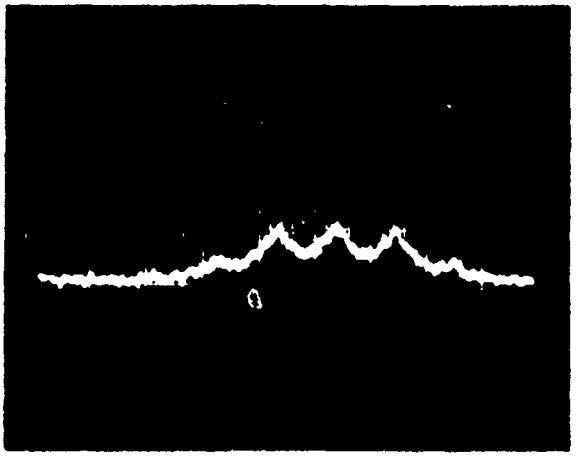


Fig. 6.5.2 — Average of 64 spectra taken from point A in Fig. 6.4.1 with 200 Hz acoustic drive. All other conditions same as in Fig. 6.5.1. [1]

6.6 DESIGN CONSIDERATIONS FOR A REMOTE-SENSING LASER HETERODYNE HYDROPHONE

In the previous section it was shown by experiment in the laboratory that an acoustic field can be detected in a fluid medium by a device based upon the principle of the coherent Doppler radar. To use the same principle to detect acoustic fields in the ocean by remote sensing requires consideration of many factors. These are discussed in the following sections.

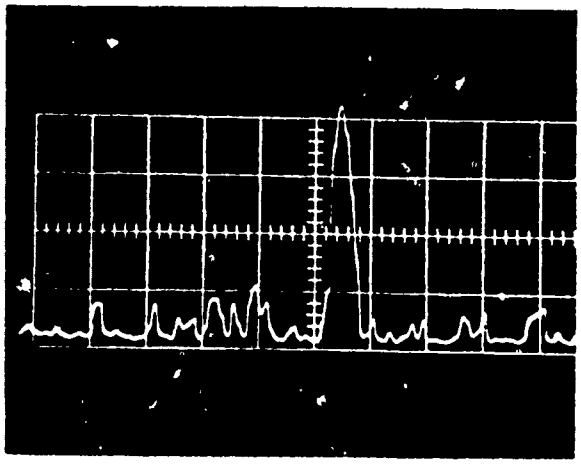


Fig. 6.5.3 — Spectrum of demodulated acoustic signal taken from point *C* in Fig. 6.4.1. Frequency range 195 – 205 Hz, with 5X magnification (0.2 Hz/cm). Vertical scale 5 dB/cm. [3]

Calculation of Back-Scattered Light

A laser beam, Fig. 6.6.1 of intensity I_0, is emitted into the ocean, travels a distance R_1 where it strikes a volume $dV = A_s l$, from which it is scattered in a conical beam to a receiver of area A_R at distance R_2. For a medium whose attenuation coefficient is α (units: m^{-1}) the intensity of light reaching the scattering volume is,

$$I_1 = I_0 e^{-\alpha R_1}. \tag{6.6.1}$$

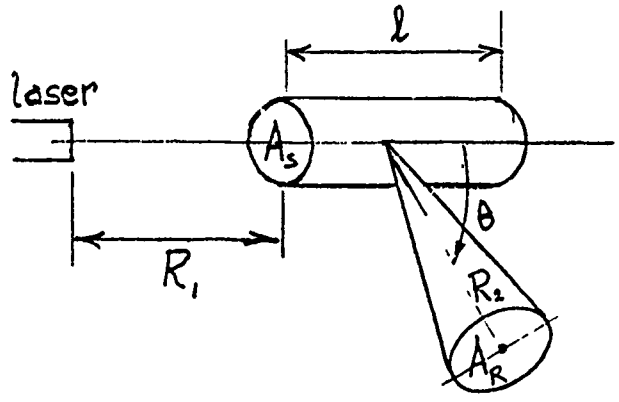


Fig. 6.6.1 — Geometric relations in the scattering of laser light by a unit volume of fluid

The scattering process itself is defined by a scattering coefficient β,

$$\beta = \frac{\text{light power scattered into solid angle } \theta}{\text{incident intensity} \times \text{volume of scattering} \times \text{solid angle}}$$

[units: m^{-1} (solid angle)$^{-1}$]. (6.6.2)

Thus the power scattered into sold angle θ is

$$P_R = \beta(\theta) \times I_1 \times e^{-\alpha R_2} \times A_s l \times \frac{A_R}{R_2^2}$$

or

$$P_R = P_0 e^{-\alpha(R_1+R_2)}\,\beta(\theta)\, l\, \frac{A_R}{R_2^2}. \tag{6.6.3}$$

The coefficients α, β are empirical. α itself depends on the wavelength of light and upon the concentration of ocean salts and particulate matter. Duntley [5] cites a value of $\alpha = 0.05$ for average sea water in the visible part of the spectrum. Similarly, for backscattering ($\theta = \pi$) he cites a value of $\beta(180°) = 6 \times 10^{-4}$. The length l of the scattering volume is set by the range gate length. For purposes of estimation this may be taken to be 1/2 acoustic wavelength at 1 kHz (= 0.750 m). The receiving area A_R is that of a converging lens. Again, for purposes of estimation this is assumed to have a diameter of 1/10 meter.

Assembling all values selected, one finds the ratio of backscattered light to laser power to be,

$$\frac{P_R}{P} = e^{-0.1R} \times 6 \times 10^{-4} \times 7.5 \times 10^{-1} \times \frac{\pi(0.1)^2}{4} \times \frac{1}{R^2} = 3.5 \times 10^{-6}\,\frac{e^{-0.1R}}{R^2}.$$

Estimates of this ratio at various ranges R are tabulated below:

Table 6.6.1

R (m)	R_R/P_0
1	3.2×10^{-6}
5	2.3×10^{-7}
10	1.28×10^{-8}
20	1.18×10^{-9}
30	1.94×10^{-10}

For other choices of laser wavelength the value of α may be obtained from Fig. 6.6.2. Similarly, for other values of scattering angle β the value of $\beta(\theta)$ may be obtained from Fig. 6.6.3.

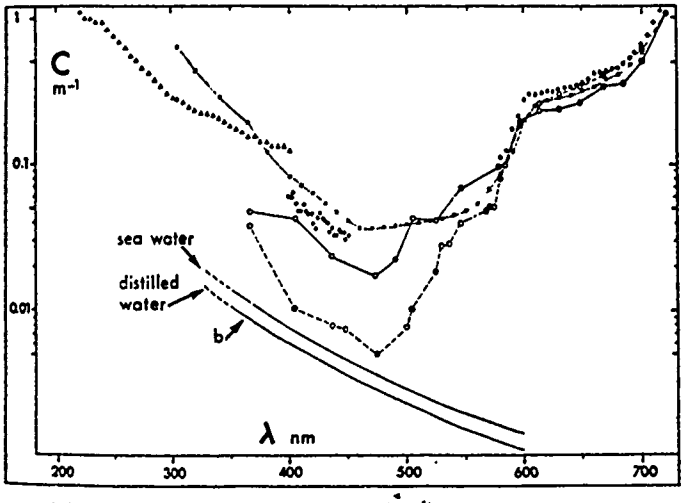


Fig. 6.6.2 — Total attentuation curves $C(m^{-1})$ in near ultraviolet and in visible part of the spectrum. Curves b are the scattering coefficients. The difference c-b is the absorption coefficient a. [after 14]

▲ Lenoble-Saint Guily (1955), path length: 400 cm;
× · · Hulburt (1934) (1945), path length: 364 cm;
● Sullivan (1963), path length: 132 cm;
○— Clarke-James (1939), path length: 97 cm (Ceresin lined tube);
○ · · · James-Birge (1938), path length: 97 cm (Silver lined tube).

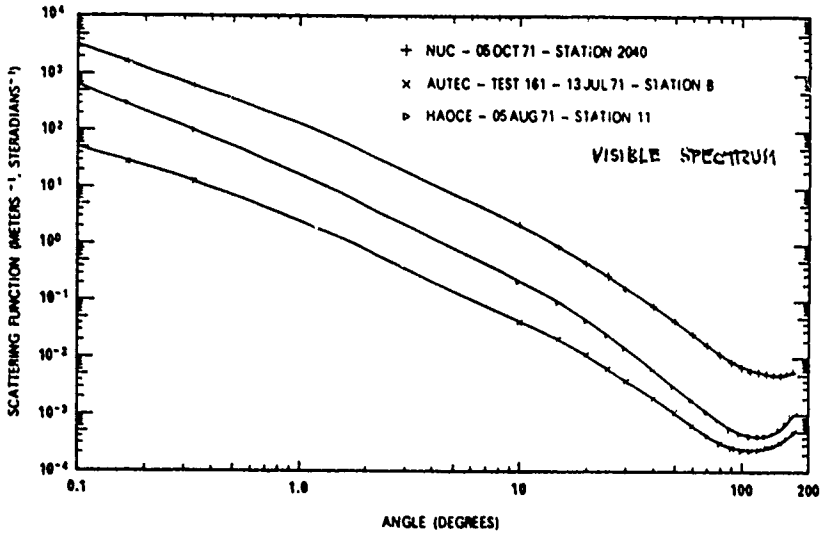


Fig. 6.6.3 — Volume-scattering function $\beta(\theta)$ (meters^{-1} steradians^{-1}) versus scattering angle θ (degrees) for three optically different water masses. AUTEC (x) = data from deep, clear ocean water of Tongue of the Ocean, Bahama Islands (24°29'N, 77°33'W); HAOCE (>) = data from moderately productive Southern California coastal water (33°30.0'N, 118°23'W); NUC (+) = data from turbid San Diego harbor water (32°42'N, 117°14'W). The symbols (x, >, +) are data points obtained from the two scattering instruments at the Visibility Laboratory. The solid curves are computer plots of $\beta(\theta)$, calculated from the raw data [*Petzold*, 1972]. Ref. "Suspended Solids In Water," R.J. Gibbs, ed., Plenum Press, p. 68.

Signal/Noise Ratio in Photon Noise Limit

According to Eq. 6.2.11 the squared electric field contains two *dc* terms and an alternating term. Dividing both sides by the characteristic impedance Z_0 of free space gives the optical intensity I (units: watts/m^2). Thus, in the absence of an acoustic signal one has,

$$I_{TOT} = I_1^2 + I_2^2 + 2\sqrt{I_1 I_2}\cos 2\pi f_0 t$$

in which f_0 is the Bragg offset frequency. We identify I_1 with the reference intensity I_{ref} and I_2 with the received signal intensity I_{sig}. Multiplying intensity by photodetector area gives the optical power. Thus

$$P_{TOT} = P_{ref} + P_{sig} + 2\sqrt{P_{ref} P_{sig}}\cos 2\pi f_0 t. \tag{6.6.4}$$

The electric current in the photodetector generated by this optical power is calculated according to the following (verbal) equations:

current i = unit charge e × number of electrons N
N = quantum efficiency η × number of photons per sec n
n = optical power P divided by energy for photon w
w = Planck's constant h × frequency of laser f
f = speed of light in a vacuum c_E divided by the laser wavelength λ_E.

Thus,

$$i = \frac{e\eta P\lambda_E}{hc_e}. \tag{6.6.5}$$

The total photodetector current is then

$$i_{TOT} = \left(\frac{e\eta\,\lambda_E}{hc_E}\right)[P_{ref} + P_{sig} + 2\sqrt{P_{ref}\,P_{sig}}\cos 2\pi f_0 t]. \tag{6.6.6}$$

Because of the quantum nature of photon-electron interaction the above total current in the photodetector is a mean (= average) value. It is accompanied by a random fluctuation which gives rise to a noise signal (= photon noise). The rms photon noise current i_N associated with the optically induced current i is measureable only over some bandwidth B. Its value is

$$i_N^2 = 2(eB)\,i_{TOT}. \tag{6.6.7}$$

In order to obtain the maximum detectability the reference power is increased until the photon noise due to it exceeds all other noises in the system. Thus, one uses only the P_{ref} term in Eq. 6.6.6. To find the photon noise power one then multiplies i_N^2 by the load resistor R of the photodetector:

$$p_{noise} = 2(eB)\left(\frac{e\eta\lambda_E}{hc_E}\right)P_{ref}\,R. \tag{6.6.8}$$

The rms ac power in the photodetector is

$$p_{sig} = (i_{TOT}^2)_{ac}R = \frac{1}{2}\left(\frac{e\eta\lambda_E}{hc_E}\right)^2\left(2\sqrt{P_{ref}\,P_{sig}}\right)^2 R \tag{6.6.9}$$

$$p_{sig} = (i_{TOT}^2)_{ac}R = \left(\frac{e\eta\lambda_E}{hc_E}\right)^2 2\,P_{ref}\,P_{sig}\,R.$$

Thus in the absence of an acoustic signal,

$$\frac{p_{sig}}{p_{noise}} = \frac{\eta\lambda_E}{hC_EB}\,P_{sig}. \tag{6.6.10}$$

When an acoustic signal modulates the signal beam the modulation amplitude is given by Eq. 6.5.1. For very small acoustic signals the ratio of the power in the sum of the *two* 1st sidebands to the power in the carrier is

$$\frac{p_a}{p_{sig}} = \left[\frac{2J_1(Kx_s)}{J_0(Kx_s)}\right]^2 \cong \left(\frac{4\pi x_s}{\lambda_E}\right)^2. \tag{6.6.11a}$$

Thus the ratio of the power in the acoustic signal to the photon noise power is

$$\frac{p_a}{p_{noise}} = \left(\frac{\eta\lambda_E P_{sig}}{hc_E B}\right)\left(\frac{4\pi x_s}{\lambda_E}\right)^2. \tag{6.6.11b}$$

Because the sum of *two* sidebands is used here this formula gives

$$(x_s)_{\min} = \frac{1}{4\pi}\left[\frac{hc_E\lambda_E B}{\eta P_{\text{sig}}}\right]^{1/2} \quad \text{(units: m)} \tag{6.6.12}$$

for $p_a/p_{noise} = 1$. This is the threshold of detection. The displacement x_s is related to the acoustic power density W(units: watt/m^2 × Hz). In a medium of density ρ_m and speed of sound c_m one has,

$$W = \frac{\rho_m c_m (2\pi f_s x_x)^2}{2B}. \tag{6.6.13}$$

Substitution into Eq. 6.6.11b then gives the ratio of acoustic power to photon noise power,

$$\frac{p_a}{p_{\text{noise}}} = \frac{8\eta W P_{SIG}}{\lambda_E h c_E \rho_m c_m f_s^2}. \tag{6.6.14}$$

Since the signal power P_{SIG} is the same as the received power P_R of Eq. 6.6.3, it is seen that the threshold equivalent noise pressure is given by

$$(a)\ (W)_{\text{threshold}} = \frac{\lambda_E h c_E \rho_m c_m f_s^2}{8\eta H \beta(\theta)}$$

$$(b)\ H = P_0 e^{-\alpha(R_1+R_2)} I \frac{A_R}{R_2^2}. \tag{6.6.15}$$

Another expression for H involving the focusing properties of the converging lens of Fig. 6.4.1 is derived in Ref. [6]. It is based on symbols d, D sketched in Fig. 6.6.4:

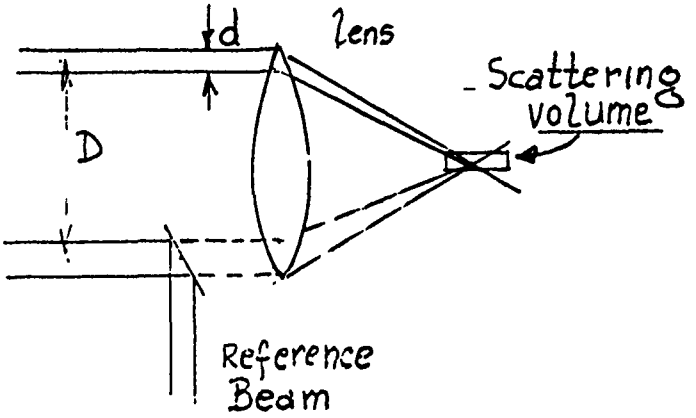


Fig. 6.6.4 — Definition of d, D

$$H = \left[\frac{d}{D+d}\right]^3 \frac{\pi}{2}\lambda_E. \tag{6.6.16}$$

A plot of threshold equivalent noise pressure for the choices,

$$\beta(180°) = 5 \times 10^{-4}(\text{m}^{-1})$$

$$d = D$$

is shown in Fig. 6.6.5. It reveals that at frequencies above (say) 100 Hz photon noise exceeds sea-state zero noise even for such laser power input as $\eta P_0 = 1$ watt.

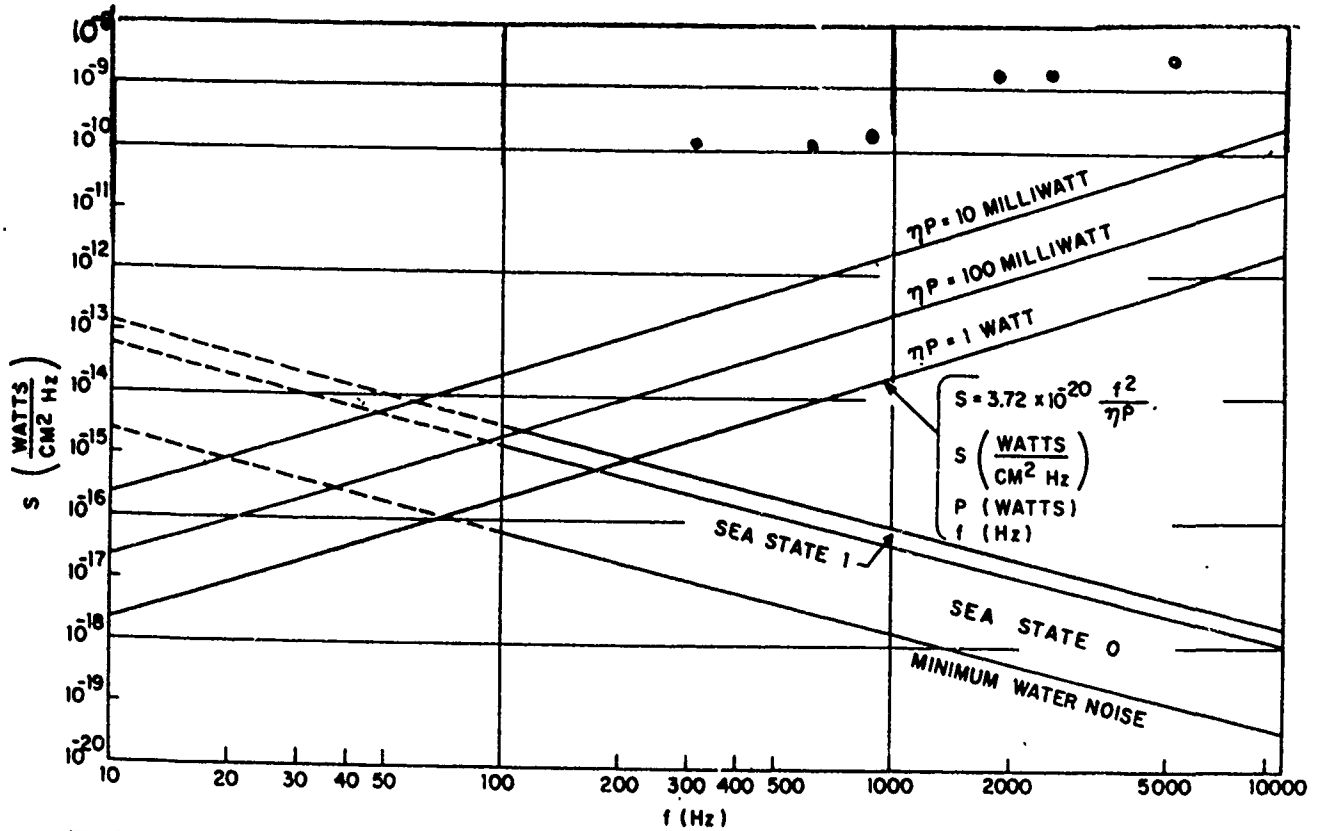


Fig. 6.6.5 — Comparison of threshold of detectability with see states versus frequency. The circled dots represent experimental based on the optical set-up of Fig. 6.4.1. [1]

Particle Size, Particle Density, Mie Scattering Cross Section

Suspended material in the ocean which is retained by a 45 micron filter is called *particulate matter.* The amount of particulate matter (in milligrams per liter) ranges from 0.04 in the surface water of the North Atlantic to 18 in the region of coastal waters. An average oceanic total is 0.8 to 2.5 (Table 6.6.2).

A statistical analysis of particle size distribution in various ocean bases leads to a statement that the mean squared particle radius is about $14 \times 10^{-12} m^2$, so that the "mean particle diameter" is about 7 microns. According to Mie theory the scattering cross-section of a single sphere (M_s) which is much larger than an optical wavelength is twice the geometric cross section. Hence $M_s = 2\pi \times 14 \times 10^{-12} = 8.8 \times 10^{-11}\ m^2$

Motion of the Scattering Particle

The mathematical model is based on the assumption that the motion of the "colloidal" particle suspended in the water faithfully records the acoustic particle velocity. To check under what conditions this can be true, we take the colloidal particle to be a sphere, radius a, density ρ_s and assume it is oscillating in a fluid medium of density ρ_f, kinematic viscosity ν_f at frequency ω_s and net amplitude V.

Table 6.6.2 — Amount of Suspended Particulate Matter [14]

Area	Depth (m)	Suspension (mg/l)
(*a*) total		
Oceanic	deep water	0·05 (average)
North Atlantic	surface water	0·04–0·15
Oceanic	—	0·8–2·5 (average)
Pacific, coast	—	1·6
Coastal	—	6·0–18·0
(*b*) organic fraction		
Atlantic	—	0·04–0·17
North Atlantic	—	0·05–0·2
North Atlantic	deep water	0·01–0·02
Central Pacific	surface water	0·02
Central Pacific	deep water	0·005
(*c*) inorganic fraction		
Atlantic, offshore	—	0·05–1·0
Coastal	—	0·16–1·20

Then the forces F exerted by the fluid on the sphere are twofold: (1) the accelerative (2) the viscous force. According to classical theory [7] the expression for F is

$$\mathcal{F} = -\frac{4}{3}\pi\rho_f a^3\left(\frac{1}{2}+\frac{9}{4\beta a}\right)\frac{dU}{dt} - 3\pi\,\rho_f a^3\omega\left(\frac{1}{\beta a}+\frac{1}{\beta^2 a^2}\right)U \tag{6.6.17}$$

in which $\beta^2 = \omega_s/2\nu$. If the period of oscillation is made infinitely long, then $\beta^2 a^2 \ll \beta a \ll 1$ and the term in dU/dt (i.e., the inertial increment due to the gross motion of the fluid) becomes negligible. Under these conditions the magnitude of the force exerted by the fluid on the sphere is $F = 6\pi\rho_f \nu a U$. This is the stokesian force resisting the slow descent of a particle in a viscous fluid under the action of gravity. The equation of forced motion arising from this resistive force is therefore

$$\frac{4}{3}\pi a^3\rho_s\frac{dU_s}{dt} = 6\pi\mu_f a U \tag{6.6.18}$$

in which $\mu_f = \rho_f\nu$ is the fluid dynamic viscosity. Thus, for particles of diameter D,

$$\frac{dU_s}{dt} = KU,\ K = \frac{18\mu_f}{D^2\rho_s}. \tag{6.6.19}$$

Since U is the differential motion of the water, i.e., $U = U_f - U_s$, we can assume U_f to be the acoustic excitation and write $U_f = U_0 \exp j\omega t$. At the steady state frequency ω the velocity U_s reduces to

$$U_s = \frac{U_0 \exp j\omega t}{\frac{j\omega}{K}+1}. \tag{6.6.20}$$

This equation defines the properties of a low-pass filter with a cut-off frequency $\omega_{c.o.} = K$. As long as $|\frac{\omega}{K}| \ll 1$ the motion of the colloidal particle will faithfully follow the motion of the acoustic wave. To calculate the magnitude of the cut-off frequency, we note that the dynamic viscosity of water at 20°C (in centipose) = 0.01 dyne sec/cm^2 = 10^{-3} Nsm^{-2}. Assuming particle sizes of order 7×10^{-6} meter, one calculates $K = \omega_0 = \left\{\frac{18}{49}\right\} 10^9/\rho_s$. If the density of the colloidal particle is the same as that of water, the cut-off frequency is

$$f_{c.o.} = \frac{18 \times 10^6}{49 \times 2\pi} = 58.5 \text{ kHz}.$$

If $|\frac{\omega}{K}| \ll 1$, then $|U_s - U_0| \simeq \frac{\omega}{\omega_0} U_0$. By choosing $\omega \ll \omega_0$, one sees that the differences between the motion of the colloidal particle and that of the acoustic wave is negligible.

It appears from the above argument that for (low-frequency) periodic motion, which is long relative to the optical process duration, the forces involved are purely resistive, and the particle motion is not sensibly different from the wave motion. However, when the wave motion is complex due to presence of soft reflective walls, diffraction, etc., the forces acting on a colloidal particle are along more than one coordinate. The motion of the particle is then oval, or elliptical, and the equations written above no longer hold. It could then be said that in complex sound fields, it can hardly be expected that a colloidal particle will faithfully follow the motion of the acoustic wave since it would then be required to be nearly indistinguishable from the medium itself, assumed free.

Brownian Motion

According to the theory of Brownian motion [8] the mean of the square of the distance travelled by a particle in a fluid during a time t is given by the equation

$$\overline{r^2} = 6\,Dt. \tag{6.6.21}$$

Here D is the diffusion coefficient (dimensions m^{2}s^{-1}). For spherical particles of radius a diffusing slowly in a medium of dynamic viscosity μ, it is known that $D = \frac{kT}{6\pi\mu a}$. Thus, the mean distance travelled in time t is

$$\sqrt{\overline{r^2}} = \sqrt{\frac{kTt}{\pi\mu a}}; \quad t = \frac{\overline{r^2}\,\pi\mu a}{kT}. \tag{6.6.22}$$

It is important to estimate the time required for the particle to move a "decorrelation distance." Arbitrarily (but reasonably), this distance is taken to be a quarter wavelength of the laser light. Let λ_E = 3860 Å, $\mu = 10^{-3}$ Nm^{-2}s, $a = 3 \times 10^{-6}$ m, Boltzman's constant = 1.38×10^{-23} NmK^{-1}, T = 300K. Then the decorrelation time is

$$t_d = \left(\frac{3.86 \times 10^{-7}}{4}\right)^2 \frac{\pi \times 10^{-3} \times 3 \times 10^{-6}}{1.38 \times 10^{-23} \times 3 \times 10^2} = 2.1 \times 10^{-2} \text{ s}.$$

The "decorrelation speed" is $\sqrt{\overline{r^2}}/t_d$ or

$$C_d = \frac{(3.86 \times 10^{-7}/4)}{2.1 \times 10^{-2}} = 4.6 \times 10^{-6} \text{ ms}^{-1}$$

Thus, C_d is of the order of 10^{-3} mm/sec.

The possibility of decorrelation of the motion due to the acoustic wave by the Brownian motion of the suspended particles must be seriously considered, if the duration of the process required to sample the wave exceeds 0.02 sec. At 100 Hz this allows about 2 complete cycles to be sampled. However, at 50 Hz only 1 cycle can be sampled. Thus, there is a threshold frequency for doppler detection of particle velocity, estimated here at 50 Hz. This conclusion is restricted to the case of a single scattering particle whose Brownian motion disturbs the acoustic particle velocity over short times, and over an assumed characteristic length of $\lambda_E/4$. In the multiple particle case the Brownian motion is random. Over long (enough) times it only adds noise to the detection process but does not set threshold frequencies. The characteristic length is then not significant.

Spectral Broadening Due to Brownian Motion

The probability of finding a Brownian particle in the distance interval r and $r + dr$ is proportional to $\exp(-r^2/4Dt)$ For two-way travel the phase change $\Delta\phi$ due to Brownian motion is $\Delta\phi = 2k\Delta r = \frac{4\pi\Delta r}{\lambda}$. Hence, the probability of finding the motion of the particle in phase $\Delta\phi$ is proportional to $\exp\{-(\Delta\phi)^2/(64\pi^2\frac{D}{\lambda^2}t)\} = \exp\left\{-\frac{(\Delta\phi)^2}{B_B t}\right\}$ where $B_B = \frac{64\pi^2 D}{\lambda^2}$. In accordance with the mathematical model sketched earlier, the spectrum of the first sideband due to acoustic modulation is 1/2 of this quantity. Thus, the spectral broadening due to Brownian Motion is

$$\frac{B_B}{2} = \frac{32\pi^2 D}{\lambda_E^2} = \frac{16}{3}\frac{\pi kT}{\lambda_E^2 \mu a} \tag{6.6.23}$$

For a laser wavelength in water of 3.86×10^{-7} m, $\mu = 10^{-3}$ Nsm^{-2}, $a = 3 \times 10^{-6}$ m $k = 1.38 \times 10^{-23}$ NMK$^{\circ -1}$, $T = 300^\circ$K the spectral broadening is 155 Hz.

Mean Distances Travelled in Significant Times Due to Brownian Motion are:

(a) in one period of acoustic wave at 100 Hz	0.7×10^{-7} m
(b) in one period of laser light	2.75×10^{-14} m
(c) in time to interrogate two quarter waves of laser wavelength (2-way travel over distance equal to a quarter wavelength)	1.9×10^{-14} m
(d) in time for acoustic amplitude to go from zero to maximum (i.e., one quarter period)	0.33×10^{-7} m
(e) the time to cover the two-way travel between laser and particle (2×30 m = 60 m)	0.341×10^{-9} m

6.7 COMPARISON OF THE LASER HETERODYNE DETECTOR WITH THE LASER DOPPLER VELOCIMETER

The method of detection of an acoustic signal by use of a laser heterodyne device can be designed to measure either of two different quantities (1) a sinusoidal displacement of particles in a fluid (2) a fluid velocity (turbulent or laminar). In the case of displacement the success in detection rests on the capability of measuring magnitude of the power spectrum of a photodetector current in the presence of noise, rather than in the capability of measuring a frequency shift. The important physical quantity in the signal processing is the modulation index or phase shift (Eq. 6.2.1) not a Doppler frequency shift. Hence the acoustic sensor in question is a true displacement device, rather than a velocity device. In the case of (steady) velocity success in detection rests on the capability of measuring Doppler frequency shift in the presence of noise (true Laser Doppler Velocimeter).

We compare goals and achievements in measuring displacement and velocity by laser heterodyne methods of several authors. As a reference goal we cite the modulation index of ambient noise in the ocean expressed as a plane wave equivalent in a one Hertz band at 100 Hz. In the absence of shipping noise this is taken to be,

modulation-index design goal: 8×10^{-6} radian

a. Under the assumption that shot noise is the only noise in the circuitry of an acoustic displacement sensor Massey [9] calculated that displacements of the order of 10^{-12} (meter) could be measured in the laboratory using a laser wavelength of 6330×10^{-10} (meter). This is equivalent to a modulation index of 2×10^{-5} radian.

b. Yeh and Cummins [10] concluded that they could detect in the laboratory constant (laminar) flow velocities as low as 4×10^{-5} meter/second at a scattering angle of 30°.

c. Edwards et al. [11] estimated that under laboratory conditions where thermodynamic diffusion of molecules was the limiting factor they could detect constant velocities as low as 10^{-5} meter/second.

d. Attempts to measure components of velocity turbulence in water by use of the laser Doppler velocimeter in the regime of dissipation spectra in high speed flows have been confronted with exceptional difficulties. The basic limit is the *Doppler ambiguity* (or uncertainty in measuring a frequency shift) due to extraneous time-varying modulation of the laser beam. These modulations are introduced by finite transit time of particles through the scattering volume, turbulent fluctuations across the scattering volume, mean velocity gradients, and circuit noise. In making measurements of turbulent flows by the optical schemes discussed above it is important to note that the only measurable velocity is the Eulerian random velocity $u_0(t)$ averaged over the scattering volume. This is the sum of a mean velocity $\bar{u}_0(t)$ and a fluctuating velocity $u_0'(t)$. The power spectrum of turbulence consists of a mean (Doppler) frequency shift broadened by the spectrum of the fluctuating components. As noted above the resolution of the power spectrum of turbulence (that is, its separation out of the noise) is limited by the Doppler ambiguity (DA). If the frequency broadening of the turbulent velocity fluctuations (namely the quantity we wish to measure) is of the same order as the broadening due to Doppler ambiguity (which is the noise we wish to avoid) then there is no way of telling them apart. If ω_0 is the mean Doppler shift due to $u_0'(t)$ then the condition of resolution is

$$\frac{u}{\bar{u}} > \frac{DA}{\omega_0}. \tag{6.7.1}$$

(This Doppler ambiguity poses a severe limit in the determination of the turbulence spectrum.) It is fundamental to recognize that the measurement of laminar flow $\bar{u}$ which is nonrandom differs from the measurement of turbulent flow $u_0(t)$ which is random. In the latter case there is a largest wavenumber (or highest cut-off frequency) that is measurable for a fixed Reynolds number and fixed scattering angle. Thus the entire power spectrum of velocity turbulence is unattainable. A simple estimate of the largest measurable wavenumber is $k_{MAX} = 2\pi/L$ in which L is the largest dimension of the scattering volume. Thus if L is a number fixed by the LDV the largest turbulence wavenumber measurable is $2\pi/L$, and the rest of the spectrum is unresolvable. Hence if the presence of submarine turbulence is to be determined by examining turbulence scale sizes less than L meters, the LDV method fails. It can be revived by reducing the scattering volume. However, such reduction is accompanied by increase in Doppler ambiguity since space is sampled over a shorter time interval. Mathematical modeling [12] shows that there is an optimum size of scattering volume L_{OPT}, given by

$$L_{OPT} = l_0 \frac{1}{\sqrt{2}} \left(\frac{1}{1.27} \right) \left(\mathrm{Re} \sin \frac{\theta}{2} \right)^{1/2}, \quad l_0 = \left(\frac{\nu^3}{\epsilon} \right)^{1/4} \tag{6.7.2}$$

(ϵ = rate of dissipation of turbulent energy per unit mass, ν = kinematic viscosity, Re = Reynolds number based on the mean velocity = $\bar{u}\lambda_E/(2\nu \sin\frac{\theta}{2})$, θ = angle of scattering). Wavenumbers greater than $2\pi/L_{OPT}$ are not resolvable because of Doppler ambiguity. The symbol l_0 is the inner scale (meters) of turbulence. When $\theta = 180°$,

$$\mathrm{Re} = \frac{\bar{u}_0\lambda_E}{2\nu \sin\frac{\theta}{2}} = \frac{\bar{u}_0(5 \times 10^{-7})}{2 \times 10^{-6}} = 0.25\,\bar{u}_0 \tag{6.7.3}$$

so that

$$L_{OPT} = l_0\,(0.57)(0.5)\,\bar{u}_0^{1/2} \approx \frac{l_0}{4}\,\bar{u}_0^{1/2} \tag{6.7.4}$$

If the turbulent velocity is 1 meter/sec, the optimum scattering volume is 1/4 of the inner scale of turbulence. This is a very severe restriction. Any attempt to decrease the scattering volume only increases the Doppler ambiguity.

e. Doppler ambiguity bandwidths have been studied in the laboratory. Bates [13] used a 10 inch pipe at flow rate of 1.4 ft/sec (Reynolds number 2.056×10^5 and found the following ratios of spectral broadening:

Table 6.7.1

		In Core	At Wall
(1)	$\frac{\text{transit time spectral broadening}}{\text{mean Doppler frequency shift}}$	0.636	0.636
(2)	$\frac{\text{turbulence spectral broadening}}{\text{transit time spectral broadening}}$	1.074	38
(3)	$\frac{\text{mean velocity gradient spectral broadening}}{\text{turbulence spectral broadening}}$	0.000719	0.75

REFERENCES

[1] General Electric Co. "VAS" The Virtual Acoustic Sensor," Document EHM-12-228-10, Feb. 1967, Electronic Systems Div., Syracus, New York.

[2] E.M. Oliver, "Signal to Noise Ratios in Photoelectric Mixing," Proc. IRE **49**, 1960 (1961).

[3] Ref. [1] p. VI-9.

[4] R. Urick, "Principles of Underwater Sound for Engineers," McGraw-Hill, 1st Ed., p. 168.

[5] S.Q. Duntley, J. Opt. Soc. Am. **53**, 214-223 (1963).

[6] Ref. 1, p. IV-14.

[7] H. Lamb, "Hydrodynamics," Dover Publications, p. 644, Eq. 26.

[8] L.D. Landau, E.M. Lifshitz, "Fluid Mechanics," p. 227. Pergamon Press, 1959.

[9] G.A. Massey, Proc. IEEE, **56**, 2157 (1968).

[10] Yeh, Cummins, Applied Phys. Letters **4**, 176 (1964).

[11] Edwards et al, J. Appl. Phys. **42**, 837 (1971).

[12] George, J.L. Lumley, J. Fluid Mech. **60**, 321 (1973).

[13] C.J. Bates, DISA INFO. No. 16, 5-10 (1974), published at 779 Susquehana Ave., Franklin Lakes, N.J. 07417.

[14] "Optical Aspects of Oceanography," N.G. Jerlov, E.S. Nielsen, Academic Press, New York, 1974, page 19 Figure 4.

Chapter 7
METALLIC-GLASS TRANSDUCER

7.1 INTRODUCTION

When a mixture of iron and one (or more) of the elements—boron, silicon, phosphorous, carbon or cobolt—is melted together, then suddenly cooled at such a rapid rate (say 10^6 K/s) as to leave insufficient time to permit crystallization, amorphous (glass-like) substances are formed which have remarkable magnetic properties. It is possible to prepare these amorphous magnetic materials in the form of long ribbons with uniform cross section by squirting the molten alloys onto a cooled rotating cylinder, or by centrifugal solidification. When so formed these metallic-glasses retain the ductility and flexibility of a metal, have high surface hardness, high tensels strength, are easily magnetized and posess large electrical resistivity.

When strips of these glossy ribbons are annealed (for some 5 to 10 minutes, at temperatures that range from 280° to 430°C, in an applied magnetic field of some 25 to 6100 oersteds directed so as to lie in the plane of the ribbon parallel to its width) and then excited by a combination of both dc and ac magnetic fields, they exhibit very high magnetostriction and elasto-magnetic coupling. Because of such properties these metallic-glasses posess special advantages for use in electromechanical transduction. In this chapter we discuss these properties in greater detail and show how this new material can be incorporated into acoustic sensors.

7.2 MAGNETOSTRICTION IN METALS—SUMMARY OF PROPERTIES OF USE IN ACOUSTIC TRANSDUCERS

To appreciate the great potential of metallic glasses as basic material for acoustic transduction it will be useful to summarize key elements in the theory of magnetostriction.

A long bar of magnetic metal (length l) with narrow cross section (A) wound with a current carrying coil changes its length by amount Δl upon being magnetized by an incremental dc magnetic field ΔH. The total change in length per unit length, $\delta l/l$ due to the total magnetic field (starting from the demagnetized condition) for iron and nickel bars is shown in Fig. 7.2.1. Roughly, in the case of *this* nickel bar the ratio $\delta l/l$ reaches the limiting (or saturation) value of $\sim -26 \times 10^{-6}$ at a magnetic field of ~ 30 oersteds. Since it is always advantageous to use MKS units we note here the conversion from Gaussian units of magnetic field to MKS units is:

$$(1 \text{ oersted}) = 4\pi \times 10^{-3} \times \left\{\frac{1 \text{ ampere–turn}}{\text{meter}}\right\}.$$

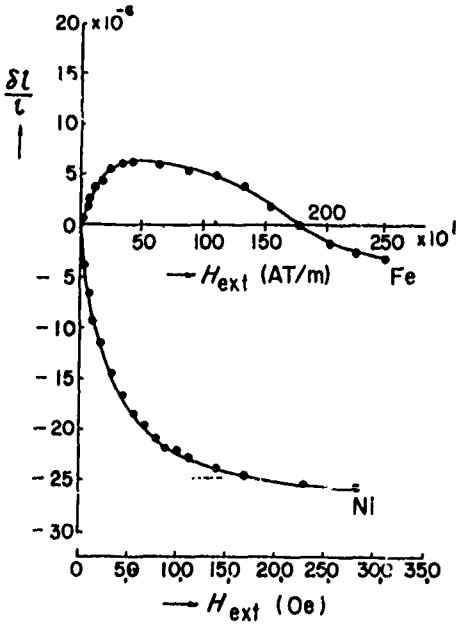


Fig. 7.2.1 — Static magnetostriction of iron and nickel as a function of external magnetic field

PREVIOUS PAGE IS BLANK

Thus 30 oersteds are equivalent to 2387 amp turns/meter. Similar values hold for nickel bars with differing anealing cycles.

Since the magnetic field H generates a magnetization M (or flux density $B \cong \mu_0 M$) this same change in length can be plotted versus magnetization, Fig. 7.2.2. It reveals that in this material there is limiting (saturation) strain $(\delta l/l)_{sat}$. The saturation magnetization corresponding to it is approximately $M_{sat} \approx 500$cgs emu. Again, it will be useful in calculation to note that the conversion from a c.g.s emu unit of magnetization to an MKS unit is

$$1 \text{ c.g.s. } emu = \left(\frac{1}{4\pi} \times 10^4\right) \times \left(\frac{\text{weber}}{\text{m}^2}\right).$$

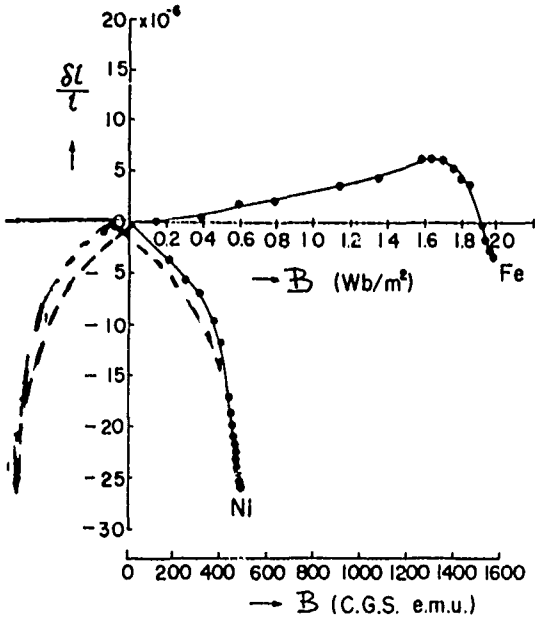


Fig. 7.2.2 — The magnetostrictive characteristics $\delta l/l$ represented as a function of flux density B(Vs/m^2)

Thus 500 c.g.s. emu are equivalent to 0.63 weber/m^2. Shown in dotted lines on the figure is the path of cyclic magnetization and demagnetization, indicating hysteresis. It is also noted that the direction of displacement is independent of the direction of the applied magnetization, from which the inference can be made that

$$\delta l/l \propto M^2.$$

Thus if the magnetization has an alternating component at frequency f the strain will have alternating components of frequency f^2, $2f$, etc.

The relation between magnetization and magnetic field for this nickel sample is shown in Fig. 7.2.3. One identifies here magnetic properties discussed in Sec. 2.2, namely:

the value of coercive force is -1.5 oersted ($= -119$ ampere turns/meter)
the value of residual induction is 150 c.g.s. emu ($= 0.19$ weber/m^2).

7.3 MAGNETOSTRICTIVITY

The ratio $\delta l/l$ is the total strain in the bar. It can be thought of as the internal strain due to an *applied* external force per unit area at the ends of the bar. If one uses the convention that an applied (external) stress is the negative of the internal stress it is seen that the force necessary to reduce the strain to zero when the bar is magnetized is given by

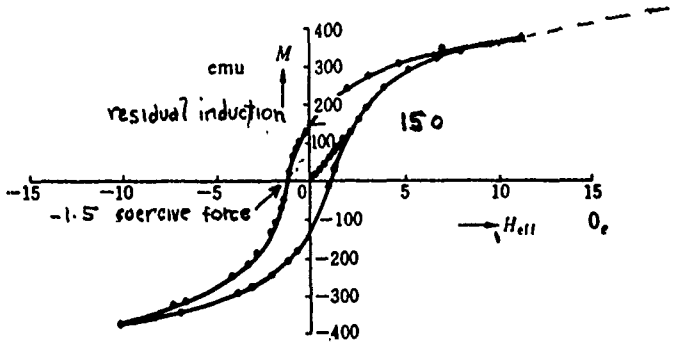


Fig. 7.2.3 — DC magnetization curve of a magnetostrictive substance

$$-\left(\tau\right)_{\text{ext}} = \left(-\frac{F}{A}\right)_{\text{ext}} = E_M \delta l/l$$

in which E_M = Young's modulus of the bar at constant magnetization. The internal stress is then,

$$(\tau)_{\text{int}} = E_M\, \delta l/l = \Gamma M \quad \text{(notation of Kikuchi [1])}$$

or

$$(T)_{\text{int}} = -hB \qquad \text{(IRE notation)}$$

As before, for metals of high magnetic susceptibility, $B \cong \mu_0 M$. The negative sign here is an IRE convention which expresses a *constitutive* relation. By definition

$$\Gamma = \left(\partial\tau/\partial M\right)_{\text{zero strain}} \quad ; \quad h = \left(\partial T/\partial B\right)_{\text{zero strain}}.$$

The units of Γ and h in the Cgs and MKS systems are:

h: Cgs emu: dyne/maxwell or dyne/gauss cm^2; MKS: Newton/weber

Γ: Cgs emu: $\dfrac{\text{dyne sec}}{\text{cm} \times \text{stat coulomb}}$; MKS: $\dfrac{Ns}{Cm}$

The conversion factors are:

$$\Gamma(\text{MKS}) \times 4\pi \times 10^{-3} = \Gamma(\text{Cgs emu})$$

$$\Gamma(\text{Cgs emu}) \times 79.577 = \Gamma(\text{MKS}).$$

$$\Gamma \simeq \mu_0 h \text{ (in [1] Kikuchi makes } \mu_0 = 1, \text{ so that } |\Gamma| = |h|)$$

Figure 7.3.1 shows a plot of the magnetostrictive dynamic constant versus magnetization. This chart may be used to calculate the magnitude of force per unit area developed in the rod if the increase in size of the rod during magnetization is completely impeded. For example, if the demagnetized rod is magnetized to a level of $\sim$ 0.42 weber/meter^2, and all displacement is completely impeded the stress developed in the rod will be

$$|T| \approx 2 \times 10^7 \frac{N}{Wb} \times 0.42 \frac{(Wb)}{\text{m}^2} = 0.84 \times 10^7 \frac{N}{\text{m}^2}$$

or

$$|T| = 0.84 \times 10^7 \times 1.450 \times 10^{-4} = 1218 \text{ psi.}$$

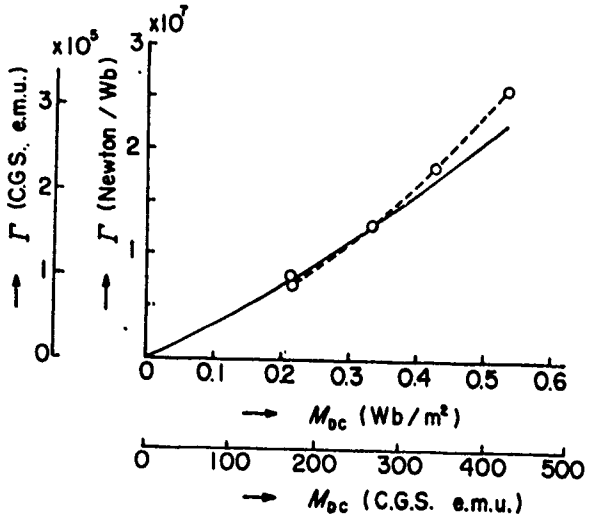


Fig. 7.3.1 — Experimental verification of Γ (= h constant) derived from static characteristics ($\delta l/l$) in nickel. Solid line, theory; dotted line, experiment [1]. (Note: Γ is calculated to be $|h|$ by making $\mu_0 = 1$).

7.4 COEFFICIENT OF MAGNETOELASTIC COUPLING

We return to the basic set of constitutive relations given by Eqs. 2.3.6. We interpret the first one as a dynamic force balance by reversing sign:

$$(a)\ \mathbf{T}_{ext} = h^{(i)}\,\mathbf{M} - c^{M}\mathbf{S} \tag{7.4.1}$$

In words,

external elastic stress = internal stress due to magnetization − internal stress due to strain.

Similarly we interpret the second one as a dynamic magnetomotive force balance:

$$(b)\ \mathbf{H} = \gamma^{S}\mathbf{M} - h\mathbf{S}. \tag{7.4.2}$$

In words,

external field = internal field due to magnetization − internal field due to strain.

Combining (a) and (b) leads to Eq. 2.3.7 with reversed sign:

$$(a)\ (\mathbf{T})_{ext} = \mathbf{h}^{(i)}\mathbf{B} - c^{S}\,\mathbf{S} \tag{7.4.3}$$

$$(b)\ c^{S} = c^{M}\left[1 - k_c^2\right]$$

$$(c)\ k_c^2 = \frac{\mu_0 \mu\, h^{(i)} h}{c^{M}}.$$

Here k_c is the coefficient of magneto-elastic coupling calculated at the value of μ, h and c^M taken at the operating point of the transducer.

In ordinary applications the internal driving magnetic induction has both a *dc* bias field and an *ac* driving field,

$$B^2 = (B_0 + B_l \cos \omega t)^2 = B_0^2 + 2B_l B_0 \cos \omega t + B_l^2 \cos^2 \omega t.$$

By making $B_o >> B_l$ and processing only the *ac* field one sets the operating point at $B_0 = B_0(H_0)$ which is a function of the bias (externally applied) magnetomotive field H. At this operating point,

$$B_l = \mu_0 \mu_l H_0 \qquad \text{(units of } \mu_0: Ns^2/C^2) \tag{7.4.4}$$

in which μ_l is the incremental, or dynamic, permeability (units: none) associated with the *ac* cycling field. An estimate of B_l for the case of annealed nickel may be obtained by setting H_0 to some arbitrary number. Let this be,

$$H_0 = 1200 \frac{\text{ampere turns}}{\text{meter}}$$

on the static $B-H$ curve. It is then experimentally found that the 'dynamic' slope at this operating point is,

$$\mu_l \approx 41.$$

Choosing the example of a long narrow bar whose Young's modulus is $E_M = c^M$, the strain is,

$$\delta l/l \sim -26 \times 10^{-6}.$$

Thus,

$$B_l = 4\pi \times 10^{-7} \times 41 \times 1200 = 6.18 \times 10^{-2} \ (Wb)/m^2.$$

The slope of the static $B - H$ curve at H_0 in relative units is scaled to be,

$$\mu = 340$$

Hence, the bias induction is,

$$B_0 = \mu_0 \mu H_0 = 4\pi \times 10^{-7} \times 340 \times 1200 = 0.512 \ (Wb)/m^2.$$

Using this value one obtains from Fig. 7.3.1 the value of the magnetostriction coefficient

$$h = |\Gamma| = 2.1 \times 10^7 \ N/(Wb) \ .$$

To calculate k_c we require a value of Young's modulus. Let us choose here its value at the demagnetized state,

$$E_M = E_0 = 2 \times 10 \qquad N/m^2.$$

Substituting these values in the expression for k_c^2 one funds that for $\mu_l = 41$

$$k_c^2 = \frac{4\pi \times 10^{-7} \times 41 \times (2.1 \times 10^7)^2}{2 \times 10^{11}} = 0.114$$

$$k_c = 0.34.$$

In terms of stored energy

$$k_c^2 = \frac{\text{energy available for doing mechanical work}}{\text{total energy input in the magnetic field}}.$$

Thus about 11% of the input energy is available for doing mechanical work. At a lower bias field (say $H_0 = 160$ amp-turns/meter) the coupling coefficient for annealed nickel is about 0.14. In this case about 2% of the input energy is available for doing mechanical work.

7.5 ΔE EFFECT

The difference between c^M and c^s shows that the magnitude of Young's modulus E of a long bar magnetized to M is lower than the value E_0 in the demagnetized state. Thus, one must write;

$$E = E(M) \leqslant E_0 . \tag{7.5.1}$$

This phenomenon of diminution in E with increasing magnetization is called the ΔE-effect. Since h and μ_l are also functions of magnetization we write,

$$k_c^2 = k_c^2 (M) \tag{7.5.2}$$

There is in every magnetostrictive material an optimum bias (M_{opt}) which gives the maximum coupling (k_{max}). For any other M the coupling is lower. Clearly the ΔE-effect and the maximum coupling coefficient are related. It is found empirically that the change in $E(= \Delta E)$ from the demagnitized state to the saturation state is given by,

$$\left(\frac{\Delta E}{E}\right)_{sat} = C\, k_{max}^2. \tag{7.5.3}$$

Tests on a variety of common iron/nickel materials shows the constant to be approximately,

$$C \approx 1.77. \tag{7.5.4}$$

in which C is a numerical constant. Thus measurement of the ΔE-effect gives a good estimate of the coupling coefficient. In particular for a value of

$$\sqrt{\left(\frac{\Delta E}{E}\right)_{sat}} \sim 1.33 \tag{7.5.5}$$

the coupling coefficient would be close to unity, which is the maximum theoretically possible. However, in certain magnetostrictive rare-earth-iron compounds the constant C has been measured and found to be approximately 2 at a bias field of kilooersteds. High coupling coefficients are anticipated for these materials [2].

Maximum Power That Can Be Delivered at a Mechanical Terminal

In a small amplitude plane elastic stress wave propagating linearly in an elastic body the stress p is related to the change in mass density δ through the propagation velocity c:

$$p = c^2 \delta$$

where

$$c^2 = 1/\kappa\rho_0; \quad \kappa = \text{compressibility}; \quad \rho_0 = \text{equilibrium mass density}.$$

The pressure is also related to the particle velocity v,

$$p = \rho_0 c \mathrm{v}$$

Thus,

$$\frac{\mathrm{v}}{c} = \frac{\delta}{\rho_0}. \tag{7.5.6}$$

Let the plane wave travel in a long bar, length l, area A. Then

$$c^2 = c_{\text{bar}}^2 = \frac{E}{\rho_0}.$$

At any point of the rod the stress $p(=\tau)$ is

$$\tau = \frac{E}{\rho}\,\delta \text{ or } \frac{\tau}{E} = \frac{\delta}{\rho_0} = \xi \tag{7.5.7}$$

where $\xi =$ strain. Hence

$$\mathrm{v} = c_{\text{bar}}\xi. \tag{7.5.8}$$

For a finite length bar one can express c_{bar} in terms of the lowest half-wave resonant frequency f_0:

$$c_{\text{bar}} = 2lf_0.$$

Thus,

$$\mathrm{v} = 2lf_0\xi = \frac{\omega_0 l}{\pi}\,\xi. \tag{7.5.9}$$

Suppose now that the bar develops a velocity v_1 against a load at one end. Then, since $l = c_{bar}/2f_0$, it is seen that

$$v_1^2 = c_b^2 \xi_1^2 P(\omega) \tag{7.5.10}$$

$$P(\omega) = \left[\frac{\omega_0}{\pi} \times \frac{1}{2f_0}\right]^2.$$

The symbol $P(\omega)$ is called the "output form-factor" by Kikuchi [1]. For the uniform long bar analyzed here it has a value of unity. Bars of nonuniform cross section display other values of $P(\omega)$ defined as,

$$P(\omega) \equiv \frac{v_1^2}{c^2 \xi_1^2} \tag{7.5.11}$$

where subscript 1 means conditions at the mechanical terminal.

Now let the real part of the load be expressed as a mechanical resistance R. In general it is a function of frequency and (sinusoidal) amplitude of velocity. The real power delivered to this load is

$$W_{mech} = \frac{1}{2} R(\omega, v_1) v_1^2.$$

In the case of the bar,

$$W_{mech} = \frac{1}{2} R(\omega, \xi_1^2) c_b^2 \xi_1^2 P(\omega), \quad P(\omega) = 1 \text{ for long bars.} \tag{7.5.12}$$

If the maximum permissible strain is ξ_{max}, the maximum possible output for the bar is

$$\left(W_{mech}\right)max = \frac{1}{2} R(\omega, \xi_{max}) c_b^2 \xi_{max}^2 P(\omega), \quad P(\omega) = 1 \text{ for long bars.} \tag{7.5.13}$$

For other structures $P(\omega)$ may differ from unity. However, the value of $P(\omega)$ for ring vibrators oscillating in the breathing mode is again unity.

The mechanical energy delivered by the bar is some fraction of the input electrical power W_{elec}. According to the definition of the coupling factor,

$$k_c^2 W_{elec} = W_{mech}.$$

Since the total energy per unit volume stored in the magnetic field is BH (units: volt coulomb/meter^3), and since $B = \mu' H$, where μ' is the dynamic permeability, it is seen that the total power per unit volume in the magnetic field at frequency ω, (where ω is much less than the resonant frequency) is,

$$W = \omega \mu' H^2.$$

Thus the mechanical energy available for doing work is

$$W_{\text{mech}} = \omega k_c^2 \mu' H^2.$$

At velocity resonance the dissipated power is proportional to the loaded Q_L of the transducer. Hence,

$$W_{\text{mech}} = \omega_r k_c^2 \mu' H^2 Q_L. \tag{7.5.14}$$

7.6 TRANSDUCTION LOSSES

Magnetostrictive transducers are constructed of a metal core wound with a coil supplying ac power, and the same coil, or another coaxial coil, supplying dc bias. Where feasible the bias can be supplied by a permanent magnet.

The blocked electrical impedance of the core is that of an inductance L_c,

$$Z_{ee} = j\omega L_c \chi.$$

Here the symbol χ is a complex quantity indicating presence of eddy-current losses,

$$Z_{ee} = R_c + jX_c = j\omega L_c |\chi| e^{-j\zeta} \tag{7.6.19}$$

$$\tan \zeta = \frac{R_c}{X_c}.$$

In dynamic biased operation the induction B executes a minor hystersis loop on the BH curve. This shows that B and H are not in phase. Thus the incremental permeability is also complex,

$$\mu_i = |\mu_i| e^{-j\beta}. \tag{7.6.2}$$

Eddy current losses in the core and in the hysteresis loops are additive. The relation between B and H then becomes

$$B = \mu' \chi \mu_0 H = |\mu_i| \mu_0 H e^{-j\phi} |\chi|, \qquad \phi = \beta + \zeta. \tag{7.6.3}$$

This relation is important in the analysis of magnetic field transducers.

7.7 TRANSDUCTION RATIO

From Eq. 7.4.3 the mechanical force F associated with the magnetic induction over area A can be calculated. First in the absence of losses:

$$F = Ah^{(i)} B \tag{7.7.1}$$

Also, from Eq. 7.4.2

$$I_{\text{blocked}} = \frac{l}{N} \gamma^S B. \tag{7.7.2}$$

The corresponding mechanical force may be represented by a force/voltage analogy through a transduction ratio α:

$$\alpha \, Z_0 \, I_{\text{blocked}} = \alpha \, V \tag{7.7.3}$$

where V is the voltage. Now the canonical equations of the magnetic field are antisymmetrical. They can be made symmetrical by changing F to $-jF$, and v to $-j$'v (see Sec. 1.48 for discussion). Thus, for canonical circuit representation the force balance is,

$$\alpha \, Z_0 I_{\text{blocked}} = -jAh^{(t)}B. \tag{7.7.4}$$

Since, for a core of length l with N turns of coil,

$$L_0 = \frac{j\omega N^2 A (\gamma^s)^{-1}}{l} \tag{7.7.5}$$

$$(\gamma^s)^{-1} = |\mu_t|\mu_0. \tag{7.7.6}$$

Solving Eq. 7.7.4 for α and substituting Eqs. 7.7.1, 5, 6, 3, one finds the circuit transduction ratio to be,

$$\alpha = -\frac{h^{(t)}}{\omega}N \quad \left(\text{units:}\frac{\text{N}}{\text{V}}\right). \tag{7.7.7}$$

Now in the presence of losses the transduction ratio becomes complex. The losses can be accounted for by use of the dip angle ϕ,

$$\alpha = -\frac{h^{(t)}}{\omega N} \, e^{-j\phi}|\chi|. \tag{7.7.8}$$

Unlike the transduction ratios of piezoceramic transducers which are constants this ratio is a complex number, and is seen to vary inversely as frequency.

7.8 MAGNETOELASTIC PROPERTIES OF METALLIC GLASSES

A. Experimental Set-Up

Figure 7.8.1 shows an apparatus for measuring magnetoelastic properties of samples of metallic glasses. The amorphous specimen 1, obtained in this case by a roller quenching technique, is wound with a detector (or 'pick-up') coil, which is connected to the terminals of a phase meter and volt meter. To excite this sample with an ac magnetic field one prepares a solenoid, 2, whose terminals are driven by a signal generator, 3. The phase and voltage of the exciting electric field are also measured by a second pair of terminals on the phase meter. The sample is slid into the solenoid and the entire structure is then placed in a strong electromagnet 4 which supplies the bias dc field. Under both dc and ac excitation the sample vibrates freely.

During measurement the magnitude of current is kept constant while the measured amplitude of the pick-up voltage $|V_p|$ varies with frequency. The phase θ between V_p and I_{ex} is measured at each increment of frequency. From this data the complex impedance at each frequency is calculated as

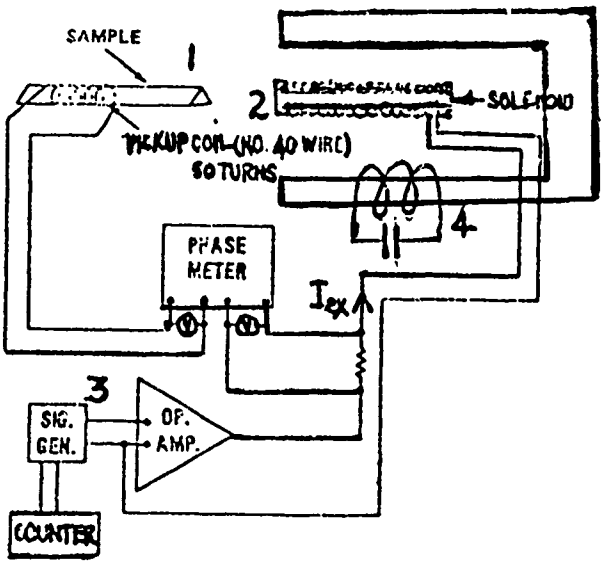


Fig. 7.8.1 — Apparatus for measuring magnetoelastic properties of metallic glasses

$$Z(\omega) \equiv \frac{|V_p|}{I_{ex}} \exp i\theta = \text{Re } Z_p + i \text{ Im } Z_p \tag{7.8.1}$$

Similarly the complex admittance Y_p is calculated from $Z(\omega)$ to be,

$$Y_p(\omega) = Z(\omega)^{-1} = \text{Re } Y_p + i \text{ Im } Y_p. \tag{7.8.2}$$

B. Theoretical Interpretation of Measurement

To find the correct expression for $Z(\omega)$ in this case of longitudinal vibration we recapitulate the derivation of the equations of motion discussed in Sec. 2.37. Let us choose a segment of the rod of volume $A_b dx$. On the cross-sectional area A_b the stress is given by the constitutive relation

$$T_3 = C_{33}^B S - h_{33}^{(i)} B_3.$$

Since we wish to specify constant current drive we substitute

$$B_3 = \frac{H_3}{\gamma_{33}^S} + \frac{h_{33}}{\gamma_{33}^S} S$$

and find

$$T_3 = C_{33}^H S - h_{33}^{(i)} \frac{H_3}{\gamma_{33}^S}$$

where

$$C_{33}^H = C_{33}^B \left[1 - \frac{h_{33}^2}{\gamma_{33}^S C_{33}^B}\right].$$

The convention of signs to be associated with forces and velocities at the ends of the bar are shown in Fig. 7.8.2. Now we make a *free-body* of this segment. The net stress across positive increment dx is

$$dx \frac{\partial T_3}{\partial x}(x_3) = dx\, C_{33}^H \frac{\partial^2 \xi(x_3)}{\partial x^2} - \frac{h_{33}^{(i)}}{\gamma_{33}^S} \frac{\partial H_3}{\partial x}(x_3)\, dx. \tag{7.8.3}$$

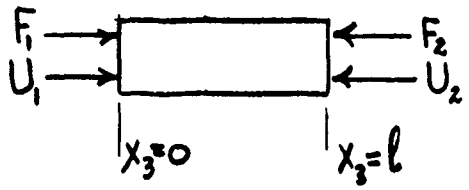


Fig. 7.8.2 — Convention of signs used in this section

$$F_1 = -A_1 T_3 \; ; \quad F_2 = -A_2 T_3$$

$$U_1 = j\omega \xi\Big|_{x_3=0} \; ; \quad U_2 = -j\omega \xi\Big|_{x_3=l}$$

Assuming there is no magnetic field leakage from the lateral edges of the bar, we set $\partial H/\partial x = 0$ at all intermediate segments of the bar. However, at the ends of the bar the applied body force due to magnetostriction is,

$$F_a = \frac{h_{33}^{(f)}}{\gamma_{33}^S} \frac{\partial H}{\partial x} = H_0[\delta(x) + \delta(x - l)] \frac{h_{33}^{(f)}}{\gamma_{33}^S} \qquad \text{(units: N/m}^3\text{)} \tag{7.8.4}$$

in which $H_0 e^{j\omega t}$ is the constant magnetic field intensity. According to Newton's law of motion as applied to the 'free-body' of one segment,

$$Adx \left(\frac{\partial T}{\partial x}\right) + Adx\, F_a = Adx\, \rho \frac{\partial^2 \xi}{\partial t^2}. \tag{7.8.5}$$

Substituting the expressions for $\partial T/\partial x$ and F_a, and choosing steady state one obtains,

$$\text{(a)} \quad \frac{\partial^2 \xi^2}{\partial x^2} + k^2 \xi = -\frac{h_{33}^{(f)} H_0}{C_{33}^M \gamma_{33}^S} [\delta(x) + \delta(x - l)] \qquad \text{(units: m}^{-1}\text{)} \tag{7.8.6}$$

$$\text{(b)} \quad k = \frac{\omega}{v_b^M}; \quad v_b^H = \sqrt{\frac{C_{33}^H}{\rho}}$$

This equation states that the rod is force-driven by the delta function distribution of magnetic field at its ends. There is no net mechanical force delivered to the bar by the magnetic field inside the bar. In the steady state the solution of the homogeneous part of Eq. 7.8.6, written as,

$$\text{(c)} \quad \frac{\partial^2 \xi}{\partial x^2} + \frac{\omega^2}{v_b^{2H}} \xi = 0, \quad v_b^{H2} = \frac{C_{33}^H}{\rho}$$

is

$$\xi = \left(A \sin \frac{\omega x_3}{v_b^H} + B \cos \frac{\omega x_3}{v_b^H}\right) e^{j\omega t} \tag{7.8.7}$$

The strain is then

$$\frac{\partial \xi}{\partial x} = \left(A \frac{\omega}{v_b^H} \cos \frac{\omega x_3}{v_b^H} - \frac{B\omega}{v_b^H} \sin \frac{\omega x_3}{v_b^H}\right) e^{j\omega t}. \tag{7.8.8}$$

We solve the inhomogeneous part of Eq. 7.8.7 by use of the appropriate Green's function $G(x|x_0|\omega)$ where x_0 is the source coordinate and x is the field coordinate. When the bar is stress-free at both ends we require from Eq. 7.8.3 that

$$\frac{dG}{dx} = \frac{h_{33}^{(f)} H_0}{C_{33}^H \gamma_{33}^S}, \quad x = 0,\ x = l \tag{7.8.9}$$

A function that satisfies this condition for source coordinate at $x = x_0 = 0$ is,

$$G(x|x_0|\omega) = -\frac{h_{33}^{(f)} H_0 e^{j\omega t}}{C_{33}^H \gamma_{33}^S} \frac{1}{k} \cos kx_0 \left| \frac{\sin k\left(\frac{l}{2} - x\right)}{\cos \frac{kl}{2}} \right|, \quad x > x_0. \qquad \text{(units: m)}$$

or

$$G(x|0|\omega) = \frac{h_{33}^{(f)} H_0 e^{j\omega t}}{C_{33}^H \gamma_{33}^S} \frac{v_b^H}{\omega} \left[\tan \frac{kl}{2} \cos kx - \sin kx\right] \tag{7.8.10}$$

Because of the delta function distributions in Eq. 7.8.6 one sees that G is identifiable with ξ. The particle velocity anywhere in the bar is then seen to be,

$$v(x) = \frac{jh_{33}^{(f)} H_0 e^{j\omega t}}{C_{33}^H \gamma_{33}^S} v_b^H \left[\sin kx - \tan \frac{kl}{2} \cos kx\right]. \tag{7.8.11}$$

An explicit form for ξ allows us to calculate the magnetic flux density,

$$B_3(x) = \frac{H_0}{\gamma_{33}^S} + \frac{h_{33}}{\gamma_{33}^S} \frac{d\xi}{dx} = \frac{H_0}{\gamma_{33}^S} + \frac{h_{33}^2 H_0}{C_{33}^H (\gamma_{33}^S)^2} \left[\cos kx + \tan \frac{kl}{2} \sin kx\right] \tag{7.8.12}$$

Using the formula

$$\tan \frac{\epsilon}{2} = \frac{1 - \cos \epsilon}{\sin \epsilon}$$

one finds the average to be,

$$(B_3)_{AV} = \frac{1}{l} \int_0^l B_3(x)\, dx = \frac{H_0}{\gamma_{33}^S} + \frac{h_{33}^2 H_0}{C_{33}^H (\gamma_{33}^S)^2} \frac{\tan \frac{kl}{2}}{\frac{kl}{2}} \qquad \left[\text{units: } \frac{A}{m}\right] \tag{7.8.13}$$

Since in this derivation the magnitude of magnetic field is kept constant the applied current is

$$I_3 = \frac{lH_0}{N} \qquad \text{(units: A)}$$

The resultant voltage varies with frequency as

$$V = j\omega NA (B_3)_{AV}$$

Thus the input electrical impedance is

$$Z = \frac{V}{I} = \frac{j\omega N^2 A}{\gamma_{33}^S l}\left[1 + \left(\frac{h_{33}^2}{C_{33}^H \gamma_{33}^S}\right)\frac{\tan\frac{k^H l}{2}}{\frac{k^H l}{2}}\right] \tag{7.8.14}$$

In the absence of losses this impedance is a maximum when

$$\frac{kl}{2} = \frac{n\pi}{2}, \quad n = 1, 2, 3 \ldots.$$

or

$$f_{\max} = n\,\frac{v_b^H}{2}\,l. \tag{7.8.15}$$

This is the frequency of velocity maximum at constant current drive as can be deduced from Eq. 7.8.11. Similarly the absolute value of electrical impedance is that of a pure inductance when,

$$\frac{k^H l}{2} = m\pi \qquad m = 1, 2, \ldots.$$

or

$$f_{\min} = \frac{m v_b^H}{l} \tag{7.8.16}$$

This is the frequency of velocity minimum (again from Eq. 7.8.11) at constant current drive. Actually, when losses are neglected, the velocity vanishes. The impedance is then the blocked value of a pure inductance:

$$Z_{\text{blocked}} = j\omega L$$

$$L = \frac{N^2 A}{l\gamma_{33}^S} \qquad \left[\text{units: } \frac{V_S^2}{C}\right]. \tag{7.8.17}$$

The tangent factor in Eq. 7.8.14 is called the motional impedance of the coil.

A similar derivation in which the bar is driven at constant magnetic flux density (that is, constant voltage) is,

$$Y = \frac{I}{V} = \frac{1}{\frac{j\omega N^2 A}{l\gamma_{33} S}}\left[1 - \frac{h_{33}^2}{C_{33}^B \gamma_{33}^S}\,\frac{\tan k^B l/2}{k^B l/2}\right] \tag{7.8.18}$$

$$k^B = \frac{\omega}{v_b^B}$$

$$v_b^B = \sqrt{\frac{C_{33}^B}{\rho}}.$$

The difference between constant-B and constant-H drive has been noted in Sect. 2.10. A similar difference between constant-V and constant-I in piezoelectric transducers is discussed in Sect. 2.19.

7.9 ALTERNATIVE SOLUTION OF THE DYNAMIC PROBLEM RAISED BY EXPERIMENT IN SECT. 7.8

Another approach in analyzing the dynamics the experiment set-up in Sect. 7.8 is taken up next. Starting with the constitutive relations

$$\text{(a)}\quad T_3 = C_{33}^B \frac{d\xi}{dx_3} - h_{33}^{(l)} B_3$$

$$\text{(b)}\quad H_3 = -h_{33} \frac{d\xi}{dx_3} + \gamma_{33}^S B_3 \tag{7.9.1}$$

and with the solution to the homogeneous wave Eq. 7.8.7

$$\xi = (\alpha \sin k_x^B + \beta \cos k^B x) e^{j\omega t}, \qquad k^B = \omega / v_b^B$$

one may set the boundary conditions at $x_3 = 0$, $x_3 = l$ in terms of the terminal forces F_1, F_2 and U_1, U_2:

$$j\omega\xi(0) = U_1;\ j\omega\xi(l) = -U_2;\ F_1 = -AT_3(0);\ F_2 = -AT_3(l) \tag{7.9.2}$$

It is then seen that

$$\text{(a)}\quad \xi = \left\{ -\frac{1}{j\omega} \left[\frac{U_1}{\tan k^B l} + \frac{U_2}{\sin k^B l} \right] \sin k^B x + \frac{U_1}{j\omega} \cos k^B x \right\}$$

$$\text{(b)}\quad F_1 = A C_{33}^B k^B \frac{1}{j\omega} \left[\frac{U_1}{\tan k^B l} + \frac{U_2}{\sin k^B l} \right] + A h_{33}^{(l)} B_3 \tag{7.9.3}$$

$$\text{(c)}\quad F_2 = A C_{33}^B k^B \frac{1}{j\omega} \left[\frac{U_1}{\sin k^B l} + \frac{U_2}{\tan k^B l} \right] + A h_{33}^{(l)} B_3.$$

In these relations we have assumed B_3 to be the driving magnetization. A second useful set is to assume H_3 to be the driving magnetic field intensity. Substitution of Eq. 7.8.12 into (a) leads to

$$\text{(a)}\quad T_3 = C_{33}^H \frac{d\xi}{dx_3} - \frac{h_{33}^{(l)} H_3}{\gamma_{33}^S};\quad \text{(b)}\quad B_3 = \frac{H_3}{\gamma_{33}^S} + h_{33} \frac{d\xi}{dx_3}$$

$$\text{(c)}\quad C_{33}^H = C_{33}^B \left(1 - \frac{h_{33}^2}{\gamma_{33}^S C_{33}^B} \right) \tag{7.9.4}$$

$$\text{(d)}\quad k_H = \frac{\omega}{v_{33}^H}$$

$$\text{(e)}\quad v_{33}^H = \sqrt{\frac{C_{33}^H}{\rho}}.$$

Thus,

$$\text{(a)}\quad \xi = -\frac{1}{j\omega}\left[\frac{U_1}{\tan k^H l} + \frac{U_2}{\sin k^H l}\right]\sin k^H x + \frac{U_1}{j\omega}\cos k^H x$$

$$\text{(b)}\quad F_1 = A\, C_{33}^H\, k^H \frac{1}{j\omega}\left[\frac{U_1}{\tan k^H l} + \frac{U_2}{\sin k^H l}\right] + \frac{A h_{33}^{(f)}\, H_3}{\gamma_{33}^S} \tag{7.9.5}$$

$$\text{(c)}\quad F_2 = A C_{33}^H k^H \frac{1}{j\omega}\left[\frac{U_1}{\sin k^H l} + \frac{U_2}{\tan k^H l}\right] + \frac{A h_{33}^{(f)} H_3}{\gamma_{33}^S}.$$

From this set it is deduced that the ratio of the force to the current transduction coefficient when there is no motion (= transducer blocked), is

$$T_{me} = \left.\frac{F}{I}\right|_{v=0} = \frac{A h_{33}^{(f)} N}{\gamma_{33}^S l} \qquad \left[\text{units: } \frac{\text{N}}{\text{A}} \text{ or } \frac{\text{Vs}}{\text{m}}\right]. \tag{7.9.6}$$

In conventional terms the magnetic-field transducer is antireciprocal so that

$$T_{em} = -T_{me}$$

The ratio of force to velocity at $x_3 = 0$ may be obtained from Eq. 7.8.11:

$$T_3\Big| = -h_{33}^{(f)}\, M_0 \text{ or } F = h_{33}^{(f)}\, M_0 A$$

$$\text{v}(0) = \frac{j\, h_{33}^{(f)}\, M_0}{C_{33}^M}\, \text{v}_b^M \tan\frac{kl}{2} \tag{7.9.7}$$

$$\text{v}(0) = j\,\frac{F\tan(kl/2)}{\rho \text{v}_b^M A}$$

so that in the absence of losses,

$$\frac{F}{\text{v}(0)} = z_m = -j(2\rho \text{v}_b^M A)\text{ctn}\left(\frac{kl}{2}\right) \tag{7.9.8}$$

The factor of 2 has been inserted to account for the impedance at the right end of the bar. From the basic theory of coupled elastic-magnetic fields, the input electrical impedance is,

$$Z_{ee} = Z_e + \frac{|T|^2}{z_m} = Z_e + Z_{MOT}$$

$$Z_{MOT} = \left(\frac{A h_{33} N}{\gamma_{33}^S l}\right)^2 \left(\frac{1}{r_m - j(2\rho \text{v}_b^M A)\text{ctn}\left(\frac{kl}{2}\right)}\right) \tag{7.9.9}$$

in which r_m is the mechanical loss. The cotangent function has the following values:

$\frac{kl}{2}$	ctn $\frac{kl}{2}$
0	$+\infty$
$\pi/2$	0
π	$-\infty$

Thus the electrical motional impedance is a maximum at the frequency of mechanical resonance.

$$\frac{k^M l}{2} = \frac{\pi}{2} \quad \text{or} \quad f_{\max} = \frac{v_b^M}{2l} \tag{7.9.10}$$

and vanishes at the frequency

$$\frac{k^M l}{2} = \pi \quad or \quad f_{\min} = \frac{v_b^M}{l} \tag{7.9.11}$$

At $f_{\min}$ the electrical impedance is the blocked value:

$$Z_e = j\omega L, \quad L = \frac{N^2 A}{l\gamma_{33}^S}$$

The alternative solution derived in this section has the advantage of more explicitly including boundary conditions at the ends of the transducer. It thus allows a more complete interpretation of experimental results.

7.10 EXPERIMENTAL RESULTS OF MAGNETOMECHANICAL TESTS ON METALLIC GLASS RIBBONS

Table 7.10.1 summarizes the magnetomechanical properties of a number of metallic glass ribbons as reported by research scientists. These ribbons are prepared in the form of strips of up to 10 cm in length, magnetized parallel to the width during annealing in a high transverse dc bias field, then driven by a low ac field at a low dc longitudinal bias field. The coefficient of electromechanical coupling was determined by the resonance method described in Sect. 7.8. The Young's modulus of elasticity is determined by use of the theoretical formulas for the mechanical resonant frequency of a long bar (Eqs. 2.10.40 or 2.10.32).

The values reported above are maximum quantities associated with particular annealing procedures and particular longitudinal dc bias fields. Figure 7.10.1 shows the variation of magnetomechanical coupling factor and relative permeability as functions of longitudinal dc bias field for samples of Metglas 2605 CO annealed at 363°C in a transverse dc bias field of 6.1 KOe. This chart shows that the coupling factor is sensitive to small changes in longitudinal bias. The question arises: how does $k_{\max}$ vary with T_a (the annealing temperature)? Figure 7.10.2 shows that below $\sim$ 378°C the value of $k_{\max}$, varies slowly with annealing temperature. However, above this annealing temperature $k_{\max}$ declines rapidly. The conjecture is that incipient crystallization is disorienting the magnetic moment alignment which is producing high values of $k_{\max}$.

Table 7.10.1 — Magnetomechanical Properties of Metallic Glass Ribbons

Metallic Glass Sample	Ref.	k_{max} / Annealing Conditions	$\Delta E/E_0$ / Long DC Bias	E_0 / ρ	Long. AC Field	Sample Ribbon Size	Q_M Impedence / Q_M Admittance
$Fe_{78}Si_{10}B_{12}$	[1]	0.82 / 373°C 5 min bias 2.0T	1.75 / 1.9 Oe		0.02 Oe P-P		
$Fe_{78}Si_{10}B_{12}$	[2]	0.75	1.9				
$Fe_{78}P_{15}C_{10}$	[3]		0.8				
$Fe_{80}P_{13}C_7$	[4]	0.53 / 350°C 20 min 1.2 k Oe	0.8 / 5.0 Oe	1.0 to 1.5 × 10^{11} N/m^2		2.0 mm × 30 μm × 6 cm long	
$Fe_{80}B_{20}$ Metglas 2605	[1]	0.64 / 376°C 6 min 2.0T	0.87 / 1.7 Oe	1.66 × 10^{11} N/m^2 / 7.4 × 10^3	0.02 Oe P-P	1.2 mm width × 0.051 mm thick	
$Fe_{67}CO_{78}B_{14}Si_1$ Metglas 2605CO	[5]	0.71 / 370°C 10 min 6.1 k Oe	10.5 Oe			1/16" × 3"	$\frac{35}{120}$
$Fe_{81}B_{13.5}Si_{3.5}C_2$ Metglas 2605SC	[5]	0.90 to 0.96 / 389°C > 1 k Oe	0.75 Oe				

(Note: T = Tesla)

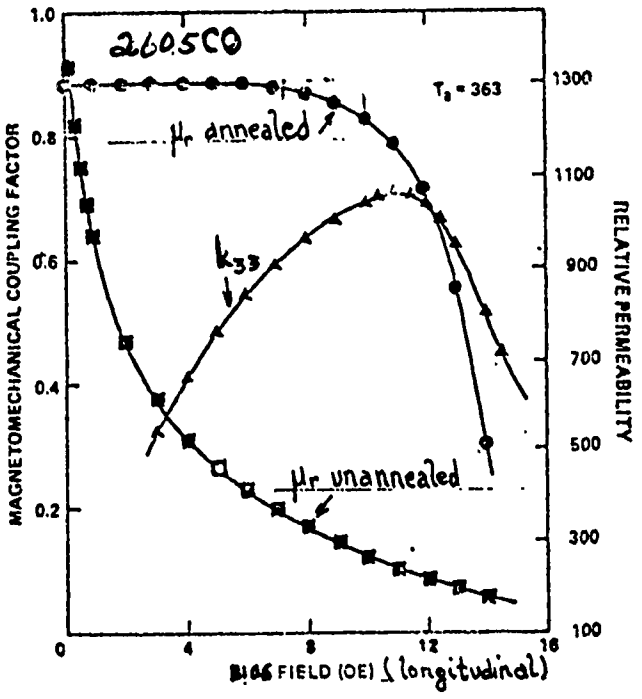


Fig. 7.10.1 — Coupling factor k_{33} (Δ) and relative permeability μ_r(O) for annealed ribbon (T_a = 363C, H_a = 6.1k0e). Also shown is the relative permeability for the unannealed ribbon (■) [7]

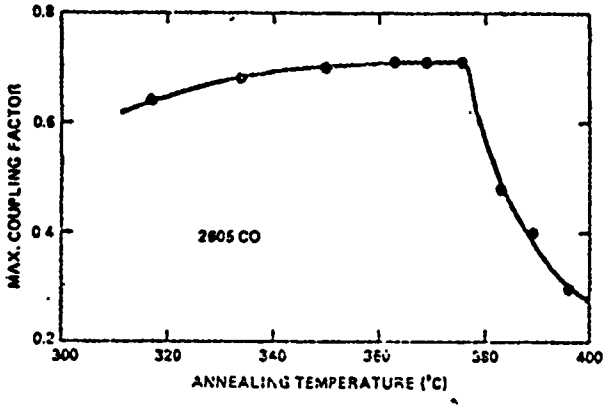


Fig. 7.10.2 — Maximum coupling factor versus annealing temperature (H_a = 6.1 k 0e). [7]

Of particular interest to transducer designers is the question whether metallic glass ribbons exhibit hysteresis and eddy current losses when driven by ac and dc magnetic fields. The answer is determined by plotting electrical impedance and admittance circles (imaginary quantities vs real quantities) and measuring dip angle of the circle diameter and blocked electrical resistance. A discussion of this procedure is given in Sect. 2.17. The results of such plotting is shown in Fig. 7.10.3. The circles, with appropriate normalization, are superimposed. The dip angles are seen to be quite small ("only a few degrees" [7]), indicating that Metglas 2605 CO, in the form of ribbons, exhibits little magnetic field losses in the frequency range of longitudinal mechanical resonance (14-32 kHz). By measuring quandrantal frequencies (see Sect. 2.17) it is found that the mehanical Q_M of the impedance circle (i.e., Q_M at constant-H) is about 35, and the Q_M of the admittance circle (Q_M at constant-B) is about 120. These high values of Q_M again indicate low mechanical losses in sweeping through the frequencies of resonance and antiresonance.

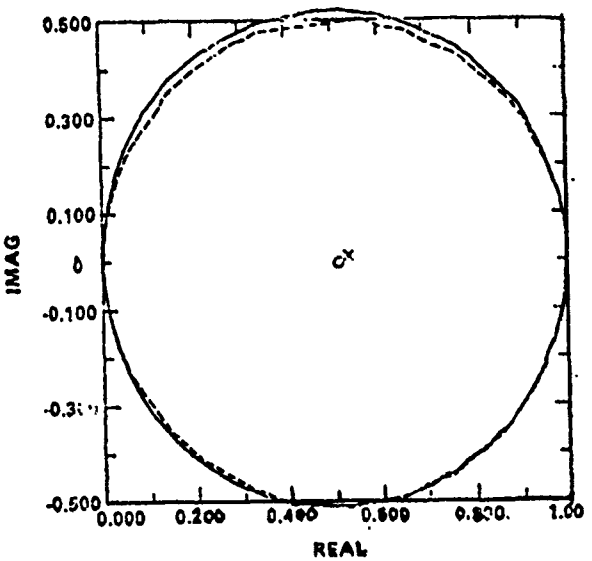


Fig. 7.10.3 — Admittance circle (dashed line) and impedance circle (solid line) of an annealed ribbon with $k_{max} = 0.71$. Data normalized so that the diameters are equal to 1. Axes are real and imaginary parts of admittance/impedance with frequency as a parameter. The high values of $k^2 Q$ causes the circles to have almost common diameters. [7]

7.11 ELECTROMECHANICAL TRANSDUCERS MADE OF MAGNETOSTRICTIVE RARE EARTH-IRON ALLOYS

A. Introduction

Rare earth-iron alloys in the compositional form *RFe* of binary, tertiary and quartenary alloys of terbium (Tb), dysprosium (Dy) and holmium (Ho) have been found to have high magnetomechanical coupling at room temperatures [8]. Other alloys, such as terbium-iron ($Tb\ Fe_2$), and samarium-iron ($Sm\ Fe_2$), also exhibit very large magnetostruction coefficients [9]. An alloy of this type that has been investigated extensively for high magnetomechanical coupling and ΔE-effect is terbium-dysprosium-iron. Its ultimate strain ($\delta l/l$) at saturation has been measured at values exceeding 1000×10^{-6}. Many experiments have been conducted to study the effects of changes in composition on its magnetomechanical properties. To illuminate these effects a variable composition has been assigned by researchers to it, of the form

$$Tb_x\ Dy_{1-x}\ Fe_{2-\delta}$$

in which x, δ are numbers chosen at will. Also chosen as parameter is the dc bias field. We discuss the electromechanical performance of the alloy next.

B. Experimental Procedure

The method pursued in studying rare-earth magnetostrictive transducers is identical with that described in Sect. 7.8. One first constructs static magnetostriction curves to find the ratio $\Delta l/l$ and relative permeability μ_r versus dc bias field. Figure 7.11.1 shows $\Delta l/l$ vs. H for terbium-iron, dysprosium-iron and terbium-dysprosium-iron. The most noticeable feature is the small dc bias field needed (1 to 3 kiloersteds) to obtain $\Delta l/l$ ratios of the order of 1000×10^{-6}. Values of relative permeability will be shown later.

After performing tests for static properties the transducer is driven through resonance. In these tests the principal goal has been to determine the coefficient of electromechanical coupling, k. As noted in Sect. 2.33, the method requires the experimenter to measure the input impedance and admittance at each frequency of forced drive. An example of an impedance plot of X vs R taken on a bar of

the tertiary compound $Tb_{0.3}Dy_{0.7}Fe_2$, biased at 150 oersteds and driven by an ac drive of 2 oersteds rms. is shown in Fig. 7.11.2. The corresponding admittance plot based on the same data is shown in Fig. 7.11.3.

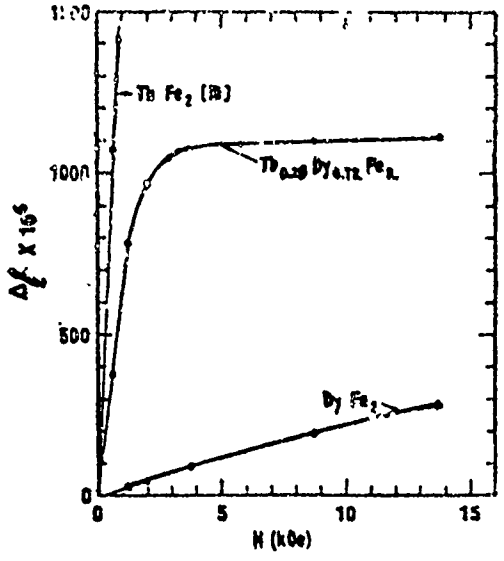


Fig. 7.11.1 — The static magnetostriction ($\delta l/l$) vs bias field (H) for $Tb_{.28}$ $Dy_{.72}$ Fe_2, Dy Fe_2, and single crystal Tb Fe_2. [10]

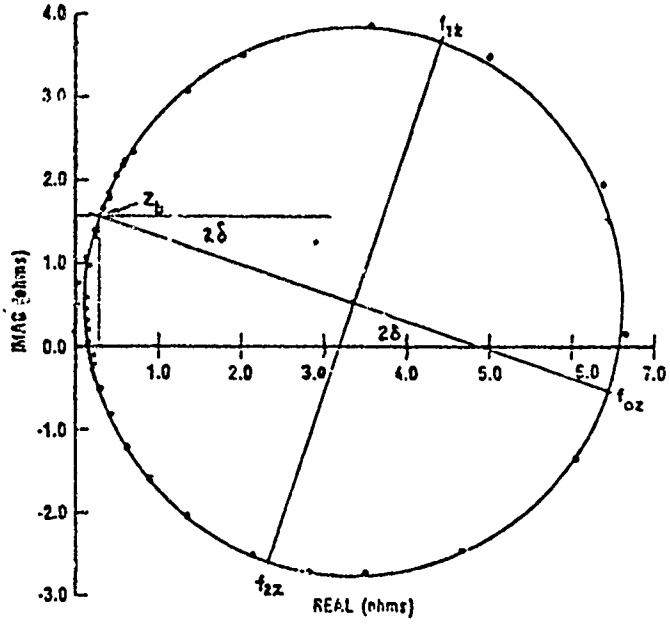


Fig. 7.11.2 — Impedance circle for $Tb_{.3}$ $Dy_{.7}$ Fe_2 at a bias field of 150 0e. The ac drive is 2 0e rms. The circle tilts at twice the loss angle $\delta(\delta \simeq 10°)$. [10]

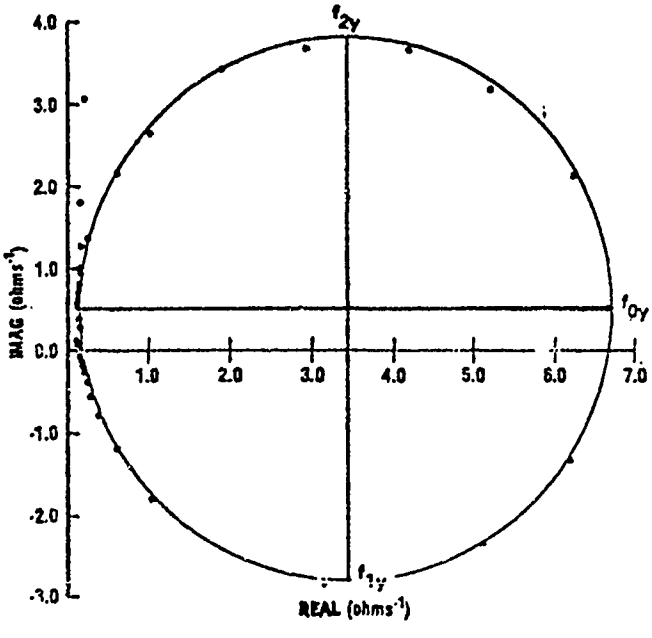


Fig. 7.11.3 — Admittance Circle fcr $Tb_{.3}Dy_{.7}Fe_2$ a a Bias of 150 0e. The same data was used to generate this circle as the one in Fig. 7.4.1. [10]

A first observation is that the impedance plot represents a drive at constant-H (that is, constant current) while the admittance plot represents a drive at constant-B (that is, constant voltage). The measured frequency f_{oy} determines the Young's modulus Y_B at constant-B which is that of the elastic bar independent of electromechanical coupling. The frequency f_{oz} determines the Young's modulus Y_H at constant-H. It includes the effect of electromechanical coupling. As explained in Sect. 2.10, the following relations of magnitude hold:

$$(1) f_{oy} > f_{oz}; (2)\, Y_B > Y_H.$$

The coupling factor itself is determinable from measurements on either plot. Referring to Eqs. 2.33.17, 2.33.20 one has:

$$k_{eff}^2 = \frac{D_Y}{B_c Q_Y}; K_{eff}^2 = \frac{1}{1 + \frac{X_c Q_Z}{D_Z}}. \tag{7.11.1}$$

D_y = diameter of the admittance circle X_c = core reactance

Q_y = $f_{oy}/f_{1y} - f_{2y}$ Q_Z = $f_{oz}/f_{2z} - f_{1z}$

B_c = core susceptance D_Z = diameter of the impedance circle

f_{1y}, f_{2y} = quadrantal frequencies on admittance circle f_{1z}, f_{2z} = quadrantal frequencies on impedance circle

From the discussion in Sect. 1.41 and Fig. 1.41.4b the frequencies f_{oz}, f_{oy} occur approximately at the maximum and minimum impedance. Hence, following the explanation given in Sect. 2.33,

$$K_{eff}^2 \simeq 1 - \left(\frac{f_{\max}}{f_{\min}}\right)^2. \tag{7.11.2}$$

The same measured data can be used to determine the material coefficient of electromechanical coupling by use of Eq. 1.42.7:

$$-R \cot R = k_{33}^2 \tag{7.11.3}$$

$$R = \frac{\pi}{2} \frac{f_{\min}(z)}{f_{\max}(z)}$$

A plot of measured Q_Y, Q_Z and computed k_{33} for $Tb_3\, D_{Y.7}\, Fe_2$ versus bias field is shown in Fig. 7.11.4. On this plot one also finds measured values of $\mu_r/10$. Compared to the relative permeability of nickel these values μ_r are very small, due physically to the very high values of $\Delta l/l$ for similar dc bias fields.

The difference between resonant frequency f_{oy} at constant induction, and resonant frequency f_{oz} at constant magnetic field intensity has been discussed in Sects. 2.10. For materials such as rare-earth magnetostrictive compounds, this difference is substantial. Figure 7.11.5 shows results of testing for this difference on $Tb_3DY_7Fe_2$. From this data one can calculate the Young's moduli Y^H, Y^B based on a knowledge of the mass density of the alloy. It is found that Y^H changes from 4.5 to 11 ($10^{10} N/m^2$) as the bias changes from zero to 4.5 *kOe*. Thus the $\Delta E/E_0$ effect is very pronounced.

Variations in alloy composition induce marked variation in (static) material coupling k_{33}. Figure 7.11.6 shows how small changes in the amount of iron in $T6_{.27}D_{Y.73}Fe$ affect this material coupling factor.

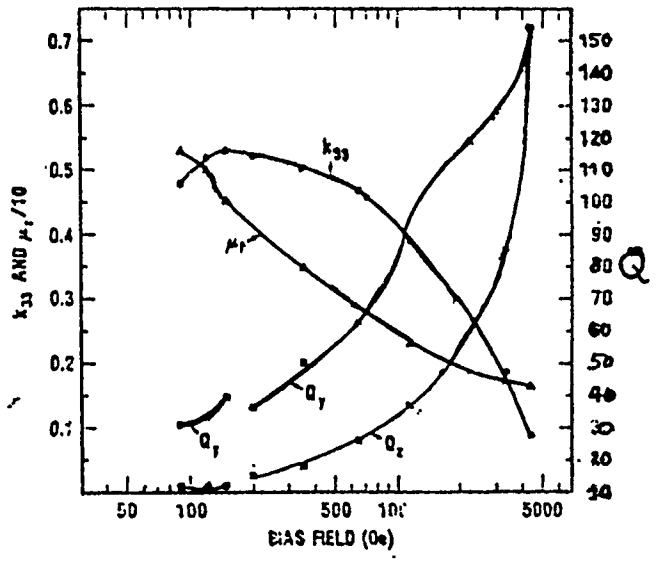


Fig. 7.11.4 — Coupling factor k_{33}, Q factor and relative permeability in $Tb_{.3}$ $Dy_{.7}$ Fe_2 as a function of bias field [10]

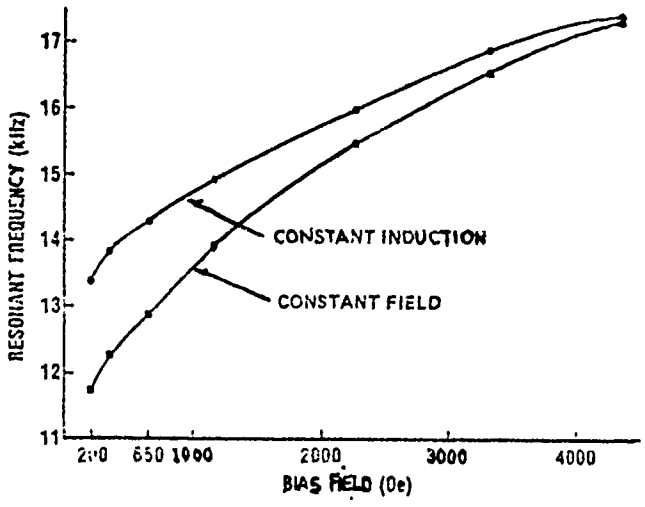


Fig. 7.11.5 — Resonant frequency at constant induction, and at constant field, vs bias field of a 3.9 inch long bar of $Tb_{.3}$ $Dy_{.7}$ Fe_2. [10]

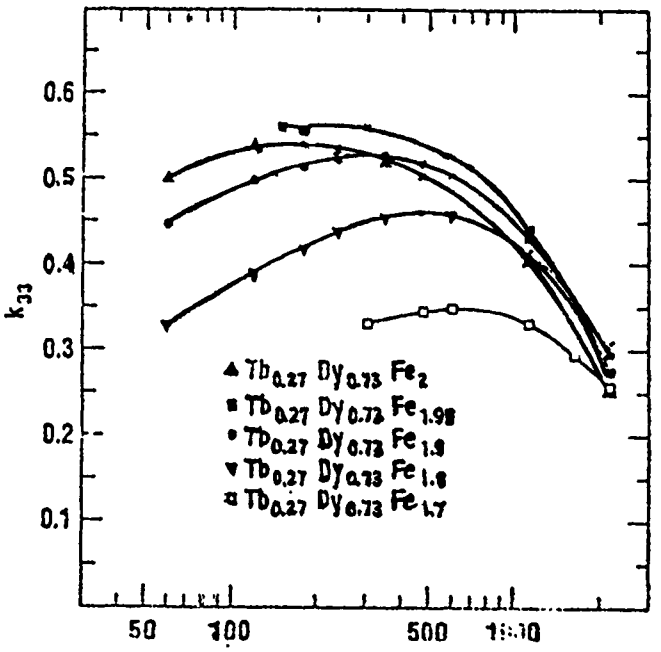


Fig. 7.11.6 — Coupling factor k_{33} vs bias field for $Tb_{.27}Dy_{.73}Fe_{2-\delta}$[10]

C. Discussion

Rare-earth magnetostriction transducers are currently constructed of short rods of the material. In them dc bias fields are provided by electric batteries or by permanent magnets. Because of the large value of material coupling there is a potential advantage of high power delivery for manageable dc bias. However the rods are quite brittle and special precautions are needed to avoid fracture at high drive.

REFERENCES

[1] "Ultrasonic Transducers," Y. Kikuchi ed., Corona Publishing Co. Ltd., Tokyo (1969).

[2] K.I. Arai et al., IEEE Trans. Mag-12, 1976, p. 936.

[3] M.A. Mitchell et al., IEEE Trans. Vol. Mag-14, p. 1169 (1978).

[4] N. Tsuya, K.I. Arai, J. Appl. Phys. Vol. 49, 1718-1720, April 1978.

[5] B.S. Berry, W.C. Pritchit, Phys. Rev. Lett. Vol. 34, p. 1022 (1975).

[6] K.I. Arai et al., IEEE Trans Mag-12, pp. 936-1018 (1976).

[7] C. Modzelewski et al., IEEE Trans Mag-17, p. 2837 (1981).

[8] A.E. Clark, H.S. Belson, Conf. on Mag. and Mag. Mat'ls, Nov. 1971, AIP Conf. Proc. **5**, 1498 (1972), Phys. Rev. B5, 3142 (1972), IEEE Trans. Mag-8. 477 (1972). N.C. Koon, A Schindler, F. Carter, Phys. Lett. **374**, 413 (1971).

[9] A.E. Clark, Conf. on Mag. and Mag. Mat'ls, Nov. 1973, AIP Conf. Proc. **18**, 1015 (1974).

[10] H.T. Savage et al., IEEE Trans. Magnetics Vol. 11, Sept. 1975, p. 1355.

Chapter 8
DIRECTIONAL HYDROPHONES

8.1 PARTICLE VELOCITY AND PRESSURE GRADIENT AT A POINT IN AN ACOUSTIC FIELD

In the small amplitude theory of acoustc fields the acoustic pressure p (r) is derivable from the velocity potential $\phi(\mathbf{r}, t)$ of the field according to the formula,

$$p(\mathbf{r}, t) = \rho_0 \frac{\partial}{\partial t} \phi(\mathbf{r}, t) \tag{8.1.1}$$

in which ϕ has the units of m^2/s and ρ_0 is the (constant) mass density of the fluid. The gradient of this pressure is then

$$\nabla p(\mathbf{r}, t) = \rho_0 \frac{\partial}{\partial t} \nabla \phi (\mathbf{r}, t). \tag{8.1.2}$$

Since the law of motion requires that the gradient of the pressure be equal to the negative of the mass acceleration,

$$\nabla p(\mathbf{r}, t) = -\rho_0 \frac{\partial}{\partial t} \mathbf{u}(\mathbf{r}, t) \tag{8.1.3}$$

it is seen that the particle velocity u is given by,

$$\mathbf{u} = -\nabla\phi. \tag{8.1.4}$$

One concludes: *a measurement of the gradient of the pressure field at a point can be interpreted as the time-derivative of the particle velocity multiplied by a constant.*

As an example we take the field of a point (monopole) source and choose its potential for outgoing waves to be,

$$\phi(r, t) = \frac{A_s}{r} \cos k(r - ct) \qquad \text{(units: } m^2/s) \tag{8.1.5}$$

in which A_s is in units of m^3/s. The the radial component of particle velocity is

$$u = -\frac{\partial\phi}{\partial r} = \frac{A_s k}{r} \sin k(r - ct) + \frac{A_s}{r^2} \cos k(r - ct). \tag{8.1.6}$$

Similarly, the pressure field developed by this monopole is,

$$p = \rho_0 A_s kc \frac{\sin k(r - ct)}{r}. \tag{8.1.7}$$

The gradient (at a point) of this pressure in the direction of the radius (going out from the source) is

$$\frac{\partial p}{\partial r} = \rho_0 A_s kc \left\{ \frac{kr \cos k(r - ct) - \sin k(r - ct)}{r^2} \right\} \tag{8.1.8}$$

By use of Eq. 8.1.6 one sees that

$$\frac{\partial p}{\partial r} = -\rho_0 \frac{\partial u}{\partial t} \tag{8.1.9}$$

as required.

A hydrophone constructed to respond to pressure gradient $\partial p/\partial r$ *at a single point* will therefore measure the temporal derivative of the radial particle velocity. This is the general case.

The case of a plane wave sound field is somewhat different. We choose a velocity potential of a single harmonic wave:

$$\phi = -A_p \exp ik(x - ct) \qquad \text{(units: m}^2\text{/s)} \tag{8.1.10}$$

from which one may find both pressure and velocity

$$p = ikc\ A_p \rho_0 \exp ik(x - ct)$$

$$u = ik\ A_p \exp ik(x - ct). \tag{8.1.11}$$

The gradient of the pressure field is then

$$\frac{\partial p}{\partial x} = \rho_0 (ikc) u. \tag{8.1.12}$$

The pressure-gradient in the direction of propagation here is directly proportional to the particle velocity. Thus a hydrophone constructed to measure pressure gradient at a point actually measures particle velocity multiplied by a frequency-dependent constant only if the sound wave is planar. Clearly Eq. 8.1.12 is a particular case of Eq. 8.1.9. Except for this case of plane waves a pressure-gradient hydrophone actually measures not the particle velocity but rather its time-derivative.

8.2 PRESSURE-DIFFERENCE BETWEEN TWO POINTS IN A SOUND FIELD

We consider next the measurement of pressures between two points in the sound field separated by a distance Δx. For simplicity we take the points to be on a radial line in a spherical sound field and imagine the hydrophone to be a small cylinder $\Delta x/2$, $-\Delta x/2$, with a local origin at its center, Fig. 8.2.1. Since the pressure at any point is given by Eq. 8.1.7 the pressure difference between two points $r \pm \Delta x/2$ is

$$p_1 - p_2 = \rho_0 A_s kc \left\{ \frac{\sin k\left[r + \frac{\Delta k}{2} - ct\right]}{r + \frac{\Delta x}{2}} - \frac{\sin k\left[r - \frac{\Delta x}{2} - ct\right]}{r - \frac{\Delta x}{2}} \right\}. \tag{8.2.1}$$

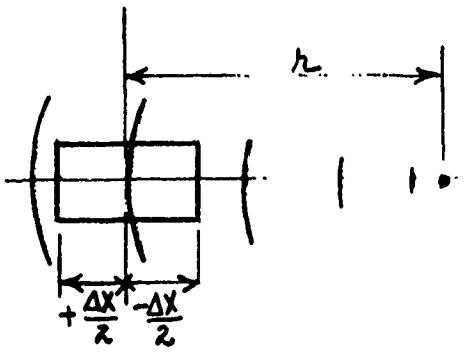


Fig. 8.2.1 — Geometrical relations of a pressure-gradient hydrophone which measures pressures at $r \pm \Delta x/2$

By use of trigomometrical identities one finds that

$$\Delta p = p_1 - p_2 = \rho_0 A_s k c \left\{ \frac{2r \cos k(r - ct) \sin \left(k \frac{\Delta x}{2} \right) - \Delta x \sin k(r - ct) \cos k \frac{\Delta x}{2}}{r^2 - \left(\frac{\Delta x}{2} \right)^2} \right\}. \quad (8.2.2)$$

If the cylinder in Fig. 8.2.1 is at angle θ with the radial line r then $\frac{k\Delta x}{2}$ is to be replaced by $\frac{k\Delta x}{2} \cos \theta$. Comparison of this result with both Eqs. 8.1.8 and 8.1.6 shows that the difference between the pressures at two distinct points not only disagrees with the pressure gradient at a point midway between them but also is not proportional to particle velocity.

In application however one usually chooses size and wavelength such that

$$r^2 >> \left(\frac{\Delta x}{2} \right)^2 ; \; k \frac{\Delta x}{2} = \frac{2\pi}{\lambda} \frac{\Delta x}{2} << 1. \quad (8.2.3)$$

Then,

$$\frac{\Delta p}{\Delta x} \simeq \rho_0 A_s k c \left\{ \frac{kr \cos k(r - ct) - \sin k(r - ct)}{r^2} \right\}. \quad (8.2.4a)$$

Since the right hand side is independent of Δx it is seen by consulting Eq. 8.1.8 that as Δx becomes infinitesimal,

$$\frac{\Delta p}{\Delta x} \text{ approaches } \frac{\partial p}{\partial x}$$

as it should. In the far-field the term in $1/r^2$ vanishes, and

$$\frac{\Delta p}{\Delta x} \simeq \rho_0 A_s k^2 c \frac{\cos k(r - ct)}{r} = -\rho_0 \frac{d}{dt} A_s k \frac{\sin k(r - ct)}{r}. \quad (8.2.4b)$$

From this one deduces that the radial particle velocity, averaged over distance Δx, is

$$u_r = A_s k \frac{\sin k(r - ct)}{r}. \tag{8.2.4c}$$

The plane-wave case exhibits other features. Suppose we *select* a velocity potential $\phi(x, t)$ at a point in a plane-wave field traveling to the right,

$$\phi = A_p \cos k(x - ct) \qquad \text{(units: } m^2/\text{s)}. \tag{8.2.5}$$

The acoustic pressure is then,

$$p = \rho_0 \frac{\partial \phi}{\partial t} = \rho_0 kc\, A_p \sin k(x - ct). \tag{8.2.6}$$

Thus, the difference in pressure between two points in the field for a plane wave incident at angle θ with the line joining the points is,

$$\Delta p = p_1 - p_2 = \rho_0 kc\, A_p \left\{\sin k\left(\frac{\Delta x}{2}\cos\theta - ct\right) - \sin k\left(-\frac{\Delta x}{2}\cos\theta - ct\right)\right\} \tag{8.2.7}$$

in which we have suppressed distance x as being common to both points. (This suppressed term can be inserted by replacing-kct with $kx - kct$ in all subsequent equations of this development.) By use of trigonometric identities one easily finds that,

$$\Delta p(\Delta x, t, \theta) = 2\rho_0 kcA_p \cos kct \sin\left(\frac{k\Delta x}{2}\cos\theta\right). \tag{8.2.8a}$$

Thus the net force acting over a small area S_x is

$$f_{\text{net}}(\Delta x, t, \theta) = S_x \Delta p. \tag{8.2.8b}$$

The sine term in Eqs. 8.2.8 is analogous to the phase delay between two point receivers in a line array. It occurs frequently in antenna theory.

We next suppose this pressure difference accelerates a mass m of fluid in the x-direction, and if there is viscosity η, overcomes (in addition) the viscous drag, so that

$$f_{\text{net}}(\Delta x, t, \theta) = m \frac{d}{dt} u_x + \eta u_x. \tag{8.2.9}$$

For simplicity we neglect viscosity. Noting that $kc \cos kct = (d/dt) \sin kct$ we solve for to average velocity of the mass,

$$u_x(\Delta x, t, \theta) = \frac{2\rho_0 S_x A_p}{m} \sin kct \sin\left(\frac{k\Delta x}{2}\cos\theta\right). \tag{8.2.10}$$

In comparison it is noted that the particle velocity in the x-direction of a plane wave incident at angle θ at a point midway between the two receivers is derived from from Eq. 8.2.5 to be

$$u_x = A_p\, k \cos\theta \sin k(x - ct). \tag{8.2.11}$$

Thus in general the average velocity of a mass m accelerated by acoustic pressure difference between two points in a plane wave field is not equal to the particle velocity of the acoustic field taken midway between. However if in Eq. 8.2.10 one allows the condition,

$$\sin\left[\frac{k\Delta x\cos\theta}{2}\right] \rightarrow \frac{k\Delta x}{2}\cos\theta$$

and if one restores kx in the manner noted earlier, one has

$$u_x = \left[\frac{\rho_0 S_x \Delta x}{m}\right] A_p k\cos\theta\sin k(x-ct). \tag{8.2.12}$$

Thus, even if the separation between points is very small the velocity of mass m is not the particle velocity of the medium in the acoustic field, unless m is exactly a unit mass of the fluid (rather than a unit mass of material other than the fluid).

8.3 PRESSURE DIFFERENCE BETWEEN TWO PAIRS OF POINTS ORIENTED IN AN ARBITRARY DIRECTION

We consider two pairs of points in a plane, located in a spherical sound field, and arbitrarily oriented relative to each other. The distance between the points of each pair is Δx, and the distance between pairs is Δx_2. The pressure difference between pairs is then *approximated* by,

$$\Delta p_{12} = \frac{\partial}{\partial r_2}\left[\left[\frac{\partial p}{\partial r_1}\right]\Delta x_1\right]\Delta x_2. \tag{8.3.1}$$

Equation 8.2.4a serves here to allow us to make the following identity for expressing the pressure difference in one pair,

$$\Delta p = \left[\frac{\partial p}{\partial r_1}\Delta x_1\right] \equiv \rho_0 A_s kc\left\{\frac{kr\cos k(r-ct) - \sin k(r-ct)}{r^2}\right\}\Delta x_1\cos\theta_1 \tag{8.3.2}$$

in which we have included the orientation angle θ_1. Between two pairs we use Eq. 8.3.1. Assuming Δx_2 very much smaller than r_1 or r_2, and assuming $r_1 \simeq r_2 = r$, one finds by a second spatial differentiation that

$$\Delta p_{12} = \cos\theta_1\cos\theta_2\,\rho_0 A_s kc\,\Delta x_1\Delta x_2\left\{\left[\frac{2-k^2r^2}{r^3}\right]\sin k(r-ct) - \frac{2kr}{r^3}\cos k(r-ct)\right\}. \tag{8.3.3}$$

When the orientation of pairs is not in a plane one can specify them by the 3 dimensional spherical angles θ, ϕ. Equation 8.3.3 defines a quadropole sound receiver in a plane. The process by which it is obtained can be repeated indefintely. Thus, writing the expression for the pressure field of a monopole point source as the real part,

$$p = \mathrm{Re}\left\{-i\rho_0 A_s kc\,\frac{e^{ik(r-ct)}}{r}\right\} \tag{8.3.4}$$

(see Eq. 8.1.7), it is seen that the nth order pressure difference is approximately,

$$\Delta p_n = \frac{\partial^n}{\partial r_1 \partial r_2 \cdots \partial r_n} \left(- i \rho_0 A_s kc \frac{e^{ik(r-ct)}}{r} \right) (\cos \theta_1 \cos \theta_2 \cdots \cos \theta_n) \Delta x_1 \Delta x_2 \cdots \Delta x_3 \quad (8.3.5)$$

provided all the pairs are arbitrarily oriented in a plane [1].

Microphones and hydrophones can be constructed to implement Eq. 8.3.5. They are called *n*th order pressure-gradient transducers. In these applications the reception of sound can be made highly directional. Hence they serve to redue noise coming from all external sources not on the main beam of reception.

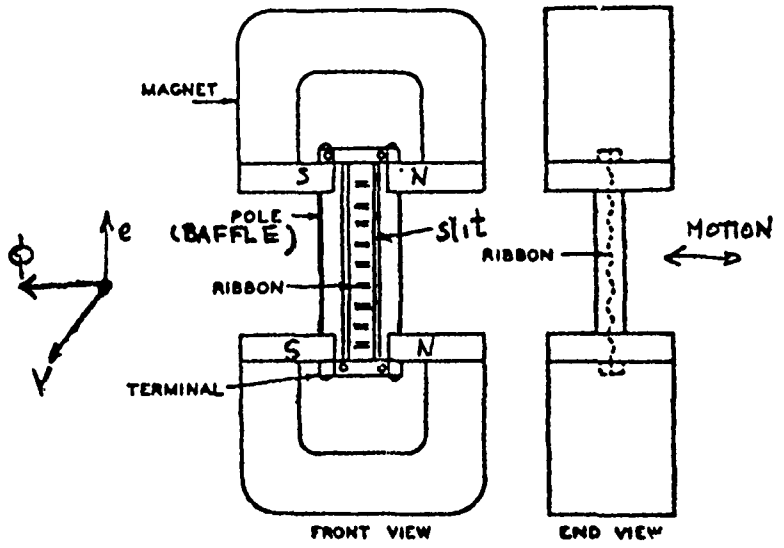


Fig. 8.4.1 — The essential elements of a velocity microphone ϕ = flux; v = velocity; e = electric potential

8.4 "PRESSURE-GRADIENT" MICROPHONE AND ITS EQUIVALENT CIRCUIT IN ELEMENTARY FORM

A thin compliant strip (or ribbon) of conducting metal is suspended in the air gap between the poles of a permanent magnet. Under the action of a differential pressure of an acoustic field it vibrates in a direction normal to the magnetic flux linkages thus generating an electric potential between its ends. Figure 8.4.1 shows the essential elements of a pressure gradient microphone constructed on this principle. To insure sufficient motion for obtaining a useful voltage output one must observe these precautions:

(a) The ribbon must be fixed in massive supports which do not move themselves in the presence of acoustic forces.

(b) The ribbon must be surrounded by a rigid baffle of large enough acoustic size (that is, large effective *ka)* to permit development of a useful pressure difference between the front and back of the ribbon.

The baffle is very important: it acts as a diffraction obstacle which increases the pressure field in the direction of greatest reflection thus enlarging the pressure difference between front and back.

The operation of this transducer in elementary form an be represented by an equivalent circut with elements of both mechanical and acoustical character. A minimum list of such elements is:

(1) The acoustic radiation impedance $\mathfrak{z}_1$, $\mathfrak{z}_2$, (units: Ns/m^5) of front and back respectively of the ribbon.

(2) The acoustic impedance $\mathfrak{z}_s$ of the slits between the ribbon and the pole pieces.

(3) The acoustic impedance $\mathfrak{z}_M$ of the ribbon.

(4) The transduced electrical impedance Z_{ME} taken to be an equivalent acoustic impedance in series with $\mathfrak{z}_M$.

The procedure for constructing the equivalent circuit follows the method outlined in Chapter 1 of this treatise (Sections 1 through 1.20):

- First, the number of 'degrees of freedom' (meaning here the number of independent volume velocities) is determined. In approximation, there are here two such velocities, that of the air in the slits, q_s, and that of the ribbon, q_M.

- The acoustic pressure relations involving the applied pressure p_1 of the frontside incident wave, p_2 of the backside diffracted wave, and the surface pressures p_f, p_b, are written out. These are,

$$\begin{aligned} &\text{(a)}\quad p_1 = \mathfrak{z}_z q_R + p_f \\ &\text{(b)}\quad p_f - p_b = z_M q_M = \mathfrak{z}_z q_s \\ &\text{(c)}\quad p_b = \mathfrak{z}_2 q_R + p_2 \end{aligned} \tag{8.4.1}$$

- The relations between acoustic volume velocities are determined. There is one (nodal) relation,

$$q_R = q_M + q_s \tag{8.4.2}$$

- An electrical/acoustical analogy is selected. Here the choice is made to allow pressure to be the across-variable and volume velocity to be the through-variable. Using this analogy one finds from Eq. 8.4.1a that $\mathfrak{z}_1$ is in series; from Eq. 8.4.1b that $\mathfrak{z}_m$ and $\mathfrak{z}_s$ are in parallel with each other but this parallel branch is in series with $\mathfrak{z}_1$; from Eq. 8.4.1c that $\mathfrak{z}_2$ is in series with this parallel branch. Figure 8.4.2 shows the equivalent circuit. The transduced impedance Z_{ME} is deliberately given a form so that it is made to be in series with z_M. While the lementary circuit is simple in appearance the values to be assigned to the circuit elements are difficult to formulate. We consider these in turn.

A. Radiation Impedance of Vibrating Strip

Let the velocity potential anywhere on the strip be $\phi(\mathbf{r}')$. This potential generates a surface pressure at point $\mathbf{r}'$ on the strip, of value

$$p(\mathbf{r}') = \rho \frac{\partial \phi}{\partial t}(\mathbf{r}'). \tag{8.4.3}$$

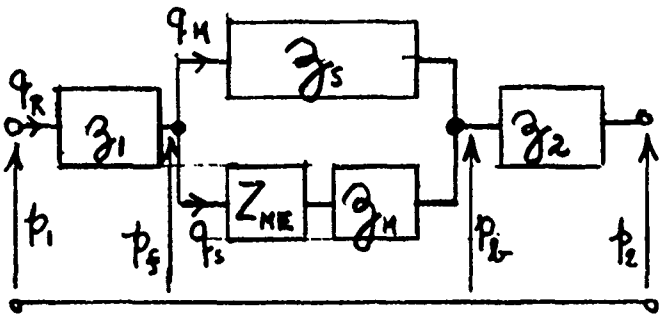


Fig. 8.4.2 — A schematic equivalent circuit of the acoustical part of a pressure-gradient microphone with coupled electrical impedance. Symbols are defined in the text.

An elementary model of ϕ assumes it to be a *simple source* in steady state. Then, for a velocity $v(r_0, \tau)$ the presure distribution on all points of the surface (both front and rear) on the surface is,

$$p(r') = \rho j\omega \iint v(r_0, \tau) \frac{\exp -jk|r' - r_0|}{4\pi|r' - r_0|} dS(r_0). \tag{8.4.4}$$

For simplicity let $v(r_0) = v_0 \exp(j\omega t)$. The total force (on surface S of both front and rear) is

$$F(\omega) = j\omega\rho v_0 \exp(j\omega t) \iint dS(r') \iint \frac{\exp(-jk|r' - r_0|)}{4\pi|r - r_0|} dS(r_0). \tag{8.4.5}$$

We define the mechanical radiation impedance as the peak force divided by the peak velocity,

$$Z_{RAD} = \frac{F(\omega)}{v_0} = R_{RAD} + j X_{RAD} \qquad \text{(units: } Ns/m\text{)}. \tag{8.4.6}$$

The acoustic (radiation) impedance is

$$\mathcal{Z}_A = \frac{Z_{RAD}}{S^2}. \tag{8.4.7}$$

An evaluation of the integral of Eq. 8.4.5 for the case of a finite length ribbon in a finite baffle is exceptionally difficult. Generally one must use the techniques of numerical integration, including special consideration for the singular point $r' = r_0$. A rough model for which Z_A is known, is the acoustic impedance for both sides of a circular disk of radius a in free space,

$$\mathcal{Z}_A = 0.01901\, a^2 \rho_0 \omega^4/c^3 + j\omega\, 0.2705\rho_0/a \qquad \text{(units: } Ns/m^5\text{)}. \tag{8.4.8}$$

At very low frequency this impedance is almost purely reactive. In this case the air load appears as an acoustic mass. While the model of Eq. 8.4.8 can serve to indicate this mass reactance another approach to modeling is to consider the load on *one* side of the ribbon to be same as that of a piston at the end of a long tube,

$$\mathcal{Z}_A \simeq j\omega M_A$$

$$M_A = 0.1952 \frac{\rho_0}{a} \quad \text{(units: } Ns^2/m^5\text{)} \tag{8.4.8b}$$

(see Fig. 1.7.6b). More accurate models are discussed in the next section.

B. Acoustic Impedance of a Slit

This is modeled on the theory of the flow of air through a very narrow duct-a process which includes consideration of viscosity effects arising from friction of the air molecules between themselves and walls. For a slit t meters wide, l meters deep (in the direction of flow) and w meters high normal to the flow the acoustic impedance is

$$z_s = \frac{12\,\eta l}{t^3 w} + j\,\frac{6\,\rho_0\,l}{5wt}\,\omega \quad \text{(units: } Ns/m^5\text{)} \tag{8.4.9}$$

[2]
where

η = dynamic viscosity coefficient (units: Ns/m^2)

At 20°C and 0.76 m Hg, the values of η for air and water are,

air: $\eta = 1.86 \times 10^{-5}$

water: $\eta = 1.0 \times 10^{-3}$.

C. Acoustic Impedance of the Ribbon

We assume the ribbon can be modeled as a flat plat length a, width b, thickness h, Young's modulus E, Poisson's ratio ν, clamped at its (long) ends, with the total mass M concentrated at the center and the total flexural stiffness K determined by the first resonant frequency ω_r in flexure,

$$\omega_r^2 = \frac{K_p}{M_p}$$

$$M_p = \rho_p ab \ (\rho_p = \text{mass of plate per unit area}) \tag{8.4.10}$$

$$K_p = D\left[\frac{b}{a^3}\right]\frac{16\pi^4}{3};\ D = \frac{Eh^3}{12(1-\nu^2)}.$$

In the analogy being used here the acoustic impedence of the ribbon is therefore,

$$\mathfrak{z}_M = j\omega\,\frac{M_p}{S^2} + \frac{K_p}{j\omega S^2} \quad \text{(units: } Ns/m^5\text{)}. \tag{8.4.11}$$

The resistance (= real part of $\mathfrak{z}_M$) of the plate due to internal frictional damping is not considered here, but may be included as a percentage (of the order of a few percent) of the stiffness reactance.

D. Transduced Electrical Impedance Z_{ME}

The appropriate form of Z_{ME} is derived from physical consideration of the transduction mechanism. For the pressure-gradient microphone shown in Fig. 8.4.1 the transduction is electrodynamic, meaning that the voltage developed (e) is proportional to the mechanical velocity (v) of the ribbon in the x-direction of motion,

$$e = Blv = Blq_R S \tag{8.4.12}$$

in which B is the induction and l is the length of conduction ribbon exposed to the flux field. In turn v is equal to the pressure difference created by the incident acoustic wave driving the ribbon, divided by the mechanical impedance of the ribbon and air composite structure. Thus the voltage e is proportional to this pressure-difference. This physical requirement leads natrally to the representation of the equivalent circuit of Fig. 8.4.2 in its dual form. To obtain the dual Eqs. 8.4.1 are inverted by solving for the volume velocity (which is taken to be the across-quantity of the dual circuit) in terms of the pressures (which are taken to be the across-quantities):

$$\text{(a)}\quad q_R = \frac{p_1 - p_f}{\mathfrak{z}_1} = \frac{p_b - p_2}{\mathfrak{z}_2}$$

$$\text{(b)}\quad q_M = \frac{p_f - p_b}{\mathfrak{z}_m} \quad ; \quad \mathfrak{z}_m = \frac{Z_{ME} z_M}{Z_{ME} + z_M} \tag{8.4.15}$$

$$\text{(c)}\quad q_s = \frac{p_f - p_b}{\mathfrak{z}_s}.$$

Here, Eq. (a) represents two branches in parallel, while (b) and (c) represent two branches in series. Since $q_R = q_M + q_s$ it is concluded that (b) plus (c) equal (a). The equivalent circuit which is the dual of Fig. 8.4.2 is shown in Fig. 8.4.3.

Equation 8.4.12 shows that the transduction ratio is $\phi = BlS$. Hence from Sects. 2.35 and 2.36 the value of Z_{ME} is $Ze'/(BlS)^2$.

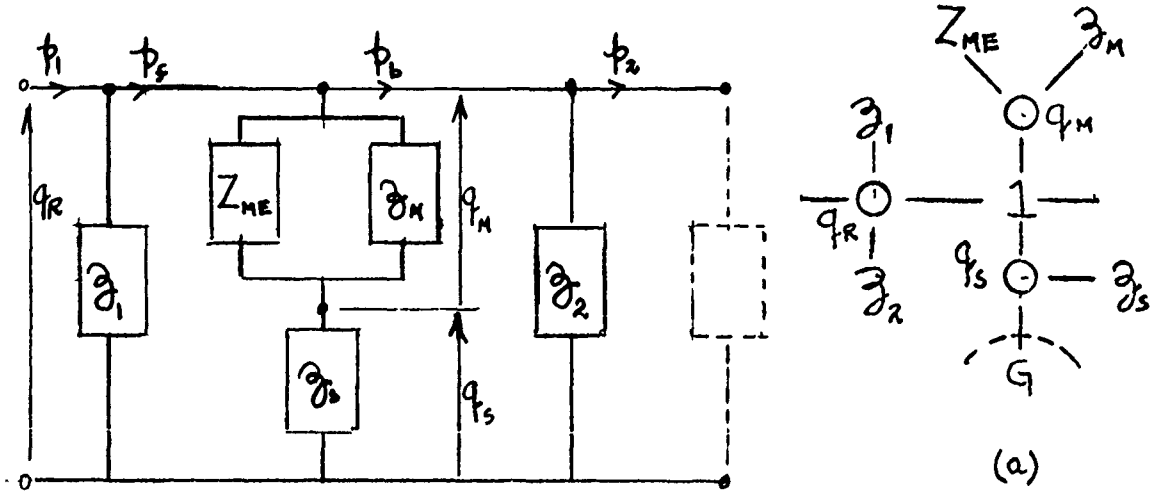


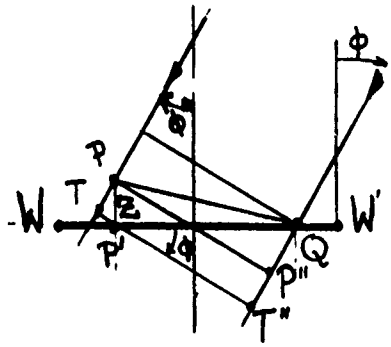
Fig. 8.4.3 — Dual of Fig. 8.4.2 with added electrical mesh. (a) Bond graph, (b) standard equivalent circuit.

8.5 DIFFRACTION EFFECTS IN PRESSURE-GRADIENT MICROPHONES

The pressure difference at the center of the ribbon, between front and rear sides caused by diffraction of an incident wave is the driving force which generates motion. The pressure on the side facing the source is increased by reflection and diffraction in a manner dependent on the ratio of the size of the ribbon relative to the wavelength, while the pressure field at the center in the rear is nearly the same as or is materially less than the incident wave. Thus the acoustic size of the ribbon and its associated baffle is crucial in the design of microphones based on the pressure-gradient principle, because it determines the magnitude of the driving force.

A. Approximate Diffraction Field of a Circular Plat

We idealize the ribbon to be a circular plate radius a, Fig. 8.5.1. When viewed on edge the plate is a line WW'. On the plate there is an arbitrary point Q which reflects the plane wave coming in at angle ϕ and direction s. The field point is taken to be P, located at distance z from the plate. Distance PP' is the *transverse* distance between the ray at P and the ray at Q.



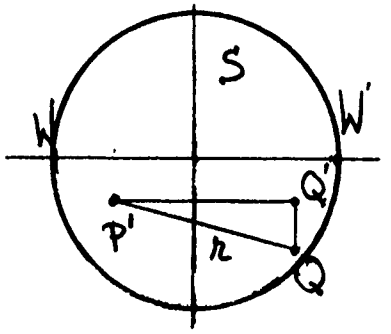


Fig. 8.5.1 — Geometrical layout of a circular plate undergoing diffraction from a plane wave of sound incident of angle ϕ

The incident plane wave is

$$\Phi_P = \Phi_0 \exp j(\omega t - \mathbf{k} \cdot \mathbf{s}) \tag{8.5.1}$$

in which $\mathbf{k}$ is the propagation wavevector. The corresponding z-component of particle velocity is,

$$\dot{w}_{inc} = jk \cos \phi \Phi_P.$$

To calculate the reflection one uses the classical procedure of endowing each point Q with an arbitrary velocity $\dot{w}_s$ normal to the plate surface S, so chosen as to satisfy a reflection boundary condition. For simplicity, let the surface be acoustically rigid. Then we choose

$$\dot{w}_s = -\frac{\partial \Phi_P}{\partial z} = jk \cos\phi \Phi_P \tag{8.5.2}$$

$$k = |\mathbf{K}|.$$

In this formula the spatial phase of Φ_P must be determined in the coordinate system shown in the figure. This is given by the product of k and distance $P''Q$. Now,

$$P''Q = P'Q \sin\phi - TP''$$

$$TP'' = TP = z \cos\phi$$

$$P'Q = r \cos\theta.$$

Thus reversing the phase of $\dot{w}_s$ in order to cancel $\dot{w}_T$ on the surface one has.

$$\dot{w}_s = jk \cos\phi \Phi_0 \exp j[\omega t - k(-r \cos\theta \sin\phi + z \cos\phi)].$$

The calculation of the scattered wave field for arbitrary baffle size is very tedious. A useful model may however be constructed by assuming this field to be the same as the field of a circular plate radiating from an infinite rigid baffle. For an arbitrary field point $P_\phi(r, z)$ at distance $\rho = \sqrt{(r - r_0)^2 + z^2}$ from (surface) point $Q(r_0, \theta_0)$ the potential function of radiation is,

$$dG(\rho) = \frac{\dot{w}_s e^{-jk\rho}}{2\pi\rho} dS(r_0, \theta_0) \qquad \text{(units: m}^2\text{/s)}. \tag{8.5.3}$$

The scattered field, approximated in this way, is found by integration over all the area of the plate

$$\Phi(r, z) = jk \cos\phi \Phi_P e^{-ikz\cos\phi} \int_0^{2\pi} \int_0^{R(\theta_0)} \frac{e^{-ik\rho}}{2\pi\rho} e^{+ikr_0\cos\theta_0\sin\phi} r_0 dr_0 d\theta_0. \tag{8.5.4}$$

The symbol $R(\theta)$ indicates the general case of a plate in which the distances from the edges of the plate vary with angle θ. For the case of a circular plate $R(\theta) = a =$ constant. Since the total field is

$$\Phi = \Phi_p + \Phi_s$$

the *relative* pressure field at any point (r, z) is given by the ratio

$$\frac{p_\phi(r, z)}{p_{\text{inc}}(\phi)} = \frac{\Phi}{\Phi_p} = 1 + \frac{\Phi_s}{\Phi_p}.$$

We choose now a field point at the center of the plate, where $r = 0$. Then, on the surface one sets $z = 0$, $\rho = r_0$. Integrating over r_0 from 0 to a, one obtains,

$$\frac{p_\phi(0, 0)}{p_{\text{inc}}(\phi)} = 1 + \frac{\cos\phi}{2\pi} \int_0^{2\pi} \frac{1 - e^{-ika(1-\sin\phi\cos\theta)}}{1 - \sin\phi\cos\theta} d\theta. \tag{8.5.5}$$

The integral can be evaluated by use of Bessel functions of the first kind. Sivian and O'Neil [3] performed the integration and obtained the result,

$$\frac{p_\phi(0,\,0)}{P_{\text{inc}}(\phi)} = 1 + \frac{\cos\phi}{\sqrt{1-\sin^2\phi}}\left[1 - e^{jka}\sum_{m=0}^{\infty}\epsilon_m j^m\left(\frac{1-\sqrt{1-\sin^2\phi}}{\sin\phi}\right)^m J_m(ka\,\sin\phi)\right]$$

$$\epsilon_0 = 1; \quad \epsilon_m = 2 \text{ for } m \neq 0. \tag{8.5.6}$$

The factor

$$\cos\phi/\sqrt{1-\sin^2\phi} = \pm 1$$

is written in the manner to indicate the two possible values shown.

Two important special cases of Eq. 8.5.5 are $\phi = 0$, $\phi = \pi$. For the choice of normal incidence at $\phi = 0$,

$$\frac{p_0(0,\,0)}{P_{\text{inc}}(0)} = 1 + \cos\phi(1 - \exp - jka) = 2 - \exp(-jka) \tag{8.5.7}$$

where

$$\left|\frac{p_0(0,\,0)}{P_{\text{inc}}(0)}\right| = \sqrt{5 - 4\cos ka}$$

while for normal incidence $\phi = \pi$,

$$\frac{P_{180}(0,\,0)}{P_{\text{inc}}(\mathbf{v})} = \exp(-jka) \tag{8.5.8}$$

where

$$\left|\frac{P_{180}}{P_{\text{inc}}(\pi)}\right| = 1.$$

Thus on the surface the ratio of acoustic pressure on the front side to that on the back side, when both are referred to the center of the circular disk, is,

$$\left|\frac{P_0}{P_{180}}\right| = \frac{\sqrt{5 - 5\cos ka}}{1}. \tag{8.5.9}$$

In particular, when ka is an odd multiple of π the magnitude $|P_0/P_{180}| = 3$, while when ka is an odd multiple of $\pi/2$ $|P_0/P_{180}| = 1$. The sinusoidally time varying pressure differential is seen to be 3× the incident pressure when the radius of the rigid circular plate is an odd number of half wavelengths. On the other hand when the radius is an even number of wavelengths the front and back pressures at the center are the same. Figure 8.5.2 is a graphic representation of these relations: curve 0° represents the surface pressure facing the oncoming wave while curve 180° represents the surface pressure on the backside, shielded from the oncoming wave.

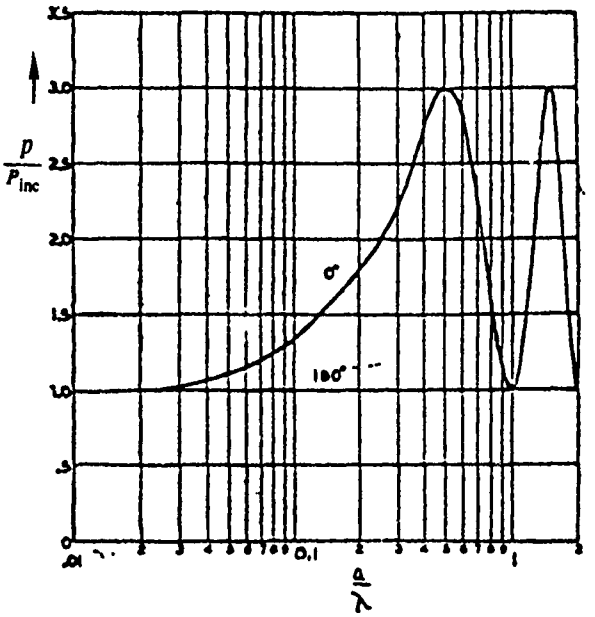


Fig. 8.5.2 — Computed pressure frequency characteristic, at the center, on the front and the back of a circular baffle for normal incidence of the impinging sound wave [4].

B. Approximate Diffraction Field of a Square Rigid Plate

From Eq. 8.5.4 it is seen that when $\phi = 0$ (normal incidence) the potential field at the center of the plate depends on the evaluation of the integral,

$$\int_0^{2\pi} e^{-jkR(\theta_0)}\, d\theta_0.$$

Reference [3] performed the evaluation by numerical means for the case of a square plate in air 11.5 cm on edge excited by a normally incident wave. Figure 8.5.3a shows the computed pressure for the case $\phi = 0$. Here curve *F* represents the pressure (ratio) facing the oncoming wave. The pressure ratio at the backside (which is shielded from the incident wave) is given by curve *I* of Fig. 8.5.3b.

C. Exact Formulas for the Diffracted Fields of Classical Shapes

A "pressure-gradient" sensor is driven by a net force generated by diffraction and reflection of the incident wave. It is necessary then to have explicit formulas for the scattering of sound waves from obstacles. In most cases it is satisfactory to model the scatterer as a simple form: a disc, a sphere, a cylinder, a strip, etc. Also, for sake of simplicity it is often useful to treat the sensor as acoustically hard.

The scattering of sound from acoustically hard obstacles has been calculated for classical shapes. We consider here several results of these analyses in connection with determining the pressure differential in pressure-gradient hydrophones.

A. Exact Solution of the Diffracted Field of an Acoustically Hard Disc

Let the disc be defined in terms of oblate spheroidal geometry (x, y, z: ξ, η, ϕ):

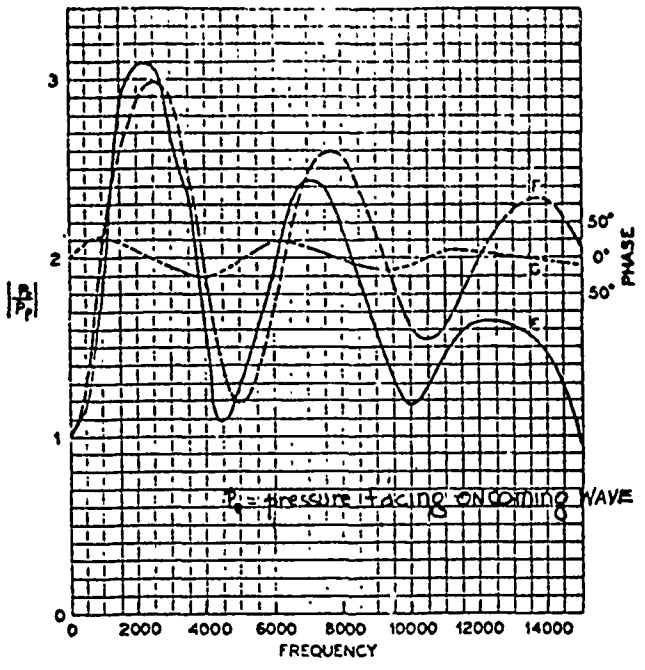


Fig. 8.5.3a — Ratio of acoustic pressure at the center of an 11.5 cm square plate at 0° azimuth (facing oncoming wave) normalized to the incident wave which strikes the plate at normal incidence, versus frequency. Curve F, computed magnitude of incident plane wave; Curve G, computed phase of incident plane wave, Curve E, observed pressure 50 cm from plate center. [3]

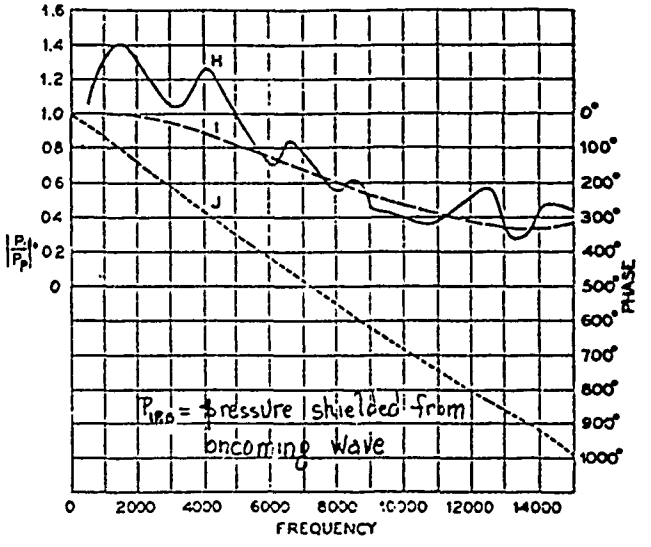


Fig. 8.5.3b — Ratio of acoustic pressure at the center of an 11.5 cm square plate at 180° azimuth (back side of the plate) normalized to the normally incident plane wave at 0° azimuth. Curves I, J, computed magnitude and phase respectively of the diffracted wave; Curve H, observed pressure 50 cm from the center, to the rear of the plate. [3]

$$x = \frac{d}{2}(\xi^2 + 1)^{1/2}(1 - \eta^2)^{1/2}\cos\phi$$

$$y = \frac{d}{2}(\xi^2 + 1)^{1/2}(1 - \eta^2)\sin\phi$$

$$z = \frac{d}{2}\xi\,\eta_3$$

shown in Fig. 8.5.4 [5]. A plane wave of sound, whose plane is parallel with the $\hat{y}$ axis, is incident upon the disc (defined by $\xi = 0$) at an angle ζ with respect to the $+\hat{z}$ axis. The velocity potential of this wave is,

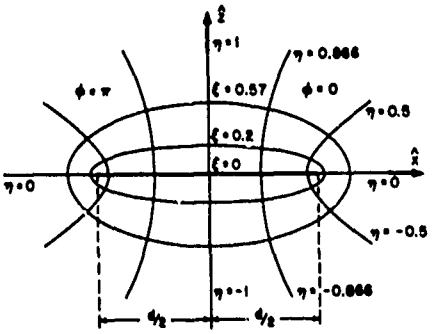


Fig. 8.5.4 — Disc ($\xi = 0$) in oblate spheroidal geometry

$$\psi^{\text{inc}} = A_0 \exp\{ik(x \sin\zeta + \cos\zeta)\}. \tag{8.5.10}$$

On the surface $\xi = 0$, the sum of incident and scattered potential is,

$$\psi_T^2 = \psi^{\text{inc}} + \psi^{\text{scat}} = \frac{2A_0}{h} \sum_{m=0}^{\infty} \sum_{n=m}^{\infty} \frac{i^n}{N_{mn}(h)} \times \left. \frac{1}{\frac{dR_{mn}^{(3)}}{d\xi}(-ih, i\xi)} \right|_{\xi}$$

$$\times S_{mn}(-ih, \cos\zeta)\, \dot{S}_{mn}(-ih, \eta) \cos n\phi \tag{8.5.11}$$

where

$$h = \frac{kd}{2} = \frac{\omega d}{2c} = \frac{\pi d}{\lambda}.$$

Here $R_{mn}^{(3)}$ is a radial function of the third kind and S_{mn} is an angle function of the first kind. These are defined and tabulated in reference [5].

Equation 8.5.11 is valid for all acoustic frequencies $\omega(=kc)$. At high "enough" frequencies one may use the Kirchoff approximations:

$$\text{double layer approximation: } \psi_T = \psi^{\text{inc}} \pm \frac{1}{2\pi} \int_S \psi^{\text{inc}} \frac{\partial}{\partial n} \left(\frac{e^{ikr}}{r} \right) dS$$

$$\text{single layer approximation: } \psi_T = \psi^{\text{inc}} \pm \frac{1}{2\pi} \int_S \frac{\partial \psi^{\text{inc}}}{\partial n} \left(\frac{e^{ikr}}{r} \right) dS \tag{8.5.12}$$

in which the $\pm$ indicate $z = 0+$ (i.e., front side) and $z = 0-$ (i.e., back side).

Severin [6] has calculated the total pressure field on a hard disc surface as a function of radial distance ρ/λ normalized to the incident field. This is shown in Fig. 8.5.5, together with experimental results, for the case of $h = 10$ (that is $(d/\lambda) = \frac{10}{\pi}$). A noticeable feature of this plot is the diffraction lobes on the front and rear faces caused by reinforcement of interfering edge-waves in particular directions.

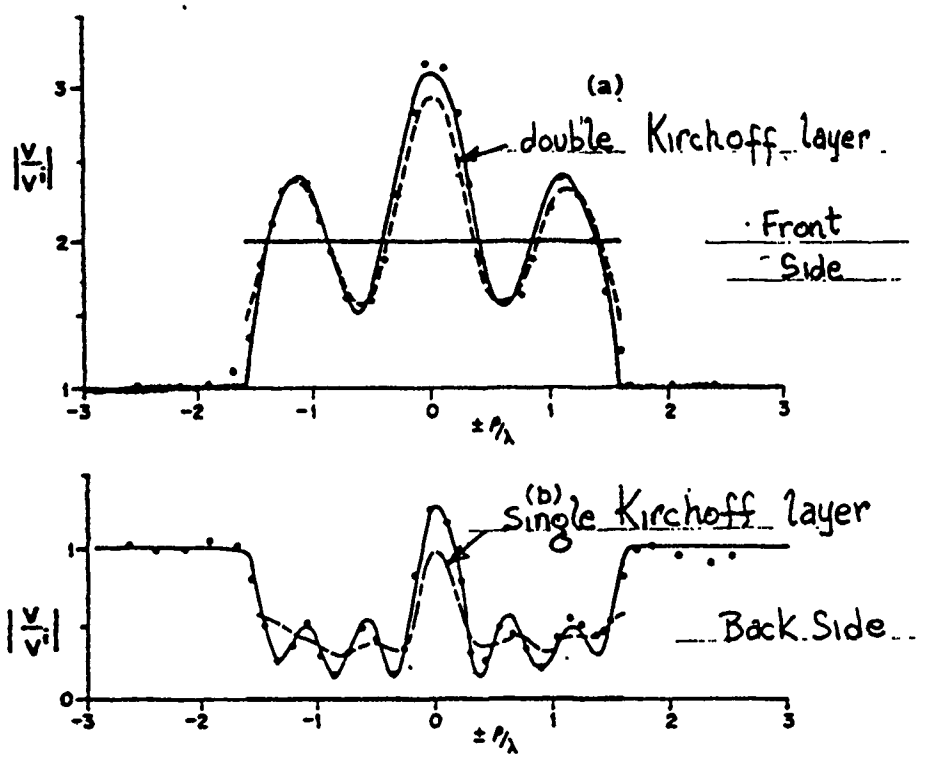


Fig. 8.5.5 — Normalized total field on surfaces, (a) $z = 0+$ and (b) $z = 0-$ for $c = 10$:—exact; ----Kirchoff double layer; -·-·-Kirchoff single layer; ··· experimental points

B. Exact Solution of the Diffraction Field of an Acoustically Hard Strip

Let the strip be defined in terms of elliptic cylindrical geometry, Fig. 8.5.6. Here,

$$x = \frac{d}{2} \cosh u \cos v$$

$$y = \frac{d}{2} \sinh u \sin v .$$

$$z = z$$

A plane wave propagating perpendicular to the z-axis in a direction forming angle ϕ_0 with the negative x-axis, and angle $\pi/2 - \phi_0$ with the negative y-axis, is represented by the velocity potential,

$$\psi^{inc} = A_0 \exp\{-ik(x \cos \phi_0 + y \sin \phi_0)\}. \tag{8.5.13}$$

A first problem is to expand this function in elliptic waves. Briefly, these waves satisfy the Helmholtz equation of steady state wave fields:

$$\frac{\partial^2 \psi}{\partial u^2} + \frac{\partial^2 \psi}{\partial v^2} + \left(\frac{dk}{2}\right)^2 [\cosh^2 u - \sin^2 v]\, \psi = 0.$$

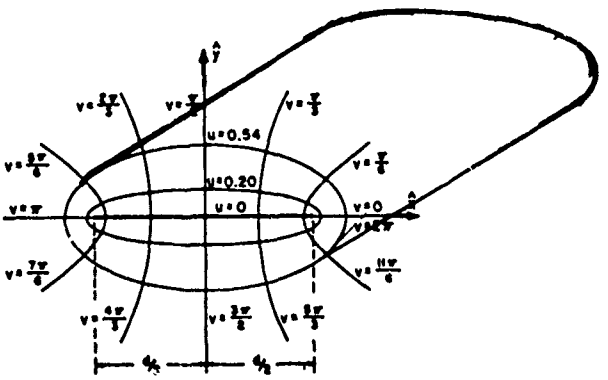


Fig. 8.5.6 — Strip, $\pm d/2$, defined in elliptical coordinates

$x = \frac{1}{2}d \cosh u \cos v,$
$y = \frac{1}{2}d \sinh u \sin v,$
$z = z,$

The solution of which is in the separable form of angle functions S and radial functions R, each satisfying Mathieu's equation [7],

$$\psi = S(\mathrm{v})\ R(u).$$

By expanding $S(\mathrm{v})$ in a Fourier series of even ($= \cos m\mathrm{v}$) and odd ($= \sin m\mathrm{v}$) functions it is found that there are four classes of solutions (designated as Mathieu functions), namely solutions periodic in π and 2π, and solutions which are even or odd. A table of them is shown below:

Table of Mathieu Functions S, R and Normalization N

	periodic in π	periodic in 2π
even	Se_{2m}, Re_{2m} N^e_{2m}	Se_{2m+1}, Re_{2m+1} N^e_{2m+1}
odd	$S0_{2n}$, $R0_{2m}$ N^0_{2m}	$S0_{2n+1}$, $R0_{2n+1}$ N_{2m+1}

$$N \equiv \int_0^{2\pi} [S(\mathrm{v})]^2 d\mathrm{v}$$

Here the radial solution can be of three types $R^{(1)}$, $R^{(2)}$, $R^{(3)}$ analogous to the Bessel funtions J, N and thc Hankel function H respectively. The choice of solution depends on the physical conditions of a particular application. In general the potential field of Eq. 8.5.13 is expandable in both even and odd functions for all m (that is, for both π, and 2π periodicity),

$$\psi^{\mathrm{inc}} = A_0 \sqrt{8\pi} \sum_m (-i)^m \left\{ \frac{Se_m(h \cos \phi_0)}{N^e_m(h)}\, Se_m(h \cos \mathrm{v})\, \mathrm{Re}^{(1)}_m(h, \cosh u) \right.$$

$$\left. + \frac{S0_m(h, \cos \phi_0)}{N^0_m(h)}\, S0_m(h, \cos \mathrm{v})\, R0^{(i)}_m(h \cosh u) \right\}. \qquad (8.5.14)$$

Let us select an application in which we are concerned only with the normal components of particle velocity on the surface of the strip. The quantity is given by the gradient of ψ,

$$\nabla_u \psi = \frac{\partial \psi}{\partial\, h_u u} = \frac{1}{\frac{d}{2}\sqrt{\sinh^2 u + \sin^2 v}} \frac{\partial \psi}{\partial u} = -V_0. \tag{8.5.15}$$

At the surface $u = 0$ it is seen that

$$\left.\frac{\partial \psi}{\partial u}\right|_{u=0} = -\frac{d}{2} V_0 \sin v. \tag{8.5.16}$$

Now sin v is an odd function which is periodic in 2π. Thus we shall be concerned only with a restricted part of Eq. 8.5.14 given by,

$$\psi_0^{inc} = A_0 \sqrt{8\pi} \sum_m (-i)^{2m+1} \frac{S0_{2m+1}(h, \cos\phi_0)}{N^0_{2m+1}(h)} S0_{2n+1}(h, \cos v)\, R0^{(1)}_{2m+1}(h, \cosh u). \tag{8.5.17}$$

The incident field given by Eq. 8.5.14 is scattered by the strip. We shall be concerned with that portion of the scattered wave which constributes to the normal particle velocioty on the surface of the strip. The (restricted) form of the scattered wave will then be that of a sum of outgoing elliptical waves:

$$\psi_u^{scat} = \sum_m D_{2n+1}\, S0_{2m+1}(h, \cos v)\, R0^{(3)}_{2m+1}(h, \cosh u). \tag{8.5.18}$$

The factor D_{2m+1} is chosen to just allow $\partial\psi^{scat}/\partial u \Big|_{u=0} = -\left.\frac{\partial \psi_0^{inc}}{\partial u}\right|_{u=0}$ that is, to satisfy the condition that the normal component of surface velocity vanishes. The total potential of the incident plus scattered field is then,

(a) $\psi_T = \psi^{inc} + \psi^{scat}$

or

$$\text{(b)}\quad \psi_T = A_0 \sqrt{8\pi} \sum_m (-i)^{2n+1} \frac{S0_{2n+1}(h, \cos\phi_0)}{N^0_{2m+1}(h)} \left[R0^{(1)}_{2m+1}(h, \cosh u) - \frac{\left(\frac{\partial R0^{(1)}_{2m+1}}{\partial u}(h, 1)\right) R0^{(3)}_{2m+1}}{\left(\frac{\partial R0^{(3)}(h, 1)}{\partial u}\right)}(h, \cosh u)\right] S0_{2m+1}(h, \cos v). \tag{8.5.19}$$

This formula, while complete, is tedious to evaluate numerically. Another approach to solution may be more useful. We return to Eq. (a) above and write it in the form,

$$p_T = p^{inc} + p^{scat}$$

or,

$$\frac{p_T}{p^{inc}} = 1 + \frac{p^{scat}}{p^{inc}}.$$

For an acoustically hard obstacle the scattered pressure may be obtained by first calculated the pressure p^{rad} radiated by the obstacle when given a surface normal velocity $-V_0$ where $+V_0$ is the normal particle velocity on the surface caused by the incident pressure. In the case of an acoustically hard strip the radiated pressure due to a surface velocity $+V_0$ on the front face and $-V_0$ on the back face is

$$p^{(rad)} = i \frac{a}{2} \rho\omega \, V_0 L$$

where,

$$L = \pi \sum_{m=0}^{\infty} \frac{B_1^0 \, (h, \, 2m+1)}{N_{2m+1}^2 \, (h)} \frac{S0_{2m+1} \, (h, \cos v)}{\left[\frac{\partial R0^{(3)} \, (h, \cosh u)}{\partial u}\right]} R0_{2m+1}^{(3)} \, (h, \cosh u) \tag{8.5.20}$$

[8] in which B_1^0 are expansion coefficients defined in the reference by the relations,

$$S0_{2m+1} \, (h, \cos v) = \sum_{n=0}^{\infty} B_{2n+1}^0 \, (h, \, 2m+1) \sin [(2n+1)v]$$

$$\sum_n (2n+1) \, B_{2n+1}^0 = 1. \tag{8.5.21}$$

The scattered pressure is simply $p^{scat} = -p^{rad}$. The incident pressure which develops a normal particle velocity $+V_0$ an the front surface is

$$p^{inc} = \frac{\rho c \, V_0}{\cos \phi_0}. \tag{8.5.22}$$

Thus on the surface $u = 0$,

$$\frac{p^{scat}}{p^{inc}} = -i \left[\frac{ka}{2}\right] \cos \phi_0 \, L_{u=0}. \tag{8.5.23}$$

In this ratio p^{scat} is a function of elliptical angle v while p^{inc} is not. The net force on the strip is due to the difference in total pressure between front and rear faces. The net force per unit of length due to the reflection and scattering of the incident wave is

$$F_{net} = \int_0^{2\pi} (-) \, p^{(rad)} \frac{a}{2} \sin v \, dv$$

$$= -\left[\frac{a}{2}\right]^2 i \rho\omega \, V_0 \pi \sum_{m=0}^{\infty} \frac{B_1^0 (h, \, 2m+1)}{N_{2m+1}^0} \frac{R0_{2m+1}^{(3)} \, (h, \, 1)}{\left[\frac{dR0^{(3)}}{du} \, (h, \cosh u)\right]_{u=0}} \int_0^{2\pi} S0_{2m+1} \, (h, \cos v) \sin v d.$$

In view of Eq. 8.5.21 the integral itself is one term, $B_1^0 \, (h, \, 2m+1)$. Hence

$$F_{\text{net}} = -i\left(\frac{a}{2}\right)^2 \rho\omega V_0 \pi \sum_{m=0}^{\infty} \frac{[B_1^0(h, 2m+1)]^2}{N_{2m+1}^0} \frac{R0_{2m+1}^{(3)}(h, 1)}{\left[\frac{dR0^{(3)}(h, \cosh u)}{du}\right]_{u=0}}, \tag{8.5.24}$$

in which the units of force are N/m. The magnitude of F_{net} is (roughly) the force driving a pressure-gradient microphone of the ribbon type, here modeled as a section of an infinite rigid strip.

A low frequency approximation of Eq. 8.5.24 valid when $\frac{ka}{2} << 1$ is useful in applications,

$$\frac{F_{net}}{-V_0} = R - iX = \left(\frac{\pi^2 a^4 \omega^3}{128\, C^3}\right) \rho c - i\omega \left(\frac{\pi}{4} a^2 \rho\right) \tag{8.5.25}$$

[9]. It is seen that the major force on the strip is the mass reactance of the fluid of value $\frac{\pi}{4} a^2\rho$ per unit of length.

C. *Exact Solution of the Diffraction Field of a Hard Cylinder of Infinite Length*

Let the axis of the cylinder be along the z-axis of cylindrical coordinates. The cross-section of the acoustically hard cylinder at $z = 0$ is shown in Fig. 8.5.7. Since the angle of incidence is arbitrary we can take the plane wave to be

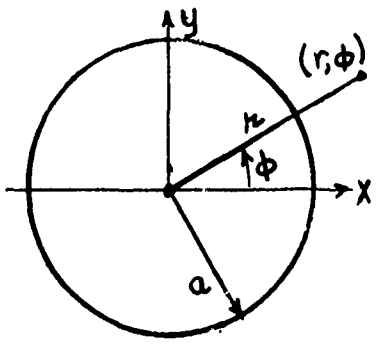


Fig. 8.5.7 — Geometry of scattering from an infinite cylinder

$$\psi^{\text{inc}} = Ae^{-ikx - i\omega t}.$$

In cylindrical waves,

$$\psi^{\text{ince}} = Ae^{-i\omega t} \sum_{m=0}^{\infty} \epsilon_m (-i) J_m(kr) \cos\phi. \tag{8.5.26}$$

The scattered field ψ^{scat} must satisfy two conditions: (1) it must be a sum of outgoing waves (2) its particle velocity on the surface $r = 0$ a must be equal in magnitude but opposite in sign to the particle velocity of the incident plane wave. A form satisfying both of these conditions is

$$\psi^{\text{sat}} = -A \sum_{m=0}^{\infty} \epsilon_m (-i)^m \frac{J_m'(ka)}{H_m^{(1)'}(ka)} H_m^{(1)}(kr) \cos m\,\phi \tag{8.5.27}$$

in which the prime signifies a derivation with respect to r. The sum of the incident acoustic pressure and the scattered pressure on the surface $r = a$ is

$$p_T = -i\omega\rho[\psi^{\text{inc}} + \psi^{\text{scat}}]$$

$$P_T = -i\omega\rho A\left[\frac{2}{\pi ka}\sum_{m=0}^{\infty}\epsilon_m(-i)^{m-1}\frac{\cos m\phi}{H_m^{(1)\prime}(ka)}\right]e^{-i\omega t}. \tag{8.5.28}$$

In which we have used the Wronskian

$$J_m(ka)H_m^{(1)\prime}(ka) - J_m'(ka)H_m^{(1)}(ka) = \frac{2i}{\pi ka}. \tag{8.5.29}$$

A plot of the ratio

$$\left|\frac{P_T}{-i\omega\rho A}\right| \text{vs } \phi$$

for $ka = 1$, 5, and 10 is shown in Fig. 8.5.8 (see Ref. 10). It shows that for large ka the ratio approaches a value of 2 at the face $\phi = 0$ and near zero at $\phi = \pi$. The argument of the ratio plus the argument of the plane wave ($= ka\cos\phi$) vs cylindrical coordinate ϕ is shown in Fig. 8.5.9.

D. Exact Solution of the Diffraction of an Acoustically Hard Sphere

The geometry of scattering from a rigid sphere is shown in Fig. 8.5.10. A plane wave incident on an acoustically hard sphere from direction θ_0 and ϕ_0 has the descriptive form of velocity potential,

$$\psi^{\text{inc}} = A\exp i\mathbf{k}\cdot\mathbf{r} = A\exp\{ikr[\cos\theta_0\cos\theta + \sin\theta_0\sin\theta\cos(\phi - \phi_\theta)]\}.$$

An expansion in spherical waves leads to the classical form [11]

$$\psi^{\text{inc}} = A\sum_{n=0}^{\infty}\sum_{m=0^n}(2n+1)i^n\epsilon_m\frac{m-m)!}{(n+m)!}\cos n(\phi-\phi_0)P_n^m(\cos\theta_0)P_n^n(\cos theta)j_n(kr) \tag{8.5.30}$$

where

$$\epsilon_0 = 1; \quad \epsilon_m = 2, \quad m \neq 0.$$

A scattered wave field which satisifes the condition of zero normal velocity must reduce to

$$\psi^{\text{scat}} = -A\sum_{n=0}^{\infty}\sum_{m=0}^{n}(2n+1)i^n\epsilon_m\frac{(n-m)!}{(n+m)!}\cos m(\phi-\phi_0)P_n^n(\cos\theta_0)P_n^n(\cos\theta)$$

$$\times\frac{j_n'(ka)}{h_n'(ka)}h_n^{(1)}(kr). \tag{8.5.31}$$

Here the prime sign means d/dkr.

The sum for ψ^{inc} and ψ^{scat} can be written directly from the above forms. However to simplify the formulas we choose a plane wave propagation in the negative z direction, Fig. 8.5.10. Then $\theta_0 = 0$ and the sum on m reduces to one term $m = 0$

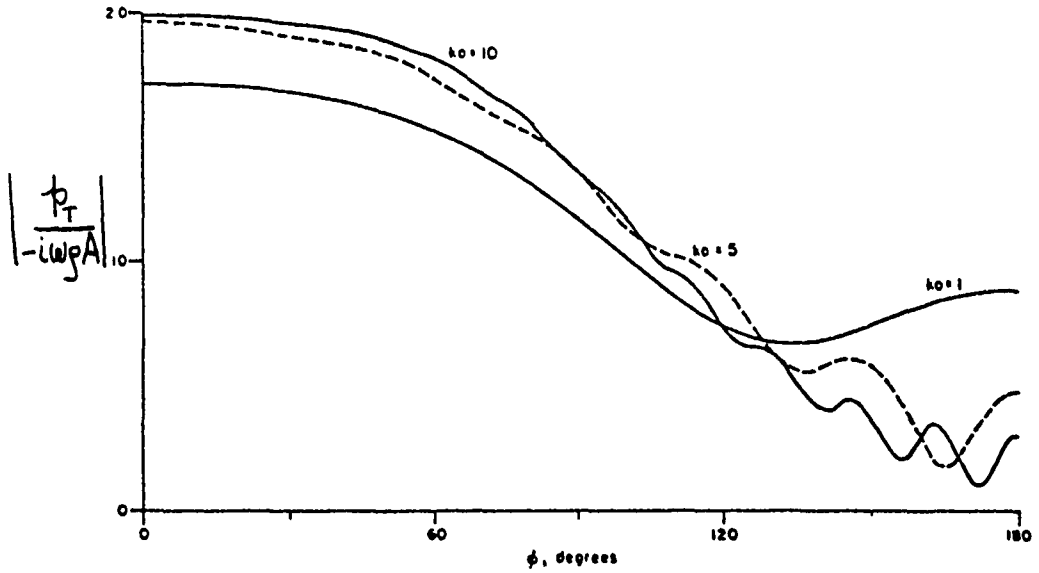


Fig. 8.5.8 — Plot of normalized amplitude of surface field produced by a plane wave incident along the x-axis [10]

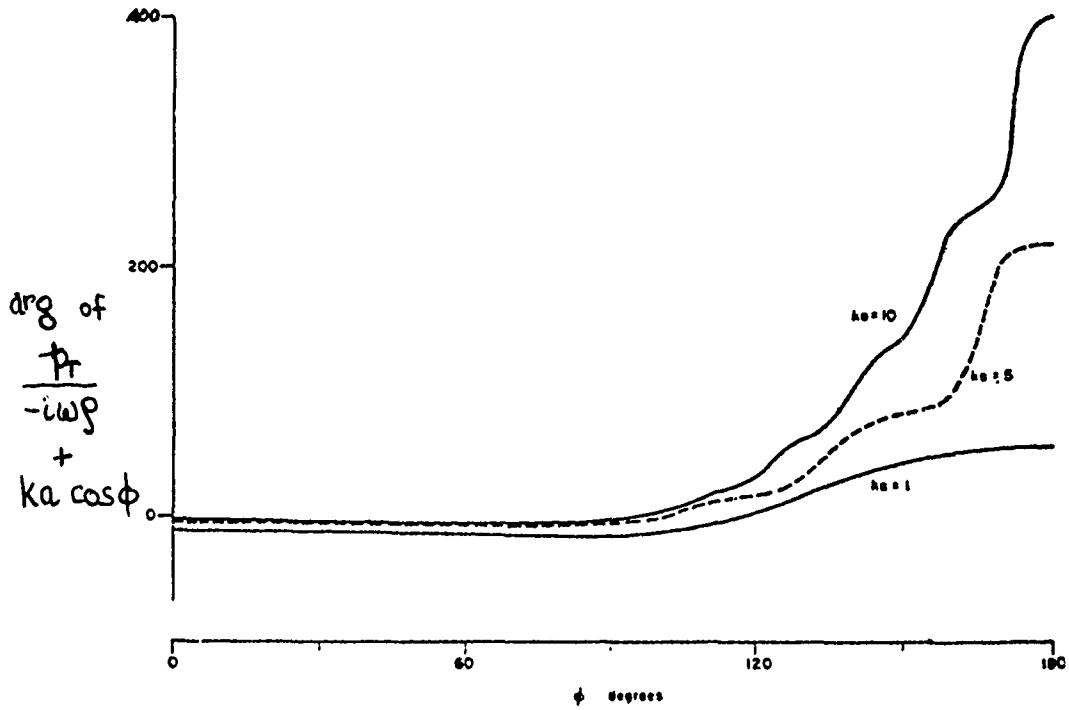


Fig. 8.5.9 — Plot of the phase of surface field (plus $ka \cos \phi$) produced by a plane wave incident along the x-axis [10]

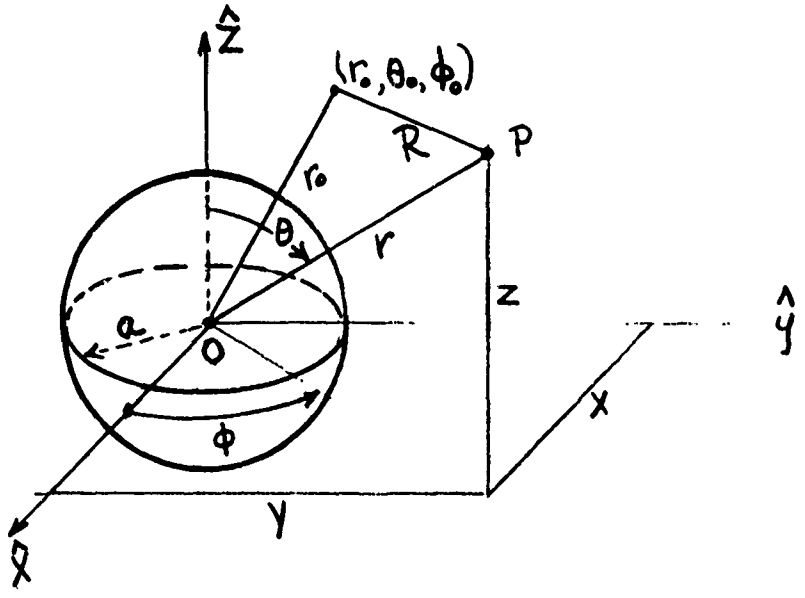


Fig. 8.5.10 — Geometry of scattering from a rigid sphere

$$\psi_T = \psi^{\text{inc}} + \psi^{\text{scat}}$$

$$\psi_T = A \sum_{n=0}^{\infty} (-i)^n (2n+1) \left[j_n(kr) - \frac{j_n'(ka)}{h_n^{(1)\prime}(ka)} h_n^{(1)}(kr) \right]$$

$$\times P_n(\cos\theta). \tag{8.5.32}$$

At the surface $r = a$ we find the total pressure to be

$$p_T = -i\omega\rho\psi_T$$

$$p_T = -i\omega\rho A \sum_{n=0}^{\infty} (-i)^n (2n+1) \left[\frac{i}{(ka)^2} \right] \frac{P_n(\cos\theta)}{h_n^{(1)\prime}(ka)}. \tag{8.5.33}$$

A plot of the ratio

$$\left| \frac{p_T}{-i\omega\rho A} \right| \text{ vs } \theta$$

is shown in Fig. 8.5.11. Again it is seen that for ka large the ratio approaches a value of 2 on the incident face at $\theta = 0$, and a value of 1 on the back face at $\theta = \pi$. A plot of the sum of the argument of the ratio and $ka \cos\theta$ vs θ is shown in Fig. 8.5.12.

$\left|\frac{p_T}{-i\omega\rho A}\right|$

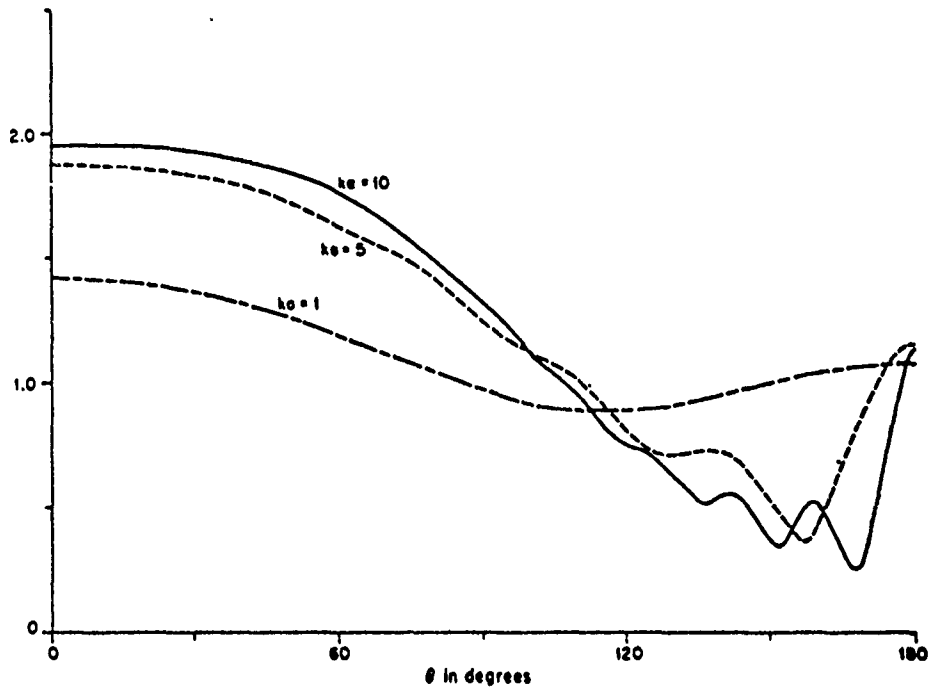


Fig. 8.5.11 — Total surface pressure field of a hard sphere caused by an incident plane wave [10]

arg of $\left(\frac{p_T}{-i\omega\rho A}\right)$ + $ka\cos\theta$

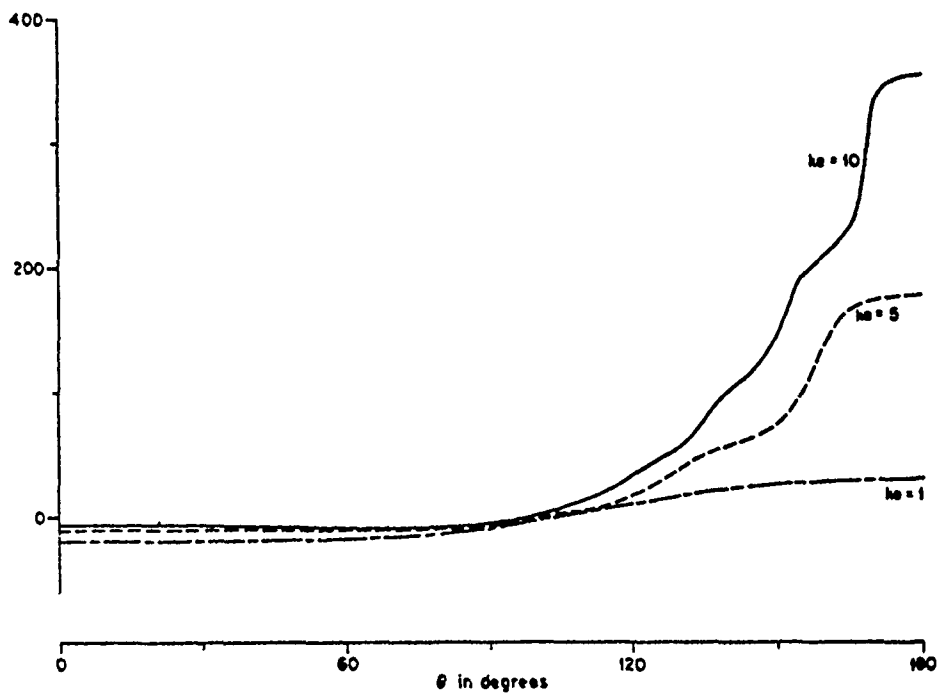


Fig. 8.5.12 — Argument of surface pressure (plus $ka\cos\theta$) vs θ [10].

8.6 DIFFRACTION CONSTANT FOR PRESSURE-GRADIENT SENSORS

The net force driving the pressure-graident sensor shown in Fig. 8.4.1, calculated by use of rigid (motionless) surface models, is the *blocked force* F_b. When the surface begins to move, and to be deflected into various shapes of deformation, the net force changes. Let us suppose that there is a velocity distribution V_n over the sensor surface either due to the blocked force, or natually occurring at the frequency of drive. The complex radiation power at the surface of the sensor, corresponding to the product of blocked pressure P_b and V_n is

$$\Gamma = \int_A P_b V_n^* dA \quad \text{(units: Nm/s)}. \tag{8.6.1}$$

In this expression we can regard $P_b(\mathbf{r}_0)$ as the pressure exerted by a constant force generator at the surface point $\mathbf{r}_0$ and $V_n(\mathbf{r}_0)$ as the normal velocity component resulting from this local force acting against the local mechanical impedance. The complex power Π is therefore an average over the entire sensor surface.

The expression for Π allows one to define an *effective blocked force* $F_{B(eff)}$ in terms of a *reference velocity* V_0. Since the choice of V_0 is arbitrary the value of $F_{b(eff)}$ is also arbitrary. Some authors choose V_0 to be the maximum of the distribution, generally at the center of the sensor face. Others choose V_0 to be the spatial average over the sensor face. However it is defined, V_0 (and Π) determine a corresponding $F_{b(eff)}$ according to the formula

$$F_{b(eff)} = \frac{\Pi}{V_0^*}. \tag{8.6.2}$$

Defined in this way $F_{b(eff)}$ is the constant force generator which drives the velocity V_0 through the mechanical system against the mechanical impedance of the system.

Actually, the origin of all force on the (passive) sensor is the incident sound pressure P_f (say that of a plane wave). This pressure acting over an area A in the absence of the sensor is AP_f. In the presence of the sensor this incident force is modified by reflection and diffraction and becomes the effective force given by Eq. 8.6.2. It seems useful, particularly in application to representation of a senor by an equivalent circuit, to relate effective force to incident force. Several such relations have been proposed in the form of dimensionless quantities called *diffraction constants D.* These are discussed next.

In a first suggestion D is taken to be the ratio of space-averaged acoustic pressure to incident acoustic pressure [12],

$$D = \frac{\int P_b dA}{AP_f}. \tag{8.6.3}$$

This relation defines D in terms of *force* delivered to the sensor as distinct from power delivered. For a piston-type surface moving with uniform velocity the distinction between force and power vanishes since they are related by a constant. If however the surface vibrates with a natural velocity distribution corresponding (say) to some flexural mode shape, the force delivered gives no indication of power delivered. To overcome this inadequacy it has be suggested that the diffraction constant be defined to include the effect of velocity distribution [13],

$$D = \frac{\Pi}{AP_f V_0^*}. \tag{8.6.4}$$

To be valid this formular requires the velocity distribution to be *fixed*, that is, the sensor surface deforms into a fixed pattern independent of angle of incidence of the exciting wave. Usually an elastic sensor surface breaks up into more than one mode of vibration when excited by arbitrary time and space varying incident waves. Formula (8.6.4) then applies only to a particular modal pattern of deformation that is effectively transduced into the electric branch of the equivalent circuit.

Formula (8.6.4) is useful to the extent that one can define a reference velocity V_0 for the surface of the sensor. A physical approach begins with the expression for local (complex) acoustic power on the surface itself,

$$\Pi = V_n Z_{\text{rad}} V_n^* \tag{8.6.5}$$

in which Z_{rad} is the mechanical radiation impedance. Thus for the general case one can define the reference velocity to be [13],

$$V_0 = \left[\frac{1}{A}\int_A |V_n|^2 dA\right]^{1/2}. \tag{8.6.6}$$

The calculation of D occupies an important step in the design of pressure-gradient hydrophones based on flexural motion of the sensing element. By use of Eqs. 8.6.4 and 8.6.6 Woollett [13] has calculated D for the three cases shown in Fig. 8.6.1.

(a) Pressure Hydrophone
fundamental resonance
$k = 0.4$, $D = 0.85$

(a) $V_n = 1.84\ V_0\left[1 - 1.2453\ \frac{r^2}{a^2} + 0.2453\ \frac{r^4}{a^4}\right.$

(b) Pressure Hydrophone
2nd resonance
$k = 0.06$, $D = 0.35$

k = coupling factor

(b) $V_n = 2.94\ V_0\ [J_0(Kr) + 4.89 \times 10^{-4}\ J_0(jKr)]$
$K = 5.455/a$

(c) Pressure Gradient
Hydrophone
$k = 0.4$
$D = 0.5\ Kb$ (typical)
$K = \omega/c$

b

$+ V_n$ $+ V_n$

(c) For V_n see Ref. 13.

Fig. 8.6.1 — A flexurally vibrating bilaminar disk under three conditions

Other constructions of pressure-gradient hydrophones have been devised. One design places the sensing element (in this case bilaminar flexural discs) inside rigid shells. Figure 8.6.2 shows an oscillating cylinder and an oscillating sphere of this construction. In the case of the cylinder the driving force is the difference in pressure between $x = 0$ and $x = l$. This is simply the pressure at $x = 0$ minus the same pressure delayed by space phase exp $(-jKl)$. The absolute value of the blocked force is

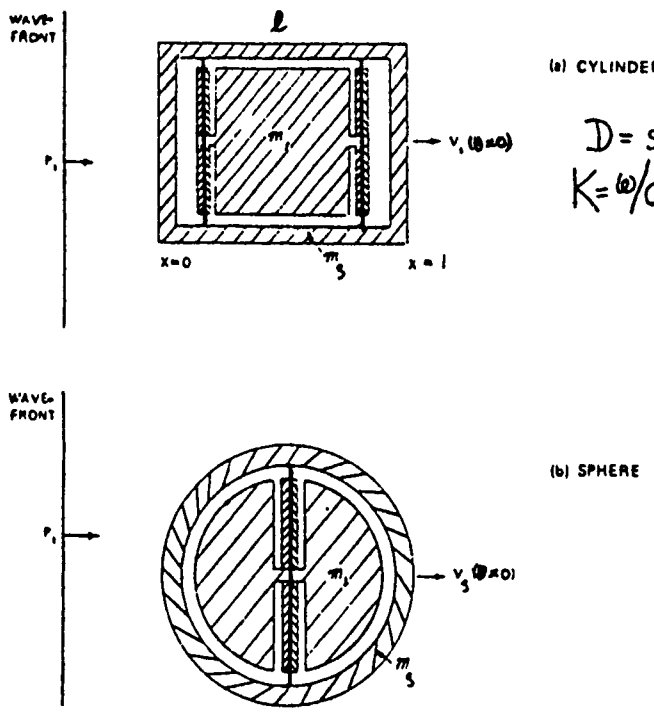


Fig. 8.6.2 — Rigid shell pressure-gradient hydrophones with internal velocity sensors. (a) oscillating cylinder, (b) oscillating sphere. The sensors are bilaminar piezoelectric disks. $\theta = 0$ defines the maximum response axis [13].

$$F_b = \phi a^2 P_f |1 - e^{-jkl}|$$

$$F_b = 2\pi a^2 P_f \sin\left|\frac{Kl}{2}\right|. \tag{8.6.7}$$

Since the active area is $A = 2\pi a^2$, it is seen that the diffraction constant is,

$$\text{(cylindrical shell):} \quad D = \sin \frac{Kl}{2}. \tag{8.6.8}$$

A similar calculation can be carried out for a rigid oscillating disc. In this structure the driving force is the scattered pressure discussed in Sect. 8.4 and 8.5. The calculation of D yields

$$\text{(oscillating disk):} \quad D = 0.42\ Ka. \tag{8.6.9}$$

In the case of the rigid spherical shell hydrophone, the rigid body velocity is

$$V_n = V_s \cos\theta. \tag{8.6.10}$$

Thus, according to Eq. 8.6.6,

$$V_0 = \frac{1}{\sqrt{3}} V_s. \tag{8.6.11}$$

The total pressure on the surface $r = a$ at angle D for a plane wave traveling in the negative z-direction is given by Eq. 8.5.3. For $ka << 1$ the sum is approximated by the first two terms,

$$p_T \rightarrow i\omega\rho A \left[1 + i \frac{3ka}{2} \cos\theta\right]. \tag{8.6.12}$$

By performing the integration called for in Eq. 8.6.1 and using it together with Eq. 8.6.11 one finds that the diffraction constant on the maximum response axis is

$$D = \frac{\sqrt{3}}{2} = ka \tag{8.6.13}$$

[13].

8.7 EQUIVALENT CIRCUIT OF A SPHERICAL-SHELL PRESSURE GRADIENT HYDROPHONE

The spherical-shell hydrophone picture schematically in Fig. 8.6.2b, consists of two masses M_s, M_l, connected through a bilaminar piezoelectric disc which acts as a spring. To construct its equivalent circuit we follow the procedure outlined in Chapt. 1, Sect. 1.20.

We first determine the number of degrees of freedom in which the transducer can exhibit motion. In practice the mass of the shell M_s can move in three possible direction of translation. Assuming the sound wave exerts not torques we omit rotation about three possible axes. The internal mass M_l is idealized in a similar way, although it may not be allowable to omit the rotation.

Of all these possible motions we select only translation in the direction of the incident plane wave. For the construction shown this is the only motion *assumed* to be coupled to the electrical system through transduction. Thus the description of operation of the hydrophone is reduced to two degrees of freedom in translation, one ($= V_s$) for mass M_s and on ($= V_l$) for mass M_l.

Following the rules outlined in Sect. 1.20, we next list the force and velocity equation based on this model of possible motion

$$\begin{aligned} &\text{(a)} \quad F_s = M_s j\omega V_s + F_l \\ &\text{(b)} \quad V_s - V_l = j\omega C_M F_l \\ &\text{(c)} \quad F_l = M_l j\omega V_l \end{aligned} \tag{8.7.1}$$

F_s = force generated by the incident wave

F_i = force coupled through the bilaminar disk to the internal mass

C_M = compliance of the internal bilaminar disk

V_s, = velocities (in translation) of the shell and the internal mass.

Let us choose an FV (force-across, velocity-through) representation. Equation (a) shows that M_s is in series and F_i is in parallel. Equation (b) is a nodal relation, and shows that if V_i flows through the parallel branch as required by Eq. (c) then compliance C_M is across F_i. Upon adding the simple representation of the piezoceramic as a capacitor in parallel position and a shell radiation impedance Z_r in the (arbitrary selected), form of a series represetation,

$$Z_r = R_r + j\omega M_r$$

one obtains the equivalent circuit shown in Fig. 8.7.1. It is noted that the force driving the shell is the incident force modified by the diffraction constant and reduced by the radiation impedance.

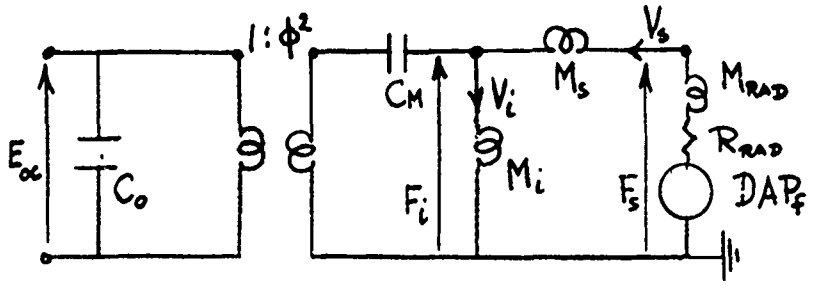
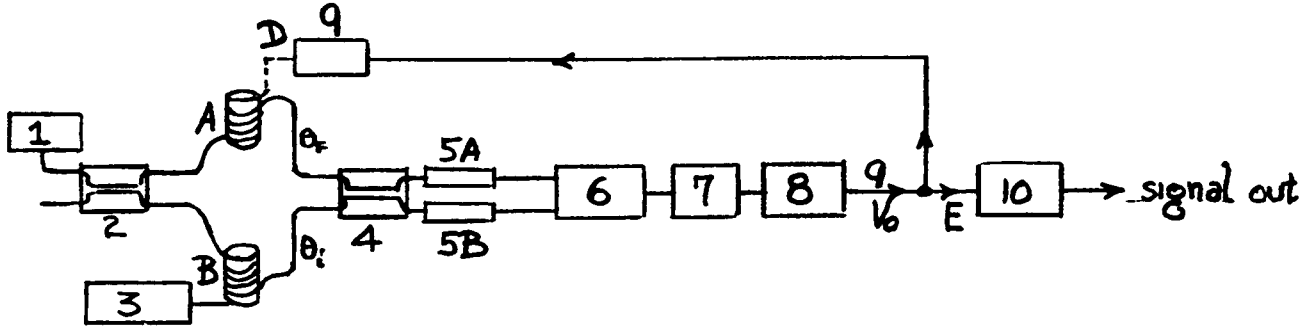


Fig. 8.7.1 — Simplified equivalent circuit of the rigid spherical shell pressure gradient hydrophone of Fig. 8.6.2(b)

8.8 FIBER OPTIC PRESSURE-GRADIENT HYDROPHONE

The construction and operation of a fiber-optic hydrophone has been presented in Chapt. 5 of this treatise. In the simplest application one (signal) arm of the interferometer (Mach-Zender type [14]) is exposed as a *point receiver* to the acoustic field while the other (reference) arm is free of signal. A procedure for mitigating the effect of environmental noise was discussed in Sect. 5.7. When the reference arm is also exposed to the acoustic field at a distance d apart from the signal arm (d much smaller than the wavelength of the field), the combination constitutes the basic elements of a pressure-gradient hydrophone. Because pressure difference is detected as phase difference and because for maximum sensitivity the two arms must be in phase quadrature it becomes imperitive to devise a compensation system which insures quadrature in the presence of phase error due to thermal disturbance. One procedure for stabilizing the phase relation of the arms of a fiber optic hydrophone in which detection is based on the homodyne principle (see Chapt. 5, Sect. 5.8 for discussion) is presented next.

Stabilization in phase relation can be achieved by a feedback correction network which (1) recognizes a phase error, (2) provides a corrective signal to cancel this error. A schematic block diagram of such a system is shown in Fig. 8.8.1. The key element here is the winding of the sensing fibers around piezoelectric cylinders B, C and cementing them in place.



1 - Single mode He-Ne laser
2 - Bottle coupler #1
A - Fiberwound piezoelectric cylinder #1
B - " " " #2
3 - Modulation signal
4 - Bottle coupler #2
5A, 5B Photo diode detector A, B
6 - Differential amplifier
7 - Lowpass filter
8 - Integrator
9 - Correction signal
10 - Band pass filter

Fig. 8.8.1 — A schematic of a pressure-gradient fiber optic hydrophone with feedback loop to maintain phase quadrature between the two point-receivers

In this digram we suppose first there is an error in phase caused by an external acoustic field, or by an internal temperature fluctuation. This appears at point D as an electrical signal at voltage V. When this voltage excites the piezoelectric cylinder it causes it to expand (or contract) radially. The result is a change in length of the fiber, hence inducing a change in the phase of the laser light in arm #1 of the interferometer. The change in phase due to the correction signal tends to cancel the error. Continuous compensation is obtained by tracking random errors in the compensator system and canceling them in the feedback loop. In the absence of stress in the fiber, and at very low frequency where the predominant mechanical impedance is that of a stiffness the constitutive relations of piezoelectric coupling requires that the strain S (which is the ratio of the change in length Δl of the cylinder to its length l) be related to the applied electric field E (which is the voltage divided by the cylinder thickness, V/t) through the piezoconstant d_{31}:

$$\frac{S}{E} = \frac{\Delta l/l}{\Delta V/t} = d_{31} \quad \text{(static condition)}$$

or (8.8.1)

$$\frac{\Delta l}{\Delta V} = \frac{l}{t}\, d_{31}.$$

For simple choices such as $l = 3$ in., $t = 0.2$ in., and $d_{31} = -274 \times 10^{-12}\ m/V$ (PZT-5H) the change in length per volt correction is,

$$\left|\frac{\Delta l}{\Delta V}\right| \sim 45 \times 10^{-10}, \quad \text{or } 45\text{Å/Volt.}$$

The change in thickness Δt per unit change in voltage is obtained from the fact that for an isotropic cylinder having Poisson's ratio = 1/3 the radial strain $\Delta t/t$ is approximately $3X$ the axial strain. In terms of magnitudes,

$$\epsilon_r = 3\,\frac{\Delta l}{l} = 3\,\frac{\Delta V}{t}\, d_{31} = \frac{\Delta t}{t}$$

or

$$\frac{\Delta t}{\Delta V} \sim 3d_{31} = 8.22 \times 10^{-10}\,\frac{m}{V} = 8.22\ \text{Å}/V.$$

In an actual device having these dimensions the voltage/phase relation proved linear over five orders of magnitude (1 to 10^{-5} rad) [15]. Thus the phase shifter has a large dynamic range. This makes it suitable for hydrophone applications.

The "error in phase" at point D of Fig. 8.8.1 is really the degree to which the two arms of the interferometer are out of quadrature. The detection of this error is the first stage of the compensator system, shown in the figure. The laser light signals from A, B are first converted into electrical signal in a pair of photodiodes. Since they are the two output beams of a Mach-Zehnder interferometer they are 180° out of phase, Fig. 8.8.2. By auxiliary apparatus the operating point OP of the system is first set to $\phi = \pi/2$. However the two intensities I_A and I_B are *always* complementary (that is, always 180° apart). If an external disturbance (such as an acoustic field, or a temperature fluctuation) induces a phase change $\Delta\phi$ between the arms of the interferometer intensities I_A and I_B become different, Fig. 8.8.2. This difference is the "error signal."

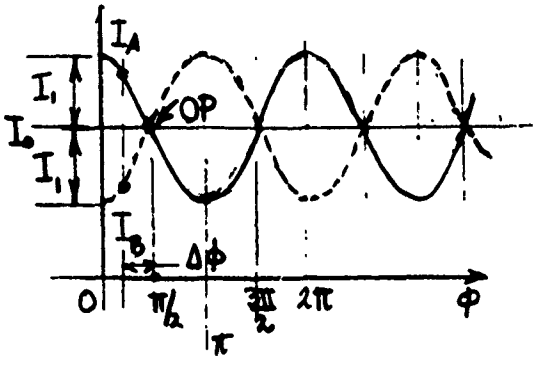


Fig. 8.8.2 — Intensity of laser beams *A*, *B* as a function of difference ϕ of arms #1, #2.

To measure the error signal, and thereby measure the external disturbance a strategy is adopted of driving intensities I_A and I_B back to the operating point *OP*, meanwhile keeping tally of how much feedback phase shifting is necessary to do this. The implementation of the strategy is this: I_A and I_B are inserted in a differential amplifier (gain K_D) whose out put is $K_D(I_A - I_B)$. High frequency noise is removed by a low pass filter. The filtered error signal is then put through two integrators. The first integrator (sometimes called the difference integrator) provides a gain $K_P(s)$ which varies inversely with the Laplace transform variable s,

$$K_P(s) = -K_1/s. \tag{8.8.2}$$

In the time domain this corresponds to an integration of the difference signal from $t = 0$ to a specified time $t = t_1$. The second integrator has a built-in "stop" required to stabilize the feedback loop. Its gain is,

$$K_1(s) = \frac{-K_2(s + a)}{s}, \quad a = \text{stop frequency}. \tag{8.8.3}$$

When $s << a$, the filtering action is simply $-K_2/s$. However, $s >> a$, the gain is simply the constant $-K_2$. The integration in time then "stops." The output of the second integrator is a voltage V_0. This is fed back as a correction signal to arm #1 where it causes the piezoceramic cylinder to expand (say) thereby causing a phase shift which drives the phase error $I_A - I_B$ toward zero. In passing through the cylinder the voltage V_0 is multiplied by the feedback gain K_F due to the electromechanical coupling response of the cylinder. At any instance the current I_A has the form,

$$I_A = V_0(s)H(s), \quad H(s) = K_F(s). \tag{8.8.4}$$

Now by definition alone it is seen that

$$V_0(s) = (I_B - I_A)G(s), \quad G(s) = K_D K_P K_I = \text{forward gain}. \tag{8.8.5}$$

Substituting of Eq. 8.8.4 leads to the feedback equation

$$V_0(s) = \frac{I_B G(s)}{1 + \dfrac{K(s + a)}{s^2}}, \quad K = K_{DK_F} K_1 K_2 = \text{loop gain}. \tag{8.8.6}$$

This is a dynamic equation in (Laplace) transform time which because of feedback locks the system to the operating point OP at the quadrature phase $\phi = \pi/2$. The running value of $V_0(t)$ is the tally of

how much phase shift is needed to keep the arms of the interferometer always at quadrature. It is reported out at point E of Fig. 8.8.1. Except for a constant it represents the pressure difference between the two "point" fiber optical sensors when they are the elements of a pressure-gradient hydrophone. Because it also contains low frequency drift it is put through a (high) band pass amplifier which cuts off the drift at the lower range roll-off.

Equation 8.8.6 predicts that the feedback loop will become unstable (that is, oscillate) when K, a, and s are such that

$$s^2 + K_s + Ka = 0. \tag{8.8.7}$$

We may think of this equation as the dynamical relation of the displacement ξ of a freely vibrating harmonic oscillator of unit mass $M(=1$ kg), damping resistance $R = MK$, and spring stiffness $k = MKa$,

$$(M \cdot s^2 + Rs + k)\xi = 0.$$

Taking $s = i\omega$ one finds the natural frequency ω_n to be,

$$\omega_n = \sqrt{\frac{k}{M}} = \sqrt{Ka}. \tag{8.8.8}$$

The damping ratio ζ of the oscillating system, defined as the ratio of R to critical damping R_c, is,

$$\zeta = R/R_{\text{critical}} = \frac{R}{\frac{2k}{\omega_m}} = \frac{K}{4\pi f_n}. \tag{8.8.9}$$

In designing the feedback loop, it is seen to be desirable to make the loop gain K large enough so that Ka is large (hence ω_n is large) and the damping ζ is near critical. However the correction circuit itself is essentially a low pass filter with response flat to zero frequency whose upper frequency roll-off is determined by K and ζ.

Minimum Detectable Signal

The self-noise of a fiber optic pressure-gradient hydrophone of identical elements is the noise of one element *increased* by the reduction in field excitation caused by taking pressure difference over small distances.

Suppose for example the instantaneous pressure variation with distance is given by

$$p(x) = p_0 \sin kx, \quad k = \frac{\omega}{c} = \frac{2\pi}{\lambda}. \tag{8.8.10}$$

Then the magnitude of pressure difference between two points separated by $\Delta X \ll \lambda$ is

$$\Delta p = p_0 k \Delta X. \tag{8.8.11}$$

In decibel units,

$$\Delta p(dB) = 20 \log_0 K\Delta X + p_0(dB).$$

Choose for example a frequency $f = 10$ Hz, and a separation distance $\Delta X = 10$ cm. Then, in water

$$20 \log_{10} \frac{2\pi \times 10 \times 0.10}{1500} = -47.6 \text{ dB}.$$

This means the pressure difference between the two in the field is −47.6 dB below the pressure midway between the points, which is very closely the pressure p_0 measured by each elementary sensor alone.

Assume now that p_0 is the minimum detectable pressure for the elementary sensor (that is, for one arm of the interferometer). Then the minimum detectable signal for the pressure-gradient sensor must be 47.6 dB *above* p_0. Thus placing both arms of the interferometer in the acoustic field and subtracting their outputs drastically reduces the signal to noise ratio and hence raises the threshold of detection by a substantial amount.

In one experimental construction 118 m of optical fiber were wound on each of two Teflon mandrels 2.5 cm in diameter spaced 0.08 m apart. The minimum detectable pressure when one arm alone of the interferometer was subject to an acoustic field of 10 Hz was measured to be ~20.5 dB *re* 1 μ*Pa* in a 1 Hz band. The reduction in signal level when both arms were subjected to the acoustic field was −49.5 dB re 1 μPa. Thus the minimum detectable signal was 49.5 + 20.5 ~70 dB re 1 μPa in a 1 Hz band. Similarly at $f = 1000$ Hz the detection threshold was ~30 dB consisting of the (constant) 20.5 dB and a 9.5 dB loss in signal due to subtraction of the pressure fields.

A plot of the threshold (in dB) versus frequency on semi-log paper is a straight-line. The calculation of threshold pressures of the 118 m fiber pressure-gradient interferometer as well as a 373 m fiber unit are shown in Fig. 8.8.3 superimposed on a Wenz-type chart of sea noise.

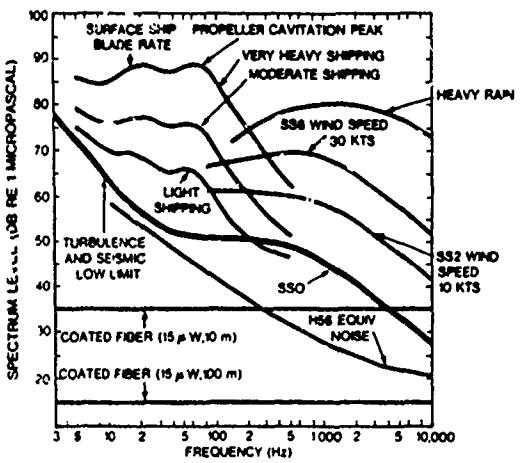


Fig. 8.8.3 — Minimum detectable pressures (dB re 1 μPa in a 1 Hz band) of two pressure-gradient hydrophones superimposed on a Wenz chart of sea noise [13c]

When the pressure field that is being measured is hydrodynamic in origin the fluctuation of pressure between two adjacent points is directly related to the fluctuation in velocity of the fluid. Pressure-gradient hydrophones are well suited to sensing such fields.

8.9 ERROR ANALYSIS IN MEASUREMENT OF PARTICLE VELOCITY BY PRESSURE GRADIENT HYDROPHONES

An important reason for conducting experiments to determine particle velocity is to derive from them a measure of acoustic intensity (= I). By definition this is the vector quantity,

$$\mathbf{I}(\mathbf{r}, t) = p(\mathbf{r}, t)\, \mathbf{u}(\mathbf{r}, t) \qquad \left[\text{units: } \frac{N-m}{m^2 s}\right]. \tag{8.9.1}$$

Using the relation (Eq. 8.1.3), one has

$$\mathbf{I}(\mathbf{r}, t) = p(\mathbf{r}, t) \left[-\frac{1}{\rho_0} \int_0^t \nabla\, p(\mathbf{r}, \tau)\, d\tau + C(\mathbf{r})\right]. \tag{8.9.2}$$

Here $C(\mathbf{r})$ is a constant (independent of time) representing the mean value of the particle velocity. In linear low amplitude acoustic theory it is zero in value and thus is omitted.

The component of I in one direction (say x) is,

$$\mathbf{I}_x(\mathbf{r}, t) = -\frac{p(\mathbf{r}, t)}{\rho_0} \int_0^t \frac{\partial p}{\partial x}(\mathbf{r}, \tau)\, d\tau. \tag{8.9.3}$$

We note that this component is a *point-function*: direction is introduced only by the gradient operator. While $p(\mathbf{r}, t)$ can be measured directly there is no practical instrument that measures $\partial p/\partial_x$ at point. However, $\partial p/\partial x$ at a point (say $\mathbf{r}_0$) can be approximated by finite differences, that is, by taking the difference between the pressures measured at two closely lying points, $\mathbf{r}_1$, $\mathbf{r}_2$:

$$\frac{\partial \tilde{p}}{\partial x} \equiv \left.\frac{\partial p}{\partial x}\right|_{\mathbf{r} = \mathbf{r}_0} \cong \frac{p(\mathbf{r}_2, t) - p(\mathbf{r}, t)}{|\mathbf{r}_2 - \mathbf{r}_1|}. \tag{8.9.4}$$

The approximation to the pressure itself at $\mathbf{r}_0$ is the average value,

$$\tilde{p} \equiv p_{\mathbf{r} = \mathbf{r}_0} \cong \frac{1}{2}\, [p(\mathbf{r}_1, t) + p(\mathbf{r}_2, t)]. \tag{8.9.5}$$

To conduct an error analysis on the measurement of intensity one begins with a Taylor-series expansion of Eqs. 8.9.4 and 8.9.5 in powers of $\Delta = |\mathbf{r}_2 - \mathbf{r}_1|$. This is the method Pavić [16]. The *tilde function* $\partial \tilde{p}/\partial x$ is an odd function, meaning it changes sign at $\mathbf{r} = \mathbf{r}_0$. In contrast to such a tilde function the *physical function* $\partial p/\partial x$ is (in general) both odd and even. Because of its definition the tilde function is expandable in odd derivatives:

$$\frac{\partial \tilde{p}}{\partial x} = \sum_{n=0}^{\infty} \left(\frac{\Delta}{2}\right)^{2n} \frac{1}{(2n+1)!} \left.\frac{\partial^{2n+1} p}{\partial x^{2n+1}}\right|_{\mathbf{r} = \mathbf{r}_0} \to \frac{\partial p}{\partial x} + \epsilon_1 \left(\frac{\partial p}{\partial x}\right). \tag{8.9.6}$$

Similarly, the *tilde function* $\tilde{p}$ is an even function, as distinct from the *physical pressure* which is both odd and even. This $\tilde{p}$ can be expanded in even derivatives,

$$\tilde{p} = \sum_{n=0}^{\infty} \left(\frac{\Delta}{2}\right)^{2n} \frac{1}{(\partial n!)} \left.\frac{\partial^{2n} p}{\partial x^{2n}}\right|_{\mathbf{r} = \mathbf{r}_0}, \to p + \epsilon_2 p. \tag{8.9.7}$$

To the extent of the validity of the approximation of a Taylor series the derivatives can be obtained from plane-wave representation, $p \propto \exp i\mathbf{k} \cdot \mathbf{r}$ (= $\exp i\ [xk \cos\alpha + yk \cos\beta + zk \cos\gamma]$, so that

$$\left|\frac{\partial p}{\partial x}\right| \propto k\cos\alpha p. \tag{8.9.8}$$

In terms of the symbols ϵ_1, ϵ_2, it is seen that

$$\epsilon_1 = \frac{\Delta^2}{24}(k\cos\alpha)^2 \propto \left[\frac{\Delta\cos\alpha}{\lambda}\right]^2 = \epsilon$$

$$\epsilon_2 = \frac{\Delta^2}{8}(k\cos\alpha)^2 \propto \left[\frac{\Delta\cos\alpha}{\lambda}\right]^2 = \epsilon. \tag{8.9.9}$$

Thus the errors in measurement of both $\tilde{p}$ and $\partial p/\partial x$ are proportional to Δ^2 and $\cos^2\alpha$, and inversely proportional to λ^2.

As an example of error estimation in the measurement of acoustic intensity by use of pressure measurement at two closely spaced points it is illuminating to take the simple case of the spherical field of a point monopole radiating harmonic waves at frequency ω and wavelength λ. The rms field intensity in the radial direction radius r_0 for rms source strength S_ω (units: m^3/s) is,

$$\mathrm{I}_r = k\omega\rho_0 |\Phi(r_0)|^2 \qquad \text{(units: } Nm/sm^2\text{)}$$

$$\Phi_0 = \frac{S_\omega}{4\pi r_0} e^{ikr_0 - i\omega t} \qquad \left(\text{units: } \frac{m^3}{s \times m} = \frac{m^2}{s}\right). \tag{8.9.10}$$

Now let us take two adjacent points $\mathbf{r}_1$, $\mathbf{r}_2$ separated by distance $\Delta = |r_2 - \mathbf{r}_1|$ and located vectorially at angle α relative to the radial direction given by vector $\mathbf{r}_0$, Fig. 8.9.1. Then

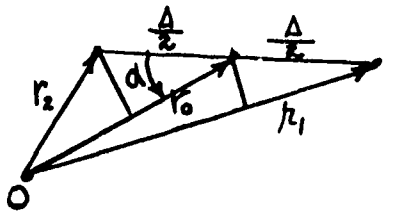


Fig. 8.9.1 — Geometrical relations defining r_1, r_2

$$r_1 = \mathbf{r}_0 + \frac{\Delta}{2}\cos\alpha$$

$$r_2 = \mathbf{r}_0 - \frac{\Delta}{2}\cos\alpha. \tag{8.9.11}$$

The rms acoustic pressures at $\mathbf{r}_1$, $\mathbf{r}_2$ are thus expressed in the

$$p(r_1, t) = -i\omega\rho_0 \Phi_0 \left(\frac{r_0}{r_1}\right) \exp\left(i \frac{k\Delta}{2} \cos\alpha\right)$$

$$p(r_2, t) = -i\omega\rho_0 \Phi \left(\frac{r_0}{r_2}\right) \exp\left(-\frac{ik\Delta}{2} \cos\alpha\right). \tag{8.9.12}$$

To calculate intensity at r_0 from these measured pressures we shall need the time-integral of $p(r_1, t)$:

$$\int_0^t p(\mathbf{r}_1, \tau) d\tau = \rho_0 \left(\frac{r_0}{r_1}\right) \Phi_0(\mathbf{r}_0) \exp\left(i \frac{k\Delta}{2} \cos\alpha\right) \tag{8.9.13}$$

The rms intensity at $\mathbf{r}_0$ in direction α, averaged over time, is

$$\mathbf{I}_\alpha = \frac{-1}{\rho_0\Delta} \left\{\left(-i\omega\rho_0 \frac{r_0}{r_2} \Phi_0(\mathbf{r}_0) \exp\frac{-ik\Delta}{2} \cos\alpha\right)\left(\rho_0 \frac{r_0}{r_1} \Phi^*_0(\mathbf{r}_0)\right) \exp\left(-\frac{ik\Delta}{2} \cos\alpha\right)\right\} \tag{8.9.14}$$

in which we have used Eqs. 8.9.3, 8.9.4, 8.9.5 , 8.9.12, and the conjugate of Eq. 8.9.13. This equation can be reduced by noting that

$$r_1 r_2 = r_0^2 \left[1 - \left(\frac{\Delta}{2r_0} \cos\alpha\right)^2\right].$$

Taking the real part of Eq. 8.9.14 one finally obtains,

$$\mathbf{I}_\alpha = \frac{\omega\rho_0}{\Delta} \frac{\sin(k\Delta \cos\alpha) |\Phi_0(\mathbf{r}_0)|^2}{\left[1 - \left(\frac{\Delta \cos\alpha}{2r_0}\right)^2\right]}, \quad \Delta/2 \ll r_0. \tag{8.9.15}$$

The ideal rms intensity at point $\mathbf{r}_0$ in the direction α averaged over time is,

$$\mathbf{I}_\alpha = k\omega\rho_0 |\Phi(\mathbf{r}_0)|^2 \cos\alpha. \tag{8.9.16}$$

Thus the ratio of approximate to ideal is,

$$\frac{\tilde{\mathbf{I}}_\alpha}{\mathbf{I}_\alpha} = \left(\frac{\sin(k\Delta \cos\alpha)}{k\Delta \cos\alpha}\right)\left[\frac{1}{1 - \left(\frac{\Delta \cos\alpha}{2r_0}\right)^2}\right]. \tag{8.9.17}$$

Now, for $\beta = k\Delta \cos\alpha \ll 1$,

$$\frac{\sin\beta}{\beta} \to 1 - \frac{\beta^2}{6};$$

and for $(\Delta \cos\alpha/2r_0)^2 \ll 1$,

$$\frac{1}{1-\left(\frac{\Delta\cos\alpha}{2r_0}\right)^2} \to 1+\frac{\Delta^2\cos^2\alpha}{4r_0^2}.$$

With these two approximate Eq. 8.9.17 further reduces to the simple ratio,

$$\frac{\tilde{I}_\alpha}{I_\alpha} = 1+\frac{\Delta^2\cos^2\alpha}{\lambda^2}\left[\left(\frac{\lambda}{2r_0}\right)^2-\frac{2\pi^2}{3}\right] = 1+\epsilon\left[\left(\frac{\lambda}{2r_0}\right)^2-\frac{2\pi^2}{3}\right] \tag{8.9.18}$$

[16]. The second term on the r.h.s is the error due to finite difference approximation. It is clear there are two sources of error: the first or *nearfield* is $[(\Delta/2)/r^2]\cos^2\alpha$, that is, it depends on the square of the ratio of separation distance Δ to radial distance r_0 from the source; the second is $(\Delta/\lambda)^2\cos^2\alpha\,(-2\pi^2/3)$, that is, it depends on the ratio squared of the separation distance to wavelength. In order for the nearfield error (due to curvature of the wavefront) to be negligible, one can estimate r_0 to be such that

$$\left(\frac{\lambda}{2r_0}\right) < const \times \frac{2\pi^2}{3}.$$

Let the constant be a factor of 2. Then $r_0 > \lambda/7 = \frac{C}{7f}$, where c = sonic velocity. Thus, to avoid nearfield error one must choose the radial distance from the source to be

$$\begin{aligned} &\text{for air:} && r_0 > \frac{330}{7f} \simeq \frac{50}{f} && \text{(units: meter)} \\ &\text{for water:} && r > \frac{1500}{7f} \simeq \frac{210}{f} && \text{(units: meter)} \end{aligned} \tag{8.9.19}$$

Upon assumption that the intensity measurement is made in the farfield of the source the magnitude of error then depends solely on the ratio of $\Delta\cos\alpha/\lambda$,

$$\text{magnitude of error relative to 1} = \left(\frac{\Delta\cos\alpha}{\lambda}\right)^2\frac{2\pi^2}{3} \tag{8.9.20}$$

[16]. The maximum error (for $\cos\alpha = 1$) versus frequency for given separation Δ (cm) is expressed as a percentage in Fig. 8.9.2. Thus at 100 Hz any separation less than 10 cm generates an error of less than 0.5%. However, at 1000 Hz a 10 cm separation leads to a measurement error of 50%.

Figure 8.9.2 is an idealized plot. It does not account for noise and phase shift. These are discussed next.

8.10 ERRORS DUE TO NOISE AND ARBITRARY PHASE SHIFT

From Eq. 8.9.14 one can express the approximated intensity by the simple form

$$\tilde{I}_\alpha = \frac{1}{\rho_0\Delta}\psi. \tag{8.10.1}$$

In the presence of noise (which contributes a term χ) this must be rewritten as,

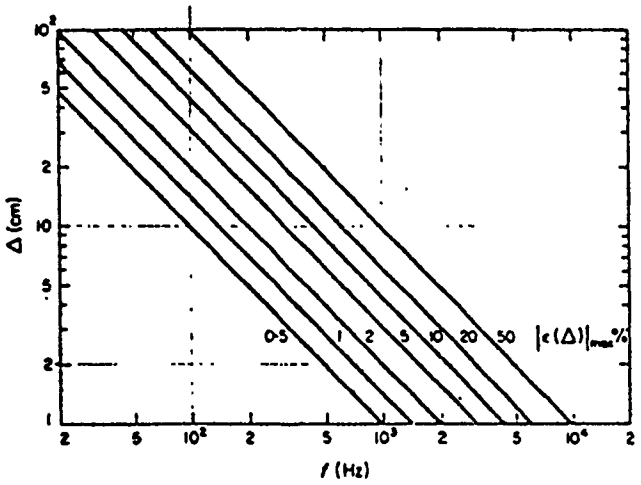


Fig. 8.9.2 — Maximum error infinite difference approximations [16]

$$\tilde{I}_{\alpha N} = \frac{(\psi + \chi)}{\rho_0 \Delta}. \tag{8.10.2}$$

Thus the error due to noise is

$$\frac{\tilde{I}_{\alpha N}}{I_\alpha} - 1 = \frac{\chi}{\psi} = \frac{\chi}{\rho_0 \Delta \tilde{I}_\alpha}. \tag{8.10.3}$$

It is seen that the error due to noise is *magnified* by making Δ smaller and smaller. In the presence of noise an arbitrary reduction of separation Δ will *deteriorate*, rather than improve, the measurement of intensity.

Similarly, when arbitrary phases, introduced by transduction, amplifiers, integrators, etc at $\mathbf{r}_1$ and $\mathbf{r}_2$, are ϕ_1, ϕ_2 respectively, the pressures become,

$$p(\mathbf{r}_1, t) \propto \exp\left(\frac{ik\Delta}{2}\cos\alpha + i\phi_1\right)$$

$$p(\mathbf{r}_2, t) \propto \exp\left(-\frac{ik\Delta}{2}\cos\alpha + i\phi_2\right). \tag{8.10.4}$$

Upon substitution in Eq. 8.9.14 it will readily be deduced that in the expressions for error (say Eq. 8.9.17), the following rule holds:

$$\sin(k\Delta\cos\alpha) \text{ is replaced by } \sin(k\Delta\cos\alpha)\,[\cos\delta\phi + ctg\ k\Delta\cos\alpha\sin\delta\phi]$$

where,

$$\delta\phi = \phi_1 - \phi_2. \tag{8.10.5}$$

When both $\delta\phi$ and $k\Delta\cos\alpha$ are very small Eq. 8.9.17 reduces to,

$$\frac{\tilde{I}_\alpha}{I_\alpha} \sim \left[1 - \frac{2}{3}\left(\frac{\pi\Delta}{\lambda}\cos\alpha\right)^2 + \frac{\delta\phi}{k\Delta\cos\alpha}\right]\left[\frac{1}{1 - \left(\frac{\Delta\cos\alpha}{2r_0}\right)^2}\right] \tag{8.10.6}$$

or

$$\tilde{I}_\alpha \sim I_\alpha\,[1 + \epsilon_1(\Delta) + \epsilon_3(\delta_\phi)]$$

in which ϵ_1 is the error due to spacing Δ and ϵ_3 is the error due to phase shift. Since ctg $\mu \to \infty$ as $\mu \to 0$ it is easily seen that making Δ arbitrarily small *in the presence of significant phase shifts* will *deteriorate* the accuracy of measurement of intensity rather than improve it. Thus phase matching of measurements at $\mathbf{r}_1$ and $\mathbf{r}_2$ is essential, particularly if the signal field contains a broadband of frequencies (that is, when the signal field is an impulse) because then Δ must be very small in order to accurately measure the high frequency end of the spectrum, which means that the error due to phase will be large (see Eq. 8.10.5). A numerical example of such phase error may be obtained from Eq. (8.10.6). There it is seen that

$$\epsilon_3(\delta\phi) \simeq \frac{\delta\phi}{\sqrt{6\,\epsilon_1(\Delta)}}.$$

Phase errors are also introduced by the diffraction effects noted in previous sections of this chapter. This is particularly true at the higher frequencies as can be seen from (say) Fig. 8.5.10. Here $\delta\phi$ is expressed in radius. When $\delta\phi$ is expressed in degrees and ϵ_3 is expressed as a percentage , the error in phase per degree is,

$$\frac{\epsilon_3}{\delta\phi(^\circ)} \simeq 100 \times \frac{\pi}{180} \times \frac{1}{\sqrt{6}} \times \frac{1}{\sqrt{\epsilon_1(\Delta)}} \simeq \frac{0.7}{\sqrt{\epsilon_1}}\%$$

Choosing $\epsilon_1 = 0.05$, the error in intensity per degree phase differential is

$$\frac{\epsilon_3}{\delta\phi(^\circ)} \cong \frac{0.7}{\sqrt{0.05}} = 3.1\%.$$

Thus in practical designs of intensity-measuring instruments it is essential to reduce diffraction effects, if only from the point of view of phase shifts and their accompanying errors.

8.11 ERRORS IN INTENSITY MEASUREMENTS DUE TO INTEGRATION TIME

In Eq. 8.9.14 the rms measured acoustic intensity is an average over time of indefinitely large duration. When the integration time is finite the intensity is

$$(I_x)_T = \frac{-1}{T}\int_0^T \frac{p(\mathbf{r}, t)}{\rho_0}\int_0^t \frac{\partial p}{\partial x}(\mathbf{r}, \tau)\,d\tau\,dt. \tag{8.11.1}$$

Pavić [16] has evaluated this integral using the approximates of Eqs. 8.9.4, 8.9.5. He finds that the approximated acoustic intensity $I_{\alpha T}$ when averaged over finite time T is related to the approximated intensity averaged over all time (I_α) by the formula,

$$I_{\alpha T} = I_{\alpha}\,[1 + \epsilon_4(T)] \tag{8.11.2}$$

in which $\epsilon_4(T)$ is the error due to finite averaging time. The maxium value of $\epsilon_4(T)$ for the condition $\Delta/\lambda << 1$ is estimated to be,

$$|\epsilon_4(T)|_{max} = \frac{1}{N\pi^2\left(\frac{\Delta}{\lambda}\right)\cos\alpha} \tag{8.11.3}$$

where N is the number of cycles used in the averaging. In terms of $\epsilon_1(\Delta)$ $\left[=\left(\frac{2}{3}\,\pi\,\frac{\Delta}{\lambda}\cos\alpha\right)\right]$

$$|\epsilon_4(T)|_{max} = \frac{0.26}{N\sqrt{\epsilon_1(\Delta)}}. \tag{8.11.4}$$

As an application, assume ϵ_4 is not be larger than ϵ_1. Then the minimum N is,

$$N = \frac{0.26}{[\epsilon_1(\Delta)]^{3/2}}.$$

If $\epsilon_1(\Delta)$ is expressed in percentage,

$$N \geq \frac{0.26}{[\epsilon_1(\Delta)]^{3/2}} \times 100 \times 10 = \frac{260}{[\epsilon_1(\Delta)]^{3/2}}.$$

Thus, in order for the error $\epsilon_4(T)$ in the measurement of acoustic intensity to be less than 5% the number of cycles must be at least,

$$N \geqslant \frac{260}{[5]^{3/2}} \sim 23 \text{ cycles}$$

provided $\Delta/\lambda << 1$.

REFERENCES

[1] H.F. Olson, J. Acous. Soc. Am. **17**, 192 (1946).

[2] L.L. Beranek, "Acoustics," McGraw-Hill, New York 1954, p. 135.

[3] L.J. Sivian, H.T. O'Neil, J. Acous. Soc. Am. **3**, p. 483 (1932).

[4] H.F. Olson, "Acoustical Engineering," D. Van Nostrand 2nd ed., p. 281 (1947).

[5] P.M. Morse, H. Feshbach, "Methods of Theoretical Physics," p. 1512, McGraw-Hill, 1953.

[6] H. Severin, Suppl. Nuovo Cimento **9**, 381-400 (1982).

[7] Ref. 5, p. 1407

[8] Ref. 5, p. 1424

[9] Ref. 5, p. 1425

[10] J.J. Bowman, ed, "Electromagnetic and Acoustic Scattering," Wiley Interscience, New York, 1969.

[11] Ref. 5, 1466

[12] R.J. Bobber, J. Acous. Soc. Am. **37**, 591-595 (1965).

[13] R.S. Woollett, J. Acous. Soc. Am. **72**, 1105-1113 (1982).

[14] "Principles of Optics," M. Born, E. Wolf, p. 312-315, Pergamon Press, Oxford 5th Ed.

[15] D.A. Jackson et al., Appl. Optics **19**, 2926-2929 (1980).

[16] G. Pavić, J. Sound and Vib **51**, 533-545 (1977).

Chapter 9
GENERAL THEORY OF ELECTROACOUSTIC TRANSDUCTION [1]

9.0 INTRODUCTION

The theory of electroacoustic transduction presented in previous chapters may be generalized to reveal an organic structure connecting its various parts. It will be useful in developing this structure to distinguish between *electroacoustic transduction* and *electromechanical transduction:* the former will include the impedance effect of the medium while the latter will exclude it. This distinction clarifies the definition of transduction parameters.

The generalization to be developed here underlies many aspects of modern electroacoustic theory.

9.1 ELECTROMECHANICAL TRANSDUCTION

We consider first a transducer designed to convert electrical current into mechanical force delivered by a flexible diaphragm. The power variables of the diaphragm are force F and normal velocity v_n while those of the electric field are voltage E and current I.

Let $\gamma(\mathbf{r})$ be the force per unit area at point r on the diaphragm (r being measured from an arbitrary origin (=0)). This force is assumed to be generated by the electrically induced motion $v_n(\mathbf{r}')$ of the diaphragm originating at some other surface point $\mathbf{r}'$, and acting against the mechanical impedance of the diaphragm structure. The diaphragm impedance function $Z_0(\mathbf{r}\,|\,\mathbf{r}_1)$ which converts $v_n(\mathbf{r}')$ into $\gamma(\mathbf{r})$ is most advantageously defined so as to have the units of acoustic impedance (= Ns/m^5). For incremental values,

$$d\gamma_v(\mathbf{r}) = Z_0(\mathbf{r}\,|\,\mathbf{r}')\, v_n(\mathbf{r}')\, dA(\mathbf{r}') \tag{9.1.1}$$

$$Z_0(\mathbf{r}\,|\,\mathbf{r}') \equiv \frac{\gamma(\mathbf{r})}{A(r')\, v_n(\mathbf{r}')}\ (Ns/m^5). \tag{9.1.2}$$

In addition to this force arising from diaphragm motion there is an additional force which is present even when motion is blocked. Choosing electric current I as the independent variable the force per unit area exerted by the surface against any restraint blocking its motion is local at r on the surface, and has the value

$$\gamma_b(\mathbf{r}) = h(\mathbf{r})\, I \tag{9.1.3}$$

(units of h: N/m^2A). The total force per unit area at r is the sum of Eq. 9.1.1, integrated over the diaphragm area, and Eq. 9.1.3:

$$\gamma(\mathbf{r}) = \int_A Z_0(\mathbf{r}\,|\,\mathbf{r}')\, v_n(\mathbf{r}')\, dA(\mathbf{r}) + h(\mathbf{r})\, I. \tag{9.1.4}$$

Since v_n is a function of the electric field it is seen that both I and v_n are coupled. A second equation is needed to complete the description of this coupling.

Again let I and v_n be independent variables. Assume first that the surface motion is blocked ($v_n = 0$). The voltage E_b associated with the current I defines the blocked electrical impedance Z_b,

$$E_b = Z_b I. \tag{9.1.5}$$

PREVIOUS PAGE IS BLANK

Assume next that the electric circuit is opened so that $I = 0$. A motion v_n then corresponds (because of electromechanical coupling) to some voltage E_v. It is useful to *define* E_v in terms of an electromechanical parameter $h'(\mathbf{r})$ (units: Vs/m^3) in such a way that an equation in increments dE_v closely parallels the formalism of Eq. 9.1.1:

$$dE_v = h'(\mathbf{r}')\, v_n(r')\, dA(\mathbf{r}'). \tag{9.1.6}$$

Thus,

$$E_v = \int_A h'(\mathbf{r}')\, v_n(\mathbf{r}')\, dA(\mathbf{r}'). \tag{9.1.7}$$

The total voltage corresponding to both v_n and I is the sum of Eq. 9.1.6 and 9.1.7,

$$E = \int_A h'(r') v_n(r')\, dA(\mathbf{r}') + Z_b I. \tag{9.1.8}$$

This is the second of two equations needed to define the coupling between v_n and I.

Equations 9.1.4 and 9.1.8 define *correspondencies*. They can also be considered to define *cause-effect relations* by choosing to regard $\gamma(\mathbf{r})$ and E as input force and voltage, and v_n and I as output normal velocity and current. Alternatively by transposing quantities in these equations one can regard current I and velocity v_n as input, and voltage E and force γ as output.

9.2 ELECTROACOUSTIC TRANSDUCTION

The transducer described above was assumed not appreciably to couple to the medium. We assume now that such coupling exists and that the medium is an infinite homogeneous isotropic fluid. The nature of the coupling described next.

The transducer diaphragm is imagined to be part of a closed surface $S(\mathbf{r})$. Outside (and on) this surface, in the absence of external sound sources, a steady state pressure field $p(\mathbf{r})$, if it exists, forms a continuum governed by the field equation,

$$p(\mathbf{r}) = \frac{1}{4\pi} \int_S \left[G(\mathbf{r} \mid \mathbf{r}') \frac{\partial p(r')}{\partial n} - p(r') \frac{\partial G(\mathbf{r} \mid \mathbf{r}')}{\partial n'} \right] dS \tag{9.2.1}$$

in which $G(\mathbf{r} \mid \mathbf{r}')$ is the Green's function appropriate to the space outside the transducer and to the surface S. The positive normal gradient is taken to point into surface S. We assume now that it is possible to *construct* G such that its normal derivative vanishes everywhere on the surface,

$$\left. \frac{\partial G(r \mid r')}{\partial n} \right|_{r' \text{ in } S} = 0. \tag{9.2.2}$$

The pressure field on the surface S then obeys the integral equation,

$$p(\mathbf{r}) = \frac{1}{4\pi} \int_S G(\mathbf{r} \mid \mathbf{r}') \frac{\partial p(\mathbf{r}')}{\partial n}\, dS\,(\mathbf{r}'). \tag{9.2.3}$$

Actually the pressure field at any point $\mathbf{r} = \mathbf{R}$ outside this surface also is governed by this equation. The function $G(R/r')$ must then be a valid description of condition $R \to \infty$, that is, it must have the form

$$G(R/r') \to \exp i\, k/\mathbf{R} - \mathbf{r}'|/|\mathbf{R} - \mathbf{r}'|. \tag{9.2.4}$$

On the surface S the acoustic field obeys the acoustic boundary condition which relates acoustic pressure gradient to particle velocity. Since the diaphragm couples to a fluid (mass density ρ) there is only one component of this velocity, namely v_n. Thus, for $v_n(r,\ t) = v_n(\mathbf{r}')e^{-i\omega t}$, one has

$$-\frac{\partial p}{\partial z} = \rho(-i\omega)v, \text{ or } \frac{\partial p}{\partial z} = i\omega\rho\ v_n e^{-\omega t} \tag{9.2.5}$$

in which normal coordinate z points into the medium. The integral equation of acoustic coupling for points $\mathbf{r}$ on S is then Eq. 9.2.3 with $+\partial p/\partial n = -\partial p/\partial z$,

$$p(\mathbf{r}) = \frac{-i\omega\rho}{4\pi}\int_S G(\mathbf{r}|\mathbf{r}')\ v_n(\mathbf{r}')\ dS(\mathbf{r}'). \tag{9.2.6}$$

It is useful to define from this equation a kernel function $Z_r(\mathbf{r}|\mathbf{r}')$ which has the units of acoustic radiation impedance,

$$Z_r(\mathbf{r}|r') = \frac{-i\omega\rho}{4\pi}\ G(\mathbf{r}|\mathbf{r}') \quad \text{(units: } N/m^5\text{)}. \tag{9.2.7}$$

It terms of this quantity the same *integral equation* may be written,

$$p(\mathbf{r}) = \int_S Z_r(\mathbf{r}|\mathbf{r}')\ v_n(\mathbf{r}')\ dS(\mathbf{r}'). \tag{9.2.8}$$

This equation states that corresponding to some (known) dis bution of pressure on S there is an (unknown) velocity distribution which can be found by solving this equation.

Equation 9.2.8 constitutes the essential contribution to formation of the equations of electroacoustic transduction. The procedure is to incorporate it into the equation of electromechanical transduction (Eq. 9.1.4). To this end the force per unit area $\gamma(\mathbf{r})$ is considered to be the sum of an applied external force Γ_0 and the medium reaction force $p(\mathbf{r})$ given by Eq. 9.2.8:

$$\gamma(\mathbf{r}) = \Gamma_0(\mathbf{r}) + p(\mathbf{r}) \tag{9.2.9}$$

Eq. 9.1.4 then reduces to,

$$\Gamma_0(\mathbf{r}) = \int_S [Z_0(\mathbf{r}|\mathbf{r}') + \frac{i\omega\rho}{4\pi}\ G(\mathbf{r}|\mathbf{r}')]\ v_n(\mathbf{r}')\ dS(\mathbf{r}') + h(\mathbf{r})I. \tag{9.2.10}$$

We can regard this result as a cause-effect relation: the cause is the applied force Γ_0 and the effect is a velocity v_n and an electrical current I, both assigned positive signs. In those applications where there is no external applied force ($\Gamma_0(\mathbf{r}) = 0$) the actual drive of the transducer is purely electrical (constant current I in Eq. 9.2.10). Then in abbreviated notation,

$$\int_S K(\mathbf{r}|\mathbf{r}')\ v_n(\mathbf{r}')\ dS(\mathbf{r}') = -h(\mathbf{r})I \tag{9.2.11}$$

where

$$K(\mathbf{r}|\mathbf{r}') = Z_0(\mathbf{r}|\mathbf{r}') + \frac{i\omega\rho}{4\pi}\ G(\mathbf{r}|\mathbf{r}'). \tag{9.2.12}$$

The negative sign before current I indicates that it is considered "a cause" of the velocity v_n. This is an integral equation in unknown $v_n(\mathbf{r})$ of the first type with kernel $K(\mathbf{r}\,|\,\mathbf{r}')$. In theory it can be solved by inversion, that is, by finding the *resolvent kernel* $L(\mathbf{r}\,|\,\mathbf{r})$ such that

$$v_n(r') = -I \int_s L(r'\,|\,r'')\, h(\mathbf{r}'')\, dS(\mathbf{r}''). \tag{9.2.13}$$

For particular cases and simple goemetries the construction of the resolvent is straightforward; however, in general, finding the resolvent may prove difficult.

Equation 9.2.11 is the first of two equations of electroacoustic transduction. The second equation is obtained by substitution of $v_n(\mathbf{r}')$ in Eq. 9.1.8. The relation $Z = E/I$ is then,

$$E = ZI, \text{ or } E = (Z_b + Z_{MOT})I \tag{9.2.14}$$

$$Z_{MOT} = -\int_{S_1}\int_{S_2} h(\mathbf{r}')\, L(\mathbf{r}'\,|\,\mathbf{r}'')\, h(\mathbf{r}'')\, dS_1(\mathbf{r}'')\, dS_2(\mathbf{r}'). \tag{9.2.15}$$

Here Z_{MOT} is the *motional* electrical impedance.

9.3 ACOUSTIC PRESSURE IN AN INFINITE MEDIUM RADIATED BY A TRANSDUCER IN A BAFFLE IN THE PRESENCE OF DISTANT SOUND SOURCES

Let A represent the vibrative surface of an acoustic transducer, and assume it is located in a baffle. For purposes of discussion the baffle is taken to be acoustically hard. In addition let there be sources of sound at some distant point, in a medium which is homogeneous, isotropic, and unbounded. It is desired then to determine the acoustic pressure at an arbitrary point in this medium, or on the surface of the transducer.

We consider first the pressure at a point $\mathbf{R}$ in the medium. This is the sum of the pressure p_{inc} coming directly from a source and the pressure field P_{reflec} *reflected* from the baffle. It will be useful to call these components the contribution of geometric acoustics (p_g),

$$p_g = p_{\text{inc}} + p_{\text{reflec}}. \tag{9.3.1}$$

A different contribution to the pressure at $\mathbf{R}$ comes from the observation that the transducer presents to the baffle an "edge" which can diffract acoustic fields. This diffracted pressure p_{diffrac} is seen to be the algebraic difference between the diffraction field of the transducer generated pressure $p(\mathbf{r})$, and the diffraction field of the geometric acoustic pressure $p_g(\mathbf{r})$ on the baffle, (with $p(\mathbf{r})$ diminishing from the surface *outward* and $p_g(\mathbf{r})$ diminishing from the distant source toward the baffle),

$$p_{\text{diffrac}}(\mathbf{R}) = \frac{1}{4\pi}\int_S \left[\left.\frac{\partial p(\mathbf{r}')}{\partial n}\right|_{\text{trans}} - \left.\frac{\partial p_g(\mathbf{r}')}{\partial n}\right|_{\text{baffle}}\right] G(\mathbf{R}|\mathbf{r}')\, dS(\mathbf{r}'). \tag{9.3.2}$$

Here the positive normal points *into* the baffle, and the condition $\partial G/\partial n = 0$ is again used to define its (assumed) acoustic hardness. When there is no transducer and when the baffle is infinite the "edges" disappear and Eq. (9.3.2) then vanishes. On the transducer surface, for time representation ($\exp -i\omega t$) one has the acoustic boundary condition Eq. (9.2.5) with $+\partial p/\partial n = -\partial p/\partial z$

$$\frac{\partial p(r')}{\partial n} = -\, i\omega\rho\, V_n. \tag{.9.3.3}$$

The total pressure at point **R** is then the sum of geometric and diffracted contributions,

$$p(\mathbf{R}) = p_g(\mathbf{R}) - \frac{ik\rho}{4\pi}\int_{\text{trans}} V_n(\mathbf{r}')\,G(\mathbf{R}|\mathbf{r}')\,dS(r') - \frac{1}{4\pi}\int_{\text{baffle}} \frac{\partial p_{\text{inc}}(\mathbf{r}')}{\partial n}\,G(\mathbf{R}/\mathbf{r}')\,dS(\mathbf{r}) \quad (9.3.4)$$

(Foldy [2], adopts the convention that $\partial p/\partial n$ is positive when directed *outward* from the surface. In addition he takes time to be exp $(j\omega t)$. Thus his Eq. (14) is the same as Eq. (9.3.4) excepting that $+i$ is replaced by $+j$.)

Equation (9.3.4) is an integral equation in the unknown field pressure $p(\mathbf{R})$ (or equivalently, in the unknown surface velocity $v_n(\mathbf{r})$). It will prove useful in determining transducer acoustic responses in subsequent derivations.

9.4 TRANSDUCER RECEIVING RESPONSE

An electroacoustic transducer (with baffle) designed for nonresonant reception of sound is placed in an acoustic field generated by a distant source. Since the motion of the transducer surfaces is purposely made small we may regard the acoustic field to be Eq. (9.3.4) without the term in v_n. This means the transducer diffraction field is negligible compared to the baffle diffraction effect,

$$p_{\text{receiver}}(\mathbf{r}) = p_g(\mathbf{r}) - \frac{1}{4\pi}\int_S \frac{\partial p_g(\mathbf{r}')}{\partial n}\,G(\mathbf{r}/\mathbf{r}')\,dS(\mathbf{r}'). \quad (9.4.1)$$

One identifies p_{receiver} with the external applied field $\Gamma_0(\mathbf{r})$ of Eq. (9.2.10). Using the notation of Eq. (9.2.12) one can then rewrite Eq. (9.2.10) in the form,

$$\int_S K(\mathbf{r}/\mathbf{r}')\,V_n(\mathbf{r}')\,dS(\mathbf{r}') = p_{\text{receiver}}(\mathbf{r}) - h(\mathbf{r})\,I. \quad (9.4.2)$$

It is important to note that no matter how small v_n is the transducer will generate no voltage unless v_n is a finite quantity.

Assuming the resolvent $L(\mathbf{r}'/\mathbf{r}'')$ of integral equation, Eq. (9.4.2) can be found one can solve for

$$v_n(\mathbf{r}') = \int_S L(\mathbf{r}'/\mathbf{r}'')\,[p^{(\mathbf{r}'')}_{\text{receiver}} - h(\mathbf{r}'')\,I]\,dS(\mathbf{r}''). \quad (9.4.3)$$

Since we are interested in voltage response we substitute this solution into Eq. (9.1.8)

$$E = \int_S h'(\mathbf{r}') \int L(\mathbf{r}'/\mathbf{r}'')\,[p_{\text{receiver}}(\mathbf{r}'') - h(r'')\,I]\,dS(\mathbf{r}'')\,dS(\mathbf{r}') + Z_b I \quad (9.4.4)$$

for materials commonly in use in electroacoustic transduction the factors $h(\mathbf{r})$, $h'(\mathbf{r})$ are small quantities. The product term in $h'h$ of Eq. (9.4.4) is therefore negligible compared to the contribution of the local receiver pressure. We will omit it in further discussion.

The voltage E and current I in Eq. (9.4.4) are *output* quantities. E itself is generally measured across the terminals of electrical load impedance Z_l,

$$E = -\,Z_l I. \quad (9.4.5)$$

Here, the negative sign indicates that E is output rather than input. Substitution for I and rearrangement of Eq. (9.4.4) lead to the (output) voltage response:

$$E = \frac{Z_l}{Z_b + Z_l} \int_S h'(\mathbf{r}') \int L(\mathbf{r}'/(\mathbf{r}'') p_{\text{receiver}}(\mathbf{r}'')\, dS(\mathbf{r}'')\, dS(\mathbf{r}'). \tag{9.4.6}$$

The open circuit response E_{oc} is obtained by allowing Z_l to become infinite.

Discussion

From the definition of the resolvent L as the operational inverse of the kernel K (see Eqs. (9.2.11), (9.2.12), and (9.2.13)) it will be seen that L contains the contributions of the diaphragm impedance Z_0 and the radiation impedance $i\omega\rho G/2\pi$. The driving force p_{receiver} is recognized as the *effective* pressure on the moving surface of the transducer, including not only the incident pressure from all external sources and their reflections from obstacles in the medium but also contributions from the diffracted field of the transducer itself calculated as if the transducer and its baffle were acoustically hard.

The receiving response is always stated relative to the electrical load impedance Z_l in units of "volts across a load resistance of (designated) ohms."

An important feature of Eq. (9.4.4) is the reciprocal relation of h, h': for reciprocal transducers (defined in Sect. 9.6 below),

$$h(\mathbf{r}) = h'(\mathbf{r}) e^{\alpha}, \quad \alpha = \text{real constant}. \tag{9.4.7}$$

This means that *symbolically* the relation of E to v_n embodied in h' and p to I embodied in h, when measured at spatial points, differ from each other only in phase (phase may be zero) but not in magnitude. Transducers obeying reciprocity in transduction factors h form a large class. They also exhibit reciprocity in the interchange of $\mathbf{r}$ and $\mathbf{r}'$ in the kernel function K and L, which comes from the defining relations for the Green's function $G(\mathbf{r}|\mathbf{r}')$,

$$K(\mathbf{r}|\mathbf{r}') = K(\mathbf{r}'|\mathbf{r}); \quad L(\mathbf{r}|\mathbf{r}') = L(\mathbf{r}'|\mathbf{r}). \tag{9.4.8}$$

These relations (Eq. (9.4.7) and (9.4.8)) are important in experimental testing and calibration of transducers that obey electroacoustic reciprocity.

9.5 TRANSDUCER TRANSMITTING RESPONSE

The electric power variables of electroacoustic transducers are taken here to be voltage E and current I. We assume the transducer is driven at constant current and ask, what is the acoustic pressure developed on the surface? This is determined from equations already derived.

From Eq. (9.2.13) the normal velocity v_n of the transducer surface generated by the constant current transduction is found in terms of the resolvent L (units: m/Ns) of the integral equation. As noted earlier L contains diaphragm (acoustic) impedance Z_0 and radiation (acoustic) impedance $\omega\rho G/4\pi$. The surface pressure developed by v_n is obtained by substitution into Eq. (9.2.6),

$$\frac{p(\mathbf{r})}{I} = \frac{i\omega\rho}{4\pi} \int_S G(\mathbf{r}/\mathbf{r}') \int_S L(\mathbf{r}'/\mathbf{r}'') h(\mathbf{r}'')\, dS(\mathbf{r}'')\, dS(\mathbf{r}'). \tag{9.5.1}$$

This is the constant current transmitting response (units: N/m^2 A) sought for.

A large class of electroacoustic transducers are driven at a constant voltage. The transmitting response of this class is determined as follows: first, Eq. (9.1.8) (with a slight change in notation to include acoustic as well as mechanical quantities) is solved for the current I and the result is substituted into Eq. (9.1.4) to obtain the surface pressure,

$$p(\mathbf{r}) = \int_S \left[Z_0(\mathbf{r}/\mathbf{r}') - \frac{h'(r')h(r')}{Z_b} \right] v_n(\mathbf{r}')\,dS(\mathbf{r}') + \frac{h(r)}{Z_b} E. \tag{9.5.2}$$

According to the acoustic boundary condition this pressure is expressible in terms of the surface velocity. Substitution of Eq. (9.2.6) and rearranging terms lead to

$$-\frac{h(r)}{Z_b} E = \int_S K^*(\mathbf{r}/\mathbf{r}') v_n(\mathbf{r}')\,dS(\mathbf{r}') \tag{9.5.3}$$

$$K^*(\mathbf{r}/\mathbf{r}') = Z_0(\mathbf{r}/\mathbf{r}') - \frac{h(\mathbf{r}')h'(\mathbf{r}')}{Z_b} + \frac{i\omega\rho G(\mathbf{r}/\mathbf{r}')}{4\pi} \quad \text{(units: Ns/m}^5\text{)} \tag{9.5.4}$$

Eq. (9.5.3) is an integral equation in the unknown velocity v_n. If the resolvent operator $L^*(\mathbf{r}/\mathbf{r}')$ (that is, the operator inverse to $K^*(\mathbf{r}/\mathbf{r}')$) can be found the solution is,

$$v_n(\mathbf{r}') = -\frac{E}{Z_b} \int h(r'') L^*(\mathbf{r}'/\mathbf{r}'')\,dS(\mathbf{r}''). \tag{9.5.5}$$

(Here the units of L^* are m/Ns.) The surface pressure, Eq. (9.2.6), then becomes the constant voltage transmitting response,

$$\frac{p(\mathbf{r})}{E} = \frac{i\omega\rho}{4\pi} \int_S G(\mathbf{r}/\mathbf{r}') \frac{1}{Z_b} \int_S h(\mathbf{r}'') L^*(\mathbf{r}'/\mathbf{r}'')\,dS(\mathbf{r}'')\,dS(r'). \tag{9.5.6}$$

The double integral is a statement that all surface points contribute a pressure to a given surface point (= first integration) and all such given points are summed over the surface (= second integration).

9.6 THE RECIPROCITY THEOREM FOR ELECTROACOUSTIC TRANSDUCERS

The electroacoustic reciprocity theorem states that the ratio of the magnitudes of the receiving and transmitting responses of an electroacoustic transducer is a constant independent of the nature and characteristics of the transducer [3].

To illustrate this theorem let a transducer, acting as a transmitter (frequency ω), centered at $\mathbf{R}_c$, radiate a field to point $\mathbf{R}$ in an infinite homogeneous isotropic fluid medium. Choosing a constant current drive we use Eq. (9.5.1) to describe the transmitted field S,

$$S(\text{transmitter centered at } R_c, \text{ field at } R) = \frac{i\omega\rho}{4\pi} \int_S G(\mathbf{R}/\mathbf{r}')$$

$$\times \int_S h(r'') L(\mathbf{r}'/\mathbf{r}'')\,dS(\mathbf{r}'')\,dS(\mathbf{r}') \tag{9.6.1}$$

in which r' and r'' are points on the surface S, the center of S being $\mathbf{R}_c$.

Now let the same transducer acting as a receiver, also centered at R_c, receive a wave field at the same frequency ω from a point source located at $\mathbf{R}$. It is useful, though not essential to the theorem, to assume the transmitted wave field is thus spherical. The incident field is then,

$$p_{\text{inc}}(r'') = \Phi \frac{e^{ik|r''-\mathbf{R}|}}{|r''-\mathbf{R}|} \tag{9.6.2}$$

in which $\mathbf{r}''$ is a point on the receiver surface and Φ is the source strength. The total field $p(\mathbf{r}'')$ on the surface on the surface is the sum of incident and diffracted fields,

$$p_{\text{receiver}}(\mathbf{r}'') = p_{\text{inc}}(\mathbf{r}'') + p_{\text{diffracted}}(\mathbf{r}''). \tag{9.6.3}$$

In the presence of the receiver and its baffle this receiver pressure is obtainable from the definition of the Green's function of the baffle,

$$p_{\text{receiver}} = \Phi G(\mathbf{r}''/\mathbf{R}). \tag{9.6.4}$$

The strength Φ of the spherical source is seen from Eq. (9.6.2) to be

$$\Phi = \frac{p_{\text{inc}}(r'')|\mathbf{r}''-\mathbf{R}|}{\exp(ik|\mathbf{r}''-\mathbf{R}|)} \quad \text{(units: N/m)}. \tag{9.6.5}$$

It is customary to refer the receiver response to the surface pressure at the center $\mathbf{R}_c$. Thus the source strength is

$$\Phi = p_{\text{inc}}(R_c)|R_c-\mathbf{R}|\exp(-ik|\mathbf{R}_c-\mathbf{R}|). \tag{9.6.6}$$

Substitution into Eq. (9.6.4) gives p_{receiver}, and substitution into Eq. (9.4.6) gives the (open circuited) voltage response M defined as,

$$M(\text{receiver centered at } \mathbf{R}_c, \text{ source at } \mathbf{R}) \equiv \frac{E_{0c}}{p_{\text{inc}}(R_c)}$$

$$= |\mathbf{R}_c-\mathbf{R}|\exp(-ik|\mathbf{R}_c-\mathbf{R}|\int_S h'(\mathbf{r}')\int_S L(\mathbf{r}'/\mathbf{r}'')G(r''/R)\,dS(\mathbf{r}'')\,dS(\mathbf{r}'). \tag{9.6.7}$$

Assume next that the reciprocity conditions, Eqs. (9.4.7) and (9.4.8) hold and that

$$G(\mathbf{r}''/\mathbf{R}) = G(\mathbf{R}/\mathbf{r}').$$

Then the ratio of transducer receiving response M to its transmitting response S is,

$$\frac{M(\text{receiver at } \mathbf{R}_c, \text{ source at } \mathbf{R})}{S(\text{transmitter at } R_c, \text{ field at } \mathbf{R})} = \frac{|\mathbf{R}_c-\mathbf{R}|\exp(-ik|R-R_c|-i\alpha)}{(i\omega\rho/4\pi)}. \tag{9.6.8}$$

The magnitude of this ratio is,

$$\left|\frac{M}{S}\right| = \frac{4\pi|\mathbf{R}_c-\mathbf{R}|}{\omega\rho} = \frac{2d}{\rho f} = \frac{2d\lambda}{\rho c} = J_s \tag{9.6.9}$$

$$d = |\mathbf{R}_c-\mathbf{R}|.$$

Discussion

The spherical wave reciprocity constant J_s depends on the distance from field point **R** to the center $\mathbf{R}_c$ of the transducer. It thus appears to be an arbitrary quantity since $\mathbf{R}_c$ can be variously defined. However, the receiving response (Eq. (9.3.7)) is itself defined only in terms of a reference point, also taken to be R_c. Thus J is not truly arbitrary.

J_s varies directly with the wavelength and inversely with the characteristic impedance ($= \rho c$) of the medium. This type of functional dependence is seen to be the result of choosing a point source of spherical waves upon which to calculate the receiver response. If the source is a line generating cylindrical waves the reciprocity constant has a different form. To derive it, it will be useful to state the electroacoustic reciprocity theorem in an alternate form. Let there be a transducer which can operate both as a receiver and as a transmitter. In the receiver mode let the transducer face be rigid so that the applied acoustic field force is the blocked force (F_b). The resultant voltage v_{0c} is then measured open circuit. In the transmitter mode let the transducer be driven by a constant-current I from a generator with zero internal impedance, thereby developing a normal velocity v_n on its surface. According to the reciprocity theorem the receiver and transmitter responses are related by a constant,

$$\left|\frac{E_{0c}}{F_b}\right| = \left|\frac{v_n}{I}\right| = J. \tag{9.6.10}$$

Now for a cylindrical transducer of length L and radius a, the blocked force in the receive mode is based on the incident force *in the absence of the transducer:*

$$F_b = 2\pi a L p_{\text{inc}}. \tag{9.6.11}$$

In the transmitter mode the pressure field at R is $p(R) = AH_0(kR)e^{-i\omega t}$ where A is the strength of the transmitter and H_0 is the Hankel function of zero order. For given normal velocity v_n on the surface $r = a$ ($\ll \lambda$) where $H_0(k) \simeq (2i/\pi) \ln r \exp -i\omega t$, one has $A = \pi^2 a f v_n \rho_0$ as may be seen from the acoustic boundary condition $(\partial p/\partial n)\big|_{r=a} = -i\omega\rho v_n$. In the farfield, $H_0(kR) = (2/\pi kR)^{1/2} \exp [ik(R - ct) - i\pi/4]$. Hence $p(R) = \pi a \rho v_n (cf/R)^{1/2} \exp [ik(R - ct) - i\pi/4]$. Substitution of F_b and v_n into Eq. (9.6.10) leads to the result,

$$\frac{E_{0c}}{p_{\text{inc}}} = \left|\frac{p(R)}{I}\right| J_c; \quad J_c = \frac{2L}{\rho c}\sqrt{\frac{cR}{f}} \quad \text{(units of } J\text{: m}^5/\text{NS)} \tag{9.6.12}$$

J_c is the desired cylindrical-wave reciprocity parameter.

Equation (9.6.9) is valid for any point **R** in the medium. From this it is deduced that the directivity pattern of the transducer acting as a transmitter is the same as its pattern when acting as a receiver. However, the reciprocity theorem requires that the orientation of the transducer relative to the field point **R** be the same whether transmitting or receiving.

9.7 PASSIVE LINEAR ACOUSTIC TRANSDUCERS WITH FIXED VELOCITY DISTRIBUTION

In Eq. (9.2.13) the (unknown) velocity $v_n(\mathbf{r})$ is obtained by inverting the integral equation (of mechanical coupling) Eq. (9.2.11). The result is then inserted into Eq. (9.3.4) thereby giving the pressure distribution $p(\mathbf{r})$ on the surface of the transducer.

Suppose now that, independent of the manner of excitation, the transducer-face normal velocity has a *fixed* spatial distribution at a particular frequency, that is,

$$v_n(\mathbf{r}) = v_{\text{ref}}\beta(\mathbf{r}), \quad \beta(\mathbf{r}) \text{ known.} \tag{9.7.1}$$

Here v_{ref} is a reference velocity, and both v_{ref} and β are complex quantities. If the transducer face is imagined to be a pair of mechanical terminals the power flow outward from these terminals is given by

$$W = \text{Re}\{fv^*\} = \text{Re}\left\{\int p(\mathbf{r})v_n^*(\mathbf{r})\,dS(\mathbf{r})\right\}$$

$$f = \int p(\mathbf{r})\beta^*(\mathbf{r})\,dS(\mathbf{r}). \tag{9.7.2}$$

Following Foldy [2] one substitutes Eq. (9.7.1) into Eq. (9.3.4), then multiplies Eq. (9.3.4) by $\beta^*(\mathbf{r})$ and integrates over the surface. The result is the force f of the medium,

$$f = f_0 - Z_r V_{\text{ref}} \tag{9.7.3}$$

$$f_0 = \int_S \beta^*(\mathbf{r})p_g(\mathbf{r})\,dS = \frac{1}{4\pi}\int \beta^*(\mathbf{r})\,G(\mathbf{r}/\mathbf{r}')\,\frac{\partial p_g(\mathbf{r}')}{\partial n}\,dS(\mathbf{r}')\,dS(\mathbf{r}) \tag{9.7.4}$$

$$Z_r = \frac{i\omega\rho}{4\pi}\int_S\int_S \beta^*(\mathbf{r})\,G(\mathbf{r}/\mathbf{r}')\beta(\mathbf{r}')\,dS(\mathbf{r}')\,dS(\mathbf{r}) \quad \left[\text{units: } \frac{\text{Ns}}{\text{m}}\right]. \tag{9.7.5}$$

The force f_0 is identified as the *generated force* of the medium considered to be a mechanical force generator. The term $Z_r\, v_{\text{ref}}$ is the *force drop* due to the velocity v_n.

Receiving Response and Transmitting Response

The quantities v_n, f, F_0, and Z_r allow us to obtain the transmitting responses of a transducer with fixed velocity distribution. To do this we return to Eq. (9.2.11), multiply by $\beta(\mathbf{r})$, integrate over the transducer surface area, then solve for V_{ref}:

$$V_{\text{ref}} = \frac{-k'I}{Z_0 + Z_r} \tag{9.7.6}$$

$$Z_0 = \int\int \beta(\mathbf{r})\,Z_0(\mathbf{r}/\mathbf{r}')\beta(\mathbf{r}')\,dS(r')\,dS(\mathbf{r}) \quad \text{(units: Ns/m)}. \tag{9.7.7}$$

$$k' = \int h(\mathbf{r})\beta(\mathbf{r})\,dS(\mathbf{r}) \quad \text{(units: N/A)}. \tag{9.7.8}$$

The transmitting response for this (known) velocity distribution $v_{\text{ref}}\beta(\mathbf{r}')$ is then given by

$$S(R) = \frac{p(R)}{I} = \frac{i\omega\rho k'}{4\pi(Z_0 + Z_r)}\int_S G(R/\mathbf{r}')\beta(\mathbf{r}')\,dS(\mathbf{r}'). \tag{9.7.9}$$

To find the receiving response of a transducer with fixed velocity distribution we return to Eq. (9.2.10) and using Eq. (9.3.4) we identify

$$\Gamma_0(\mathbf{r}) = p_g(\mathbf{r}) - \frac{1}{4\pi} \int G(\mathbf{r}/\mathbf{r}') \frac{\partial p_g(\mathbf{r}')}{\partial n} dS(\mathbf{r}'). \tag{9.7.10}$$

Substitution in Eq. (9.2.10), followed by multiplication of the result by $\beta^*(\mathbf{r})$ and integration over surface area, then solving for v_{ref} lead to

$$v_{\text{ref}} = \frac{f_0 - k'I}{Z_0 + Z_r}. \tag{9.7.11}$$

Now from Eq. (9.1.8)

$$E = kv_{\text{ref}} + Z_b I \tag{9.7.12}$$

$$k = \int h'(\mathbf{r})\beta(\mathbf{r})dS(\mathbf{r}). \tag{9.7.13}$$

Choosing an electrical load impedance $Z_l = -E/I$, one substitutes Eq. (9.7.11) and (9.7.13) into Eq. (9.7.12), which then gives the output voltage

$$E = \frac{kZ_l f_0}{(Z_l + Z_b)(Z_0 + Z_r) - kk'}. \tag{9.7.14}$$

(Note again that Z_b refers to the transducer and Z_l to the electric generator, both expressed as electrical ohms.) In order for this expression to be reduced to the receiving response, E must become the open-circuit E_{0c} by making $Z_l \to \infty$. Also f_0 must become the free field incident pressure p_g. The latter transformation requires the calculation of f_0 for a specific acoustic field. Let this field be due to a point source with strength Φ at distance $\mathbf{R}$, and let the center of the receiver be at $\mathbf{R}_c$. Then employing the definition of the Green's function and using Eq. (9.6.4) and (9.6.5) as models, one has

$$f_0 = \Phi \int G(\mathbf{r}/\mathbf{R})\beta^*(\mathbf{r})dS(\mathbf{r}) \tag{9.7.15}$$

$$\Phi = \frac{p_g(r)|\mathbf{R} - \mathbf{R}_c|}{\exp(ik|\mathbf{R} - \mathbf{R}_c|)}. \tag{9.7.16}$$

The receiving response of the transducer with fixed distribution of velocity then reduces to

$$M(R) = \frac{E_{0c}}{p_f(\mathbf{R}_c)} = \frac{k|\mathbf{R} - \mathbf{R}_c| \exp(-ik|\mathbf{R} - \mathbf{R}_c|}{Z_0 + Z_r} \int G(\mathbf{r}/\mathbf{R})\beta^*(\mathbf{r})dS(\mathbf{r}). \tag{9.7.17}$$

This formula for M together with the formula for S (Eq. (9.7.9)) from the basis of the reciprocity theorem discussed in the next section.

Electroacoustic Reciprocity for Transducers with Fixed Velocity Distribution

Division of Eq. (9.7.17) for $M(\mathbf{k})$ and Eq. (9.7.9) for $S(\mathbf{R})$ gives the reciprocity theorem for electroacoustic transducers with fixed velocity distribution. If one sets the conditions of reciprocity,

$$|k| = |k'| \tag{9.7.18}$$

and

$$\beta^*(r) = e^{i\gamma}\beta(\mathbf{r}) \tag{9.7.19}$$

then

$$\frac{|M(\mathbf{R})|}{|S(\mathbf{R})|} = \frac{2d\lambda}{\rho c}, d = |\mathbf{R} - \mathbf{R}_c|. \tag{9.7.20}$$

Thus reciprocity is established, provided conditions Eqs. (9.7.18) and (9.7.19) hold. Furthermore if one writes

$$\beta(r) = g(r)e^{i\phi(r)} \tag{9.7.21}$$

then condition (9.7.19) leads to

$$i(\gamma + 2\phi(\mathbf{r})) = \pm 1$$

or

$$\phi(\mathbf{r}) = n\pi - \gamma/2, \; n = 0, \; 1, \; 2 \ldots . \tag{9.7.22}$$

Since γ is independent of $\mathbf{r}$, then ϕ must also be independent of $\mathbf{r}$. Hence the phase of any two adjacent points on the transducer surface must be 0° or 180° [2].

Directivity Factor

A transducer moving with face-velocity v_n radiates a pressure $p(\mathbf{R})$ to a field point $\mathbf{R}$ given by Eq. (9.2.6). Choosing $\mathbf{R}$ to be a surface point $\mathbf{r}$ one finds the real power radiated is given by Eq. (9.7.2),

$$W_{\text{rad}} = \text{Re}\left\{\int\int \frac{-i\omega\rho}{4\pi} G(\mathbf{r}/\mathbf{r}')v_n(\mathbf{r}')dS(\mathbf{r}')v_n^*(\mathbf{r})dS(\mathbf{r})\right\} = v_{\text{ref}}^2 r_r \tag{9.7.23}$$

in which

$$r_r = \text{Re}Z_r$$

where Z_r is Eq. (9.7.2).

Now by definition the directivity factor of a transducer is the ratio,

$$DF = \frac{|p(\mathbf{R})|^2}{\rho c}\frac{A(\mathbf{R})}{W_{\text{rad}}} \quad \text{(units: none)}. \tag{9.7.24}$$

Here, $A(\mathbf{R})$ is the area of a sphere of radius $\mathbf{R}$. Thus the DF is not specified unless the radius vector $\mathbf{R}$ is specified in magnitude and direction. It is customary to take $\mathbf{R}$ in the direction of maximum transmitting (or receiving) response, and to choose its magnitude to be a unit distance (say one yard or one meter). Substituting of Eqs. (9.7.23) and (9.2.6) lead to

$$DF = \frac{\omega^2 |\mathbf{R}|^2 \rho}{4\pi c r_r} \left| \int G(\mathbf{R}/\mathbf{r}')\beta(\mathbf{r}')\, dS(\mathbf{r}') \right|^2, \quad |\mathbf{R}|^2 \gg 1. \tag{9.7.25}$$

It is clear from the structure of this equation that the transmitting and receiving factors of a reciprocal transducer are equal.

Available Acoustic Power Upon Reception

Let the origin of coordinates of a receiving transducer be at its acoustic center. Assume a point source (strength Φ (units: N/m)) at a (great) distance $\mathbf{R}$ is radiating a plane wave field which is incident on the receiver at some angle relative to the coordinate system. According to Eq. (9.3.4) the field a $\mathbf{R}$ in the presence of the transducer moving at velocity v_n is

$$p(\mathbf{r}) = \Phi G(\mathbf{r}/\mathbf{R}) - \frac{i\omega\rho v_{\text{ref}}}{4\pi} \int G(\mathbf{r}/\mathbf{r}')\beta(\mathbf{r}')\, dS(\mathbf{r}'). \tag{9.7.26}$$

Here, as always, G is the Green's function associated with the medium *and* the baffle structure of the receiver.

The net force f on the transducer face is the medium force which generates acoustic power (Eq. (9.7.2)) in the receiver

$$W = \text{Re}\{f v_{\text{ref}}^*\} = \text{Re}\left\{\frac{|f|^2}{Z}\right\} \tag{9.7.27}$$

$$Z \equiv \frac{f}{v_{\text{ref}}^*}.$$

The symbol Z is the mechanical impedance of the transducer face calculated with reference to velocity v_{ref}. Integrating Eq. (9.7.2) with $p(\mathbf{r})$ given by Eq. (9.7.26), then using $v_{\text{ref}} = f/z$, one obtains the net force f,

$$f = \frac{\Phi \int \beta^*(\mathbf{r}) G(\mathbf{r}/\mathbf{R})\, dS}{1 - \frac{i\omega\rho}{4\pi z} \int\int \beta^*(r) G(\mathbf{r}/\mathbf{r}')\beta(\mathbf{r}')\, dS(\mathbf{r}')\, dS(\mathbf{r})}. \tag{9.7.28}$$

Using the definition of Z_r (Eq. (9.7.5)) one readily derives the real power absorbed by substituting Eq. (9.7.28) into (9.7.29) and taking the real part,

$$W = \frac{\rho c |\mathbf{R}|^2 r \mathscr{I} \left| \int \beta^*(\mathbf{r}) G(\mathbf{r}/\mathbf{R})\, dS \right|^2}{|z + z_r|^2} \tag{9.7.29}$$

$$r = \text{Re}Z$$

$$\mathscr{I} = \frac{|\Phi|^2}{\rho c} \frac{1}{|\mathbf{R}|^2}.$$

The absorbed power is a maximum when $z = z_r^*$, that is, when

$$r = r_r, \quad x = -x_r. \tag{9.7.30}$$

Then, using the definition of the directivity factor, Eq. (9.7.25), one finds

$$W_{\max} = \frac{\pi \oint c^2 (DF)}{\omega^2} = \frac{\lambda^2 (DF) \oint}{4\pi}. \tag{9.7.31}$$

Discussion

The maximum power that can be absorbed by a receiver from a plane wave incident in a given direction is seen to depend on three factors. A first factor is the intensity of the incident wave, which is to be expected. However, because the receiver is directional this intensity must be modified by the directivity factor of the receiver which magnifies (or reduces) it depending on direction. This also is an expected result. It is important to note that this receiving directivity is calculated relative to the direction of incidence of the plane wave. The third factor is the square of the wavelength. Its appearance is due to the fact that $W_{\max}$ varies inversely as frequency squared. Since however DF varies directly as frequency squared, the wavelength dependency is seen to be directly the result of including the DF explicitly in Eq. (9.7.31).

Available Power Efficiency

In an electroacoustic receiver, the transfer of power from the acoustic field into the electric field may be visualized in an ideal way. In the acoustic field one may take the force of the medium on the transducer face to be f_0 in Eq. (9.7.3), neglecting the term $Z_r v_{\text{ref}}$ since v_{ref} is small enough to render this term negligible. If the impedance imposed by the medium on the face is the acoustic radiation impedance $z_r (= r_r - ix_r)$, and if the power transfer between the acoustic field and the electric field is ideal (= matched) then $Z_l (= R_l - iX_l)$ of the electric load approaches $2R_l$ and z_r approaches $2r_r$. The ideal acoustic power transferred is $|f_0|^2/4r_r$ and the ideal electrical power generated is $|E_{0c}|^2/4R_l$.

The ratio of the two ideal powers gives the available power efficiency $(\eta_{\text{ideal}})_{\text{rec}}$. Using Eq. (9.7.14) with $E = E_{0c}$ one finds:

$$(\eta_{\text{ideal}})_{\text{rec}} = \frac{|E_{0c} I|}{|f_0 v_{\text{ref}}|} = \left| \frac{E_{0c}^2}{Z_l} \times \frac{k^2 Z_l^2 f_0^2}{(Z_b + Z_l)(Z_0 + Z_r) - kk')^2} \right| \times \left| \frac{1}{f_0^2/4r_r} \right|$$

or

$$(\eta_{\text{ideal}})_{\text{rec}} = \frac{4|k|^2 r_r R_l}{|(Z_l + Z_b)(Z_0 + Z_r) - kk'|^2}. \tag{9.7.32}$$

In the case of an electroacoustic transmitter f_0 is replaced by $f_0 - Z_r v_{\text{ref}}$ in both the acoustic field and in Eq. (9.7.14). The available power efficiency for transmission is again Eq. (9.7.32), excepting that k' replaces k,

$$(\eta_{\text{ideal}})_{\text{transmit}} = \frac{4|k'|^2 r_r R_l}{|(Z_l + Z_b)(Z_r + Z_0) - kk'|^2}. \tag{9.7.33}$$

If the transducer is reciprocal, $|k'|^2 = |k|^2$; then the available power efficiency is the same for transmitting or receiving modes.

For perfect matching the electrical terminating impedance of the electric generator is made the complex conjugate of the transducer electrical terminating impedance. Under this condition of matching the above ratios of ideal powers are called *standard available power efficiency* in each case.

Threshold Pressure of a Receiver

Assume a condition of ideal power transfer from an incident plane wave to an electrical load resistance R_l. Then the electrical power absorbed for the lowest detectable acoustic pressure p_T can be written in terms of the threshold open circuit voltage E_T. The maximum acoustic power ideally transferred is given by Eq. (9.7.31). Hence, by definition of the available power efficiency, the threshold pressure is

$$|p_T|^2 = \frac{|E_T|^2}{4R_l} \frac{\rho c 4\pi}{\lambda^2 (DF)}. \tag{9.7.34}$$

Now $|E_T|^2/4R_l$ must be equal to the averaged noise power $<E_N^2/R_l>$ due to noise in the receiver circuitry. Such noise is a sum of ambient noise in the medium and thermal noise in the transducer. Since ambient noise itself may be the desired signal pressure we consider here only thermal noise. For a receiving band Δf Hz wide, at absolute temperature T (units: °K) this is given by,

$$\frac{<E_N^2>}{R_l} = 4\kappa T \Delta f \tag{9.7.35}$$

$$\kappa = \text{Boltzman's constant} = 1.38 \times 10^{-23} \frac{Nm}{°K}.$$

From the definition of threshold voltage one sets $<E_N^2> = |E_T|^2$. Then the threshold pressure becomes:

$$|p_T| = \left[\frac{4\pi \rho c \kappa T \Delta f}{\lambda^2 (DF) (\eta_{\text{ideal}})_{\text{rec}}} \right]^{1/2} \tag{9.7.36}$$

It is immediately seen that by making the directivity factor indefinitely large the threshold pressure may be made indefinitely small. An empirical formula for the directivity factor of a plane-surface transducer in an infinite baffle is known to be [4],

$$DF = 4\pi \frac{A}{\lambda^2} - \frac{2\sqrt{A}}{\lambda} + 2. \tag{9.7.37}$$

When $A << \lambda^2$ then $DF = 2$. The threshold pressure is then

$$p_T \propto \frac{1}{\lambda} \propto \omega \quad \text{for } (\eta_{ideal})_{\text{rec}} = \text{constant}. \tag{9.7.38}$$

When, however, $A/\lambda^2 >> 2$ then the threshold pressure is independent of frequency but varies inversely as the square-root of the transducer face area

$$p_T \propto (A)^{-1/2}. \tag{9.7.39}$$

The use of threshold pressure as a criterion of excellence in receiver design is seen to be wanting because a mere increase in receiver area reduces the reception threshold regardless of any other electromechanical, or electroacoustic feature of the transducer. A more significant criterion of goodness is the available power efficiency, Eqs. (9.7.32) or (9.7.33), which involves electrical, mechanical and acoustic parameters in a meaningful way.

Receiver Capture Area

The maximum power that can be extracted from a plane wave by a transducer with directivity factor DF is given by Eq. (9.7.31). Assume now that A/λ^2 is large enough so that

$$DF \simeq 4\pi \frac{A_c}{\lambda^2}. \tag{9.7.40}$$

Substitution into Eq. (9.7.31) leads to the formula

$$W_{max} \approx A_c \mathscr{I}, \quad \text{or } A_c \approx W_{max}/\mathscr{I}. \tag{9.7.41}$$

The symbol A_c is the *capture area* of the receiver. Its significance is this: if the frequency is "high enough" such that DF is approximately equal to the first term in Eq. (9.7.37), and $A = A_c$ = actual face area of the transducer then the available acoustic power for reception is the product of A_c and the intensity of the incident plane wave. The capture area is then related to the directivity factor by the formula,

$$A_c = \frac{(DF)\lambda^2}{4\pi} = \frac{(DF)c^2}{4\pi f^2}. \tag{9.7.42}$$

If DF is proportional to f^2 then A_c could be independently of f. A_c is thus seen to be a significant design parameter of receivers.

Generator Force (f_0) of the Medium

From the concept of available acoustic power upon reception (Eq. (9.7.31)) and discussion thereafter) one may deduce from the formula for the power matched ideal transducer that

$$\frac{|f_0|^2}{4r_r} = \frac{\lambda^2(DF)\,\mathscr{I}}{4\pi}$$

or (9.7.43)

$$|f_0| = \sqrt{\frac{\lambda^2(DF)\,\mathscr{I} r_r}{\pi}}.$$

Thus a plane wave of intensity $\mathscr{I}$ incident upon a receiver develops a generator force f_0 given by Eq. (9.7.43). This is equivalent to an "open-circuit force" exerted by the medium on the transducer face. The face responds with motion v_{ref}, and the force f actually delivered to the transduction mechanism through the radiation impedance Z_r is given by,

$$f_0 = f + Z_r v_{ref}. \tag{9.7.44}$$

In an equivalent circuit, constructed with "force across" and "velocity through," the generator force f_0 is seen to be in series with the radiation impedance Z_r while the delivered force f is across the terminals of the medium force generator.

Transmitting Response of Transducers In the Presence of Volume Distributed Sources

Equation 9.3.4 predicts the steady state pressure field p of a transducer with normal surface velocity V_n in the presence of a second field p_g generated by external sources. A more general formulation predicts the pressure field under transient excitation $p_g(\mathbf{r}, t)$. In this case the Green's function for unbounded space is,

$$g = \frac{\delta[(R/c) - (t - t_0)]}{R}$$

$$R = |\mathbf{r} - \mathbf{r}'|$$

and integration is with respect to time to as well as space $\mathbf{r}'$. The source incident pressure (p_{inc}) is taken to be due to volume distributed sources q. In this general case q may be monopole sources M, dipole sources F_i, and quadrupole sources T_{ij}. Integration with respect to time then changes time dependency of these volume sources (as well as of equivalent surface sources) into dependency on *retarded time*, i.e.,

$$q\left(\mathbf{r},\ t - \frac{R}{A_0}\right),\ A_0 = \text{speed of wave propagation}$$

written briefly as $[q]$. Of particular interest is the volume source T_{ij} of a turbulent fluid whose velocity structure is characterized by a velocity field C_i, and by shear stress τ_{ij},

$$T_{ij} = \rho C_i C_j - \tau_{ij}.$$

All sources $q(r',\ t_0)$ generate a pressure p on the surface of the transducer, which, together with the fluid shear stress τ_{ij}, makes up the stress vector $P_i = n_j(p\delta_{ij} - \tau_{ij})$. Following Eq. 9.3.4 (in its transient form) the pressure fluctuation above ambient pressure (p_0) at field point $\mathbf{r}$ is,

$$(p - p_0)4\pi = \frac{\partial^2}{\partial x_i \partial x_j}\int_V \frac{[T_{ij}]}{R}\,dV(\mathbf{r}') - \frac{\partial}{\partial x_i}\int_V \frac{[F_i]}{R}\,dV(\mathbf{r}') + \int_V \frac{1}{R}\left[\frac{\partial M}{\partial t}\right]dV(\mathbf{r}')$$

$$+ \frac{\partial}{\partial x_i}\int_S \frac{1}{R}[P_i]\,dS + \frac{\partial}{\partial x_i}\int_S \frac{1}{R}[\rho C_i V_n]\,dS - \int_s \frac{1}{R}\left[\frac{\partial \rho V_n}{\partial t}\right]dS.$$

Here, the term in P_i represents diffraction from the transducer considered to be a solid body, and the terms in V_n represent acoustic radiation due to the normal surface velocity on the moving part of the transducer surface. V_n is caused both by the external sources q and by internal drive forces of transduction (such as voltage, amperage, etc).

REFERENCES

[1] L.L Foldy, H. Primakoff, J. Acous. Soc. Am. **17**, 109-120 (1945).

[2] L.L. Foldy, J. Acous. Soc. Chem. **21**, 595-604 (1949).

[3] H. Primakoff, L.L. Foldy, J. Acous. Soc. Am. **19**, 50-58 (1947).

[4] J.W. Horton, "Fundamentals of Sonar," U.S. Naval Institute Annapolis 1957 (p. 200).

Chapter 10
HYDROPHONES CONSTRUCTED OF PIEZOELECTRIC COMPOSITE MATERIALS

10.0 INTRODUCTION

The use of polarized piezoactive ceramic materials as the principal ingredients in hydrophones is widespread. They can be produced in large quantities at economical prices, have good receiving sensitivity and dynamic range, require no dc polarizing current (or voltage), have a reasonable life expectancy and can be built in many shapes.

In applications important to undersea surveillance of potentially hostile navies there is a need for hydrophone with large capture areas. While such a hydrophone can be constructed of groups of piezoelectric ceramics these tend to be heavy in weight, brittle and therefore easily damaged, requiring careful matching of component ceramics to ensure phase and sensitivity uniformity, exhibit deterioration of performance with depth of submersion, and are likely to be bulky.

A new material (generally called piezoelectric ceramic/polymer composite) which is inherently lightweight and compliant, with improved piezoelectric properties, and which can be built into large area hydrophone receivers in ways that make them relatively insensitive to hydrostatic pressure, has been the focus of research. The goals of such research and the achievements to'date are discussed in this chapter.

10.1 HYDROPHONE FIGURE-OF-MERIT

The concept of available power efficiency of a transducer acting as receiver is discussed in Sect. 9.7. There it was defined as the ratio of (ideal) electrical power developed in the electric load to incident acoustic power developed on the face of the transducer. This ratio, given by Eq. (9.7.32), is chosen here to be the figure-of-merit of a hydrophone. For purposes of providing a useful guide in materials research Eq. (9.7.32) can be reduced to a simpler form closely related to piezoelectrics.

We assume first that the transduction properties of material in question can be described by the linear static equations of piezoelectricity. Two alternate sets of coupled equations are chosen in order to interrelate piezoconstants:

$$(1)\ \begin{cases} S_l = s_{lj}^E T_j + d_{ml} E_m \\ D_m = d_{mnl} T_l + \epsilon_{mk}^T E_k \end{cases} \qquad (2)\ \begin{cases} S = s_{lj}^D T_j + g_{ml} D_m \\ E_m = -\, g_{ml} T_l + \beta_{mk}^T D_k \end{cases} \tag{10.1.1}$$

Here d_{ml} is the charge density-stress constant and g_{ml} is the electric field-stress constant. In these (tensor) equations let the stress T_l be the component external hydrostatic pressure p_h. Considering only electromechanical conversion with both D and E measured in the 3-direction one deduces that in terms of the hydrostatic piezoelectric coefficient d_h and g_h,

$$D_3 = d_h p_h \qquad \left(\text{units of } d_h\text{: } \frac{C}{m^2} \times \frac{m^2}{n} = C/N \right) \tag{10.1.2}$$

PREVIOUS PAGE IS BLANK

$$E_3 = -g_h p_h \quad \left[\text{units of } g_h\text{: } \frac{V}{m} \times \frac{m^2}{N} = \frac{Vm}{N}\right].$$

Cady [1] notes that

$$d_h = d_{31} + d_{32} + d_{33} = 2d_{31} + d_{33}; \quad g_h = 2g_{31} + g_{33}. \tag{10.1.3}$$

The electric energy stored because of hydrostatic deformation is

$$\mathscr{E}_{\text{elec}} = E_3 D_3 = -g_h d_h p_h^2 \quad (\text{units: Nm/m}^3). \tag{10.1.4}$$

Now under static conditions, for a transducer structure with mechanical compliance C_M (units: m^2/N), the mechanical energy supplied by the medium is

$$E_{\text{mech}} = p_h^2 C_M \quad (\text{units: Nm/m}^3). \tag{10.1.5}$$

Thus, the magnitude of the ratio of energies is,

$$\frac{\mathscr{E}_{\text{elec}}}{\mathscr{E}_{\text{mech}}} = \frac{g_h d_h}{C_M} \quad (\text{units } g g_h d_h\text{: m}^2/\text{N}). \tag{10.1.6}$$

If the transduction were matched (= ideal coupling) this ratio would be the available power efficiency on reception. As it is, it can serve as a figure-of-merit even though the transduction is nonideal. For brievity, the figure-of-merit is taken to be the $g_h d_h$ product for transducers operating in the hydrostatic mode. It is related to the usual definition of coefficient of electromechanical coupling on reception, k_c^2 in the following way:

$$k_c^2 = \frac{\mathscr{E}_{\text{elec}}}{\mathscr{E}_{\text{elec}} + \mathscr{E}_{\text{mech}}} = \frac{g_h d_h / C_M}{1 + g_h d_h / C_M}. \tag{10.1.7}$$

The figure-of-merit is also related to open-circuit receiving sensitivity, M_0 defined by Eq. (9.7.18). In the case of a simple receiver structure composed of a plate or shell, of thickness t and receiver area A, Eq. (10.1.4) takes the form

$$\frac{V}{t} \times \frac{C}{A} = -g_h d_h p^2.$$

Since

$$C = \left(\frac{\epsilon A}{t}\right) V = C^T V, \quad (C^T = \text{free capacity})$$

it is seen that

$$\left(\frac{V}{p}\right)^2 \frac{1}{\mathscr{V}} C^T = -g_h d_h, \quad \mathscr{V} = At.$$

By choosing $V = V_{0c}$, one may generalize the left-hand side of this formula to apply to any mode of piezoelectric coupling:

$$f_H = \frac{M_0^2 C^T}{\mathscr{V}} \quad \text{(units: m}^2\text{/N)}. \tag{10.1.8}$$

This is the figure-of-merit derived by Woollett [2], who takes $\mathscr{V}$ however to be the totally enclosed volume.

Evidently one goal of research in piezoelectric composities is to maximize $g_h d_h$ for given C_M.

We now return to Eq. (10.1.1) and consider the purely electric field relation,

$$D_3 = \epsilon_{33}^T E_3.$$

This equation states that the generation of a time-varying voltage in the receiver circuit at zero mechanical stress is accompanied by time-varying accumulation of charge (i.e., electric current). In order to realize the maximum electric energy the current should be maximum. This requires a large ϵ_{33}^T. Thus, a second goal of research in piezoelectric/polymer composites is to obtain as large a permittivity as possible.

Since light weight of hydrophone structure is desirable a third goal of research is to reduce the mass density of the composite. A fourth goal of research is to make the piezoactive material more elastically compliant so that it is a better impedance match to water.

Any achievement of these goals must compete with existing, highly serviceable materials.

To provide a reference for the achievements of recent research we list here in Table 10.1.1 those properties of polarized piezoceramic materials (and polymer film) that are appropriate to this chapter.

Table 10.1.1 — Piezoelectric Ceramic Materials for Hydrophones [3]

Property / Material	ρ (kg/m^3)	K_{33}^T	Curie Point (°C)	$g_{31} \cdot d_{31}$	$g_{33} \cdot d_{33}$	$g_h \cdot d_h$	$g_{15} \cdot d_{15}$
				10^{-15} m^2/N			
Type I	7500	1300	320	1,365	7,543	168	19,542
Type II	7750	1700	350	1,840	8,875	70	22,309
Type II-M	7450	3400	190	2,253	11,135	112	19,859
Type III	7600	1000	300	976	5,341	112	—
Type IV	5500	1200	115	319	2,101	102	5,082
$PbNb_2O_6$	6000	225	570	41	3,612	2,244	—
Flexible Ceramic	4000	30	—	—	112*	38*	—
PVF_2	1800	10	100+	3,480*	—	343*	—

*estimated value; maximum temperature

10.2 CONNECTIVITY OF PHASES OF COMPOSITE STRUCTURES

The word "phase" that appears in desciption of piezoelectric/polymer composites is defined as one component material of a system of several possible components. Thus for example a biphasal system consists of two distinct component materials of different physical and chemical structures. Similarly, a multiphased system consists of several distinct components.

In the formation of multiphase composites it has been found useful to distinguish between systems with the same phases but different structures among the phases. For example, the biphasal system piezoelectric/polymer can be different from polymer/piezoelectric. Position in the word sequence serves to distinguish them. The distinction is brought out by the concept of *connectivity.* This is described next.

The component material in each phase may be dispersed throughout the volume of the composite in various ways. It may be *self-connected in one-dimension,* meaning that the component material appears essentially as thin linear rods (or fibers) pointing in one direction of a rectangular coordinate system. It may be *self-connected in two-dimensions,* meaning that the component material accupies two dimensions of (say) a rectangular block. This may be a two-dimensional layer of the material of phase 1 or alternatively, a group of linear rods (or fibers) pointing in the x-direction, and a second group of identical rods (or fibers) pointing in the y-direction. It may be *self-connected in three dimensions,* meaning that the component is an isotropic block of material, or alternatively, three groups of linear rods pointing in the x, y, and z coordinate directions. Finally, the component may not be self-connected in any direction, like a random dispersion of voids in a cube of material.

To identify a composite and thereby describe its essential phasal construction, a numerical value chosen from 0, 1, 2, 3 is assigned to the phase. These numbers mean: 0 = not self-connected; 1, 2, 3 connected in one, two or three directions respectively. As an example of such composite connectivity identification we choose the verbal sequence "elastomer /*PZT*/ spheres" and assign the numbers, 3-1-0. This sequence means the following: the elastomer phase is self-connected in 3 dimensions (most likely a block); the *PZT* phase is self-connected in 1-dimension (most likely a collection of linear rods (or fibers)) pointing (say) along the x-direction and embedded in the elastomer; the "spheres" phase is a collection of spherical bodies randomly dispersed throughout the elastomer.

A second example helps distinguish between 0-0 and 3-3 connectivity. A 0-0 composite consists of particles of phase 1 and phase 2 randomly dispersed in each other in a volume. By contrast a 3-3 composite consists of a 3-dimensional skeleton of phase 1 interwoven with a skeleton of phase 2.

This numbering scheme in conjunction with a verbal sequence, though not without its ambiguities, serves to label a particular composite. More complete descriptions are always possible.

Figure 10.2.1a, b, c, and d are four examples of connectivity of piezoceramic/polymer types.

10.3 SERIES, PARALLEL CONNECTIVITIES; HYDROSTATIC PIEZOELECTRIC CONSTANTS

Figure 10.3.1 shows two disphasic composites with 1-1 connectivity, if phases 1 and 2 are rods (or fibers); or 2-2 connectivity, if phases 1 and 2 are layers. In (a) the phases are connected *in series* with the electrodes (that is, the electrodes form layers parallel with the phases). The composite piezoelectric constants (marked with an overhead) are written in terms of volume fractions ν:

$$\text{series connection} \begin{cases} \bar{\mathbf{d}}_{33} = \dfrac{\nu_1 d_{33}^{(1)} \epsilon_{33}^{(2)} + \nu_2 d_{33}^{(2)} \epsilon_{33}^{(1)}}{\nu_1 \epsilon_{33}^{(2)} + \nu_2 \epsilon_{33}^{(1)}} \\ \bar{\mathbf{g}}_{33} = \nu_1 g_{33}^{(1)} + \nu_2 g_{33}^{(2)} \end{cases} \tag{10.3.1}$$

in which 1 and 2 indicate phase 1 and phase 2.

In (b) the phases are connected in parallel relative to the electrodes (that is, phases 1 and 2 are perpendicular to the electrodes). The composite piezoelectric constants are:

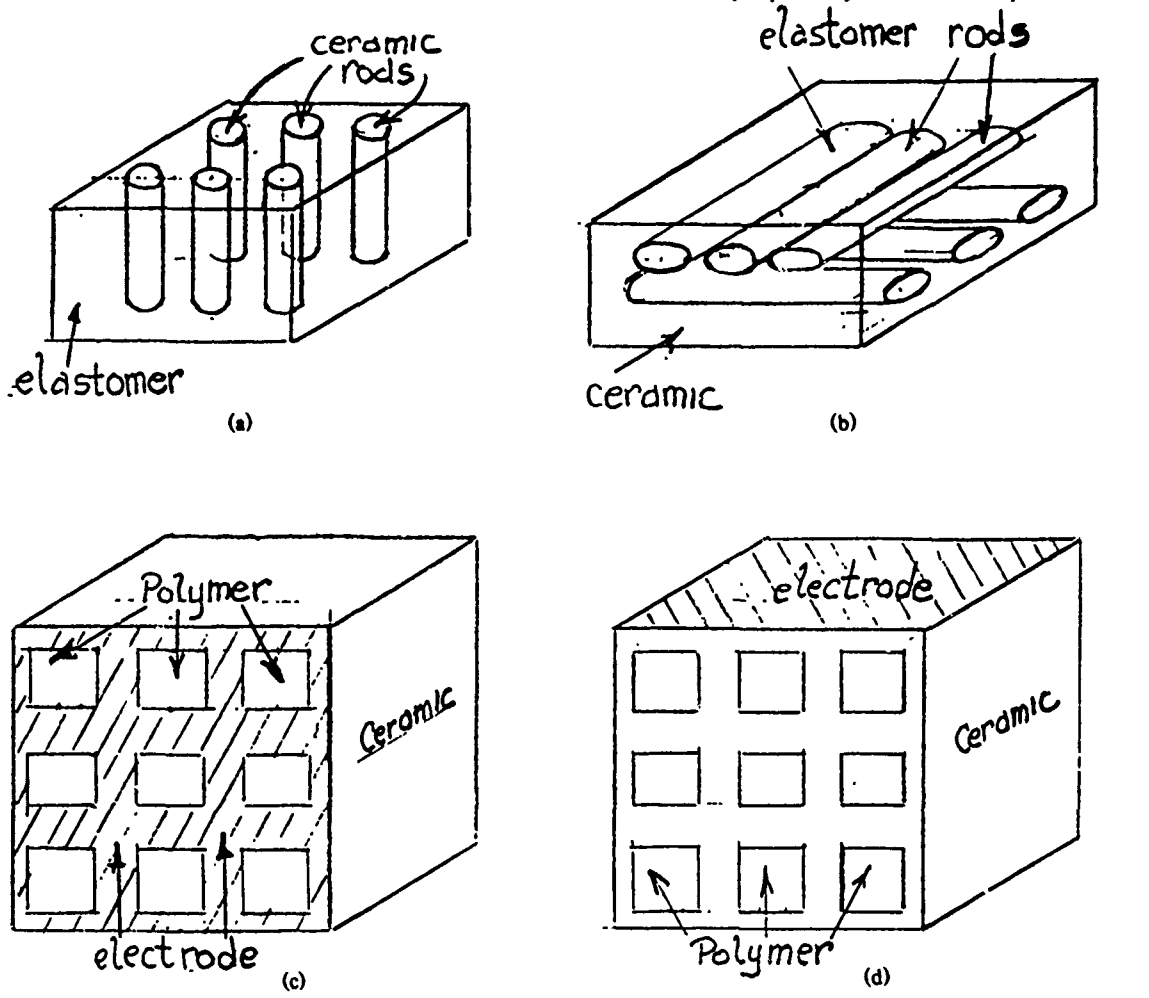


Fig. 10.2.1 — Example of connectivity of composite materials. (a) piezoceramic/elastomer, 1-3 connectivity, (b) piezoceramic/elastomer, 3-2 connectivity, (c) piezoceramic/elastomer, 3-1P connectivity, (d) piezoceramic/elastomer, 3-1s connectivity.

$$\text{parallel connection} \begin{cases} \bar{\mathbf{d}}_{33} = \dfrac{\nu_1 d_{33}^{(1)} s_{33}^{(2)} + \nu_2 d_{33}^{(2)} s_{33}^{(1)}}{\nu_1 s_{33}^{(2)} + \nu_2 p_{33}^{(1)}} \\ \bar{g}_{33} = \dfrac{\nu_1 d_{33}^{(1)} s_{33}^{(2)} + \nu_2 d_{33}^{(2)} s_{33}^{(1)}}{(\nu_1 d_{33}^{(2)} + \nu_2 s_{33}^{(1)})(\nu_1 \epsilon_{33}^{(1)} + \nu_2 \epsilon_{33}^{(2)})} \end{cases} \tag{10.3.2}$$

As will be noted later in this chapter composites with parallel connection show sizable $\mathbf{g}_{33}$ constants. The *hydrostatic* sensitivity $\mathbf{d}_h$ for such a parallel connection is a combination of $\mathbf{d}_{33}$ and $\mathbf{d}_{31}$:

$$\bar{\mathbf{d}}_h = \bar{\mathbf{d}}_{33} + 2\bar{\mathbf{d}}_{31} \cong \frac{\nu_1 d_{33}^{(1)} s_{33}^{(2)} + \nu_2 d_{33}^{(2)} s_{11}^{(1)}}{\nu_1 s_{33}^{(2)} + \nu_2 s_{33}^{(1)}} + 2(\nu_1 d_{31}^{(1)} + \nu_2 d_{31}^{(2)})$$

where

$$\bar{\mathbf{d}}_{31} \cong \nu_1 d_{31}^{(1)} + \nu_2 d_{31}^{(2)}. \tag{10.3.3}$$

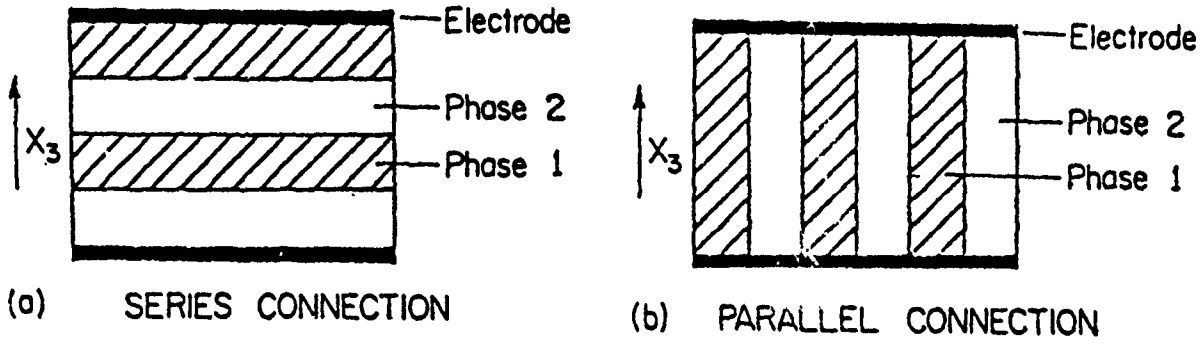


Fig. 10.3.1 — Sketches of composites which define series, parallel connection

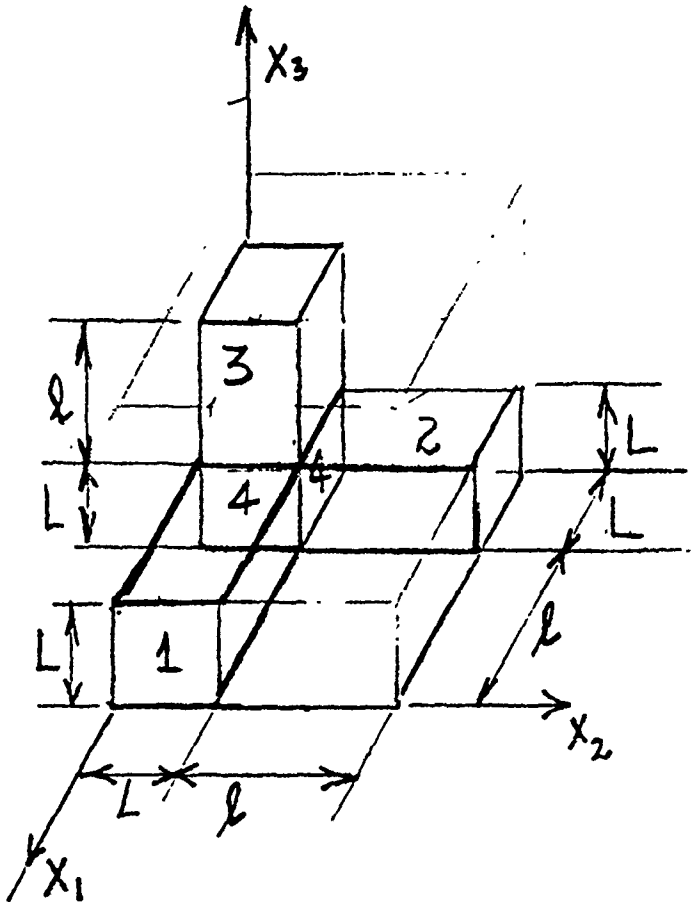


Fig. 10.3.2 — Theoretical model of a repeating cube in a 3-3 composite

When 3-3 composites are considered, the phase are neither all parallel or all series connected. A theoretical model is useful in estimating electric permittivity and piezoelectric constants. A simple model [4] is based on a lattice of cubic building blocks, each block $L + l$ units on edge, Fig. 10.3.2. Here parallelopipeds 1, 2, and 3 are phase 1 piezoceramic blocks parallel to X_1, X_2, and X_3 respectively. Cube 4 is also a piezoceramic block. The total volume of piezoceramic is $L^3 + 3L^2l$. Since the remainder of the $L + l$ cube is filled with polymer the volume fraction of piezoceramic is

$$\nu = \frac{L^3 + 3L^2l}{(L + l)^3}. \tag{10.3.4}$$

Assume now that the composite is poled in the X_3 direction. Only block #3 then is piezoelectrically coupled. The volume fraction ν_1^*, of active piezoceramic is then

$$\nu_1^* = \frac{L^3 + L^2 l}{(L + l)^3} \tag{10.3.5}$$

while the volume fraction of polymer in the building block cube is

$$\nu_2^* = 1 - \nu_1^*.$$

The formula for $\bar{\mathbf{d}}_{33}$ in this model is then

$$\bar{\mathbf{d}}_{33} = \frac{\nu_1^* d_{33}^{(1)} s_{33}^{*(2)}}{\nu_1^* s_{33}^{*(2)} + \nu_2^* s_{33}^{(1)}}. \tag{10.3.6}$$

Here $s_{33}^{*(2)}$ is the compliance of nonactive piezoceramic with associated polymers. In making estimates it is useful to choose

$$s_{33}^{(1)} \cong 0.1\ s_{33}^{*(2)}. \tag{10.3.7}$$

In a similar manner

$$\bar{\mathbf{d}}_{31} = \frac{L^3 d_{31}^{(1)}}{(L + l)^3}. \tag{10.3.8}$$

The dielectric constant of the components may be estimated in the same way,

$$\bar{\mathbf{K}}_{33} \cong \bar{\mathbf{K}}_{33}^{(1)} L^2. \tag{10.3.9}$$

Note that l and L in these formulas are expressed as fractions of a unit cell.

Figure 10.3.3 is a (calculated) plot of $\bar{\mathbf{d}}_{33}$, $\bar{\mathbf{k}}_{31}$, $\bar{\mathbf{d}}_h$, and $-\bar{d}_{31}$ versus volume fraction ν_1 (of piezoceramic) of a unit cell based on the cubic array model [5].

Other models can similarly be constructed, such as one based on rectangular parallelopiped. As before, they can be used to give phenomenological explanations of measured values of composite properties.

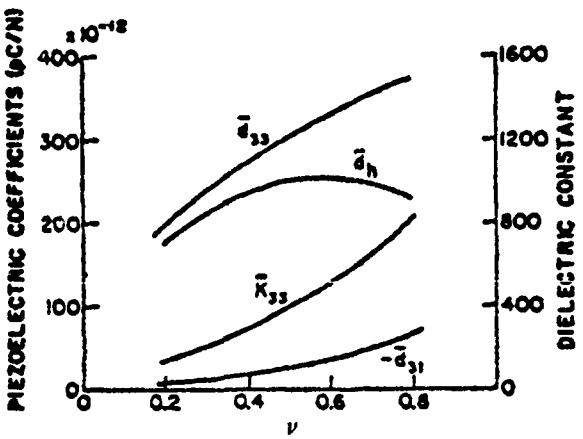


Fig. 10.3.3 — Piezoe ectric and dielectric coefficients calculated from the cubic array model

10.4 PREPARATION PROCEDURES FOR COMPOSITE MATERIALS

Composite structures designed to be the piezoactive materials of hydrophones are prepared in various ways. We note here four commonly used procedures.

(1) Embedding

Two phases of a multiphase composite are embedded in each other when one of the phases, generally in liquid form is poured around the second phase, generally in rod, fiber, crystal, etc. form, and harded in-situ.

(2) Perforation

The first phase, generally in block form, is drilled in different patterns of long, thin, straight holes which are then filled with the second phase, possibly in liquid form, in which case the liquid is hardened in-situ, or in solid form, in which case a close fitting is required.

(3) BURPS (Burned-out Plastic Spheres)

One phase, say a piezoactive ceramic, is ground to a powder, mixed with a volume of small plastic spheres, cemented with a binder, then fired (sintered). The plastic spheres burn out leaving a porous ceramic skeleton. The cavities of this skeleton are then back-filled with polymer, generally in liquid form, which is hardened in place.

(4) Replamineform [4]

A piece of coral skeleton is shaped by machining to a desired geometry. It is then vacuum-impregnated with Kerr Inlay casting wax and the wax is allowed to harden. The coral skeleton is then leached away in hydrochloric acid leaving a wax negative. The negative is invested with piezoceramic slip fluid by vacuum impregnation with vibratory action. The composite is heated at 300°C which burns off the wax negative. The coral-like piezoceramic structure is then sintered at 1280°C for one hour. The replica is back-filled with a suitable polymer (say Dow Corning MDX-4-4210 elastomer (silicone rubber)). Poling is done at 14 kV/cm for 5 min at 100°C. When desired the composite is crushed to break the connectivity leaving a flexible composite.

10.5 SUMMARY OF MEASUREMENTS ON FERROELECTRIC COMPOSITES FOR HYDROPHONES

With the definition of connectivity given in Sects. 10.2 and 10.3 and with a brief note of preparation methods given in Sect. 10.4 we turn now to record measured results on a variety of composites. Since the construction of hydrophones is currently based (to great extent) on polarized lead zirconate titanate material it will useful to list in Table 10.5.1 the physical and piezoelectric properties of those most commonly in use. For nomenclature see [3].

Included for comparison are three other materials: lead niobate, flexible components, and polyvinyldifluoride polymers. These are currently under investigation.

To assess the relative usefulness of these materials in hydrophone design we choose the figure-of-merit f_H discussed in Sect. 10.1, namely

$$f_H = \frac{M_0^2 C^T}{\mathscr{V}}.$$

Table 10.5.1 — Piezoelectric Ceramic Materials for Hydrophones [3]

Property / Material	g_{31}	g_{33}	k_{31}	k_{33}	S^E_{11}	S^E_{12}	S^E_{13}	S^E_{33}	$\tan\delta_b$	Q^E_M	Aging (%)		
	10^{-3} V–m/N				10^{-12} m²/N				(%)		K^T_{33}	k_p	f_1
Type I	−11.1	26.1	0.33	0.66	12.3	−4.0	−5.3	15.5	0.5	500	−5.0	−2.3	+1.5
Type II	−11.5	25.0	0.34	0.70	16.4	−5.7	−7.2	18.8	1.4	75	−1.0	−0.3	+0.2
Type II-M	−8.6	19.1	0.38	0.75	16.5	−4.8	−8.4	20.7	2.0	65	−2.7	−1.4	+0.9
Type III	−10.5	24.5	0.31	0.62	11.1	−3.7	−4.8	13.9	0.5	960	−4.0	−1.5	+1.0
Type IV	−5.5	14.1	0.19	0.47	8.6	−2.6	−2.7	9.1	0.6	400	−1.6	−1.4	+0.6
$PbNb_2O_6$	-4.5	42.7	0.05	0.38	–	–	–	25.4	–	11	–	–	–
*Flexible	-4.0	20.0	<0.01	–	–	–	–	–	15.0	<10	low	–	–
*PVF_2	-250	–	-0.001	–	–	–	–	–	2.0	<10	low	–	–

$g_h = g_{33} + 2g_{31}$; $\sigma^E = -\dfrac{S^E_{12}}{S^E_{11}}$; $\sigma^2 = \dfrac{k^2_{31} + \sigma^E}{(1 - k^2_{31})}$; $k_p^2 = \dfrac{2k^2_{31}}{(1 - \sigma^E)}$

$S^D_{11} = S^E_{11}(1 - k^2_{31})$; $S^D_{33} = S^E_{33}(1 - k^2_{33})$; *estimated values

In all practical cases, the design features a single mode of piezoelectric coupling so that the product of the square of the hydrophone sensitivity (M_0^2) and the free capacity C^T becomes,

$$M_0 C^T \propto g_T d_T \text{ or } g_p d_p \text{ or } g_h d_h.$$

A highly desirable mode of coupling is the hydrostatic mode in which the piezoactive material is subject to hydrostatic pressure *on all sides:* no pressure release is needed, whether inherent in the structure (such as hollow cylinders or spheres) or furnished with air-backed cavities in the form of sponge-rubber etc. Hence the advantage of possible submergence of this material in the ocean to limitless depths. In pursuit of such a design it is noted from Table 10.1.1 that the magnitude of $g_h d_h$ for commonly used hydrophone materials lies between 100 and 200 × 10^{-15} (in units of m^2/N). This is judged to be quite low, and is attributed to the fact that d_h (= $d_{33} + 2d_{31}$) is small because d_{31} (about 1/2 d_{33}) is opposite in sign to d_{33}. Also because $g_h = d_h/K^T_{33}$, and because K^T_{33} is large the value of g_h is low.

To improve the design of hydrophones operating in the hydrostatic mode one must seek two goals: (1) to decouple the d_{33} from the d_{31} piezoconstant, and (2) simultaneously lower the dielectric constant so that g_{33} is increased. There is however a price paid for low dielectric constant, namely adverse electric loading of the electric cable to the hydrophone, which can only be overcome by use of a preamplifier between hydrophone and cable. A material which offers promise to achieve both of these goals is a composite of piezoceramic and polymer elastomers in diphasal structure combined in a variety of connectivities. To assist in the discussion we note that the subject of connectivity has been derived in Sects. 10.2 and 10.3, and methods of preparation of composites are briefly summarized in Sect. 10.4. The new material itself can best be described by experiments on various compositions.

We consider next experimental results of measurements of piezoelectric properties of piezoelectric polymer composites with various connectivities. The cases considered are a few of the many types of connectivity possible.

Case #1 Lead Zirconate Titanate/Epoxy Composites in 1-3 Connectivity

The structure of this composite is shown in Fig. 10.2.1(a). In the final assembly the piezoceramic rods were 3 cm long and 840, 600, 400, and 254 μm in diameter—rods of any one diameter making up a particular composite. Fixtures were designed to give the composites 10, 20, 30, 40, and 50% piezoceramic by volume. Epoxy was then poured around each fixture under a vacuum to remove air bubbles

and cured at 70°C for 16 h. The resultant 3 cm long slug (mass density 1.3×10^3 kg/m^3) was cut into sections 1, 2, 3, and 4 mm thick, and silver electrodes were applied to them, and they were poled in a 75°C oil bath with a field of 22 KV/cm for 5 min. Permittivity was measured on a bridge at 1 kHz; d_{33} was measured with a d_{33} meter (Model CPDT 3300 of Channel Industries, Chagrin Falls, Ohio) and d_h was measured by changing pressure in an oil chamber at a rate of 3.5 MPa/s and collecting charge in an integrating electrometer.

Figure 10.5.1(a) shows measured d_{33} (in units of coulomb/newton) as a function of volume percent of lead zirconate titanate for three diameter rods (400, 600, and 840 μm). Figure 10.5.1(b) gives the standard deviation in these measurements.

Figure 105.2 shows measured d_h versus thickness of sample with volume percentage of lead zirconate titanate as parameter. A noticeable feature of plot (C) is that for a 4 mm thick sample d_h of the composite was some 3X the value of d_h for Clevite PZT 501A.

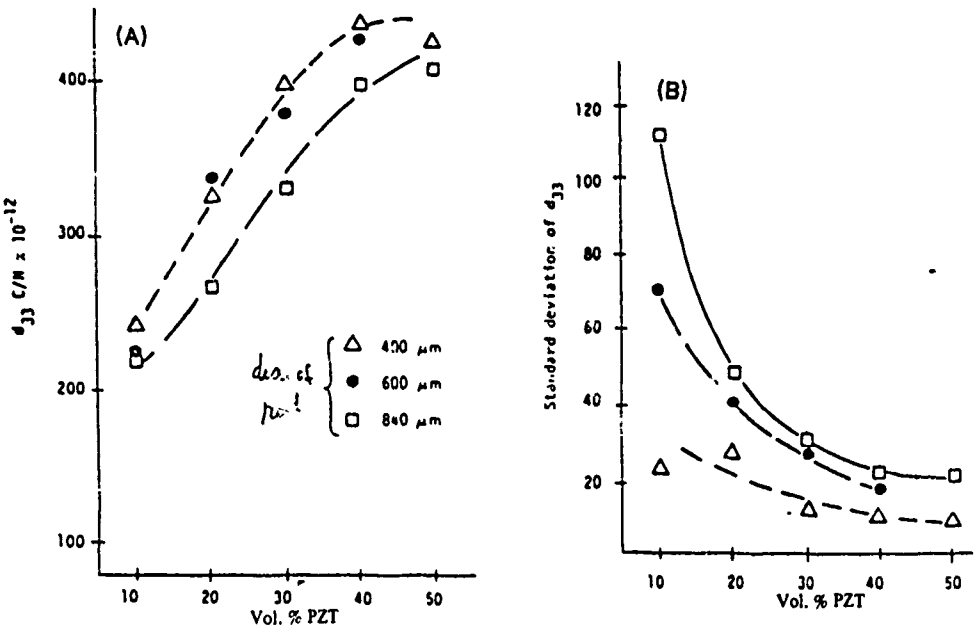


Fig. 10 5.1 — Plots of (A) d_{33} and (B) standard deviation of d_{33} vs vol % of PZT [7]

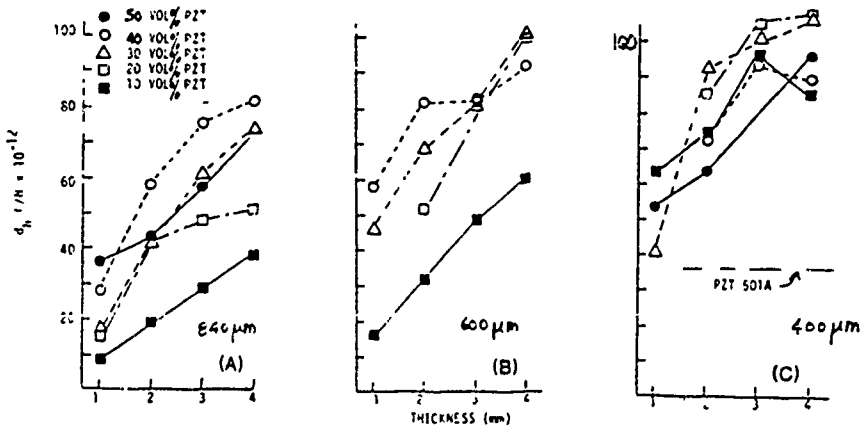


Fig. 10.5.2 — Variation of d_h with vol % PZT and composite thickness for rod diameters of (A) 840 μm (B) 600 μm, and (C) 400 μm [7]

Figure 10.5.3 shows measured values of K_{33}^{T} versus volume percentage of of lead zirconate titanate. The variation is seen to be nearly linear.

Figure 10.5.4 shows measured values of "voltage piezoconstant" g_h (units: Vm/N) versus volume percentage of lead zirconate titanate.

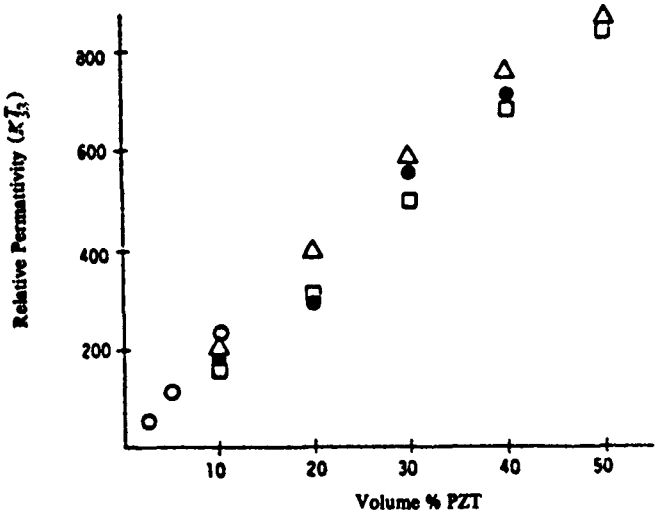


Fig. 10.5.3 — Relative permittivity vs vol % PZT; symbols as in Fig. 10.5.1 [7]

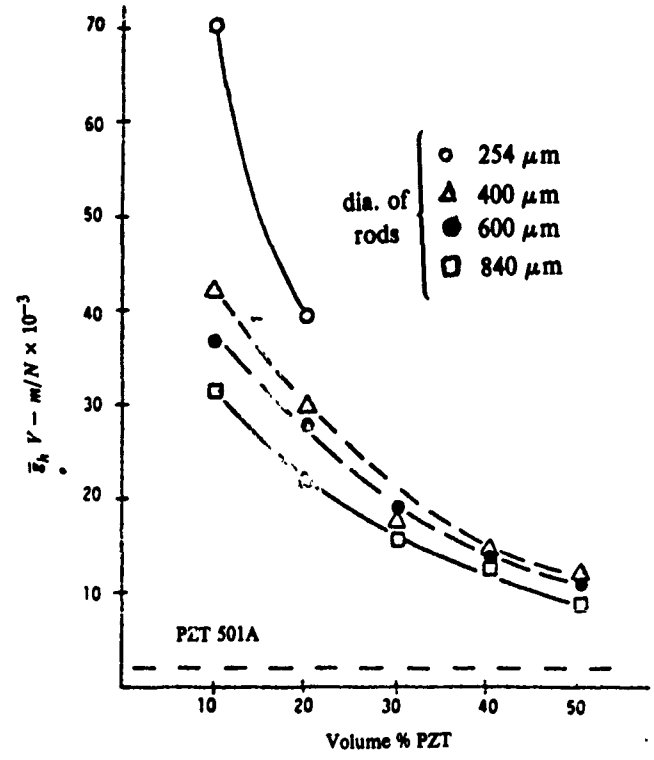


Fig. 10.5.4 — Plot of g_h vs vol % PZT; symbols as in Fig. 10.5.1 [7]

All these figures give a variety of figure-of-merit (taken here to be the g_h and d_h product). An example will show what can be achieved. We choose,

10% PZT by volume
400 μm diameter of rod
1 mm thickness

The values of parameters for this composite are then:

$$d_{33} \simeq 235 \times 10^{-12}\ \text{C/N} \qquad \text{(Fig. 10.5.1)}$$

$$d_h \simeq 63 \times 10^{-12}\ \text{C/N} \qquad \text{(Fig. 10.5.2)}$$

$$K_{33}^T \simeq 200 \qquad \text{(Fig. 10.5.3)}$$

$$g_h \simeq 43 \times 10^{-3}\ \frac{V_m}{N}. \qquad \text{(Fig. 10.5.4)}$$

Hence,

$$g_h d_h \simeq 2709 \times 10^{-15}\ (\text{m}^2/\text{N}).$$

This product is roughly some 20× larger than piezoelectric ceramic materials currently in use (see Table 10.1.1).

Case #2 Lead Zirconate Titanate/Epoxy Composites in 0-3, 1-3, 3-3, 3-1 and 3-2 Connectivities

A summary of the piezoelectric properties of these composites prepared by Perforation, Burps, Replamine or Embedding procedures (see Section 10.4) is presented in Tables 10.5.2 and 10.5.3. Some remarkable figures-of-merit are achieved. In Table 10.5.2 a polyurethane matrix drilled with a row of holes in one direction, and then backfilled with piezoceramic rods to make a 1-3 connectivity, showed a $g_h d_h$ product of $42,100 \times 10^{-15}$ m^2/N. Similarly a composite prepared by the BURPS procedure which gave a 3-3 connectivity (= skeleton of piezoceramic intertwined with a skeleton of silicone rubber) showed a $g_h d_h$ product of $26,000 \times 10^{-15}$ m^2/N. Again this should be compared to a value of 168×10^{-15} m^2/N Type I Piezoelectric Ceramic (Table 10.1.1).

Table 10.5.3 lists results of measurements on composites of 3-1 and 3-2 connectivity prepared by perforation. In one case of a 3-2 connectivity (see Fig. 10.2.1b), with the piezoceramic block polarized and electroded along the z-axis, and holes backfilled with epoxy along both x and y axes, the epoxy-filled hole size was 3.2 mm, separated from adjacent holes by $X = 4.5$ mm. The composite thickness was 5.8 mm. Upon measurement on an automated capacitance bridge at 1 kHz the dielectric constant $\bar{\mathbf{K}}_{33}$ came to a value of 290. The piezo charge constant $\bar{\mathbf{d}}_{33}$ was measured on the d_{33} meter noted above to be 290×10^{-12} C/N. From these two values one deduced that $g_{33} = d_{33}/K_{33} \sim 114 \times 10^{-3}$ Vm/N. Thus the product $\bar{\mathbf{g}}_{33}\bar{\mathbf{d}}_{33} \simeq 33,000 \times 10^{-15}$m^2/N. Similarly the hydrostatic constant $\bar{\mathbf{d}}_h$ was measured to be 329×10^{-12}C/N by use of an electrometer method described above. The voltage piezoconstant was deduced to be 128×10^{-3} Vm/N, from which the $g_h d_h$ product calculated out to be about $42,000 \times 10^{-15}$m^2/N. These are extraordinary values.

Table 10.5.2 — Piezoelectric Properties of PZT-Polymer Composites

	$\bar{K}_{33}$	$\bar{d}_h$ (PCN^{-1})	$\bar{g}_h$ (10^{-3} VmN^{-1})	$\bar{d}_h\bar{g}_h$ (10^{-15} m^{2}N^{-1})
PZT	1600	50	4	200
PZT particles in silicone rubber matrix (0-3 connectivity)	100	28.3	32	900
PZT replamine in a silicone rubber matrix (3-3 connectivity)	50	35.8	80	2800
PZT rods in an epoxy matrix (1-3 connectivity)	200	77.6	40.4	3138
PZT rods in a polyurethane matrix (1-3 connectivity)	83	176.2	239	42100
Burps composite (epoxy matrix) (3-3 connectivity)	500	120	27	3200
Burps composite (silicon rubber matrix (3-3 connectivity)	300	260	100	26000

(after [8]).

Table 10.5.3 — Measurements on 3-1 and 3-2 Composites

	Hole Size (mm)	Composite Thickness (mm)	$X^\dagger$ (mm)	K_{33}	$\bar{d}_{33}$ (PCN^{-1})	$\bar{g}_{33}$ (10^{-3} VmN^{-1})	$\bar{d}_h$ (PCN^{-1})	$\bar{g}_h$ (10^{-3} VmN^{-1})	$\bar{d}_h\bar{g}_h$ (10^{-15} M^{2}N^{-1})
Perforated PZT/epoxy (3-1 connectivity)	3.2	6.5	4.25	810	340	47	210	29	6000
Perforated PZT/epoxy (3-1 connectivity)	3.2	6	4.25	760	350	52	230	34	7800
Perforated PZT/epoxy (3-1 connectivity)	3.2	5.5	4.25	740	330	50	206	30	6000
Perforated PZT/epoxy (3-1 connectivity)	3.2	4.5	4.25	680	320	53	190	31	5900
Perforated PZT/epoxy (3-1 connectivity)	4.2	6.8	4.75	470	290	70	190	46	8600
Perforated PZT/epoxy (3-1 connectivity)	4.2	6.5	4.75	450	290	73	222	56	12300
Perforated PZT/epoxy (3-1 connectivity)	4.2	6	4.75	425	280	74	170	45	7600
Perforated PZT/epoxy (3-1 connectivity)	4.2	5.5	4.75	410	275	76	120	33	3950
Perforated PZT/epoxy (3-2 connectivity)	3.2	6.7	4.5	360	290	90	238	74	17600
Perforated PZT/epoxy (3-2 connectivity)	3.2	6.2	4.5	330	290	99	294	100	29000
Perforated PZT/epoxy (3-2 connectivity)	3.2	6	4.5	320	300	105	322	113	36300
Perforated PZT/epoxy (3-2 connectivity)	3.2	5.8	4.5	290	290	114	329	128	42000
Perforated hollow PZT scaled with polymer (3-2 connectivity)	3.2	6.2	4.5	340	340	112	372	123	45700

(after [8])

(†X is the center-to-center distance of adjacent holes.)

In composites prepared by perforation it is clearly seen that hole size, hole separation and composite thickness play a role. Figure 10.5.5 shows the variation of d_h with composite thickness. This is a 3-1 composite prepared by perforating a solid block of piezoactive ceramic (PZT) with 3.2 mm diameter holes parallel to the x-axis, separated in three samples by x = 3.25, 3.75 and 4.25 mm distances respectively. Polarization (prior to perforation) was along the z axis, carried out in an oil bath at 140°C in a field of 25 kV/cm for 3 minutes. The perforations were backfilled with commercial epoxy and cured at 70°C for 8 hours. The effect of hole size on $\bar{d}_{33}$ for various hole separation distances in shown in Fig. 10.5.6. The value of d_{33} is seen to rise linearly with hole separation distance and then level off to about 350-400 × 10^{-12} C/N.

An example of a piezoceramic/polymer in 3-1 connectivity of the honeycomb type shown in Fig. 10.2.1c has been reported by Shrout et al. [10], the results of which are shown in Table 10.5.4. Mass densities of 2.9 × 10^3 kg/m^3 were achieved in these structures. Table 10.5.5 gives the electromechanical properties of these honeycomb composities.

10.6 LEAD ZIRCONATE TITANATE/POLYMER COMPOSITES HIGH FREQUENCY APPLICATIONS

Polarized lead zirconate titanate ceramic materials are often used in thin slabs to radiate (and receive) ultrasonic pulses in liquid media. Because of their high mass density and nonuniform face motion they are mismatched in impedance to liquids and therefore do no load well. Since their internal losses are negligible they usually operate over narrow (resonance) bandwidths with mechanical Q above 100. Distortion of pulse shape is then expected. To improve the bandwidth of pulse projection the designs usually employs Langevin techniques of adding backing plates of appropriate materials and thickness, and adding quarter-wave layers to the radiating face thus achieving better impedance match. This is the conventional sandwich construction.

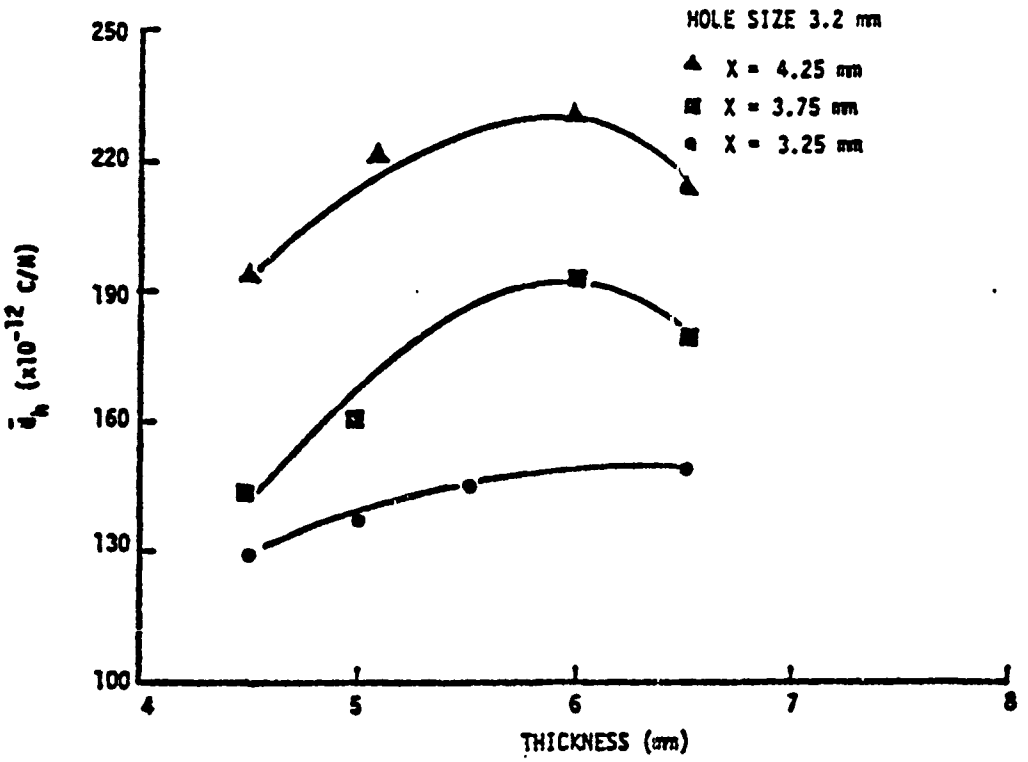


Fig. 10.5.5 — Hydrostatic piezoconstant d_h versus composite thickness for fixed hole size and three hole separation distances for a 3-1 connected composite [8]

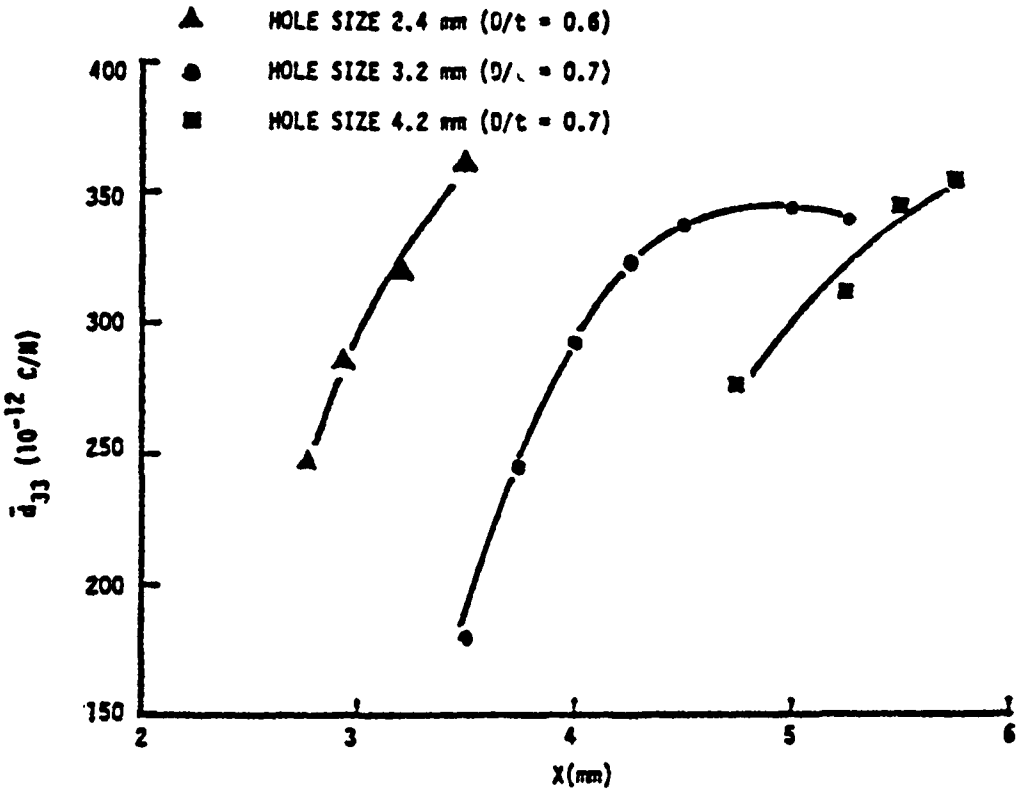


Fig. 10.5.6 — Piezoconstant d_{33} vs hole separation X for three hole sizes [8]

Table 10.5.4 — Electromechanical and Physical Properties of PZT/Polymer Composites [10]

Property	Homogeneous PZT 501A[a,b]	1-3* Composities	
		PZT/Spurrs	PZT/Flexane
density (kg/m^3)	7900	2900	2600
dielectric constant (K)	2000 (1800)[b]	(unpoled) 340-370 (poled) 450-500	390-460 480-520
tan δ	0.014	0.017	0.025
piezo d_{33} ($\times 10^{-12}$ C/N)	400	240-300	260-340
piezo d_h ($\times 10^{-12}$ C/N)	50	10-20	15-20
piezo d_{31} $-(\times 10^{-12}$ C/N)	175	115-140	120-160
voltage coef. g_{33} ($\times 10^{-3}$ Vm/N)	22	60-70	60-70
voltage coef. g_{31} ($\times 10^{-3}$ Vm/N)	10	29-32	28-35

[a]Ultrasonic Powder, Inc., "Piezosonic Powders" data sheet.
[b]Properties measured on PZT-50A disks were found to be in good agreement with expected values. However typical values of dielectric constants were found to be lower ~1800 ± 10%.
*(same as 3-1 in the nomenclature of this treatise.)

Table 10.5.5 — Electromechanical and Physical Properties Determined by Resonance [10]

Property	Homogeneous PZT 501A[a,b]	1-3* Composites	
		PZT/Spurrs	PZT/Flexane
Frequency constant $N_{thickness}$ (Hz-m)	1740	1600	1600
Elastic stiffness C_{33}^{D} (G Pa)	96	81	81
Thickness coupling coefficient, k_t (%)	45	55-65	55-58
Planar coupling coefficient, k_p (%)	63	35	—[c]

[c]Note: The PZT/Flexane composites did not give distinct planar mode resonances due to difficulties in processing uniform disks.

*(Same as 3-1 in the nomenclature of this treatise.)

An alternative approach to achievement of lower mechanical Q is the use of piezoceramic/polymer composites. Because their mass density and sonic speed are inherently lower than conventional piezoceramic materials they make a better match to liquids. In ultrasonic applications Qs less than 20, and even less than 10, can routinely be obtained.

Several types of piezoceramic/polymer composites for ultrasonic use have been investigated. These are (1) lead zirconate titanate/polymer in 1-3 connectivity similar to Fig. 10.2 1(a); (2) in 3-3 connectivity replamine form (see Sect. 10.4) in which a skeleton of piezoceramic is interwoven with a skeleton of polymer epoxy; (3) in honeycomb 3-1P connectivity of the type shown in FIg. 10.2.1(c); (4) or in piezoceramic tapes laminated with epoxy in a 2-2 connectivity similar to Fig. 10.3.1(a).

These composites were tested by various methods with various results. These are discussed next.

Case #3 Lead Zirconate Titanate/Polymer Composite in 1-3 Connectivity for Ultrasonic Application

The composite slug constructed in the manner shown in Fig. 10.2.1(a) was sliced into thin disks such that the thickness resonance mode occurred in the 1-5 MHz region. They were poled at 20 KV/cm for 5 min in an oil bath at 75°C. To measure their transmitting response characteristics Ref. 9 used the tone-burst pulse-echo method, the set-up of which is shown in Fig. 10.6.1. Each disk of composite was sealed at the end of a steel tube and inserted in the system as the "transducer." The disk was then driven at 10 volts peak in a tone-burst lasting 15-20 cycles of a selected frequency. The pulse traversed the water tank, struck a stainless steel block, and was perfectly reflected back to the disk. The disk transduced the echo into an electrical signal which was measured either across a diode isolation, or across 50 ohms, and was made visible on an oscilloscope. To reduce near field diffraction effects of the disk, radius a, at wavelength λ, the reflecting block was placed at distance $D = a^2/\lambda$. Although all disks had a 1-3 connectivity, the piezoceramic (phase 1) was in the form of rods, or spheres, or triangular prisms.

Dielectric constant K_{33} and piezoconstant d_{33} were measured by methods described in Sect. 10.5. Mechanical Q, thickness coupling K_T, resonance frequency, bandwidth, echo signal level were measured by the electrical admittance technique. To compare various composites the product of the bandwidth and the echo voltage signal across 50 ohms was chosen as a figure-of-merit. Table 10.6.1 gives measured results on piezoceramic/polymer composites of 1-3 connectivity.

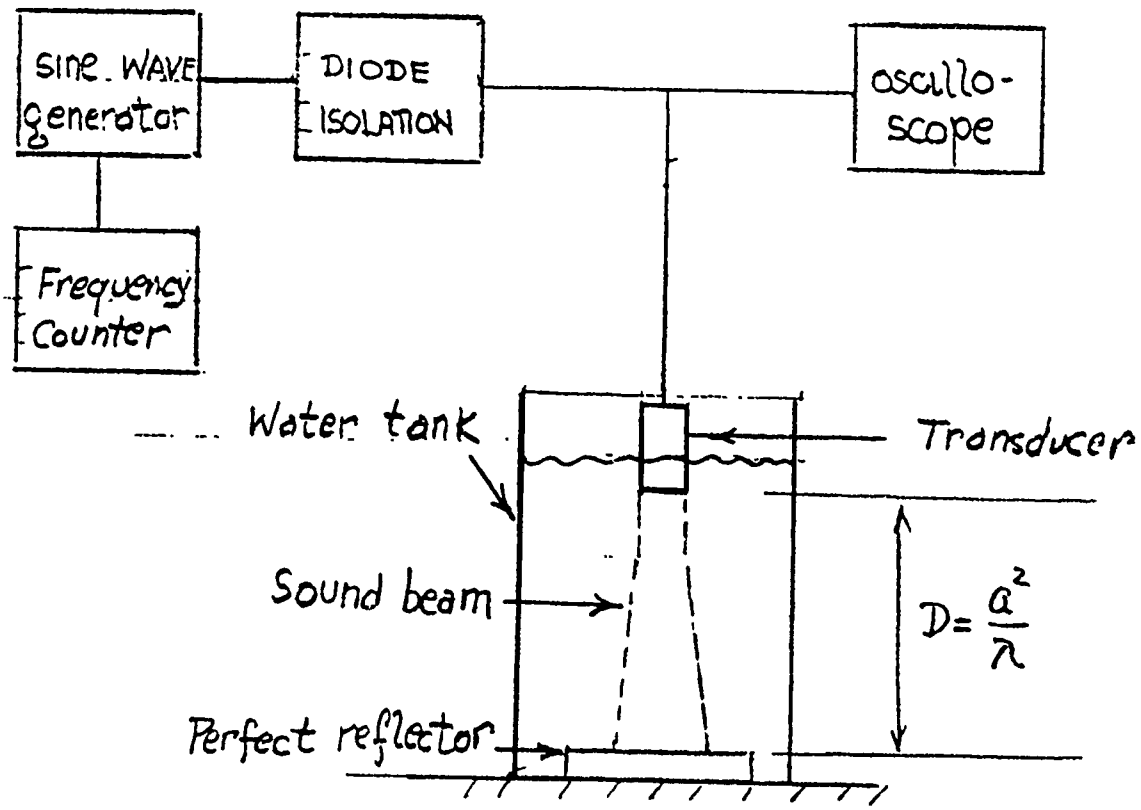


Fig. 10.6.1 — Pulse echo that set-up

Table 10.6.1 — Electromechanical Properties and Pulse Fcho Response of Composite in Piezoceramic/Polymer 1-3 Connectivity [9]

composite type	Pulse % PZT	Dielectric constant k	d_{33} $\times 10^{12}$ C/N	Thickness coupling $k_t(z)$	mechanical Q	Frequency constant N(Hz-M)	Resonance frequency f(MHz)	Bandwidth (BW) MHz (6 dB)	Echo Signal (50 Ω load) V_{50} (volts)	Figure of merits V_{50}-BW	Echo Signal (diode isolation) V_D (volts)
3-1* with 0.45 mm rods	10	117	110	70	4-5	1324	2.4	0 4	0.8	0.32	
	20	244	174	67	14	1290	2.55	0.3	2.8	0.84	3.4
		233	225	—	—	—	3.2	1	1.2	1.2	—
		153	101	—	—	1-60	4.4	1.25	0.4	0.50	—
	30	335	183	72	3	—	2.65	0 7	2.4	1.7	—
		249	123	67	19	1051	4.15	1.3	0.8	1.0	—
3-1* with 0.28 mm rods	10	87	129	59	4.6	1335	2.6	0.65	0.3	0.20	0.7
		237	277	—	—	1221	1.17	0.26	0.7	0.18	3.8
	20	211	195	68	11	1310	2.18	0.45	1.25	0.56	2.2
		158	122	78	10	1071	4.4	1.2	1.12	1.3	1.16
3-1* with 1.5 mm spheres	10*	180	60	60	6	1100	0.915	0.29	0.80	0.23	—
	30**		140					0 24	0.72	0.17	—
3-1* with triangular prims (0.85 τ)	12*	270	153	—	—	101*	1 13	0.35	0.32	0.11	—
	60**		2.5					0°	0.3	0.14	—

*In Ref. 9 a 3-1 connectivity has the same meaning as a 1-3 connectivy in this treatise.

Table 10.6.2 gives similar test results on piezoceramic/polymer composites with 2-2 connectivity of the type shown in Fig. 10.3.1a, with layers of piezoceramic and epoxy, and a honeycomb composite with 3-1P connectivity of the type shown in Fig. 10.2.1(c).

Table 10.6.2 — Electromechanical Properties and Pulse Echo Response of Composite in Piezoceramic/Polymer 1-3 P Connectivity [9]

composite type	Pulse % PZT	Dielectric constant k	d_{33} $\times 10^{12}$ C/N	Thickness coupling $k_t(z)$	mechanical Q	Frequency constant N(Hz-M)	Resonance frequency f(MHz)	Bandwidth (BW) MHz (6 dB)	Echo Signal (50 Ω load) V_{50} (volts)	Figure of merits V_{50}-BW	Echo Signal (diode isolation) V_D (volts)
2-2 with 0.38 mm tapes	27	155	126	52	14	1894	3.00	0.76	0.65	0.5	1.20
1-3 honey-comb	30	273	175	65	12	1530	2.4	0.3	0.8	0.24	–

*In Ref. 9 a 1-3 connectivity has the same meaning as a 3-1 P connectivity in this treatise.

REFERENCES

[1] W.G. Cady, "Piezoelectricity," Dover Publications New York (1946) p. 194.

[2] R.S. Woollett, J. Acous. Soc. Am. **34**, 522 (1962).

[3] "Handbook of Hydrophone Element Design Technology," Ed. C.L. LeBlanc, 1978. Naval Underwater Systems Center New London. NUSC Tech. Document 5813 [Note: Materials designated Type I through IV are described in U.S. Mil-Std-1376].

[4] D. Berlicourt, "Properties of Sponge Ceramics," Clevit Corp. Internal Report Dec. 1960.

[5] K. Rittenmeyer et al., "Targeted Basic Studies of Ferroelectric and Ferroelastic Materials for Piezoelectric Transducer Applications," Mat. Res. Lab. Penn. State, University Park, Penn. Nov. 1981, Appendix 6.

[6] D.P. Skinner, Nat. Res. Bull. **13**, 599-607 (1978).

[7] K.A. Klicker et al., J. Am. Ceramic Soc. **46**, 5(1981).

[8] A. Safari et al., See Appendix 5 of Reference 5.

[9] T.R. Gururajer et al., Ferroelectrics **39**, 1245-1248 (1981).

[10] T.R. Shrout et al., Mat. Res. Bull. **15**, 1371-1379 (1980).

INDEX

Acoustic loading, 8, 145
Acousto-Optic materials, 347
Acoustical networks, 23
Analogies, electroacoustic, 33
Analysis of transducers
  abstract form of, 114
  Green's function approach, 115
  state system model, 119, 176
  variational methods, 97-109
  equivalent circuits, 146
  impedance/admittance plots, 225
  transmission line, 269
  signal flow graphs, 109
Bandwidth of transducers, 69, 76
Blackbox description of transducer components, 45
Boundary conditions in analysis, 211
Bond graphs, 148
  notation, 149
  power flow in, 149
  causality in, 149, 153
    integral causality, 154, 168
    differential causality, 154
  for interconnected systems, 156
  relation to impedance, 178, 182
  examples of, 157 to 176
  flow charts, 21
  of equivalent sources, 58
  and formulation of dynamic equations, 170
Canonical circuits of 2-mesh systems, 91
Coefficient of electromechanical coupling, 79
  experimental determination of, 81
  material coupling coefficient, 84
  effective coupling coefficient, 87
  static and dynamic coupling factors, 89
  measure of work done, 84
  for dielectric transducers, 196
  magnetoelastic, 402
Composite materials, Chap. 10
  connectivity of, 487-491
  preparation of, 492
  hydrophone of, 492
  measurements, 487, 494, 495
Constant-B drive, 203
Constant-H drive, 203
Constant voltage drive, 229
Constant current drive, 229
Coupled circuits, 68
  mutual inductance type, 69
  capacitive type, 76
  2-mesh electrical type, 90
Design aids, 220
  motional impedance plots, 224
  motional admittance plots, 224
  geometrical considerations of impedance and admittance plots, 225
Diffraction constant in pressure-gradient sensors, 448
Duality, 77
  contrasted to series/parallel inversions, 18, 17
ΔE effect, 404
Equivalent circuits, 2
  construction of, 35
  for mechanical networks, 36
  examples of, 8
  of continuous elastic systems, 49
Figure-of-merit for hydrophones, 485
  gd product, 486
Filters
  mechanical, 254
  acoustical, 254
  described by bond graphs, 265
Fixed velocity distribution, general theory of transducers with, 475
Four-pole (impedance) parameters, 62, 63, 64
FV plots, 42
General theory of transduction, Chap. 9
  electroacoustic transduction, 468
  electromechanical transduction, 467
  transducer receiving response, 471
  transducer transmitting response, 472
  reciprocity, 473
  fixed velocity distribution, 475
  available acoustic power, 480
  threshold pressure, 481
Grounding of mass element, 8
Helmholtz resonator (Underwater) transducer, Chap. 3
  analysis, 310
  construction, 309
  spherical type, 316
  cylindrical type, 320
  generic model, 314
Homodyne, heterodyne reception, 377

Hydrophone
polymer film, 340
optical fiber, 357, 452
laser doppler, Chap. 6
metallic glass, 408
composite material type, 492
Ideal transformer transduction, 94
Laser-doppler hydrophone, Chap. 6
homodyne, heterodyne, 377
minimum detectable signal, 381
laboratory demonstration, 382
design considerations, 385
comparison with laser-dopper velocimeter, 394
Magnetic fields, 187
maximum power in magnetic field transducers, 405
magnetic field transduction losses, 407
transduction ratio, 407
Magnetostriction, 400
nickel, 399
metallic glass, 415
rare-earth alloy, 418
Mason equivalent circuit of a
bar transducer, 232-243
clamped at one end, loaded at the other end, 239
one end free, other end loaded, 240
examples and cases, 213
Matrix modeling of transducers, 30, 124
examples of, 31, 32
Mechanical circuit elements, 5
Metallic glass transducer, Chap. 7
magnetostriction property of, 408
coupling coefficient, 416
ΔE effect, 416
transduction losses, 416
transduction ratio, 416
experimental results, 415
Mechanical mutual mass, 5
Mechanical networks, 3
Nonreciprocal transduction, 96
Norton's equivalent source
Bond graph of, 58
One-connection systems, 57, 59
Thevenin's equivalent source, 58
Norton's equivalent source, 58
Optical fibers as pressure sensors
properties, 347
stress-strain relations, 349
pressure effects on, 351
Optical fiber hydrophone
construction, 357
theory of operation, 358
experimental results, 359
protection against environmental noise, 362
lowest detectable signal, 360
intensity modulated types, 373
SNR, 366
Particle velocity determined by
pressure-gradient sensor, 423
error analysis, 458
Piezomagnetic activity, 192
Piezomagnetic coupling, equations, 194
Polymer film
phenomenological theory, 331, 339
31 mode, 333
33 mode, 337
Polymer film hydrophone, 340
structure, 341
analysis, 342
Pressure-gradient in an acoustic field
relation to particle velocity at a point, 423
between two points, 424
between two pairs of points, 427
Pressure-gradient microphone
diffraction effects, 428
diffraction constant, 433
Pressure-gradient hydrophone
spherical shell, 450, 451
mass suspended inside a cylindrical shell, 450
fiber-optic type, 452
Primary circuit model, 132
Rare-earth alloy magnetostrictive
transducers, 418
theory, 418
measurements, 419
Receivers
moving armature, 293
length expander, 296
electrostatic, 299
standard hydrophone designs of, 303
Reciprocal transduction, 93
Resonance
velocity, 200
electrical/mechanical, 200
multiple, 198
nomenclature summary, 209
quarter-wave, 230
half-wave, 231
series-connected, 248
parallel-connected, 243
series/parallel connected, 252
Standard equivalent circuits, 213, 216
State system model, 133
theory, 119

trees, cotrees, system graphs, 128
supernode (cut-set), 131
examples, 139
Secondary circuits, 2
Series/parallel form, 18
Signal flow graphs, 109
Sources, exchange of, 15
Helmholtz equivalent, 16
Norton, Thevenin Equivalent, 58
Thevenin equivalent source
bond graph of, 58
Transduction types
ideal transformer, 54
ideal gyrator, 52
antireciprocal, 96
Transmission line analysis
lumped parameter, 269
distributed parameter, 280
examples of, 283, 284
resonant circuit comparison, 287
Turns-ratio, 228
Two-Connection systems, 60, 126
Unification of coupled circuits, 52
example, 55
Variational principle, 97
VF representation of systems, 19, 40

☆ U.S. GOVERNMENT PRINTING OFFICE: 1984-428-696